

# Graduate Schools Yearbook **2013**



**Editors:**

Kim Dam-Johansen  
Sindhu Vudayagiri  
Krist V. Gerbaey

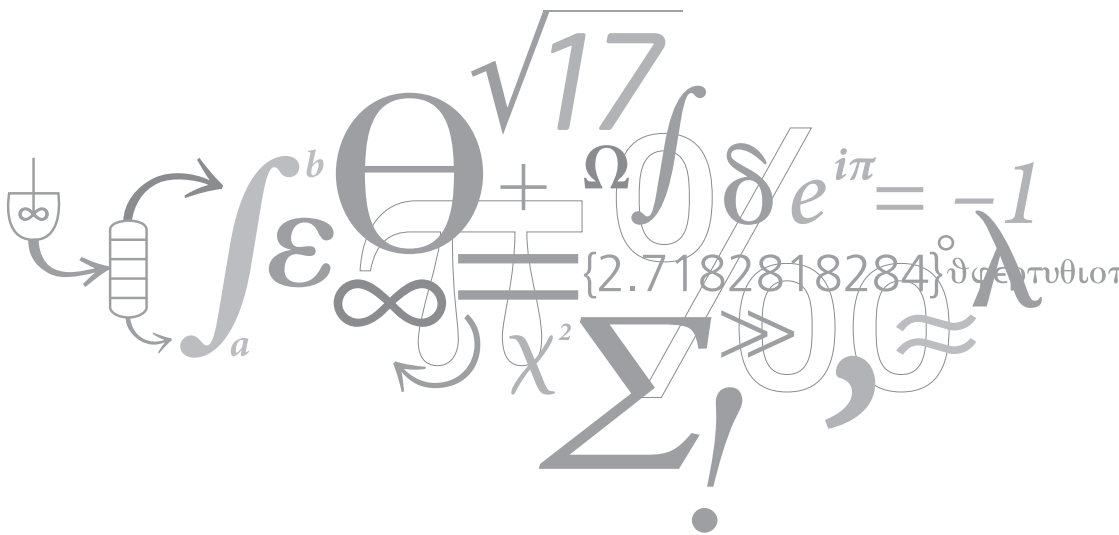
# Graduate Schools Yearbook **2013**

**Editors:**

Kim Dam-Johansen

Sindhu Vudayagiri

Krist V. Gernaey



Address: Department of Chemical and Biochemical Engineering  
Søltofts Plads, Building 229  
Technical University of Denmark  
DK-2800 Kgs. Lyngby  
Denmark

Telephone: +45 4525 2800

Fax: +45 4588 2258

E-mail: [kt@kt.dtu.dk](mailto:kt@kt.dtu.dk)

Internet: [www.kt.dtu.dk](http://www.kt.dtu.dk)

Print: J&R Frydenberg A/S  
København  
January 2014

Cover: Suzanne Fog

Cover photo: Christian Ove Carlsson

ISBN-13: 978-87-93054-24-0

## **Preface**

In this Graduate Schools Yearbook 2013 the PhD students of the Department of Chemical and Biochemical Engineering at the Technical University of Denmark (DTU) present their research projects. Some of the students have just initiated their research and therefore provide a short description of their research project in the Yearbook, whereas others are close to concluding their work and present the most significant project results. We hope that you will find the Yearbook interesting, and we invite you to contact us in case you would like to receive additional details about one of the projects or topics described in the Yearbook.

The PhD projects in the Yearbook cover all areas where the Department is active, both at Campus Lyngby and Campus Risø. We have managed to consolidate our level of activity at the Department in 2013, meaning that we have kept our total number of PhD students significantly higher than 100. Our focus is still on the initiation of an increased number of industrial PhD projects. Specifically for 2014, the Department also has focus on exploring the new opportunities in the frame of the recently launched Horizon2020 Research Programme.

We wish you a pleasant reading.

Yours Sincerely

Kim Dam-Johansen  
Professor, Head of Department

Krist V. Gernaey  
Professor, Editor



## Contents

Design and Evaluation of Multi-enzyme Processes <i>Rohana Abu</i>	1
Low Salinity Waterflooding and Mineral Dissolution <i>Artem Alexeev</i>	3
Predictive Modeling of Gas Diffusion and Solubility in Polymers for Offshore Pipelines <i>Susana Almeida</i>	5
Combined Silage Pretreatment and Enzymatic Hydrolysis of Energy Grasses for Lignocellulosic Biofuel Production <i>Morten Ambye-Jensen</i>	7
Generic Model-Based Tailor-Made Design and Analysis of Biphasic Reaction Systems <i>Amata Anantpinijwatna</i>	9
Bioprocess Engineering for the Application of P450s <i>Marie Andersson</i>	11
Process Intensification: A Phenomena-based Approach <i>Deneesh K. Babi</i>	13
Dipolar Cross-linkers for PDMS Elastomers with Enhanced Dielectric Permittivity <i>Frederikke Bahrt Madsen</i>	17
Operation and Design of Diabatic Distillation Processes <i>Thomas Bisgaard</i>	21
CO <sub>2</sub> -Hydrates - Challenges and Possibilities <i>Martin Gamél Bjørner</i>	23
Integrated Microfactories <i>Vijaya Krishna Bodla</i>	27
Plant-wide Modelling and Control for Nitrous Oxide Emissions from Wastewater Treatment Plants <i>Riccardo Boiocchi</i>	31
Fermentation Processes at Small Scale <i>Andrijana Bolic</i>	33
Early Stage Design of Wastewater Treatment Plants: A Mathematical Programming Approach <i>Hande Bozkurt</i>	37

Process Synthesis and Design of the Future Biorefineries: Uncertainty Analysis on Raw Material and Utility Cost <i>Peam Cheali</i>	39
Symbiotic Growth Depressions in Bioenergy and Forage Crops <i>Signe Sandbech Clausen</i>	41
Interactions Between Solid Fuels and Raw Materials in Cement Rotary Kilns <i>Maria del Mar Cortada Mut</i>	43
Data, Analysis and Modeling of Physical Properties for Process Design of Systems Involving Lipids <i>Larissa Peixoto Cunico</i>	47
Systematic Methods and Tools for Computer Aided Modeling <i>Marina Fedorova</i>	49
Measurements and Modelling of Phase Equilibrium of Oil-Water-Polar Chemicals <i>Michael Frost</i>	53
Sustainable Design of Biorefinery Systems for Biorenewables <i>Carina Lira Gargalo</i>	57
Rate Based CO <sub>2</sub> Post-Combustion Modelling in Aspen Plus Using CERE Cape Open Modules <i>Jozsef Gaspar</i>	59
Reinforced Poly(Propylene Oxide): A Soft and Extensible Dielectric Electroactive Polymer <i>Kaustav Goswami</i>	61
Online Trace Gas Analysis for Biomass Gasification <i>Helge Grosch</i>	65
Evaluating Enzymatically Assisted CO <sub>2</sub> Removal from Flue-Gas with Carbonic Anhydrase <i>Maria Gundersen</i>	67
Novel Clay/Nanocellulose Biocomposite Films and Coatings in the Context of New Packaging Materials <i>Jon Trifol Guzmán</i>	69
Exploiting <i>Aspergillus Niger</i> Pelleting Behavior for Morphology Control in Order to Correlate it to Productivity in Industrial Fermentation <i>Timo Hagemann</i>	73
Microbial Enhanced Oil Recovery for North Sea Oil Reservoir <i>Amalia Halim</i>	75

Synthesis and Design of Integrated Process and Water Networks <i>Zainatul Bahiyah Handani</i>	79
Development of New Automotive Diesel Oxidation and NH <sub>3</sub> Slip Catalysts <i>Thomas Klint Hansen</i>	81
Combustion Characterization of Bio-derived Fuels and Additives <i>Hamid Hashemi</i>	83
Lamination of Polydimethylsiloxane Films Using an Open-Air Plasma Treatment System <i>Suzan Sager Hassouneh</i>	87
A Miniaturized Experimental Platform for Development of Recovery Processes <i>Søren Heintz</i>	89
The Effect of Nematic Interactions in Uniaxial Extension of Polymer Blends <i>Ludovica Hengeller</i>	93
Thermodynamic and Process Modelling of Gas Hydrate Systems in CO <sub>2</sub> Capture Processes <i>Peter Jørgensen Herslund</i>	95
Considerations for an Equilibrium Shifting Cascade Selection in $\omega$ -Transaminase Systems <i>Krešimir Janež</i>	99
Biomass Burners for Biodust Combustion <i>Joakim M. Johansen</i>	103
Property Modeling and Tailor-Made Mixture Design Involving Complex Chemical Systems <i>Sawitree Kalakul</i>	105
Determination of Core-Shell Content of Liquid Core Microcapsules <i>Malgorzata Kostrzewska</i>	107
Discovery and Engineering of a Bacterial Rhamnogalacturonan I Lyase <i>Dorte Møller Larsen</i>	109
Modeling Oxygen Transfer in Small Scale Reactors using Computational Fluid Dynamics <i>Hilde Larsson</i>	113
Phase Equilibria and Speed of Sound in Binary Systems of 1-Alcohols and n-Alkanes from the Simplified PC-SAFT Equation of State <i>Xiaodong Liang</i>	115
Catalytic Materials for Combined Particulate and NO <sub>x</sub> Removal from Vehicles <i>Kasper Linde</i>	119



Fuel Efficiency and Fouling Control Coatings in Maritime Transport <i>Asger Lindholdt</i>	121
Preparation and Characterization of Poly (Methyl Methacrylate) (PMMA) Microcapsules for PDMS Crosslinking Reaction <i>Baoguang Ma</i>	123
Inhibition of Gas Hydrate Formation by Antifreeze Proteins <i>Christine Malmos</i>	127
Design, Control and Analysis of Intensified Biochemical Processes <i>Seyed Soheil Mansouri</i>	131
A Systematic Methodology for Design of Emulsion-Based Chemical Products <i>Michele Mattei</i>	133
Thiol-ene “Click Chemistry” as a Powerful Tool for Preparation of Lab-on-Chip Flow Focusing Microfluidic Devices <i>Piotr Mazurek</i>	137
Multi-Dimensional Population Balance Models of Crystallization Processes <i>Kresten Troelstrup Meisler</i>	141
Enzymatic Production and Purification of Prebiotic Oligosaccharides by Chromatography and Membrane Systems <i>Malwina Michalak</i>	145
Operational Aspects of Continuous Pharmaceutical Production <i>Aleksandar Mitic</i>	149
Development of an Electrolyte CPA Equation of State for Applications in the Petroleum and Chemical Industries <i>Bjørn Maribo-Mogensen</i>	153
Obtaining a Piecewise Linear Model of the Sewer System for Control Purposes <i>Ane Loft Mollerup</i>	157
Stability and Resistance of Catalysts for Hydrodeoxygenation of Bio-oil <i>Peter Mølgaard Mortensen</i>	159
Biorefining of Lignocellulosic Biomass <i>Line Munk</i>	163

Ash Chemistry in Circulating Fluidized Bed <i>Vikas Narayan</i>	165
Synthesis of Novel Biobased Binders for Alkyd Paint Systems <i>Hiep Dinh Nguyen</i>	169
Phytase-Mediated Phytate Dephosphorylation to Improve Bioavailability of Iron <i>Anne Veller Friis Nielsen</i>	173
Direct Liquefaction of Lignin: Solvent Effects <i>Joachim Bachmann Nielsen</i>	175
Understanding Agglomeration Behavior in Fluidized Bed Gasification <i>Mads Willemoes Nordby</i>	177
Design and Testing of Efficient and Robust Intumescent Coatings <i>Kristian Petersen Nørgaard</i>	179
Mixing and Oxygen Transfer Processes in Bioreactors <i>Anders Nørregaard</i>	183
Deactivation of Selective Catalytic Reduction Catalysts in Biomass Fired Power Plants <i>Brian Kjærgaard Olsen</i>	185
Modeling and Synthesis of Pharmaceutical Processes: Moving from Batch to Continuous Manufacturing <i>Emmanouil Papadakis</i>	189
Design of Continuous Reactor Systems for API Production <i>Michael Jønch Pedersen</i>	191
Model of Stickiness in Spray Drying <i>Thomas Petersen</i>	193
Fed-Batch Feeding Strategies for Enzymatic Biodiesel Production <i>Jason Price</i>	195
Linking Strain Morphology to Rheology and Mass Transfer as a Means to Improve Fermentation Processes <i>Daniela A. Quintanilla Hernández</i>	199
Identification of Bottlenecks for Biocatalytic Oxidations <i>Hemalata Ramesh</i>	201
Selective and Efficient Synthesis of Ethanol from Dimethyl Ether and Syngas <i>Dominik Bjørn Rasmussen</i>	205

Degradation Products from Pretreated Biomass <i>Helena Rasmussen</i>	209
Time of Harvest Affects the Yield of Soluble Polysaccharides Extracted Enzymatically from Potato Pulp <i>Helle Christine Ravn</i>	211
$\mu$ -Tools for Development of $\omega$ -Transaminase Processes <i>Rolf H. Ringborg</i>	213
Optimisation of a Microbioreactor Configuration for Enzymatic Production of Chiral Amines <i>Inês Pereira Rosinha</i>	215
Land Use in Life Cycle Impact Assessment: Terrestrial Carbon Pools Modeling for Prediction of Impacts on Climate and Biotic Production <i>Koldo Saez de Bikuña Salinas</i>	219
Bioprocess Evaluation Tools <i>Catarina Seita</i>	221
Supramolecular Polymeric Rheology <i>Aamir Shabbir</i>	223
Practical Application of Models in the Urban Water System: Simulation Based Scenario Analysis <i>Laura Snip</i>	225
Establishment of Bioelectrochemical Systems (BESs) for Production of Electricity and Hydrogen Peroxide from Pretreated Energy Crops <i>Guotao Sun</i>	229
Bioenergy from Lignocellulosic Waste Resources in Ghana <i>Sune Tjalfe Thomsen</i>	231
Single Biomass Particle Combustion and Fuel Characterization <i>Anna Trubetskaya</i>	235
Process Synthesis and Design Using Process Group Contribution Methodology <i>Anjan Kumar Tula</i>	237
An Experimental and Theoretical Study of CO <sub>2</sub> Hydrate Formation Systems <i>Fragkiskos Tzirakis</i>	239
Surfactants to Ease the Release of Thin Polydimethylsiloxane Films from Difficult Substrates <i>Sindhu Vudayagiri</i>	241

Reaction and Reactor Design for Multi-step Biocatalysis <i>Rui Xue</i>	245
The Electrical Breakdown of Thin Dielectric Elastomers: Thermal Effects <i>Shamsul Bin Zakaria</i>	249
Optimizing the Biocatalytic Productivity of an Engineered Sialidase from <i>Trypanosoma Rangeli</i> for 3'-Sialyllactose Production <i>Birgitte Zeuner</i>	253
Wind Turbine Blade Coatings with Anti-Erosion Properties <i>Shizhong Zhang</i>	255
Fast Pyrolysis of Wood and Lignin Using the New Pyrolysis Centrifuge Reactor <i>Guofeng Zhou</i>	257
Modeling and Operation of Diesel Engine Exhaust Gas Cleaning Systems <i>Andreas Åberg</i>	259



**Rohana Abu**

Phone: +45 4525 2926  
E-mail: roha@kt.dtu.dk

Supervisors: John M. Woodley  
Krist V. Gernaey

PhD Study

Started: October 2013  
To be completed: September 2016

## Design and Evaluation of Multi-enzyme Processes

### Abstract

Biocatalysis is attracting significant attention from both academic and industrial scientists due to its excellent capability to accept a wide variety of complex molecules as substrates and catalyze exquisitely selective reactions. This makes biocatalysis an attractive and alternative tool for industrial chemical synthesis and for creating new biosynthetic pathways of industrial interest. Moreover the use of multiple enzymes has been exploited and can show clear advantages over single step conversions carried out by biocatalytic methods. These numerous studies provide several technology choices that create a challenge in process design and development of effective multi-enzyme processes.

### Introduction

There are many published papers on the role of one enzyme in a single step conversion [1]. Currently, there is a clear opportunity for the use of more than one enzyme that works sequentially, parallel or in complex reactions that exhibit the excellent advantages over the single step system [2-4]. These multi-enzyme processes can incorporate the complexities of reactions that the single enzyme system cannot. This benefit could provide the results to organic synthesis problems to produce more complex compounds especially as pharmaceutical intermediates and provide more efficient reactions compared to single-step conversion.

Two mechanisms can be classified for the multi-enzymatic reactions; domino (or cascade) and tandem processes. In domino (or cascade) reactions, the intermediate products cannot be singled out because of the spontaneously fast reactions take place for intermediate production (formation of an unstable intermediate) and later used for the next step. Here, the individual steps cannot be performed separately [5]. Tandem processes use isolated enzymes coupled with a one-pot system (one synthetic operation) that sequentially catalyse transformations which in principle could also be carried out separately [6]. These two mechanisms significantly contribute to the remarkable applications in multi-enzyme processes.

### Applications of multi-enzyme systems

The use of biocatalysis is now seen in broader applications, not only in pharmaceutical industry but

also in other areas such as specialty and bulk chemical, food processing, biofuel, biopolymer, biomedical processes and environmental purposes. Bruggink and his colleagues have reviewed the multi-enzyme systems in various applications of biocatalysis [7]. Through

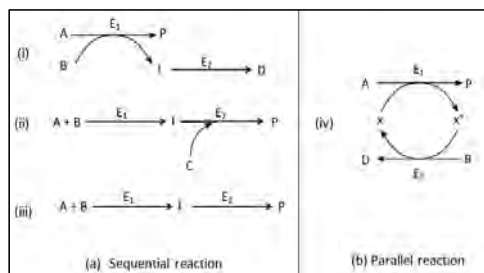


**Fig. 1:** Possible mechanisms for bi-enzymatic reactions.  $E_1$  and  $E_2$ : Enzyme, A, B, C: substrates, I: intermediate, P: product and D: by-product. (a) Sequential reaction and (b) parallel reaction with co-factor regeneration, x.

these applications, it can be concluded that enzymes can be exploited to work in sequence (Fig. 1a) or in parallel (Fig. 1b), or by a combination of both, in a system to catalyse several reactions not only to produce the desired products **P** but also at the same time are used to generate co-factors **x** and/or to remove by-products or intermediates **I**. Theoretically, for two step multi-enzymatic reaction, the number of possible processes is 2 as shown in Fig. 2a and Fig. 2b. Nonetheless, there is

**Fig. 2:** Possible reactor configuration for bi-enzymatic reactions in stirred tank reactor. (a) One-pot system, (b) two reactors in series and (c) compartmentalization of one-pot.  $\Theta$  Enzyme 1 and Enzyme 2  $\curvearrowright$

**Table 1:** Application of bi-enzymatic processes

Biocatalysis	Bi-enzymatic mechanism	Biocatalyst	Reactor system	Refs
Oxidative deamination of amino acids	i	E <sub>1</sub> : D-amino acid oxidase (EC1.4.3.3) and E <sub>2</sub> : catalase (EC1.11.1.6)	One-pot system	[8]
Conversion of polyunsaturated fatty acid triacylglycerols to hydroperoxidase	ii	E <sub>1</sub> : lipase (EC3.1.1.3) and E <sub>2</sub> : lipoxygenase (EC1.13.11.12)	Two-phase, in one-pot system (compartmentalized medium, octane/buffer)	[9]
Production of fructose syrup	iii	E <sub>1</sub> : glucoamylase (EC3.2.1.3) and E <sub>2</sub> : glucose isomerase (EC5.3.1.5)	One-pot system	[10]
Reductive amination of trimethylpyruvate	iv	E <sub>1</sub> : leucine dehydrogenase (EC1.4.1.9) and E <sub>2</sub> : formate dehydrogenase (EC1.2.1.2) is used to generate cofactor NADH, x	Multiple reactors (two enzyme membrane CSTRs in series)	[11]

a clear opportunity to separate the activity of the two enzymes using a two-phase system in one-pot or a two-compartment system separated by a sieve plate in one-pot (Fig. 3c). Table 1 represents the good examples of the applications of bi-enzymatic processes according to the mechanism in Fig. 1 and reactor configuration in Fig. 2.

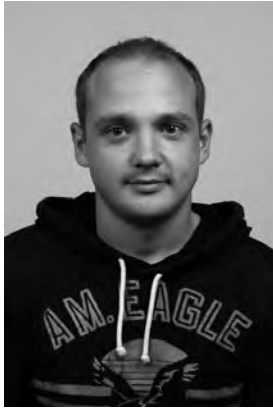
### Process design and challenges

Although the concept of a multi-enzyme system have been shown to benefit organic synthesis in general, very few studies on the topic exist at pilot and industrial scale, while it is important that multi-enzyme systems be used successfully on the large scale thus enabling compete with conventional chemical approaches. Therefore, the decisions about the choice of biocatalyst format (whole cells, cell-free extract, immobilized or soluble enzymes) and reactor configuration (batch/continuous stirred tank reactor or packed-bed reactor) for designing the process flowsheet for development in multi-enzyme processes require extensive evaluation and consideration. Hence, the design and evaluation of bi-enzymatic processes will be studied in this project. A process flowsheet will be designed and used as a guideline for developing a bi-enzymatic processes from the upstream process to downstream processing operations based on technology options. Engineering tools such as process and kinetic modelling, sensitivity and uncertainty analysis, will be used to assist process

development. The feasibility study for all possible designs will be done to evaluate the process performance and to eliminate the unfavourable reactions in order to guide process decision making (process metric evaluation – yield on substrate, yield on enzyme, product concentration, and space time yield).

### References

1. J. M. Woodley. *Advances in biochemical engineering/biotechnology* 70 (2000) 93–108.
2. P. A. Santacoloma, G. Sin, K. V. Gearney and J. M. Woodley. *Organic Process Research & Development*, 15 (2011) 203–212.
3. R. Xue and J. M. Woodley. *Bioresource technology*, 115 (2012), 183–195.
4. Z. Findrik, *Chem. Biochem. Eng. Q.* 23(4) (2009) 545–553.
5. E. Ricca, B. Brucher and J. H. Schittwieser. *Advanced Synthesis & Catalysis*, 353(13) (2011) 2239–2262.
6. I. Oroz-Guinea and E. García-Junceda. *Current opinion in chemical biology*, 17(2) (2013) 236–249.
7. A. Bruggink, R. Schoevaart and T. Kieboom. *Organic Process Research & Development*, 7(5) (2003), 622–640.
8. N. Nakajima, D. Conrad, H. Sumi, K. Suzuki, N. Esaki, C. Wandrey and K. Soda. *Journal of Fermentation and Bioengineering*, 70(5) (1990) 322–325.
9. M. Gargouri and M. D. Leqoy. *Enzyme*, (21) (1997) 79–84.
10. Y. Ge, Y. Wang, H. Zhou, S. Wang, Y. Tong and W. Li. *Journal of biotechnology*, 67(1) (1997), 33–40.
11. U. Kragl, D. Vasic-Racki and C. Wandrey. *Bioprocess Engineering*, 14 (1996) 291–297.



**Artem Alexeev**  
Phone: +45 4525 2886  
E-mail: arta@kt.dtu.dk

Supervisors: Alexander Shapiro  
Kaj Thomsen

PhD Study  
Started: September 2012  
To be completed: August 2015

## Low Salinity Waterflooding and Mineral Dissolution

### Abstract

Low salinity waterflooding is one of the modern applied enhanced oil recovery (EOR) techniques. The process involves a number of physico-chemical fluid-rock interactions which in a complex manner depend on the external conditions and component composition of brine and are not very well understood. In this paper we study waterflooding together with mineral dissolution which is very likely to occur in lab experiments. The results obtained reflect real system behavior though we claim that the only possible way to account for low salinity effects is to investigate pore-scale mechanisms during displacement.

### Introduction

In the last decade considerable research on the possibility of improving oil recovery by means of altering the injected brine composition has been conducted. Low salinity improved recovery has been discussed in the literature, both in laboratory core experiments, single and inter-well tests, however relatively few low salinity modeling works have been reported. The underlying mechanisms both with favorable conditions leading to an increase in oil recovery still remain unclear.

One of the effects on low salinity waterflooding is related to the change of ion content of the effluent brine noticed in the number of studies [1]. This may indicate that mineral dissolution takes place.

### Specific Objectives

The main goal of the project is to understand the governing mechanisms behind the Low Salinity Effect in carbonate reservoirs and determine the conditions for which low salinity waterflooding would be an effective EOR technique.

The aim of this study is to develop and implement an appropriate physico-chemical model. This implies both realizations of reservoir scale and inter-pore simulations. The first is aimed to provide predictive capabilities for the practical implementation of low salinity waterflooding, while the second – to reveal physics behind phenomena that is later to be incorporated into large scale simulations.

The model will be validated against the experimental data from laboratory waterflood experiments focusing

on two types of sedimentary rocks in the Danish part of the North Sea: chalk and greensand.

### Study on mineral dissolution

Our first study was carried out to quantify the effect of mineral dissolution on the waterflooding on the laboratory scale tracking the displacement, pressure and species concentration profiles throughout the core sample

The description derived below is similar to that given by Aharonov et al. [2]. The approach is based on the macroscopic approximation of mechanics of continuous medium. Solid phase, i.e. matrix of porous material and the two fluid phases, water and oil, are all situated at the same point. Each phase contains a number of components which cause physico-chemical interactions between phases. Introduced chemistry is expected to influence both flow and reservoir parameters, such as porosity, residual oil saturation, relative permeability curves, etc. Governing system of equations consists of phase mass conservation laws, equations for transport of components, momentum equation in the form of generalized Darcy law and chemical kinetics. The primary variables for the system are chosen to be porosity  $\phi$ , saturation  $s$ , pressure  $P$  and components mass fractions  $w_i$ :

To relate induced heterogeneity of the porous matrix to hydrodynamic properties of the rock we use well known Kozeny empirical relation for the absolute permeability:

$$K \sim \phi^3 / a^2, \quad (1)$$

where  $a$  is the specific surface (ratio of matrix surface to its volume).

One of the peculiarities of the model is that we use equation of state for brine which density depends both on pressure and composition. It is clear that dissolution of external species in water affects its density, moreover the molar volume of species on dissolution/precipitation processes may change leading to forced expansion/contraction of aqueous phase. Compressibility due to composition change is much larger compared to compressibility due to the pressure change, thus the goal was to check the possibility of emergence of pressure effects to adjust for change in density caused by physic-chemical interactions between the rock and aqueous phase. For the purpose of estimation the significance of the effect we used linearized dependences, rather than full correlations available for specific ions [2]:

$$\rho_w(P, w_i) = \rho_w(1 + c_p \Delta P + c_{w_i} \Delta w_i), \quad (2)$$

These correlations were used to provide us with the characteristic values that were included in the model.

We apply spatial discretization to reduce the problem to a system of semi-discrete ordinary differential equation. We use finite volume method (FVM). The interface flux between neighboring finite volume elements is computed by the two point flux approximation (TPFA).

For the time integration of semi-discrete system of nonlinear ODEs we use fully implicit scheme. Early approach based on explicit scheme showed that above system is badly conditioned which resulted in requirement for a very small time step. Implementation of implicit scheme is computationally costly per unit time step, however due to better stability allow for significantly larger time stepping making temporal integration more robust and efficient.

The two main parameters are the Damköhler number  $Da$  – the ratio between the rate of chemical reaction and convection, and  $\gamma$  – the ratio between the molecular volume of the dissolved species before and after dissolution. We tested the numerical model for a number of sets of two parameters.

## Results and Discussion

Results obtained indicate that alteration of brine density and volumetric non-additivity doesn't affect the global picture of the displacement process. Rather than affecting pressure the liquid is pushed forward or backward depending in the sign of the volume disbalance thus affecting insignificantly the velocity of the displacement front.

Rock dissolution affects mainly porosity, absolute permeability and hence pressure drop over the region of dissolution. Changing the Damköhler number  $Da$  we were able to observe different scenarios: at low values of  $Da$  the active component in the brine was penetrating the whole length of the sample for relatively small pore volumes injected. Thus the pressure gradient was altered throughout the whole sample to adapt to the absolute

permeability change. In the opposite extreme case of significantly large  $Da$  the active component was not able to penetrate far from the inlet unless the entire dissoluble mineral was dissolved. Thus we were observing formation of the wormholes corresponding to growth of pore sizes in the direction perpendicular to the flow. These results are visualized in Fig. 1.

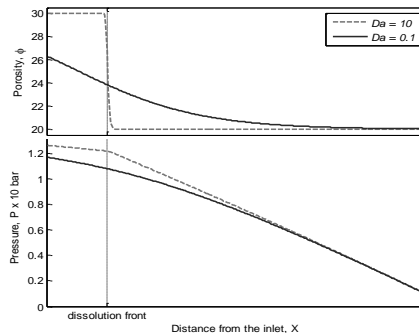


**Figure 1:** Porosity and pressure profiles after injection of 5 porous volumes.

This study cannot be claimed to account for the low salinity effect but rather an investigation on the importance of accompanying effects during the waterflooding. Introduction of residual oil saturation dependence on brine composition in the model would give us a predictive tool for verification purposes, and the next task is to reveal this dependence through pore scale physico-chemical model.

## Conclusions

Successful modeling of EOR process by low salinity waterflooding requires understanding the mechanism of how additional oil is released. Numerical models can account for dependence of residual oil saturation on brine composition using empirical dependences but cannot be treated as sufficient description of the effect. We therefore claim that a pore-scale model of low salinity effect is required to be later incorporated in laboratory scale simulations.

## Acknowledgements

This PhD study is part of the Smart Water project which is funded by industrial partners: DONG Energy and Mærsk, the Danish EUDP program (a program for development and demonstration of energy technology) under the Danish Energy Agency and by the Danish research councils.

## References

1. H. Pu, X. Xie, P. Yin, and N.R. Morrow, SPE 134042.
2. E. Aharonov, M. Spiegelman, P. Kelemen, J. Geophys. Res. 102 (1997) 14,821–14,833.
3. Lam, E. J., Alvarez, M. N., Galvez, M. E., & Alvarez, E. B. (2008). Journal of the Chilean Chemical Society, 53(1), 1393-1398.





**Susana Almeida**

Phone:

E-mail:

susal@kt.dtu.dk

Supervisors:

Nicolas von Solms

Adam Rubim

PhD Study

Started:

December 2013

To be completed:

November 2016

## **Predictive Modeling of Gas Diffusion and Solubility in Polymers for Offshore Pipelines**

### **Abstract**

The carbon dioxide (CO<sub>2</sub>) has two distinct applications in the field of gas and oil industry, the first one is in the production from ultra-deep water high pressure reservoirs with high CO<sub>2</sub> contents, and the second one in reinjection of CO<sub>2</sub>. The reinjection can be driven by a wish to reduce CO<sub>2</sub> emissions as in Carbon Capture and Storage (CCS) projects, but also as a method for Enhanced Oil Recovery (EOR) [1]. In all cases it is likely that CO<sub>2</sub> will be present in supercritical state. The main objective of the project is the prediction of solubility and diffusion of gases and gas mixtures in polymers used as liner materials in flexible pipelines for transporting fluids in offshore applications.

### **Introduction**

For the last 35 years flexible pipes have been a key component in offshore oil and gas production. This kind of pipes presents advantages when compared with rigid pipes such as the faster installation time and the better adaptation to the changes in field layout, being a more economical solution [1]. The pipeline has a polymeric inner liner that has the function of prevent the escape of the gases and the damage of the other layers in the structure. Inside the pipeline the carbon dioxide will be transported at high temperature and pressure, reaching the supercritical stage ( $T_c = 30.98\text{ }^\circ\text{C}$  and  $P_c = 73.77\text{ bar}$ ) [1]. In the laboratory the reproduction of these extreme conditions can be achieved using specific equipments such as a Magnetic Suspension Balance and a 2-D permeation cell for measuring the solubility and the permeability, respectively. The main problem of the use of carbon dioxide in the supercritical stage is that can promote a swelling phenomenon of the polymer which could conduct to its damage.

Many polymers have a high degree of swelling and plasticize at high pressures in the presence of carbon dioxide. The solubility of carbon dioxide in many polymers is substantial; this depends on pressure and temperature, but also on the interactions with the chain group in the polymer. The carbon dioxide dissolved in the polymer causes a considerable reduction in the viscosity of molten polymers due to an increase of free volume. Several other physical properties of polymers are altered such as the density, diffusivity and the swollen volume [1].

It is intended to measure and modeled the solubility and the diffusion of some gases (CH<sub>4</sub>, CO<sub>2</sub> and H<sub>2</sub>O) as well as their mixtures in some polymers (MDPE, HDPE, XLPE, PA11 and PVDF) at a range of temperatures up to 90 °C and pressures up to 650 bar.

### **Transport Phenomena**

The phenomena of gas transport through a polymer can be decomposed into 5 steps. The steps are as follows:

- Diffusion through the limit layer on the side corresponding to the higher partial pressure (upstream side);
- Absorption of the gas (by chemical affinity or by solubility) by the polymer;
- Diffusion of the gas inside the membrane polymer;
- Desorption of the gas at the side of lower partial pressure;
- Diffusion through the limit layer of the downstream side [2].

The transport phenomena can be grouped into three transport coefficients: diffusion, solubility, and permeability.

### **Specific Objectives**

The purpose of this study is:

1. Experimental measurements of solubility and permeability of carbon dioxide in different types of polymers (as function of temperature, pressure, pressure drop and composition).

2. Modelling the above properties based on the equation of state sPC-SAFT. It is the intention that the model will also account for volumetric properties of the polymer gas mixture (such as polymer swelling).

### Measurements and Modeling of Solubility

To measure the solubility is used an Magnetic Suspension Balance (MSB), the MSB is suitable to measuring solubilities up to 350 bar. Figure 1 shows a picture of the MSB without the heating system and with all the components identified.

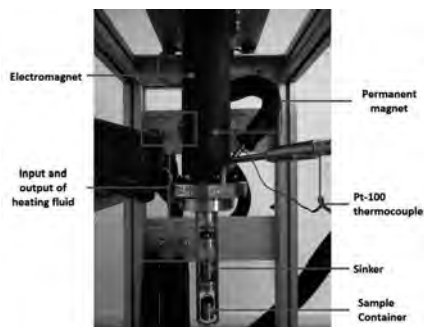


Figure 1: Picture of the open MSB [3]

The most versatile and successful models for predicting and correlating the thermodynamic properties (solubility and swelling) of gas/polymer mixtures, especially at elevated pressures, are equations of state [4]. In particular, the equation of state sPC-SAFT, suitable for polymers and developed at DTU [5] has been applied to these and other similar systems with success – see figure 2.

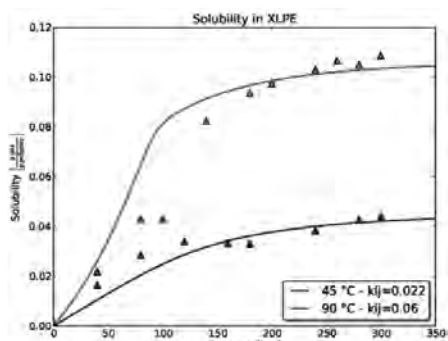


Figure 2: sPC-SAFT correlations for solubility of CO<sub>2</sub> in XLPE at 45 °C and 90 °C. The dots are the average of experimental results [3].

### Measurements and Modelling of Diffusion

The permeability is obtained from a 2-D permeation cell. The high pressure 2-D permeation cell was designed and manufactured by the Department of Chemical and Biochemical Engineering at Technical University of Denmark. The operating conditions of the

cell are up to 150 °C and 700 bar absolute. The set-up of the equipment is shown in Figure 3.



Figure 3: 2-D permeation cell assembled prior to a run [3].

Predictive theories for diffusion in polymers are rare, although Vrentas and Duda [6] have proposed a model based on the concept of free volume in a polymer, where the free volume is divided into interstitial free volume and “hole” free volume, where only the hole free volume is available for solvent diffusion. This is usually taken from a model such as Flory-Huggins, although an equation of state such as sPC-SAFT can also be used [5].

### Future Work

- Further experiments with MSB and 2-D permeation cell to measure the solubility and diffusion, respectively, in several polymers and gases
- Modeling the experimental results

### Acknowledgements

We would like to thank National Oilwell Varcofor funding this PhD project.

### References

1. A. Rubim, C. Wang, Qualifications of Flexible Dynamic Risers for Supercritical CO<sub>2</sub>, Offshore Technology Conference, Houston, USA, 2012
2. M. Klopffer, B. Flaconnèche, Transport Properties of gases in polymers: Biographic Review, Oil & Gas Science and Technology, 56, (2001), 223-244.
3. S. Almeida, Measurement and Modeling of Supercritical CO<sub>2</sub> Solubility and Permeability in Polymers for Offshore Applications, M.Sc. thesis, DTU Chemical Engineering (2012).
4. N. von Solms, M. L. Michelsen, G. M. Kontogeorgis, Prediction and Correlation of High-Pressure Gas Solubility in Polymers with Simplified PC-SAFT, Ind. Eng. Chem. Res. 44, (2005), 3330.
5. N. von Solms, M. L. Michelsen, and G. M. Kontogeorgis, Computational and Physical Performance of a Modified PC-SAFT Equation of State for Highly Asymmetric and Associating Mixtures, Ind. Eng. Chem. Res. 42, (2003), 1098.
6. J.S. Vrentas, J.L. Duda, Free-Volume Interpretation of Influence of Glass-Transition on Diffusion in Amorphous Polymers, J. Appl. Polym. Sci., 22, (1978), 2325.



**Morten Ambye-Jensen**

Phone: +45 2132 8032  
 E-mail: morj@kt.dtu.dk

Supervisors: Anne Meyer  
 Katja Salomon Johansen, Novozymes A/S  
 Thomas Didion, DLF TRIFOLIUM A/S

PhD Study  
 Started: November 2010  
 To be completed: January 2014

## Combined Silage Pretreatment and Enzymatic Hydrolysis of Energy Grasses for Lignocellulosic Biofuel Production

### Abstract

Pretreatment and enzymatic hydrolysis for conversion of lignocellulosic biomass to fermentable sugars is often the most expensive steps in 2<sup>nd</sup> generation bioethanol production. The aim of this project is to develop a pretreatment method using ensiling combined with enzymatic hydrolysis. Ensiling of biomass has a great potential as storage method for bioenergy feedstock. At the same time the silage process might function as a simple pretreatment method given its moist acidic conditions, and hereby facilitate better enzymatic hydrolysis of the lignocellulosic structure.

### Introduction

Ensiling is an anaerobic biological process that conserves biomass. This method of moist forage preservation is widely used for fodder preservation all over the world. The aim of producing silage is to preserve the crop with minimum loss of nutrients and carbohydrates. In a successful silage process, lactic acid bacteria dominate the fermentation process; fermenting free sugars into lactic acid and acetic acid causing the pH to drop which inhibits microbes that decompose polysaccharides, in that way effectively minimizing the degradation of sugars and polycarbohydrates in a crop [1]. The main products from the anaerobic metabolism by lactic acid bacteria can be seen in Figure 1.

biomass losses during harvest, (iii) no need for energy intensive drying, and (iv) possibilities of combined storage and pretreatment. The combination of storage and pretreatment at ambient temperature and pressure holds considerable potential cost and energy savings compared to common and more severe pretreatments of chemical or physicochemical means [2].

Four studies on ensiling as a biological pretreatment have reported results of cellulose conversion through enzymatic hydrolysis, all with the aim of producing energy carriers of either ethanol or biogas and the studies have consistently been reporting improved enzymatic saccharification for the ensiled biomass [2-5]. Ensiling in combination with hydrothermal treatment was also found to improve cellulose convertibility of wheat straw [6].

The objective of the study [7] was to investigate the relations of three factors; biomass composition, initial DM, and addition of LAB inocula, upon enzymatic saccharification of cellulose after ensiling, using the grass *Festulolium Hykor*.

*Festulolium Hykor* is a high yielding forage grass, developed and produced by DLF TRIFOLIUM A/S. It is a cross hybrid between the species *Festuca* and *Lolium*. It grows well in northern temperate regions due to high resistance against cold conditions and yields around 15-17 ton DM/hectare.

The Silage treatment is carried out using vacuum packaging according to the method of H.E. Johnson *et al.* [8], performed on a Variovac EK10, see Figure 2 (left). Freshly harvested *Festulolium Hykor* is chopped into 2-5 cm pieces and packed in plastic bags, see Figure 2 (right).

Main products of anaerobic sugar metabolism by lactic acid bacteria (Seale, 1989)

Homofermentative	
1 Glucose (or 1 fructose)	2 Lactic acid
	1 Lactic acid + 1 Acetic acid
Heterofermentative	
1 Glucose	1 Lactic acid + 1 Ethanol + CO <sub>2</sub>
3 Fructose	1 Lactic acid + 2 Mannitol + 1 Acetic acid + 1 CO <sub>2</sub>
2 Fructose + 1 Glucose	1 Lactic acid + 2 Mannitol + 1 Acetic acid + 1 CO <sub>2</sub>
1 Pentose	1 Lactic acid + 1 Acetic acid

**Figure 1:** Main products of anaerobic metabolism by lactic acid bacteria

Ensiling has gained increased focus as a biomass feedstock for biofuel production in recent years. The method poses several potential advantages as opposed to dry storage. The main advantages include (i) less dependence on dry weather conditions, (ii) reduced



**Figure 2:** Left: Vacuum packaging machine, Variovac EK10. Right: Grass silage bag

## Results

The results in Figure 4 indicate a negative correlation between DM at ensiling and the production of organic acids during storage. Lactic acid concentration was found to decrease linearly with increasing DM ( $p < 0.05$ ). The acetic acid and propionic acid concentrations were also decreasing with increasing DM at ensiling, however much less than what was seen for lactic acid, and the linear correlations were not statistically significant ( $p > 0.05$ ).

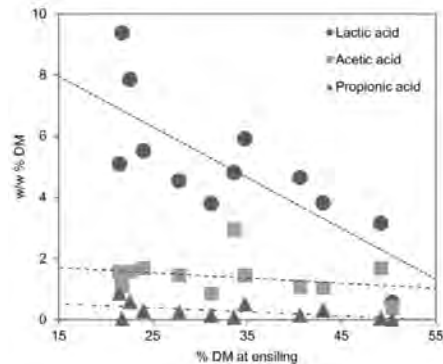


**Figure 3:** Organic acid concentration in grass silage as a function of grass DM at ensiling.

The pretreatment effect of ensiling was measured by enzymatic hydrolysis and the glucose yield (GY) were compared to that of the dried grass. The GY results showed that ensiling had a positive effect on the sugar release by generally yielding higher amounts of sugar per g biomass DM. For all cuts the low DM silage treatments gave higher GYs than the high DM silage treatments. However, as discussed above the compositional differences of the grasses caused deviations between the four cuts.

The results of higher concentrations of hydrolysing organic acids produced at lower DM (Figure 4) corroborate that the pretreatment effect of ensiling improves at lower DM. This also confirms that the organic acids produced during ensiling promote a gentle hydrolysis of lignocellulosic structures, which in turn appear to increase the access of the cellulose enzymes to the cellulose. Furthermore the present study

demonstrate that maximising organic acid production in the silage, by ensiling at low DM, leads to a better pretreatment effect.

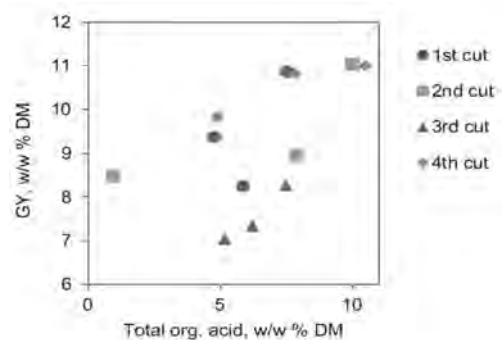


**Figure 4:** Enzymatic hydrolysis and total organic acid. Total organic acids vs. Glucose yield, w/w % of DM;

## Conclusions

Ensiling improved cellulose convertibility compared to dry storage, through acid hydrolysis of the lignocellulosic matrix. Dry matter and chemical composition of the biomass affected the ensiling which affected cellulose convertibility. Low DM ensiling (<25%) resulted in highest glucose yield and cellulose convertibility for all cuts of grass. The composition is largely determined by the maturity; less mature grass resulted in higher cellulose convertibility both with and without ensiling, due to the lower lignin content. However, less mature grass have also lower cellulose content. This suggests an optimum stage of maturity for grass, where cellulose content and convertibility results in an optimal sugar release.

## Acknowledgements

The project is financially supported by The Danish Energy Agency under the programme of EUDP (Energiteknologisk Udviklings- og Demonstrationsprogram)

## References

1. D.N. Thompson, J.M. Barnes, T.P. Houghton. *Appl Biochem and Biotech* (2005) 121-124.
2. Chen Y, Sharma-Shivappa RR, Chen C. *Appl Biochem Biotechnol* 2007;143:80-92.
3. Digman MF, Shinnors KJ, Casler MD, Dien BS, Hatfield RD, Jung HG et al. *Bioresour Technol* 2010;101:5305-14.
4. P Oleskowicz-Popiel, A.B. Thomsen, J.E. Schmidt, *Biomass Bioenergy* (2011)
5. Pakarinen A, Majjala P, Jaakkola S, Stoddard F, Kymäläinen M, Viikari L. *Biotechnol Biofuels* 2011;4:20.
6. Ambye-Jensen M, Thomsen ST, Kádár Z, Meyer AS. *Biotech for Biofuels* 2013, 6(1):116.
7. Ambye-Jensen M, Johansen KS, Didion T, Kádár Z, Schmidt JE, Meyer AS. *Biomass Bioenergy* 2013, 58:303-312.
8. H.E. Johnson, R.J. Merry, D.R. Davies, D.B. Kell, M.K. Theodorou, G.W. Griffith, *J Appl Microbiol* (2005) 98(1):106-13.



**Amata Anantpinijwatna**

Phone: +45 4525 2912  
E-mail: amatana@kt.dtu.dk

Supervisors: Rafiqul Gani  
Gürkan Sin

PhD Study  
Started: August 2013  
To be completed: July 2016

## Generic Model-Based Tailor-Made Design and Analysis of Biphasic Reaction Systems

### Abstract

In biphasic reacting systems, the reactor contain two immiscible solvents, in which, the active catalyst is embodied in only one phase and can be recycled without additional treatment. Therefore, it offers the possibility of making organic synthesis route feasible through higher product yield, easier separation, or more flexible operation of the system. The modeling of biphasic reacting systems is difficult due to the complex of the systems and the lack of experimental data. In the first stage of project, the framework for modeling biphasic reacting system is developed and applied with pseudo-PTC case.

### Introduction

Biphasic reaction systems contain two immiscible liquid phases such as aqueous/organic, ammonium/organic, supercritical-CO<sub>2</sub>/ionic liquid, or two liquid membrane-separated phases. In biphasic systems, reactants and catalyst (include biocatalysts and enzymes) could come in difference phase, allowing novel synthesis path; as well as, higher selectivity, conversion, and yield can be achieved by manipulating the reaction conditions. Furthermore, after the reaction, reactants, catalyst and products might end up in different liquid phases causing easier separation. There are plenty applications of biphasic reaction such as: (1) phase transfer catalyst involved systems; (2) epoxidation of unsaturated fatty acid by hydrogen; (3) hydroformylation of olefins, that produce aldehydes, which is performed successfully in industrial scale; (4) furan production from biomass in aqueous/organic solvent for biodiesel production, etc.

Modeling can be a valuable tool to help with efficient analysis and development of processes employing biphasic reaction systems. However, the model that describes chemical equilibrium, thermodynamic equilibriums, reactions kinetic, and unit operations altogether is inadequately studied.

### Objectives of the research project

- To propose a framework for modeling biphasic reaction systems.
- To develop a model of interested biphasic reaction systems.
- To use developed models for designing, optimizing, and analyzing the system.

### Framework

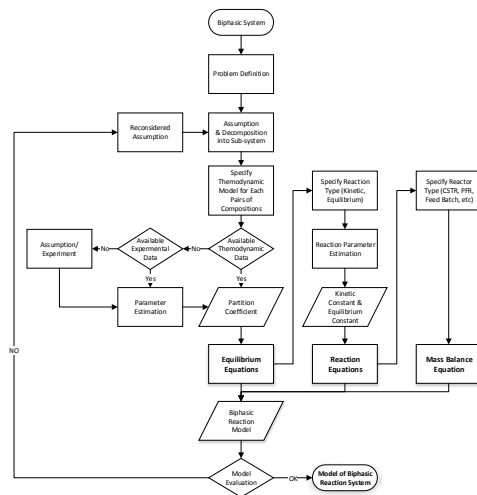


**Figure 1:** Framework for modeling biphasic reaction systems

Figure 1 presents framework for modeling of biphasic reaction systems. Starting from the problem definition; then, assumptions based on how accurate the result required to be is posed. 3 sets of equations, equilibrium, reaction, and mass balance, are required to make an

entire model, but not mandatory since there are cases that only some part of model is under interested.

The equilibrium equations set tell how components distribute between phases by partition coefficient shown in equations (1) and (2):

$$K_i^E = \frac{\gamma_i^\alpha}{\gamma_i^\beta} \quad (1)$$

$$x_i^\alpha K_i^E = x_i^\beta \quad (2)$$

where  $K_i^E$  is partition coefficient of  $i$  component between phases  $\alpha$  and  $\beta$ ,  $\gamma_i$  is activity coefficient, and  $x_i$  is mole fraction.

As for the reaction equations set, there are 2 types of reaction: kinetic reaction, where the equation be derived from:

$$r_i = \frac{dc_i}{dt} \quad (3)$$

While, for the equilibrium reaction equations set will be derived from chemical equilibrium equation:

$$K_j = \Pi \left( \frac{f_i}{f_i^0} \right)^{v_{i,j}} \quad (4)$$

$$f_i = x_i \gamma_i \quad (5)$$

where  $r_i$  and  $c_i$  are rate of reaction and concentration respectively,  $K_j$  is equilibrium constant of reaction  $j$ ,  $v_{i,j}$  is stoichiometric coefficient,  $f_i$  and  $f_i^0$  are fugacity and standard state fugacity respectively.

Whereas, mass balance equations set is depended on reactor geometry. The model needed to be evaluated for its accuracy before further applications.

### Case Study: Pseudo PTC

Mechanism of benzoin condensation from benzaldehyde with tetrabutylammonium-cyanide ( $TBA^+CN^-$ ) as a catalyst is shown in **Figure 2**.

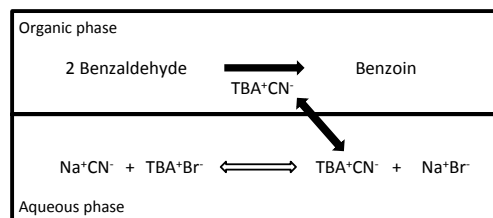


**Figure 2:** Pseudo-PTC reaction mechanism

Solvents used in this case are toluene and water; it is assumed that reactant, product, and sodium salt are not distributed between phases. TBA, as pseudo phase transfer catalyst, help bringing cyanide ion from sodium cyanide in aqueous phase to act as catalyst for reaction in organic phase; the concentration of sodium salt and TBA-PTC are constant over all the reaction time. The reaction in aqueous phase is equilibrium reaction while reactions in organic phase are set of equilibrium and kinetic reactions together [1]; while, the reactor is a batch reactor.

For distribution of active catalyst ( $TBA^+CN^-$ ) between two phase, there is no database's parameter or experimental data available; the main assumption in this case is the active catalyst, after formed by reaction in aqueous phase, will all inhibit in aqueous phase.

Therefore, the model for this reaction system are shown as following equation (6) to (10).

$$K_1 = \frac{[TBA^+CN^-]^A [Na^+Br^-]^A}{[TBA^+Br^-]^A [Na^+CN^-]^A} \quad (6)$$

$$K_2 = \frac{[B^+TBA^+CN^-]^O}{[B^+]^O [TBA^+CN^-]^O} \quad (7)$$

$$K_3 = \frac{[PTBA^+CN^-]^O}{[B^+]^O [TBA^+CN^-]^O} \quad (8)$$

$$\frac{d[P]}{dt} = k_4 [PTBA^+CN^-] \quad (9)$$

$$K_{QCN} = \frac{[TBA^+CN^-]^A}{[TBA^+CN^-]^O} \quad (10)$$

Where superscript  $A$  and  $O$  indicate aqueous and organic phase respectively,  $K_1 - K_3$  are equilibrium constants,  $k_4$  are reaction constant of the kinetic reaction, and  $K_{QCN}$  is partition coefficient of the active catalyst.

The early result shows agreement between predicted conversion and experimental at different starting concentration as shown in

**Figure 3.**

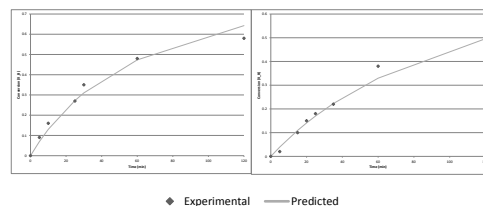


**Figure 3:** Comparison of benzaldehyde conversion between prediction and experimental

### Conclusion

The framework for modeling of biphasic reaction systems is developed and successfully applied to a cases study dealing with benzoin condensation from benzaldehyde. Although, there are still rooms for improvement such as limited database of equilibrium and kinetics data; predictions of the model are in acceptable range. The framework will be applied for further various cases to further develop and extend the range of applications including epoxidation of soybean oil and hydroformylation of higher olefin process; which are in the process of study.

### Acknowledgements

First of all, I'd like to thank Professor Felipe Lopez-Isunza for guidance in the first month of my project and Professor John P. O'Connell for guidance during my research stay at University of Virginia. I also would like to thank Thai's OCSC for a financial support.

### References

- 1 Yadav, Ganapati D. and Kadam, Anup A. *Org. Process Res. Dev.*, 16 (2012), 755.



**Marie Andersson**

Phone: +45 4525 2958  
E-mail: mande@kt.dtu.dk

Supervisors: John M. Woodley  
Ulrich Krühne

PhD Study

Started: February 2012  
To be completed: January 2015

## Bioprocess Engineering for the Application of P450s

### Abstract

Cytochrome P450 monooxygenases perform selective hydroxylation of non-activated hydrocarbons. That makes them interesting from an industrial perspective and the fact that they are involved in human drug metabolism is interesting in pharmaceutical research. The characteristics of this group of enzymes makes them suitable as catalysts in a whole cell format and to identify the bottleneck of a potential whole cell P450 process, CYP153 expressed in *E. coli* was used as model system. It can be concluded that the enzyme needs to be improved in several aspects to become industrial feasible especially with in terms of stability and activity.

### Introduction

Cytochrome P450 monooxygenases (P450 or CYP) is a very interesting group of enzymes found in all kingdoms performing specific hydroxylations. The involvement of P450s in drug metabolism in the human liver makes them interesting to the pharmaceutical industry. Furthermore, the difficulties related to the conventional chemical synthesis also make them interesting in the field of white biotechnology. Cytochrome P450s are heme-containing, cofactor dependent and requires corresponding electron transporting proteins (reductases). Besides these characteristics, the poor stability motivates the use of a whole cell system. The challenges don't stop with the biochemical characteristics; the reactants often have poor water solubility and are inhibitory to the enzyme and toxic to the cells at relevant process concentrations. Due to the many challenges this system is facing, the limiting parameter is important to identify for a potential process in order to improve the bottleneck.

As a first model system for the thesis CYP153A from *Marinobacter Aquaeolei* fused to the reductase domain of CYP102A1 was used, illustrated in Figure 1 [1]. The fusion construct can be soluble expressed in the industrial relevant host *E. coli* HMS174(DE3). The whole cell catalyst was used for terminal hydroxylation of lauric acid. Terminal hydroxylated fatty acids are relevant in the fragrance industry and can also be used for high-end polymers.

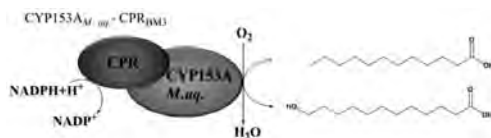


**Figure 1:** CYP153A fused to the reductase partner from CYP102A1 forming the model system used for terminal hydroxylation of lauric acid. (Picture modified from D. Scheps, University of Stuttgart)

### Specific objectives

The objectives of the project are to:

- define the requirements and bottlenecks for an industrial relevant process involving P450 monooxygenase
- evaluate mode of operation (growing or resting cells)
- evaluate 2-phase systems involving water immiscible organic solvents
- explore oxygen supply strategies
- perform environmental and economic evaluation of a selected process

## Results and Discussion

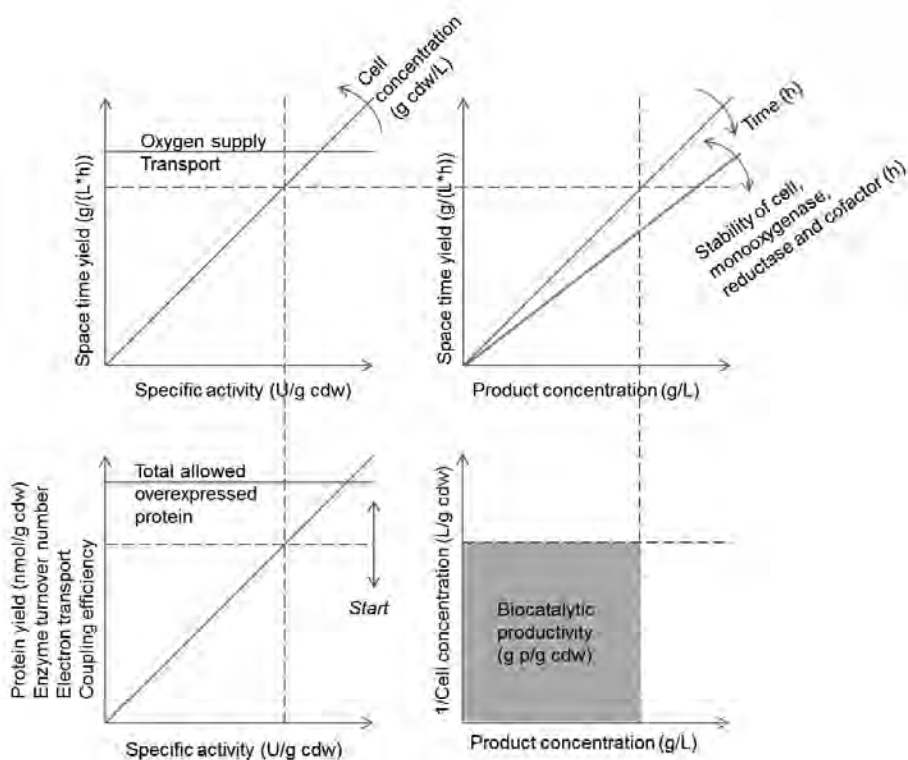


**Figure 2:** Influence of the typical biochemical parameters presented in P450 whole cell processes on economic important parameters and limitations

In Figure 2 typical parameters presented in most publications about P450 monooxygenases can be related to economic important parameters to evaluate a process such as space time yield, product concentration and biocatalytic productivity. Starting in the lower left corner the rate related parameters are listed (protein yield, enzyme turnover number, electron transport and coupling efficiency) influencing the specific activity that in the upper left corner together with the cell concentration results in the space time yield. The space time yield can be limited by the possible oxygen supply by the reactor and the transport of reactants between phases or across the cell membrane. From the space time yield, the possible final product concentration is determined by the stability of the whole cell system including the host cell, the monooxygenase, reductase and cofactors, shown in the upper right corner. The lower right corner illustrates how the cell concentration together with the final product concentration determines the biocatalytic productivity.

The many theoretical limitations of the whole cell biocatalytic P450 processes need to be verified and the bottleneck identified in practice in order to improve

the system. For this purpose, the fusion construct with CYP153A shown in Figure 1 expressed in *E. coli* was used as a model system for terminal hydroxylation of lauric acid.

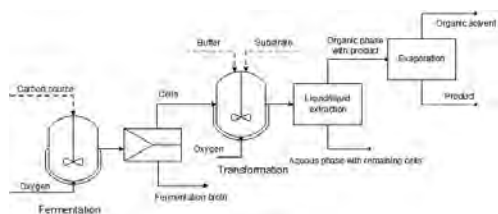


**Figure 3:** Flow sheet of a resting cell process where the transformation is separated from the fermentation process.

The process characterized for the selected case study is shown in Figure 3, where fermentation and transformation is separated, enabling optimization of the two steps. The fermentation was performed as a fed-batch process with minimal media, yielding a



biocatalyst concentration of around 25 g cdw and up to 1 g correctly folded enzyme per liter media. The cells were then harvested by centrifugation and washed prior to resuspension in potassium phosphate buffer for biotransformation.

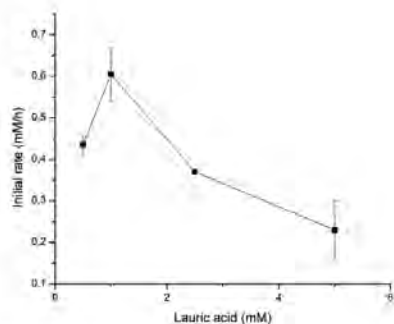


**Figure 4:** Substrate inhibition profile of lauric acid on CYP153A.

Substrate inhibition was shown to occur in shake flask transformations already above 1mM substrate concentration, as shown in Figure 4. However, the inhibition profile and reaction rate was shown to be different in stirred tank reactors compared to shake flasks, probably due to different mixing and oxygen supply. Feeding experiments trying to circumvent the inhibition by high substrate concentration showed a higher initial rate but did however not show any improvement of the final product concentration.

Potential cofactor and transport limitations were also investigated by addition of external cofactor and by different disruption methods of the cell membrane. The presence of NADPH in the reaction media was monitored spectrophotometrically at 340 nm and it could be seen that the added cofactor is taken up by the cells within 30 min regardless of the treatment (data not shown). Progress curves of the reaction course are shown in Figure 5 and the highest final concentration was reached by intact cells without additional cofactor added. It can however be seen that the fastest initial rates are achieved by the intact cells (control), cells permeabilized with acetone and frozen cells where cofactor is added indicating that the cofactor regeneration is limiting the reaction rate. No permeabilization method without addition of cofactor increased the reaction performance, indication that the reaction is not limited by substrate transport across the cell membrane.

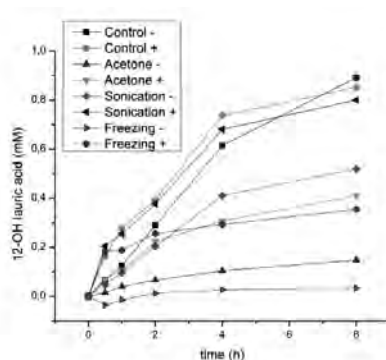


**Figure 5:** Progress curves of biotransformation in shake flasks after different permeabilization methods of cell membrane. + and - indicates cofactor or no cofactor added. Substrate and cofactor was added in equal concentrations, 1.5mM.

Enzyme inactivation was studied spectrophotometrically where the reduced form of the correctly folded heme domain of the enzyme binds to CO and absorbs at 450nm. In Figure 6 it can be seen that the whole cell is intact during the reaction course but 50% of the correctly folded enzyme has been lost already after 2h.

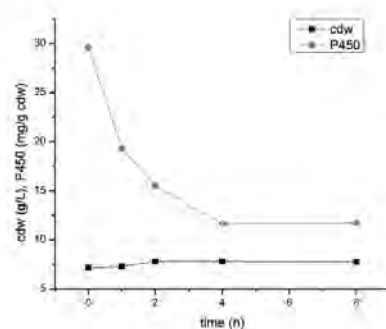


**Figure 6:** Cell dry weight and correctly folded P450 during transformation performed in 1L reactor. Reaction conditions: 50 g cww/L, 100 mM potassium phosphate buffer pH 7.4, 30°C, pO<sub>2</sub> 30%, initial substrate concentration 5 mM.

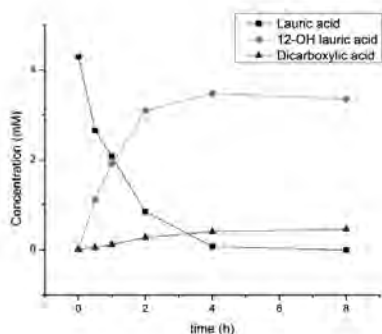


**Figure 7:** Progress curve of biotransformation performed in 1L bioreactor. Reaction conditions as described in Figure 6.

Figure 7 shows progress curves of a biotransformation performed in a 1L bioreactor and the data of the first 4h is summarized in Figure 8 and presented in relation to set targets for economic feasibility. The biocatalytic productivity is determined by the cost of the catalyst and requires a successful fermentation step with good protein expression [2]. Product concentrations between 50 and 100 g/L as well as productivities of around 1 g/L/h characterize industrial biocatalytic processes [3]. It can be seen that the biocatalyst needs to be improved to reach the economic targets for a feasible industrial process.

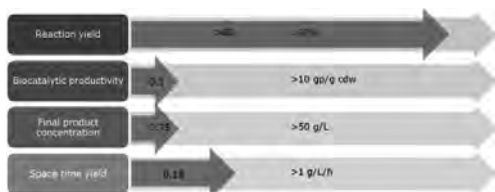


**Figure 8:** Reached economic parameters in relation to targets set for an economic feasible process.

## Conclusions

The terminal hydroxylation of lauric acid using CYP153A expressed in *E. coli* has been characterized and a resting cell process evaluated at 1L scale. It has been found that cofactor regeneration limits the initial rate but does not limit the final conversion when supplied in stoichiometric amounts. Limitation of the reaction due to transport of the substrate lauric acid across the cell membrane was ruled out.

To be in the range of an economic feasible process the specific activity of the model system needs to be improved 5 times and the stability needs to allow a 24h process. The biomass concentration for the biotransformation step needs to be increased to 50 g cdw/L and the oxygen demand of >1 g/L/h at this

concentration will be a challenge to meet with standard bioreactors.

## Acknowledgement

The research leading to these results has received funding from the People Programme (Marie Curie Actions) of the European Union's 7th Framework Programme (FP7/2007-2013) under REA Grant Agreement 289217.

## References

- [1] Scheps, D., Honda Malca, S., Richter, S. M., Marisch, K., Nestl, B. M., Hauer, B., Synthesis of  $\omega$ -hydroxy dodecanoic acid based on an engineered CYP153A fusion construct. *Microbial biotechnology* 2013, 6, 694-707.
- [2] Tufvesson, P., Lima-Ramos, J., Nordblad, M., Woodley, J. M., Guidelines and cost analysis for catalyst production in biocatalytic processes. *Organic Process Research & Development* 2011, 15, 266-274.
- [3] Straathof, A. J. J., Panke, S., Schmid, A., The production of fine chemicals by biotransformations. *Curr. Opin. Biotechnol.* 2002, 13, 548-556.



**Deenesh K. Babi**

Phone: +45 45 25 29 59  
E-mail: dkbabi@kt.dtu.dk

Supervisors: Rafiqul Gani  
John M. Woodley

PhD Study  
Started: September 2011  
To be completed: August 2014

## Process Intensification: A Phenomena-based Approach

### Abstract

Process Intensification (PI) is a means by which the overall improvement of a process can be sustainably achieved through the improvement of key elements within the process, for example energy efficiency and waste reduction. In order to go beyond existing Unit-Ops and therefore be predictive; one has to operate at a lower level of aggregation. Previously different PI methodologies operated at the Unit-Ops (Jakslund *et al.* 1995) and task levels (Sirola *et al.* 1995) and it was shown how PI can be achieved, but these methods were only able to find solutions based on existing Unit-Ops. Therefore to go beyond the existing Unit-Op solutions one has to operate at the phenomena level which uses key knowledge obtained from the previous developed methodologies. The objective of this work is the development of a systematic, multi-level framework which integrates process synthesis and PI.

### Introduction

Process Intensification (PI) can be defined as the improvement of a process at the operational level, functional level and/or phenomena level. That is the operational level is related to the integration of unit operations (Unit-Ops) for example reaction and separation, the functional (task) level is related to the enhancement of functions for example the finding of a new solvent for an extractive distillation process and the phenomena level is related to the integration or targeted enhancement of phenomena which has an overall impact at the functional level and operational level. The objective of PI is the improvement of a process with respect to waste reduction, energy efficiency and cost, subjected to predefined performance criteria. The objective of process synthesis is to find the best processing route, among numerous alternatives for converting given raw materials to specific desired products subject to design constraints and predefined performance criteria. Therefore by considering process synthesis and process intensification together sustainable process design can be achieved. Sustainable design can be defined as the design of process alternatives that correspond to lower values of set targeted performance criteria related to economics, sustainability and/or life cycle assessment factors. The objective of this work is the development of a systematic, multi-level framework for process synthesis-intensification that achieves more sustainable process designs. At the highest level of aggregation, process

flowsheets are synthesized in terms of a sequence of unit operations that correspond to acceptable values for a set of targeted performance criteria. This defines the upper-bound of the performance criteria and is therefore the base-case design. At the next lower level, tasks representing unit operations are identified and analyzed in terms of means-ends to find more flowsheet alternatives that improve the base-case design and correspond to lower values of the set of targeted performance criteria. At the lowest level, phenomena employed to perform the specific tasks are identified and manipulated to find intensified operations, leading to more flowsheets that further improve the base-case design and correspond to even lower values of the set of target performance criteria.

### Discipline

The research conducted in this field is primarily within the field of process systems engineering (PSE).

### Process Synthesis-Intensification Framework

The framework allows process synthesis-intensification at the Unit-Ops level (Jakslund *et al.* 1995), the task level (Sirola *et al.* 1995) and the phenomena level (Lutze *et al.* 2013). An overview of the phenomena-based synthesis-intensification method is given.

#### Concept-Phenomena-based Synthesis

Consider as analogy, the design of chemicals based products, where a set of target properties of the product are matched by considering a set of molecules available

in the database; and/or by considering functional groups (of atoms) that can be combined to form existing as well as new molecules that match the specified targets; and/or by considering a set of atoms that can be combined to generate even more existing as well as new molecules that match the specified targets. This is the reason behind phenomena-based synthesis.

#### Phenomena-based process flowsheet representation

Based on a study of chemical processes, it was found that most chemical processes can be represented through the following 9 phenomena building blocks (PBBs): mixing (M), two-phase-mixing (2phM), heating (H), cooling (C), reaction (R), phase contact (PC), phase transition (PT), phase separation (PS), dividing (D). Second, each task is replaced by the phenomena associated with it.

#### Combination of phenomena to represent tasks, unit operations and flowsheets

One or more phenomena are combined which fulfill the objectives of any task subject to connectivity rules for ignoring/accepting certain combinations. First the PBB are combined to form simultaneous phenomena building blocks (SPBs). For example, by combining mixing, 2-phase mixing, reaction, phase contact, phase transition and phase separation phenomena, a reaction-separation SPB  $[M=2phM=R=PC(VL)=PT(VL)=PS(VL)]$  is generated, where  $PT(VL)$  is a PBB representing a VL-separation task. Second, SPBs are combined to form operations that are translated to known or new Unit-Ops which constitute the final flowsheet. An example of the representation of a distillation through the combination of 3 SPBs is shown in Figure 1.

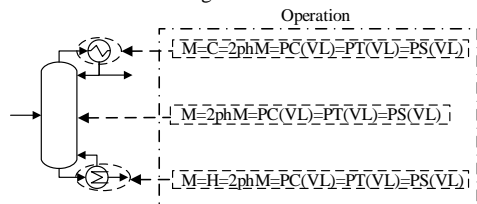


**Figure 1:** Distillation column representation using SPB's

#### The Framework

The synthesis-intensification framework is shown in Figure 2 which is an extended version of the phenomena-based synthesis methodology developed previously (Lutze *et al.*). The first stage of the framework determines a base case design at the Unit-Ops level considering a superstructure of all possible alternatives based on known technologies. The second stage performs a sustainability analysis (Carvalho *et al.* 2013, Gani *et al.* 1997) to systematically and logically identify process hotspots, which sets the targets for process improvement. The inputs to the analysis are detailed mass and energy balance data and the base case process flowsheet information. The third stage performs phenomena-based synthesis subject to the following conditions: the new flowsheet should have a smaller number of Unit-Ops for all synthesized alternatives compared to the base case. Analysis of the chemical

system is performed using ICAS tools (Jaksland *et al.* 1995, Gani *et al.* 1995). The unit operation based flowsheet is translated to a task-based flowsheet that is further translated to a phenomena-based flowsheet. Then all the phenomena found in the flowsheet are listed and using combination rules, SPBs are generated and screened. Next, SPBs are combined to form operations (tasks), which are combined to form unit operations (see Figure 3).

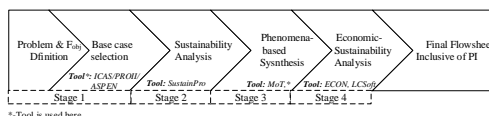


**Figure 2** Synthesis, Design and Intensification Methodology

Only those operations and their combination to flowsheets are retained if they satisfy all constraints and move the objective function in the desired direction.

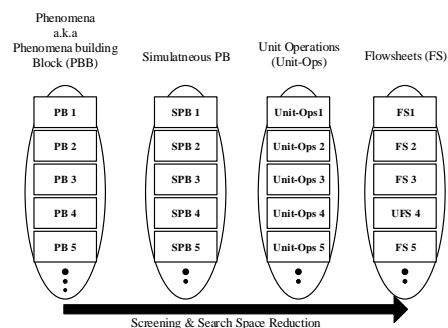


**Figure 3:** Connection of PBBs to flowsheet alternatives

#### Tools

In applying this framework different tools are used and are classified as follows:

- Property prediction: ProPred
- Modelling-MoT
- Economic Evaluation: ECON
- Sustainability Analysis: LCSof/SustainPRO
- Rigorous simulation: PROII/ASPEN

These tools are available in the updated version of ICAS (Gani *et al.* 1997), except for process simulators (PROII and ASPEN).

#### Case study Application

The key steps of the framework are highlighted through this case study involved with the production of methylacetate (MeOAc) from an equilibrium-limited reaction between methanol (MeOH) and acetic acid (HOAc) with water (H<sub>2</sub>O) as a by-product. The reaction is a liquid phase reaction catalysed by Amberlyst 15. A molar feed ratio of 2:1 for the base case design for MeOH and HOAc are used respectively (Agregda *et al.* 1986, Huss *et al.* 2003).

#### Stage 1

The synthesis problem is defined as: Find intensified process design options for the production of MeOAc

having a conversion of HOAc $\geq$ 92% by maximising the objective function related to utility cost (Eq. 1) subject to:

$$F_{obj}(C_{Ut}) = Opt \left\{ \sum E_j C_{U_i,j} / kg \text{ Pr od} \right\} \quad (1)$$

C, and E represent cost and energy flows, respectively. Compared to the base case design, the generated feasible intensified alternatives must satisfy the following design constraints ( $\theta$ ) and performance criteria ( $\phi$ ), reduction in energy consumption ( $\theta$ ), use of solvents should be avoided ( $\phi$ ), the number of Unit-Ops must be less ( $\phi$ ), sustainability and LCA factors must be the same or better ( $\phi$ ). From a literature survey a base-case design is available (Agreda et al 1986) and it consists of ten unit operations (one reactor, five distillation columns, one liquid-liquid extractor and decanter). It should be noted that if a base-case design does not exist, the framework has the option to generate one. The base case design is then simulated to obtain detailed mass and energy balance data.

### Stage 2

Sustainability analysis is performed and two potential process hotspots are identified: the reaction does not go to full completion (limited-equilibrium) and high energy consumption for product and raw material recoveries. These process hotspots are then used as the targets that must be overcome subject to the design constraints and performance criteria.

### Stage 3

**Identification of tasks and phenomena:** Using the appropriate tools the chemical system pure component and mixture properties are analyzed and the following minimum boiling binary azeotropes are found: HOAc/H<sub>2</sub>O, MeOH/MeOAc and MeOAc/H<sub>2</sub>O. Next, the base-case flowsheet is represented in terms of tasks and then in terms of phenomena, resulting in the following 15 PBBs: R, M (assuming four types, ideal, flow, rectangular, vapor), 2phM, PC(VL), PS(VL), PS(VV), PT(VL), PT(P:VL), PT(V:V) (key phenomena for a vapor permeation membrane), H, C and dividing (D) phenomena. Considering all possible combinations of the identified PBBs resulted in 16278 SPBs, out of which 64 were found to be feasible.

**Generation of more sustainable alternatives:** Only a brief overview of the flowsheet generation procedure is highlighted here. The system contains four compounds and therefore 6 binary pairs exist: MeOH/HOAc, MeOH/MeOAc, MeOH/H<sub>2</sub>O, HOAc/MeOAc, HOAc/H<sub>2</sub>O and MeOAc/H<sub>2</sub>O. Starting with the first task of reaction, a second task, *in situ* removal of water (see Figure 4a) could be added to obtain a SPB that translates into a membrane reactor at the Unit-Ops level. This increases the conversion of MeOH and HOAc to MeOAc by removing the water *in situ*. Figure 4b shows that this would be feasible if a pervaporation membrane (P:VL) is employed to remove water from the 2-phase reacting system (R=PT), thereby avoiding solvent-based separation for the azeotropes HOAc/H<sub>2</sub>O and MeOAc/H<sub>2</sub>O. The resulting SPB is R=PT(P:VL). Note that additional mixing, heating or cooling phenomena

could also be added to this SPB. Due to the feed ratio, the outlet of the membrane reactor also contains MeOH therefore a separation task using VL-separation that is a PT(VL) PBB is identified for recovering MeOH.

From the top product of the membrane reactor (see Figure 3), according to thermodynamic insights (Jakslund et al. 1995) HOAc should be removed first before separating the pressure-sensitive azeotrope of MeOH/MeOAc. The first separation task is easily accomplished by a VL-separation, that is, using a PT(VL) PBB. Two VL-separation tasks operating at different pressures are employed to first separate MeOH and then MeOAc, thereby avoiding the use of solvents. The final flowsheet (alternative 1- satisfies the specified constraints) is shown in Figure 5.

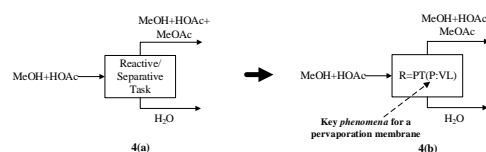


**Figure 4:** Identified task (4a) translated into phenomena (4b) to overcome process hotspot for increasing the conversion of HOAc

Using the presented concepts of flowsheet generation, 3 other feasible flowsheet alternatives were generated, including the well-known reactive distillation (Agreda et al. 1986) that is alternative 4 in Table 1.

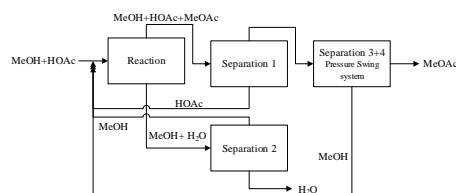


**Figure 5:** Flowsheet alternative 1

Alternatives 2 and 3 are generated by further reducing the flowsheet of alternative 1 by changing the MeOH-HOAc feed ratio resulting in easier and lesser separation tasks after the membrane reactor. Among the different SPBs that can be generated, only those that have the potential to overcome the process hot-spots are considered.

### Stage 4

Selection of the best alternative is dependent on economic factors, sustainability metrics and LCA factors in addition to the objective function value. Table 1 gives values of a selected set of performance criteria for the base-case design and the four alternative (intensified) designs. For each alternative the conversion of HOAc $\geq$ 92% has been achieved, no solvents have been used and the number of unit operations have been reduced from 10 (the base case) to

1 (alternative 4). The concept of generation of more sustainable process designs by matching a set of targeted performance criteria is illustrated through Figure 6, where, the ratios of different performance criteria with respect to the base-case multiplied by 100 have been plotted (for profit, the inverse has been taken). It can be noted that the base-case design is at the boundary while the more sustainable alternatives are all within the boundary, indicating quite clearly that these alternatives are more sustainable than the base-case. Alternative 3 and alternative 4 give the best results.

**Table 1:** Selected performance criteria for base-case and 4 more sustainable alternatives

Performance Metrics	Base case	Alternatives			
		1	2	3	4
Feed Ratio	2:1	2:1	2:1	1:1	1:1
Energy Usage (MJ/kg MeOAc)	21.9	20.6	19.1	3.6	2.2
Raw material (kg/kg MeOAc)	0.88	0.87	0.87	0.87	0.88
Carbon Footprint (eq. kg of CO <sub>2</sub> )	0.92	0.56	0.52	0.09	0.05
Fobj (Eq. 1)	0.101	0.088	0.08	0.012	0.008

production of MeOAc, highlighting the workflow of the framework has been presented.

#### Future Work

The future work related to this thesis is to further apply the framework to other case studies related to bio-based chemicals in order to realize the possible benefits of process synthesis-intensification.

#### References

- A. Carvalho, H. A. Matos, R. Gani, 2013, *Computers & Chemical Engineering*, 50, 8-27  
 C.A. Jaksland, R. Gani, K.M. Lien, 1995, *Chemical Engineering Science*, 50, 511-530.  
 J. J. Sirola, 1996, *Computers & Chemical Engineering, Supplement 2*, 20, S1637-S1643  
 K.P. Papalexandri, E.N. Pistikopoulos, 1996, *AIChE Journal*, 42, 4, 1010-1032  
 P. Lutze, D. K. Babi, J. M. Woodley, R. Gani, 2013, *Industrial Engineering & Chemistry Research*, 52, 7127-7144  
 R. Gani, G. Hytoft, C. Jaksland, A. K. Jensen, 1997, *Computers & Chemical Engineering*, 21, 1135-1146  
 V. H. Agreda, L. R. Partin, W. H. Heise, 1986, *Chemical Engineering Progress*, 2, 40-46

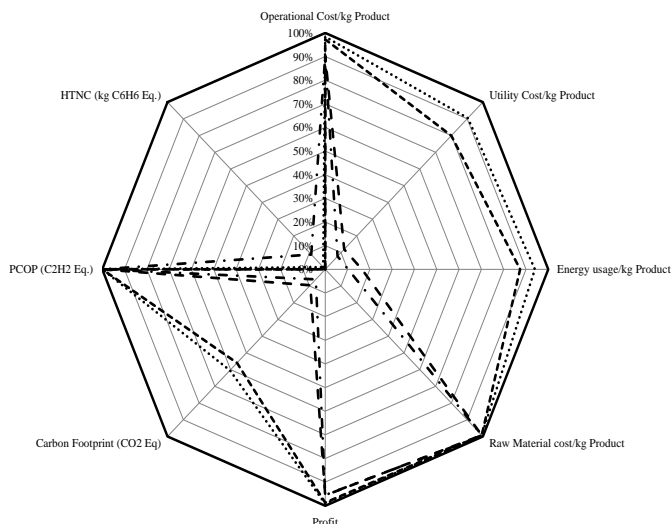


**Figure 6:** Economic and LCA improvements relative to the base case design. HTNC-human toxicity (carcinogenic effects); PCOP-Photochemical Oxidation Potent

#### Conclusion

A framework for performing process synthesis and intensification has been developed. The framework is multi-level and therefore operates at different levels of aggregation and the benefit of the framework is that it provides the opportunity for generating sustainable intensified process designs which include hybrid/intensified Unit-Ops. The framework has been applied to other case studies and the results from the

**Frederikke Bahrt Madsen**

Phone: +45 4525 6809  
E-mail: frbah@kt.dtu.dk

Supervisors: Anne Ladegaard Skov  
Søren Hvilsted  
Anders Egede Daugaard

**PhD Study**

Started: August 2011  
To be completed: August 2014

## Dipolar Cross-linkers for PDMS Elastomers with Enhanced Dielectric Permittivity

**Abstract**

Dipole grafted cross-linkers were utilized to prepare PDMS elastomers with various chain lengths and with various concentrations of functional cross-linker. The grafted cross-linkers were prepared by reaction of two alkyne-functional dipoles with a synthesized silicone compatible azide-functional cross-linker by click chemistry. The electromechanical properties were investigated for PDMS films of 0 to 3.6 wt% of dipole cross-linker. The relative dielectric permittivity was found to increase by ~20% at only 0.46 wt% of incorporated dipole. Furthermore dielectric losses were proved to be remarkably low while the electrical breakdown strengths were high, which are sought after properties for dielectric electro active polymers.

**Introduction**

Dielectric electro active polymers (DEAPs) are promising materials for advanced electromechanical applications such as actuators, sensors and generators. DEAPs usually consist of a thin filled elastomer film sandwiched between two compliant electrodes [1]. When an external voltage is applied to the electrodes, the electrostatic pressure acting on the film will squeeze the elastomer in thickness and the film is consequently expanded in planar directions. The electrical energy has thus been converted into mechanical energy. When the external voltage is switched off, the elastomer film returns to its original shape.

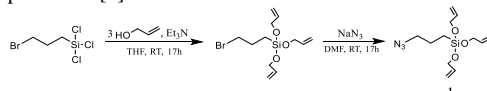
Polydimethylsiloxane (PDMS) is one of the most utilized polymers for DEAP applications due to its high efficiency and fast response [2,3]. PDMS, however, suffers from low dielectric permittivity and thus high voltage is required to obtain a large strain.

The permittivity is generally improved by the use of fillers resulting in elastomer composites of metal oxides such as TiO<sub>2</sub> and BaTiO<sub>3</sub>. These types of composite systems can, however, exhibit drawbacks such as large dielectric losses and reduced electric breakdown strengths due to agglomeration of fillers and consequent significant changes in mechanical properties. A controlled system which allows for an increase in permittivity even at low concentration of added filler materials would make it possible to achieve and maintain good material properties as well as low

dielectric losses. The aim of this work is to investigate the impact of two different dipolar cross-linkers on the dielectric permittivity of PDMS elastomers. The PDMS networks will be prepared with varying content of the two dipole-functional cross-linkers using two different lengths of PDMS chains thus varying the network densities and thereby the mechanical properties. Networks prepared with high molecular weight PDMS create softer, highly stretchable films with potential uses as actuators where large strains are desired. Low molecular weight PDMS elastomers are stiffer and less stretchable and therefore find applications within the area of generators.

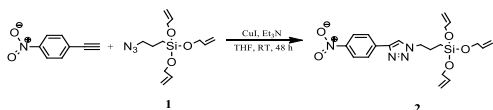
**Results and discussion**

An azide-functional vinyl cross-linker was synthesized according to Scheme 1 using a recently published procedure [4].

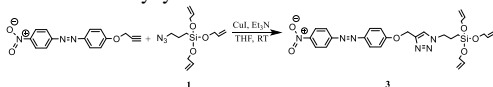


**Scheme 1:** Synthetic scheme for the preparation of the azide-functional vinyl cross-linker.

The cross-linker was hereafter used in click reactions (the copper(I)-catalyzed azide-alkyne cycloaddition (CuAAC)) with 1-ethynyl-4-nitrobenzene and a nitroazobenzene using a Cu/Et<sub>3</sub>N catalytic system according to Scheme 2 and 3.

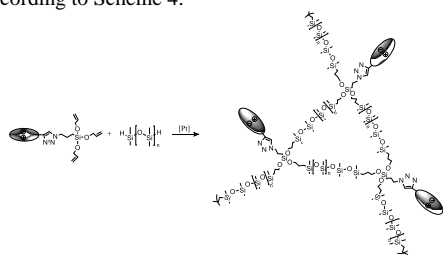


**Scheme 2:** Click reaction of azide-functional cross-linker and 1-ethynyl-4-nitrobenzene.



**Scheme 3:** Click reaction of azide-functional cross-linker and a nitroazobenzene.

Dipole-functional PDMS networks were created using the two cross-linker, hydride terminated PDMS of 28000 g/mol or 6000 g/mol and a platinum catalyst according to Scheme 4.



**Scheme 4:** PDMS cross-linking reaction between functional dipole cross-linkers and hydride terminated PDMS.

The ratio between the three-functional dipole cross-linkers and a commercial cross-linker was varied to create PDMS films of 0.23 to 3.6 wt% of dipolar cross-linker. Reference films prepared solely with 16-functional commercial cross-linkers were also made. The impact of the type of push-pull dipole cross-linker on the dielectric properties was determined by dielectric relaxation spectroscopy. The frequency dependent relative permittivity ( $\epsilon'$ ), loss tangent ( $\tan \delta$ ) as well as the electrical breakdown strength,  $E_B$ , for films with cross-linker **2** and **3** are presented in Table 1. For both

cross-linkers an increase in dielectric permittivity is observed upon the addition of dipole-functional cross-linker. In all cases, the effect is largest at the lowest amount of added dipole cross-linker. Compared to pure PDMS with commercial cross-linker only for which  $\epsilon'=2.8$  at 100 Hz, the film prepared with 6000 g/mol PDMS containing 1.35 wt% of cross-linker **2** has a  $\epsilon'=3.3$  at 100 Hz. This corresponds to an increase of ~20% at only 0.46 wt% of pure dipole. For all films, the dielectric loss remains exceptionally low after addition of dipole cross-linkers which means that all films exhibit very low dissipation of energy.

For films with cross-linker **3**, an increase in the breakdown field strength was observed with addition of low amount of cross-linker for both 28000 g/mol and 6000 g/mol films. In both cases, the measured values of 95.0 V/ $\mu\text{m}$  and 124 V/ $\mu\text{m}$ , respectively, are remarkably high. For cross-linker **2**, the electrical breakdown strengths decrease with increasing concentration of dipolar cross-linker but remain high at low concentrations. The reduction in breakdown strength at high concentration of functional cross-linker could be caused by the reduction in the stiffness. For all films the breakdown strength stays above ~40 V/ $\mu\text{m}$  which is high enough for most DEAP applications and in the range of commercially available products such as Elastosil RT625 from Wacker Chemie AG as stated by the manufacturer.

## References

1. R. Pelrine, R. Kornbluh, Q. Pei, J. Joseph, *Science* 287 (2000) 836–9.
2. C. Löwe, X. Zhang, G. Kovacs, *Adv. Eng. Mater.* 7 (2005) 361–7.
3. P. Brochu, Q. Pei, *Macromol. Rapid Commun.* 31 (2010) 10–36.
4. F. B. Madsen, I. Dimitrov, A.E. Daugaard, S. Hvilsted, A.L. Skov, *Polym. Chem.* 4 (2013) 1700–1707.

**Table 1:** Dielectric permittivity ( $\epsilon'$ ) and loss tangent ( $\tan \delta$ ) at 100 Hz as well as the breakdown strength ( $E_B$ ) for films with different type and weight percent of cross-linker.

Dipole content [wt%]	Films with cross-linker 2			Films with cross-linker 3		
	$\epsilon'$	$\tan \delta$	$E_B$ [V/ $\mu\text{m}$ ]	$\epsilon'$	$\tan \delta$	$E_B$ [V/ $\mu\text{m}$ ]
28000 g/mol:						
0.00	2.8	$2.69 \times 10^{-4}$	91.8	2.8	$2.69 \times 10^{-4}$	91.8
0.23	3.2	$5.78 \times 10^{-4}$	88.2	3.1	$5.25 \times 10^{-4}$	95.0
0.45	3.2	$4.54 \times 10^{-4}$	49.9	3.0	$6.33 \times 10^{-4}$	88.9
0.72	3.0	$5.24 \times 10^{-4}$	39.0	3.0	$7.03 \times 10^{-4}$	85.9
6000 g/mol:						
0.00	2.8	$3.45 \times 10^{-4}$	111.0	2.8	$3.45 \times 10^{-4}$	111.0
1.35	3.3	$6.01 \times 10^{-4}$	91.9	3.2	$5.21 \times 10^{-4}$	124.2
2.25	3.1	$3.34 \times 10^{-4}$	71.8	3.1	$4.04 \times 10^{-4}$	68.2
3.60	3.0	$10.5 \times 10^{-4}$	na <sup>a</sup>	3.2	$7.16 \times 10^{-4}$	57.0

<sup>a</sup> Attempts to obtain the electrical breakdown strength were unsuccessful as the prepared 150  $\mu\text{m}$  film was too sticky to be handled.





**Thomas Bisgaard**

Phone: +45 4525 2810  
E-mail: thbis@kt.dtu.dk

Supervisors: Jens Abildskov  
Jakob Kjøbsted Huusom  
Nicolas von Solms  
Kim Pilegaard

PhD Study  
Started: September 2012  
To be completed: October 2015

## Operation and Design of Diabatic Distillation Processes

### Abstract

Diabatic operation of distillation columns can lead to significant reductions in energy and operation cost compared to conventional (adiabatic) distillation columns, at an expense of an increased complexity of design and operation. The earliest diabatic distillation configuration dates back to the late 70's, and various different configurations have appeared since. However, as it is today, no full-scale diabatic distillation columns are currently operating in the industry. The aim of this project is to shed light on the potential benefits of diabatic operation and to handle some of the barriers for industrial application/acceptance of diabatic distillation columns.

### Introduction

Conventional Distillation Columns (CDiC) are energy intensive and operate at Second-Law efficiencies as low as 5-20 % [1]. Despite the fact that distillation is considered a mature technology, alternative configurations are under consideration. This is primarily due to increasing attention paid to environmental issues and resource management. Alternative column configurations, which reduce the amount of external energy utility, are the heat-pump assisted distillation columns. These configurations do, however, not fundamentally change the fact the energy is degraded through the column, which causes low Second-Law efficiencies.

Diabatic distillation has been proposed as a means to increase the Second-Law efficiency and hence the reversibility of the process. In this type of operation, the heat required to perform the separation is added and/or removed throughout the column. An example is the heat-integrated distillation column (HIDiC). Internal heat transfer in the HIDiC is realized by operating the rectifying section at a higher pressure than the stripping section by employing vapor recompression, thereby enabling heat transfer between the sections. This heat transfer facilitates gradual boil-up throughout the stripping and condensation throughout the rectifying section leading to an improved Second-Law efficiency [2]. The HIDiC uses significantly less utility in form of steam and cooling water compared to the CDiC. Instead, electrical energy needs to be supplied to the compressor. Even though electricity is several times more expensive

than supplying energy by steam, this operation may significantly reduce the operation cost of separation [3].

As a result of the promising features of the HIDiC, extensive efforts have been made to develop this technology during the past 15 years, both theoretically and experimentally. However, despite demonstrations of large energy savings of the HIDiC compared to the CDiC, it has not yet been accepted by industry. This could be due to lack of mature methods for designing and analyzing these more complex configurations, although such methods are beginning to appear. Furthermore, operation becomes more complex as a result of the higher degree of process integration.

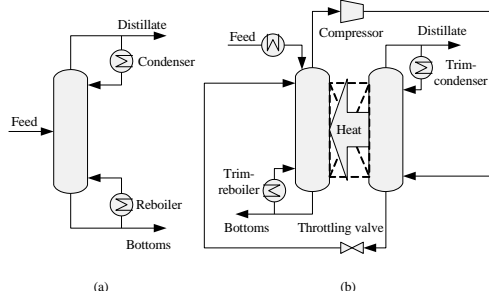


**Figure 1.** CDiC (a), HIDiC (b).

### Specific Objectives

There is a need for research and comparative studies that can help to provide analysis of the pros and cons of novel and intensified distillation processes compared to conventional columns, while considering a broader range

of separations. These studies must address both static as well as dynamic analysis. Carrying out work in the following topics have been identified to comprise an important contribution:

1. **Modeling** of the HIDiC is an important task, since the use of simplistic models can comprise a problem. For example in dynamic models, pressure dynamics or sensible heat effects are often ignored, but how will these assumption affect the HIDiC. Furthermore, only few experimental studies are carried for the HIDiC and therefore a great need for experimental validation of existing models exists.
2. Analysis of **potential benefits** of novel distillation solutions due to the applications of different means of analysis in literature of e.g. energy efficiencies. This can lead to bias towards one given configuration. Current studies report very different figures for potential energy savings, which clearly constitutes a problem in relations to achieving industrial acceptance. Few authors have addressed this issue by proposing systematic evaluations. Furthermore, it is planned to include sustainability metrics in the analysis as well.
3. Published **case studies** of industrial relevance are limited to a quite narrow range of separations. Most attention has been directed to ideal, binary systems of close boiling mixtures of hydrocarbons such as separations of equimolar mixtures of benzene/toluene or propane/propene.
4. Knowledge and experience on conceptual **design** of heat-integrated distillation columns is scarce compared to conventional distillation columns. A promising conceptual design method for the HIDiC is the Ponchon-Savarit method. Furthermore, the sizing of the internals in the internally heat integrated columns still appears to be a challenge.
5. A complete mapping of the **operation** by rigorous simulations, considering a HIDiC in operation taking into account all control loops etc., has not been published in literature. It is also planned to employ advanced control strategies (e.g. model predictive control), since the dynamic interactions are stronger in diabatic processes.

## Results and Discussion

The dynamics of the HIDiC have been studied [i, ii] and the design (see Figure 2) in order to reassess conclusions presented in literature.

A model framework has been developed [iii], being capable of describing both adiabatic and diabatic distillation columns. The model framework enables studies to gain insights into e.g. static properties and the dynamic behaviors. These insights can cover utility consumption accounts, energy efficiencies, operation expenses, as well as dynamics and control. In addition, the framework offers a flexibility of extending current configuration libraries due to the modular structure. An example study is shown in Table 1.

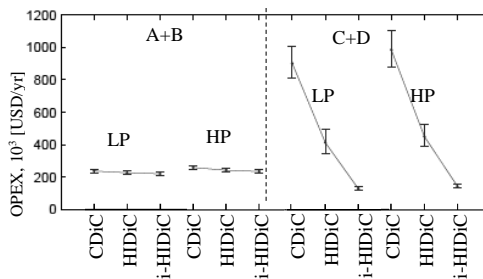


**Figure 2.** Uncertainty of operation expenditure  $OPEX$  of four different separations: Two different mixtures (A+B and C+D) with two different specifications, low purity (LP) or high purity (HP).

**Table 1.** Capital expenditures ( $CAPEX$ ), operational expenditures ( $OPEX$ ), and total annualized cost ( $TAC$ ) for the separation of benzene-toluene.

	CDiC	HIDiC
$CAPEX$	330,000 USD	1,500,000 USD
$OPEX$	280,000 USD/yr	133,000 USD/yr
$TAC$	346,000 USD/yr	433,000 USD/yr

## Conclusions

Diabatic distillation offers promising features in terms of energy usage and operation costs. It is thus an attractive technology from economical and an environmental point of view. The main barriers for industrial implementation, identified in this study, are the design and the operation aspects.

## Acknowledgement

The author would like to thank the Technical University of Denmark for financing of the study.

## References

- [1] G.M. de Koeijer, S. Kjelstrup, Minimizing Entropy Production Rate in Binary Tray Distillation 3 (3) (2000) 105-110
- [2] M. Nakaiwa, K. Huang, M. Owa, T. Akiya, T. Nakane, M. Sato, T. Takamatsu, H. Yoshitome, Potential energy savings in ideal heat-integrated distillation column 18 (11) (1998) 1077-1087
- [3] Z. Olujic, F. Fakhri, A. de Rijke, J. de Graauw, P.J. Jansens, Internal heat integration -- the key to an energy-conserving distillation column 78 (2-3) (2003) 241-248

## List of Publications

- [i] T. Bisgaard, J.K. Huusom and J. Abildskov, Dynamic Effects of Diabatization in Distillation Columns, Proceedings of ACD2012, 2012.
- [ii] T. Bisgaard, J.K. Huusom and J. Abildskov, Dynamic Effects of Diabatization in Distillation Columns, Proceedings of ESCAPE, 2013.
- [iii] T. Bisgaard, J.K. Huusom and J. Abildskov, A Modeling Framework for Conventional and Heat Integrated Distillation Columns, Submitted for proceedings of DYCOPS 2013.



**Martin Gamél Bjørner**

Phone: +45 4525 2886

E-mail: mgabj@kt.dtu.dk

Supervisors: Georgios Kontogeorgis

PhD

Started: June 2012

To be completed: June 2015

## CO<sub>2</sub>-Hydrates - Challenges and Possibilities

### Abstract

Despite its importance, accurate modeling of carbon dioxide (CO<sub>2</sub>) and in particular mixtures of CO<sub>2</sub> is still a challenge. Traditional approaches model CO<sub>2</sub> either as an inert or as a solvating molecule. Rigorously, however, CO<sub>2</sub> is a quadrupolar molecule and should in principle be modeled as such. In this work a quadrupolar contribution to the Helmholtz energy, inspired by recent advances within the statistical association fluid theory (SAFT), is proposed and combined with the well-known cubic plus association (CPA) equation of state (EoS). The new model is applied to the prediction of second virial coefficients of CO<sub>2</sub> and prediction of binary vapour-liquid equilibria (VLE) of CO<sub>2</sub>/hydrocarbon mixtures.

### Introduction

Carbon dioxide, as a solvent or refrigerant, is considered an environmentally harmless chemical. Nevertheless, in recent years CO<sub>2</sub> has received a significant amount of negative attention due to its contribution to the global warming and the fact that the amount of CO<sub>2</sub> in the atmosphere continues to rise. This is believed to be largely due to the high amounts of CO<sub>2</sub> emitted to the atmosphere as a result of e.g. electricity production from the combustion of fossil fuels. Alone in Denmark about 50 million tons of CO<sub>2</sub> are emitted each year. The reduction of the CO<sub>2</sub> emission is considered a high priority.

To understand the problems caused by CO<sub>2</sub>, high quality experimental data and accurate models, valid over a wide range of conditions and chemicals, are necessary. For example a novel technique for CO<sub>2</sub> capture using gas hydrates has recently been patented [1]. The operative pressure of the technique, however, is currently too high to be economically profitable. It is believed this pressure could be reduced by specific additives. Such a screening process, however, is expensive and time consuming, and accurate models for CO<sub>2</sub> in mixtures would greatly facilitate this process.

Mixtures of CO<sub>2</sub> and gas hydrates are also a nuisance in the petroleum industry, where the phase equilibrium of mixtures of CO<sub>2</sub> in hydrocarbons, water and glycols are of particular importance [2].

In an effort to improve current models a quadrupolar term is, in this contribution, combined with the CPA EoS (Kontogeorgis et al. [3]) and partly evaluated by

calculation of second virial coefficients of pure CO<sub>2</sub> and prediction of binary VLE of CO<sub>2</sub>-hydrocarbon mixtures.

### Specific Objectives

The purpose of the overall FTP project is to acquire a solid experimental and theoretical basis for understanding and addressing the problems of CO<sub>2</sub> and CO<sub>2</sub> hydrates, for the possible utilization of hydrate formation as a CO<sub>2</sub> capture technology.

More specifically a molecular thermodynamic model for CO<sub>2</sub> will be developed, based on the CPA EoS. The model is expected to include a specific quadrupole term and possibly other polar and/or induction terms. These terms should originate from statistical thermodynamic considerations.

It is expected that the applicability of several different terms, related to varying theoretical approaches such as those of Karakatsani et al. [4] and Gross [5], may be evaluated in combination with the CPA EoS.

The proposed model will be first tested for various pure compound bulk properties such as the second virial coefficients (this work), heat capacities and speed of sound, and for regular mixtures containing CO<sub>2</sub> and alkanes (this work), water and/or glycols. Finally the model will be incorporated in an improved van der Waals-Platteeuw theory for describing CO<sub>2</sub> hydrates.

Complex mixtures containing CO<sub>2</sub> hydrates and inhibitors will be studied both experimentally and using the new model.

## Results and Discussion

Despite the importance of CO<sub>2</sub> containing mixtures, accurate predictive modeling of such mixtures still poses a challenge [2]. A reason for this may be, that traditional approaches such as the Soave-Redlich-Kwong (SRK) [6] EoS treat CO<sub>2</sub> as an inert. Even in modern equations of state such as the Statistical Association Fluid Theory (SAFT) only dispersive forces are usually considered. The continued use of such procedures may be attributed to the fact that the mixture behavior usually is captured quite well when correlating with a (relatively large) interaction parameter ( $k_{ij}$ ), some predictive character is lost in this way, however, and it is uncertain how well such procedures work when extended to ternary or higher systems.

Other more pragmatic approaches tend to treat CO<sub>2</sub> as a self-associating (hydrogen bonding) or solvating molecule, such procedures often works well resulting in better correlations with smaller interaction parameters [2]. Unfortunately the improvement is obtained at the cost of additional pure component parameters and, in some cases, an extra parameter for the binary mixtures. Moreover, as we demonstrate in this work (see Figure 1), the second virial coefficient of CO<sub>2</sub> seems to be predicted significantly less accurately than when CO<sub>2</sub> is treated as an inert.

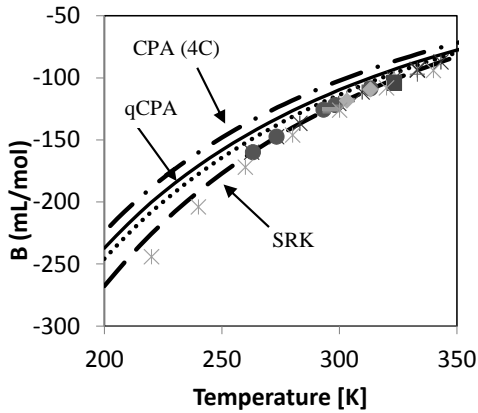


**Figure 1:** Model predictions and experimental values of the second virial coefficient of CO<sub>2</sub> in a limited temperature interval. From the top: CPA (scheme 4C), qCPA, regular CPA and classical SRK.

Rigorously, however, CO<sub>2</sub> has a large quadrupole moment (i.e. a concentration of charges at four separate points in the molecule). While quadrupolar forces are small short ranged forces, relative to regular van der Waals forces, they may become important for molecules with a significant quadrupole such as CO<sub>2</sub>. The effect of a quadrupole is that certain molecular conformations are favored more than others. That is, the quadrupole moment causes some local structuring in the fluid. This is believed to be the reason for the unusual phase behavior of mixtures containing CO<sub>2</sub>.

For these reasons several quadrupolar terms have been suggested, mainly based on the statistical mechanical theories for polar and quadrupolar fluids developed by Stell et al. [8] and Rushbrook et al. [9] (the so-called u-expansion). Gubbins and Twu presented the first equation applicable for calculation of the phase equilibrium of real mixtures [10], and later models are greatly inspired by their approach.

In recent years several research groups have exploited, the fact that the Helmholtz energy contributions are (assumed to be) independent of each other, that is:

$$A^{res} = A^{disp} + A^{Assoc} + A^{chain} + A^{pol} + A^{quad} \quad (1)$$

Equation 1 is used to combine the quadrupolar terms with the SAFT framework.

This approach has been utilized with varying degrees of success. To the best of our knowledge the first attempt was made by Walsh et al [11] for a general multipole. Gross [5] used an energetic term very similar to that used by Gubbins and Twu, without adding any extra pure component parameters. Improvements are observed for mixtures of CO<sub>2</sub>/hydrocarbons, however, model performance seem to deteriorate for mixtures where cross-interactions are of importance. Two quadrupolar (and polar) terms (a “full” expression and a truncated version) were utilized by Karakatsani et al. based on the theory of Stell et al. [8]. The truncated version, which seems to be the more useful of the two, is more computationally efficient at the cost of an additional pure compound parameter. The model has mainly been investigated for complex mixtures of cross interacting systems. While demonstrating the strength of the approach, this unfortunately makes it quite difficult to assess the model performance for specific system classes. Other authors have contributed with similar terms, mostly taking their basis in the model of Gubbins and Twu rather than the original papers by Stell et al.

Unfortunately it is difficult to compare the different models directly, since the various authors tend to test their own theory on different systems, thus making a comparison difficult. Moreover, the results are often not even compared to those of the unmodified SAFT version, which is crucial in order to properly evaluate the possible improvements from the theory.

We have recently developed a new (unpublished) quadrupolar term which is directly applicable in equations of state such as the CPA EoS. The term is set in a Padé approximation of the Helmholtz energy so that:

$$\frac{A^{quad}}{RT} = \frac{A_2}{1 - A_3 / A_2} \quad (2)$$

where the reduced residual Helmholtz energy expressions for the second order and third order terms are given as:

$$A_2(T, V, \mathbf{n}) = c_1 \frac{n^2 b}{V} \Theta^4(T) \quad (3)$$

$$A_{3,2}(T, V, \mathbf{n}) = c_2 \frac{n^2 b}{V} \Theta^6(T) \quad (4)$$

$$A_{3,3}(T, V, \mathbf{n}) = c_3 \frac{n^3 b^2}{V^2} \Theta^6(T) \quad (5)$$

and

$$A_3 = A_{3,2} + A_{3,3} \quad (6)$$

Where  $n$  is the number of moles,  $b$  is the co-volume,  $V$  the volume of the fluid and  $\Theta$  is a dimensionless quadrupolar moment given as:

$$\Theta(T) = c_4 \frac{Q}{\sqrt{T} b^{5/3}}$$

Where  $Q$  is the quadrupolar moment,  $T$  the temperature and  $c_1, \dots, c_4$  are numeric constants.

The CPA is an equation of state, which combines the simplicity of the Soave Redlich Kwong (SRK) EoS with the association term from Wertheim's theory. That is  $A^{CPA} = A^{SRK} + A^{assoc}$ . This allows for the modeling of many complex systems due to the association term, while the CPA EoS reduces to the computationally simple SRK EoS for non-associating systems. As  $\text{CO}_2$  is strictly speaking a non-associating species the regular CPA EoS in fact reduces to the SRK EoS for this compound. The expression for the Helmholtz energy of the SRK EoS is:

$$\frac{A^{SRK}}{RT} = -n \ln(1 - bn/V) - \frac{na(T)}{RTb} \ln(1 + bn/V)$$

where

$$a(T) = a_0 \left(1 + c_1(1 - \sqrt{T_r})\right)^2$$

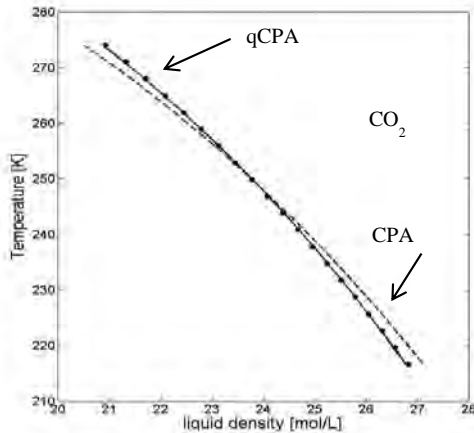


**Figure 2:** Model correlations for the liquid density of  $\text{CO}_2$  to pseudo experimental data obtained from the DIPPR database. Full lines are the quadrupolar CPA and dotted lines the regular CPA.

The Helmholtz energy term of the CPA EoS is coupled with the quadrupolar term assuming additivity

of the energy terms. The adjustable parameters  $a_0$ ,  $b$ ,  $c_1$ , and  $Q$  have been estimated by weighted least squares minimization of the saturated liquid density ( $\rho_{sat}$ ) and saturated vapor pressures ( $P_{sat}$ ) using the objective function:

$$Q = \sum_i \left( \frac{\rho_{sat,i}^{exp} - \rho_{sat,i}^{calc}}{\rho_{sat,i}^{exp}} \right)^2 + \sum_i \left( \frac{P_{sat,i}^{exp} - P_{sat,i}^{calc}}{P_{sat,i}^{exp}} \right)^2$$

Figure 2 shows both the correlations of the quadrupolar CPA (qCPA) and the regular CPA to the experimental liquid density as a function of temperature. It can be seen that the qCPA is capable of correlating the liquid density extremely accurately, while the regular CPA also captures the data quite well, it does deviate systematically at either endpoints. Table 1 shows the regressed parameters of the two models, and Table 2 shows their deviation from experimental data.

**Table 1:** Estimated pure compound parameters of the CPA and qCPA for  $\text{CO}_2$ . For  $T_r = [0.7-0.9]$ .

Model	$a_0$ [L <sup>2</sup> bar/mol <sup>2</sup> ]	$b$ [L/mol]	$c_1$	$Q$ [DÅ]	Ref
CPA	3.508	0.0272	0.76	-	2
qCPA	2.39	0.0285	0.63	3.47	This work

**Table 2:** Percentage absolute average deviations (AAD) from experimental data for  $\text{CO}_2$  with the CPA and qCPA.

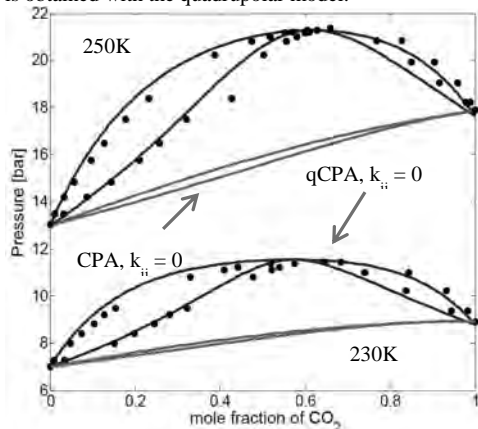
Model	%AAD in $\rho^{liq}$	%AAD in $P^{sat}$	Ref
CPA	0.80	0.20	2
qCPA	0.08	0.08	This work

Obviously the improvement is most significant for the liquid density where deviations are reduced by an order of magnitude. However, we should keep in mind that the improvement is obtained at the cost of an extra adjustable parameter (the quadrupole moment). As the CPA EoS already correlates the data quite well, identification of 'unique' parameters may be an issue, since the data used for parameter estimation is sparse in relation to the model. That is, good agreement between correlated and experimental pure compound properties is not a sufficient condition for a good predictive model, but certainly a necessary one.

In an attempt to validate the parameters second virial coefficients were calculated and compared to the regular CPA. Additionally second virial coefficients for  $\text{CO}_2$  treated as a pseudo-associating compound were calculated, using pure compound parameters from [2] (see Figure 1). Somewhat surprisingly we can see from Figure 1 that both the qCPA and CPA with  $\text{CO}_2$  treated as an associating compound yields worse second virial coefficients than the regular CPA or the SRK EoS. Clearly the poorest results are obtained when  $\text{CO}_2$  is treated as an associating species.

To evaluate the predictive capability of the qCPA for mixtures of CO<sub>2</sub>, compared to the regular CPA, the predicted VLE of a few simple CO<sub>2</sub>/hydrocarbon mixtures have been performed. We stress that while both models may accurately correlate the VLE of such mixtures, using a binary interaction parameter, the VLEs shown in this contribution are pure predictions (i.e.  $k_{ij} = 0$ ).

Figure 3 compares the predicted VLE of the binary mixture CO<sub>2</sub>/ethane with experimental data using either the qCPA or the CPA. It is clear from Figure 3 that significant improvements can be obtained compared to the regular CPA EoS. That is, without the quadrupolar term an almost ideal Raoult's law type VLE is predicted, while an almost perfect match to the experimental data is obtained with the quadrupolar model.



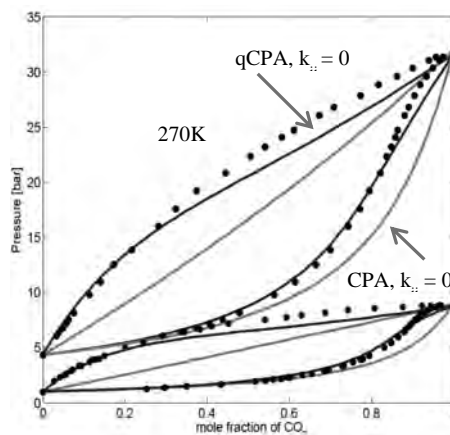
**Figure 3:** Prediction of the VLE for CO<sub>2</sub>/ethane at two different temperatures. Full lines are the quadrupolar CPA, while dashed lines are the CPA. The experimental data is taken [12].

Figure 4 demonstrate a similar trend for CO<sub>2</sub>/propane where in particular the CO<sub>2</sub> rich vapor phase is captured very well.

### Conclusions

In an effort to improve the predictive capabilities of classic thermodynamic models for mixtures containing CO<sub>2</sub> a novel quadrupolar term, developed from statistical mechanics, have been proposed and combined with the CPA EoS. It has been found that the model may significantly improve the prediction of simple CO<sub>2</sub>/hydrocarbon mixtures. The prediction of second virial coefficients of pure CO<sub>2</sub>, however, becomes slightly deteriorated compared to the regular CPA.

Further investigation on more challenging systems and improved parameter estimation is necessary to fully evaluate the applicability of the suggested term. Future work will estimate other pure compound properties and, if possible, include some of these in the parameter estimation to increase identifiability. Moreover the performance of the term should be tested in mixtures which form LLE and for mixtures of CO<sub>2</sub>/water.



**Figure 4:** Prediction of the VLE for CO<sub>2</sub>/propane at two different temperatures. Full lines are the quadrupolar CPA, while dashed lines are the CPA. The experimental data is taken from [13].

### Acknowledgements

The author is grateful to the Danish Research Council for Independent Research – Technology and Production Sciences for funding this project.

### References

1. D.F. Spencer, Methods of selectively separating CO<sub>2</sub> from a multicomponent gaseous stream, US Patent 5700311 (1997) and 6106595 (2000).
2. I. Tsvintzelis, G.M. Kontogeorgis, M.L. Michelsen, E.H. Stenby, Fluid Phase Equilibria 306 (1) (2011) 38-56.
3. G.M. Kontogeorgis, E.C. Voutsas, I.V. Yakoumis D.P. Tassios, Ind. Eng. Chem. Res 35(11) (1996) 4310-4318
4. E.K. Karakatsani, T. Spyriouni, I.G. Economou, AIChE Journal 51 (8) (2005) 2328-2342.
5. J. Gross, AIChE Journal 51 (9) (2005) 2556-2568.
6. G. Soave, Chem. Eng. Sci. (27) (1972) 1197-1203.
7. D.Y. Peng, D.B. Robinson, Ind. Eng. Chem. Fundamen. 15 (1) (1976) 59-64.
8. G. Stell, J.C. Rasaiah, H. Narang, Mol. Phys. 27 (5) (1974) 1393-1414
9. G.S. Rushbrooke, G. Stell, J.S. Høye, Mol. Phys. 26 (5) (1973) 1199-1215
10. K.E. Gubbins, C.H. Twu, Chem. Eng. Sci. (33) (1978) 863-878
11. J.M. Walsh, H.J.R. Guedes, K.E. Gubbins, J. Phys. Chem. 96 (26) (1992)
12. M.S.-W. Wei, T.S. Brown, A.J. Kidnay, E.D. Sloan, J. Chem. Eng. Data, 40 (1995) 726-731.
13. L.A. Webster, A.J. Kidnay, J. Chem. Eng. Data 46 (2001) 759-764.



## Vijaya Krishna Bodla

Phone: +45 4525 2967  
E-mail: vikb@kt.dtu.dk

Supervisors: Krist V. Gernaey  
Ulrich Krühne  
John M. Woodley

### PhD Study

Started: March 2011  
To be completed: May 2014

## Integrated Microfactories

### Abstract

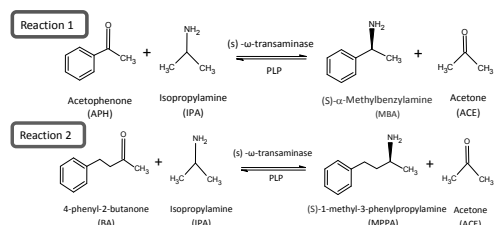
This project aims to demonstrate for the first time that fermentation and biocatalysis can be integrated. The hypothesis is to construct and operate integrated microscale reactors – so-called microfactories – using a transaminase model system (adapted to the specific microorganism and the biocatalytic reaction) in an intensified process. The integrated microfactory can be used to quickly and effectively screen different process conditions. The first part of this study is to evaluate the effect of miniaturization on biocatalytic reactions and to design and construct a miniaturized reactor, comparing its performance to a lab scale reactor. The second part includes the integration of the reaction and extraction to form an integrated and intensified process for efficient operation.

### Introduction

Biocatalysis is becoming increasingly attractive for the production of pharmaceutical intermediates and other products. However, significant efforts are needed to develop processes and biocatalysts to achieve an economically feasible process and to increase the biocatalyst productivity<sup>1</sup>. Miniaturization can help in gaining more process understanding and thus significantly enhance the productivity of some processes<sup>1</sup>. The potential of high throughput experimentation for rapid screening of biocatalysts, substrates, reaction conditions, kinetics, reactor and process design is of particular interest. An integrated microfactory has a number of features that are advantageous for rapid screening with respect to improved economy of the proposed process and process development: (1) the method for preparing the catalyst is considerably cheaper as no intermediary purification steps are needed; (2) the system process intensity is inherently enhanced through the continuous operation; (3) large sets of data can be obtained while consuming significantly lower amounts of expensive catalysts. The aim of this study is to design a microfluidic system, for rapid screening, that can mimic or improve the performance of the reaction at larger scale using biocatalytic transamination as a model reaction.

Transaminases (TAMs) (also known as aminotransferases) catalyze the transfer of an amino group from an amine donor, usually an amino acid or a simple amine such as isopropylamine, to an acceptor

molecule yielding a chiral amine as well as a co-product ketone (or alpha-keto acid), and require the cofactor pyridoxal phosphate (PLP) to act as a shuttle to transfer the amine group.



The main challenges are: (1) an unfavourable thermodynamic equilibrium position, requiring processes to shift the equilibrium; (2) substrate and product inhibition; (3) low substrate solubility, giving low volumetric productivities; (4) high biocatalyst cost<sup>2</sup>. The performance is evaluated by varying the operation conditions, i.e. parallel flow, multi-phase system for controlled supply of substrate, varying flow rate, residence time, enzyme concentration etc., which influences the performance of the reaction, and to study the reaction rate and mass transfer rate limitations observed under these conditions.

Initial reactions at batch scale, performed at different substrate and product concentrations, show the effect of substrate and product inhibitions on the biocatalyst activity (Fig. 1). Product inhibition has a more pronounced effect than substrate inhibition. These

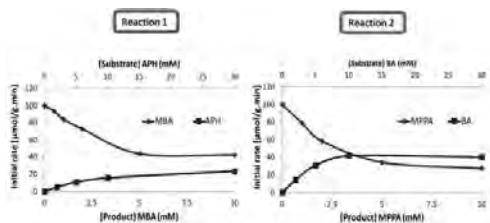


**Figure 1:** Effect of substrate and product concentrations on initial rates using ATA-47 (cLecta) (0.85g/L cell-free extract), 1M IPA, 2mM PLP, 100 mM phosphate potassium buffer (pH 7) at 30 deg.C and 400 rpm. For product inhibition 10 mM substrate ketone was used 2-30 mM ketone substrate for substrate inhibition assay. Data obtained from Dr. Watson Neto.

graphs also yield operational targets for substrate and product concentrations which are about 10-15 mM for the substrate and less than 2.5 mM for the product. The initial rate for reaction 1 is also slower than reaction 2 because of the smaller  $K_{eq}$  (Fig. 1)

### Material selection and Design formats

Poly(methyl methacrylate) (PMMA) is widely used and considered a biologically compatible material also for medical applications, and is therefore used for our application. Reactor configurations that are fabricated and tested are shown in Fig 2.

### Computational Fluid dynamics (CFD) simulations

CFD is used to predict the flow behaviour inside the micro-channels and is further also applied to improve our understanding of the diffusional properties of the substrate and product.

### Reactor configurations

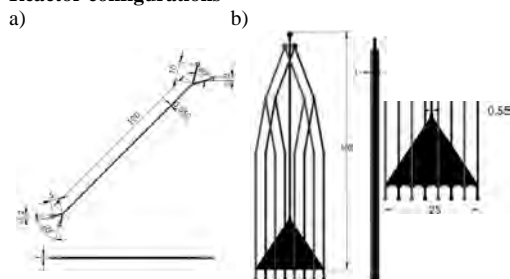


**Figure 2:** Reactor configurations: a) YY channel reactor, volume 50  $\mu$ L and b) 8 stream reactor (8S), volume 245.5  $\mu$ L. The dimensions of the reactors are mentioned along with the front and side views. A detail of the bottom part of the 8S reactor is also shown

### Residence time distribution (RTD) – YY channel

The CFD model of the reactor configuration was established, simulated and analyzed using the software ANSYS Fluent 12.1. Transient CFD simulations were performed by testing 2 different diffusion coefficients of a diffusing species in water. A surface monitor was set to calculate the vertex average mass fractions at the outlet at the specified time intervals. They are presented as a function of time in order to obtain the RTD profiles

(Fig 3). Comparing the experimental data from transient experiments to the RTD curves from simulations can give an insight into the diffusional properties of the compounds. The simulation of MBA (Fig. 3) corresponds well to the data indicating that the diffusion coefficient of MBA is in the order of  $10^{-9}$   $m^2/s$ . From the simulation for APH (Fig. 3), it can be concluded that the simulation doesn't fit with the data at the beginning. The simulation corresponds well with the data at the end where the normalized concentration was closer to 1. Based on understanding that this lag is caused by a slow diffusing species it can be anticipated that the diffusion coefficient of APH is in the order of  $10^{-12}$   $m^2/s$ . However this can also be the effect on the profile of other influential parameters such as the volatility and the permeability through PMMA.

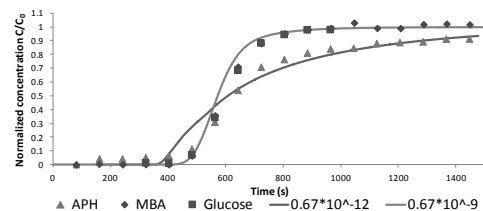


**Figure 3:** CFD simulations with tested diffusion coefficients of  $0.67 \cdot 10^{-9}$  and  $0.67 \cdot 10^{-12}$  plotted as continuous lines; Experimental results plotted as dots

A reactor configuration with 8 streams was built, as shown in Fig 2, where the 2 inlet streams are subdivided into 8 sub streams and combined to form an interdigitated flow (Fig. 4). Thus, the 8 stream reactor has 6 more contact surface areas for diffusion compared to the YY channel. This enables a much faster mixing of streams by diffusion due to the reduced diffusion length. The interfaces where the substrate and enzyme concentrations are non-zero also grow wider along the length of the reactor compared to the YY-channel. A reasonable expectation is that the product formation should increase with a factor 6 as there are 6 more contact surfaces for diffusion if the species transport was the bottleneck rather than the reaction kinetics. These studies also help in understanding the interaction between the species transport and the kinetic limitations. Experimental results show an increased production compared to the YY-channel reactor and the batch reactor (Fig. 5). However the yield was not 6 times higher as expected before. This indicates the shifting of the bottleneck from the species transport limitation to a kinetic limitation.

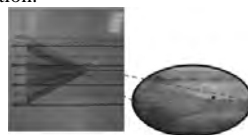


**Figure 4:** Interdigitated flow of the 8 stream reactor represented by two coloured dyes



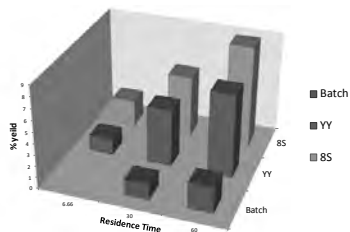
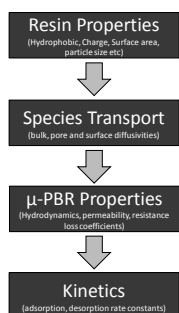


**Figure 5:** Comparison of experimental results for batch, YY-channel and 8 stream reactors for different residence times

Microreactors can prove to be an effective tool as they can be easily fabricated and tested. Experiments at microscale thus will also reduce the process development times for scale-up while consuming significantly lower amounts of expensive reagents. It is further intended to integrate the reaction together with product extraction to intensify the process and optimize the performance by using an auxiliary phase such as resins for product extraction.

### Screening and Characterization of Resins

Solid-liquid extraction using particles (resins etc.) is an attractive alternative option to processes where organic solvents exhibit operational challenges such as biocompatibility, phase toxicity, emulsification etc.



Porous resins, in general, are inert, easy to handle and simplify product isolation. The technology as such is widely used in the chemical and pharmaceutical industry.

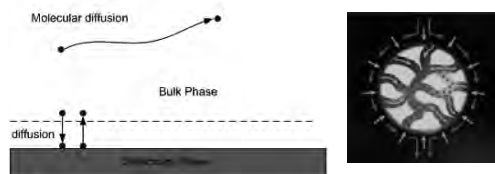


**Figure 6:** Species transport in the bulk phase and in a resin particle. The image was taken from the website of Pall Corporation.

It is important to identify resins with high loading capacity (based on hydrophobicity or charge),

selectivity etc. to minimize the effective loading for efficient operation. The mechanism of resin operation is based on bulk, surface and pore diffusivities (Fig. 6) and various models describing these are discussed in the literature<sup>3</sup>.

### Scaled down model:

Experiments done with scaled-down set-ups can be used to validate CFD models and also require less computational power for CFD simulations. Experiments were performed with 14 resin particles in a PTFE tube to obtain the adsorption breakthrough curve. The results are then used to validate the CFD models (Fig. 7).

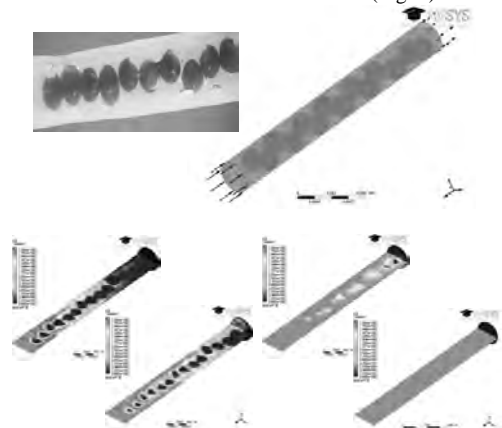


**Figure 7:** CFD simulations with resin and bed properties, species transport and kinetics

### μ -Packed bed reactor (μ -PBR)

A μ-packed bed reactor (Fig. 8) can be used as effective tool to screen and characterize these resins under operational conditions. Compared to its macro-scale counterpart, Losey et al. reported an increase in mass transfer by more than 2 orders of magnitude for cyclohexene hydrogenation in a μ-PBR using an activated carbon catalyst<sup>4</sup>.

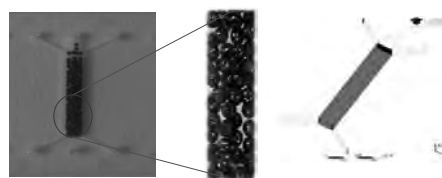


**Figure 8:** μ -PBR with resins (Lewatit AF5)

Experiments were performed by varying the process conditions and the flow rates, to check for the loading that could be obtained under process conditions. A higher loading is achieved at smaller flow rates (Fig. 9), as expected, because of better mass transfer. Validated CFD models from scaled-down experimental set-ups can be used to perform simulations of a μ-PBR to further understand the mechanism of resin operation.

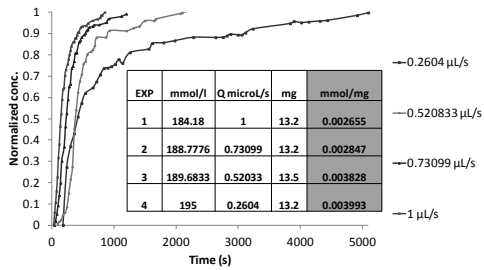


**Figure 9:**  $\mu$ -PBR with resin loading at different flow rates

Comparing CFD models with experimental data, more process knowledge can be gained, to understand which parameters (surface area, kinetics, diffusional velocities etc.) have a higher influence on the resin loading.

### Integrated Micro Membrane Packed Bed Reactor

This part of the work is focused on overcoming process related challenges such as thermodynamic equilibrium, substrate and product inhibitions, low aqueous substrate solubility and limitations with respect to enzyme stability and activity. This is achieved through developing an integrated micro membrane packed bed reactor (IMMPBR) that can be operated in fed-batch mode to overcome the above-mentioned limitations, and can be used as an effective screening tool for screening various process conditions, substrate and enzyme concentrations (Fig. 10). The aim is to continuously extract the product (using resins), with recycling of the waste stream, while continuously supplying the substrate. The microsystem is operated with a total volume of ~1.5 ml and a reactor volume of ~600  $\mu$ L. Polytetrafluoroethylene (PTFE) membrane is used to separate the enzyme from the resin.

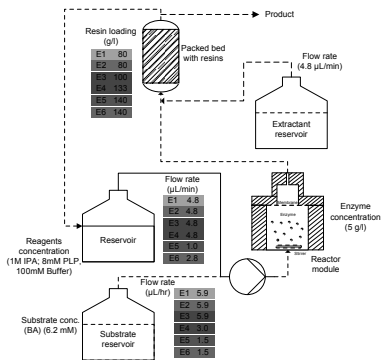


**Figure 10:** IMMPBR with different modules; Experiments performed at 5 g/l of crude enzyme extract, except for E2 where 10 g/l of dried cells was used

Experiments were performed with varying substrate flow rates, recycling rates and packed bed resin loading, the values of which are shown in Fig. 10. The reactor is operated for 37 hours while the substrate is continuously supplied as fed-batch and product continuously extracted into the resins. However after 37 hrs, based on the amount and the selectivity of the resins, product is

split between the resin phase and the aqueous phase. The results are plotted as the product produced per total final volume for different experimental scenarios (Fig. 11). The target concentrations for these were obtained from inhibition curves (Fig. 1).

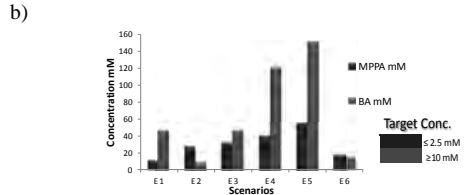
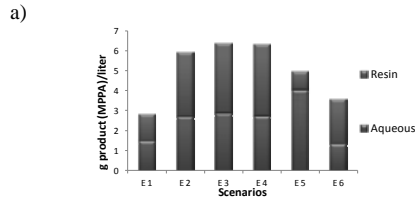


**Figure 11:** a) Product concentration in the resin phase and the aqueous phase for different experimental scenarios b) Substrate and product concentrations in the aqueous phase for different experimental scenarios

### Conclusions and Outlook:

- A YY reactor and 8 stream reactor, built for gaining more process knowledge, were shown to perform better than the traditional well-mixed batch reactors
- IMMPBR can be used as an effective tool for gaining process understanding and screening various process conditions while consuming lower amounts of enzyme compared to batch scale experiments.
- It has been demonstrated that microreactor technology and computational fluid dynamics (CFD) can be used as tools for rapidly acquiring process data and gaining more process knowledge
- A microbioreactor for the production of the enzyme, needs to be developed and integrated with the IMMPBR

### Acknowledgement

The work is financed by the Danish Research Council for Technology and Production Sciences (FTP), project no. 10-082388

### References

1. Pollard D.J., Woodley J.M., Trends Biotechnol., (2007) 25(2), 66-73.
2. Matosevic S., Szita N., Baganz F., J. Chem. Technol. Biotechnol., (2011) 86, 325-471.
3. Medved I., Cerny R., Microporous Mesoporous Mater., (2011) 142, 405-422.
4. Losey M.W., Schmidt M.A., et al., Ind. Eng. Chem. Res., (2001) 40, 2555- 2563.



**Riccardo Boiocchi**

Phone: +45 4525 2910  
E-mail: ricca@kt.dtu.dk

Supervisors: Gürkan Sin  
Krist V. Gernaey

PhD Study

Started: October 2013  
To be completed: September 2016

## Plant-wide Modelling and Control for Nitrous Oxide Emissions from Wastewater Treatment Plants

### Abstract

There are increasing evidences showing that nitrous oxide ( $N_2O$ ), a greenhouse gas with a global warming potential (GWP) 300 times larger than the one of carbon dioxide ( $CO_2$ ) and an ozone-depleting substance, is emitted in a considerable amount from domestic wastewater treatment plants (WWTPs). For this reason, development of WWTP control strategies is nowadays focused on finding strategies that can accomplish the legal effluent quality standards while minimizing greenhouse gas emissions as well.

### Introduction

Nitrous oxide ( $N_2O$ ) is well-known as the dominant ozone-depleting substance and a harmful greenhouse gas with a global warming potential 300 times larger than the one of carbon dioxide ( $CO_2$ ) [1]. In literature there is substantial published evidence demonstrating that wastewater treatment plants treating mainly wastewater from households contribute considerably to the global  $N_2O$  emissions [2]. In particular, biochemical studies have shown that  $N_2O$  can be produced in the liquid phase during the biochemical processes responsible for biological nitrogen removal. These processes are: heterotrophic denitrification [3] and autotrophic nitrification [4, 5]. The first is the oxidation of the organic biodegradable matter with nitrogen compounds such as nitrate ( $NO_3^-$ ) and nitrite ( $NO_2^-$ ) as electron acceptors [6], whereas the latter is the oxidation of total ammonia nitrogen to nitrate with oxygen as electron acceptor [7]. There are many environmental parameters which affect the  $N_2O$  production during these two processes. For instance, with regard to heterotrophic denitrification it is well-known that a too high concentration of dissolved oxygen can lead to incomplete reduction of the previously-mentioned nitrogen compounds. As a consequence, an accumulation of  $N_2O$ , an intermediate in the reduction of nitrate to nitrogen gas, can occur [8]. Moreover, low availability of organic biodegradable carbon can lead to the same negative consequence [9]. With regard to autotrophic nitrification, oxygen is one of the main factors [10]. As a matter of fact, a lack of oxygen during autotrophic nitrification is shown to force ammonia-

oxidizing bacteria (AOB) to use nitrogen compounds as electron acceptors for ammonia nitrogen oxidation. In this case,  $N_2O$  is formed simply as a consequence of nitrogen compound reduction.

As can be deduced, accomplishing environmental conditions in the WWTPs that minimize the formation of  $N_2O$  is the route towards mitigating the emissions of  $N_2O$ . Process control is widely used to support achieving the legal effluent quality requirements of the WWTP. Up to now, several control strategies have been designed with control objectives such as maintaining the oxygen concentration at a set point, or maintaining the internal recycle proportional to the influent flow rate (ratio control), or keeping the ammonium effluent concentration below effluent limits. However, thus far no specific control strategies have been design the minimization of the amount of  $N_2O$  emitted as the control objective. This PhD project aims at filling this gap.

### Methodology

The development of control strategies will be performed on an extension of the Benchmark Simulation Model n°2 (BSM2). As a consequence, the preliminary step to be done before the control design will be to extend the BSM2. This extension will regard both the plant configuration and the description of the biochemical processes. In particular, the plant configuration will be extended with side-stream systems such as SHARON & Anammox processes, and membrane filtration. The biochemical model, on the other hand, will be modified by including  $N_2O$  production by denitrifying

heterotrophs and AOB. The biochemical models describing these dynamics will be developed in DTU Environment with respect to observations made at the Department of Biology of the University of Southern Denmark. The new BSM will be used as reference for the development of the control strategies mentioned in the introduction. In order to achieve this, the scheme below will be followed:

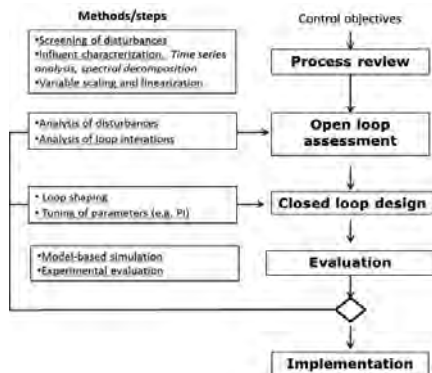


**Figure 1:** Control design methodology

As can be seen, the first step for the design of a control strategy is to define its objectives and constraints. Here, the objective is the minimization of  $N_2O$  emitted. The definition of constraints has to deal with boundaries such as legal limits for the effluent and economic management chances. Afterwards, a process review has to be performed, which consists mainly in identifying, among the system inputs, the disturbances to be overcome through the control and the possible manipulated variables. A global sensitivity analysis is the next step, to analyze the effect of the disturbances on the system. Moreover, if the control strategy will involve more than one controlled variable, an analysis of the loop interactions will be made. Once the open loop assessment has been performed, the closed loop(s) control structure will be decided. It is worth to mention that there exist different kinds of controllers which can be used. There are for example Proportional Integral Derivative (PID) and fuzzy-logic controllers. PID controllers provide a single control action on the basis of the predicted effect of the disturbances on the process. There are different tuning strategies which provide optimal values of PID controller parameters such as the Internal Model Control (IMC) which requires a linearization of the process model. The fuzzy-logic controllers are based on expert knowledge and in this case there are no deterministic rules to tune the different parameters for an optimal control performance. However, for specific process systems it is important to determine the effect of the different tuning choices on the control performance, and to define the criteria to follow when making decisions during the fuzzy-logic control design. There is evidence showing that in cases such as wastewater control a fuzzy-logic controller can have better performance and has a better chance to be

realizable compared to a PID controller [11]. For this reason, during this PhD project the fuzzy-logic control approach will be taken into consideration.

Both situations, i.e. either adopting a PID or a fuzzy-logic controller, include a relatively large number of choices that can be made, and as a result of such choices different control strategies will be produced. Each of these control strategies will be simulated in the previously-extended BSM2, and the results will be used as basis for the evaluation of control performance in order to choose the best control strategy. This evaluation will be performed according to a large number of criteria which take into account the environmental impact and technical-economical objectives. With regard to the environmental impact, and in view of controlling the  $N_2O$  emissions, what has to be paid attention to are the liquid effluent quality and the emissions of other gases such as nitric oxide (NO) and  $CO_2$ , which have a considerable negative environmental impact. It is furthermore also important that the minimization of  $N_2O$  is achieved within contained management costs, and that the control strategy is technically feasible in view of future application on the plants. Once the best control strategy has been selected, it will be implemented in different plant configurations to test the compatibility of the control scenario with the reality. In case of incompatibility, the possibility of retuning controller parameters and/or reshaping the controllers will be evaluated. At the end of the project, optimal control strategies minimizing  $N_2O$  emissions from WWTPs while respecting the economical and environmental constraints will be available for WWTP managers.

#### References:

1. A. R. Ravishankara, J. S. Daniel and R. W. Portmann , Science 326 (2009) 123-125.
2. M. J. Kampschreur, H. Temmink, R. Kleerebezem, M. S.M. Jetten, M. C. M. van Loosdrecht, Water Research 43 (2009) 1093-1103.
3. K. Hanaki, Z. Hong, T. Matsuo, Water Science and Technology 26(5) (1992) 1027-1036.
4. L. J. Shaw, G. W. Nicol, Z. Smith, J. Fear, J. I. Prosser, E. M. Baggs, Environmental Microbiology 8(2) (2006) 214-222.
5. H. Zheng, K. Hanaki, T. Mtsuo, Water Science and technology 30(6) (1994) 133-141.
6. Knowles R. Microbiological reviews 46 (1) (1982) 43-70.
7. U. Wiesmann: Advances in Biochemical Engineering Biotechnology 51 (1994) 114-153.
8. S. Otte, N.G. Grobben, L. A. Robertson, m.S. Jetten, J. G. Kuene, Applied and Environmental Microbiology 62(7) (1996) 2421-2426.
9. H. Itokawa, K. Hanaki, T. Matsuo Water Research 35 (3) (2001) 657-664.
10. M. J, Kampschreur, N.C.G. Tan, R. Kleerebezem, C. Picioareanu, M. S. M. Jetten, M.C. M. van Loosdrecht, Environmental Science and Technology 42 (2) (2008) 429-435.
11. R. M. Tong, M. B. Beck, A. Latten, Automatica 16 (1980) 659-701.



**Andrijana Bolic**

Phone: +45 4525 2958  
E-mail: anb@kt.dtu.dk

Supervisors: Krist V. Gernaey  
Anna Eliasson Lantz

PhD Study  
Started: March 2010  
To be completed: February 2014

## Fermentation Processes at Small Scale

### Abstract

At present, research in bioprocess science and engineering requires fast and accurate analytical data (rapid testing) that can be used for investigation of the interaction between bioprocess operation conditions and the performance of the bioprocess. Miniaturization could result in a set of attractive tools necessary for obtaining a vast amount of experimental data in a short time. The main objective of this project is to develop a microbioreactor platform for continuous cultivations of *Saccharomyces cerevisiae*, where NIR spectroscopy could be further implemented for rapid on-line measurement of process variables like substrate and biomass.

### Introduction

Conventional microbial cell cultivation techniques are not sufficient anymore considering the fast development of tools for genetic manipulation of biological systems resulting in large numbers of strains and conditions that need to be screened. Usually bench-scale reactors, flasks and tubes are used for obtaining relevant experimental data of microbial cultivations. Although bench-scale reactors have efficient control of process variables and yield valuable data, they are expensive, labor intensive and they provide a relatively small amount of data.

sufficient. Beside the above-mentioned vessels, today, microtiter plates are increasingly used for screening experiments considering that they provide easy handling, low cost and high throughput. Nevertheless, the process control in microtiter plates is often not reliable enough to provide realistic numbers in view of later scale up which is affecting the overall value of data. Different reactor configurations and their positioning according to throughput and data quality are presented in Figure 1.

There is a big driving force and interest in the last decade for development of new techniques which could provide both high quality data and also a high quantity of experimental data. In recent years microbioreactors and other small scale systems have been researched intensely due to their clear advantages like small volume, little or no need for cleaning (one time usage), high throughput (multiple bioreactors in parallel), high information content and control capabilities [1]. Small scale systems together with analytical methods are providing the opportunity for a potentially automated and well defined experimental system, which can deliver results that are more comparable to bench-scale reactors in comparison to e.g. a shake flask.

Even though microbioreactors have many advantages, it is important to bear in mind that they also have issues related to their size and handling. Evaporation, proper and reliable stirring, interconnections between micro-scale features and the 'macro world' are just some of the burning problems that need to be solved. In addition, measurements of several process variables at small scale are not

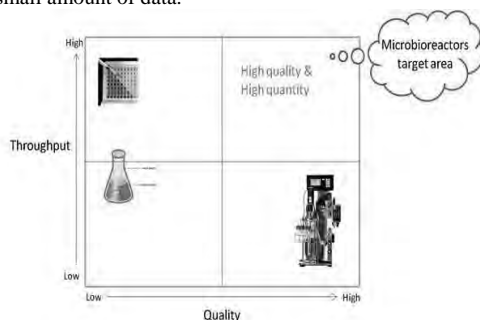


**Figure 1:** Different vessels (microtiter plates, flasks and bench-scale bioreactor) and their positioning according to throughput and data quality.

Regarding microbial cultivations in flasks and tubes, there is a general lack of control and the amount of data collected per experiment is usually not

straightforward to implement. They rely on analytical methods, which are not sufficiently developed for such a small scale at this point. If the measurements are possible, they are not cheap either.

Another important issue that needs to be addressed is determining the optimal working volume while keeping in mind the final objective – application. Does one need a sample or not? Does one talk about cells in suspension or adhered to a substrate? The final microbioreactor design should thus strongly depend on the goal of a specific microbioreactor application.

### Micro- and milliliter scale reactor design

To address some of the previously mentioned questions, a bioreactor platform with 1-2 ml working volume is developed. Considerable effort is placed in development a system that could provide reproducibility and easy handling at a reasonable cost.

### Platform

The reactor surrounding is equally important as the reactor itself. Keeping this in mind, a platform with gas connections, optical fibers for sensing, a specially designed heater and standard temperature sensor was designed and fabricated. It can be seen in Figure 2.

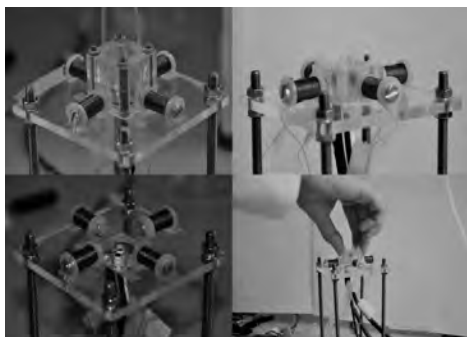


**Figure 2:** Microbioreactor together with platform

The reactor can be placed on a platform using a ‘Lego’ approach, which ensures reproducibility in sensing and establishing connections. Furthermore, this configuration lowers the cost per microbioreactor, considering that expensive parts of the system are reusable and placed in the platform, while the bioreactor is mostly made from cheap PMMA and has one magnetic ring and two sensor spots.

### Reactor and stirrer design

The bioreactor, made in PMMA, consists of a bottom and one or two upper parts as shown in Figure 3. This enables change in volume, by adding or removing one of the upper parts. The bottom part is made as a negative to the platform and has a thin optically transparent layer to make sure that measurements based on optical sensing are possible (pH, DO, OD).

The top part is a cylinder with a shaft in the middle on which a magnetic stirrer is mounted. The bioreactor can have two tubes for optional aeration (upper picture in Figure 3). Beside air sparging, there is also the possibility for exploiting surface aeration in which case aeration tubes are removed and connectors are made on the top of the microbioreactor (lower picture in Figure 3).

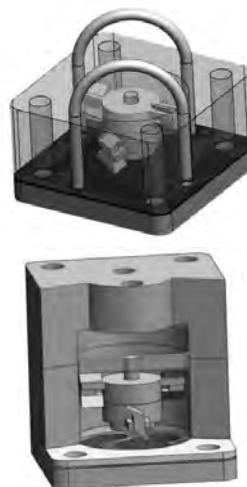


**Figure 3:** Two options for bioreactor design

The shaft is closed by a cap which prevents the stirrer to fall off from the shaft. The outer surface of the cap is covered with aluminum foil which serves as a mirror. Therefore, when light at 610 nm is sent into the reactor through a bundle of optical fibers, it is reflected by the aluminum foil and it reaches the detector. In this way the optical density is measured with a good linear range up to 20 g/L, which can be seen in Figure 4.

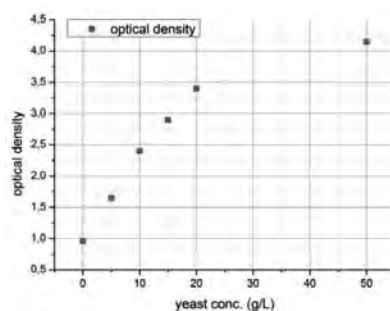


**Figure 4:** Measured optical density as a function of yeast concentration

The stirrer has two pairs of impeller blades placed at two levels, which can be seen in Figure 5. Each blade can be removed in order to create a different mixing behavior. A permanent magnetic ring, which is

magnetized across its diameter, is placed inside the stirrer and is driven by a rotating magnetic field.

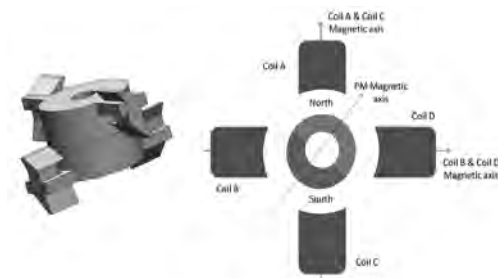


**Figure 5:** Stirrer design

Electromagnets were incorporated in the mixing device, in order to obtain control over the mixing by changing the speed and direction of the stirrer rotation. In this way, it is possible to prevent formation of a vortex without usage of baffles. The mixing device consists of a base fabricated by micromilling in PMMA (non-magnetic material and part of the platform), illustrated in Figure 2, on which 4 coils (electromagnets) are mounted. The coils are connected to a switch mode power supply, which is controlled by a PC running LabView software. The basic principle of the mixing control is presented in Figure 6.

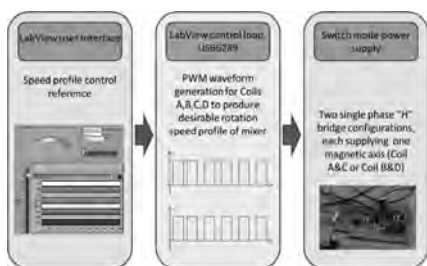


**Figure 6:** Mixing control principle

## Results

The mixing capability of the microbioreactor was quantified by experiments where mixing time and volumetric mass transfer coefficient ( $k_L a$ ) were evaluated against different stirrer rotational speeds.

The mixing time was determined by a colorimetric method based on acid-base reaction [2]. The change in color was filmed and the time needed to reach a homogeneous liquid phase was measured. Afterwards, the movie was analyzed frame by frame in order to determine the exact time when the color changed from pink to transparent. As expected, the mixing time in a 1 ml microbioreactor was significantly reduced with an increase of the rotational speed. Thus, 2 s mixing time at 200 rpm was reduced to 0.4 s at 1000 rpm, which can be observed in Figure 7.

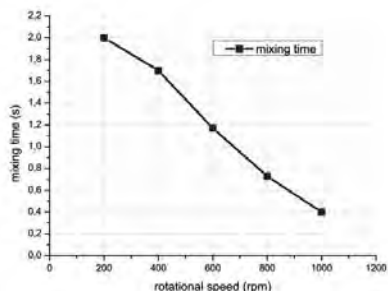


**Figure 7:** Mixing time at different rotational speeds

The volumetric mass transfer coefficient ( $k_L a$ ) is one of the most critical parameters during aerobic fermentation processes. Therefore, the influence of air sparging, surface aeration, one- and bi-directional mixing on  $k_L a$  value was evaluated using the gassing-out method[3,4]. First, nitrogen was continuously flushed through the medium until the oxygen concentration in the reactor dropped to zero. Subsequently, air was introduced and the change in the oxygen concentration was measured by a PreSens sensor spot at the bottom of the reactor. The response time of the DO sensor ( $t_1$ ) was evaluated and it was taken into account during the development of best correlation for estimating the transfer of oxygen from air to water ( $t_2$ ):

$$DO = A_1 \left( 1 - (t_1 + \exp(-t/t_1)) - t_2 + \exp(-t/t_2) \right) / (t_1 - t_2); t_1 = 11.6s$$

The correlation between the volumetric mass transfer coefficient and the rotational speed during surface aeration, sparging and bidirectional mixing in a 1 ml microbioreactor is presented in Figure 8.

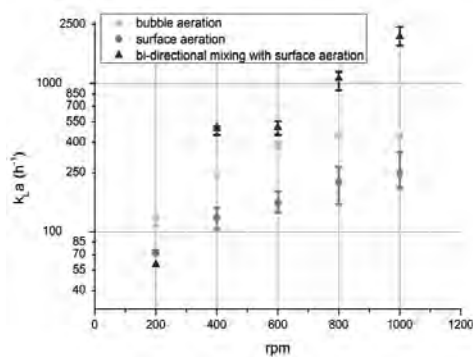


**Figure 8:**  $k_L a$  values at different stirrer rotational speeds and aeration methods

The highest  $k_L a$  values ( $k_L a > 1000$  h<sup>-1</sup>) were obtained by bidirectional mixing in combination with surface aeration, where the spinning direction was changed every 2 s at different rotational speeds. In the case where air sparging with only one direction of rotation

was applied, the maximum  $k_{LA}$  value obtained was  $450 \text{ h}^{-1}$ , while with surface aeration the  $k_{LA}$  was around  $300 \text{ h}^{-1}$ . A larger difference between sparging and surface aeration was expected, but the size of the bubbles and the stirrer were not holding and dispersing bubbles sufficiently long in the liquid phase. Beside the mentioned parameters, the influence of viscosity and reactor volume on the  $k_{LA}$  was also examined and results are presented in Figure 9.

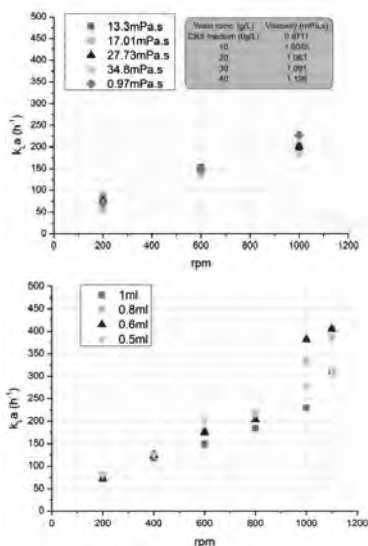


**Figure 9:** Influence of viscosity and reactor volume on the measured  $k_{LA}$

From the results presented in the upper graph of Figure 9, it is obvious that the influence of viscosity is negligible, especially for the cultivations with yeast. In the second graph of Figure 9, it can be seen that a decrease of the volume didn't have a major influence on the  $k_{LA}$  value, although this would be expected due to an increased surface to volume ratio. The major reason explaining this result is that the decrease of the volume in the reactor means that the stirrer is not completely submerged, and thus doesn't participate anymore in the mixing. The available surface for oxygen transfer doesn't change that much either due to the specific size and geometry of the stirrer.

After all mixing characterization and evaluation, a first series of cultivations were performed. An anaerobic batch cultivation with *Lactobacillus paracasei* as a model organism was performed. Comparison was made between 2 mL (batch 3 and 4) and 2L (batch CL0481-3E) scale. The end point measurements of glucose and lactic acid concentrations together with the optical density (OD) measurement are presented in Table 1.

The OD and lactic acid concentration values were significantly lower and the glucose concentration was higher after 10 and 11 hours in the 2 L fermentations

compared to the 2 mL fermentations. The same levels of OD, glucose, and lactic acid were achieved after 12 – 13 hours in the 2L fermentor. This could indicate that the lag phase of the 2 mL fermentations was shorter or that the growth in the exponential growth phase was faster.

**Table 1:** Cultivations at 2mL and 2L (CL0481-3E) scale [5]

Fermentation	Sample time (hours)	OD (external)	Glucose (g/L)	Lactic acid (g/L)
CL0481-3E	10	2.227	15.6	3.3
	11	3.397	14.9	5.3
	12	4.837	11.7	7.1
	13	6.577	8.70	9.9
3	11	4.334	11.5	8.7
4	10	4.573	13.3	9.2

The first results regarding the application of the small scale reactor in fermentations with anaerobic cultivations are promising. Naturally, the next step is to test the whole system with aerobic cultivations, where evaporation can be a potential problem.

## Conclusion

A flexible, disposable and cheap microbioreactor with supporting platform was developed. It has a small footprint. The system shows high level of flexibility:

- ✓ Surface or bubble aeration
- ✓ One- or bi- directional mixing
- ✓ Volume (0.5 - 2 mL)

The magnetic stirrer with adjustable geometry is low cost and maintenance free. It is a standalone mixing system, and consequently there is no need for external plate shakers and motors. Mixing can be considered almost instantaneous. Bi-directional mixing eliminates the need for baffles and drastically improves the  $k_{LA}$  value ( $k_{LA} > 1000 \text{ h}^{-1}$ ). The volumetric mass transfer coefficient obtained by surface aeration is sufficient for a standard fermentation.

## Acknowledgements

This project is supported by the Danish Council for Strategic Research in the frame of the project "Towards robust fermentation processes by targeting population heterogeneity at microscale" (project number 09-065160).

## References

1. D. Schäpper, M. N. H. Z. Alam, N. Szita, A. E. Lantz, K. V. Gernaey, Anal. Bioanal. Chem. (2009) 395:679–695
2. Paul, EL.; Atiemo-Obeng, VA.; Kresta, SM. Handbook of Industrial Mixing: Science and Practice, John Wiley & Sons, 2004
3. Suijdam JCV, Kossen NWF, Joha AC. Biotechnol Bioeng XX: (1978)1695–1709
4. Stanbury PF, Whitaker A, Hall SJ. Principles of fermentation technology: Oxford, UK: Elsevier Science Ltd. 1995, Pp 243-253
5. R.A.Prior, T.Vilby. Validation of 2 mL microbioreactors and near-infrared spectroscopy monitoring, bachelor thesis, 2012, DTU





**Hande Bozkurt**

Phone: +45 4525 5510  
E-mail: hboz@kt.dtu.dk

Supervisors: Gürkan Sin  
Krist V. Gernaey

PhD Study  
Started: December 2011  
To be completed: December 2014

## Early Stage Design of Wastewater Treatment Plants: A Mathematical Programming Approach

### Abstract

In this study we propose a new approach based on mathematical programming to manage the optimal process selection and early stage design of wastewater treatment plants (WWTP). To this end, a superstructure optimization approach -formulating the design problem as a Stochastic Mixed Integer (Non)linear Programming (MI(N)LP) problem- is used to generate novel and optimal wastewater treatment process selection under uncertainty. Treatment alternatives are described in terms of input-output mass balance using a generic process interval model. The application of the problem is highlighted using a case study with the objective of designing a new WWTP under different objective function scenarios, taking into account different sources of uncertainty.

### Introduction

Wastewater treatment process synthesis can be defined as the step in the design of a WWTP where the design engineer selects unit processes from a number of alternatives and interconnects them to create the process flow diagram. Considering the process selection and network design for WWTPs have evolved recently from being a simple technical problem to a complex decision making task, which needs to contemplate many criteria such as nutrient recovery, energy efficiency, water and sludge reuse in addition to cost and effluent quality; wastewater treatment process synthesis has become one of the most challenging steps in WWTP design. Another consideration in design studies is that the plant design should be robust and feasible over the lifetime of the project; therefore data and model uncertainty need to be considered in the design phase. Currently, wastewater treatment process synthesis is mainly based on expert decisions and previous applications; however this approach might not fit to handle such complex problems hence is expected to provide sub-optimal solutions. This study, therefore, proposes an alternative approach to cast the decision making problem using mathematical programming techniques for process synthesis and design of domestic WWTP under uncertainty.

several steps. The first step is where the problem is defined and its mathematical formulation is developed. Moreover, for each treatment technology system specific data are collected and used to calculate the design parameters (volumes, utility consumptions etc.) as well as performances (contaminant removals, sludge production etc.). Then, the domain of uncertainty is defined with respect to selected uncertain parameters. The future scenarios are generated by sampling the uncertain space uniformly using Latin Hypercube Sampling (LHS). After formulating the optimization problem and performing the deterministic solution; it is solved for the defined number of scenarios which are generated with regard to the uncertain data. Finally, the stochastic problem is formulated and solved to find the optimal treatment network under uncertainty. The details of the framework can be found elsewhere [1].

### The Framework

A schematic representation of the framework for superstructure based optimization methodology is shown in Figure 1 [1]. The framework is composed of

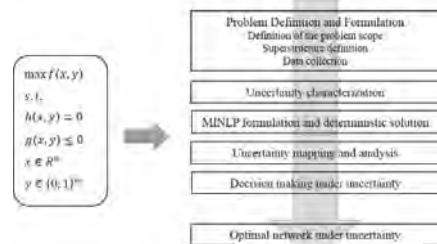


**Figure 1:** The superstructure based optimization framework for WWTP design [1]

## Case Study

The problem is defined as the design of a WWTP for the treatment of a given wastewater composition [2] in compliance with the emission limits defined by the EU Urban Wastewater Treatment Directive. The objective of the design is the minimization of the total annualized cost (TAC). The superstructure developed for the problem is seen in Figure 2 [3].

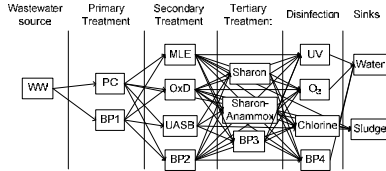


**Figure 2:** Case study superstructure [3]

The uncertain domain is defined under two scenarios; the first scenario deals with uncertainty with respect to cost parameters and effluent total nitrogen limitation; the second scenario deals with the effect of uncertainty in influent wastewater characterization. In the first scenario, the parameters alpha, beta and fouling factor (Eq. 1) are considered uncertain which defines the relation between actual (AOTR) and standard oxygen transfer rate (SOTR) together with standard oxygen transfer efficiency, price of electricity, price of landfilling and total nitrogen effluent limitation. For the second scenario on the other hand, the possible change in the COD fractionation is taken into account together with the change in influent ammonium nitrogen ( $S_{NH}$ ) concentration. Four different COD fractions ( $S_I$ ,  $S_S$ ,  $X_I$  and  $X_{BH}$ ) were sampled and the resulting  $X_S$  concentration was calculated assuming that the total COD in the influent wastewater is constant.

$$AOTR = SOTR \left( \frac{\beta + C_{s,T}H - C_L}{C_{s,20}} \right) (1.024^{T-20}) (\alpha) (F) \quad (1)$$

## Results and Discussion

The deterministic problem was formulated as an MILP problem and solved by using GAMS using CPLEX as the solver; the resulting process flow diagram is shown in Figure 3. The value of the objective function for the highlighted network selection is 970.75 (unit cost) whereas effluent COD and total nitrogen values are 43.15 mg COD/L and 13.62 mg N/L, respectively.

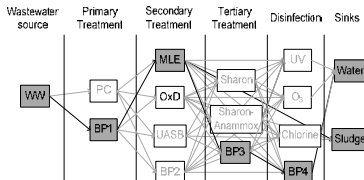


**Figure 3:** Resulting WWTP process flow diagram [1]

Next, the uncertain domain was sampled by LHS to create 100 future scenarios. For each of the scenarios, the optimization problem was solved resulting in 100 different solutions. The results are presented in Table 1.

Accordingly, the value of the objective function changes from 818 to 1,530 (unit cost) for scenario 1 with the realization of 3 different selected configurations; whereas in scenario 2 the objective function value differs between 978 and 1,402 (unit cost) with 2 possible process flow diagram configurations.

**Table 1:** Uncertainty mapping results

Scenario	Realization	Selected intervals
1	41 %	WW-BP1-MLE-BP3-BP4-Water-Sludge
	9 %	WW-BP1-MLE-Shar/An-BP4-Water-Sludge
	50 %	WW-BP1-OxD-BP3-BP4-Water-Sludge
2	98%	WW-BP1-MLE-BP3-BP4-Water-Sludge
	2 %	WW-BP1-MLE-Shar/An-BP4-Water-Sludge

In the last step, the optimization problem is formulated and solved using sample average approximation (SAA), and the results presented in Table 2.

**Table 2:** Summary of SAA results

	Scenario 1	Scenario 2
Network	WW-BP1-MLE-BP3-BP4-Water-Sludge	WW-BP1-MLE-Shar/An-BP4-Water-Sludge
Utility cost (unit cost)	71.391	119.933
Landfill cost (unit cost)	263.676	286.187
Capital cost (unit cost)	1044.944	957.271
Objective function (unit cost)	1,380.1	1,363.391

## Conclusion and Future Work

A superstructure based optimization methodology is developed which is used to deal with the early stage WWTP design/retrofit problem under uncertainty. The uncertainty analysis resulted in different possible network configurations and objective function values which proved the importance of considering the sources of uncertainty in the early design studies. The presented framework with its models and database comprises a tool which is expected to assist the decision making by generating novel ideas for the WWTP process selection problem. The future work will focus on further expansion of the superstructure and its database and applying it to real case studies.

## References

1. H. Bozkurt, A. Quaglia, K.V. Gernaey and G. Sin. Superstructure Development and Optimization under Uncertainty for Design and Retrofit of Municipal Wastewater Treatment Plants. Submitted to ESCAPE24 conference, 2013.
2. J.B. Copp. The COST Simulation Benchmark Description and Simulator Manual, Luxembourg, 2002.
3. H. Bozkurt, A. Quaglia, K.V. Gernaey and G. Sin. Early stage design of wastewater treatment plants: A mathematical programming approach. Submitted to Environmental Modeling and Software, 2013.

**Peam Cheali**

Phone: +45 4525 2911  
E-mail: pche@kt.dtu.dk

Supervisors: Gürkan Sin  
Krist V. Gernaey

**PhD Study**

Started: May 2012  
To be completed: April 2015

## Process Synthesis and Design of The Future Biorefineries: Uncertainty Analysis on Raw Material and Utility Cost

**Abstract**

This study presents the impact of uncertain data on the optimal solution obtained from superstructure-based optimization approach in synthesis and design of biorefinery. In the early stages of biorefinery design, many of the data required for the formulation of the design problem are characterized by considerable uncertainty. These uncertainties might have significant impact on the solution, and therefore need to be carefully evaluated and managed, in order to generate candidates for robust design. In this contribution, we study the effect of data uncertainty on the design of a biorefinery process network.

**Introduction**

In a typical biorefinery, a bio-based feedstock is processed to produce various products such as fuel, chemicals, feed or power/heat. As there are several feedstock, many alternative conversion technologies and a wide range of products, this creates a number of potential processing paths for biorefinery. Therefore, during the early stage of design, it is important to identify the optimal biorefinery processing path with respect to techno-economic criteria. Moreover, during the early design stage, accurate input data are usually scarce, and some design decisions are taken by considerable uncertainties [1].

A framework to generate and identify optimal processing networks under uncertainty [3] is used. The framework, based on superstructure-based optimization coupled with a generic modeling approach and Monte Carlo simulation, consists of tools, databases, models to represent and identify the optimal pathway among the potential alternatives. In this study, the optimal processing path(s) at minimum total annualized cost under uncertainty of raw material and utility cost are identified.

**Framework**

*2.1 Step 1: Problem formulation: (i) problem definition; (ii) superstructure definition and data collection; (iii) model selection and validation.*

This step consists of defining the problem scope by selecting objective functions with respect to economic/engineering metrics. The superstructure is

also defined, the necessary data are collected, then, the models are verified for a consistency check.

*2.2 Step 2: Uncertainty characterization.*

This step, the domain of uncertainty is defined and characterized. Monte Carlo simulation and Latin Hypercube Sampling with correlation control are then used to sample uncertain data.

*2.3 Step 3: Deterministic formulation and solution.*

The optimization problem which is formulated in step 1 is performed and solved using the nominal values for the parameters. The result is the deterministic optimal processing path.

*2.4 Step 4: Uncertainty mapping and analysis.*

The deterministic problem is performed separately for each sample generated from Step 2. The results are the probability distribution of the objective function value and the number of optimal processing path candidates that are selected for given uncertain inputs.

*2.5 Step 5: Decision making under uncertainty*

The optimization problem is modified as a stochastic problem and the objective function is reformulated as to minimize/maximize the expected value of the objective function over the uncertain domain.

*2.6 Step 6: Report generation*

A number of suggested indicators [1] used to analyze the solution under uncertainties. EVPI indicates the cost relevant to the lack of knowing the exact data during the decision making process. VSS indicates the cost relevant to the performance of stochastic and deterministic solutions. UP indicates the cost relevant to the impact of uncertainty.

## Uncertainty analysis of a superstructure-based optimization

The specified objective function is to minimize the total annualized cost. The superstructure (Figure 1) of the biorefinery processing network is to convert corn stover and wood to bioethanol developed from the previous study [2]. The data management and model verification performed in the previous study [2] also formed the basis for this study.

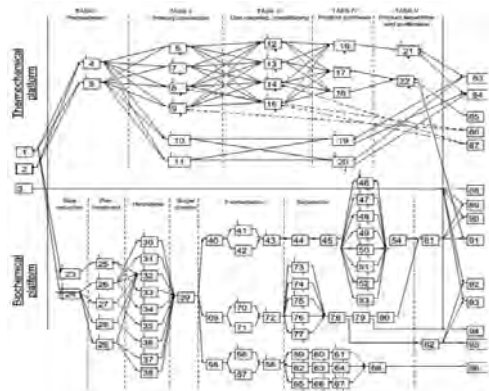


**Figure 1:** The combined superstructure.

In this study, the uncertainties of market prices (raw material and steam cost) were identified as the important sources of uncertainty affecting the decision concerning the biorefinery design. A summary of the input uncertainties and the correlation control information used here is presented in Table 1. These data were then used to generate 200 samples of the uncertain inputs using Latin Hypercube Sampling (LHS) technique.

**Table 1:** Input uncertainty and correlation matrix.

Input uncertainty	Min.	Max.	Reference
Corn stover cost (\$/dry ton)	60	100	NREL
Wood cost (\$/dry ton)	60	100	NREL
Steam cost (\$/ton)	65	90	U.S. EIA
Correlation matrix	Stover	Wood	Steam
Corn stover cost	1	0	0
Wood cost	0	1	0
Steam cost	0	0	1

Consequently, the formulated MIP/MINLP was solved for the deterministic case (mean input values). Then, the deterministic problem was solved again using 200 samples generated from the LHS as the input data, resulting in 200 optimal solutions. Lastly, the stochastic problem was formulated and solved over the specified uncertainty domain. The optimization results of the deterministic problem, the deterministic under uncertainty and stochastic problem are presented in Table 2 and 3. Table 2 and 3 present the optimal processing paths under uncertainty. As can be seen, the biochemical conversion platform requires less operating cost and a lower capital cost. Corn stover is the favorable feedstock for the biochemical platform as well as Lime pretreatment, enzymatic hydrolysis and

molecular sieve. As regards the optimal network solution under uncertainty, the same process topology was selected (Table 3) as for the deterministic case, thus confirming the robustness of the deterministic solution. This is also shown by uncertainty indicators VSS and UP, which were zero and close to zero respectively. The reason is because of the linearity and symmetry of the problem.

**Table 2:** The frequency of selection of the optimal processing paths for 200 scenarios.

Network no.	Processing path	Frequency of selection	TAC (MM\$/a)
1	1 24 29 37 39 40 41 42 43 44 45 53 54 81 91	140/200	50-80
2	1 24 29 38 39 40 41 42 43 44 45 53 54 81 91	38/200	56-76
3	2 5 8 14 17 22 85 91	21/200	56-77
4	2 5 9 14 17 22 85 91	1/200	65

**Table 3:** The optimization results.

Solution	Network	TAC (MM\$/a)	
Optimal network (step3)	1 24 29 37 39 40 41 42 43 44 45 53 54 81 91	65.16	
Network under uncertainty (Step 5)		65.09	
Scenarios	EVPI (MM\$/a)	VSS (MM\$/a)	UP (MM\$/a)
Network under the effect of uncertainty (Step 3-5)	2.1	0	0.07

## Conclusion

In this study, the impact of data uncertainties on design of optimal biorefinery networks using superstructure-based approach is discussed. The combination of the deterministic problem, the deterministic problem under uncertainty and the stochastic problem was used to effectively identify the impact of uncertainty on the optimal solution. Biochemical platform using corn stover, lime pretreatment, enzymatic hydrolysis and molecular sieve was found optimal with respect to total annualized cost. Moreover on the effect of uncertainty, the indicators show that the uncertainty of raw material and utility cost has an impact on the expected performance of optimal biorefinery design, however, the optimal process topology did not change under the given/defined domain of market uncertainty. This confirms the robustness of the deterministic solution.

## References

1. J. K. Birge, F. Louveaux, Introduction to stochastic programming (springer series in operations research and financial engineering), Springer, New York, 1999.
2. P. Cheali, K. V. Gernaey, G. Sin, ACS Sustainable Chem. Eng., dx.doi.org/10.1021/sc400179f, 2013.
3. A. Quaglia, B. Sarup, G. Sin, R. Gani, Computers & Chemical Engineering, 59 (2013), 47-62.

**Signe Sandbech Clausen**

Phone: +45 4525 4213  
E-mail: sic1@kt.dtu.dk

Supervisors: Iver Jakobsen  
Mette Grønlund  
Ingo Lenk, DLF Trifolium

**PhD Study**

Started: April 2011  
To be completed: January 2015

## Symbiotic Growth Depressions in Bioenergy and Forage Crops

**Abstract**

Phosphorus (P) is an essential nutrient for plant growth. Because P is one of the least plant-available nutrients in the soil, it is often growth limiting. As a result, most plants engage in a symbiotic relationship with arbuscular mycorrhizal (AM) fungi. The symbiosis is usually mutualistic and increases plant uptake of mineral nutrients, especially P, and thereby also increases growth. This is, however, not always the case as some grasses exhibit symbiotic growth depressions when colonized by certain AM fungi. Currently the P rock reserves used in fertilizer production are depleted in parallel with the increasing global demand for food and bioenergy production. A part of the solution to mitigate this shortage is to increase the Pi acquisition capacity and efficiency of crop plants. To do this, a better understanding of the Pi uptake pathways and regulatory mechanisms in crop plants is required. In this project we aim to characterize putative direct Pi uptake transporters in the model grass *Brachypodium distachyon*. We will also test the hypothesis that AM-colonized plants become P limited due to impaired function of direct Pi uptake at the root surface, leading to growth depression in the plant.

**Introduction**

Phosphorus (P) is one of the major macronutrients for plant growth and development. Plant roots acquire P from the soil as inorganic phosphate (Pi), which is actively taken up via Pi transporter (PT) proteins. PTs play a critical role in both Pi acquisition from soil solution, and Pi translocation within the plant. Even though P may be present in relatively large amounts in the soil, it can still be limiting for plant growth. This is mainly because of very low solubility and mobility in the soil [1]. To overcome this, plants have evolved a range of strategies that increase Pi uptake capacity or Pi availability in the soil. One strategy is to establish a symbiosis with arbuscular mycorrhizal (AM) fungi. This is an advantage to the plant as the AM fungi offer an alternative and very effective P uptake pathway. In AM colonized plants two Pi uptake routes are present: the mycorrhizal pathway and the direct root uptake pathway. The symbiotic association occurs in roots of most soil grown plants, and approximately 80% of all terrestrial plants are colonized by AM fungi [2]. AM colonization often leads to dramatically increased plant growth, primarily because of the fungal mycelium, which reaches further into the soil and assists the plant in scavenging P and other nutrients from larger soil volumes than exploited by the root system itself.

Nevertheless, there is considerable functional diversity in the outcome of the symbiosis, ranging from positive to negative effects [3, 4]. Negative effects are often observed in some grasses and such symbiotic growth depressions are conventionally assigned to the result of carbon drain by the fungi. However, an alternative hypothesis is that the direct Pi uptake in plants is repressed during AM colonization. This is based on results showing that PT genes in the direct pathway are suppressed in AM plants, and that some AM non-responsive plants have a high mycorrhizal Pi uptake. Therefore, the direct uptake is assumed to be down-regulated. This will lead to P limitations in the plants if the reduced direct Pi uptake is not fully compensated by the AM mediated Pi uptake. Since modern crop plants are supplied with excess amount of P fertilizer and have been bred at high nutrient level in the soil, they may not be very efficient in relation to uptake of P or other nutrients. This provides a global challenge, as the mineral phosphate rock (PR) reserves used for fertilizers are non-renewable. Although there is considerable debate about the size of the PR reserves, they must be utilized in a sustainable manner to avoid their long-term depletion. To maintain optimal crop yields using a reduced amount of P fertilizer, it is necessary to work towards new crop varieties with superior capacity for

acquisition and utilization of P. This could potentially be obtained by breeding plants in which direct and AM mediated Pi uptake become additive rather than complementary. For this reason, an important issue is to clarify how Pi is acquired and how the uptake is regulated in plants.

### Plant species

The fully sequenced model grass *Brachypodium distachyon* (Bd) is used to investigate the activity of the two Pi uptake pathways under different growth conditions and selected AM fungi. *B. distachyon* was first proposed as a model system by Draper et al. in 2001 [5]. Like Arabidopsis, *Brachypodium* has no agricultural significance, but offers many advantages over current model systems for plant genetic, cellular and molecular biology studies in monocots. Also, the phylogenetic position of *Brachypodium* makes it a convenient model for functional genomics studies in temperate grasses, cereals, and dedicated biofuel crops. A growing list of genomic resources has been established and is currently under development (see [brachypodium.org](http://brachypodium.org)).

### Method and perspective

A transformation approach is used to test the activity of the Pi transport pathways and the role of the selected PT in the model plant. First, by generating over expression (OE) and knock down (RNAi) lines of two putative direct phosphate transporters *BdPT4* and *BdPT8*. Secondly, the sub cellular localization of the *BdPT4* and *BdPT8* proteins will be determined in stable transgenic lines expressing GFP tagged versions of the proteins. Along with our own transgenic *B. distachyon* lines, five T-DNA mutant lines of *BdPT1*, *BdPT8*, *BdPT9*, and *BdPT11* obtained from the WRRC *Brachypodium distachyon* T-DNA collection, will be characterized. The transgenic *B. distachyon* lines will be used to investigate the roles of the phosphate transporters in Pi uptake. Based on the expression of the gene of interest, which should be up or down regulated as expected in the transgenic lines, specific lines are selected for further studies. The expression patterns in the transgenic and wild type plants in combination with physiological isotope tracer uptake studies will allow discrimination between Pi uptake via the mycorrhizal and direct pathways. In the selected lines, it will be determined how Pi uptake and/or translocation is affected by the change in expression and the potential for increasing Pi uptake efficiency in plants will be evaluated. Pi uptake efficiency of crops might be improved if a high activity of the direct uptake pathway in mycorrhizal plants is maintained, thereby making the two pathways additive instead of complementary. Finally, the sub cellular localization of the selected genes will be investigated in transgenic lines, which express the genes fused to GFP. When identified, these lines will be imaged using confocal microscopy for localization.

### Results

Thirteen PT genes have been identified in *B. distachyon* and their expression pattern analyzed by qPCR in non-mycorrhizal and mycorrhizal plants grown at different phosphate levels. Based on the expression levels and phylogenetic relationship to other known monocot phosphate transporters, two putative direct transporter genes *BdPT4* and *BdPT8*, which were found to be down-regulated at high phosphate levels and in mycorrhizal plants have been selected for further investigation. A transformation approach using *Agrobacterium tumefaciens*-mediated transformation of embryogenic *B. distachyon* callus was used to manipulate the activity of the Pi transporters. Over-expression and knockdown lines of the two transporters were produced. The produced transgenic *B. distachyon* lines will be used to investigate the specific roles of the phosphate transporters in Pi uptake. At present initial molecular studies are being performed to determine the expression profiles of *BdPT4* and *BdPT8* in the produced transgenic lines. Based on these profiles, some lines will be selected for additional molecular studies and elaborate physiological studies. The potential for increasing Pi uptake efficiency in plants will be evaluated, as Pi uptake efficiency of crops might be improved if a high activity of the direct uptake pathway in mycorrhizal plants is maintained. Additionally, two GFP tagged lines (translational fusion to fluorescent marker) were produced in collaboration with Professor Maria Harrison at Boyce Thompson Institute for Plant Research, Ithaca, New York, for subcellular localization studies of the transporter proteins.

### Acknowledgements

The PhD project is part of the Research Project *Can we prevent symbiotic repression of crop performance?* Funded by The Danish Council of Independent Research | Technology and Production Sciences. It involves close collaboration with plant breeders at DLF TRIFOLIUM A/S and plant scientists at Boyce Thompson Institute for Plant Research, Ithaca NY and The University of Adelaide.

### References

1. D.P. Schachtman, R.J. Reid, S.M. Ayling, *Plant Physiol* (116) (1998) 447-453
2. S.E Smith, D.J. Read, *Mycorrhizal Symbiosis*. Ed 3. Academic Press-Elsevier, 2008
3. S. Ravnskov, I. Jakobsen, *New Phytologist* 129 (1995) 611-618
4. S.E Smith, F.A. Smith, I. Jakobsen, *New Phytol.*, 162 (2004) 511-524
5. J. Draper, L.A. Mur, G. Jenkins, G.C. Ghosh-Biswas, P. Bablak, R. Hasterok, & A.P. Routledge, *Plant Physiol.* 127 (2001) 1539–1555



**Maria del Mar Cortada Mut**

Phone: +45 4525 52920  
 E-mail: mmarc@kt.dtu.dk

Supervisors: Kim Dam-Johansen  
 Peter Glarborg  
 Linda Kaare Nørskov, FLSmith

PhD study  
 Started: September 2011  
 To be completed: August 2014

## Interactions Between Solid Fuels and Raw Materials in Cement Rotary Kilns

### Abstract

The cement industry has an interest in replacing fossil fuels with alternative fuels due to economical considerations and environmental concerns. The combustion of alternative fuels may increase the internal circulation of sulphur and may cause blockages and corrosion. A preliminary mathematical model is set up to predict the SO<sub>2</sub> formation caused by CO released from devolatilization of a fuel particle buried under the cement raw materials in the inlet of the rotary kiln.

### Introduction

The cement industry is an energy intensive industry and the energy costs account for 30-40 % of the total costs of the cement production [1]. In the past decades, the cement industry has had a great interest in replacing fossil fuels with alternative fuels (waste from other industries), partly minimize production cost due to the increase of the fuel prices and partly to minimize the environmental impact.

Alternative fuels cover a large range of fuels, such as industrial and municipal waste, tire derived fuels, plastic and wood waste. The fuels have typically relatively large particles, with different chemical and physical properties. Some of the characteristics of alternative fuels are that they are partial or fully CO<sub>2</sub>-neutral, cheap and available in large quantities. The most important fuel characteristics to consider when selecting alternative fuels are the heating value, the ash and the moisture content.

The process flow sheet of a modern cement kiln system is illustrated in Figure 1. The traditional firing points in a cement plant are the calciner and the kiln burner. Additional combustion equipments for combustion of coarse alternative fuels have been developed, such as the HOTDISC [2]. However, several cement plants are firing the alternative fuels directly into the material inlet end of the rotary kiln because it requires a minimum of investments. Therefore, the combustion of alternative fuels in these conditions has some consequences, which are:

- Direct physical contact between the fuels and the cement raw materials.
- Local reducing conditions in the material inlet end of the rotary kilns.
- Potential of increase internal circulation of sulphur, chlorine and alkali metal species.

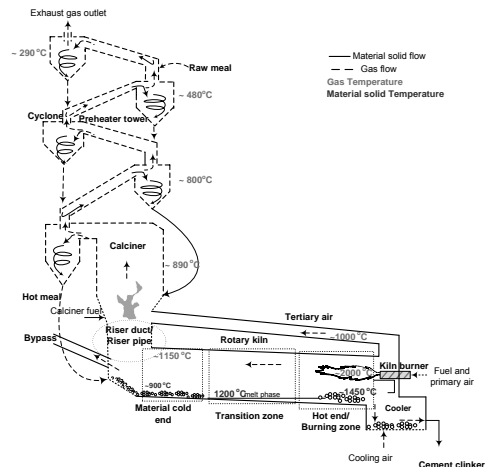


**Figure 1:** Scheme of a modern In-Line Calciner cement kiln system.

The modification of process conditions due to the combustion of alternative fuels may affect the clinker quality and the process operation. As a consequence of

the local reducing conditions and high temperature, the sulfates in the raw meal may decompose to release SO<sub>2</sub>, which will potentially circulate in the kiln system.

High levels of sulphur enhance deposit build-ups and corrosion of the kiln shell in a long term. These deposits accumulate typically in the material inlet end of the rotary kiln, or in the riser duct between and the rotary kiln the calciner, where they may cause blockages. Under such conditions, the plant must sometimes be temporarily shut-down in order to remove the deposits [2].

### Specific Objectives

The specific objectives of this project are:

- Improve the understanding of the interactions between solid fuels and the raw materials.
- Development of a mathematical model predicting sulfur release from the raw materials due to the direct combustion of alternative fuels or partially combusted calciner fuels in the kiln material inlet.
- Suggestion of new methods to combust large alternative fuels.

### Model development

A mathematical model that enables prediction of SO<sub>2</sub> formation caused by CO only as volatiles gas released from a fuel particle buried under the cement raw materials in the inlet of a rotary kiln is being developed. The modelling approach consists of a single spherical wood particle under the bed material which releases CO into a column of hot meal particles in the kiln inlet. The spherical particle is placed in the worst possible scenario, which is under the bed material (no oxygen present) and in the middle point of the cross-section kiln bed material (obtaining the highest column of bed material). The release of the gases is considered perpendicular to the surface bed, as illustrated in Figure 2. The column of bed particles is placed on top of the wood particle. The column has a rectangular shape and is divided in  $N$  layers.

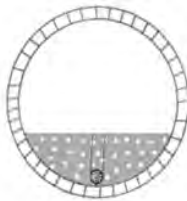


**Figure 2:** Schematic of the bed column considered in the middle point of the cross-section kiln bed material.

This model has been formulated taking into account the following assumptions:

- The rotation of the bed is neglected.

- The fuel particle is spherical and is fired directly into the rotary kiln from the surroundings (no preheating).
- The physical properties of the fuel are considered constants.
- The released volatile gas from the fuel considered in the model is only CO.
- There are no gas velocities in the material bed, only molecular diffusion is considered.
- The hot meal particles consist only of CaO particles with the same diameter.
- Sulfur is assumed to be found as CaSO<sub>4</sub> and is distributed evenly on the CaO particles as a shell.
- CO reacts with CaSO<sub>4</sub> at the surface of the particles according to reaction 1.  

$$CO + CaSO_4 \rightarrow CaO + CO_2 + SO_2 \quad [\text{Reaction 1}]$$
- The hot meal particles are assumed to be distributed in even layers where each particle is lying next to its six neighboring particles.

The model is divided in 3 steps: temperature profile of the fuel particle, release of CO from the pyrolysis of the fuel and the cross-section kiln bed model, which calculates the CO consumption, the CaSO<sub>4</sub> layer decrease by the shrinking core model and the SO<sub>2</sub> formation.

The heat up of a large, spherical particle is determined by solving numerically the unsteady heat transfer differential equation 1 with the boundary conditions (equations 2 and 3).

$$\frac{\partial T(r,t)}{\partial t} = \frac{1}{r^2} \frac{\partial}{\partial r} \left( r^2 \frac{k_p}{\rho_p C_p} \frac{\partial T(r,t)}{\partial r} \right) \quad [1]$$

$$\frac{\partial T(t,r=0)}{\partial r} = 0 \quad [2]$$

$$k_p \frac{\partial T(t,r=R)}{\partial r} = h_{cond} (T - T_{bed}) \quad [3]$$

where  $T_{bed}$  is the bed temperature in K, which will be the final temperature of the particle, and  $h_{cond}$  is the heat transfer coefficient for conduction in W/(m<sup>2</sup> K).

The temperature profiles for the wood particle are used to predict the release of volatiles as a result of the ongoing pyrolysis. Equation 4 describes the mass based conversion of the particle due to pyrolysis [3].

$$\frac{dw}{dt} = -k_{pyrolysis} (w - w_\infty) \quad [4]$$

where  $w$  denote the remaining mass of wood at time  $t$  in kg,  $w_\infty$  is the mass which cannot be pyrolysed in kg,  $w_0$  is the initial mass in kg, and  $k_{pyrolysis}$  is kinetic constant for the pyrolysis, which has a form of 1<sup>st</sup> order Arrhenius equation [3].

The difference between the initial mass and the mass of the particle at any time is the cumulative amount of volatiles released.



The shrinking core model [4] for the  $\text{CaSO}_4$  layer is considered. By the analysis of the limiting rates for the reaction between  $\text{CaSO}_4$  and CO the terms regarding the gas film and product layer diffusion are neglected because the resistance towards chemical reaction composed the greatest resistance. Consequently, the shrinking core model relates only to the reaction between CO and  $\text{CaSO}_4$ , as expressed in equation 5.

$$\frac{dr_{\text{CaSO}_4,i}}{dt} = \frac{C_{\text{CO},i}}{\rho_{\text{CaSO}_4}} \cdot k_{\text{CO} \rightarrow \text{SO}_2} \quad \text{for } i = 1, \dots, N \quad [5]$$

where  $r_{\text{CaSO}_4}$  is the radius of the shrinking core in m,  $C_{\text{CO}}$  is the concentration of CO in  $\text{mol/m}^3$ ,  $\rho_{\text{CaSO}_4}$  is the molar density of  $\text{CaSO}_4$  in  $\text{mol/m}^3$ ,  $k_{\text{CO} \rightarrow \text{SO}_2}$  is the reaction constant for reaction 1, which has a form of 1<sup>st</sup> order Arrhenius equation [5].

The simultaneously diffusion of CO through the bed and reaction with  $\text{CaSO}_4$  is described by equation 6 for CO. In order to simultaneously be able to solve the consumption of CO and the shrinking core, equation 6 is converted into a set of ordinary differential equations by the method of finite volume.

$$\frac{\partial C_{\text{CO}}}{\partial t} = D_{\text{CO}} \frac{\partial^2 C_{\text{CO}}}{\partial x^2} + R(C_{\text{CO}}) \quad [6]$$

$$R(C_{\text{CO},i}) = \frac{4\pi\rho_{\text{CaSO}_4} \cdot r_{c,i}^2}{V_{\text{layer}}} \frac{dr_{c,i}}{dt} \quad \text{for } i = 1, \dots, N \quad [7]$$

where  $x$  is the length scale in m,  $R(C_{\text{CO}})$  is the consumption term for CO in  $\text{mol}/(\text{m}^3 \cdot \text{s})$ - expressed by equation 7,  $N$  is the number of equations to solve,  $N_{\text{layer}}$  is the number of particles in each layer,  $i$  is discretization points, and  $D_{\text{CO,eff}}$  is the effective diffusion coefficient of CO in  $\text{m}^2/\text{s}$ .

The boundary conditions for equation 6 are mathematically expressed by equation 8 and 9.

$$\text{at } x=0; \quad \frac{dC_{\text{CO}}}{dx} = 0 \quad [8] \quad \text{at } x=L; \quad C_{\text{CO}} = 0 \quad [9]$$

Thereby, each control volume is described by 2 ordinary first order equations: 1) for the change in CO concentration and 2) for the decrease of  $\text{CaSO}_4$  layer.

The formation of  $\text{SO}_2$  will be calculated based on a mass balance for the decrease of the  $\text{CaSO}_4$  particle radius.

$$n_{\text{SO}_2,i} = (R_{\text{CaO}}^2 - r_{\text{CaSO}_4,i}^2) \cdot \frac{4}{3} \pi \rho_{\text{CaSO}_4} \cdot N_{\text{layer}} \quad \text{for } i = 1, \dots, N \quad [10]$$

## Model results

The model has been applied to a fir wood particle of 1 cm of diameter [6]. The heat transfer through the fuel particle and the rate of release of CO will depend on the physical properties of the wood.

The material bed considered in this case is the 5 % volumetric fill degree, having a column length of 0.46 meters.

The temperature profiles for a spherical fir wood particle at 5, 10 and 30 seconds are shown in Figure 3.]

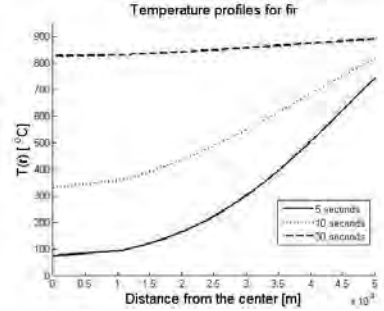


**Figure 3:** Temperature profiles for fir wood particle of 1cm diameter at 20, 40 and 60 s.

The mass loss of the fir particle corresponding to the CO release is 15 wt.% of the wood [7]. The cumulative release of CO can be seen in Figure 4.

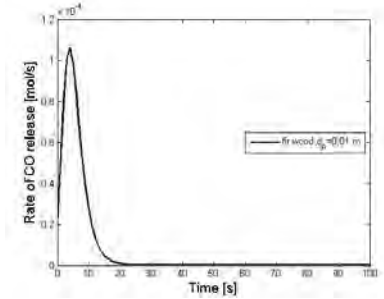


**Figure 4:** Rate of release of CO from fir wood particle.

From the fir wood particle, a total of  $7.86 \cdot 10^{-4}$  mol CO is released during its lifetime and the total  $\text{SO}_2$  released from the bed is  $2.46 \cdot 10^{-4}$  mol. The total amount of  $\text{SO}_2$  released as function of time is illustrated in Figure 5.

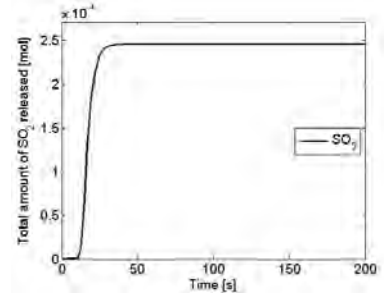


**Figure 5:** Total formation of  $\text{SO}_2$  for the amount of CO release from wood particle.

## Model expansion

The model has been extended to cover the whole cross section of the bed of the rotary kiln. The principle is to the width of the kiln into a convenient number of columns. This model can consider more than 1 particle

and the bed material moves the axial direction of the kiln.

The model is solved considering 1 t/h of fir wood (55 particles of 5 g each every second) distributed evenly through the material bed with 15 % fill degree. The kiln model considers half of the width of the kiln and the CO release from 27.5 wood particles due to symmetry. The half-width of the kiln is divided into 9 columns as can be seen in Figure 6.

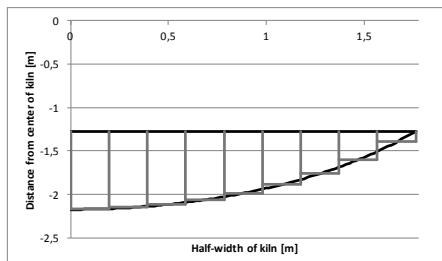


**Figure 6:** The material bed and the wall of the kiln (black) and the 9 columns (red).

The SO<sub>2</sub> release in the bed is released to the kiln freeboard gas and to calculate its concentration, the molar flow of flue gas is taken into account. The flue gas coming from the main burner is assumed to have a concentration of 0 ppmv SO<sub>2</sub> and the SO<sub>2</sub> in gas phase does not react with dust or other gaseous species.

The concentration of SO<sub>2</sub> in the flue gas of the kiln is calculated and presented in Figure 7. The concentration of SO<sub>2</sub> in the counter flowing flue gas in the rotary kiln reaches 300 ppmv in the kiln inlet.

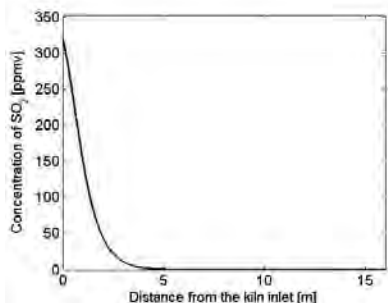


**Figure 7:** SO<sub>2</sub> concentration in the flue gas from 55 fir wood particles of 5 g as a function of the distance from the kiln inlet.

### Conclusions and Future work

The sulfur release during combustion of fuel particles in the bed material is caused by the reaction between the reducing gases from the fuel devolatilization and CaSO<sub>4</sub>. The degree of sulfur release is strongly influenced by the fuel particle size.

A mathematical model to predict the SO<sub>2</sub> formation caused by CO from a wood particle has been developed.

The model calculates the temperature profile of the particle, release of CO from the fuel pyrolysis, the CO consumption, the CaSO<sub>4</sub> layer decrease by the shrinking core model and the SO<sub>2</sub> formation.

The model was extended to cover to whole bed of the rotary kiln with 9 columns in half-width. It can be used for multiparticles and the SO<sub>2</sub> release from the bed material to the freeboard flue gas is included. In the cases of 55 fir wood particles of 5 g each fired in a bed material of 15 % fill degree, the SO<sub>2</sub> concentration in the kiln inlet reached 300 ppmv.

The model needs to be validated against experimental data and it may be extended to other type of fuels and other reducing agents.

### Acknowledgements

This project is part of a research platform on future cement technology financed by The Danish National Advanced Technology Foundation, DTU and FLSmidth A/S.

### References

- [1] Cembureau, Activity Report 2008. <http://www.cembureau.be/> (Accessed on 2/12/2011).
- [2] FLSmidth HOTDISC™ combustion device. <http://www.flsmidth.com> (Accessed on 2/12/2011).
- [3] Di Blasi, C.; Modeling chemical and physical processes of wood and biomass pyrolysis. *Progress in Energy and Combustion Science*, 34, 47–90, 2008.
- [4] Levenspiel, O.; *Chemical Reaction Engineering*. Third Edition, 1999. ISBN: 978471254249
- [5] Xiao, R., Song, Q.; Characterization and kinetics of reduction of CaSO<sub>4</sub> with carbon monoxide for chemical-looping combustion. *Combustion and Flame*, 158, 2524–2539, 2011
- [6] Guo, W., Lim, C. J., Bi, X., Sokhansanj, S., and Melin, S.; Determination of effective thermal conductivity and specific heat capacity of wood pellets. *Fuel*, 103, 347-55, 2013.
- [7] Nunn, T., Howard, J.; Product compositions and kinetics in the rapid pyrolysis of sweet gum hardwood. *Industrial & Engineering Chemistry Process Design and Development*, 24, 836–844, 1985.

**Larissa Peixoto Cunico**

Phone: +45 4525 5510  
E-mail: lacu@kt.dtu.dk

Supervisors: Rafiqul Gani  
Roberta Ceriani, UNICAMP  
Bent Sarup, Alfa Laval Copenhagen A/S

**PhD Study**

Started: February 2012  
To be completed: January 2015

## **Data, Analysis and Modeling of Physical Properties for Process Design of Systems Involving Lipids**

**Abstract**

Pure component and mixture properties are necessary for synthesis, design, and analysis of processes for the production of edible oils, fats, biodiesel, and other lipids. The lack of measured data for these systems makes it necessary to develop reliable predictive models based on limited data. We have systematically collected vapor–liquid equilibrium (VLE), solid–liquid equilibrium (SLE) and related pure component properties involving lipid systems as a first step toward developing relevant property models. The established consistency tests to evaluate the VLE data of lipid systems as well as lipid properties are briefly reviewed. For SLE systems, where consistency tests based on the Gibbs–Duhem equation cannot be implemented, a consistency test has been developed. It involves limiting conditions and regression of the parameters for a new thermodynamic model that combines solute activity coefficients in the liquid phase at infinite dilution and a theoretically based term to account for the non-ideality in dilute solutions. This model gives noticeably better descriptions of experimental data in lipid systems than do traditional models. Examination of various objective functions for regressing model parameters showed that some variation of parameter values and differences in accuracy can be found, though they are not large. Some original UNIFAC group contribution parameters for lipids have been revised by fitting to the lipid database.

**Introduction**

Lipids are often not tabulated in common property databases and their polyfunctional structure requires careful model analysis. This work considers the main classes of lipids present in edible oils and biodiesel production systems, namely fatty acids, esters (methyl and ethyl), triacylglycerols (TAGS), diacylglycerols (DAGS), monoacylglycerols (MAGS), phospholipids, tocopherols, squalenes, among others. The analysis of the availability and reliability of data and modeling of the properties and phase equilibria for pure lipids and their mixtures is summarized in this work. Given the importance of predictive models once verified the lack of measured data for lipids systems, the role of database, property models, and analysis of property models in terms of accuracy, reliability, predictive power, and thermodynamic consistency is discussed.

**Database**

The database contains about 4500 measured data points for 332 different phase equilibrium data-sets, including binary and multicomponent systems (92 VLE, 91 LLE, 70 SLE and 79 solubility data). For VLE data, PTx and PTxy data were considered. Uncertainties of experimental measurements or quality estimates given

by the authors of the experimental were also considered. The published activity coefficients and parameter values from fitting different GE models (UNIQUAC, original UNIFAC and NRTL) for VLE and SLE binary systems are stored in the database. In our previous work [1], these models were used in parameter regressions for fine-tuning existing model parameters, improving VLE, and obtaining model parameters not available in the literature, which has been extended to include SLE data. A total of 358 data sets from the DECHEMA® database for solid solubility systems, mainly for components important in the pharmaceutical industry were included in this work aims to analyze the proposed SLE consistency tests.

**Data analysis and consistency tests for VLE systems**

For VLE data, several thermodynamic consistency tests have been proposed. In this work, VLE data have been evaluated following the consistency tests recommended by NIST [2], based on the Gibbs–Duhem equation, pure component limits, and accuracy in regressing excess Gibbs Energy models.

### Data analysis and consistency tests for SLE systems

For most SLE systems, the entire composition range is not covered, so the Gibbs–Duhem equation cannot be applied. To address this situation, we have proposed an alternative set of consistency tests, including a new approach for modeling dilute solution SLE. Two tests for quality were developed for SLE data sets and applied to the binary systems of the CAPEC Lipids Mixtures Database and DECHEMA® database. Test 1 for SLE data is similar to the  $Q_{\text{test5}}$  of the TDE program for VLE data. It evaluates whether the mixture data asymptote to the pure component melting points. Test 2 is similar to that of Van Ness [4] for VLE systems where the ability of a model to describe the data is assessed. The usefulness of this test depends on the reliability of the model for the description. In order to evaluate whether any data might be given a lower quality factor because of model insufficiency instead of data error, alternative activity coefficient model (Test 3) was developed. The proposed new thermodynamic model combines solute infinite dilution activity coefficients in the liquid phase with a theoretically based term to account for the non-ideality for dilute solutions relative to infinite dilution. This model was found to give noticeably better descriptions of experimental data than do traditional thermodynamic models (NRTL, UNIQUAC and UNIFAC) for lipid systems [3]. Results for both the NRTL and FST models for some representative systems are shown in Figure 1.

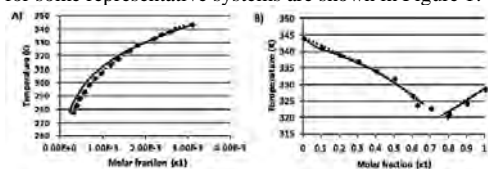


**Figure 1:** A) Solubility of L-Aspartic acid(1) in water(2); B) Myristic acid(1) and stearic acid(2) SLE ♦Experimental data; — NRTL model; - - - FST Model.

### Objective Functions for Parameter Regression and Performance Statistics

Since Test 2 cited previously requires regression to determine the quality of parameter fits for models in solutions where both T and x are varying, options exist for selection of the objective function to be minimized. An objective function that considers the measurement uncertainties would be desirable when the experimental data contains random errors. The derivative of the probability density function of the measurement errors are considered in the parameter estimation using maximum likelihood estimation (MLE). The experimental temperature, solute liquid mole fraction, or activity coefficient were considered depending on the selected objective function for MLE parameter estimation. The well-known thermodynamic models such as NRTL, UNIQUAC and UNIFAC give only slightly different average absolute deviations (AAD) values, with the FST model regression giving the lowest AAD and the original UNIFAC giving the highest, though the values are reasonably good. The parameter

values found from the different objective functions are also similar.

In addition, we have worked to improve the performance of the original UNIFAC group contribution model. Since the original UNIFAC model parameters were not regressed with data from lipid systems, a possible way to improve the UNIFAC performance is to fine-tune the group interaction parameters using the lipid SLE data-sets with their quality factors. We did this by regressing the interaction parameters for the functional group with the chain group, such as COOH with the CH<sub>2</sub>/CH<sub>2</sub> group for fatty acids. One example is given in Table 1 below.

**Table 1:** UNIFAC model performance for lipid systems from regression of group interaction parameters for myristic acid(1) + stearic acid(2), P = 101.3kPa and T from 328.88 – 343.98 K

Objective Function	AAD	Parameters	
MLE <sub>T</sub> (Modified UNIFAC)	0.33	-9093.35	-3536.5
MLE <sub>x</sub> (Modified UNIFAC)	4.477	-7377	-1169.82
MLE <sub>T</sub> (Modified UNIFAC)	0.220 / 2.409	-5521.76	-4705.49

### Uncertainty analysis of thermodynamic models

To estimate the uncertainty of the predicted temperature or molar fraction calculated using the thermodynamic models (NRTL, UNIQUAC, UNIFAC, FST), we use the information of the covariance  $COV(P^*)$  of the parameters, and the local sensitivity  $J(P^*)$  of the thermodynamic models. For non-linear models, such as the thermodynamic models, the local sensitivities are obtained by differentiating the property model with respect to the estimated final model parameters. The results of the uncertainty analysis for the different models can be seen in Figure 2 for the SLE binary system containing myristic acid(1) and stearic acid(2).

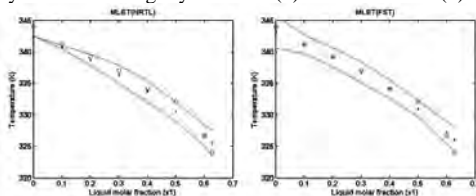


**Figure 2:** Uncertainty analysis: myristic acid(1) + stearic acid(2) SLE. ○Experimental data; •Thermodynamic models; — ±95% Confidence interval

### References

1. L.P. Cunico, A. S. Hukkerikar, R. Ceriani, B. Sarup, R. Gani, Fluid Phase Equilibria, 357 (2013) 2-18.
2. V. Diky, R. D. Chirico; C. D. Muzny; A. F. Kazakov; K. Kroenlein; J. W. Magee; I. Abdulagatov; J.W. Kang; M. Frenkel, J. Chem. Inf. Model 52 (2011) 260-276.
3. L.P. Cunico, R. Ceriani, B. Sarup, J. P. O’Connell, R. Gani, Fluid Phase Equilibria, 2013 (in Press).
4. H.C. Van Ness; S. M. Byer; R. E. Gibbs, AIChE J. 19 (1973) 238-244.



**Marina Fedorova**

Phone: +45 4525 2911  
E-mail: mfad@kt.dtu.dk

Supervisors: Rafiqul Gani  
Gürkan Sin

PhD Study  
Started: April 2012  
To be completed: March 2015

## Systematic Methods and Tools for Computer Aided Modeling

### Abstract

The proposed project is developing methods and tools that will allow systematic development of models and their solution. It is based on the modeling framework, which represents a knowledge-based system that is built on a generic modeling language and structured based on workflows for different general modeling tasks. This framework is to be extended in terms of development of new models, re-use of models and development of model-based solution techniques. A template-based approach for model development is presented in this work. Based on a model decomposition technique, the computer-aided template concept has been developed. This concept is implemented as a software tool, which provides a user-friendly interface for following the workflow steps, as well as the guidance through the steps providing additional information and comments. The application of the tool is highlighted with a multiscale modeling case study involving a catalytic membrane fixed bed reactor.

### Introduction

Models are playing important roles in design and analysis of chemical processes and products. They help to reduce the number of expensive and time consuming experiments and to give better understanding of the process domain. However, when the required models are complex, and require multiple time and/or length scales, their development and application for product-process design is not trivial. Also, once a model (or a template) is developed, it should be possible to adapt it for various similar modeling objectives with a minimum of effort. Therefore, a modeling framework with the associated tools can contribute by reducing the time and resources needed for model development and application. Moreover, better application of the developed models can be achieved by reusing them through a specially developed modeling framework. This will allow one to make a proper documentation of the created models, will increase reuse of the models and also will allow different users to exchange and work with a variety of models. The main objectives of this computer-aided modeling framework are to provide structure, guidance and support during model development and application; increase the efficiency of the modeling process; and, improve the quality and reliability of the models.

### Computer-Aided Modeling Framework

The main objectives of the developed computer-aided modeling framework are to provide structure, guidance

and support during model development and application, increase the efficiency of the modeling process, improve the quality and reliability of the models.

This is achieved by structuring the computer-aided modeling framework based on workflows for different general tasks related to model development and application. The modeler is systematically guided through the steps of the different workflows and, at each step, the framework identifies and integrates the required guidance, tools, database and library connections. The new addition to this framework is the integration of systematic model derivation tools including ModDev and generic template models into the framework as shown in Figure 1.

Proposed modeling framework allows the user to develop new, improve existing, solve and export validated models for third party applications. The framework contains three parts: (i) Model development, (ii) Model identification and validation, (iii) Application using a domain-specific generic template. Depending on the modeling needs and goals, the modeler has a possibility to create a new model in case there is no existing problem-specific model in the library, identify, validate and solve the new model or use existing model from templates library.

The whole structure contains modeling framework, computer-aided tools, methods and libraries including application templates and problem-specific models.

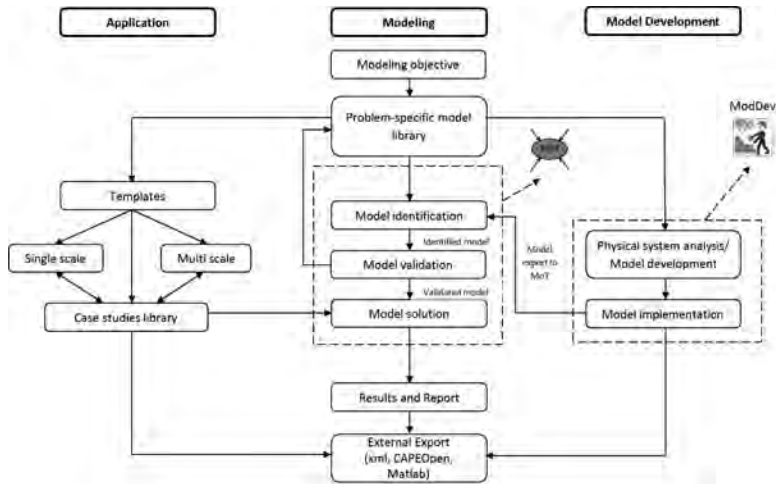


**Figure 1:** Computer-aided modeling framework with systematic model derivation methodologies.

#### *Model development*

This part of the modeling framework is using the model development tool – ModDev, which is the part of ICAS.

ModDev is a knowledge-based system that is based on a generic modeling language. It provides a base for manual definition of new variable types and new model blocks as well as a set of fundamental building blocks that assists with knowledge-based information in the creating of new building blocks [1].

Using ModDev modeler is able to describe his case system and the model equations will be obtained by the tool. The resulting mathematical equations can be translated to an appropriate computer language, e.g. mot file, and sent to internal MoT solver or to be exported to another tool. After creation and validation the model is adding to problem-specific model library. And that will give an opportunity to use this model as a template in other cases.

#### *Modeling part*

This part is based on a generic computer-aided modeling tool named ICAS-MoT [2] developed earlier. It is a computer-aided modeling framework that is structured based on the modeling methodology of in-depth work-flows and data-flows for the different generic modeling tasks required for model development, analyses, identification, discrimination, documentation and application for simulation and optimization.

Following the workflow of this part of the framework user will be able to change existing modeling templates, to pick one of the templates for the case under study, to implement the model that is developed already as well as create a new mathematical model.

#### *Application and templates library.*

This part of the framework describes the using of generic modeling templates, which can be chosen from the templates library that includes validated models.

Modeler can use the template for his case problem or use the template or its part for extending a model. This is based on idea of model reuse, which emphasizes using a model not only for one specific application but also for future applications involving different needs and levels of details to match different purposes.

The purpose of the template approach is to enable modeler to create a general model (with all known phenomena and assumptions) for a given system, which will be used later to generate problem-specific models. To achieve this, the template approach guides systematically the modeler through the steps of the different workflows and, at each step, the framework identifies and integrates the required guidance, tools, database and library connections. Depending on the modeling needs and goals, the modeler has the possibility to create a new model when the needed problem-specific model is not available in the library. The modeler has also the possibility to identify, validate and solve the new models or use existing models from the templates library. The model templates are a part of the model generation feature of the framework. The templates aim to provide structured domain-specific knowledge, speed-up of the model development/derivation process and improve model quality. This modeling template includes model equations, model description, solution strategy among others. Modeler can use the template for a new modeling problem or can update it in order to extend its application range. As the template library includes validated models, the creation of a new template-based model will reduce the modeling time and increase efficiency in the subsequent steps of model analysis, solving and identification.

In the template, a model is decomposed into three sets of equations: balances, constitutive relations and connection and/or conditional equations. This decomposition is based on the hierarchy given by Cameron & Gani [3].

The workflow of template use consists of 6 general steps (as shown in Fig. 2):

1. Select a template from a library of templates, e.g. catalytic membrane fixed bed reactor.
2. Define process system. What is the system volume, number of phases, presence or not of reactions, accumulation, number of components, number of scales etc.? Information from this step is used in the subsequent steps.
3. Define balance volumes, the model type (steady state, dynamic state), etc. This step includes generation of mass, energy and momentum balance equations. Every template has default option for model type, but user can apply his/her preference and the equations will be changed accordingly.
4. Define constitutive equations. In this step user identifies the models needed to describe the system volume behavior, such as thermodynamic relations, transport and reaction rates, diffusion, phase equilibrium, etc.
5. Define connection and conditional relations. These are equations describing surroundings and system connections, such as summation of mole fraction, etc. Equations given in this step are mostly generated by default. User can define additional boundary and/or initial conditions if necessary and also the connection between different system volumes.
6. Generation of the final set of model equations by aggregating all the model specifications done in previous steps. In this step a model is ready to be sent to the solver or for further identification and analysis.

### Software Implementation

In this section we present the implementation of the template framework as a computer-aided tool providing the user an easy and simple interface to follow the workflow.

Software implementation includes several libraries, which provide building blocks for the templates. Schematic architecture of the implementation is shown in Figure 3.

In the process of following the template workflow step by step, model equations, which in this case are building blocks for the future model, are taken from the certain libraries of balance, constitutive or connection equations. Regarding the user changes (for example, dynamic state

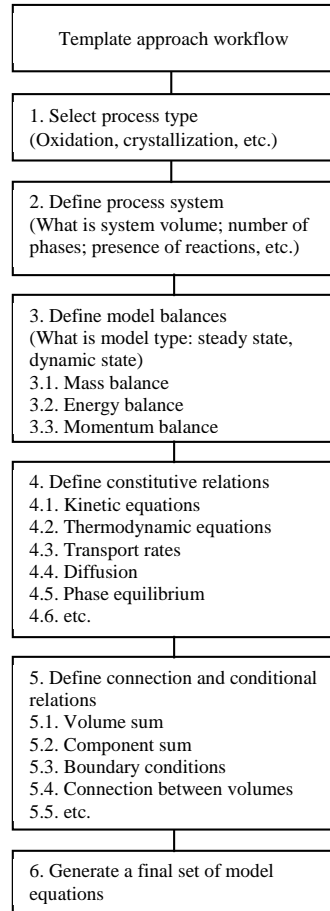


**Figure 2.** Workflow for the template use instead of steady state), the program engine modifies chosen equations and includes them in the final model.

In the end all equations from the previous stages are collected together and combined in a final model, which is translated to an MoT object and can be solved and identified in the ICAS-MoT modeling platform or can be transferred to a text or xml file in order to use it in external programs. Moreover, the newly created model can be added to the model library and can be as well used

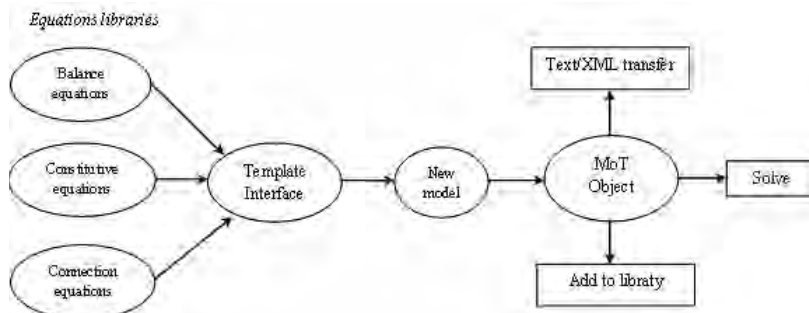


**Figure 3.** Architecture of the software implementation of the template tool.

for template creation and/or updates.

The creation of template building blocks is based on the models, which are related to the certain phenomena and have already been verified. This makes possible for the program engine to connect different equations after modifying them. However, it is always required for a new model to be checked in order to prevent potential mistakes in equations linking, e.g. use of different names for the same variable.

### Case study application

The application of the modeling template is highlighted with a case study related to the modeling of a catalytic membrane fixed bed reactor coupling dehydrogenation of ethylbenzene with hydrogenation of nitrobenzene (model is taken from Abo-Ghander et. al [4]).

The reactor is composed of two compartments within a shell containing a bundle of hydrogenation tubes. On the shell side, dehydrogenation of ethylbenzene takes place producing styrene and hydrogen. Five side reactions also occur, producing benzene, toluene, and non-condensable gases like ethylene, methane, carbon monoxide, and carbon dioxide. Inside the membrane tubes, cocurrently flowing nitrobenzene reacts with hydrogen to produce aniline as a second major useful product from the integrated membrane reactor [4]. The schematic view of the reactor is shown at the Figure 4.

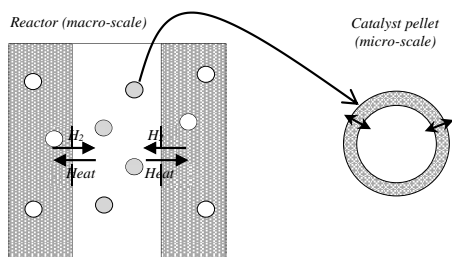


**Figure 4.** Schematic sketch of the reactor and catalyst pellets in it.

The workflow to be employed in this case study is the following.

1. Template for the catalytic membrane fixed bed reactor is chosen.
2. System has two volumes, separated by membrane; one vapor phase; 6 reactions on the dehydrogenation side and one reaction on the hydrogenation side. Every volume is considered as 2-scale system with catalyst particles as micro-scale and reactor as macro-scale. Other options in template are to have one volume, e.g. catalytic fixed bed reactor without membrane, and to use one-scale model only for reactor.
3. For both volumes models are in steady state, distributed in angular direction, for mass, energy and momentum balances (the independent variable is the reactor length). No external mass or heat loss. Catalyst pellets are isobaric.
4. Reaction rates are chosen based on the original model of Abo-Ghander et al. [4].

Catalyst pellets are isothermal. Diffusion inside catalyst pellets is represented by Fick's law. Ideal gas behavior in both volumes.

5. Two volumes are connected by hydrogen transfer across membrane from volume 1 to volume 2 and by heat transfer from volume 2 to volume 1.
6. Final model is constructed based on answers from steps 1-5. It contains 46 ODE and 582 AE, including all constitutive and connection equations of both volumes and both macro and micro scales. After generating the final model, it has been translated into a model object and solved by using ICAS-MoT.

### Conclusions

A computer-aided modeling framework integrating systematic model derivation and development tools has been developed that includes features for model development, model identification and solution, model templates library. Template based approach has been presented and implemented as a computer-aided software tool, which guides user through workflow steps in order to generate a problem-specific model based on the available template. The possibility of combination and modification of the modeling templates is making the model development process easier and more efficient.

Current and future work is extending the application range for the template approach including unsaturated fatty acid oxidation, as well as improving the different aspects of workflow and its software implementation.

### Acknowledgements

This PhD project is funded by EU FP7 OPTICO Project.

### References

- [1] Jensen A.K., Gani R., 1999, A Computer Aided Modeling System, Computers and Chemical Engineering, 23, 673-678.
- [2] Heitzig M., Sin G., Sales-Cruz M., Glarborg P., Gani R., 2011, Computer-Aided Modeling Framework for Efficient Model Development, Analysis, and Identification: Combustion and Reactor Modeling, Industrial and Engineering Chemistry Research, 50(9), 5253-5265.
- [3] Cameron I., Gani R., 2011, Product and Process Modelling. A Case Study Approach., Elsevier.
- [4] Abo-Ghander N.S., Logist F., Grace J.R., Van Impe J.F.M., Elnashaie S.S.E.H., Lim C.J., 2012, Computers and Chemical Engineering, 38, 11-23.

### List of Publications

Fedorova M., Sin G., Gani R., 2013, Computer Aided Chemical Engineering, 32, 775-780.



**Michael Frost**

Phone: +45 4525 2876  
E-mail: mifro@kt.dtu.dk

Supervisors: Georgios M. Kontogeorgis  
Nicolas von Solms

**PhD Study**

Started: June 2011  
To be completed: May 2014

## Measurements and Modelling of Phase Equilibrium of Oil-Water-Polar Chemicals

**Abstract**

As the exploitable oil resources decrease, more advanced recovery methods are employed in the oil industry. This has led to an increase in used chemicals, in order to ensure a constant and safe production. These chemicals have many applications, and are part of different families like alcohols, glycols, alkanolamines etc.

Due to rising demands from environmental agencies and a wish for a more refined product, it is becoming increasingly important for downstream processing to know/predict the solubility of oil and gas with different complex chemicals. The objective of this project is to further develop the CPA equation of state for use in calculation of solubility between oil and polar chemicals.

**Introduction**

Chemicals are added in almost all stages of oil and gas production. It is generally accepted that efficient and cost effective oil and gas production is not possible without the use of chemicals. Monoethylene glycol (MEG) and methanol are two of the most widely used production chemicals. They are used as gas hydrate inhibitors to ensure safe production and transportation. The prediction of the distribution of chemicals in oil, water and gas streams is important for the oil industry to ensure reliable production and processing. It is also important information to fulfill the demand from environmental authorities, in order to know the amounts of chemicals and hydrocarbons in a processed water stream for ensuring safety of marine life. Furthermore it is important for efficient design/operation of separation equipment. The partitioning of the chemicals can either be measured experimentally or predicted using a suitable thermodynamic model. The experimental method is expensive and challenging, partly due to the difficulties involved in measurements of such low solubilities. The CPA equation of state proposed by Kontogeorgis et al. [1] has been successfully applied in the past to well defined systems containing associating compounds (such as water, methanol and MEG). It has also, to a first extend, been successfully applied to reservoir fluids in presence of water and polar chemicals, using a characterization method (Pedersen et al. [2]), modified by Yan et al. [3]. In order to understand these complex systems and to further develop/validate CPA, more experimental data is

desirable. This work focuses on producing new experimental data for both well defined multi-component mixtures, as well as for systems containing oil-water-polar chemicals.

**Specific Objectives**

As basis for the further development of CPA, the aim of this project is threefold:

- Produce experimental data (VLE/LLE/VLLE) for well-defined systems (containing water, hydrocarbons and polar chemicals).
- Further development of equipment for high quality VLE/LLE/VLLE measurements.
- Carry out oil-water-MEG measurements for oil systems not previously studied – emphasis to heavy oils and those with high aromatic/naphthenic content.
- Develop and validate the CPA equation of state based on data generated and relevant literature data.
- It is of special importance to develop an oil characterization method which can be used for a wide range of oils and conditions. This method should account for paraffinic (P), naphthenic (N) and aromatic (A) contents of a reservoir fluid.

**Experimental work**

Experimental work has been carried out at Statoil research facility in Norway, over the past years. The goal

has been to focus on different reservoir fluids from the North Sea, with varying PNA distributions.

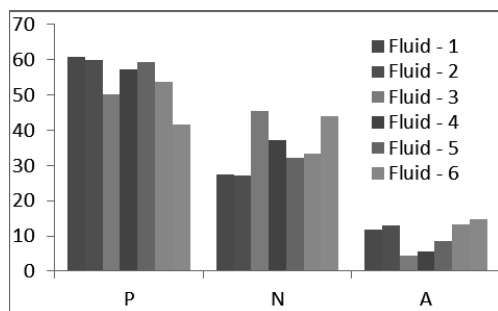


**Figure 1:** The PNA distribution of 7 reservoir fluids from Statoil operated fields in the North Sea.

The properties of the reservoir fluids such as mean molecular weight (MMW), density and  $C_{10+}$  fraction is given in table 1. Mutual solubility data and thermodynamic modeling are presented here only for one of the systems (Fluid – 6 which was investigated summer 2013). Example of the composition of Fluid – 6 can be seen in table 2.

**Table 1:** Properties of reservoir fluids investigated

Reservoir fluid	MMW g/mol	Density Kg/m <sup>3</sup>	C <sub>10+</sub> Mole%
Fluid – 1	112.7	0.7562	24.25
Fluid – 2	106.9	0.7385	5.88
Fluid – 3	97.37	0.7205	6.84
Fluid – 4	266	0.9055	76.64
Fluid – 5	135.2	0.7784	31.9
Fluid – 6	157.54	0.8016	40.58
Fluid – 7	336.56	0.9416	91.44

#### Apparatus and procedures

A sketch of the experimental setup used in this work is shown in figure 2.

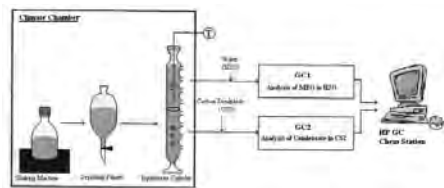


**Figure 2:** Sketch of experimental setup.

#### Mixing and Equilibrium

MEG, water and reservoir fluid were mixed at a fixed temperature for 24 hours using a mixing machine in an air heated oven. For binary systems, approximately equal mass of MEG and reservoir fluid were added for mixing. The ternary system consists of MEG, water and reservoir fluid, where the hydrocarbon phase was 50%

(mass) and the polar phase also 50% (mass). The polar phase composition was ranged from 40% - 80% MEG, which is the area of interest to the industrial applications in the North Sea.

**Table 2:** Composition of a North-sea condensate

Component	Mole%	Density	Mol.Wt
C2, (P)	0.09	0.3580	30.07
C3, (P)	1.57	0.5080	44.10
i-C4, (P)	0.90	0.5630	58.12
n-C4, (P)	3.98	0.5850	58.12
2,2-DM-C3 (P)	0.02	0.5970	72.15
Ic5 (P)	2.54	0.6250	72.15
nC5 (P)	4.10	0.6310	72.15
Hexanes Total	6.82	0.6676	85.01
Hexanes - P	6.32	0.6629	86.18
Hexanes - N	0.50	0.7500	70.13
Heptanes Total	14.06	0.7418	90.79
Heptanes - P	4.96	0.6876	100.20
Heptanes - N	7.69	0.7663	87.05
Heptanes - A	1.41	0.8840	78.11
Octanes Total	16.34	0.7668	103.59
Octanes - P	4.41	0.7068	114.23
Octanes - N	8.65	0.7727	102.49
Octanes - A	3.28	0.8710	92.14
Nonanes Total	8.99	0.7733	118.86
Nonanes - P	4.22	0.7214	128.08
Nonanes - N	1.88	0.7877	117.69
Nonanes - A	2.89	0.8721	106.17
Decanes Plus	40.58	0.8528	253.8
Totals	<b>99.99</b>	-	-

After mixing the mixture was transferred to a glass equilibrium cylinder and was kept for at least 18 hours to ensure equilibrium. The equilibrium cylinder contains holes and caps fitted with septa for sampling.

#### Sampling and Analysis

At equilibrium, samples from both phases were drawn manually using preheated syringes. A preheated needle was used to avoid phase separation due to temperature gradient. Two Agilent gas chromatographs (GCs) with different column specifications were used for composition analysis: one for the polar phase, while another for the organic phase.

#### Polar phase Analysis

For the polar phase analysis, hydrocarbons were extracted using the solvent extraction method. The solvent used in this work for the extraction of hydrocarbons from the polar phase is carbon disulphide (CS<sub>2</sub>), which has negligible solubility in MEG but is soluble with hydrocarbons. The extract phase is then analyzed on the GC, with an internal standard of 1-heptane diluted in 1-dodecane.

#### Organic phase Analysis

MEG dissolved in hydrocarbons was extracted using water and analyzed on GC. The water content of hydrocarbon rich phase were analyzed using Karl Fischer Coulometer, which provides very fast and reliable results, especially for systems with low solubility's.

### Thermodynamic Modeling

Thermodynamic modeling is carried out using the CPA equation of state, with the characterization method described by Yan et al.[3]. To be able to use equations of state (EoS) for complex hydrocarbon mixtures, the acentric factor ( $\omega$ ), critical pressure ( $P_c$ ) and critical temperature ( $T_c$ ) must be provided for all components in the mixture. Reservoir fluids may contain thousands of different components. Such high numbers are impractical to handle in phase equilibrium calculations. Some components are therefore lumped together and represented as pseudo components. The  $C_{7+}$  characterization consists of representing the hydrocarbons with seven or higher carbon atoms as a convenient number of pseudo components and finding the corresponding EoS parameters for each component. Table 3 presents Fluid – 6 after characterization.

**Table 3:** Characterization of Fluid - 6

Components	Mole %	Tc (K)	Pc (bar)	$\omega$
Ethane	0.01	305.4	48.8	0.0980
Propane	1.57	378.6	47.2	0.1048
i-Butane	0.90	415.8	40.1	0.1508
n-Butane	3.98	436.3	43.6	0.1575
i-Pentane	2.54	460.4	33.8	0.2270
n-Pentane	4.11	479.4	38.0	0.2172
C6	6.83	522.3	34.9	0.2439
C7	14.08	562.3	36.5	0.2259
C8	16.36	593.0	34.8	0.2552
C9	9.00	619.1	31.6	0.2985
C10-C11	8.16	655.3	28.4	0.3517
C12-C14	9.27	707.2	24.5	0.4320
C15-C16	4.66	754.3	21.4	0.5113
C17-C18	3.72	785.6	19.6	0.5661
C19-C21	4.23	816.0	18.1	0.6186
C22-C25	3.83	855.7	16.2	0.6932
C26-C30	2.90	899.4	14.4	0.7811
C31-C37	2.10	944.2	12.7	0.8717
C38+	1.75	1023.8	9.9	1.0421

Both MEG and water have been modeled using four association sites (so-called 4C scheme).

The CPA equation of state uses five pure component parameters, including three for non associating compounds and two for associating compounds. For mixtures containing more than one associating compound, a combining rule is needed for the association parameters. In this work the Elliot Combining Rule (ECR) has been used.

A binary interaction parameter ( $k_{ij}$ ) is needed for each binary system. For binary interaction parameters between

MEG-hydrocarbons and between water-hydrocarbons generalized expression using a correlation in terms of molecular weight has been developed, based on data for well-defined systems.

$$\begin{aligned} \text{MEG-HC:} & \quad k_{ij} = -0.0701 \cdot \ln(\text{MW}_{\text{HC}}) + 0.3521 \\ \text{Water-HC:} & \quad k_{ij} = -0.1533 \cdot \ln(\text{MW}_{\text{HC}}) + 0.7055 \end{aligned}$$

Where  $\text{MW}_{\text{HC}}$  is the molecular weight of the carbon fraction (Pseudo Component). The used binary interaction parameter between MEG and water is -0.115 using ECR.

### Results and discussions

In the binary systems only one associating compound (MEG) is present, which means that the only binary interaction parameters needed are those between MEG and each HC fraction. The binary interactions between hydrocarbons are all set to zero.

The mutual solubility of MEG, water and reservoir fluids using the CPA EoS is shown in table 4. In the case of the ternary mixtures of MEG, water and reservoir fluids, the cross association between water and MEG must be taken into account. The Elliot combining rule is used for the MEG/water system, with a  $k_{ij} = -0.115$ . Using correlations for all binary interaction between all MEG-HC and all water-HC pairs, satisfactory results are obtained for the solubility of water and MEG in the organic phase and for the solubility of hydrocarbons in the polar phase.

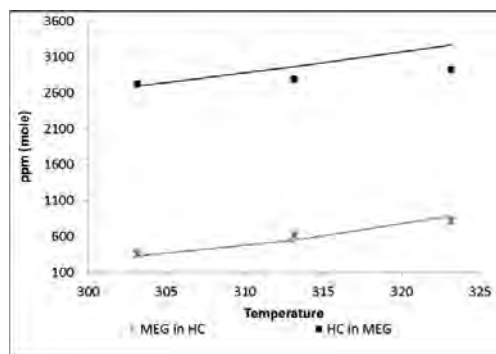
**Table 4:** Average deviation for experimental data using the CPA EoS

Reservoir fluid	HC in polar phase	MEG in HC phase	Water in HC phase
Fluid – 1	21	47	21
Fluid – 2	67	14	28
Fluid – 3	18	21	17
Fluid – 4	41	57	14
Fluid – 5	26	40	27
Fluid – 6	46	39	11
Fluid – 7	95	52	19
Average	45	39	20

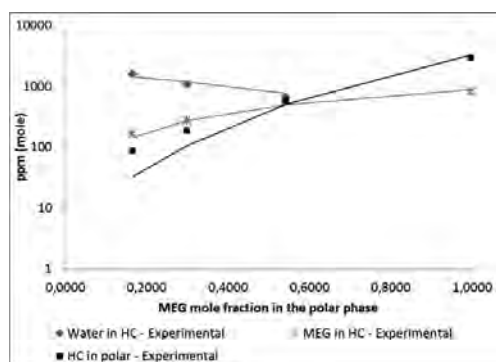
The CPA EoS can satisfactorily predict the experimental trends and describe the solubility's in both phases with reasonable accuracy. A slight under prediction is observed for the MEG concentration in the hydrocarbon rich phase, the water content in the hydrocarbon rich phase and the hydrocarbon concentration in the polar phase. The under prediction of reservoir fluid solubility in the polar phase, and of water solubility in the hydrocarbon rich phase, can to some degree be explained by solvation, which is not explicitly accounted for.

Figure 3+4 presents experimental data and predictions made with the CPA EoS for a mixture of Fluid – 6 with MEG and Fluid 6 with MEG and water. This shows that the solubility of hydrocarbons and MEG decreases with

increasing water content in the polar phase. It is important to mention, that predictions are as good as for well-defined hydrocarbons with MEG and water, as can be seen in table 5:



**Figure 3:** Mutual solubility of MEG – Fluid 6. The points are experimental data and the lines are CPA predictions.



**Figure 4:** Mutual solubility of MEG - water – Fluid 6. The points are experimental data and the lines are CPA predictions.

**Table 5:** Average deviation for well-defined systems using the CPA EoS

Reservoir fluid	HC in polar phase	MEG in HC phase	Water in HC phase
n-hexane	44	42	44
Benzene	71	14	4
n-nonane	35	50	9
Ethylbenzene	33	35	20
C1/C3/C7	50	26	31
C3/Toluene	16	8	12
Average	42	29	20

## Conclusions

The CPA equation of state has been applied to the systems containing reservoir fluids, MEG and water. The critical properties were calculated using a previously

developed characterization method, which uses the CPA EoS monomer values.

Using newly developed correlations for binary interaction parameters between all MEG/HC and Water/HC pairs, the CPA EoS satisfactorily describes the mutual solubility of the reservoir fluids with MEG and the mutual solubility of reservoir fluid with MEG and water.

Some under prediction are observed for the solubility of MEG and water in the hydrocarbon rich phase and the solubility of hydrocarbons in the polar phase. The results are in the right order of magnitude, and the predictions are as good as for well-defined hydrocarbons with MEG and water.

Improved results might be achieved by further investigating the effect of PNA distribution in the calculations, so that solvation effect is accounted for explicitly.

## Acknowledgements

The authors wish to thank the industrial partners in the CHIGP (Chemicals in Gas Processing) consortium for financial support.

## References

1. G. M. Kontogeorgis, E. C. Voutsas, I. V. Yakoumis, D. P. Tassios, *Ind. Eng. Chem. Res.* 35 (1996) 4310.
2. K. S. Pedersen, P. Thomassen, A. Fredenslund, *Characterization of gas condensate mixtures, Advances in thermodynamics*, Taylor & Francis, New York, 1989
3. W. Yan, G. M. Kontogeorgis, E. H. Stenby, *Fluid Phase Equilib.*, 276 (2009) 75-85.

## List of publications

1. M. Frost, G.M. Kontogeorgis, E.H. Stenby, M.A. Yussuf, T. Haugum, K.O. Christensen, E. Solbraa, T.V. Løkken, *Fluid Phase Equilib.* 340 (2013), 1-6
2. M. Frost, E. Karakatsani, N. von Solms, D. Richon, G.M. Kontogeorgis, *Journal of Chemical Engineering Data*, Accepted



**Carina Lira Gargalo**

E-mail: carlour@kt.dtu.dk

Supervisors: Gürkan Sin  
Rafiqul Gani

PhD Study

Started: November 2013

To be completed: November 2016

## Sustainable design of Biorefinery Systems for Biorenewables

### Abstract

Governments around the globe are setting an ambitious target to reduce the greenhouse gases (GHG) emissions and oil dependence. Therefore, replacing oil in all applications (including plastics, chemicals and other value-added products) by biomass-derived products could be the key to achieve this goal (de Jong *et al.*, 2009). Therefore, the objective of this project is to develop a framework that allows the user to systematically generate competing solutions and optimal biorefinery options. The framework will be validated through several case studies on the integrated biorefinery concept, such as the production of biodiesel and value-added derivatives from vegetable oil or lignocellulosic biomass.

### Introduction

The sustainable design of a biorefinery system aims to achieve lower water, energy and raw material consumption than the petrochemical refinery producing the same chemical or range of chemicals using fossil-fuels as feedstock. Consequently, a major challenge is to develop the ability to sustainably convert different biorenewables into different value-added products as efficiently as the current petrochemical industry.

Several studies have developed methods to create new designs or improve an already existing design by retrofit techniques with the objective of decreasing for instance the energy, water or raw material consumption. Among them, Uerdingen *et al.* (2003), El-halwagi (1998), Rapoport *et al.* (1994) and Cheali *et al.* (2013). Carvalho *et al.* (2008) took it further by establishing the link between the identification of the process hot spots and the related sustainability metrics to further improve the process design.

Therefore there is a need to collectively apply previous concepts of sustainability, superstructure optimization and retrofit design. The objective of the present project is to propose a systematic multi-level framework which uses superstructure optimization to obtain a base-case design subject to design constraints and a set of performance criteria. The base-case design will be evaluated through sustainability analysis in order to logically

identify the process hot spots. The obtained information is then used to set design targets for achieving a more sustainable design through retrofitting techniques.

### Discipline

The research is mainly conducted within the field of process systems engineering and sustainable design.

### Research Methodology & Tasks

The objective of this work is achieved by developing a systematic step-by-step methodology as follows.

(1) to integrate superstructure generation, (2) to perform sustainability and economic analysis under uncertainty and sensitivity analysis, (3) to perform environmental impact analysis applying proactively life cycle assessment (LCA) models under uncertainty and sensitivity analysis, and (4) to validate the framework applying it to generate the superstructures of lignocellulosic and vegetable oil biorefinery to biofuels and bioproducts, and identify the respective optimal solutions with respect to the selected set of constraints.

In Figure 1 it is depicted a superstructure for the production of biodiesel and derivatives from waste palm oil and methanol, as an example of the biorefinery complexity that will be faced in the current project.

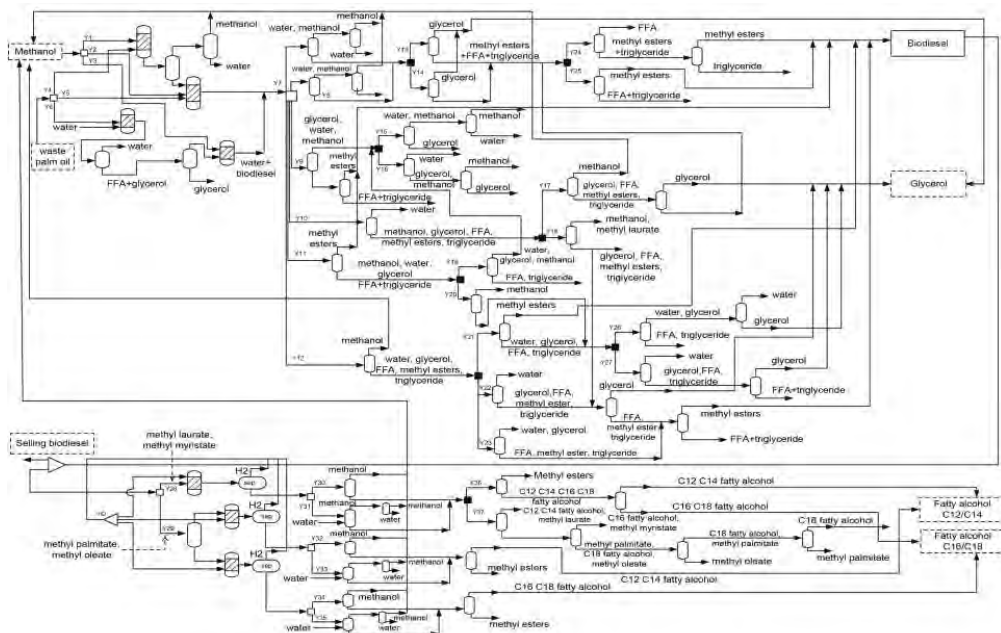


**Figure 1:** Overview of an Integrated Biorefinery: biodiesel, glycerol and fatty acid production from waste palm oil. (Simasatitkul *et al.*, 2013)

## Conclusions

Biorefineries have been synthesized by superstructure optimization followed through more detailed design subject to predefined performance criteria related to environmental targets. However, the use of detailed sustainability analysis and life cycle assessment models in selecting the best design has not yet been proposed. Therefore, the framework objective is to systematically generate and identify the optimal flowsheet alternative(s) with respect to the objective function subject to a set of performance criteria involving sustainability metrics and life cycle assessment factors. In order to verify the framework, it will be applied to several case studies, among them, the production of (1) biodiesel, glycerol, fatty acids and other value-added chemicals from vegetable oil, and (2) by the production of lignocellulosic bioethanol, biobutanol and respective derivatives from lignocellulosic biomass.

## References

- Carvalho, A., Gani, R., & Matos, H. (2008). Design of sustainable chemical processes: Systematic retrofit analysis generation and evaluation of alternatives. *Process Safety and Environmental Protection*, 86(5), 328–346. doi:10.1016/j.psep.2007.11.003
- Cheali, P., Germaey, K. V., & Sin, G. (2013). Towards a computer-aided synthesis and design of biorefinery networks – data collection and management using a generic modeling approach.
- De Jong, Ed, René van Ree, and I. K. K. 2009. (2009). Biorefineries: Adding Value to the Sustainable Utilisation of Biomass. *IEA Bioenergy*.
- El-halwagi, M. M. (1998). Pollution prevention through process integration, 1(July), 5–19.
- Rapport, H., & R. Lavie. (1994). Retrofit Design of New Units into an Existing Plant. *Computers & Chemical Engineering*, 18, 743–753.
- Simasatitkul, L., Arpornwichanop, A., & Gani, R. (2013). Design methodology for bio-based processing: Biodiesel and fatty acid production. *Computers & Chemical Engineering*, 57, 48–62. doi:10.1016/j.compchemeng.2013.01.018
- Uerdingen, E., Fischer, U., & Hungerbuhler, K. (2003). Screening for Profitable Retrofit Options of Chemical Processes : a New Method, 49(9).

**Jozsef Gaspar**

Phone: +45 4525 28 76  
E-mail: joca@kt.dtu.dk

Supervisors: Philip Loldrup Fosbøl  
Kaj Thomsen  
Nicolas von Solms

**PhD Study**

Started: December 2012  
To be completed: March 2016

## Rate Based CO<sub>2</sub> Post-Combustion Modelling in Aspen Plus Using CERE Cape Open Modules

Sustainable energy infrastructure development is a key challenge of our society. In order to reach the Zero CO<sub>2</sub> Emission policy, carbon capture has to be integrated with power production. CO<sub>2</sub> post-combustion capture is a mature, end-of-pipe capture technology. However, the feasibility of the process has to be demonstrated. Plant wide process studies might help to identify improvements opportunities and can lead to more efficient and profitable operation. As part of my PhD project, a generic communication protocol was implemented with the purpose of preparing the simulations for plant wide process analyses and optimization. Process developments will be investigated and possible improvements identified. This study is part of the EU FP7 OCTAVIUS benchmarking project for large scale capture plants.

**Introduction**

Availability, relatively low cost and existing infrastructure for delivery and distribution of fossil fuels makes them a major player in the world energy and greenhouse gas production [1]. In order to reach the Zero CO<sub>2</sub> Emission policy, carbon capture has to be integrated with power production. Scale-up, validation and verification are required for the deployment of a large scale industrial capture plants.

The focus of the present work is to illustrate the way of interoperability between the DTU in-house capture unit and Cape Open compliant simulation engines, such as Aspen Plus. General modelling principles are discussed. A post-combustion plant, design for an 800 MWe bituminous coal power plant is simulated. This work is part of the OCTAVIUS benchmarking task. The present simulation study aims to underline the benefits of using generic communications standards for plant wide process simulation, analyses, and optimization.

**DTU Cape Open module**

The intention of the Cape Open initiative is to define common communication standards for information exchange in computer aided process engineering [2]. Cape Open is a tool which enables automatic transfer of calculation results between simulation engines, in-house unit operations models, and property packages.

The Cape Open Standards consist of the technical architecture, interface and implementation specifications. It relies on modern development tools as object oriented paradigm, component-based approach, middleware technology, etc. This communication protocol uses the Unified Modeling Language [3].

Cape Open puts the technology in focus instead of the general modelling principles. Cape Open plays an essential role not only in the interoperability but also in the accelerated developments of complex technologies. The process is simulated as a whole, which it should be, and not as independent separated process islands.

In this work the CAPCO2 software is used. It is a versatile tool developed at the Technical University of Denmark (DTU) for calculating rate based absorption and desorption. The high performance of the calculations is secured by incorporation of the extended UNIQUAC thermodynamic model [4] and accurate estimation of mass transfer and hydraulic properties. The mass transfer model is applied in a film model approach. A flexible enhancement factor model valid at both absorption and desorption conditions is used. The physical property package was validated at both absorber and desorber conditions within a loading range of 0.15 – 0.55 mole CO<sub>2</sub>/mole MEA, at a temperature range of 25 – 140 °C. The model performance is validated against various experimental datasets [5, 6] which cover the whole operational window of post-combustion plants.

### Post combustion simulation

The simulation is shown of a post-combustion capture plant designed for an 800 MWe bituminous coal based power plant, incorporating lean vapor re-compression (LVC).

The capture process is simulated in Aspen Plus using the CAPCO2 Cape Open compliant module in conjunction to built-in heat exchange, mixers, boilers, and compressors. The operational parameters and design conditions are in accordance with the EU FP7 OCTAVIUS project guidelines.

### Results and discussions

The accuracy of the stand-alone CAPCO2 model and of the integrated post-combustion model has been evaluated against experimental data published by Notz [6]. The predicted and measured temperature as function of the column height for experimental run 2 is shown in Figure 1. This figure underlines that the stand-alone approach predicts more accurately the absorber temperature but does not catch the shape of the temperature curve for the desorber. It has to be said that flashing of the desorber feed stream might occur resulting in erroneous concentration readings. In overall, it can be concluded that the integrated model predicts well both, absorber and desorber temperature and composition.

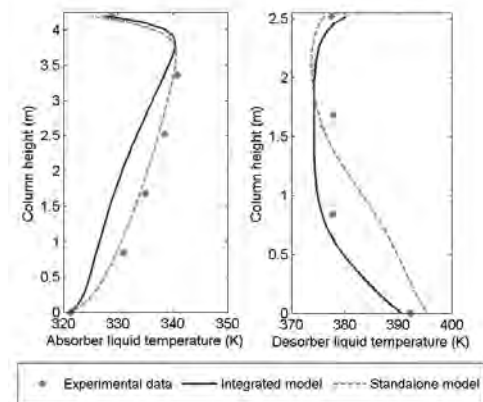


**Figure 1:** Post-combustion flowsheet for CO<sub>2</sub> capture simulation.

In order to show the performance of the demonstrated technologies and aspects in the OCTAVIUS project, benchmarking is performed. This work is based on comparison of performance parameters like loading, L/G ratio, removal rate, reboiler duty, and etc. The results obtained with DTU CAPCO2 model and NTNU CO2SIM model is shown in Table 1. One might note the good agreement of the mass balance around the absorber, desorber and connected units. The reboiler duty is 201.79 MW per train. With the flow-rate of CO<sub>2</sub> leaving the stripper equal to 67.21 kg/s, this corresponds

to 3.00 MJ/kg CO<sub>2</sub> captured. This is in a good correlation with the results found with CO2SIM software.

**Table 1.** Main benchmarking parameters with CAPCO2 and CO2SIM in the OCTAVIUS benchmarking project

Comparison parameters	CAPCO2	CO2SIM
Lean loading (mol/mol)	0.1951	0.1939
Rich loading (mol/mol)	0.4790	0.5043
Reboiler duty (MW)	201.8	209.3
CO <sub>2</sub> captured (kg/h)	67.21	72.9
Reboiler SP* (MJ/kg CO <sub>2</sub> )	3.00	2.87
Hot rich temperature (°C)	95.88	94.30
Reboiler temperature (°C)	121.0	120.3
Blower SP* (MJ/kg CO <sub>2</sub> )	0.0242	0.0273
LVC SP* (MJ/kg CO <sub>2</sub> )	0.0694	0.0693
All pumps SP* (MJ/kg CO <sub>2</sub> )	0.0244	0.0252

\*SP : specific duty (MJ/kg CO<sub>2</sub> captured)

The above presented data shows a good agreement between the CO2SIM and CAPCO2 simulation results. The main performance indicators of the capture and regeneration sections underline the reliability of the models. The absolute relative deviations between the CO2SIM and CAPCO2 models are less than 10%.

### Conclusion

The Cape Open generic interface for unit operations was implemented in Visual C#. The methodology of Cape Open interface implementation was illustrated through a post-combustion capture case study. The developed capture unit was tested at various conditions and the interoperability with Aspen Plus has been demonstrated. The evaluation of the model substantiates the good agreement with experimental data. Furthermore, the accuracy of the whole post-combustion model has been demonstrated.

As part of the OCTAVIUS benchmarking project the developed post-combustion model will be integrated with power plant simulation in collaboration with Technical University of Hamburg.

### References

1. J. Gaspar, A.M. Cormos, International Journal of Greenhouse Gas Control, 8(2012), 45-55
2. R. Morales-Rodriguez, R. Gani, S. Dechelotte, A. Vacher, O. Baudouin, Chemical Engineering Research & Design, 86, (7A) (2008),823-833.
3. Cape Open Standards and Supporting Documents, [www.colan.org](http://www.colan.org)
4. K. Thomsen, P. Rasmussen, Chemical Engineering Science, 54, (12) (1999), 1787-1802 T.L.
5. Sonderby, K.B. Carlsen, P.L. Fosbol, L.G. Kiorboe, N. von Solms, International Journal of Greenhouse Gas Control, 12, (2013) 181-192.
6. R. Notz, H.P. Mangalapally, H. Hasse, Journal of Greenhouse Gas Control, 6 (2012) 84-112.





**Kaustav Goswami**

Phone: +45 4525 6885  
E-mail: kago@kt.dtu.dk

Supervisors: Anne Ladegaard Skov  
Anders Egede Daugaard

PhD Study  
Started: August 2011  
To be completed: July 2014

## Reinforced Poly(Propylene Oxide): A Soft and Extensible Dielectric Electroactive Polymer

### Abstract

Poly(propylene oxide) (PPO), a novel soft elastomeric material, and its composites were investigated as a new dielectric electroactive polymer (EAP). The PPO networks were obtained from thiol-ene chemistry by photochemical crosslinking of  $\alpha,\omega$ -diallyl PPO with a tetra-functional thiol. The elastomer was reinforced with hexamethylenedisilazane treated fumed silica to improve the mechanical properties of the PPO. The mechanical properties of PPO and composites thereof were investigated by shear rheology. Dielectric spectroscopy of PPO revealed high relative dielectric permittivity of 5.6 at  $10^3$  Hz. The relative permittivity decreased slightly upon addition of fillers, but remained higher than the commonly used acrylic EAP material VHB4910. The electromechanical actuation performance of both PPO and its composites showed properties as good as VHB4910 and a lower viscous loss.

### Introduction

The interest in using elastomers for electromechanical transducers has increased during the last decade due to their large strains, frequency responses of the order of milliseconds, work densities higher than human muscle, and high degree of electromechanical coupling [1,2]. A special class of elastomers known as dielectric electroactive polymers (DEAPs) has emerged as a strong candidate in this field due to their low density, fast response time, low cost of production, low energy consumption and low heat generation. It has been found that the DEAPs possess mechanical properties very similar to human muscle and can mimic human muscular function, and thus they are commonly nicknamed artificial muscles [3].

In a typical configuration for DEAP transducers, a thin film of dielectric elastomer is sandwiched between very thin layers of compliant electrodes, which are connected to the power supply for transduction. The equation governing the actuation of a DEAP actuator is given as [4],

$$P = \epsilon_0 \epsilon_r E^2 = \epsilon_0 \epsilon_r \left( \frac{V}{d} \right)^2 \quad (1)$$

where  $P$  is the electrostatic pressure acting on the dielectric elastomer due to an applied electric field  $E$ ,  $V$  is the applied voltage,  $d$  is the thickness of the dielectric

elastomer,  $\epsilon_0$  is the vacuum dielectric permittivity ( $8.85 \times 10^{-12}$  F m<sup>-1</sup>) and  $\epsilon_r$  is the relative permittivity of the elastomer. At equilibrium, the electrostatic pressure equals the internal stress in the material so that the strain produced on the elastomer ( $S$ ) can be written as,

$$S = \frac{\epsilon_0 \epsilon_r}{Y} \left( \frac{V}{d} \right)^2 \quad (2)$$

where  $Y$  is the elastic modulus of the elastomer. The first elastomeric material to be used successfully as dielectric elastomer was the acrylic VHB tape from 3M. In an article on dielectric elastomers, it was reported that this material showed extraordinarily high strain and high electrostatic pressure. It was also shown in the same article that the performance could be increased manifold by applying prestrain in planar direction [5]. However, the long response time and need for prestrain of VHB are the reasons for the decreasing trend of using VHB as DEAP material.

In this study PPO has been investigated as a new DEAP material against commercially available acrylic (VHB4910). The aim was to develop a new DEAP material with enhanced electromechanical response, compared to VHB. In the presented work, a novel, fast and efficient UV photo-crosslinking was employed to crosslink PPO and its composites with treated fumed silica. Rheological, dielectric, and electromechanical

characterizations were performed on both this new material and its composites in order to evaluate the potential of PPO as a new electroactive polymer.

## Experimental

### Materials

Allyl terminated PPO of approximate molecular weight 16500 g/mol (Kaneka Silyl ACS 003) was obtained from Kaneka Corp., Japan. 2,4,6-trimethylbenzoylphenylphosphinic acid ethyl ester (Lucirin TPO-L) was purchased from BASF. VHB 4910 was obtained as 1 mm and 0.5 mm thick films with polyethylene backing material from 3M. The filler used for the elastomeric composites was hexamethyldisilazane (HMDS) treated fumed silica AEROSIL® R812, from Evonik Industries. The reported Brunauer, Emmett and Teller (BET) surface area of AEROSIL® R812 was  $260 \pm 30$  m<sup>2</sup>/g. All the other chemicals used in this work were purchased from Sigma-Aldrich.

### Methods

Rheological tests were performed in a stress controlled rheometer (AR2000) from TA Instruments, with 25 mm parallel plate geometry. Measurement conditions were set to controlled strain mode at 1% strain, which was ensured to be within the linear viscoelastic region as determined from initial strain sweeps. Frequency sweep experiments were performed from 100 Hz to 0.001 Hz at 25°C. Broadband dielectric spectroscopy was carried out on disc-shaped samples of both the pure matrix and the composites (diameter of 25 mm and thickness 1 mm) at 25°C in the frequency range 20 Hz to 2 MHz by means of an ARES G2 rheometer equipped with DETA accessory including an inductance (L)-capacitance (C)-resistance (R) (LCR) meter (Agilent E4980A). The electromechanical response of the PPO films, shaped in rectangular material strips of dimension  $20 \times 25$  mm<sup>2</sup> and thickness varying between 80-226  $\mu$ m, was studied after they were provided with opposed compliant electrodes by smearing a carbon based conductive grease (Nyogel 755G, TecnoLube Seal, USA) on both their major surfaces. For each sample a vertical prestrain of 100% and a dc high voltage with stepwise increment of 250V were applied across the elastomer by means of power supply (HV-DC 205A-30P, Bertan, USA). At each voltage level isotonic transverse strains were measured by a displacement transducer and waited until a constant deformation was obtained.

### Standard procedure for preparation of PPO network.

Pentaerythritol tetrakis (3-mercaptopropionate) (4 functional crosslinker, 0.244 g, 0.5 mmol) and 2,4,6-trimethylbenzoylphenylphosphinic acid ethyl ester (Lucirin TPO-L) (photo initiator, 0.192 g, 0.6 mmol) were added to  $\alpha,\omega$ -diallyl PPO (10 g (0.6 mmol of allyl groups)  $M_n = 16500$  g/mol) and mixed in a SpeedMixer™ (DAC 150 FVZ, Hauschild Co., Germany) at 3500 rpm for 5 minutes. The mixture was poured into an 8 cm  $\times$  10 cm steel mould placed over a glass plate lined with Parafilm® M. This setup was kept in a well-ventilated place for 45-60 minutes and

subsequently transferred to the UV chamber ( $\lambda = 365$  nm, 4.5 mW/cm<sup>2</sup>) and irradiated for 45 minutes in ambient atmosphere.

*Standard procedure for filled PPO system.* The system was prepared as above for PPO networks. The filler was added with 40-60 wt% toluene directly into the PPO-crosslinker mixture prior to speed mixing, otherwise, the procedure was unchanged. The resulting films were studied by scanning electron microscopy (SEM) to ensure proper mixing of the fillers into the elastomer.

## Results and Discussions

The linear viscoelastic (LVE) properties of pure and composite PPO networks were measured in order to characterize the material response in the low strain limit. Figure 1a shows the storage modulus ( $G'$ ) and Figure 1b shows loss tangent ( $\tan \delta$ ) of the materials.  $\tan \delta$  is also known as the damping of the material. It is obvious that, with respect to the viscous loss in the investigated frequency regime, all PPO networks are superior to VHB (see insert in Figure 1b for comparison).

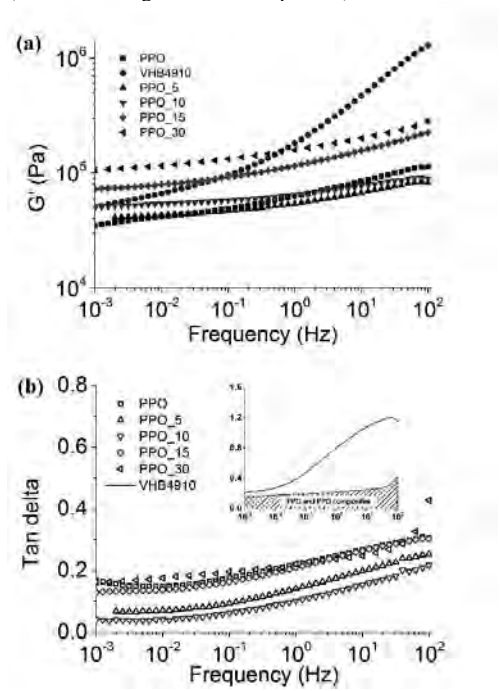


**Figure 1:** (a) Storage modulus and (b) tan delta versus frequency for pure PPO and filled PPO networks at 25°C. Inset shows the difference in tan delta between the PPO formulations (shaded region) and VHB

From Figure 1a it can be seen that the storage modulus ( $G'$ ) at the plateau (terminal) region ( $10^{-3}$  Hz) is approximately 35 kPa for pure PPO which is very low compared to VHB as well as for non-filled silicone elastomers [6]. On addition of treated fumed silica into the soft PPO network, the storage modulus ( $G'$ ) at low frequencies gradually increases from 35 kPa to 106 kPa

due to the hindrance in chain movement imposed by the filler. The tan delta plots (Figure 1b) also give some insight into the molecular motion and damping behaviour of the polymers. At 5 phr treated fumed silica loading, the viscous loss of pure PPO is reduced significantly in the entire frequency range, and it continues to decrease as the filler content is raised up to 10 phr. However, upon addition of 15 and 30 phr treated fumed silica the composites show increased tan delta, indicating prominent damping behavior of the composites and hence a possible destruction of the network properties [6]. Moreover, at low frequencies the samples containing treated fumed silica exhibit an almost stable tan delta, as is typical for a loaded crosslinked rubber in which chain movements are further restricted due to the presence of filler particles. Compared to PPO, VHB remains a material with a significant loss, a higher tan delta and showing a much more dispersive behavior than PPO and any of the composites (Figure 1b).

One aspect of this study is to measure the effect of incorporating treated fumed silica as a reinforcing agent on dielectric permittivity of PPO. Figure 2a and Figure 2b show dielectric spectra for PPO and its composites.

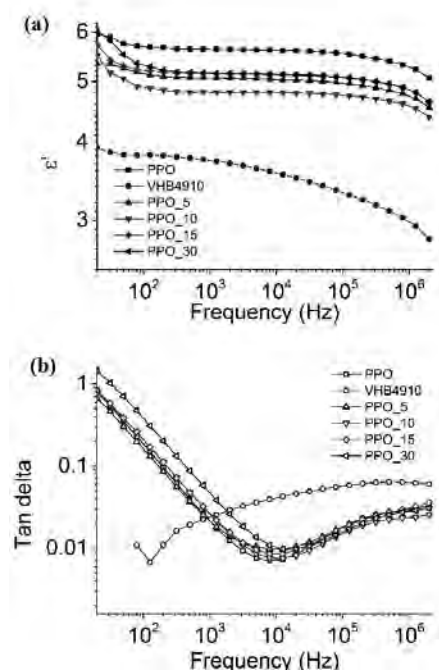


**Figure 2:** Dielectric spectroscopy plot (a) real part of permittivity versus frequency and (b) imaginary part of permittivity versus frequency for PPO and the composites.

At low frequencies, an increase in the dielectric constant of both PPO and its composites is observed as frequency is progressively lowered from about  $10^2$  down to 20 Hz (Figure 2a), which is accompanied by a parallel increase

of the tan delta (Figure 2b). Such an increase, which shows up as a low frequency dispersion in all the dielectric spectra, can be ascribed to a Maxwell-Wagner polarization, which is caused by a limited displacement of charges induced by the electric field in correspondence of interfaces between different phases. While in the case of pure PPO such dispersion could arise only from a polarization contribution at the level of the sample/electrode interface and in the composites it could be indicative of the presence of further interfaces. Indeed, the fact that in the composites such polarization effects are more significant than in pure PPO is likely due to the presence of interfaces between the PPO matrix and the filler. Coherently, it is also found that as the filler amount is increased the interface polarization effect increases. In the region of the medium-high frequencies ( $10^2 - 10^6$  Hz), where the dielectric response mainly depends on the bulk polarization processes [7], there are no significant changes in the  $\epsilon'$  (Figure 2a) for all the materials. However, the dielectric constant varies with the composites compared to that of the pure matrix. From Figure 2a the relative dielectric constant for pure PPO at 1 kHz can be determined to be 5.6, which is higher than the value reported for VHB4910 (3.21 at 1 kHz). Treated fumed silica was used as a filler for reinforcing purposes, and since it is a low dielectric constant filler ( $\epsilon_r = 3.9$ ) it gives a minor decrease in the dielectric permittivity, as predicted by common mixing rules [8]. Although, at higher treated fumed silica contents the bulk permittivity of PPO\_15 and PPO\_30 becomes higher than PPO\_5 and PPO\_10, it remains lower than the pure matrix. This change in the behavior of the dielectric properties at higher filler loading factors could be the result of a larger contribution from interfaces at filler/matrix boundaries as the filler volume fraction is increased. Some studies have already revealed that the presence of such boundary layers inside a material increases the dielectric permittivity. For instance, at the interface between matrix and filler in a particulate composite or between two immiscible phases in a polymer blend, intermediate interaction regions can provide additional polarization properties, which can play a major role in determining the final permittivity of such material [9,10].

Electromechanical tests were performed on 100% prestretched samples of both PPO and its composites, and the results are presented in Figure 3. The electromechanical response of prestretched VHB4910 is included in Figure 3 for easy comparison. Due to the detection of a partial electrical conduction at fields over  $20 \text{ V}/\mu\text{m}$  in samples containing treated fumed silica, the effective electric field acting on these samples was not considered reliable beyond this threshold value. Therefore, data have been reported only for reliable values below  $20 \text{ V}/\mu\text{m}$  (with the exception of PPO\_30, which showed reliable actuation at electric field as high as  $27 \text{ V}/\mu\text{m}$ ). For pure PPO the sample failed at fields around  $17 \text{ V}/\mu\text{m}$ , while VHB4910 did not show any such failure.

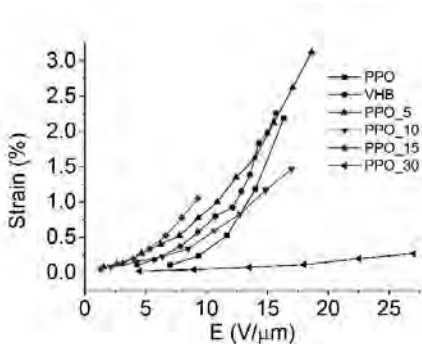


**Figure 3:** Electromechanical response of PPO and the composites.

As seen in Figure 3, the electromechanical response of pure PPO is very close to that of VHB4910. Addition of filler significantly reduces the stickiness of PPO and improves its mechanical performance manifold (Figure 1). From Figure 3, it can be seen that PPO\_5 shows the maximum actuation strain among the studied PPO composites, followed by PPO\_10 and PPO\_15. The relatively low actuation strain of PPO\_10 and PPO\_15 is due to the higher modulus and lower dielectric permittivity compared to pure PPO and PPO\_5. At higher content of treated fumed silica the strain induced by the electrostatic pressure becomes very small as can be seen for PPO\_30. These observations are in good agreement with equation 2 and all measurements agree well at low voltages whereas the different losses start to play an important role at higher voltages for all types of materials investigated here. Considering the results obtained from electromechanical tests, PPO filled with small amounts of filler has very good actuation behavior and good mechanical properties. Higher filler content gave better mechanical property, but severely hindered the electromechanical performance of the material. Therefore a convenient tradeoff between the required mechanical reinforcement of PPO composites and the electromechanical response opens a pathway into the development of stacked actuators [11,12]. The PPO samples possess natural adhesiveness, which would be beneficial for sandwiching several actuators on top of each other. Future development of this material would be to strike a balance between improving mechanical properties and electromechanical response by either employing chemical modification of the base polymer or using novel filler materials. However, the filler selection is limited to fillers with little UV absorption.

## Conclusion

This study reveals the potential of PPO reinforced with treated fumed silica filler as a new dielectric electroactive polymer actuator. A novel PPO elastomer and its composites were developed by a simple and easily manageable processing scheme. Shear rheology showed enhancement in the mechanical stability of PPO composites over the mechanically weak pure PPO

network, and additionally both PPO and its composites showed significantly less viscous loss as compared to the widely used VHB elastomer. The relative permittivity of pure PPO at  $10^3$  Hz was found to be 5.6, and all the PPO composites showed permittivities above 4.8, which is significantly higher than VHB4910. The electromechanical test showed that PPO composites with small amounts of filler (5-10 phr) have the best electromechanical behavior. The observed performance, combined with their intrinsic stickiness, suggest that these materials have great potential in the application area of stacked actuators. PPO composites were also found to be similar to VHB4910 in their electromechanical response with the added advantage of possessing very low viscous dissipation. Furthermore the PPO presents another advantage over VHB4910 since further optimization of the PPO networks is allowed due to the reactive handles resulting for the excess of thiol groups. In addition, a thorough electrical breakdown measurement of this system could also be done in future in order to investigate the effect of filler addition on electrical breakdown strength, as it is known that such particulate filled system could suffer from low breakdown strength.

## References

- [1] J. D. W. Madden, in *Dielectr. Elastomers as Electromechanical Transducers* (Eds.: F. Carpi, D. De Rossi, R. Kornbluh, R. Pelrine, P. Sommer-larsen), Elsevier, Amsterdam, **2008**, pp. 13–21.
- [2] R. Pelrine, R. Kornbluh, G. Kofod, *Adv. Mater.* **2000**, *12*, 1223–1225.
- [3] R. Shankar, T. K. Ghosh, R. J. Spontak, *Soft Matter* **2007**, *3*, 1116–1129.
- [4] R. E. Pelrine, R. D. Kornbluh, J. P. Joseph, *Sensors Actuators A Phys.* **1998**, *64*, 77–85.
- [5] R. Pelrine, R. Kornbluh, Q. Pei, J. Joseph, *Science.* **2000**, *287*, 836–839.
- [6] S. M. G. Frankær, M. K. Jensen, A. G. Bejenariu, A. L. Skov, *Rheol. Acta* **2012**, *51*, 559–567.
- [7] F. Carpi, G. Gallone, F. Galantini, D. De Rossi, in *Dielectr. Elastomers as Electromechanical Transducers* (Eds.: F. Carpi, D. De Rossi, R. Kornbluh, R. Pelrine, P. Sommer-Larsen), Elsevier, Amsterdam, **2008**, pp. 51–68.
- [8] G. Gallone, F. Carpi, D. De Rossi, G. Levita, A. Marchetti, *Mater. Sci. Eng. C* **2007**, *27*, 110–116.
- [9] M. S. Ozmusul, R. C. Picu, *Polym. Compos.* **2002**, *23*, 110–119.
- [10] M. G. Todd, F. G. Shi, *J. Appl. Phys.* **2003**, *94*, 4551–4557.
- [11] G. Kovacs, L. Düring, S. Michel, G. Terrasi, *Sensors Actuators A Phys.* **2009**, *155*, 299–307.
- [12] Y. Bar-Cohen, in *Proc. SPIE* (Eds.: Y. Bar-Cohen, T. Wallmersperger), **2009**, pp. 728703–1–728703–6.

**Helge Grosch**

Phone: +45 4677 5417  
E-mail: hgch@kt.dtu.dk

Supervisors: Alexander Fateev  
Sønnik Clausen

**PhD Study**

Started: December 2011  
To be completed: November 2014

## Online Trace Gas Analysis for Biomass Gasification

**Abstract**

In the process of biomass gasification often unwanted low concentrated by-products (trace gases) are produced. In order to be able to handle the by-products, an on-line, in-situ analysis of these trace gases is necessary. Due to their advantages ultraviolet and infrared spectroscopy are used for this purpose in this project. To obtain quantitative results a database of different chemical compounds at various temperatures has been built up and applied in the analysis of experimental data obtained at the pilot-scale low temperature circulating-fluidized bed gasifier at DTU Risø Campus.

**Introduction**

Due to its renewability, the interest in biomass as a source of energy and chemicals increases. While gasification seems to be an attractive way of the utilization of biomass, some problems still have to be addressed. By now the producer gases (e.g. H<sub>2</sub>, CO, CH<sub>4</sub> and CO<sub>2</sub>) still lack of the necessary purity to be utilized in a broader fashion. In some cases, even the combustion of the producer gas, still creates some hazardous gases. In general, the by-products of the gasification can be responsible for a decrease in conversion efficiency, corrosion and environmental issues. Some trace gases can already create problems at concentrations in the parts-per-million (ppm) range. These concentrations are difficult to detect, especially if low detection time is desired. As important compounds, SO<sub>2</sub>, and other sulfur containing compounds such as OCS, CS<sub>2</sub> and H<sub>2</sub>S [1] as well as aromatic compounds such as phenol or naphthalene [2] were identified in different gasification processes.

Thus, the analysis techniques play an important role in process control and optimization. Traditional methods, such as gas chromatography coupled with mass spectrometry (GC-MS), have the drawbacks of long analysis times and the necessity of a gas extraction system. With the extraction of the gas a change in temperature and therefore a change in the chemical composition of the gas may occur. A possibility to circumvent these problems is to use an in-situ optical analysis with high resolution infrared (IR) and/or ultraviolet (UV) spectroscopy. These methods can provide real-time analysis at low concentrations.

However, the drawback is that optical access on site and a gas database for absorption cross-sections for quantification are necessary. Not only does this mean that the optical behavior of each chemical compound must be known but also its change with temperature. These databases are in most cases not available and must be built up.

In order build up a high resolution database, a special, heated gas cell was developed and used for the quantification of the previously mentioned chemical compounds at different temperatures in the laboratory. Besides this, the results from the lab were used for quantification in the pilot sized low-temperature circulating fluidized bed reactor (LT-CFB) on DTU Risø-Campus.

**Experimental Techniques**

For the build-up of a database a hot gas flow cell was developed and quantified [3]. This gas cell allows the measurement of reactive gas at temperatures up to 800 K. As it is used for varies wavelength (from UV at 190 nm to IR at 20.000 nm), it has exchangeable optical windows depending on their transmission in the specific spectral range and two so-called flow windows. At the flow windows a nitrogen flow ensures, that the reactive gas flow does not come in contact with the optical windows. This is necessary, because the reactive gases might react with the optical windows and change their optical characteristics. A detailed description is given in [3]. Both techniques, the UV and the IR spectroscopy, use the Lambert-Beer Law. In the following, only the results for the UV spectroscopy will be given.

For the quantification of the gas concentration two methods were used. In case of the sulfur containing compounds, a commercially available gas mixture with known concentration was used and, if necessary, diluted before it was introduced into the gas cell. This is however not possible for aromatic compounds, because these mixtures are not stable and cannot withstand higher pressures. Therefore, in the case of naphthalene and phenol, an unknown concentration was introduced into the gas cell. At the exit of the gas cell the aromatic compounds were captured and their concentration determined by GC-MS.

## Results and Discussion

For the UV spectroscopy the behavior of SO<sub>2</sub>, OCS, CS<sub>2</sub> and H<sub>2</sub>S as sulfur containing compounds and phenol and naphthalene as aromatic compounds were investigated by now. To assure the reliability of the system and the acquired data, the data obtained for room temperature were compared to previously published data. In all cases a very good agreement between literature and experiment could be found. In Figure 1 and 2 the behavior of the absorption cross-sections of OCS and phenol at different temperatures are shown.

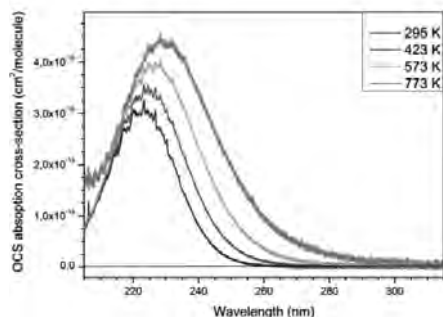


**Figure 1** Absorption cross-section of OCS at room temperature (blue), 423 K (green), 573 K (orange) and 773 K (red).

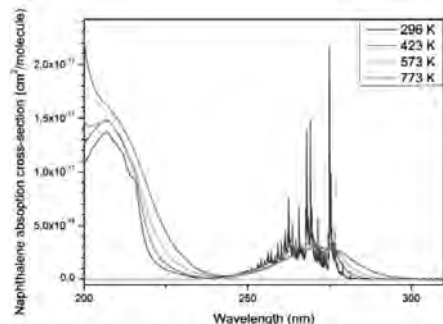


**Figure 2:** Absorption cross-section of phenol at room temperature (blue), 423 K (green), 573 K (orange) and 773 K (red).

In general, the fine structures of the cross-sections disappear with higher temperature and only the coarse

structures remain. Besides this, the structure broadens. In case of OCS one can also see that the maximum of the cross-section shifts to higher wavelength and the area under the curve increases.

The disappearing fine structure can cause problems for the analysis, when multiple gas compounds absorb at similar wavelength regions. In order to handle this problem not the absolute intensities, but the absolute change at a sharp peak (differential absorption) can be analyzed to obtain a quantitative result. This has already been applied successfully in case of measurements of phenol at the LT-CFB on Risø Campus (see Fig.3). The measured peaks coincide and the relative peak heights at 275 nm show a good agreement between laboratory and real application. Here, it could also be shown, that the actual amount of phenol in the producer gas was significantly higher than measurements with traditional methods (sampling, GC-MS) suggested.

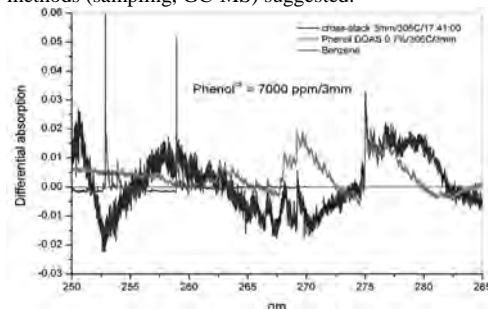


**Figure 3:** Differential absorption cross section of phenol measured in the laboratory (red) and at the gasifier (blue).

## Conclusion and future goals

An UV database for various compounds at different temperatures has been build-up and the results have been or will soon be published in scientific journals. Besides this, the results have been applied on first measurements at a pilot-scale gasifier. In the future, the IR database has to be build-up and more measurements on the gasifier with a high resolution FTIR spectrometer have to be made.

## Acknowledgements

Project acknowledgments to Energinet.dk Project Nr. 2011-1-10622.

## References

1. R. Ma, R. M. Felder, J. K. Ferrell, Ind. & Eng. Chem. Res., 28 (1) (1989) 27-33
2. P. Ståhlberg, M. Lappi, E. Kurkela, P. Simell, P. Oesch, M. Nieminen, Sampling of contaminants from product gases of biomass gasifiers, Research Notes 1903, VTT Energy, 1998
3. H. Grosch, A. Fateev, K.L. Nielsen, S. Clausen, J. of Quant. Spect. & Rad. Trans. 130 (2013) 392-399.



**Maria Gundersen**

Phone: +45 4525 2926  
E-mail: mgun@kt.dtu.dk

Supervisors: John M Woodley  
Nicolas von Solms

PhD Study

Started: September 2013  
To be completed: September 2016

## Evaluating Enzymatically Assisted CO<sub>2</sub> Removal from Flue-Gas with Carbonic Anhydrase

### Abstract

Atmospheric CO<sub>2</sub> is one of the leading causes of global warming. Therefore the restriction of CO<sub>2</sub> released into the atmosphere is an urgent issue of great importance. Here we focus on using enzyme assisted technologies for CO<sub>2</sub> removal from flue-gas, one of the leading contributors towards greenhouse gasses. Here we aim to optimize the technology solvent scrubbing, by facilitating the issue of new energy efficient solvents on an industrial scale, by enzyme activation.

### Introduction

It is well established that greenhouse gasses are a major contributor towards climate change. This is an urgent issue to address, as studies have shown that even with today's level of CO<sub>2</sub> in the atmosphere, these changes may jeopardize human viability on the planet [1]. About 40% of CO<sub>2</sub> from fossil fuel related emissions originate from coal-fired power plants [2].

The leading technology for CO<sub>2</sub> removal from flue-gas is amine scrubbing. Here amine solvents with a high capture capacity are used to remove CO<sub>2</sub> from the gas at relatively low temperatures in an absorption unit. The highly loaded solvent is then transferred to a desorption unit, where the CO<sub>2</sub> is removed by heating (Figure 1). A limitation of this technology is the solvents used. They are often simple affordable amines, which have a high capacity for absorption, as the CO<sub>2</sub> tightly binds to the solvent, such as monoethanolamine (MEA). However this strong association means that a high amount of energy (high temperatures) must be employed desorb the CO<sub>2</sub>. In addition solvents like MEA carry several other unfavourable properties: They are associated with solvent degradation losses through evaporation and they are corrosive in the presence on oxygen, thus causing damage to the equipment [3]. Especially the high temperatures required are problematic in this setting, because of the large carbon footprint, the very issue this technology is aiming to solve.

Our aim is to facilitate more energy efficient carbon capture by enabling the use of new solvents through enzyme assisted technologies.

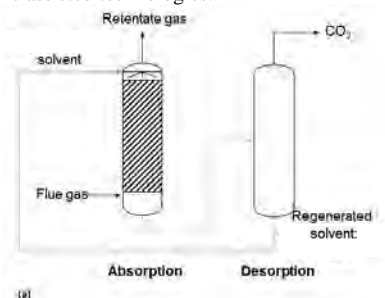


**Figure 1:** Example of an amine scrubbing unit, used for capturing CO<sub>2</sub> from flue-gas.

Biocatalysis is the use of biological materials to produce chemical products, and has been around for millennia in the form of brewing [4]. Today it offers a wide range of new catalytic options for industrial applications [5]. Enzymes are now extensively applied in many processes for single step conversions [6]. Furthermore, new opportunities are arising in enzymatic removal of toxic or harmful substances, where the exquisite selectivity and activity of enzymes at low concentrations are utilized. CO<sub>2</sub> removal from flue-gas is such a problem.

## Specific Objectives

In collaboration with the world leading enzyme producer Novozymes A/S, we are aiming to use enzymes to enhance carbon capture, where solvents with a slow absorption rate will be assisted by enzyme technology, to load faster and reach higher loading and therefore function better under the absorption step. Specifically, the enzyme Carbonic Anhydrase (CA) hydrates CO<sub>2</sub> to bicarbonates, which in turn then will associate with the solvent. In fact the CA is one of the fastest known catalysts, with a reaction rate close to 10<sup>6</sup>/s [2]. We therefore believe that even present in small quantities it can make great improvements in absorption rate. By enabling the use of solvents which are more energy efficient in the desorption step it leads to increased overall energy efficiency (Figure 2). Thus, facilitating increased use of carbon capture technologies. Enzyme assisted CO<sub>2</sub> capture technology has previously shown great potential, but has yet to be fully developed [2]. The implementation of this technology is part of a wider EC funded project (INTERACT) [7] we will focus on evaluation and implementation of this technology in relation to other technologies developed by the project partners for removal of CO<sub>2</sub> from flue-gas.

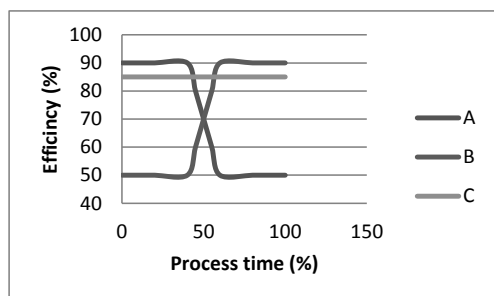


**Figure 2:** Relative efficiency of CO<sub>2</sub> capturing solvents during the process cycle. A high efficiency means that the solvent is optimal for this step of the process. A) Simple solvents like MEA, has a high loading capacity but also requires high energy input during desorption. The solvent is therefore optimal for the first phase of the process but suboptimal for the second step. B) Complex solvents have lower loading capacity, but lower energy requirements for stripping. Thus, is suboptimal for phase one and optimal for phase two of the process. C) Expected result for enzyme assisted technologies, with high loading capacity and low energy required for stripping, therefore an optimal solvent for the entire process.

## Conclusions

We offer here a promising solution to an increasingly pressing problem, namely reduction of CO<sub>2</sub> from the atmosphere. Which is one of the major contributors to atmospheric CO<sub>2</sub> and global warming. We believe that

enzyme assisted technologies have the potential to greatly improve CO<sub>2</sub> removal from flue-gas, by lowering the energy penalty for solvent regeneration. Thus, it reduces both the carbon footprint and the operating cost.

## Acknowledgements

The research leading to these results has received funding from the European Union Seventh Framework Programme FP7/2007-2013 under grant agreement n°608535.

## References

1. J. Rockström, et al. *Ecol. Soc.* 14, (2009).
2. C.K. Savile, J.J. Lalonde, *Curr. Opin. Biotechnol.* 22 (2011) 818–823.
3. R.J. Hook, *Ind. Eng. Chem. Res.* 36 (1997) 1779–1790.
4. F.G. Meussdoerffer, *A Comprehensive History of Beer Brewing*, Royal Society of Chemistry, Cornwall, UK, 2009.
5. U.T. Bornscheuer, et al. *Nature* 485 (2012) 185–194
6. J.M. Woodley, *Trend. Biotechnol.* 26 (2008) 321–327
7. <http://www.interact-co2.eu>





**Jon Trifol Guzmán**

Phone: +45 4525 6196  
E-mail: jotg@kt.dtu.dk

Supervisors: Ole Hassager  
Anders Egede Daugaard  
Peter Szabo

PhD Study  
Started: September 2012  
To be completed: August 2015

## **Novel Clay/Nanocellulose Biocomposite Films and Coatings in the Context of New Packaging Materials**

### **Abstract**

During recent years several efforts have been made into bio-based and renewable resources. Among all the resources the packaging and more specifically the packaging for food application has started to awake the interest of the scientific community. Although currently there are biopolymers available at the market, there is still some work to do in the optimization of some technical properties, such as mechanical properties and barrier properties. The addition of novel nanoreinforcements as nanocellulose, cellulose nanofibers or whiskers, organically modified layered silicates or other kind of nanoreinforcements could promote the properties of the biopolymer enough to have the right technical parameter for this application.

### **Introduction**

The use of petrol-based products for packaging applications represents a serious global environmental problem, not only from the point of view of the raw material but also due to the lack of biodegradability of the most part of the petrol-based products. In recent years novel bio-based materials have been exploited to develop edible and biodegradable materials.

However, the use of edible and biodegradable polymers as PLA has been limited because of challenges related to material performance (such as brittleness, poor gas and moisture barrier), processing (such as low heat distortion temperature) and cost<sup>1</sup>. The addition of some nanoreinforcements such as nanocellulose<sup>2</sup>, nanoclays<sup>3</sup> and others<sup>4</sup> could possibly enhance enough the biomaterials properties for these applications. Nowadays a big effort is being made into the field of reinforced composites for food packaging applications<sup>5</sup>

During recent years several researches into cellulose nanofibers reinforced polymers have been done<sup>6</sup>. There are several publications reporting the influence of the nanocellulose into the mechanical properties of the polymers<sup>7,8</sup>. Apart from the mechanical properties an improvement on barrier properties has been reported<sup>9</sup>. There is no uniformity of results in cellulose nanofibers based composites since there are several factors which can affect the result of the composites: a) the aspect ratio and nature of the cellulose nanofiber, b) the

compatibility, dispersion and load of the reinforcing agent and c) the nature of the matrix, among others.

The first nanoclay composite was obtained by Toyota in 1993<sup>10</sup> but improvement in nanocomposite properties has not been reported until 2002<sup>11</sup>. The addition of small amounts of nanoclays in the polymeric matrix has been reported to improve some properties<sup>12</sup> such as the barrier properties (up to 60%<sup>13</sup>), mechanical properties<sup>14</sup> especially at low clay loading that also gives fire retardant behavior. The barrier properties especially for oxygen are key parameters to develop edible films for food packaging applications since the permeability to oxygen is related to the shelf life of the food.

Recently novel nanoclay/nanofibers nanopapers have been developed which are reported to have great mechanical and gas barrier properties<sup>15</sup>. This material has been reported to have fire retardant effect<sup>16</sup>.

### **Specific Objectives**

The research will be focused on the development of nanoclay/nanofiber reinforced films for food packaging applications. The cellulose nanofibers could enhance the mechanical properties of the films meanwhile the nanoclays could improve the barrier properties.

### **Results**

First a DSC test was performed to study the crystallinity of the nanocomposites. The crystallinity is a parameter

which might play a very important role in some properties such as mechanical and barrier properties, hence a very important parameter to study.

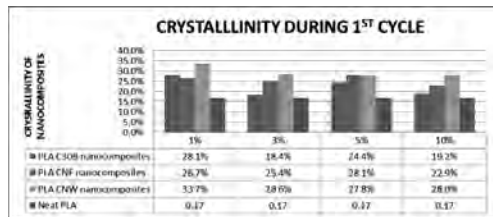


**Figure 1:** Crystallinity of the films. 1st heating cycle of DSC

The main conclusion is that always the CNW (nanocrystalline cellulose) based nanocomposites showed a higher degree of crystallinity than the CNF (cellulose nanofibers) and both of them have higher crystallinity than the clay based composites. This really does not mean that the clays are worse nucleating agent that the cellulose based nanoparticles, since here the processing method has a very critical influence, and the processing method has not been the same for all of the composites. Instead an optimized method for each of nanofiller has been used.

Something to remark is that the 5% load nanocomposites have the same crystallinity, so is a good point to compare the barrier properties of the single nanofiller composite.

The crystallinity is suspected to have a very important role in crystallinity since the crystalline domains are almost impermeable, so, a small amorphous phase will lead to a very high tortuous path for the molecules, which will cause a delay which could explain the behaviour on mass transport in the nanocomposite.

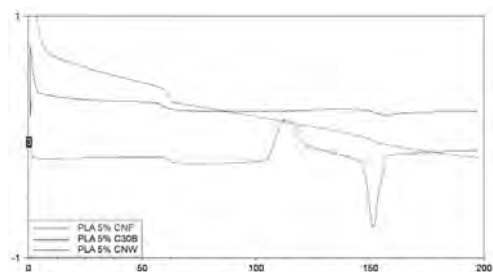


**Figure 2:** Crystallinity of the films. 2nd heating cycle of DSC

The 2<sup>nd</sup> heating cycle of the DSC is more comparable than the 1<sup>st</sup> heating cycle since all of the thermal history of the sample is removed. Here it can be seen that the cellulose nanocrystals look to be a very good nucleating agents, since a crystallization peak appears during 2<sup>nd</sup> heating something that is hard to see in clay and CNF based nanocomposites. This does not really necessarily

means that the CNW are better nucleating agent, since for that further studies should be carried.

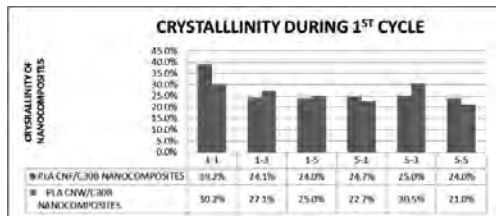


**Figure 3:** Crystallinity of the films. 1st heating cycle of DSC)

In the case of the hybrid composites, the CNF/C30B at 1%/1% load, is observed a very high crystallinity, which might be difficult to explain. But all of the other composites shows a crystallinity around 25% which makes very easy to compare them especially on terms of barrier properties.

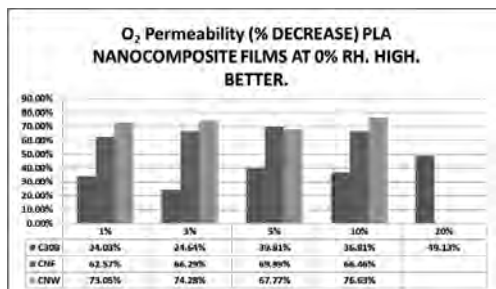


**Figure 4:** Improvement on oxygen barrier properties. (Higher the better, positive: improvement on barrier properties respect PLA, 100% completely impermeable barrier).

The Oxygen permeability test shows an unexpected result. The cellulose based nanocomposites have a bigger improvement on barrier properties than clay based nanocomposites. After looking at the literature in the most part of the articles shows a slight increase/decrease, but, very few one speak about a big increase on the barrier properties. The fact here is to achieve a very nice dispersion of the nanocomposite, reason for which the DMF and not the DCM was used as solvent.

The role of the crystallinity anyway is not completely clear in this case. All of the composites at 5% shows more or less the same crystallinity, but the point here is that this does not tell us the whole history since other parameters as spherulites shape, size, allomorphic phase, distribution, location ... and so on are parameters that they are currently under research.

Something interesting for these properties was to see if the clay addition to the cellulose based nanocomposites could enhance or decrease the barrier properties of the nanocomposite.

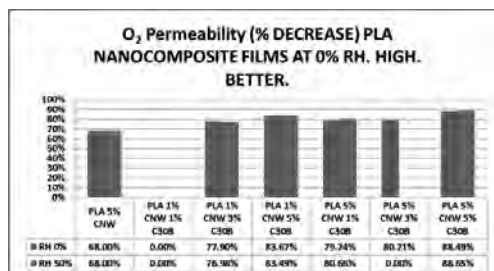


**Figure 5:** Improvement on oxygen barrier properties. (Higher the better, positive: improvement on barrier properties respect PLA, 100% completely impermeable barrier).

It can be seen clearly that the addition of clays enhance the barrier properties, thanks to a synergistic addition. The reason of this synergistic effect is currently under research, but what could happen is that the clay, which main reason to increase barrier properties is enhancing the tortuous path of the molecules, can be kept into the cellulose nanofiber network, “closing” the holes of this network.

A point to be raise here is that the PLA/clay based composites was made using DCM as solvent. An the rest of the nanocomposites were made using DMF. The point here is how we should compare all of the nanocomposites, with the same processing method, or with the best processing method for each of them. To our understanding, the best option is the second one. For that reason we could not compare directly these results of hybrid nanocomposites with the hybrid one, but, fortunately there is quite a literature about PLA/clay nanocomposites, and for a simple solvent casting method it is hard to find an improvement on barrier properties higher than 60%. For PLA/C30B, the clay used in our experiments, the main improvement is about 35 ~ 40 %.

So we can think that these composites in terms of oxygen barrier properties shows a simple synergistic behavior.

The food packaging requires protection against food and water, so the water permeability was also tested.

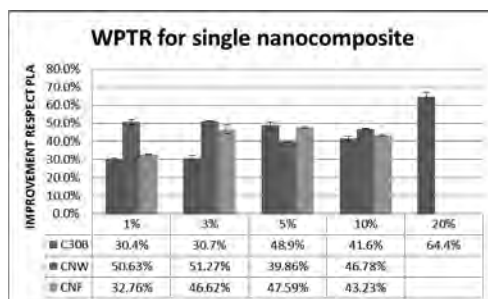


**Figure 6:** Improvement on water vapor barrier properties. (Higher the better, positive: improvement on barrier properties respect PLA, 100% completely impermeable barrier).

In this case the improvement of the cellulose based nanocomposites, was smaller compared with oxygen meanwhile the clay performance was better than for oxygen. The fact here is that the permeability is a mass transport process which is governed by diffusivity and solubility. The cellulose based nanoparticles are very hydrophilic, meanwhile the C30B it is not. The clays are hydrophilic but in this case this clay was grafted with tetraalkyl ammonium chain, which made it hydrophobic. So, a different behavior on the barrier properties was expected.

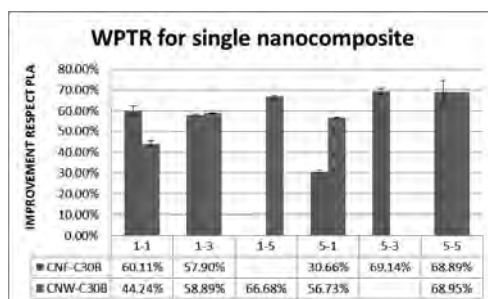


**Figure 7:** Improvement on water vapor barrier properties. (Higher the better, positive: improvement on barrier properties respect PLA, 100% completely impermeable barrier).

In the case of the hybrid nanocomposites, the performance is worse than for oxygen barrier properties, but still, the effect of clay and nanofiber and crystals is also synergistic. The CNF/C30B nanocomposite shows a much better barrier properties than CNW/C30B but this might be attributed to the higher crystallinity of this film respect the CNW based one.

### Conclusions

Although nowadays the use of biopolymers for food packaging applications has some difficulties for some

technical parameters, the addition of nanofillers can enhance the properties, especially barrier properties, of these bio based materials enough to be able to be used in this application.

### Acknowledgements

The author wants to thank the Marie Curie Initial Training Network for funding the research. The PhD fellow is very grateful to Professor Iñaki Mondragón Egaña whom dedication to science during his life is an example for everybody.

1.Madhavan Nampoothiri, K., Nair, N. R., & John, R. P. (2010). An overview of the recent developments in polylactide (PLA) research. *Bioresource technology*, 101(22), 8493–501. doi:10.1016/j.biortech.2010.05.092

2.Eichhorn, S. J., Dufresne, a., Aranguren, M., Marcovich, N. E., Capadona, J. R., Rowan, S. J., Weder, C., et al. (2009). Review: current international research into cellulose nanofibres and nanocomposites. *Journal of Materials Science* (Vol. 45, pp. 1–33). doi:10.1007/s10853-009-3874-0

3.Sinha Ray, S., & Okamoto, M. (2003). Polymer/layered silicate nanocomposites: a review from preparation to processing. *Progress in Polymer Science*, 28(11), 1539–1641. doi:10.1016/j.progpolymsci.2003.08.002

4.Aider, M. (2010). Chitosan application for active bio-based films production and potential in the food industry: Review. *LWT - Food Science and Technology*, 43(6), 837–842. doi:10.1016/j.lwt.2010.01.021

5.Azeredo, H. M. C. D. (2009). Nanocomposites for food packaging applications. *Food Research International*, 42(9), 1240–1253. doi:10.1016/j.foodres.2009.03.019

6.Abdul Khalil, H. P. S., Bhat, a. H., & Ireana Yusra, a. F. (2012). Green composites from sustainable cellulose nanofibrils: A review. *Carbohydrate Polymers*, 87(2), 963–979. doi:10.1016/j.carbpol.2011.08.078

7.Kowalczyk, M., Piorkowska, E., Kulpinski, P., & Pracella, M. (2011). Mechanical and thermal properties of PLA composites with cellulose nanofibers and standard size fibers. *Composites Part A: Applied Science and Manufacturing*, 42(10), 1509–1514. doi:10.1016/j.compositesa.2011.07.003

8.Liu, D. Y. (2009). Characterisation of solution cast cellulose nanofibre - reinforced poly(lactic acid). *eXPRESS Polymer Letters*, 4(1), 26–31. doi:10.3144/expresspolymlett.2010.5

9.Lavoine, N., Desloges, I., Dufresne, A., & Bras, J. (2012). Microfibrillated cellulose - its barrier properties and applications in cellulosic materials: a review.

*Carbohydrate polymers*, 90(2), 735–64. doi:10.1016/j.carbpol.2012.05.026

10.Kojima, Y., Usuki, A., Kawasumi, M., Okada, A., Kurauchi, T. and Kamigaito, O. (1993). One-pot synthesis of nylon 6–clay hybrid. *J. Polym. Sci. A Polym. Chem.*, 31: 1755–1758. doi: 10.1002/pola.1993.080310714

11.Sinha Ray, S., Maiti, P., Okamoto, M., Yamada, K., & Ueda, K. (2002). New Polylactide/Layered Silicate Nanocomposites. 1. Preparation, Characterization, and Properties. *Macromolecules*, 35(8), 3104–3110. doi:10.1021/ma011613e

12.Alexandre, M., & Dubois, P. (2000). Polymer-layered silicate nanocomposites: preparation , properties and uses of a new class of materials, 28(March), 1–63.

13.Svagan, A. J., Åkesson, A., Cárdenas, M., Bulut, S., Knudsen, J. C., Risbo, J., & Plackett, D. (2012). Transparent films based on PLA and montmorillonite with tunable oxygen barrier properties. *Biomacromolecules*, 13(2), 397–405. doi:10.1021/bm201438m

14.Sengupta, R., Chakraborty, S., Bandyopadhyay, S., Dasgupta, S., Mukhopadhyay, R., Auddy, K., & Deuri, A. S. (2007). A Short Review on Rubber / Clay Nanocomposites With Emphasis on Mechanical Properties, 21–25. doi:10.1002/pen

15.Wu, C.-N., Saito, T., Fujisawa, S., Fukuzumi, H., & Isogai, A. (2012). Ultrastrong and high gas-barrier nanocellulose/clay-layered composites. *Biomacromolecules*, 13(6), 1927–32. doi:10.1021/bm300465d

16.Liu, A., Walther, A., Ikkala, O., Belova, L., & Berglund, L. a. (2011). Clay nanopaper with tough cellulose nanofiber matrix for fire retardancy and gas barrier functions. *Biomacromolecules*, 12(3), 633–41. doi:10.1021/bm101296z

**Timo Hagemann**

Phone: +45 30 77 14 20  
E-mail: timoh@kt.dtu.dk

Supervisors: Krist V. Gernaey  
Ulrich Krühne  
Stuart Stocks (Novozymes A/S)

PhD Study (with Novozymes A/S)

Started: November 2013

To be completed: November 2016

## **Exploiting *Aspergillus niger* Pelleting Behavior for Morphology Control in Order to Correlate it to Productivity in Industrial Fermentation**

### **Abstract**

The existence of a company like Novozymes A/S demonstrates the added value that can be obtained by production of enzymes with *Aspergillus niger*. Deeper knowledge about its behavior is of interest though. The aim of this project is therefore to follow the particle size development of the biomass, beginning with spores and up to fully mature biomass. With manipulations of the fungus (fermentation) environment in terms of ion strength, pH value and mechanical power input by agitation as well as aeration and back pressure, the biomass configuration will be designed with the aim of finding an answer to the question of how important the morphology is for productivity in an industrial strain.

### **Introduction**

This PhD project is done in cooperation between the DTU and Novozymes A/S. The work is a continuation of academic work that has been started as part of an employment at the Institute of Biochemical Engineering at the Technische Universität Braunschweig. This project will build on the findings of this previous work, with the final goal of answering a question that is important both from an industrial and an academic point of view.

The academic strain *Aspergillus niger* AB1.13 [1] was researched during this first part of the project. Along with the common fermentation analysis, like biomass and metabolites, online laser diffraction analysis was the main means to follow biomass development under specific fermentation conditions. On the basis of the different factors that were varied in the fermentations, one important result is that the biomass reaction can be predicted in order to design the amount and the state of the biomass and the respective expected particle size for future fermentations with *Aspergillus niger* AB1.13.

The latter is important in order to keep the broth's rheology in control in order to keep the OTR in the fermentation at the desired/highest possible level, for example in a seed tank. In this way, the subsequent main fermenter can be optimized in terms of biomass morphology and/or productivity.

Additional experiments have already been conducted at Novozymes pilot plant as a design of experiment set

up to investigate the influence of power input by agitation as well as back pressure and aeration on particle size development and productivity of an industrial *Aspergillus niger* strain. With the particle size distributions as linking factor, a model should now be established for precise predictions of biomass behavior/productivity. This will be verified with additional fermentations in a final screening design in order to connect a chosen morphology with the productivity of an industrial strain.

### **Methods**

The results from the previous work were mainly achieved by introducing step changes to the fermentation system. The biggest contribution to manipulating the morphology at the onset of the fermentation directly after inoculation is the pH of the broth: Cultivations were started with non-aggregating behavior resulted by maintaining a pH of 3, and were then later shifted to aggregating conditions by changing the pH set point to 5.5.

Besides the normal sampling for HPLC and biomass determination, a Malvern MasterSizer 2000 was installed in a bypass to a 2 L fermenter. Measurements were taken every five minutes over a time frame of 20 h. The resulting particle size distributions were split into the volume shares of spores only and biomass aggregates (later pellets) (see fig. 1) to differentiate between particle size growth due to aggregation and biomass growth.

## Results and Discussion

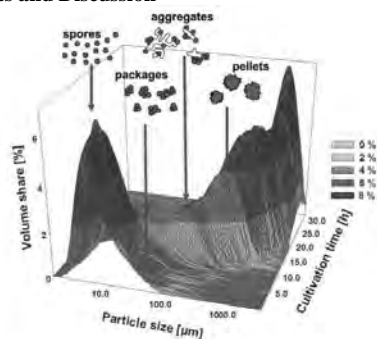


**Figure 1:** Display of the volume share (Y-axis) over the particle size class (X-axis) during the course of the fermentation (Z-axis): At time = 0, i.e. at the start of the fermentation, only spores can be detected with laser diffraction while at time = 8 h and with a pH of 5.5 in the broth, spore packages can be seen. Aggregates consisting of hyphae and spores are detected after growth began.

The split of volume shares of different particle classes allows tracking the spore development.

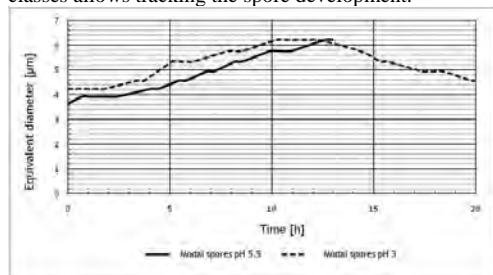


**Figure 2:** Particle size of mode of spores over time at different inoculation pH: At pH 5.5, the spores are smaller compared to the ones at pH 3 and after 12-13 h, they are completely aggregated towards growing biomass (hence no longer detectable).

Measurements show that *A. niger* spores desorb melanin at a pH around 5-6. That could mean that a sterical hindrance for aggregation is removed. Also, the surface charge of the biomass is altered by changing the pH, which can be seen by performing zeta-potential measurements.

As a consequence, changing pH can be used to alter aggregation. Fig. 3 displays the results of different long durations of the shifts which each started at 8 h. Fermentations started with pH 5.5 were the first to show aggregates and the first when the aggregate mode dominates the measured particle sizes. With longer pH shift durations, the detectability of aggregates and them dominating the particle distribution is postponed and the resulting particle size is smaller.

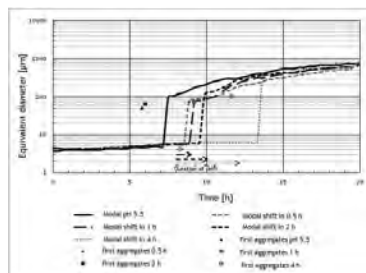


**Figure 3:** Display of particle sizes of the modes over time; during the first hours, spores form the majority of measured particles. The “jump” in particle size indicates the point in time when biomass aggregates form the majority. The single dots mark their first appearance.

## Conclusions

Spore aggregations can take place at the onset of the cultivation and it is dependent on particle concentration, the power input, the ion strength and the pH of the broth [2,3]. This study showed thus far that pH is the most powerful handle at the beginning of a batch: Spores clinging together can be prevented and/or employed to design the basis for a later pellet. Prolonging the pH shift duration from non to aggregating conditions resulted in later aggregate formation with a smaller overall particle size compared to faster shifts.

## Publications

None yet.

## Acknowledgements

The presented results were achieved through research at the Technische Universität Braunschweig and were funded by the German Research Foundation via the “SFB578” [4].

## References

1. I. E. Mattern, J.M. van Noort, P. van den Berg, D.B. Arbacher, I.N. Roberts, C.A.M.J.J. van den Hondel, Isolation and characterization of mutants of *Aspergillus niger* deficient in extracellular proteases, *Molecular Genetics and Genomics* 234 (1992) 332-336.
2. L.H. Grimm, S. Kelly, J. Hengstler, A. Göbel, R. Krull, D.C. Hempel, Kinetic studies on the aggregation of *Aspergillus niger* conidia, *Biotechnology and Bioengineering* 87/2 (2004) 213-218.
3. A. Wargenau, A. Kwade, Determination of adhesion between single *Aspergillus niger* spores in aqueous solutions using an atomic force microscope, *Langmuir* 26/13 (2010) 11071-11076.
4. C. Wittmann, D. Jahn, R. Krull, From gene to product - Development of biotechnological processes by integrating genetic and engineering methods, Cuvillier Verlag, Göttingen, Germany, 2012.

**Amalia Halim**

Phone: +45 4525 2892  
E-mail: amah@kt.dtu.dk

Supervisors: Alexander Shapiro  
Sidsel M. Nielsen  
Anna E. Lantz, DTU Systems Biology

**PhD Study**

Started: February 2012  
To be completed: January 2015

## Microbial Enhanced Oil Recovery for North Sea Oil Reservoir

**Abstract**

Some microorganisms living in petroleum reservoirs produce substances like gases, surfactants, polymers and/or acids, facilitating enhanced oil recovery (EOR). Therefore, selective stimulation of certain microbial species may be an inexpensive method for additional oil recovery. In addition, microbes can selectively plug reservoir formation, thus divert the flow of the injected water into regions of the reservoir with low permeability-high oil saturations. However, plugging effect by bacteria may also cause reduction in reservoir formation permeability. The first experimental study focused on bacteria penetration in core plug samples to understand how deep bacteria can travel through porous media and the effect of bacterial plugging.

**Introduction**

It was credited to Beckman in 1926, who found that microorganism could be used to release oil from porous media [1]. Numerous mechanisms have been proposed in the literature through which microorganism can be used for enhanced oil recovery process [1]. However, the mechanism are poorly understood and the effectiveness of each mechanism for different reservoir parameters is also unknown [2, 3]. Recent publications on the bacteria-fluid-porous media interaction classified the mechanisms into two broad categories: 1) alteration of oil/water/rock interfacial properties and/or wettability [2-5], 2) changes in flow behaviour due to bioclogging or selective plugging [2-4, 6]. The initial study focused on bacteria penetration as the North Sea chalk reservoir formation has relatively small size of pore throats, which is almost comparable with the bacteria cell size. The plugging effect caused by bacteria is also investigated by monitoring the pressure during bacteria injection.

**Specific Objectives**

The main goal of the project is to understand the factors that influence the growth, propagation, and movement of bacteria within porous formations; and how this may aid in improving oil production.

The preliminary test focused on core flooding experiment to investigate whether bacteria can pass through the porous media and the mechanism of the bacteria movement within porous media. Two bacteria species, *Bacillus licheniformis* 421 and *Pseudomonas*

*putida* K12, representing spore forming and non-spore forming bacteria, were used for this purpose.

**Experimental Work**

Each individual core was then cleaned by flooding with toluene and absolute ethanol to remove any organic material inside the core. After cleaning, the core was dried in the oven at 80°C overnight. The dry weight and wet weight were measured in an analytical balance to calculate core porosity. The dry core was assembled in sterile Hassler core holder. Approximately 7 pore volume (PV) of 75% ethanol were injected in order to sterilize the core plug. The saturated 75% ethanol core was left overnight inside the core holder. The core was then flooded with sterile 7 PV MQ water to displace the 75% ethanol and the effluent was collected every PV to cross check for possible contamination. Injection pressure and pressure difference were monitored throughout this process. The recorded pressure difference during MQ flooding was used to calculate initial permeability using Darcy's Law. The core was injected with bacteria inoculum in synthetic seawater (SS) media. Various bacteria concentrations were tested to see the plugging effect of the bacteria. The effluent was collected every PV for bacteria enumeration. An illustration of core flooding experiment is depicted in figure 1

*Inoculum preparation and bacteria enumeration*

The bacteria inoculum were grown in the enrichment media for 24 hours then diluted with 0.85% NaCl. The optical density (OD) of the bacteria solution was

adjusted to the desired value at the wave length 600 nm using a spectrophotometer. Approximately 10% (v/v) bacteria solution was inoculated into SS media for core flooding experiment. The bacteria and SS media were homogenized by a vortex for 3 minutes. Bacteria

enumeration was conducted by serial dilution plate method using enrichment media. In addition, the effluent was also analyzed under fluorescence microscopy. The effluent was subject to 4',6-diamidino-2-phenylindole (DAPI) staining.

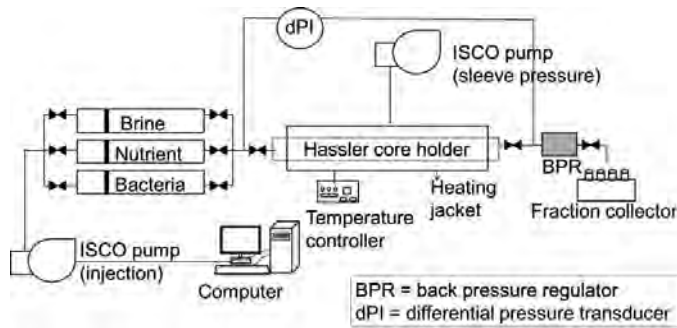


**Figure 1.** Core flooding experiment

### Result and Discussion

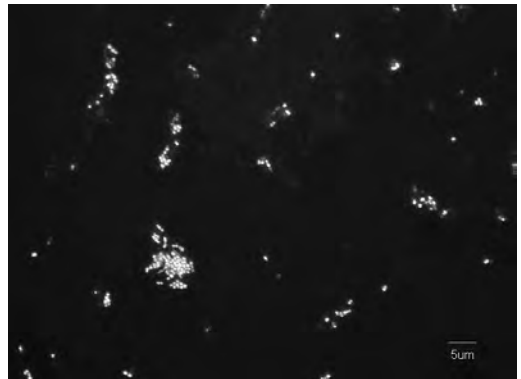
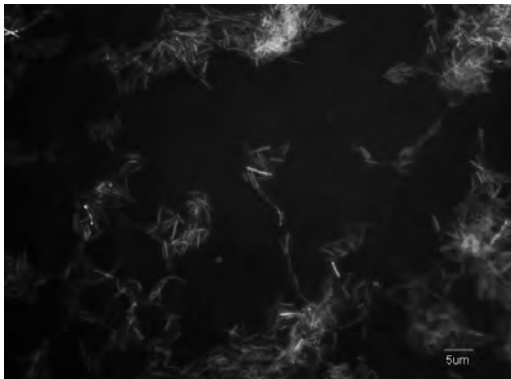


**Figure 2.** *B. licheniformis* 421 cells under DAPI staining (a) before injection into a chalk core plug, cell size  $0.5 \times 3\mu\text{m}$  (b) in the effluent from a chalk core plug, spore formation

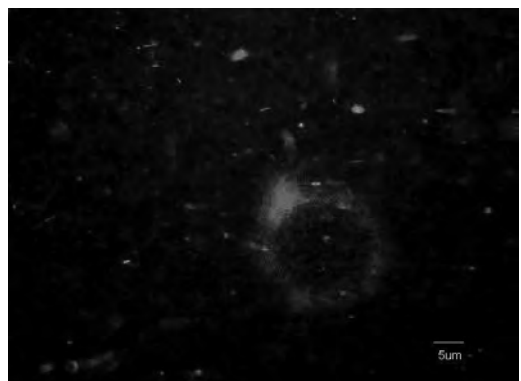
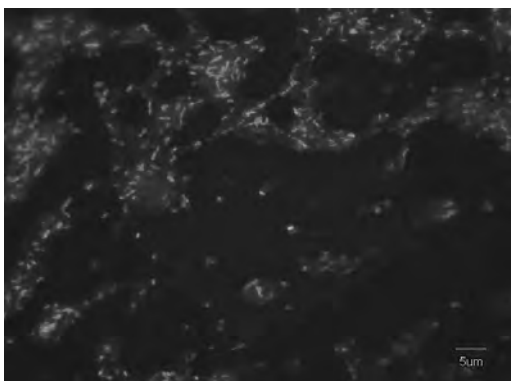


**Figure 3.** *P. putida* K12 cells under DAPI staining (c) before injection into chalk core plug cell size  $0.5 \times 1.5 \mu\text{m}$ , (d) in the effluent from a chalk core plug, some cells were slightly elongated and slender



Our results showed that both bacteria types were able to penetrate through the cores, even when the core permeability was below 4 mD and the mean values of the pore throat sizes were approximately 0.5  $\mu\text{m}$  [7], which is comparable to the sizes of the specific bacterial strains used in this study. This means that the 1/3 – 1/7 rule commonly used for straining [8] is not applicable for bacteria penetration, since bacteria are not rigid as particles. Photos of the bacterial cells are shown in growth media and in the effluent in Fig. 2 and Fig. 3. It can be seen from the sizes and the shape that the bacteria injected into the core were in form of vegetative cells for both *B. licheniformis* 421 and *P. putida* K12. The vegetative *B. licheniformis* 421 had an approximate cell size of 0.5  $\mu\text{m}$  in diameter and 2-4  $\mu\text{m}$  in length (Fig. 2a). In the collected effluent after injection, no vegetative cells were seen when samples from *B. licheniformis* 421 experiments were investigated in microscope. Instead, small round particles with a size of approximately 0.5  $\mu\text{m}$  were found, which are likely to be spores (Fig. 2b). The vegetative *P. putida* K12 in the growth media had an approximate cell size 0.5  $\mu\text{m}$  in diameter and 1-2  $\mu\text{m}$  in length (Fig. 3a). In the effluent after injection, exposure to high salinity and high pressure, the *P. putida* K12 became slender (Fig. 3b).

To evaluate to what extent bacteria can penetrate chalk rock, the total number of bacterial cells passing through the cores (bacteria breakthrough concentration) was determined. An initial *B. licheniformis* 421 concentration of  $3.8 \times 10^7$  cfu/ml in the injected inoculum resulted in concentration in the order of  $10^1$  cfu/ml in the effluent (Fig. 4, core 10). These were much lower than the concentrations in the order of  $10^4$ - $10^6$  cfu/ml obtained in the effluents, when an inoculum with bacterial cell concentration of  $8.8 \times 10^7$  cfu/ml was injected (Fig. 4, core 2). After 12 days of incubation without extra addition of nutrients, an increase in cell numbers in the effluents compared to before incubation was detected.

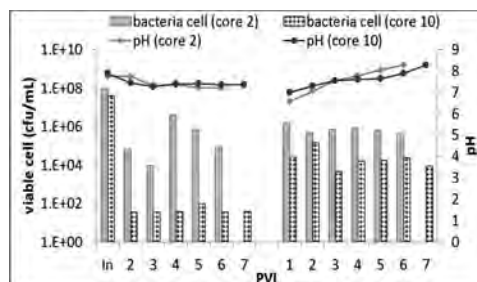


**Figure 4.** Viable *B. licheniformis* 421 cells detected in the effluent during injection of bacteria suspension (left) and after 12 days of incubation (right) of the core 2 and core 10. The injection and incubation were conducted at 50°C. (In: concentration of injected bacteria/inoculum)

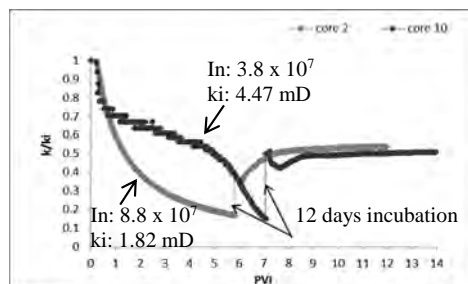


**Figure 5.** Permeability changes by *B. licheniformis* 421 during injection of bacteria suspension and after 12 days of incubation of the core 2 and core 10. The injection and incubation were conducted at 50°C. (In: bacteria inoculum in cfu/ml; ki : initial permeability).

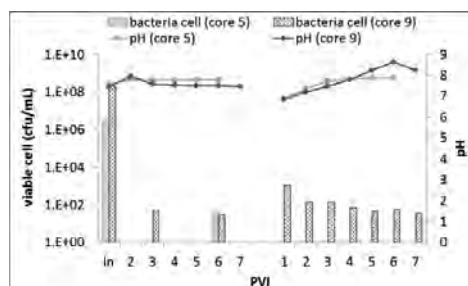


**Figure 6.** Viable *P. putida* K12 cells detected in the effluent during injection of bacteria suspension (left) and after 12 days of incubation (right) of the core 5 and core 9. The injection and incubation were conducted at 50°C. (In: concentration of injected bacteria/inoculum)

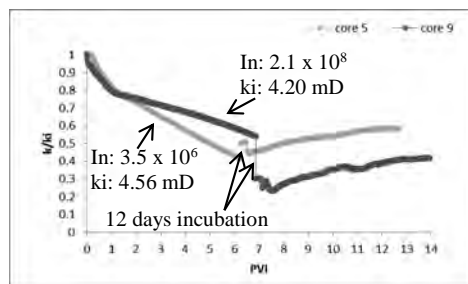


**Figure 7.** Permeability changes by *P. putida* K12 during injection of bacteria suspension and after 12 days of incubation of the core 5 and core 9. The injection and incubation were conducted at 50°C. (In: bacteria inoculum in cfu/ml; ki: initial permeability)

Penetration behavior of the *P. putida* K12 was a function of the inoculum concentration with a higher amount of cells detected in the effluent when higher inoculum concentrations were used (Fig. 6). When the inoculum concentrations were as low as  $3.5 \times 10^6$  cfu/ml, bacterial cells were only detected in one of the effluent fractions collected (Fig. 6, core 5). On

the other hand, when higher inoculum concentrations were used, bacteria were detected in more than one effluent fraction meaning improved penetration of the bacteria (Fig. 6, core 9). In general, the pH of the collected effluents decreased during bacterial injection. This might indicate production of organic acids and/or CO<sub>2</sub> by the bacteria. After 12 days of incubation, the pH of the collected effluents increased. This might be due to release of Ca<sup>2+</sup> ions from the rock.

For all four core flooding experiments the core permeability was reduced continuously in the course of injection; and permeability reduction was influenced by the bacterial inoculum concentration. Fig. 5 shows the effect of *B. licheniformis* 421 injection on the chalk permeability. The injection rate was kept constant, and injection pressure increased, as plugging occurred. Fig. 7 shows the effect of *P. putida* K12 injection on the chalk permeability. In contrast to permeability damage by *B. licheniformis* 421, the permeability reduction by *P. putida* K12 injection occurred at a much slower rate and plugging curve had a different shape. Further SS flooding after 12 days of incubation did not allow permeability to return to the initial value for any of the bacterial strains. This means that bacteria remained trapped inside the core and/or bacterial metabolites might precipitate and cause plugging in some pore channels. In the case of *P. putida* K12 injection, permeability restoration after incubation was lower as the bacterial inoculum concentration increased.

## Conclusions

In this work we have shown that bacteria were able to penetrate and to be transported through the chalk porous rocks even though the permeability is as low as below 4 mD and the pore sizes are comparable to bacterial sizes. The spore-forming *B. licheniformis* 421 predominantly penetrates in form of spores while the *P. putida* K12 penetrate as vegetative cells, however, smaller in size than during normal growth conditions due to the high salinity conditions. The number of cells being able to penetrate the core depended on the bacteria inoculum concentration. The higher the injected inoculum, the higher the number of cells was found in the effluent. Retention of bacteria and, probably, of produced metabolites in the cores caused irreversible permeability damage, which could not be repaired by further brine flooding after a 12-day waiting (no addition of nutrients).

## References

1. Lazar, I., I.G. Petrisor, and T.F. Yen, *Petroleum Science and Technology*, 25 (2007) 1353-1366.
2. Kowalewski, E., I. Rueslåtten, K.H. Steen, G. Bødtker, and O. Torsæter, *Journal of Petroleum Science and Engineering*, 52 (2006) 275-286.

3. Armstrong, R.T. and D. Wildenschild, *Transport in Porous Media*, 92 (3) (2012) 818-835.
4. Afrapoli, M.S., C. Crescente, S. Alipour, and O. Torsæter, *Journal of Petroleum Science and Engineering*, 69 (2009) 255-260.
5. Karimi, M., M. Mahmoodi, A. Niazi, Y. Al-Wahaibi, and S. Ayatollahi, *Colloids and Surfaces B: Biointerfaces*, 95 (2012) 129-136.
6. Afrapoli, M.S., S. Alipour, and O. Torsæter, *Transport in Porous Media*, 90 (2011) 949-964.
7. Tweheyo, M.T., P. Zhang, and T. Austad, *The Effect of Temperature and Potential Determining Ions Present in Seawater Recovery From Fractured Carbonates*, Society of Petroleum Engineers, Tulsa, Oklahoma, 2006
8. van Oort, E., J.F.G. van Velzen, and K. Leerlooijer, *Impairment by Suspended Solids Invasion: Testing and Prediction*, in *SPE Production & Facilities* 1993, Society of Petroleum Engineers. p. 178-184.



## **Zainatul Bahiyah Handani**

Phone: +45 4525 5510  
E-mail: zbha@kt.dtu.dk

Supervisors: Rafiqul Gani  
Gürkan Sin

### **PhD Study**

Started: May 2013  
To be completed: April 2016

## **Synthesis and Design of Integrated Process and Water Networks**

### **Abstract**

A simultaneous synthesis and design of process and water networks is a complex task which involves many decisions making in business and engineering levels. Many alternatives in process and wastewater treatment technologies are available to enable the industrial practitioners to select the optimum technology network in early stage by representing them in a superstructure. In this work, a new systematic framework for synthesis and designing process and water networks for process industries is proposed. A simultaneous optimization approach mathematically combines the problem of process and water networks into a single step. The interaction between two elements in the networks is visualized via selection appropriate technologies and alternatives for process and water treatment.

### **Introduction**

Water is an important substance and is used extensively in the process industries. Water can be supplied as raw material, solvent, cleaning agent or utility (steam and cooling water). Minimization of freshwater consumption and wastewater generation are being critical concerns in process industries due to the rise of freshwater and effluent treatment costs and stringent regulations. Over the last few decades, many synthesis and design techniques have been developed to minimize water consumption and wastewater generation in process industries either using pinch analysis [1-3] or mathematical programming techniques [4-6]. In order to reduce freshwater consumption in the process, wastewater generated from the process or utility could be reused after being treated in the wastewater treatment plant to acceptable limits by using various treatment technologies and alternatives. In addition, different process technologies and design alternatives will also be considered in the processing network to transform raw materials/feedstocks into products/byproducts while reducing freshwater consumption and wastewater generation.

Conventionally, in process synthesis and design, subsystems (eg. water network and heat exchanger network) are dealt and solved sequentially or separately after process flowsheet is being developed [7]. It is important to note that the simultaneous process and water network synthesis is regarded as a difficult and complex task which involves a combination of strategic

decisions (selection of product portfolio, raw materials, process technology and treatment technology) and tactical decisions (considering synthesis, design and optimization of production technology etc.). The aim of this work is to develop a systematic framework using the superstructure - optimization approach for the optimal synthesis and design of processing plant network that connected with water/wastewater treatment network. The strategy accounts explicitly for the interactions between both networks. The optimal raw material, product portfolio, process technology and wastewater treatment strategies as well as material flows can be achieved simultaneously by implementing the systematic approach through interaction between the process and water networks (so called as *a network within a network*). The main advantage of the integrated approach is that it enables the simultaneous synthesis and design of overall systems where water network models will be included within the process models.

### **Objective**

In this PhD project, a generic model-based framework will be developed for integrated analysis of process synthesis and water/wastewater treatment network synthesis problems. The integration of water consumption early at process synthesis and design stage is expected to reduce the consumption of freshwater and reusing more processed water. A systematic approach is used to manage the complexity and solving simultaneously process synthesis and water synthesis

network problem with respect to economics, resources consumption and sustainability. In order to achieve this task optimally and efficiently, a new superstructure will be proposed and formulated for the simultaneous synthesis of the process and water network.

Overall, the main tasks of the PhD-project:

- a) Development of a systematic framework for integrated synthesis and design of process and water networks
- b) Development of library models and database for the assessment of performance of the process and water network
- c) Development of models for the simultaneous synthesis of process and water networks based on the superstructure
- d) Feasibility assessment and comparison of the candidates at their optimality
- e) Application of the optimization models of industrial case studies illustrate the effectiveness of the approach

### Methodology

As a basic formulation processing network, the systematic framework recently developed by Quaglia et al. [8] (Figure 1) will be applied and extended, to enable a simultaneous synthesis of process and water network. The methodology is based on the development and synthesizing of a generic process and water network superstructure involving all design possibilities; its modelling; determining the optimal network from the feasible set generated from the superstructure; and finally, designing and optimizing the final selected network. Since data related to water/wastewater (contaminants concentration, treatment and industrial usage) and process (raw material and product prices, performance of new processes) can be subjected to high levels of uncertainty, hence the effect of these uncertainties on the final design of the network will also be investigated.

The optimization problem will be formulated as Mixed Integer Non Linear Programming (MINLP) and different variations of it. Process synthesis methods based on thermodynamic insights and means-end-analysis will be employed to generate the superstructure process and water network in order to find the optimal network.

### Conclusion

It is expected that a systematic approach is used to manage the complexity and solving simultaneously process synthesis and water synthesis network problem with respect to economics, resources consumption and sustainability. In order to achieve this task optimally and efficiently, a new superstructure is proposed and formulated for the simultaneous synthesis of the process and water network

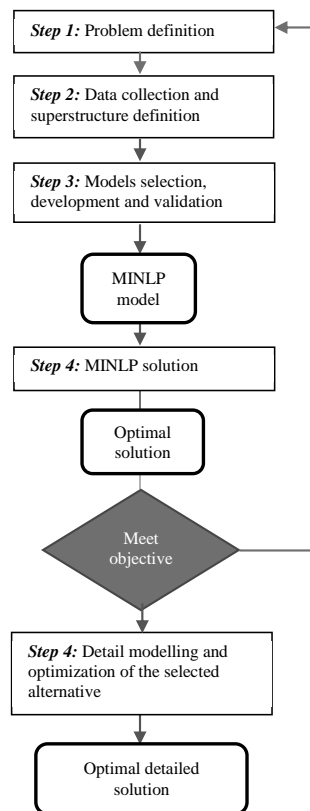


**Figure 1:** Systematic framework for synthesis and design of processing network [8]

### References

- [1] Y.P. Wang, R. Smith. *Chemical Engineering Science*. 49 (1994) 981-1006.
- [2] S.R. Wan Alwi and Z. A. Manan. *Industrial and Engineering Chemistry Research*. 47 (2008) 2762-2777.
- [3] D.C.Y. Foo. *Ind. Eng. Chem. Res.* 5125-5159.
- [4] N. Takama, T. Kuriyama, K. Shikoko, T. Umeda. *Computers and Chemical Engineering*. 4 (1980) 251-258.
- [5] Z. B. Handani, S.R. Wan Alwi, H. Hashim, Z.A. Manan. *Ind. Eng. Chem. Res.* 49 (12) (2010) 5742-5751.
- [6] A. Quaglia, A. Pennati, M. Bogataj, Z. Kravanja, G. Sin, R. Gani. *Ind. Eng. Chem. Res.* [dx.doi.org/10.1021/ie401379](https://doi.org/10.1021/ie401379).
- [7] L. Čuček, M. Martin, I.E. Grossmann, Z. Kravanja. *Computers and Chemical Engineering*. 35 (2011)1547-1557.
- [8] A. Quaglia, B. Sarup, G. Sin, R. Gani. *Computers and Chemical Engineering*. 38 (2012). 213-223.



**Thomas Klint Hansen**

Phone: +45 4525 2952  
E-mail: tkli@kt.dtu.dk

Supervisors: Anker D. Jensen  
Brian B. Hansen  
Ton V.W. Janssens, Haldor Topsøe A/S

PhD Study  
Started: April 2013  
To be completed: March 2016

## Development of New Automotive Diesel Oxidation and NH<sub>3</sub> Slip Catalysts

### Abstract

Catalytic diesel exhaust aftertreatment (DEA) systems are an essential part of emission control from heavy duty diesel (HDD) vehicles. These systems are under constant development in order to meet the stringent emission limits of the Euro VI and future regulations. The focus of this project is the development of a highly selective NH<sub>3</sub> slip catalyst (ASC) and a low cost diesel oxidation catalyst (DOC). A selective ASC could enable the use of higher NH<sub>3</sub> loads in the Selective Catalytic Reduction (SCR) unit and thereby a higher NO<sub>x</sub> removal. The research and development of these units will include optimization of the dual layer ASC design and identification and screening of new formulations. A catalyst testing unit has been prepared for investigation of reaction kinetics and screening of new catalyst formulations.

### Introduction

Heavy duty diesel (HDD) vehicles handle a substantial part of the world's transport and logistics. Harmful pollutants are however formed, such as nitrogen oxides (NO<sub>x</sub>), hydrocarbons (HC), particulate matter (PM), and carbon monoxide (CO). The diesel exhaust aftertreatment (DEA) system has been developed to treat the pollutants in the exhaust gas [1].

Figure 1 illustrates the current standard DEA system consisting of a series of catalytic units. The Diesel Oxidation Catalyst (DOC) oxidizes CO and HC to CO<sub>2</sub> and H<sub>2</sub>O, as well as generates NO<sub>2</sub> from NO. The Diesel Particulate Filter (DPF) is a wall-flow filter, entraining PM in its monolith walls. The DPF can be regenerated actively by increasing the exhaust gas temperature using post-injection of fuel, or passively using a catalyst. NO<sub>2</sub> generated by the DOC also assists regeneration. NO<sub>x</sub> is treated through Selective Catalytic Reduction (SCR) using NH<sub>3</sub> as the reducing agent. NH<sub>3</sub> is supplied to the system through urea dosing, regulated by the onboard Model Predictive Control (MPC) unit. Excess NH<sub>3</sub> is controlled with the Ammonia Slip Catalyst (ASC). Upon exiting the DEA system, the emissions should meet the restrictions imposed by the Euro VI regulations [1].

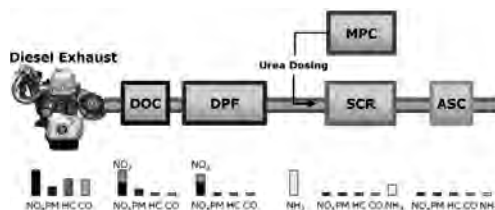


**Figure 1:** Example of a standard design of the DEA system, consisting of the DOC, DPF, SCR component, urea dosing MPC unit, and the ASC.

The DEA system is very complex, requiring efficient exhaust treatment for a wide range of operating conditions, corresponding to cold start, stop-and-start driving (inner city), and high speed driving (highways). As a result, DTU Chemical Engineering and Haldor Topsøe A/S are collaborating on the development of the next generation DEA system, with funding from The National Danish Advanced Technology Foundation. The underlying PhD projects concern the development of new DOC and ASC formulations (Thomas Klint Hansen, pg. 81-82), the combination of the DPF and SCR components (Kasper Linde, pg. 117-120), and the development of the MPC unit for efficient regulation of urea dosing (Andreas Åberg, pg. 259-260).

## Specific Objectives

The overall objective of the project is to develop new DOC and ASC formulations for the next generation of DEA systems. New catalyst formulations will be identified and screened, and the kinetics investigated using a recently modified catalyst testing unit. Full scale monolith samples will be prepared based on the most promising formulations and tested in a full-scale engine testing unit at Haldor Topsøe A/S.

The purpose of the ASC is the Selective Catalytic Oxidation (SCO) of  $\text{NH}_3$  to  $\text{N}_2$ . Figure 2 illustrates the dual layer design used in the ASC. The upper layer is a SCR catalyst (Cu-beta zeolite) and the lower layer is an Ammonia Oxidation Catalyst (AOC) (Pt/TiO<sub>2</sub>).

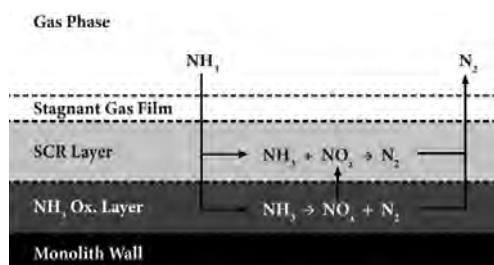


**Figure 2:** The dual layer design of the ASC. The lower layer oxidizes  $\text{NH}_3$  to  $\text{N}_2$  and  $\text{NO}_x$ . The  $\text{NO}_x$  produced in the lower layer reacts with  $\text{NH}_3$  in the upper layer, over the SCR catalyst, increasing overall  $\text{N}_2$  selectivity.

A model developed for the monolithic dual layer ASC will be used to optimize the catalyst design parameters, such as layer thicknesses and noble metal loading. The optimized design will then be the basis for catalyst preparation [2]. The reaction kinetics used in the dual layer ASC model will be developed through kinetic parameter investigations of the AOC and the SCR catalytic materials.

New formulations of the AOC will also be investigated. A formulation of interest could be a mixture of Pt and CuO on  $\text{Al}_2\text{O}_3$  support, which has been seen to have higher  $\text{N}_2$  selectivity compared to the Pt/ $\text{Al}_2\text{O}_3$  catalyst [3]. Additionally, alternative Cu-zeolites varying in zeolite framework may be investigated since the Cu-BEA catalyst has been seen to achieve lower  $\text{NO}_x$  conversion and higher  $\text{N}_2\text{O}$  formation compared to Cu-ZSM-5 and Cu-SSZ-13 [4].

The DOC is commonly a Pd-Pt based catalyst and is therefore quite expensive to produce [1]. The next generation DOC will be developed with the goal of reducing the component price, by reducing the dependency of the catalyst on noble metals. The new formulations will be based on the information gathered through a literature study. To better understand the DOC, a kinetic model will be developed accounting for the oxidation reactions of CO, representative HC's, and NO, as well as interactions between the CO, representative HC's, and  $\text{NO}_2$  [5].

## Conclusions

Improved DEA systems are needed to meet future emission regulations. The next generation of DOC and ASC formulations will be designed based on literature studies, mathematical modelling of the respective systems, and experimental investigations, including kinetic studies and activity screenings. The dual layer ASC design will be optimized through mathematical modelling and by investigation of alternative AOC and SCR catalyst formulations. The DOC will be improved through the reduction of the noble metal content and the lower component price. The next generation DOC and ASC will contribute to the overall improvement of the DEA system.

## Acknowledgements

This project is a collaboration between the CHEC research center at DTU Chemical Engineering and Haldor Topsøe A/S, and The National Danish Advanced Technology Foundation.

## References

1. W. A. Majewski, M. K. Khair, Diesel Emissions and Their Control, SAE International, 2006.
2. A. Scheuer, W. Hauptmann, A. Drochner, J. Gieshoff, H. Vogel, and M. Votsmeier, Dual layer automotive ammonia oxidation catalysts: Experiments and computer simulation. Applied Catalysis B: Environmental 111-112 (2012) 445–455.
3. S. Shrestha, M. P. Harold, K. Kamasamudram, A. Yezerets, Ammonia Oxidation on Structured Composite Catalysts. Topics in Catalysis 56 (8) (2013) 182–186.
4. J. H. Kwak, R. G. Tonkyn, D. H. Kim, J. Szanyi, C. H. F. Peden, Excellent activity and selectivity of Cu-SSZ-13 in the selective catalytic reduction of  $\text{NO}_x$  with  $\text{NH}_3$ . Journal of Catalysis 275 (2) (2010) 187–190.
5. M. Ahmadinejad, T. C. Watling, M. Țuțuianu, M. A. Paterson, Å. Johansson, Development and validation of a Pt-Pd diesel oxidation catalyst model. SAE Technical Papers 5 (3) (2012) 1420–1442.

**Hamid Hashemi**

Phone: +45 4525 2809  
E-mail: hah@kt.dtu.dk

Supervisors: Peter Glarborg  
Jakob M. Christensen

**PhD Study**

Started: May 2011  
To be completed: April 2014

## Combustion Characterization of Bio-derived Fuels and Additives

**Abstract**

Combustion characterization of bio-derived fuels including methane and alcohols with different additives at high pressures and intermediate temperatures is the major aim of this project. For this purpose, experiments have been conducted in a high pressure laminar flow reactor. Based on the obtained data from experiments on H<sub>2</sub>, CH<sub>4</sub>, DME, and ethanol, a reaction mechanism has been developed. The mechanism was able to reproduce ignition of the listed fuels very well and can be used to predict other combustion characteristics of the fuels.

**Introduction**

In recent years, fuels produced from bio-sources have generated considerable research and practical interests. Less net production of greenhouse gases and independency from the natural reservoirs are leading causes for this emerging attention.

Methane, as one of the bio-derived fuels, benefits from its wide range of bio-sources in addition to its abundant natural reservoirs. Even when produced from the fossil sources, burning methane releases 30% to 45% less carbon dioxide per unit of energy compared to petroleum and coal. However, longer ignition delay time and lower flame speed of methane may result in pollutants and performance deficiencies if used directly in conventional mobile and stationary energy plants. One solution to address these challenges is to adjust the combustion properties of methane by additives, e.g. dimethyl ether (DME), which itself can be produced from bio-sources as well.

Hydrogen has been considered as an energy carrier to be used in conventional engines while it is a major component of syngas (H<sub>2</sub>+CO) produced from bio-sources. Burning syngas has been believed to be an alternative way of using biofuels in conventional energy plants. Furthermore, hydrogen reactions are among the most sensitive reactions controlling ignition of different hydrocarbon fuels which make understanding of H<sub>2</sub>/O<sub>2</sub> combustion chemistry a vital step in development of hydrocarbon fuel models.

Alcohols have been used as additives or even as the main fuel to replace petroleum in many combustion devices. Burning alcohols results in less soot formation

while alcohols as liquid fuels remove logistic problems encountered in the use of methane.

Dimethyl ether (DME) is another bio-derived fuel with the potential for use especially in high speed diesel engines when residence time is too short so fast ignited fuels are desired. Additionally, DME is a soot-free fuel ignited at low temperatures making NO<sub>x</sub> control easier. As mentioned earlier, DME has been believed to be a suitable candidate for addition to methane to promote combustion properties.

Knowledge of combustion characteristics of the mentioned fuels and their combination will facilitate developing chemical models of combustion engines and other industrial applications. Even though all the discussed fuels have been studied extensively in recent years (e.g. see [1-8]), data for the high pressure and medium temperature, ignition range encountered in many industrial/engine applications, are rare. Furthermore, effect of additives on methane has not been understood well.

**Specific Objectives**

The main aim of this work is to measure combustion characteristics of H<sub>2</sub>, CH<sub>4</sub>, DME and ethanol at high pressures and intermediate temperatures. In a unique high-pressure flow reactor setup at DTU Chemical Engineering, it is possible to investigate combustion of different liquid/gas fuels at pressures and temperatures up to 100 bar and 900 K respectively. Furthermore, it is desired to develop and validate a reaction mechanism for combustion of the mentioned fuels and their combination at the discussed conditions. Finally, the model will be used for prediction of other

characteristics of the fuels and the implication for use of the selected fuels in diesel engines will be addressed.

## Results and Discussion

Figures 1-3 show results of hydrogen experiments at four different stoichiometries. At the reducing conditions ( $\Phi = 12$ ), oxidation started at 748–775 K while it was shifted to 798–823 K for stoichiometric and oxidizing conditions ( $\Phi = 1.03$  and 0.05). At very oxidizing conditions ( $O_2$  atmosphere,  $\Phi = 0.0009$ ), the temperature for onset of reaction was reduced to 775–798 K. The data were interpreted in terms of a detailed chemical kinetic model. The reaction mechanism was based on recent work of Burke et al. [4], updating the rate constants for  $OH + OH$ ,  $HO_2 + OH$ , and  $HO_2 + HO_2$  based on recent determinations. As can be seen from figures 1-3, the modeling predictions were in good agreement with the measurements in the flow reactor. Further comparison and discussion can be found in [9].

Figures 4-5 represent results of methane ignition as well as the effect of doping with DME at 100 bar pressure and under stoichiometric conditions. For pure methane, the first sign of fuel conversion was observed at 775 K while replacing just 1.8% of methane by DME expands the onset of fuel conversion to 725 K. Although DME was very effective in modifying the ignition temperature, it had an insignificant effect on the final products of the combustion at higher temperatures. The model used here is based on the models in [1-3]. The hydrogen subset was updated according to [9] and several other reactions were modified according to new determinations. As can be seen, agreement between the developed model and measured values has been very good for major components.

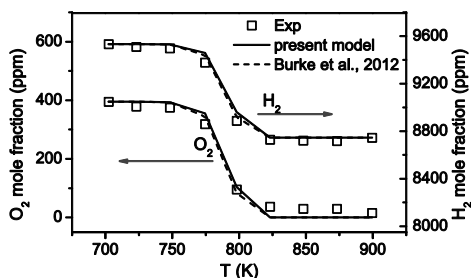


**Figure 1:** Results of reducing experiments on hydrogen (0.95%  $H_2$  and 0.04%  $O_2$  in  $N_2$ ,  $\Phi=11.9$ ) at 50 bar pressure. The residence time is given by  $\tau [s] = 5661/T [K]$ . Symbols mark experimental results and lines denote predictions of the present model and the model by Burke et al. [4].

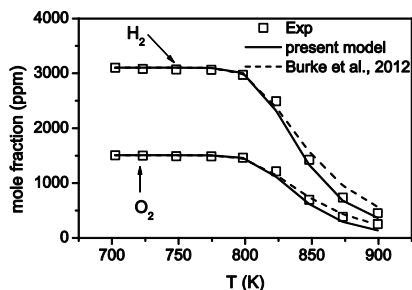


**Figure 2:** Results of stoichiometric experiments on hydrogen (0.31%  $H_2$  and 0.15%  $O_2$  in  $N_2$ ,  $\Phi=1.03$ ) at 50 bar pressure.

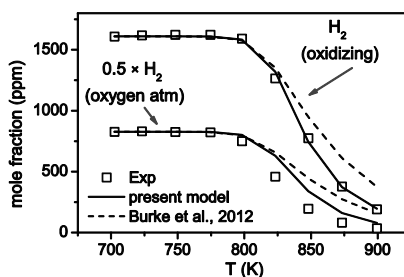


**Figure 3:** Results of oxidizing experiments on hydrogen (0.16%  $H_2$  and 1.60%  $O_2$  in  $N_2$ ,  $\Phi=0.05$ ) and experiments in oxygen atmosphere (0.17%  $H_2$  and 93.92%  $O_2$  in  $N_2$ ,  $\Phi=0.0009$ ) at 50 bar pressure.

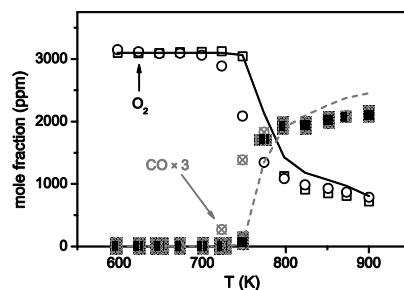


**Figure 4:** Results of stoichiometric experiments on methane (0.15%  $CH_4$  and 0.32%  $O_2$  in  $N_2$ ,  $\Phi=1.0$ ) at 100 bar pressure. Squares represent pure  $CH_4$  experiment while circles show  $CH_4$  doped by DME (DME/ $CH_4=1.8\%$ ) experiments. The residence time is given by  $\tau [s] = 9586/T [K]$ . Symbols mark experimental results and lines denote predictions of the present model for pure  $CH_4$ .



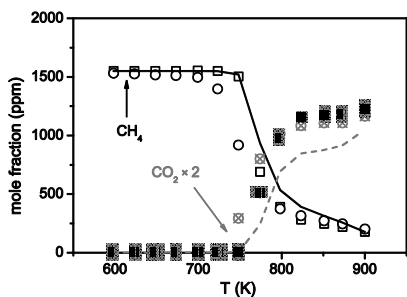


**Figure 5:** Results of stoichiometric experiments on methane at 100 bar pressure. Squares represent pure CH<sub>4</sub> experiment while circles show CH<sub>4</sub> doped by DME experiments. Symbols mark experimental results and lines denote predictions of the present model for pure CH<sub>4</sub>.

Experiments on pure DME also has been conducted in the flow reactor. It was found that DME conversion could start at a much lower temperature of 500 K. Furthermore, it seemed that starting temperature for conversion is independent of stoichiometry. Negative temperature dependency has been observed for all investigated stoichiometries although it is more obvious in stoichiometric conditions. A recent comprehensive work on DME combustion from Zhao et al. [5] has been selected as a starting point for the simulation. Although the model showed a good ability in prediction under stoichiometric conditions, it seemed that reactivity of DME was overestimated at reducing conditions. Moreover, CO production in oxidizing atmosphere was far from perfect. Future work will therefore focus on improving the DME model.

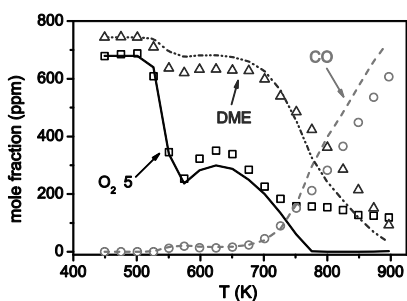


**Figure 6:** Results of reducing experiments on DME (0.07% DME and 0.01% O<sub>2</sub> in N<sub>2</sub>,  $\Phi=16.44$ ) at 50 bar pressure. The whole temperature profile of the reactor is considered in modeling. Symbols mark experimental results and lines denote predictions of the model by Zhao et al. [5].

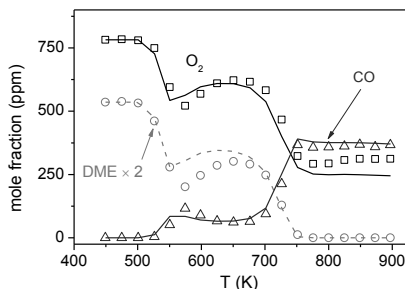


**Figure 7:** Results of stoichiometric experiments on DME (0.03% DME and 0.08% O<sub>2</sub> in N<sub>2</sub>,  $\Phi=1.03$ ) at 50 bar pressure. Symbols mark experimental results and lines denote predictions of the model by Zhao et al. [5].

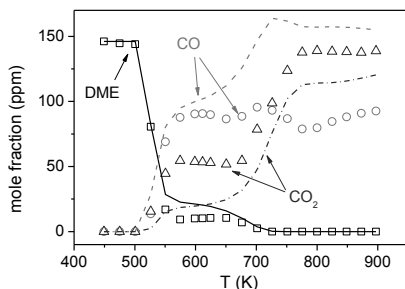


**Figure 8:** Results of oxidizing experiments on DME (0.01% DME and 1.08% O<sub>2</sub> in N<sub>2</sub>,  $\Phi=0.04$ ) at 50 bar pressure. Symbols mark experimental results and lines denote predictions of the model by Zhao et al. [5].

Results of measurements of ethanol conversion in the flow reactor are shown in figures 9-11. Under reducing conditions, fuel consumption started above 675 K while it was postponed to 700 K for stoichiometric and oxidizing conditions. Although the model predictions for the fuel and the oxidant were in good agreement with the measurements, it was less accurate for CO concentration. In general, the model overestimated the CO which is likely because of underestimated CO consumption rate at current conditions. It seems that further work especially on CO/CO<sub>2</sub> subset is required to acquire a better prediction for ethanol combustion.

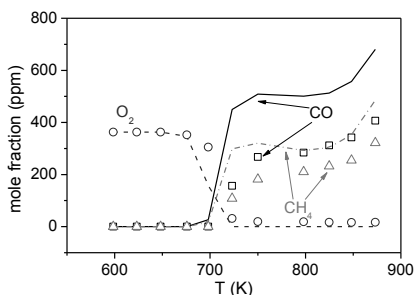


**Figure 9:** Results of reducing experiments on ethanol (0.53% EtOH and 0.04% O<sub>2</sub> in N<sub>2</sub>,  $\Phi=43.4$ ) at 50 bar pressure. The residence time is given by  $\tau$  [s] = 3841/T [K]. Symbols mark experimental results and lines denote predictions of the present model.

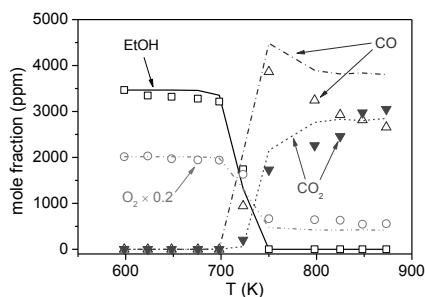


**Figure 10:** Results of stoichiometric experiments on ethanol (0.35% EtOH and 1.01% O<sub>2</sub> in N<sub>2</sub>,  $\Phi=1.03$ ) at 50 bar pressure. Symbols mark experimental results and lines denote predictions of the present model.

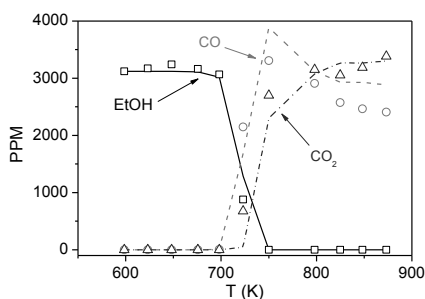


**Figure 11:** Results of oxidizing experiments on ethanol (0.31% EtOH and 9.83% O<sub>2</sub> in N<sub>2</sub>,  $\Phi=0.10$ ) at 50 bar pressure. Symbols mark experimental results and lines denote predictions of the present model.

## Conclusion

Oxidation of hydrogen, methane, ethanol, and dimethyl ether (DME) was investigated in a laminar flow reactor at intermediate temperatures and high pressures. Results provided information about the onset temperature for reaction and the fuel consumption rate upon initiation. A detailed reaction kinetic model mainly based on previous work from the current laboratory has been developed and validated with comparison to the measured data and other available combustion characteristics. It was found that onset temperature for consumption of the investigated fuels showed a low sensitivity to the extreme changes in the stoichiometries. Furthermore, DME was shown to be a very efficient in promoting ignition of methane. Pure DME itself has shown to have negative temperature dependency of conversion in a range of temperatures. All in all, agreements between the model and the experimental data were very good while further improvement in prediction of CO is desired.

## Acknowledgement

Funding from the European Graduate School is gratefully acknowledged.

## References

1. C. L. Rasmussen, J. Hansen, P. Marshall, P. Glarborg, *Int. J. Chem. Kinet.* 40 (2008) 454–480.
2. C. L. Rasmussen, J. G. Jakobsen, P. Glarborg, *Int. J. Chem. Kinet.* 40 (2008) 778–807.
3. V. Aranda, J. M. Christensen, M. U. Alzueta, P. Glarborg, S. Gersen, Y. Gao, P. Marshall, *Int. J. Chem. Kinet.* 45 (2013) 283–294.
4. M. P. Burke, M. Chaos, Y. Ju, F. L. Dryer, S. J. Klippenstein, *Int. J. Chem. Kinet.* 44 (2012) 444–474.
5. Z. Zhao, M. Chaos, A. Kazakov, F.L. Dryer, *Int. J. Chem. Kinet.* 40 (2008) 1–18.
6. F. M. Haas, M. Chaos, F. L. Dryer, *Combust. Flame* 156 (2009) 2346 – 2350.
7. M. Abian, C. Esarte, A. Millera, R. Bilbao, M. U. Alzueta, *Energy Fuels* 22 (2008) 3814–3823.
8. T. Mendiara, P. Glarborg, *Combust. Flame* 156 (2009) 1937–1949.
9. H. Hashemi, J.M Christensen, S. Gersen, P. Glarborg, *Hydrogen Oxidation at High Pressure and Intermediate Temperatures: Experiments and Kinetic Modeling*, (submitted to) *Proc. Combust. Inst.* 35, 2014.



**Suzan Sager Hassouneh**

Phone: +45 4525 6195  
E-mail: shas@kt.dtu.dk

Supervisors: Anne Ladegaard Skov  
Anders Egede Daugaard

PhD Study  
Started: August 2012  
To be completed: January 2015

## Lamination of Polydimethylsiloxane Films Using an Open-Air Plasma Treatment System

### Abstract

The DEAP technology was originally developed with artificial muscles as the main purpose due to their ability to mimic biological muscles. This is due to their electro-responsive properties and very similar properties with real muscle, which is in strong contrast to other types of actuators. It later turned out that DEAP had broad industrial and commercial applicability. The aim of this project is to adhere the DEAP films in multiple layers to make the elements more robust, prolong the life time and increase the energy density of the final product.

### Introduction

In recent years, the interest in smart materials has increased. Smart materials respond to external stimuli such as electric field, temperature and pH, to name a few, by changing their e.g. size and shape [1]. Dielectric electroactive polymers (DEAP) are in the category of smart materials. DEAP are thin elastomeric films sandwiched between compliant electrodes and can be used as transducers, which converts one form of energy to another. As an actuator, it converts an electrical energy to a mechanical deformation. It can also work in the reverse mode, i.e. convert a mechanical deformation to an electrical energy, and work as sensors and generators [2].

Due to this versatility, the DEAP can be used in many different applications as shown in figure 1.



**Figure 1:** Different applications of DEAP, such as thin lightweight loudspeakers, e-books for blind people, wave energy harvesters and bandages to increase the blood circulation and ease the recovery e.g. after surgeries.

### Specific Objectives

The DEAP films are stacked, rolled or folded in multiple layers to prolong the lifetime and to increase both the energy density and robustness of the transducer. These multiple layers are independent of each other, which can influence the overall performance and lifetime of the transducer. Friction between the layers could cause a reduction in lifetime. Furthermore, the electrical breakdown strength would be decreased due to air trapped between the layers.

Danfoss Polypower A/S (DPP) produces DEAP-films; using polydimethylsiloxane (PDMS).

The films have a corrugated surface on one side and a flat surface on the other side. The corrugated side is sputtered with metal electrodes [3]. Due to the DPP design of the elastomers, the films can be laminated in three different configurations as illustrated in figure 2.



**Figure 2:** The different configurations for the adhesion of the films. The back-2-back configuration is where the flat sides are adhered together. The corrugated sides are adhered together in the front-2-front configuration and for the front-2-back configuration, a corrugated side is adhered with a flat side.

This study focuses on the Back-2Back-configuration (B2B) where the films are adhered by plasma treating

the flat surface before adhering them together. This study investigates the possibilities of using open-air plasma treatment for DPP materials and investigating the different parameters for the adhesion. The electrical breakdown strength and peel force of the laminates are investigated.

### Experimental

The plasma treatment is performed in open-air to decrease the processing costs compared to using the conventional method, with plasma treatment performed in vacuum.

The plasma treater is attached to an arm that can be moved at a given speed across the sample and the sample can be placed with different distances to the plasma treater.

The plasmatreater is a Plasmatreater RD1004 with nozzlehead 22892 attached, both from Plasmatreater GmbH and the DEAP-films are supplied by DPP.

The plasma treatment exchanges the methyl groups in the PDMS with silanol groups (-OH) [4]. After the plasma treatment the films are placed on top of each other, a condensation reaction occurs, and the films are adhered covalently together.

The plasma treatment is performed at different speeds and distances to investigate if the intensity of the plasma treatment has an influence on the adhesion and the electrical breakdown strength. The distances investigated are 5-15 mm in an increment of 5 and for all the distances the speeds measured are 5-20 m/min in increments of 5.

### Results and discussion

For all the distances and speeds the electrical breakdown strength and peel force are measured.

The breakdown is measured on single films and laminates. For the single films the breakdown is measured on both plasma treated and non-treated films. The breakdown values for the different samples are shown in figure 3.

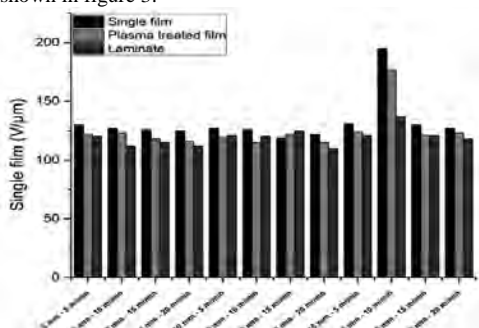


**Figure 3:** The breakdown values of the plasmatreated films and laminates compared with a non-treated single film.

Figure 3 shows that the breakdown strength decreases after the plasma treatment for both single films and laminates for all distances and speeds except the 10 mm

and 15m/min sample where the breakdown strength is increased with 4% for the single film and 6 % for the laminate. There are no obvious correlation between the decrease in breakdown strength and the speed and distance the samples are treated.

The force used to peel the films in the laminate from one another is measured and the values can be seen in figure 4.

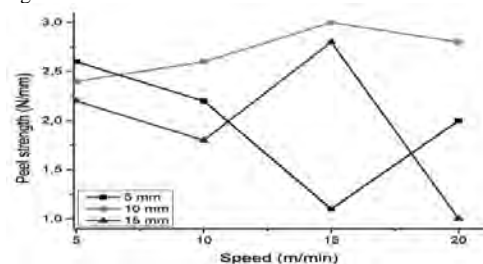


**Figure 4:** The peel strength values of the laminates at the different speeds for the different distances.

Figure 4 illustrates that there are no obvious correlation between the measured peel force and the distance and speed. The peel strength values for the samples performed at distances of 5 mm and 15 mm and speeds of 15 m/min and 20 m/min respectively, are lower than the rest of the samples. This difference can be due to experimental errors. The rest of the values are in the same range and the differences could be experimental uncertainties.

### Conclusions

To optimize the overall performance of the transducers the films are laminated using an open-air plasma treatment system. The plasma treatment is performed at different speeds and distances from the films and the electrical breakdown strength and peel force were investigated. The study showed that the different speeds and distances do not influence the peel force and that the peel force is high enough so that the laminates will not detach during operation. The electrical breakdown strength is decreased for single plasma treated films and laminates compared to a non-treated single film, which is unfavorable for DEAPs.

### Acknowledgements

The author would like to thank the Danish National Advanced Technology Foundation for the financial support.

### References

- [1] X. Zhang, C. Löwe, M. Wissler, B. Jähne, G. Kovacs, *Advanced Engineering Materials* 7 (5) (2005) 361-367
- [2] [http://www.eurocap.eu/epedia/index.php?title=Introduction to the EAP field](http://www.eurocap.eu/epedia/index.php?title=Introduction_to_the_EAP_field) (10.12.13)
- [3] H.-E. Kiil, M. Benslimane, *Proceeding SPIE*, vol 7287, (2009)
- [4] M. A. Eddings, M. A. Johnson, B. K. Gale, J. Micromec. *Micromec* 18 (2008) 067001

**Søren Heintz**

Phone: +45 4525 2949  
E-mail: shein@kt.dtu.dk  
Supervisors: Krist V. Gernaey  
John M. Woodley  
Ulrich Krühne  
Pär Tufvesson

**PhD Study**

Started: September 2012  
To be completed: August 2015

## Miniaturized Experimental Platform for Development of Recovery Processes

**Abstract**

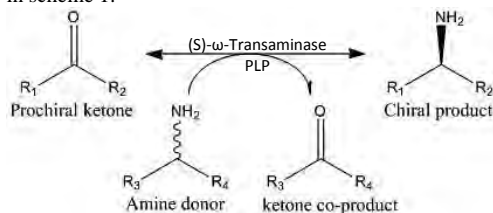
The scope of this project is the use of automated microsystems as novel tools to accelerate the development of biocatalytic processes. The intention is for the microsystems to serve multiple purposes enabling full process characterization in a fast, easy and cheap manner. For example, the systems are intended for characterization of different promising biocatalysts, characterization of different process options and process optimization. The main focus of this PhD study is on the application of these microsystems to test, optimize and identify economically feasible product recovery options, e.g. different downstream processing scenarios and *in-situ* (co-)product removal strategies. As case studies, for the evaluation of the potential of such microsystem as process development tools, three  $\omega$ -transaminase catalyzed model reactions are used. These three case studies impose different challenges to both the biocatalytic reaction performance as well as to the following product recovery. The challenges cover unfavorable thermodynamic equilibrium, product inhibition, low aqueous solubility and similar physicochemical properties of the reaction species. Addressing these challenges will ensure that the microsystems are really put to a test.

**Introduction**

Chiral amines are important building blocks for many pharmaceuticals and precursors [1]. As a consequence of their role in such applications it is, in most cases, required to ensure production of enantiomerically pure compounds for patient safety reasons, as defined by regulatory authorities [2]. However, the production of enantiomerically pure chiral amines, i.e. achieving a high enantiomeric excess (*e.e.* > 99%), can be quite a challenging task.

An alternative to conventional chemical synthesis methods is synthesis using biocatalysis. Biocatalysis is organic synthesis mediated by an isolated enzyme, or an immobilized enzyme, or alternatively a whole-cell catalyst containing one or more enzymes. Biocatalysts have the advantage of enabling high selectivity (high *e.e.* values); they can potentially use a range of substrates while forming relatively few by-products, and potentially allow the establishment of simplified process routes [3]. Other drivers for industrial implementation of biocatalytic processes are the potential of improved process economy and a better environmental profile than conventional chemical processes [3-7]. All these factors make biocatalysis attractive for the production of chiral amines.

There are multiple types of biocatalysts enabling the synthesis of chiral amines, where one is the asymmetric synthesis using  $\omega$ -transaminases [8].  $\omega$ -transaminases (E.C.2.6.1.1) are quite attractive as they potentially enable asymmetric synthesis of pure chiral amines with *e.e.* > 99%, under mild reaction conditions [9].  $\omega$ -transaminases facilitate the transfer of an amino group from a primary amine to a carbonyl compound mediated by pyridoxal-5'-phosphate (PLP) [10]. The general reaction scheme of  $\omega$ -transaminase reactions is shown in scheme 1.



**Scheme 1:** General reaction scheme for the asymmetric synthesis of chiral amines using  $\omega$ -transaminases.

Despite all the benefits related to applying  $\omega$ -transaminases for the synthesis of chiral amines, the

application of such biocatalytic processes is not very common. This is a consequence of the many challenges related to operating these biocatalytic processes, making it difficult to achieve economically feasible processes. The challenges related to  $\omega$ -transaminase applications are in many cases related to unfavorable thermodynamic reaction equilibrium, low solubility of reaction species and different inhibition effects, to name a few [11]. The effect of such process limiting challenges can be reduced in different ways during the development of a biocatalytic process, such as biocatalyst and process engineering. Well-known examples are the modification of the biocatalyst to improve process compatibility and/or exploiting different *in-situ* co-product (IScPR) and/or product removal (ISPR) options [9]. The general principles of the development of biocatalytic processes are illustrated in the development cycle in figure 1. The development cycle identifies the major areas of development and the key decisions which have to be taken during the development and optimization phase of a process [4].

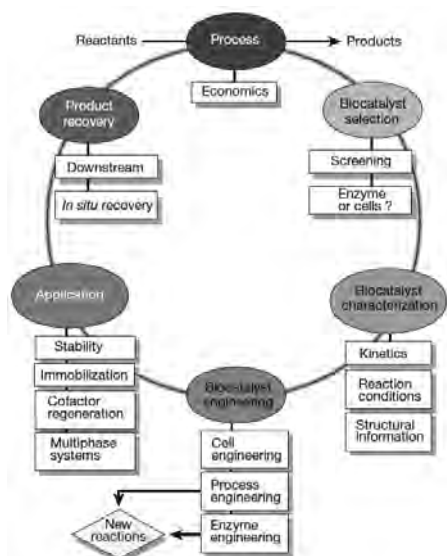


**Figure 1:** Development cycle of biocatalytic processes [4].

Currently, it is quite time demanding to develop new biocatalytic processes, imposing a need for better and faster technologies to ensure faster process development. The EU FP7 financed project BIOINTENSE (grant agreement n°. 312148) intends to provide such technologies with the aim of ensuring accelerated process development, in the form of automated microsystems. Such automated microsystems should provide tools to achieve fast screening, characterization and optimization of new processes, with a low consumption of expensive and scarce resources.

This PhD study will mainly concern the development of different process options for product recovery using microsystems, i.e. characterization and evaluation of different downstream processing (DSP), IScPR and ISPR methods.

### Aspects of product recovery

In addition to the importance of improving the performance of the biocatalytic reaction it is equally important to consider the following downstream recovery. Downstream recovery of products from biocatalytic reactions can be quite challenging, due to the complexity of the reaction mixtures. Also, the recovery procedures vary dependent on the biocatalytic reaction. For  $\omega$ -transaminase reactions the recovery can be quite problematic as a consequence of the very similar physicochemical nature of substrates and products making selective and efficient separation challenging. The latter is especially due to the fact that many separation techniques exploit differences in physicochemical properties of the species to be separated.

The function of the microsystems in this relation is to aid in fast identification of the most feasible separation method, i.e. the method enabling the highest economical profit.

In some cases it will be required to exploit the separation methods to improve the biocatalytic reaction performance, i.e. by combining the separation and reaction referred to as *in-situ* removal (IScPR and ISPR). Implementation of IScPR and/or ISPR will aid in reducing effects such as product degradation, inhibition and unfavorable thermodynamic equilibrium [4]. IScPR and ISPR methods will always have a positive influence on such process limiting effects and can potentially simplify the following product purification.

However, the implementation of different *in-situ* removal methods is not straightforward. There is the issue of achieving selective and efficient removal as with conventional downstream processing options, but there are also issues such as the compatibility of the removal method with the biocatalyst and vice versa. An overview of some general aspects which influence the ISPR and IScPR options applicable for any given biocatalytic process is given in figure 2 [3].

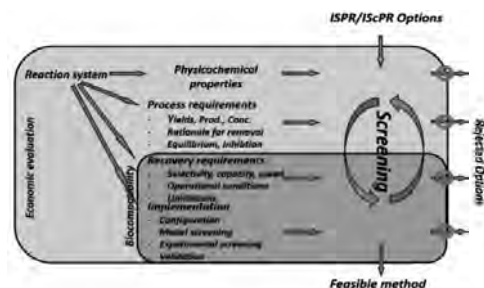


**Figure 2:** Overview of some general aspects of ISPR/IScPR development for biocatalytic processes [3].

A good example of the complexity of applying *in-situ* removal options is the implementation strategy. The implementation strategy is highly dependent on the compatibility of the biocatalyst and the selected *in-situ* removal option. For example, dependent on their compatibility with one another it will either be necessary to have them in direct contact or in indirect contact with one another. Also, there is the possibility to implement the removal option internal or external of the reactor, dependent on the specific requirements, e.g. operating conditions, cost of implementation and configuration limitations. The described implementation scenarios are illustrated in figure 3.

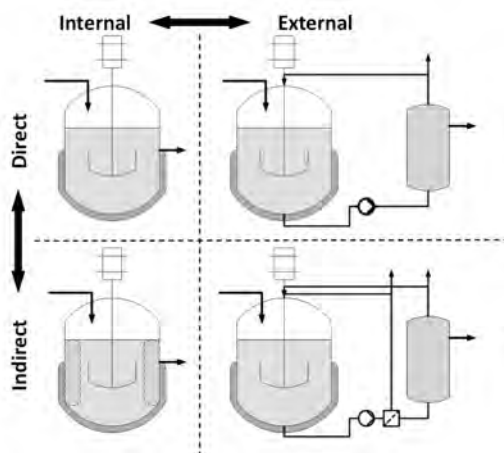
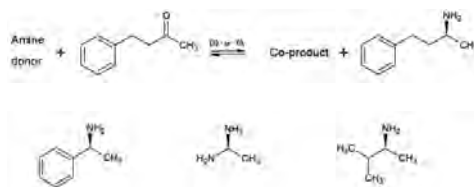


**Figure 3:** Implementation options of biocatalyst based processes with *in-situ* removal [12].

Flexible microsystems will make it possible to test the influence of different separation options on the biocatalyst, enabling fast identification of potentially feasible *in-situ* removal options.

### Case studies

During this PhD project the main focus will be kept to three specific reaction systems using  $\omega$ -transaminase ATA-50. These three case studies will be used to validate the use of microsystems for process development. The overall reaction scheme which is in focus is the formation of 1-methyl-3-propylphenylamine (MPPA) from benzylacetone (BA) using three different amine donors: Methylbenzylamine (MBA), isopropylamine (IPA) and alanine (ALA), i.e. the three case studies. The general reaction schemes of these model reactions are highlighted in scheme 2.



**Scheme 2:** General reaction scheme for the asymmetric synthesis of 1-methyl-3-propylamine from benzylacetone using  $\omega$ -transaminases and three different amine donors: methylbenzylamine, isopropylamine and alanine.

These case studies impose different challenges which have to be addressed in order to improve the reaction performance. These challenges are also the motivation for the selection of precisely these case studies as they will put the application of microsystems for process development to the test. The challenges related to the case studies cover different equilibrium scenarios, i.e. favourable and unfavourable scenarios, potential inhibiting effects, low solubility of certain reaction species and separation of reaction species with very similar physicochemical properties. The thermodynamic equilibria of each of the reactions are roughly: ~30:1 (MBA-donor), ~1:1 (IPA-donor) and ~1:1000 (ALA-donor) [13].

### Analytics

An important factor for the successful application of microsystems is the implementation of analytics enabling on-line measurements. Working in such small scales, manual sampling gives large uncertainties as a consequence of handling difficulties. Having flexible microsystems where it is possible to implement different standard analytical methods (e.g. NIR, UV, HPLC) and/or novel sensor technologies is of utmost importance for the microsystems to reach their full potential. It should be aimed at having on-line monitoring in the systems not only to avoid the uncertainties resulting from manual sampling, but also to overcome some of the current analytical bottlenecks and thereby enabling high throughput characterization systems. The focus will mainly be kept on the implementation of optical sensors, so the impact of the sensors on the process is avoided as much as possible.

### Influence of scale

An important cornerstone of this PhD project is the transfer of the knowledge obtained from process characterization in microsystems across scales. The different dominant phenomena across scales make this knowledge transfer difficult. It is the hypothesis that fundamental process knowledge, e.g. kinetic parameters, is transferable across scales as long as the influence of the scale, e.g. mass transfer limitations, is taken into account. The intention of this work is also to investigate this hypothesis based on a combination of experiments at various scales in combination with

modelling, e.g. computational fluid dynamics (CFD) simulation, to obtain more detailed process knowledge.

### Specific objectives

The main objectives which will be covered in this project are:

- Propose general protocols for the evaluation of various standard separation options using microsystems in combination with biocatalytic processes. Focus both on traditional downstream and *in-situ* development applications.
- Provide standard automated microsystems with integrated on-line monitoring using both standard analytical methods as well as novel sensors.
- Combine modelling tools with experimental investigations to improve the basis for obtaining process knowledge.
- Propose procedures for transferring knowledge obtained in microsystems across scales. Evaluate and validate the proposed procedures.

### Conclusion

Currently, development and optimization of industrially relevant biocatalytic processes is quite time consuming, and in some cases the available quantities of substrates and/or catalyst are quite sparse and expensive. It is therefore evident to develop new technologies which can aid in accelerating the process development and at the same time ensure better use of available resources. The application of automated microsystems is in this context recognized as potential technological solution to these requirements.

In order to exploit the full potential of automated microsystems it is required to successfully implement on-line analysis methods to ensure high throughput along with reduced experimental uncertainty. Another important factor for the success of such microscale technologies is successful demonstration that it is possible to transfer the obtained process knowledge in microsystems across scales.

The technology and procedures developed during this project will entirely be based upon  $\omega$ -transaminase applications, but the intention is that the technologies, methods and procedures should be generally applicable.

### Acknowledgements

This Ph.D.-project is financially supported by the European Union 7<sup>th</sup> Framework Program: BIOINTENSE – Mastering Bioprocess Integration and Intensification across Scales (grant agreement n<sup>o</sup>. 312148).



### References

1. S. Panke, M. Held, M. Wubbolts, Current Opinion in Biotechnology 15 (2004) 272-279.
2. U.S. Food and Drug Administration (FDA), Development of new Stereoisomeric Drugs, <http://www.fda.gov/drugs/guidancecompliance/regulatoryinformation/guidances/ucm122883.htm>.
3. J.M. Woodley, Synthetic Methods for Biologically Active Molecules, Wiley-VCH (2013) 263-284. ISBN:978-3-527-33387-5
4. A. Schmid, J.S. Dordick, B. Hauer, A. Kiener, M. Wubbolts, B. Witholt, Nature 409 (2001) 258-268.
5. J.M. Woodley, Trends in Biotechnology 26 (2008) 321-327.
6. U.T. Bornscheuer, G.W. Huisman, R.J. Kazlauskas, S. Lutz, J.C. Moore, K. Robins, Nature 485 (2012) 185-194.
7. J.M. Woodley, Current Opinion in Chemical Biology 17 (2013) 310-316.
8. M. Höhne, U.T. Bornscheuer, ChemCatChem 1 (2009), 42-51.
9. P. Tufvesson, J. Lima-Ramos, J.S. Jensen, N. Al-Haque, W. Neto, J.M. Woodley, Biotechnology and Bioengineering 108 (2011) 1479-1493.
10. M.S. Malik, E.-S. Park, J.-S. Shin, Applied Microbial Biotechnology 94 (2012) 1163-1171.
11. S. Mathew, H. Yun, ACS Catalysis 17 (1999) 395-402
12. J.M. Woodley, M. Bisschops, A.J.J. Straathof, M. Ottens, Journal of Chemical Technology and Biotechnology 83 (2008) 121-123
13. P. Tufvesson, J. S. Jensen, W. Kroutil, J. M. Woodley, Biotechnology and Bioengineering 109 (2012) 2159-2162

### List of publications

1. Mitic, S. Heintz, R.H. Ringborg, V. Bodla, J.M. Woodley, K.V. Gernaey, Chimica Oggi – Chemistry today 31 (2013) 4-8
2. U.Krühne, S. Heintz, R.H. Ringborg, I.P. Rosinha, P. Tufvesson, K.V. Gernaey, J.M. Woodley, Green Processing and Synthesis (2013) (in press) (doi:10.1515/gps-2013-0089)
3. U.Krühne, H. Larsson, S. Heintz, R.H. Ringborg, I.P. Rosinha, V.K. Bodla, P. A. Santacoloma, P. Tufvesson, J.M. Woodley, K.V. Gernaey, Chemical and Biochemical Engineering Quarterly (2013) (submitted)
4. U.Krühne, S. Heintz, I.P. Rosinha, R.H. Ringborg, P. Tufvesson, K.V. Gernaey, J.M. Woodley, Dansk kemi 94 (11) (2013) 18-22
5. Poulsen, S. Heintz, R.H. Ringborg, J.M. Woodley, K.V. Gernaey, U. Krühne, Dansk kemi 94 (10) (2013) 32-34





## Ludovica Hengeller

Phone: +45 45256813  
E-mail: luhe@kt.dtu.dk

Supervisors: Ole Hassager  
Anne Skov Ladegaard  
Kristoffer Almdal

### PhD Study

Started: April 2013  
To be completed: March 2016

## The Effect of Nematic Interactions in Uniaxial Extension of Polymer Blends

### Abstract

The purpose of the present study is to investigate the existence of nematic interactions, namely polymer-polymer, in strong elongational flow using two bi-disperse polystyrene blends of 95K and 545K Mw with different weight ratios. Preliminary investigations focus on the shear rheology of these binary blends and the linear viscoelastic behavior of such systems will be illustrated by experimental measurements. Future works will focus on uniaxial extension and stress relaxation experiments to determine if orientation and extension of long PS chains induce orientation and extension in shorter chains (whose orientation should be unaffected by the flow).

### Introduction

Industrial polymers are largely polydisperse systems. One step towards understanding polydisperse polymers is the characterization of bi-disperse blends. Even though linear viscoelastic properties of bi-disperse polystyrene blends have been investigated thoroughly both theoretically and experimentally in recent years [1], both nonlinear shear and extensional flow properties are lacking. In a recent study on solvent effects in mono-disperse concentrated polymer solutions, Huang et al. [2] introduced a hypothesis that there exists nematic interactions between solvent-polymer and polymer-polymer molecules. However, this hypothesis needs further testing and is still an open question.

### Specific Objectives

The purpose of the present work is to make well-defined experiments to evaluate the influence on the rheological properties of bi-disperse entangled polymer melts due to the interaction between long and short polymer molecules.

Two nearly mono-disperse polystyrenes of molecular weight of 95 kg/mol and 545 kg/mol have been used to prepare the two binary blends, the first one with 10% of 545k and the second one with 50% of the high Mw polystyrene. The two melts are measured in shear flow and later measurements will be done in extensional flow. In the latter and more interesting case the hypothesis is that the stretching of the long chains in fast extensional flows can induce the alignment of the short ones even if the extensional rate is not enough

high to influence the orientation of the lower molecular weight chains.

### Synthesis and Chromatography

The two polystyrenes PS-95k and PS-545k with narrow molecular weight distributions have been synthesized by living anionic polymerization according to the standard procedure. Size exclusion chromatography (SEC) was employed for sample characterization.

Stabilized tetrahydrofuran (THF) was used as the eluent. Table 1 summarizes the weight-average molecular weight Mw and the glass transition temperature Tg of the synthesized polystyrenes.

**Table 1:** Molecular Weight and Glass Transition Temperature of the mono-disperse Polystyrenes.

Sample name	Mw[g/mol]	T <sub>g</sub> [°C]
PS-545k	545000	106.5
PS-95k	95000	109

### Preparation of Blends

Two polystyrene blends were made using either PS-95k or PS-545k and were prepared by dissolving both the polystyrenes in THF and stirring at room temperature overnight. When the components were well dissolved and mixed, the THF solution was carefully put into methanol drop by drop and the blends were recovered by precipitation and filtration. Finally the blends were dried under vacuum at 70 °C for 2 weeks. The concentrations of all the polystyrene blends were

determined by the peak areas of the bimodal curve in SEC. For each sample, two randomly picked parts were checked in SEC in order to ensure the concentration is homogeneous throughout the sample. Table 2 summarizes the components and the weight fraction  $\phi$  in % of the bi-disperse blends.

**Table 2:** Compositions of the polystyrene blends.

Sample name	95000 [g/mol]	545000 [g/mol]
Blend 1	90%	10%
Blend 2	50%	50%

## Results and Discussion

The linear viscoelastic properties of the polystyrene melts were obtained from small amplitude oscillatory shear flow measurements. An 8 mm plate-plate geometry was used on an ARES-G2 rheometer from TA Instruments. The measurements for the two blends were performed at temperatures between 130 °C and 170 °C under nitrogen. For each polystyrene sample, the data were shifted to a single master curve at 130 °C using the time-temperature superposition procedure.

The shift factor  $a_T$  is reported in Table 3 for different temperatures.

**Table 3:** Temperature Shift Factor  $a_T$  for the blends.

Sample name	150 to 130 °C	170 to 130 °C
Blend 1	0.020124	0.001417
Blend 2	0.020124	0.001242

We analyze the LVE data by plotting separately the loss modulus  $G''$  and the storage modulus  $G'$  for both the mono-disperse melts and the two blends as illustrated in Figure 1 and 2.

In both graphs it is clear how the relaxation behavior of the moduli in the high frequency region is essentially the same for all the samples analyzed. That is in agreement with the theory since the Rouse time (which express the shortest mechanism of relaxation of a polymer chain) is an essentially constant material parameter that is unaffected by the distribution and the polydispersity of the polymer.

On the other hand, both the moduli show a dependence on the molecular weight distribution in the so called terminal region, at low frequencies. In fact, if we compare the curves of the blends with the ones of the mono-disperse samples, shoulders are highly visible on the moduli of the blend 1 although the high molecular weight component only represent 10% of the total. The influence of the long chains on the relaxation mechanism of the short ones is even more evident for the blend 2, where the amount of the high molecular weight polymer is 50%.

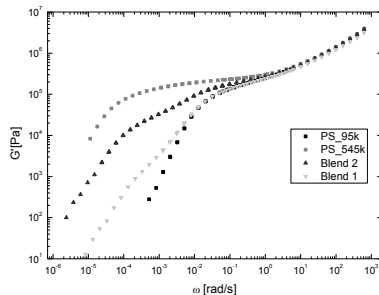


**Figure 1:**  $G'$  data for PS-95k, PS-545k, Blend 1 and Blend 2 at 130 °C.

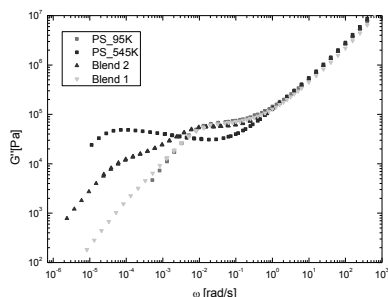


**Figure 2:**  $G''$  data for PS-95k, PS-545k, Blend 1 and Blend 2 at 130 °C.

## Conclusions

In summary, the molecular weight and polydispersity of linear polymers are strongly reflected in the linear viscoelastic response. It is clear that the low frequency response is sensitive to a small high molecular weight tail of the distribution due to the very strong molecular weight scaling of relaxation times.

Next step of this work will be the investigation on how these systems behave when they are subjected to fast extensional flows in order to explore their dynamic in the non-linear regime.

## Acknowledgements

I would like to express my sincere gratitude to my main supervisor Prof. Ole Hassager for his support and encouragement throughout this project. I am grateful to Dr. Qian Huang and Dr. Nicolas J. Alvarez for their guidance and help from the beginning of my Ph. D. I would also like to thank all the people at the Danish Polymer Centre.

## References

1. J. K. Nielsen., H. K. Rasmussen, O. Hassager, and G. H. McKinley, *J. Rheol.* 2006, 50, 453–476.
2. Q. Huang, N. J. Alvarez, Y. Matsumiya, H. K. Rasmussen, H. Watanabe and O. Hassager *ACS Macro Lett.* 2013, 2, 741–744.



**Peter Jørgensen Herslund**

Phone: +45 4525 2863  
E-mail: pjhe@kt.dtu.dk

Supervisors: Nicolas von Solms  
Kaj Thomsen  
Jens Abildskov

PhD Study  
Started: February 2010  
To be completed: December 2013

## Thermodynamic and Process Modelling of Gas Hydrate Systems in CO<sub>2</sub> Capture Processes

### Abstract

The fluid phase behaviour, of the binary system comprised of water and tetrahydrofuran (THF) is modeled by use of the Cubic-Plus-Association (CPA) equation of state. It is found that only by for allowing cross-association between water and THF, may the full qualitative behaviour of the fluid phase equilibria in this system be described by CPA. Based on the results presented in this work, it is suggested to model this binary system considering THF as cross-associating only, with two association sites. The use of a temperature dependent binary interaction parameter and a correlated binary cross-association volume then allows for both accurate vapour-liquid and liquid-liquid equilibria descriptions over large ranges of temperature and pressure. Hydrate formation pressure is modeled in promoted hydrate systems with THF.

### Introduction

Tetrahydrofuran (THF) is a cyclic ether compound with the chemical formula  $c\text{-(CH}_2\text{)}_4\text{O}$ . THF is, among others, used as a precursor in polymer production, a solvent for polymers, e.g. poly vinyl chloride (PVC) and also as a cleaning agent for semi-conductors [1]. However, THF has recently received growing attention due to its ability to form gas clathrate hydrates at moderate conditions of temperature and pressure.

Several publications are available in the literature, presenting THF as a potential thermodynamic promoter in hydrate-based pre- [2-5] or post combustion [2,3,6-9] capture of carbon dioxide (CO<sub>2</sub>).

In this work the Cubic-Plus-Association (CPA) equation of state (EoS) is used to model both the vapour-liquid equilibria (VLE) and the liquid-liquid equilibria (LLE) of the binary system.

Modelling results for both VLE and LLE behaviour are presented. This work presents only a condensed part of a thorough investigation, which is currently under preparation for publication.

### Model

The CPA equation of state combines the physical term from the cubic Soave-Redlich-Kwong (SRK) EoS with an association term similar to that found in the Statistical Associating Fluid Theory (SAFT) models.

On pressure explicit form, the CPA EoS may be expressed as Eq. 1 [10]:

$$P = \frac{R \cdot T}{V_m - b} - \frac{\alpha(T)}{V_m \cdot (V_m + b)} \quad (1)$$

$$- \frac{R \cdot T}{2 \cdot V_m} \left[ 1 + \frac{1}{V_m} \cdot \frac{\partial \ln g}{\partial (\frac{1}{V_m})} \right] \times \sum_i x_i \sum_A (1 - X_A)$$

Where  $R$  is the universal gas constant and  $T$  is temperature.  $V_m$  denotes the molar volume,  $\alpha(T)$  is the temperature dependent SRK energy parameter and  $b$  is the SRK co-volume parameter.  $g$  is the hard sphere radial distribution function.  $A_i$  denotes association site  $A$  on component  $i$ .  $x_i$  is the mole fraction of component  $i$ ,  $X_{A_i}$  is the fraction of sites, type  $A$  on component  $i$ , not bonded to other sites.

When extending CPA to binary or multi component mixtures, the classical van der Waals one fluid mixing rules, with “classical” combining rules, are applied for the SRK parameters,  $\alpha(T)$  and  $b$ , whereas the CR1 combining rules are applied for the two association parameters. Further details of the model and the applied mixing- and combining rules may be found elsewhere in the literature [10].

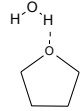
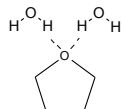
### Association

Here, association defines hydrogen bonding occurring between electron donating sites and electron accepting sites on two molecules.

Water is modeled as a self-associating compound using the 4C association scheme as defined by Huang and Radosz [11]. When using this association scheme, water is assigned two electron donating sites and two electron accepting sites. The five CPA pure component parameters for water are available elsewhere in the literature [10] and these have been adopted in this work.

THF is modeled as a non self-associating compound but is allowed to cross-associate with water via either one or two electron donating sites situated on the oxygen atom. The modelling scenario, where THF is assigned a single association site, is named Model 1. The other scenario, with two association sites on THF, is denoted Model 2. Table 1 illustrates the types of association allowed between water and THF in the two investigated scenarios.

**Table 1:** Cross-association allowed in the two modelling approaches presented. Model 1 has a single electron donating site on THF, whereas Model 2 has two electron donating sites on THF.

Model	Cross-association
1	
2	

In addition to the cross-association illustrated in Table 1 water molecules are always allowed to self-associate.

### Parameter Regression

Three pure component parameters for THF have been regressed as a part of this work. These parameters are obtained by correlating the CPA EoS to pure component vapour pressure- and saturated liquid density data [12]. The reference data have been limited, in terms of reduced temperature, to the interval  $0.30 < T/T_c < 0.93$ , where  $T_c$  equals 540.2 K for THF.

With THF being a non self-associating compound, the two self-association parameters,  $\epsilon^{AiBj}$  and  $\beta^{AiBj}$ , take values of zero for this compound. When applying the standard CR1 combining rules in order to estimate the binary cross-association parameters with water,  $\beta^{AiBj}(cross)$  takes a value of zero, inhibiting all cross-association. In order to solve this, the modification to the CR1 combining rule, presented by Folas et al. [13], is utilized in this work.

The binary parameters that can be correlated thus become the binary interaction parameter,  $k_{ij}$ , and the binary cross-association volume,  $\beta^{AiBj}(cross)$ .

Since the obtained  $k_{ij}$ 's turned out to be highly temperature dependant, attempts were made applying a temperature dependency on the correlated  $k_{ij}$ 's. By doing this, a total of 3 binary parameters are finally

adjusted simultaneously. In the following sections, Model 1 with a constant value for  $k_{ij}$  is denoted Model 1A. When a temperature dependent  $k_{ij}$  is used, the notation is changed to Model 1B. The same goes for Model 2 that changes notation to 2A and 2B.

A constrained optimisation algorithm has been implemented in order to regress binary parameters in CPA and thereby to correlate the experimental VLE data available in the literature [14-21]. The optimisation algorithm is based on a FORTRAN implementation of the simulated annealing (SA) global optimisation algorithm presented by Goffe et al. [22] (source code available via [23]). The objective function, to which the SA algorithm is applied, is defined by the sum of absolute differences between calculated and experimental boiling point temperatures, or boiling point pressures as well as calculated and experimental vapour phase compositions (if available). As an example, when correlating  $P_{xy}$  data, the objective function is defined by Eq. 2.

$$OBJ = \sum_i \left( \left| \frac{P_{calc,i} - P_{exp,i}}{P_{exp,i}} \right| + \left| \frac{y_{calc,i} - y_{exp,i}}{y_{exp,i}} \right| \right) \quad (2)$$

If  $T_{xy}$  data are available, the pressures in Eq. 2 are exchanged with temperatures. If only  $T_x$  or  $P_x$  data are available, the second term in the sum is omitted.

In order to assure complete miscibility in the liquid phase at low pressures, constraints have been applied in the form of stability tests (Gibbs energy minimisation) on the liquid phase in temperature and pressure regions close to the experimental boiling point data. A penalty function has been imposed such that any finding of liquid-liquid phase splits, where the experimental data show a single liquid phase, results in a step increase in the objective function.

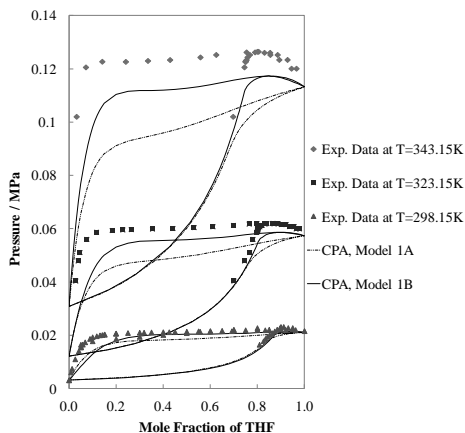
Finally the experimental LLE data at approximately 0.5 MPa presented by Riesco and Trusler [24] have been considered. A constraint has been set assuring liquid phase stability at 0.5 MPa up to temperatures of approximately 345 K. This constraint has been implemented in the form of stability tests for multiple compositions at the above conditions of temperature and pressure.

### Results and Discussion

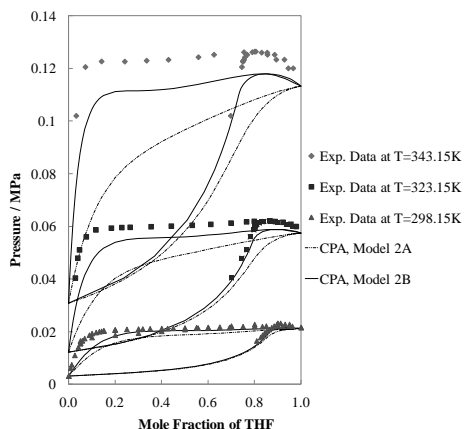
The obtained model parameters will be presented elsewhere in the literature in a publication currently under preparation. Here, only a selection of the obtained results is presented in graphical form. Figure 1, Figure 2 and Figure 3 compares the model performances with a selection of the experimental data used in the binary parameter regression.

Figure 1 clearly shows how CPA Model 1A (dashed lines) performs well at the lowest temperature ( $T = 298.15$  K) but loses accuracy as the temperature increases. By applying a temperature dependency on the regressed  $k_{ij}$  (CPA Model 1B – solid lines), the azeotrope in the experimental data is well described in terms of composition and the boiling point pressure

descriptions at the two high-temperature data sets are significantly improved.



**Figure 1:** Comparison of Model 1A and 1B with experimental boiling point and dew point pressures as functions of the tetrahydrofuran (THF) mole fraction in the binary system of water and THF. Experimental data from [14,15,17,19].

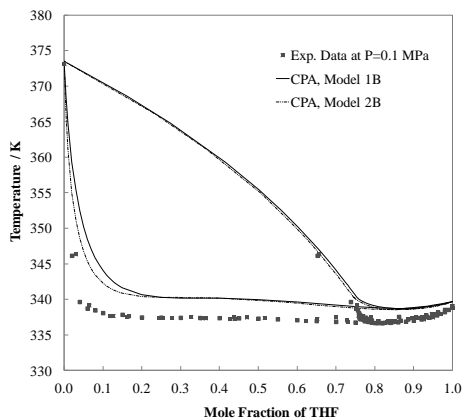


**Figure 2:** Comparison of Model 2A and 2B with experimental boiling point and dew point pressures as functions of the tetrahydrofuran (THF) mole fraction in the binary system of water and THF. Experimental data from [14,15,17,19].

Similar results are seen in Figure 2 for CPA Model 2A (dashed lines) and 2B (solid lines). Generally, both Model 1B and Model 2B underestimate the boiling point pressures at the two high-temperature data sets. This is a direct cause of the liquid-phase stability criterion set in the parameter regression work. By lowering the temperature in this criterion, the high temperature VLE descriptions may be improved, however the cost will be a liquid-liquid split stretching

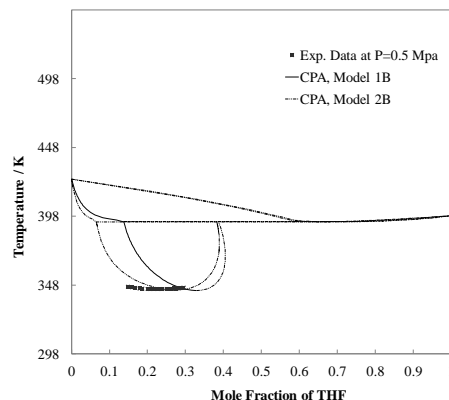
into the VLE region at  $T = 343.15$  K. Hence the above results are the best possible compromise enabling a description of both VLE and LLE with a single set of parameters.

Figure 3 shows  $T_{xy}$  descriptions of the VLE at a pressure of 0.1 MPa. Model 1B and Model 2B are compared in this figure. Despite Model 2B having two sites for cross-association with water, and Model 1B only a single site, the two models perform almost identical. Only in the low THF concentration region, at THF mole fractions below 0.2, does the differences between the two models become visible.



**Figure 3:** Comparison of Model 1B and 2B with experimental boiling point and dew point temperatures as functions of the tetrahydrofuran (THF) mole fraction in the binary system of water and THF. Experimental data from [14,18,20,21].

It is seen that Model 2B describes the boiling point temperature more accurately than Model 1B in systems with low THF content.



**Figure 4:** Comparison of Model 1B and 2B with experimental liquid-liquid separation temperatures as functions of the tetrahydrofuran (THF) mole fraction in

the binary system of water and THF. Experimental data from [24].

No actual LLE data were included in the binary parameter regression. Hence the LLE descriptions of Model 1B and Model 2B illustrated in Figure 4 are true predictions made by the CPA EoS. Only when using a temperature dependant  $k_{ij}$  does CPA predict LLE with the obtained parameters. Hence Model 1A and 2A predicts no LLE in the illustrated conditions of temperature and pressure.

Figure 5 now incorporates hydrate modeling and shows formation pressure as a function of THF concentration. The model clearly shows the optimum concentration at a ratio of 1 THF molecule to 17 water molecules

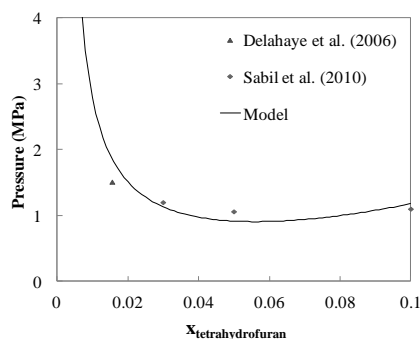


**Figure 5:** Hydrate formation pressure as a function of THF concentration. The model clearly shows the optimum concentration at a ratio of 1 THF molecule to 17 water molecules. Data from [25,26].

### Conclusion

Based on the results of this work, it is suggested to model this binary system considering THF as cross-associating only, with two cross-association sites. The use of a temperature dependent binary interaction parameter,  $k_{ij}$ , and a correlated binary cross-association volume,  $\beta^{Aij}$ , then allows for both accurate VLE and LLE descriptions over large ranges of temperature and pressure. A total of three binary parameters were regressed to experimental VLE data. Combining CPA with a van der Waals-Platteeuw model for hydrates can accurately predict hydrate formation pressure in promoted hydrate systems.

### Acknowledgements

The financial contributions to this work from the iCap project (EU FP7) and the Department of Chemical and Biochemical Engineering (MP<sub>2</sub>T) at The Technical University of Denmark, are greatly appreciated.

### References

1. H. Matsuda, N. Kamihama, K. Kurihara, K. Tochigi, K. Yokoyama, Journal of Chemical Engineering of Japan 41 (3) (2011) 131-139.
2. P. Linga, R. Kumar, P. Englezos, Chemical Engineering Science 62 (2007) 4268-4276.

3. P. Linga, R. Kumar, P. Englezos, J. of Hazardous Materials 149 (2007) 625-629.
4. J. Zhang, P. Yedlapalli, J. W. Lee, Chemical Engineering Science 64 (2009) 4732-4736.
5. H. J. Lee, J. D. Lee, P. Linga, P. Englezos, Y. S. Kim, M. S. Lee, Y. D. Kim, Energy 35 (2010) 2729-2733.
6. S.-P. Kang, H. Lee, Environ. Sci. Technol. 34 (2000) 4397-4400.
7. S.-P. Kang, H. Lee, C.-S. Lee, W.-M. Sung, Fluid Phase Equilibria 185 (2001) 101-109.
8. P. Linga, A. Adeyemo, P. Englezos, Environ. Sci. Technol. 42 (2007) 315-320.
9. C. Giavarini, F. Maccioni, M. L. Santarelli, Fuel 89 (2010) 623-628.
10. G.M. Kontogeorgis, M.L. Michelsen, G.K. Folas, S. Derawi, N. von Solms, E.H. Stenby, Ind. Eng. Chem. Res. 45 (2006) 4855-4868.
11. S. H., Huang, M., Radosz, Ind. Eng. Chem. Res. 29 (11) (1990) 2284-2294.
12. Design Institute for Physical Property Data (DIPPR). Diadem Pro.
13. G. K., Folas, G. M., Kontogeorgis, M. L., Michelsen, E. H., Stenby, Ind. Eng. Chem. Res. 45 (2006) 1527-1538.
14. V. A., Shnitko, V. B., Kogan, Journal of Applied Chemistry of the USSR (Zhurnal Prikladnoi Khimii) 41 (6) (1968) 1235-1242.
15. R., Signer, H., Arm, H., Daeniker, Helvetica Chimica Acta 52, 8 (1969) 2347-2351.
16. H. M., Lybarger, H. L., Greene, Advances in Chemistry Series 115 (1972) 148-158.
17. J., Matous, J. P., Novak, J., Sobr, J., Pick, Collection Szechoslov. Chem. Commun. 37 (1972) 2653-2663.
18. W., Hayduk, H., Laudie, O. H., Smith, Journal of Chemical and Engineering Data 18 (4) (1973) 373-376.
19. C., Treiner, Journal de Chimie Physique 70 (9) (1973) 1183-1187.
20. E., Sada, T., Morisue, K., Miyahara, Journal of Chemical and Engineering Data 20 (3) (1975) 283-287.
21. J., Lampa, J., Matous, J. P., Novak, J., Pick, Collection Czechoslov. Chem. Commun. 45 (1980) 1159-1167.
22. W. L., Goffe, G. D., Ferrier, J., Rogers, Journal of Econometrics 60 (1/2) (1994) 65-99.
23. SIMANN.F, <http://www.netlib.no/netlib/opt/simann.f> (Acquired July 2012).
24. N., Riesco, J. P. M., Trusler, Fluid Phase Equilibria 228-229 (2005) 233-238.
25. A. Delahaye, L. Fournaison, S. Marinhas, I. Chatti, J.-P. Petitot, D. Dalmazzone, W. Fürst, Ind. Eng. Chem. Res. 45 (2006) 391-397.
26. K. M. Sabil, G.-J. Witkamp, C. J. Peters, Fluid Phase Equilibria 290 (2010) 109-114.



**Krešimir Janeš**

Phone: +45 4525 2992  
E-mail: kreja@kt.dtu.dk

Supervisors: Krist V. Gernaey  
John M. Woodley  
Pär Tufvesson

PhD Study

Started: December 2010  
To be completed: February 2014

## Considerations for an Equilibrium Shifting Cascade Selection in $\omega$ -transaminase Systems

### Abstract

Production of optically pure chiral amines using transaminases is an attractive alternative to conventional synthetic methods, which yield low enantio-purity and require costly purification processes. The asymmetric synthesis approach promises higher yields compared to the kinetic resolutions, however many industrially interesting cases have been reported to have unfavourable equilibrium as a major challenge [1]. In order to achieve high enough yields at conditions typical for pharmaceutical processes (>50 g product/L, etc.) the product and/or co-product formed during the reaction must be selectively removed (so called *in-situ* co-product removal (ISCPR)). The implementation of different ISCPR technologies varies on a case-to-case basis. However, severely thermodynamically challenged systems require a second enzyme reaction to remove the co-product in a so called enzymatic cascade [2]. Several different enzymatic systems have been suggested for implementation, but still, there are no decision tools available to help select the most appropriate cascade systems.

### Introduction

The usage of the biocatalysis is continuously increasing in the pharmaceutical industry due to the greater availability of the enzymes and the diversity of the reactions enzymes can catalyze [3]. Regioselectivity of the biocatalysts offers the process simplification compared to the organic synthesis routes (reduction of protective/deprotective steps) and stereoselectivity enables production of desired chiral compounds, often chiral building blocks of the APIs, e.g. the production of chiral amines by  $\omega$ -transaminase. Currently there are many established processes in the industry using biocatalysis ( $\approx 300$ ) e.g. the usage of lipases, esterases, ketoreductases and proteases and many more emerging biocatalysts such as monoamine oxidases, transaminases and P450 monooxygenases to name a few.

The production of optically pure amines is an interesting topic for the pharmaceutical industry, particularly via biocatalysis when using, e.g.  $\omega$ -transaminases as an emerging technology. There are many challenges following the realization and implementation of these technologies and attempts of tackling them have been numerous. In some cases  $\omega$ -transaminase catalyzed reactions are thermodynamically challenged and equilibrium shifting strategies are required. Proposed equilibrium strategies are the selection of an amino

donor, excess of an amino donor, *in-situ* product removal (ISPR) and *in-situ* co-product removal (ISCPR). The last three strategies are based on the Le Chatelier's principle and there are many technologies available. However the implementation depends on the physical properties of the reaction mixture components and the  $K_{eq}$  value of the reaction.

For severely thermodynamically challenged reactions (Figure 1) ISCPR by enzymatic cascades provides the only option as equilibrium shifting strategy due to the very high substrate selectivity of the enzymes. In the literature several enzymatic cascades have been reported as an ISCPR for the  $\omega$ -transaminase systems. However no process considerations for selecting a cascade in an industrial process have been given. It is therefore, the main objective of this work to consider different aspects of shifting the equilibrium in the  $\omega$ -transaminase system by enzymatic cascades. Considerations are based on the conditions typical for industrial process implementation, e.g. > 50 g product/L.

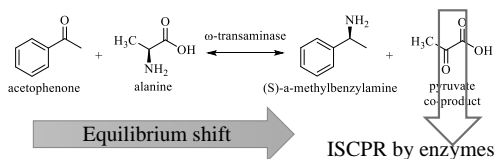


**Figure 1:** General figure of ISCPR by enzymes for shifting the equilibrium in the  $\omega$ -transaminase system

### Specific Objectives

In this research lactate dehydrogenase (LDH) (E.C. 1.1.1.27), alanine dehydrogenase (E.C. 1.4.1.1) (AlaDH) and yeast alcohol dehydrogenase (E.C. 1.1.1.1) (YADH) have been researched as co-product degrading enzymes and glucose dehydrogenase (GDH) (E.C. 1.1.1.47) and formate dehydrogenase (E.C. 1.2.1.2) (FDH) as co-factor regeneration enzymes. Additionally pyruvate decarboxylase (E.C. 4.1.1.1) (PDC) and acetolactate synthase (E.C. 2.2.1.6) (ALS) have been considered as co-product degrading options. All enzymes have been put in the context of an industrial process and dehydrogenases have been compared and evaluated experimentally to identify possible candidates for industrial application.

### Considerations for a Cascade Selection

The implementation of different cascades for shifting the equilibrium in the  $\omega$ -transaminase systems will result in a different process with different reaction components at the end of the reaction, different pH changes and DSP options to name a few considerations. Building a database of different process and enzyme considerations help describe each cascade option however it doesn't directly indicate which cascade is feasible for the industrial implementation. To develop a cascade selection process, several important considerations have been identified as feasibility considerations indicating whether or not the given cascade is applicable: thermodynamics, substrate selectivity and operational stability of the cascade enzymes.

## Results and Discussion

### Thermodynamics

For the severely thermodynamically challenged systems, e.g. the reaction system shown in the Figure 1, where the  $K_{eq}$  value is  $4.03 \cdot 10^{-5}$  [4] ISCPR by enzymatic cascades is the only option.

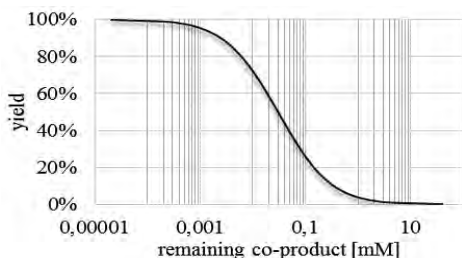


**Figure 2:** Desired yield as a function of allowed co-product remaining in the reaction mixture for the

equilibrium value  $K_{eq} = 4.03 \cdot 10^{-5}$  and one time excess (1X) of amino donor

As shown in the Figure 2, the amount of allowed residual co-product in the reaction mixture decreases significantly with the increase of the yield. For the industrially relevant yields, e.g. 95 % and for the given conditions from Figure 2 the allowed residual co-product concentration is 1.11  $\mu$ M. To investigate the additive effect of a possible secondary (ISPR) and tertiary (Amino Donor Excess) equilibrium shifting strategy, similar calculations can be made.

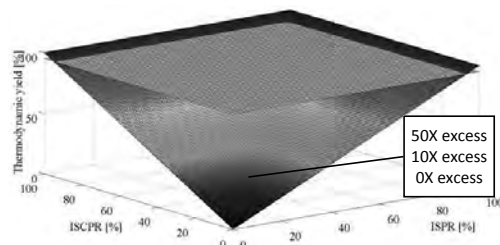


**Figure 3:** Thermodynamic yield as a function of ISPR (x axis), ISCPR (y axis) and Amino Donor Excess (0X lower surface, 10X and 50X upper surface); due to the low  $K_{eq}$   $4.03 \cdot 10^{-5}$  the difference between Amino Donor Excess surfaces (0X, 10X and 50X) is almost indistinguishable meaning that the Amino Donor Excess does not contribute significantly to the increase of the yield; the horizontal flat surface indicates 95 % yield.

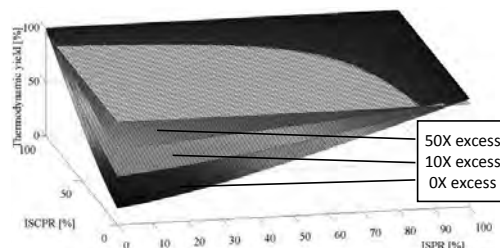


**Figure 4:** Thermodynamic yield as a function of ISPR (x axis), ISCPR (y axis) and Amino Donor Excess (0X lower surface, 10X and 50X upper surface) for the case where 2-propylamine is used as an amino donor with  $K_{eq}$   $3.33 \cdot 10^{-2}$ ; the contribution of Amino Donor Excess has increased compared to the previous case due to more favorable  $K_{eq}$  value; horizontal flat surface indicates 95 % yield.

Taking into consideration the conditions from Figure 2, it is possible to set a limit for thermodynamic yield expressed in terms of the allowed residual co-product concentration which all cascades have to satisfy. This limit is case dependent and varies with the  $K_{eq}$  which is the case for the YADH cascade or when alanine recycling is present in the case of AlaDH. The next step is to calculate the thermodynamic ability of the cascade. The  $K_{eq}$  is calculated for every cascade reaction based on the literature [5], and an iterative program has been made to calculate how much of residual co-product is left after thermodynamic equilibrium is established.



**Table 1:** Allowed residual co-product vs. the thermodynamic ability of the individual cascade system and the resulting thermodynamic conversion

Enzymatic cascade	Allowed co-product [ $\mu\text{M}$ ]	Thermodynamic ability (co-product [ $\mu\text{M}$ ])	Thermodynamic conversion
LDH/GDH	1.11	$1.10 \cdot 10^{-7}$	> 99.99 %
LDH/FDH	1.11	$1.25 \cdot 10^{-7}$	> 99.99 %
AlaDH/GDH	2.11	$9.28 \cdot 10^{-2}$	99.77 %
AlaDH/FDH	2.11	$1.66 \cdot 10^{-8}$	> 99.99 %
YADH/GDH	$9.21 \cdot 10^2$	$1.65 \cdot 10^{-1}$	99.12 %
YADH/FDH	$9.21 \cdot 10^2$	$1.81 \cdot 10^{-1}$	99.12 %
PDC	1.11	$7.89 \cdot 10^{-25}$	> 99.99 %
ALS	1.11	N.A.	N.A.

Simulations showed that all cascades satisfy the thermodynamic consideration for cascade selection and none can be discarded at this point.

### Substrate Selectivity Considerations

One of the considerations that will determine the feasibility of a given cascade is the substrate selectivity. In this case two types of substrate selectivity can be observed and the first type is the cascade selectivity. A cascade enzyme that consumes the co-product, e.g. pyruvate or acetone could, if lacking sufficient selectivity, consume other ketones in the reaction mixture, e.g. acetophenone. This would result in two parallel competing reactions where the  $\omega$ -transaminase ketone substrate would be consumed both by  $\omega$ -transaminase and a cascade enzyme resulting in an unfavorable shift of the thermodynamic equilibrium and possible loss of the desired amine product. None of the investigated cascades showed an observable reaction with the undesired ketone. The second type of the substrate selectivity is the selectivity of the  $\omega$ -transaminase towards the products of the cascade reactions.

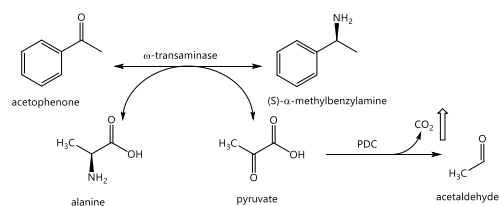


**Figure 5:** PDC cascade for shifting the equilibrium in an  $\omega$ -transaminase system

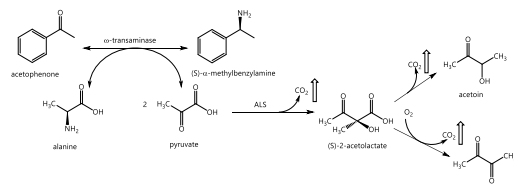


**Figure 6:** ALS cascade for shifting the equilibrium in an  $\omega$ -transaminase system

As shown in Figure 5 and Figure 6, products of the PDC and ALS cascades are aldehydes, ketones or diketones which are preferred or possible substrates for most of the transaminases [6]. In this type of process a sequential reaction would follow the main  $\omega$ -transaminase reaction. This reaction would produce an undesired amine product consuming the keto- or aldehyde substrate (produced by PDC or ALS cascade) and the consumed amino donor would be either the amino donor alanine or more likely, the desired amino product S- $\alpha$ -methylbenzylamine. Another consequence would be a resulting reaction mixture containing different amines and separating the desired one would prove to be difficult. Taking into consideration the negative effects described, it is reasonable to exclude the PDC and ALS enzymatic cascades from the process implementation until the selectivity of the  $\omega$ -transaminase can be improved.

### Operational Stability of the Enzymes

The reaction conditions in the industrial process are usually harmful to the enzymes and to maintain the desired rate of the reaction often additional quantities of enzymes must be added. It is therefore very desirable to have an enzyme with sufficient stability towards the industrial conditions. Ideally, to evaluate stability of the enzymes under industrial conditions, operational stability experiments would have to be performed under such conditions [7]. However, a compromise has been made by simulating the process conditions by preparing a reaction mixtures consisting of averaged concentrations corresponding to the beginning and the end of the reaction based on 50 g/L of product formed. Different reaction mixtures have been prepared to simulate different cascade systems and the stability of the corresponding enzymes has been measured after 0, 4 and 24 hours (Figure 7).

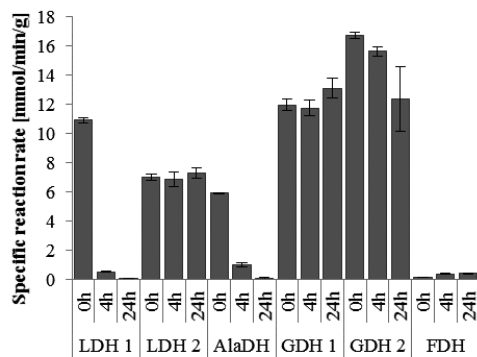


**Figure 7:** Cascade enzyme stability under the corresponding industrial conditions; LDH 1 and LDH 2 represents the same enzyme from two different sources as well as GDH 1 and GDH 2

As shown in Figure 7 LDH 1 and AlaDH have shown insufficient stability towards the process conditions. The experiments with YADH showed no observable activity at time 0 hours leaving only two

possible cascade systems for industrial implementation: LDH/GDH and LDH/FDH. In the first cascade system, the co-factor recycling enzyme GDH has an obvious advantage over FDH in terms of the relative activity, meaning less of the enzyme is needed to achieve the desired reaction rate. However, GDH is a pH changing enzyme (gluconic acid production) and pH regulation is necessary. Moreover, the product of FDH is CO<sub>2</sub> which facilitates the DSP. The summary of the selection process is shown in Figure 8.

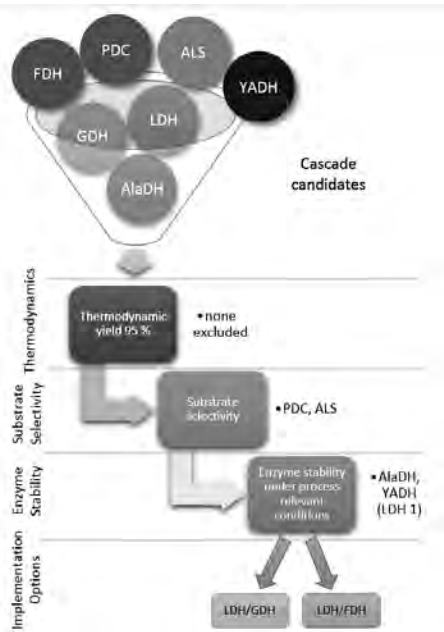


**Figure 8:** An overview of the selection process of the cascades in the  $\omega$ -transaminase systems; two possible cascade systems LDH/GDH and LDH/FDH are candidates for industrial implementation.

### Conclusions

The selection process based on process considerations was created and was successfully implemented on eight cascade systems suggested in the literature to shift the equilibrium in  $\omega$ -transaminase systems. Two cascade systems were identified as promising candidates for industrial implementation. However, further investigation of the process set-up and the optimization of the enzyme concentrations are necessary to select one cascade system over another.

### Future Work

- Development of the kinetic models for both implementation candidates
- Validation of the models and further investigation of the process set-up implementation based on the simulations

### Acknowledgments

The support from the AMBIOCAS project financed through the European Union 7<sup>th</sup> Framework Programme (Grant agreement no.: 245144) is acknowledged as well to the Codexis for supplying some of the enzymes

### References

1. Tufvesson P, Lima-Ramos J, Skibsted J J, Al-Haque N, Neto W, Woodley J M. Process considerations for the asymmetric synthesis of chiral amines using transaminases. *Biotech. Bioeng.* (2011) Vol. 108: 1479-1493
2. Koszelewski, D.; Tauber, K.; Faber, K.; Kroutil, W.,  $\omega$ -Transaminases for the synthesis of non-racemic  $\alpha$ -chiral primary amines. *Trends in Biotechnology* (2010) Vol. 28, 324-332.
3. Sutton, P. W.; Adams, J. P.; Archer, I.; Auriol, D.; Avi, M.; Branney, C.; Collis, A. J.; Dumas, B.; Eckrich, T.; Fotheringham, I.; ter Halle, R.; Hanlon, S.; Hansen, M.; Holt-Tiffin, K. E.; Howard, R. M.; Huisman, G. W.; Iding, H.; Kiewel, K.; Kittelmann, M.; Kupfer, E.; Laumen, K.; Lefèvre, F.; Luetz, S.; Mangan, D. P.; Martin, V. A.; Meyer, H.-P.; Moody, T. S.; Osorio-Lozada, A.; Robins, K.; Snajdrova, R.; Truppo, M. D.; Wells, A.; Wirz, B.; Wong, J. W., *Biocatalysis in the Fine Chemical and Pharmaceutical Industries. In Practical Methods for Biocatalysis and Biotransformations 2*, Whittall, J., Ed.: John Wiley & Sons, Ltd. (2012) 1-59.
4. Tufvesson, P.; Jensen, J. S.; Kroutil, W.; Woodley, J. M., Experimental determination of thermodynamic equilibrium in biocatalytic transamination. *Biotech. Bioeng.* (2012) Vol. 109, 2159-2162.
5. Alberty, R. A., Calculating apparent equilibrium constants of enzyme-catalyzed reactions at pH 7. *Biochem. Ed.* (2000) Vol. 28, 12-17.
6. Höhne, M.; Bornscheuer, U. T., *Biocatalytic Routes to Optically Active Amines. Chem. Cat. Chem* (2009) Vol. 1, 42-51.
7. Gardossi, L.; Poulsen, P. B.; Ballesteros, A.; Hult, K.; Svedas, V. K.; Vasic-Racki, D.; Carrea, G.; Magnusson, A.; Schmid, A.; Wohlgemuth, R.; Halling, P. J., Guidelines for reporting of biocatalytic reactions. *Trends Biotechnol.* (2010), 28, 171-180.

**Joakim M. Johansen**

Phone: +45 4525 2830  
E-mail: jjoha@kt.dtu.dk

Supervisors: Peter Glarborg  
Peter A. Jensen

**PhD Study**

Started: September 2011  
To be completed: Fall 2014

## Biomass Burners for Biodust Combustion

**Abstract**

In the strive for a CO<sub>2</sub>-neutral energy profile the exploitation of biomass in central and decentral heat and power plants has continuously increased in recent decades. This PhD-project aims to establish a scientific basis for the development of a new generation of biodust burners for utility boilers. The project focuses on particle ignition and flame stabilization through parametric studies both in full-scale measurements and from a CFD (Computational Fluid Dynamics) point of view. This article will introduce the reader to the work flow established to fulfill this goal.

**Introduction**

In recent decades, central power and heat production through thermal conversion of biomass has gained ground concurrently with the political agenda both on a national and an international level. The development of high efficiency biomass plants are required in order to balance the fluctuating power production from wind mills and other alternative energy sources, while still striving towards a CO<sub>2</sub>-neutral energy profile. In addition, thermal plants are a necessary need in the provision of district heating.

Development and implementation of high efficiency biomass combustion technology is arguably the best near-term solution to provide stable and CO<sub>2</sub>-neutral centralized power and district heating to larger cities and industrial areas.

Biomass differs from conventional solid fossil fuels (traditionally coal) in a number of essential areas including both chemical composition and physical structure and appearance. Thus, direct utilization of existing high efficiency pulverized power or combined heat and power facilities is not an option when considering biodust as an energy source.

The fibrous nature of the biomass complicates particle pretreatment implying larger and oddly shaped fuel particles; changing the aerodynamics and particle size distributions. In addition, the larger fraction of volatile matter changes the conditions at which a stable flame is achieved. A turbulent development of the technology aiming to convert existing high efficiency burner installations has been conducted in Denmark throughout the past couple of decades. However, technical difficulties lower the efficiency and limit the

operation flexibility both with regards to biomass type and quantity.

**Objectives**

This work aims to establish a scientific basis for the development of a new generation of biomass burners designed to facilitate simultaneous high power efficiency and fuel flexibility combined with good particle burn-out and stable flame capabilities of dedicated biodust fueled plants. The project will link fuel properties to flame properties, considering both fluid dynamic effects due to the differences in particle characters and chemical effects due to changes in the chemical composition and kinetics.

**Content**

The project will include full scale combustion measurements from relevant plants operated by the industrial partners: Dong Energy Power and Vattenfall. This will include advanced in-situ high speed thermal imaging, optical and extractive probe measurements of the flame, burner area, and fuel conveying system. Close coordination with other work-packages will ensure thorough fuel characterization of a range of different biomass fuels. Flame detection by state of the art diagnostic techniques will be evaluated for optimized operational control.

Fundamental research will be conducted in lab and pilot-scale forming the basis for the modeling work applicable to computational fluid dynamics calculations taking both chemical kinetics and aerodynamic differences between fossil fuels and biodust into account, for the development of novel burner designs.

### Devolatilization Kinetics at High Heating Rates

Devolatilization experiments at high heating rates aim to mimic the conditions seen by particles entraining e.g. a pulverized fuel flame. This is typically described by heating rates in the order of  $10^5$ - $10^6$  K/s which can be achieved in entrained flow reactors. Figure 1 shows the conversion degree as function of residence time when rapidly heating a woody and an energy crop at high heating rates and reducing conditions.

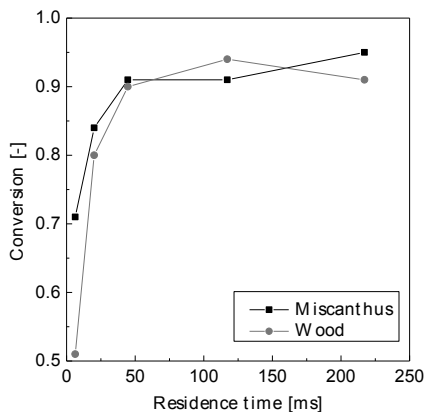


**Figure 1:** Devolatilization progression as function of residence time for two different fuels heated in a laminar entrained flow reactor in reducing conditions.

From such data the devolatilization kinetics can be extracted and used in CFD modeling.

### Evaluation of the kinetic data

Kinetic data is evaluated in pilot scale facilities employing a 15 kW drop tube furnace allowing for in-situ temperature and gas concentration measurements as well as particle extraction. The validity of the determined devolatilization kinetics may then be evaluated by comparing the observed flame characteristics with corresponding CFD simulations.

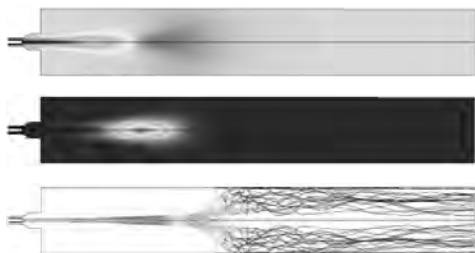


**Figure 2:** CFD calculations of (top) temperature, (middle) CO mass fraction, and (bottom) particle trajectories and mass loss of wood particles burning in a 15 kW entrained flow reactor.

### Extrapolating Numerical Models

Because the issue of scaling is a broadly accepted phenomenon, creating guidelines for novel technology development based on either numerical simulations or experimental studies the final result will benefit from the study being carried out at the scale intended.

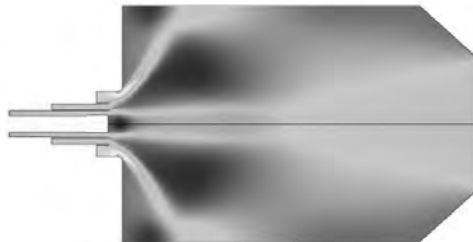


**Figure 3:** Axial velocity predictions of 2D-axisymmetric full-scale burner modeling firing 30MW of wood dust.

Figure 3 shows a velocity prediction of a scaled up numerical simulation of a full-size biodust burner. These models, with sub-routines developed on the basis of the lab-scale data, can be used to simulate a broad range of scenarios of operating conditions leading to the development of guidelines for burner construction.

### Full-Scale Measurements

Because scaling issues are not specific to experimental setups but also applies to numerical simulations. The full-scale CFD models are validated against in-situ power plant measurements, e.g. temperature profiles as presented in Figure 4.

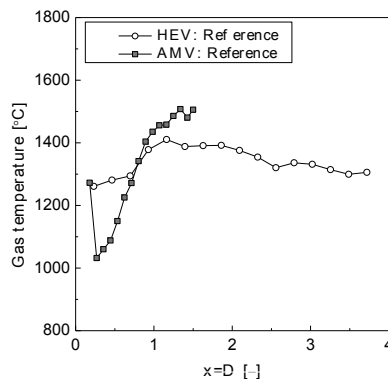


**Figure 4:** Gas phase temperature profiles along the flame center axis for HEV: Herningværket and AMV: Amagerværket.

### Acknowledgements

This PhD project is part of the GREEN Research Center (Center for Power Generation from Renewable Energy) financed by the Danish Strategic Research Council.

**Sawitree Kalakul**

Phone: +45 5024 2872  
E-mail: sawit@kt.dtu.dk

Supervisors: Rafiqul Gani  
Georgios Kontogeorgis

**PhD Study**

Started: 1 June 2013  
To be completed: 30 May 2016

## Property Modeling and Tailor-Made Mixture Design Involving Complex Chemical Systems

**Abstract**

This project deals with modeling to predict properties of chemical systems (liquid mixtures containing combinations of lipids, solvents, inorganic salts and water), the further development of model-based design of liquid formulated products and the implementation of the models and the model-based design methods in a product-process design software, the Virtual Product-Process Design Laboratory (VPPD-Lab). The application of the developed models, methods and tools will be highlighted through different case studies, for example, tailor-made design of jet-fuels and design of formulated liquid products-processes involving lipids.

**Introduction**

Complex chemical systems are typically encountered in processes handling lipids, such as in edible oil production, production of crude gaseous or liquid fossil fuels, biodiesel production, and pharmaceutical product manufacturing. The growth rates of products with complex chemical systems such as oils and fats have been remarkable in the past few years. Also, the demand for jet-fuel has been steadily increasing, raising concerns about greenhouse gas emissions by the aviation sector. The resulting growth in the production of oils, fats and fuels together with consumer's increasing preference for better quality products offer major challenges to the lipid processing industry and the concept of tailor-made fuel blends, such as jet-fuel and gasoline.

The VPPD-Lab is a computer-aided product-process engineering toolbox that has been developed as an aid to product-process development. Rather than design chemicals based products through an experiment-based trial and error approach, the VPPD-Lab offers a quick and thorough search of the alternatives through a model-based approach to be followed by experiment-based validation and evaluation of the most promising candidates for eventual selection of the final product. In this way, VPPD-Lab performs virtual experiments to identify the products that satisfy property requirements and the design of process that can manufacture them with the same qualities [1]. The current version of VPPD Lab consists of templates for the design of

microcapsules, and homogeneous liquid formulated products. Yunus et al. (2013) and Mattei et al. (2013) have developed methods for the design of blended and emulsified products, respectively, that also need to be incorporated as new design templates in VPPD-Lab.

Property models for different chemical types and algorithms for mixture (blend) design have been developed and these need to be incorporated within the VPPD-Lab toolbox. To make the VPPD-Lab generic and widely applicable, a wide range of property prediction models need to be developed and integrated to the different steps of the design algorithm. Also, the template for each type of products requires databases of chemicals as well as properties that also need to be incorporated in a flexible and efficient manner.

**Objectives of the project**

- (i) Evaluate the requirements of property models together with the available data to determine the property model needs for use in design-analysis of products-processes handling lipids and other complex chemicals.
- (ii) Extend the application range of VPPD-Lab with new models, methods and tools, and, apply the developed property models for the tailor-made design of jet-fuel and other blended liquid formulations.

**Framework of VPPD-Lab**

The framework for property modeling and extension of VPPD-Lab is illustrated in Figure 1.

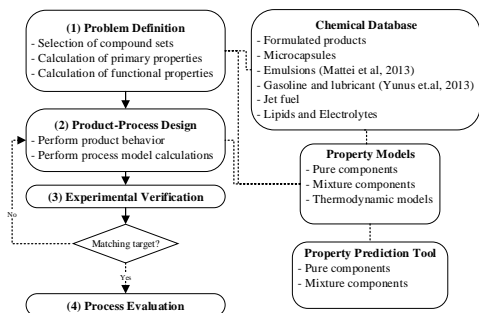


**Figure 1:** Framework for property modeling and extension of VPPD-Lab

(1) *Problem Definition:* the product needs are identified by selection of compound sets and translated to the target property values. This step requires data from chemicals databases that contain molecular information, property values and model parameters for available property models, which may be used to predict the defined property targets. In case that the property values or model parameters are not available, the property prediction models will need to be adopted/extended to handle the new chemicals. In this step, available property models for the complex chemicals system such as lipids, electrolytes, and jet-fuel will be implemented together with emulsions [2], and gasoline blends, lubricant and other liquid formulated products [3].

(2) *Product-Process Design:* The analysis of product behavior or performance involves the calculation of various mixture properties and the verification of the mixture stability. The process evaluation also needs a set of mixture properties so that the ability of the process to produce the designed product can be verified.

(3) *Experimental verification:* The desired products are verified experimentally.

(4) *Process Evaluation:* A process that can produce the designed product is identified and its feasibility evaluated.

### Case Study: Blend design of jet-fuel

In this case study only steps 1 & 2 are highlighted.

(1) *Problem Definition:* For jet-fuel, the following two issues, among others, need to be considered: (i) consistency of crude-oil supply; (ii) the harmful impurities. Therefore, the substitution of jet-fuel components with new chemicals is needed and stability of the blend is the most important issue since all the components must form a single phase liquid with the desired properties. Also, adding bio-based compounds would directly reduce the fossil fuel crude oil consumption and the environmental impacts. The bio-based chemicals are mainly ester converted from an organic compound (alcohols, ethers, ketones, acids and furan derivatives). The blended jet-fuel should meet the standard specifications of performance and safety. The common and problem specific properties for blended jet-fuel are listed in Table 1. LB/UB are the allowed lower/upper limits of the property values. In this step

the properties of selected jet-fuel compositions are calculated, large numbers of candidate chemicals are reduced by analyzing the miss-match of the target properties. The remaining chemicals are considered in the next step.

**Table 1:** Standard specification of jet fuel

Product needs:	Target properties:	Unit	LB	UB
Combustion ability	Net heat of combustion	MJ/kg	42.8	-
	Smoke point	mm	25	-
Volatility	Flash point	°C	38	-
Fluidity	Viscosity at -20 °C	mm <sup>2</sup> /s	-	8
	Freezing point	°C	-	-47
Stability	JFTOT ΔP at 260 °C	mmHg	-	25
Blend regulatory issues and emissions	Aromatic content	vol%	-	25
	Sulphur content	wt%	-	0.3
	Naphthalene content	vol%	-	3
	Acidity	mg KOH/g	-	0.015

### (2) Product-Process Design:

The jet-fuel blend problem is formulated as a Mixed Integer Non-Linear Programming (MINLP) problem, where the jet-fuel composition is optimized. The objective of this case study is to design the blended jet fuels that are suitable for commercial use (jet A-1) that satisfy the target properties listed in Table 1.

### Conclusions

The property modeling framework within the VPPD-Lab is extended and adopted to handle a wider range of liquid blended products. It is expected to make the chemicals based product design faster and at reduced cost by converting some of the time consuming experiment-based design steps to accurate and reliable model-based design steps. In this way, model-based techniques are employed for initial screening and for identifying a small number of potential candidates, while the experiments are used for verification and final selection.

### Future Work

Property models for jet-fuels related chemicals and formulated liquid products-processes involving lipids will be developed in order to predict their primary and functional properties. Also, the models will be extended to the specific design procedures. The chemical databases and calculation models for each type of product will be revised and managed through the system information and integrated in order to design a wide range of chemicals based liquid products.

### References

- 1 E. Conte, R. Gani, K.M. Ng. *AIChe J.* (57) (2011) 2431.
- 2 M. Mattei, M. Hill, G.M. Kontogeorgis, R. Gani. *Computer Aided Chemical Engineering* (32) (2013) 817-822.
- 3 N.A. Yunus, K.V. Gernaey, J.M. Woodley, R. Gani. *Computer Aided Chemical Engineering* (32) (2013) 835-840.



**Malgorzata Kostrzewska**

Phone: +45 4525 6195  
E-mail: malko@kt.dtu.dk

Supervisors: Anne Ladegaard Skov  
Søren Hvilsted

PhD Study  
Started: September 2013  
To be completed: September 2016

## Determination of Core-Shell Content of Liquid Core Microcapsules

### Abstract

Reactive liquid cross-linker molecules are encapsulated in PMMA microcapsules by use of the solvent extraction/evaporation technique. This report describes and compares three methods for determination of core content. Integration of peaks in NMR spectrum of microcapsules revealed to be a convenient way to establish the core-shell content as it involves only the dissolving of sample. This method allows for fast and accurate calculation of core content.

### Introduction

Encapsulation is a powerful tool for design of novel materials. Solid, liquid and gaseous ingredients can be packed within a second material, which protects the inner part from the surrounding environment. Thus the inner part is called core, and the outer part is designated as shell [1]. The morphology, size and shape of microcapsules depend on the applied materials and preparation techniques. There are many well-described techniques in the literature for preparation of microcapsules. The solvent extraction/evaporation method is one of the most well-known techniques and basically consists of four steps [2]. Firstly shell and core materials are dissolved in a highly volatile organic solvent. The mixture is then dispersed in an immiscible continuous phase to form an emulsion. The third step is an evaporation of solvent which leads to solidification of the shell material and formation of microcapsules. Washing and drying of microcapsules are the terminal step in the process. The technique has been chosen for preparation of microcapsules in this project because it is relatively easy to scale-up and previous studies have shown it is a suitable way to synthesis PMMA shell microcapsules with liquid, low viscosity core [2-4].

### Specific objectives

The aim of this project is to design microcapsules and then to upscale the preparation process to the best performing system. The first part will include preparation of microcapsules under varying conditions and characterization of them. Mainly core content, size distribution and release mechanism will be investigated. In the second part the optimal conditions established in

the previous experiments will be used to upscale the production of microcapsules.

### Preparation of samples

Poly(methyl methacrylate) (PMMA) and HMS-301 were used for preparation of microcapsules as shell and core material, respectively. Proper amounts of PMMA ( $m_{\text{PMMA}}$ ) and HMS-301 ( $m_{\text{HMS-301}}$ ) were dissolved in 75 mL of dichloromethane (DCM). The mixture was then slowly added during mechanical stirring (2000 rpm) to an equal volume of 1% surfactant solution. Two kinds of surfactants were used – poly(vinyl alcohol) (PVA) and poly(methacrylic acid) (PMAA). In some cases acetone was added to aim the emulsification process. When the emulsion was formed, the agitation speed was decreased to 750 rpm and kept for further 1 hour. In order to evaporate the DCM, emulsion was diluted with 120 mL of surfactant solution and rotary evaporated for 1.5 hour. Microcapsules were then washed with water and heptane to ensure no cross-linker left on the surface of microcapsules. In table 1 all studied microcapsules formulations are listed.

**Table 1:** Prepared microcapsules formulations

entry	$m_{\text{PMMA}}$ [g]	$m_{\text{HMS-301}}$ [g]	S	acetone	$\emptyset$ [ $\mu\text{m}$ ]
1	1	1.5	PVA	No	13.1
2	1	1.5		Yes	13.3
3	2.55	3.9		No	19.9
4	2.55	3.9		Yes	12.9
5	1	1.5	PMAA	No	13.6
6	1	1.5		Yes	11.9
7	2.55	3.9		No	10.5
8	2.55	3.9		Yes	9.3

## Results and the discussion

As it can be seen from table 1, the average diameters ( $\varnothing$ ) of the microcapsules are in the range of 9.3 to 19.9  $\mu\text{m}$ . The diameter of microcapsules depends on the used surfactant solution, while addition of acetone and the concentration of shell and core materials to the organic phase does not influence the average size of capsules. The microcapsules are slightly bigger when the PVA solution was used.

The weight percent of core material ( $W\%_{\text{HMS-301}}$ ) was determined by three techniques: TGA, NMR and extraction. Figure 1 presents TGA plots of pure HMS-301, PMMA and microcapsules, respectively.

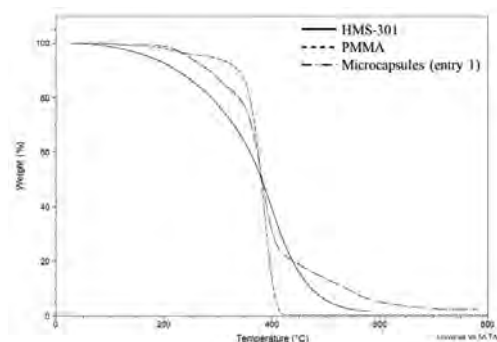


**Figure 1:** TGA plots of PMMA, HMS-301 and microcapsules.

The major thermal decomposition of PMMA starts around 270°C and at 430°C all PMMA is decomposed. Degradation of HMS-301 starts at 165°C and ends above 600°C. As the decomposition of those compounds takes place in the same temperature range up to 430°C, in order to determine the core content physical mixtures of PMMA and HMS-301 with different concentrations were prepared. From the knowledge of the residue at 430°C ( $R_{430^\circ\text{C}}$ ) the proportional factor  $K$  can be calculated from equation 1.

$$W\%_{\text{HMS-301}} = K * R_{430^\circ\text{C}} \text{ "eq. 1"}$$

$K$  was plotted as a function of residue at 430°C, and the calibration equation was established. By using the  $R_{430^\circ\text{C}}$  of microcapsules and replacing the  $K$  with the calibration equation, the content of encapsulated HMS-301 was calculated.

$^1\text{H}$  NMR spectra of the microcapsules were recorded and analyzed. Peaks at 4.6 ppm were observed and ascribed to protons which are directly linked with Si atom in the cross-linker molecule. Additionally, signals at 3.6 ppm were assigned to H atoms of the methyl groups attached to ester in PMMA. From integration of the areas of those peaks, the  $W\%_{\text{HMS-301}}$  was estimated. In table 2 results obtained from both investigated methods are gathered.

**Table 2:** Core content of microcapsules

Entry	$W\%_{\text{HMS-301}}$		
	TGA	NMR	Extraction method
1	48	53	-
2	51	55	-
3	41	42	47
4	50	58	-
5	10	26	-
6	21	43	-
7	35	50	51
8	25	32	-

When the PVA solution was used the microcapsules contained more HMS-301 than those prepared in 1% PMAA solution (expect entry 3 – NMR column). It must be underlined that results calculated by TGA and NMR techniques differ from each other. For further verification a third method was applied.  $W\%_{\text{HMS-301}}$  of two microcapsules formulations was investigated by an extraction method. Firstly, microcapsules were grounded on a filter paper and inserted into an oven for 5 hours at 120°C. The crushed microcapsules were then washed with heptane (100 mL) to remove the HMS-301 and dried in the oven at 80°C overnight. From the initial weight of microcapsules ( $W_i$ ) and the weight of the residual PMMA shell ( $W_s$ ),  $W\%_{\text{HMS-301}}$  of the microcapsules was calculated as:

$$W\%_{\text{HMS-301}} = 1 - (W_s/W_i) * 100\% \text{ "eq. 2"}$$

In table 2 it can be seen that NMR and extraction methods results are in good agreement. TGA method was found to be inaccurate as some reactions can occur between HMS-301 molecules at high temperatures. It was confirmed by repeating TGA measurements of pure cross-linker few times. The residue at 430°C varied between 24 and 45%.

## Conclusions

Microcapsules were prepared by the solvent evaporation method. Determination of core content was investigated by three methods. The integration of peaks by NMR technique was found to be the most convenient technique. It is fast and accurate as it involves only the dissolving of the sample. The validity of this technique was confirmed by the extraction method.

## References

1. R. Dubey, T.C. Shami, K.U. Bhasker Rao, Defence Science Journal 59 (1) (2009) 82-95
2. J. Wang, X. Dong, S. Chen, J. Lou, Colloid Journal 75 (1) (2013) 26-33
3. A. Loxley, B. Vincent, Journal of Colloid and Interface science 208 (1) (1998) 49-62
4. Q. Li, A. K. Mishra, N. H. Kim, T. Kuila, K. Lau, J. H. Lee, Composites: Part B 49 (2013) 6-15





## Dorte Møller Larsen

Phone: +45 4525 2705  
E-mail: dml@kt.dtu.dk

Supervisor: Jørn Dalgaard Mikkelsen

### PhD Study

Started: March 2008  
To be completed: February 2014

## Discovery and Engineering of a Bacterial Rhamnogalacturonan I Lyase

### Abstract

Thermostable enzymes are required, to allow processing at elevated temperatures at which the substrate viscosity and risk of contamination are lower, the enzymatic rates are higher, mixing are easier and the substrate solubility is better. A relatively thermostable rhamnogalacturonan I (RGI) lyase (EC 4.2.2.-) from *Bacillus licheniformis* has been identified, codon optimized and successfully expressed in *Pichia pastoris* and biochemically characterized. The optimal reaction conditions for the RGI lyase were established to be 61 °C, pH 8.1 requiring 2 mM of both Ca<sup>2+</sup> and Mn<sup>2+</sup> (specific activity: 18.4U/ mg, Km: 1.2 mg/mL) with a half life of 15 min at 61 °C. The RGI lyase was optimized further with respect to thermal stability by targeted single point mutations for site-saturated mutagenesis. A library was constructed for expression in *Bacillus subtilis*. The best mutant Glu434Leu produced a half life of 31 min at 60 °C, correspondingly a 1.6 fold improvement of thermal stability.

### Introduction

Conversion of side-streams biomass into valuable prebiotics by enzymatic catalysis is promising due to enormous amounts from the agriculture such as sugar beet and potato pulp. In order to obtain those compounds with reduced energy consumption, carbohydrate active enzymes can be used as catalysts. Pectin from sugar beet pulp or potato pulp can be converted into beneficial polymeric and oligomeric carbohydrates requiring enzymes such as pectin lyases, rhamnogalacturonan I (RGI) lyases, polygalacturonases, galactanases and arabinases [1-3, 3]. The RGI lyase catalyzes the cleavage of  $\alpha$ -(1,4)-bonds between rhamnose and galacturonic acid in the rhamnogalacturonan I backbone chain of pectins by  $\beta$ -elimination [4]. The action results in the release of oligomers containing  $\Delta$ -(4,5)-unsaturated galacturonic acid moieties at the non-reducing end.

It is of great advantage that above enzymes exhibit high thermal stability as the substrate availability becomes higher, pectin is less viscous and microbial contamination minimizes [5]. Several web servers consists of an enormous amount of available sequenced genes mainly derived from whole genome sequences predicted to exhibit putative enzyme activities. Every day new genomes are sequenced and released which gives an opportunity to extract this data for phylogenetic analysis with the purpose of finding robust enzymes with required enzyme activities. Their encoding genes can be

optimized for expression in a heterologous host for production and purification for biochemical characterization.

In order to meet the requirements of thermal stability, engineering of enzymes can be necessary. Directed evolution is the most common method although it is costly, time consuming and requires a high-throughput assay as it generates high molecular diversity using random mutagenesis. Although it doesn't require any structure based knowledge. Rational design of enzymes is less costly and time consuming as you minimize your dataset by selection of single sites for site saturation mutagenesis but then it requires knowledge regarding structure-function relationships. Alternatively, when it is desired to enhance the thermal stability of an enzyme, a semi-rational design strategy can be worked out based on sequence alignment of homologous proteins for identifying amino acids (AA) related to thermal stability, i.e., the so-called consensus approach [6]. This consensus approach assumes that amino acids occurring more frequently in a certain position within the protein family contribute to the overall stability. Consequently, replacement of non-consensus amino acids by the consensus ones is presumed to enhance thermostability. Several computational methods for prediction of candidate site can be used in combination with 3D models to make the sites more plausible. Two examples of in silico methods are prediction of protein mutant stability changes (PoPMuSiC) and the B-factor iterative

test (B-FIT). The PoPMuSiC algorithm can predict the changes in folding free energy (ddG) for all possible single mutations in a protein [7] whereas the B-FIT test is based on crystallographic B-factor data that can give insight into the protein flexibility. Making a protein more rigid can improve stability, and therefore, amino acids in areas exhibiting high flexibility values (high B-factor) are potential targets for site saturation mutagenesis in optimization of thermostability [8]. This study of the my PhD project covers discovery and heterologous expression of a putative bacterial RGI lyase following successfully engineering of its thermal stability by targeted single point mutations.

### Specific Objectives

The objectives of this study are to:

1. Identify a thermostable or relatively RGI lyase
2. Enhance the thermal stability of a RGI lyase if necessary by rational protein design
  - a. Express the original RGI lyase and its mutants in *P. pastoris* and *B. subtilis*

### Methodology

Database screening in UniProtKB (ExPasy Proteomics Server) following phylogenetic analyses was performed to identify and select the RGI lyase for synthesis and expression. Codon optimization was worked out to increase the level of heterologous protein in both *P. pastoris* and later on *B. subtilis*(ref). *P. pastoris* expression system (picZalphaC) was used due to its ability to produce and secrete high quantities of foreign enzymes under carbon-source feed control (glycerol-to-methanol feed switch) with relatively low amounts of native secreted enzymes [9]. *B. subtilis* was chosen as the host for expression of the RGI lyase library using pDP66K-PM[10] in frame with the CGTase signal peptide. A multiple sequence alignment approach was used as one of the methods for prediction of possible candidates [6]. The frequencies of each amino acid in the original RGI lyase and the consensus sequence, respectively, were calculated. For each position in the alignment, the frequency of the RGI lyase was divided by the frequency of the consensus. If this value was below 1, the amino acid was defined as not conserved and further compared with PoPMuSiC (predictions of mutant stability changes) [7] results as well as with the aligned amino acids in the putative RGI lyase (uniprot A5INB0) from *Thermotoga petrophila* RKU-1 included in the multiple alignment. A 3D model of the RGI lyase was predicted and used to study alpha-helix projections in for selection of candidates. B-FIT predictions [8] were used on the basis of B-values from PDB structures of *B. subtilis* RGI lyase YesW. The final list of candidates was made by combining and comparing the results of B-FIT, PoPMuSiC, and the consensus approach. The candidate for alpha-helix stabilization was selected only from 3D model projections.

Biochemical characterizations of the original RGI lyase and its mutants were performed by Ines R. Silva

performing multivariate regression analysis [11]. The biological parameter half-life ( $t_{1/2}$ ) was used to evaluate the thermostability of the mutant variants [12].

### Results and discussion

All proteins from the PL11 family were compared in a phylogenetic tree. The putative RGI lyase from *B. licheniformis* was identified in the same group as the well characterized endo-acting YesW and exo-acting YesX from *B. subtilis*. In addition proteins from *Thermotoga petrophila* (A5INB0 THEP1) and *Thermobaculum terrenum* (D1CB51 THET1) had a short distance to this group. A5INB0 THEP1 and Q65KY1 BACL D were selected for gene synthesis and expression as they probably would exhibit potential thermostability. The putative RGI lyase encoded a protein of 596 AA including the histidine-tag with a deduced molecular weight and pI of 65072.8 Da and 5.68, respectively. The codon bias can often be a limiting factor for the expression of heterologous genes, and the gene encoding the putative RGI lyase was therefore subjected to a high degree of codon optimization. The native DNA sequence of the RGI lyase encoding gene had a codon adaption index (CAI) to *P. pastoris* at 0.655 whereas after optimization the codon adaption index was calculated to 0.928.

Expression in *P. pastoris* gave rise to a high yield (1.07 g/l). The expression level was also relatively high in comparison with that of other heterologous bacterial genes expressed in *P. pastoris* [9]. The strong codon optimization may be the key reason for this achievement as previously described for several other recombinant proteins [13, 14].

Characterization of RGI Lyase was carried out to evaluate the effect of temperature, pH and ions such as  $Mn^{2+}$  and  $Ca^{2+}$  using potato rhamnogalacturonan as the substrate. The set of experiments gave rise to a surface with a bell shaped structure that allowed the determination of optimum pH and temperature of the reaction.  $Mn^{2+}$  strongly increased the enzyme activity. The optimum conditions was determined to be 61 °C, pH 8.1 in reaction with 2 mM concentrations of both  $Ca^{2+}$  and  $Mn^{2+}$  with a RGI lyase activity of 17.8 U/mg. When plotting Ln (activity) versus incubation time a linear relationship was observed showing that the thermal inactivation of RGI lyase followed first order reaction kinetics. At 55 °C the RGI lyase had a half life of 25 min and at 61 °C of 15 min. With temperatures higher than 61 °C the RGI lyase activity decreased significantly with incubation time. The half life of RGI lyase decreased at 65 °C (10 min), 75 °C (5 min), and 80 °C (3 min). The enzyme completely lost catalytic activity after half an hour at 80 °C (see figure 1).

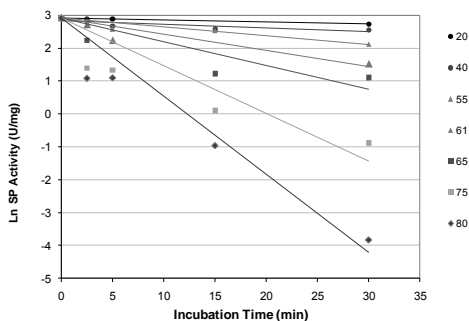


**Figure 1:** The temperature stability of RGI Lyase evaluated incubating the enzyme for 2.5, 5, 15 and 30 minutes at several temperatures. The plot was obtained representing the Ln of the activity at the different temperatures as a function of time [11].

The RGI lyase was subjected to optimization of its thermal stability by targeted single residues for site-saturation mutagenesis to reinforce protein packing or protein-protein interactions.

Nine sites were selected for site-saturated mutagenesis. From a multiple sequence alignment, Gly25, Asp158, Lys243, Gly326, Glu434, and Val541 were selected on the basis of a low occupancy of these amino acids compared to the consensus AAs. Furthermore, structural prediction and comparison to the suspected thermostable, putative RGI lyase from *T. petrophila* RKU-1 was performed. Positions were highly prioritized if a consensus amino acid was also found in the sequence at the same position. The selection was thus a compromise between different methods, and several of the selected positions had ratios (consensus approach) that were high compared to the criteria [6], because the PoPMuSiC predictions with one or more substitutions at these positions with negative ddG values were also taken into account. The structural predictions concerned one or more substitutions with low ddG values (<0) having a relatively high solvent accessibility. The rationale for favoring solvent accessibility was that surface-exposed positions can accommodate more different amino acids and exhibit only few intraprotein interactions, and candidate positions would therefore likely contribute an additive stabilization effect. Finally, loop regions with high flexibility (high B-factor) in the homologous *B. subtilis* RGI lyase YesW were identified. PoPMuSiC was also used as a guideline to decide on positions most likely to stabilize the loops leading to selection of Gly55 and Ala67. Finally, position Gly558 associated with the alpha-helix was chosen based on the 3D model of the RGI lyase. Mutation of Gly558 would have the potential to fill a cavity in the protein interior and, depending on the nature of the substitution, make additional interactions that could provide additional rigidity to the enzyme.

Our strategy was to increase the chance of finding stabilizing mutations using semi-rational approaches

allowing a reduction in library size. In this way, we made a more functional library with a reduced number of variants that were inactive or with lower thermal stability. This led to a reduced number of mutants to screen while increasing the probability of finding improved mutants. All the mutations were located at the surface except for position Gly558. Mutagenesis at the surface can often be stabilizing when exposed residues are not involved in strong interactions with other residues and hence are often additive [15].

The analysis of purified enzymes showed lower variability: The replicates of the half-life measurements had a variation of 7 % for the WT and was between 1 and 10 % for the mutants. The mutants were considered relevant if the half-life was higher than 24 min (20 % higher than the WT). In general, the Glu434 mutations appeared to be most stabilizing with several mutants displaying significantly increased thermostability at 60 °C. The mutant Glu434Leu had a half life of 30.9 min, corresponding to a ~1.6-fold increase in thermal stability at 60 °C (equal to a 55 % increase) compared to the WT. Gly55Val was the second best mutation with an increase of 35 % (27.0 min). The next best mutations were Glu434Trp, Glu434Phe, and Glu434Tyr with a half-life of 26.6 (33 %), 26.5 (33 %), and 26.3 min (31 %), respectively (see figure 2).

The specific activity of the WT at 40 °C (with no incubation) was thus 7 U/mg, and the average activity of the mutants was not statistically different from this activity (data not shown).

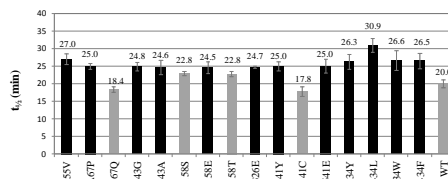


**Figure 2:** Results after scale-up production. Plot of half-life values of the 16 mutants selected. Mutants shown in black have a  $t_{1/2}$  at least 20 % higher than the WT [12]

## Conclusions

This is the first report of a prokaryotic thermostable RGI lyase expressed in *P. pastoris*. Using synthetic biology, the gene sequence encoding the RGI lyase from *B. licheniformis* was optimized with respect to codon usage. This resulted in a high yield of pure, active RGI lyase with a relatively high temperature (61 °C) and high pH (8.1) optimum. The RGI lyase was enhanced by targeted single point mutations. The most pronounced increase in thermal stability, increasing the RGI lyase half-life at 60 °C from 20 to 31 min (1.6-fold higher), took place with the mutation Glu434Leu. Other mutations, Gly55Val and Glu434Trp, enhanced significantly RGI lyase stability by 35 and 33 %, respectively. Although the increments made by the remaining mutations were smaller, the fact that they

occurred at six different positions located at the protein surface might enable combination of the mutations with an additive effect on protein thermostability.

### Acknowledgements

This study was partially supported by the Danish Strategic Research Council's Committee on Food and Health (FøSu) Project "Biological Production of Dietary Fibres and Prebiotics" (no.2101-06-0067).

### References

[1] Holck J, Hjerno K, Lorentzen A, Vignsnaes LK, Hemmingsen L, Licht TR et al. Tailored enzymatic production of oligosaccharides from sugar beet pectin and evidence of differential effects of a single DP chain length difference on human faecal microbiota composition after in vitro fermentation. *Process Biochemistry* 2011;5:1039-49.

[2] Thomassen LV, Vignsnaes LK, Licht TR, Mikkelsen JD, Meyer AS. Maximal release of highly bifidogenic soluble dietary fibers from industrial potato pulp by minimal enzymatic treatment. *Appl Microbiol Biotechnol* 2011;3:873-84.

[3] Otten H, Michalak M, Mikkelsen JD, Larsen S. The binding of zinc ions to *Emericella nidulans* endo-beta-1,4-galactanase is essential for crystal formation. *Acta Crystallographica Section F-Structural Biology and Crystallization Communications* 2013:850-4.

[4] Mutter M, Colquhoun IJ, Beldman G, Schols HA, Voragen AGJ. Rhamnogalacturonan alpha-L-rhamnopyranosyl-(1->4)-alpha-D-galactopyranosyluronide lyase, a new enzyme able to cleave RG regions of pectin. *Pectins and Pectinases* 1996:783-6.

[5] Eijssink V, Gaseidnes S, Borchert T, van den Burg B. Directed evolution of enzyme stability. *Biomol Eng* 2005;1-3:21-30.

[6] Davidson AR. Multiple sequence alignment as a guideline for protein engineering strategies. *Methods Mol Biol* 2006:171-81.

[7] Dehouck Y, Grosfils A, Folch B, Gilis D, Bogaerts P, Rooman M. Fast and accurate predictions of protein stability changes upon mutations using statistical potentials and neural networks: PoPMuSiC-2.0. *Bioinformatics* 2009;19:2537-43.

[8] Reetz MT, D Carballeira J, Vogel A. Iterative saturation mutagenesis on the basis of B factors as a strategy for increasing protein thermostability. *Angewandte Chemie-International Edition* 2006;46:7745-51.

[9] Macauley-Patrick S, Fazenda ML, McNeil B, Harvey LM. Heterologous protein production using the *Pichia pastoris* expression system. *Yeast* 2005;4:249-70.

[10] Obro J, Sorensen T, Derkx P, Madsen CT, Drews M, Willer M et al. High-throughput screening of *Erwinia chrysanthemi* pectin methylesterase variants using carbohydrate microarrays. *Proteomics* 2009;7:1861-8.

[11] Silva IR, Larsen DM, Meyer AS, Mikkelsen JD. Identification, expression, and characterization of a novel bacterial RGI Lyase enzyme for the production of

bio-functional fibers. *Enzyme Microb Technol* 2011;2:160-6.

[12] Silva IR, Larsen DM, Jers C, Derkx P, Meyer AS, Mikkelsen JD. Enhancing RGI lyase thermostability by targeted single point mutations. *Appl Microbiol Biotechnol* 2013;22:9727-35.

[13] Yang Y, Malten M, Grote A, Jahn D, Deckwer W. Codon optimized *Thermobifida fusca* hydrolase secreted by *Bacillus megaterium*. *Biotechnol Bioeng* 2007;4:780-94.

[14] Chang SW, Lee GC, Shaw JF. Codon optimization of *Candida rugosa* lip1 gene for improving expression in *Pichia pastoris* and biochemical characterization of the purified recombinant LPI1 lipase. *J Agric Food Chem* 2006;3:815-22.

[15] Schmid F. Lessons about Protein Stability from in vitro Selections. *ChemBiochem* 2011;10:1501-7.

### List of Publications

1. L.V. Thomassen, D.M. Larsen, J.D. Mikkelsen, A.S. Meyer, Definition and characterization of enzymes for maximal biocatalytic solubilization of prebiotic polysaccharides from potato pulp, *Enzyme Microb. Technol.* 49 (2011) 289-297.
2. I.R. Silva, D.M. Larsen, C. Jers, P. Derkx, A.S. Meyer, J.D. Mikkelsen, Enhancing RGI lyase thermostability by targeted single point mutations, *Appl. Microbiol. Biotechnol.* 97 (2013) 9727-9735.
3. I.R. Silva, D.M. Larsen, A.S. Meyer, J.D. Mikkelsen, Identification, expression, and characterization of a novel bacterial RGI Lyase enzyme for the production of bio-functional fibers, *Enzyme Microb. Technol.* 49 (2011) 160-166.
4. M. Michalak, D.M. Larsen, Carsten Jers, J.R.M. Almeida, M. Willer, H. Li, F. Kirpekar, L. Kjærulff, C.H. Gotfredsen, R.T. Nordvang, A.S. Meyer, J.D. Mikkelsen. Biocatalytic production of human milk oligosaccharides by use of a sialidase mutant with superior trans-sialidase activity. *Process biochemistry* (1359-5113). In press, accepted manuscript, available online
5. J. Holck, D.M. Larsen, M. Michalak, H. Li, L. Kjærulff, F.Kirpekar, C.H. Gotfredsen, S. Forssten, A.C. Ouwehand, J.D. Mikkelsen, A.S. Meyer. Characterization and enzyme catalyzed production of 3'-sialyllactose from casein glycomacropeptide and lactose by *Trypanosoma cruzi* trans-sialidation. *New biotechnology* (1871-6784). In press, accepted manuscript, available online
6. C. Jers, M. Michalak, D.M. Larsen, K. P. Kepp, Haiying Li, Y. Guo, F. Kirpekar, A. S. Meyer, J. D. Mikkelsen. Rational design of a new *Trypanosoma rangeli* trans-sialidase for efficient sialylation of glycans. *PLoS one*. In press, accepted manuscript, available online.



**Hilde Larsson**  
Phone: +45 4525 2993  
E-mail: hila@kt.dtu.dk

Supervisors: Ulrich Krühne  
Krist V. Gernaey  
Anne Ladegaard Skov

PhD Study  
Started: December 2012  
To be completed: November 2015

## Modeling Oxygen Transfer in Small Scale Reactors using Computational Fluid Dynamics

### Abstract

In this project, oxygen transfer is being modeled in small scale reactors with the purpose of developing a simulation tool for reactor design and optimization. Computational fluid dynamics is being used for this purpose, and a method, able to predict the oxygen transfer and mixing time in different kinds of miniaturized reactors, is currently being developed. Based on these models, improved reactor designs will finally be fabricated and evaluated experimentally.

### Introduction

It is important to know the transient concentrations of oxygen and other chemical substances in a fermentation broth in order to interpret experimental results correctly. The amount of dissolved oxygen available to a microorganism has for example an enormous impact on its growth and productivity. The most common way to describe oxygen transfer in bioreactors is to use the oxygen transfer coefficient,  $k_{La}$ , which describes the dynamic relationship between the oxygen concentration ( $C$ ) and the oxygen saturation concentration ( $C^*$ ) in a perfectly mixed liquid according to the following equation:

$$\frac{dC}{dt} = k_L a (C^* - C(t))$$

However, the simplification of assuming perfect mixing in the liquid is introducing an inaccuracy and an alternative modeling approach is therefore suggested where concentration gradients in the liquid are taken into account.

In this project, computational fluid dynamics (CFD) is being used with the intention to model the spatial distribution of dissolved chemicals dissolved in a liquid considering phenomena such as convection, diffusion and chemical reactions.

### Specific objectives

The focus of this project is to improve the productivity and reliability of small scale reactors used for

fermentation processes through process modeling and reactor optimization. The project is initially focusing on modeling oxygen transfer in small scale reactors, and these models will then be used to theoretically improve the design of the reactors. Improved reactor designs will finally be fabricated and evaluated experimentally.

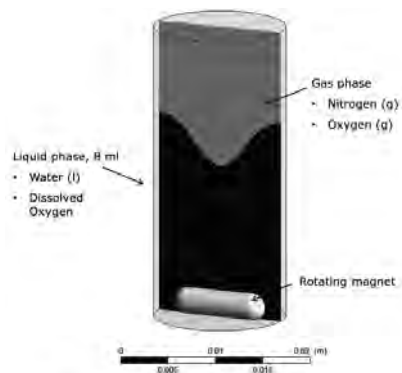


**Figure 1:** Small-scale reactor model simulated in ANSYS

### Method

8 ml distilled water with a low concentration of dissolved oxygen was transferred into a small vessel and stirred using a rotating magnet. The dissolved oxygen recovery profile in the liquid was then recorded using an optical sensor from PyroScience GmbH, Germany.

The CFD software ANSYS CFX-14.0 was used to simulate the system using the two phase model shown in Figure 1. The mixing in the liquid was evaluated as well as the interfacial area between the phases and the oxygen recovery profile in the liquid.

## Results and Discussion

### Oxygen Transfer Experiments

The experimental oxygen recovery profiles for 300, 600, and 900 rotations per minute (rpm) are presented in Figure 2 together with their calculated  $k_L a$  values.

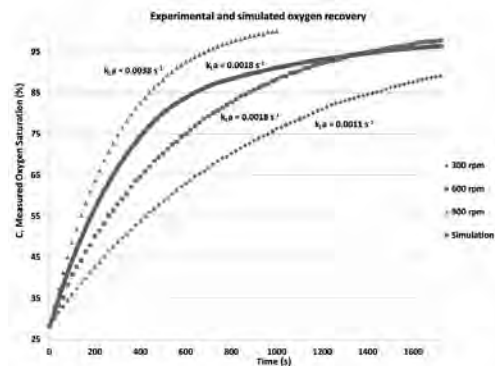


**Figure 2:** Experimental oxygen recovery profiles and calculated  $k_L a$  values

### Oxygen Transfer Simulations

In the oxygen transfer simulations the amount of dissolved oxygen in the liquid and the gas phase were allowed to vary over time. The oxygen transfer between the phases was then modeled using Henry's law as an interfacial equilibrium model. The mass transfer coefficient between the phases was set to  $2.57 \cdot 10^{-4}$  m/s, which is in the same range as reported in literature for a similar system [1].

The appearance of the simulated oxygen concentration in the liquid for 600 rpm is similar to the experimental results, and is shown as the solid line in Figure 2.

**Table 1:** Summary of the oxygen transfer simulations and experiments at different rotational speed

Revolutions per minute (rpm)	300	600	900
Interface area, simulated (cm <sup>2</sup> )	2.85	2.99	3.58
Area, percent of 600 rpm	95%	100%	120%
$k_L a$ from experiments (s <sup>-1</sup> )	0.0011	0.0018	0.0038
$k_L a$ , percent of 600 rpm	60%	100%	207%

### Gas-Liquid interface

Table 1 reports the simulated surface areas of the gas-liquid interface as well as the experimental values of  $k_L a$ . It can be seen that the change of rotational speed

has a larger impact on the  $k_L a$  values than on the surface areas. It is therefore suggested that there is at least one more parameter than surface area influencing the oxygen transfer, which is most likely the mixing of the fluid since this should have an impact on the renewal of the liquid boundary layer closest to the interface.

### Mixing simulations

The value of an additional variable, representing a color dye, was set to unity in the bottommost fraction of the liquid and transient simulations were performed in order to evaluate the mixing characteristics for different rotational speeds. The mixing was evaluated as the time it took for the additional variable to reach at least 90% of its final concentration in the entire liquid volume. Simulations showed that for 900 rpm, this was achieved after 1.45 s. For the 600 rpm simulation it took 2.65 s and for 300 rpm it took 4.65 s. This clearly shows that the level of applied stirring has got a large impact on the resulting mixing.

## Conclusion

According to Table 1, the surface area of a gas-liquid interface is not the only parameter affecting the oxygen mass transfer into the liquid in the system described. In addition, ANSYS 14.0 has shown to be a good simulation tool for describing oxygen transfer in this system.

## Future work

The oxygen transfer model will be improved with the intention to more accurately capture the differences between varying rotational speeds. The separate influences of the parameters surface area, mixing and oxygen gradient over the interphase will also be investigated in order to see which one has got the largest impact on the oxygen transfer.

The developed model will also be evaluated by using it to simulate oxygen transfer in another small scale fermentation system.

An optimization algorithm will be developed where the 3D shape of the reactor will be automatically varied and optimized with respect to its oxygen transfer characteristics, i.e. the parameter surface area, mixing time or oxygen gradient which has shown to have the largest effect on it.

The design performing best in the simulations will subsequently be fabricated with the aid of 3D printing and evaluated experimentally.

## Acknowledgements

This PhD project is funded by Novo Nordisk Foundation

## Reference

1. Brüning, S., Weuster-Botz, D, Chem. Eng. Res. Des. (2013), <http://dx.doi.org/10.1016/j.cherd.2013.07.024>

**Xiaodong Liang**

Phone: +45 4525 2891  
E-mail: xlia@kt.dtu.dk

Supervisors: Georgios Kontogeorgis  
Kaj Thomsen  
Wei Yan (DTU Chemistry)

PhD Study  
Started: August 2011  
To be completed: August 2014

## Phase Equilibria and Speed of Sound in Binary Systems of 1-Alcohols and n-Alkanes from the Simplified PC-SAFT Equation of State

**Abstract**

The Perturbed-Chain Statistical Associating Fluid Theory (PC-SAFT) equation of state is considered as one of the most successful SAFT variants. It, however, has difficulties in describing the second-order derivative properties, such as speed of sound. This work models the vapor-liquid equilibria and speed of sound in binary mixtures of 1-alkanols and n-alkanes using the simplified PC-SAFT equation of state with pure component parameters estimated in different ways. All results are straight predictions, i.e. no binary interaction parameters are used. The results reveal that it is possible to simultaneously model the vapor-liquid equilibria and speed of sound with a satisfactory accuracy for 1-alkanols and n-alkanes binary systems within the PC-SAFT framework.

**Introduction**

Speed of sound modeling is a challenging task for any equation of state because the first- and second-order derivatives of the Helmholtz free energy with respect to both temperature and total volume are needed. Equally challenging is the simultaneous modeling of phase behavior and speed of sound with satisfactory accuracy over wide composition, temperature, and pressure conditions.

As pointed out by Gregorowicz et al. [1], it a challenge for any EoS model to precisely describe the first- and second-order derivatives of Helmholtz free energy with respect to temperature and total volume. For instance, most of the classical equations of state (EoS), such as SRK [2] and PR [3], fail in describing speed of sound reliably in wide temperature and pressure ranges. This may be due to the intrinsic nature of these EoS, usually applied only to phase equilibria calculations, and also due to the sensitivity of the second-order derivative properties performed to a given function, or to the physics behind these properties. A way to discern some of these uncertainties could be to use a molecular-based EoS; these equations should ideally not depend on the particular properties under study and should retain the microscopic contributions considered when building the equation.

The Perturbed-Chain Statistical Associating Fluid Theory (PC-SAFT) equation of state [4-6], has been widely applied for systems with chemicals, polymers, petroleum, biochemicals, electrolytes, pharmaceuticals

and ionic-liquids [7-10]. This model, however, has difficulties in describing the second-order derivative properties [11-13]. In order to improve the capability of modeling speed of sound, the dispersion term of the PC-SAFT EoS, more specifically its universal constants [4], have been revised while maintaining acceptable accuracy for vapor pressure and liquid density for pure normal hydrocarbons [14].

In the current study, the performance of the PC-SAFT EoS, in the simplified form [6] with the original [4] and new universal constants [14], will be evaluated based on the quality of predictions of the vapor-liquid equilibria and speed of sound in binary systems of 1-alkanols and n-alkanes using parameters from different sources.

**Specific Objectives**

The purpose of this work is to investigate if it is possible to obtain simultaneously good predictions of phase equilibria and speed of sound within the PC-SAFT framework [4-6].

**Discipline**

Engineering thermodynamics

**The PC-SAFT EoS**

The PC-SAFT EoS [4,5] can be expressed in terms of residual Helmholtz free energy as:

$$\frac{a^r}{RT} = \frac{a^{hc}}{RT} + \frac{a^{disp}}{RT} + \frac{a^{assoc}}{RT} \quad (1)$$

Where subscripts *hs*, *chain*, *disp* and *assoc* denote the contributions, respectively, from hard-sphere, chain formation, dispersion and association. In this work, the simplified PC-SAFT EoS, proposed by von Solms et al. [6] is used.

$$\frac{a^{hc}}{RT} = \bar{m} \frac{a^{hs}}{RT} - \sum_i x_i (m_i - 1) \ln g_i^{hs}(d_{ii})$$

$$= \bar{m} \frac{4\eta - 3\eta^2}{(1-\eta)^2} - (\bar{m}-1) \frac{2-\eta}{2(1-\eta)^3} \quad (2)$$

$$\frac{a_1^{disp}}{RT} = -2\pi\rho I_1(\eta, \bar{m}) \sum_i \sum_j x_i x_j m_i m_j \left( \frac{\epsilon_{ij}}{kT} \right) \sigma_{ij}^3 \quad (3)$$

$$\frac{a_2^{disp}}{RT} = -\pi\rho\bar{m} \left( 1 + Z^{hc} + \rho \frac{\partial Z^{hc}}{\partial \rho} \right)^{-1} I_2(\eta, \bar{m})$$

$$\sum_i \sum_j x_i x_j m_i m_j \left( \frac{\epsilon_{ij}}{kT} \right)^2 \sigma_{ij}^3 \quad (4)$$

$$\frac{a^{assoc}}{RT} = \sum_i x_i \sum_A \left( \ln X^A - \frac{X^A}{2} + \frac{1}{2} \right) \quad (5)$$

The detailed expressions of these terms can be found in original literature [6] or the book of Kontogeorgis and Folas [7].

This simplified version was proposed in order to simplify and reduce the computational time. In this aspect, it is not a new EoS, rather a simplified version in terms of mixing rules of the original PC-SAFT EoS [4]. The pure component parameters of the original and simplified PC-SAFT are essentially same. However, a simple conversion is needed for the association volume parameter due to a slightly different expression for the association strength employed in the simplified version:

$$\Delta^{A_i B_j} = N_{av} \sigma_{ij}^3 g^{hs} \frac{\pi}{6} \kappa^{A_i B_j} \left[ \exp\left(\frac{\epsilon^{A_i B_j}}{kT}\right) - 1 \right] \quad (6)$$

In another word, the association volume  $\kappa^{A_i B_j}$  from the original PC-SAFT EoS should be divided by  $\pi/6$  when used in the simplified PC-SAFT EoS. It is mainly for consistency with the simplifications of hard sphere term and radial distribution function, and of course more efficient practical implementation. More details can be found in the work of von Solms et al. [6] and Grenner et al. [15].

### Equations

The speed of sound can be calculated from an EoS model as [16]:

$$u = \sqrt{-\frac{V^2 C_P}{M_w C_V} \left( \frac{\partial P}{\partial V} \right)_{T,n}} \quad (7)$$

Where  $V$ ,  $M_w$ ,  $C_P$ ,  $C_V$  and  $(dP/dV)_{T,n}$  are, respectively, total volume molecular weight, isobaric heat capacity, isochoric heat capacity and the derivative of pressure with respect to total volume.

The calculations of  $C_P$  and  $C_V$  can be done as:

$$C_V = (C_P^{ig} - R) - T \left( \frac{\partial^2 A^r}{\partial T^2} \right)_{V,n} \quad (8)$$

$$C_P = (C_P^{ig} - R) - T \left( \frac{\partial^2 A^r}{\partial T^2} \right)_{V,n} + T \left( \frac{\partial P}{\partial T} \right)_{V,n} \left( \frac{\partial V}{\partial T} \right)_{P,n} \quad (9)$$

### Average Absolute Deviation (%AAD)

In this work, the percent average absolute deviation of the speed of sound ( $u$ ) is defined as:

$$\% \text{AAD}(u) = \frac{1}{N^{\text{exp}}} \sum_{i=1}^{N^{\text{exp}}} \left| \frac{u^{\text{calc}}}{u^{\text{exp}}} - 1 \right| \times 100\% \quad (10)$$

## Results and Discussion

### Speed of sound in pure substances

The modeling results of the speed of sound in pure n-heptane and 1-alcohols with both original and new universal constants are presented in Figures 1 and 2. It is shown that the new universal constant performs better from both qualitative and quantitative point of view.

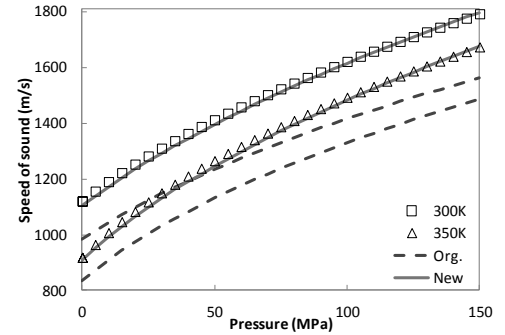


**Figure 1:** Speed of sound in n-heptane at 300K and 350K. Solid and dash lines (New and Org.) denote the calculation results from the new and original universal constants, respectively. Data is taken from NIST [17].

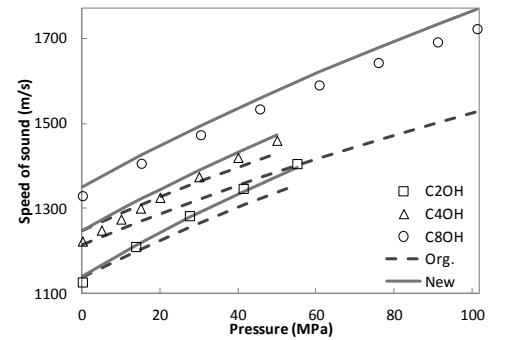


**Figure 2:** Speed of sound in ethanol, 1-butanol and 1-octanol at 303K. Line symbols are the same as Figure 1. Data is taken from Sun et al. [18] and Plantier et al. [19]

### Speed of sound in binary systems

Figure 3 shows measured and predicted speed of sound in the binary system of ethanol with n-alkanes at 298.15K at atmospheric pressure. Both parameter sets capture to some extent the local minimum in the variation of the speed of sound with the composition.



Even though there is no doubt that the model with the new universal constants shows better quantitative speed of sound description, it performs not very well from a qualitative point of view. Figure 3 also shows that the deviations from the model with the original universal constants become larger when the n-alkane gets heavier. The calculations of the speed of sound in the binary systems of 1-propanol and 1-decanol with n-heptane are performed in the temperature range of 293-318K, and pressure ranges of 0.1-122MPa and 15-101MPa, respectively. Typical results at different temperature and pressure conditions are plotted in Figures 4 and 5. It is clearly seen that the model with the new universal constants leads to a significantly improved modelling of the speed of sound both qualitatively and quantitatively, and the improvements become more pronounced as the chain length gets longer.

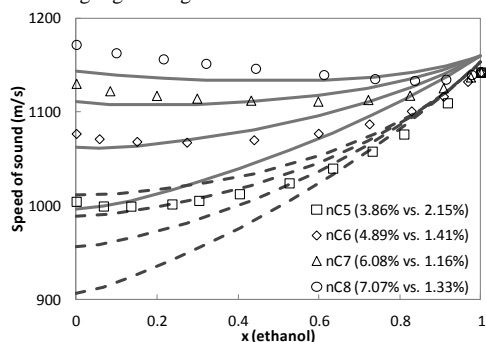


**Figure 3:** Speed of sound in binary systems containing ethanol at 298.15K and atmospheric pressure. Line symbols are the same as Figure 1. Data is taken from Orge et al. [20]

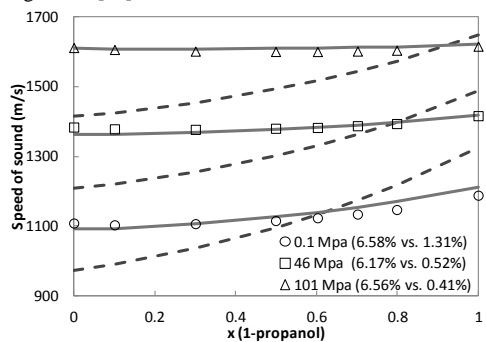


**Figure 4:** Speed of sound in binary systems of 1-propanol and n-heptane at 303.15K and three different pressures. Line symbols are the same as Figure 1. Data is taken from Dzida et al. [21]

For the speed of sound in the binary system of 1-propanol with n-heptane, as shown in Figure 4, the deviations from the model with the new universal constants become smaller as the pressure increases at constant temperature. While for the speed of sound in

the binary system of 1-decanol with n-heptane, as shown in Figure 5, the deviations from the original universal constants become smaller and those from the new universal constants become larger as the temperature increases at constant pressure, respectively. The deviations, however, do not vary very much with temperature and pressure. It can be anticipated that the new universal constants can predict speed of sound in other mixtures of 1-alcohols and n-alkanes with equally good accuracy.

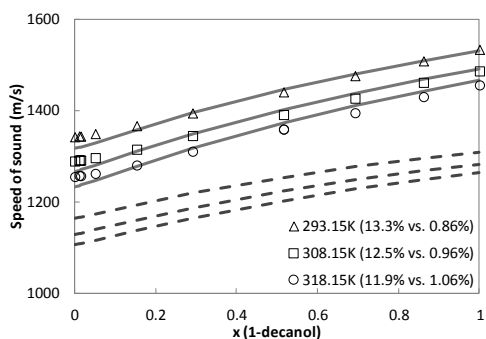


**Figure 5:** Speed of sound in binary systems of 1-decanol and n-heptane at 30MPa and three different temperatures. Line symbols are the same as Figure 1. Data is taken from Dzida [22].

#### Vapor-liquid equilibria

Some typical VLE ( $P_{xy}$  or  $P_x$ ) diagrams of 1-alkanols with n-alkanes are plotted in Figures 6-8. The model with the new universal constants perform overall better than the original one. It is shown in Figure 6 that both models capture the azeotrope point successfully in the binary mixture of 1-butanol and n-hexane at 333.15K. The original model, however, fails to capture the azeotrope point in the binary mixture of 1-pentanol and n-heptane at 368.15K, as shown in Figure 7. In both cases, the new model has much smaller deviations of predicted saturation pressure. Figure 8 presents the VLE ( $P_{xy}$ ) diagrams of binary mixture of 1-octanol and n-heptane at 333.15K. The results reveal again that the new model describe the system with high accuracy.

#### Conclusion

The simplified PC-SAFT EoS with the original and new universal constants has been applied to model the vapor-liquid equilibria and speed of sound in binary systems of 1-alkanols and n-alkanes with the pure component parameters estimated in different ways. The systematic investigation results show that the model with the new universal constants provides significantly improved qualitative and quantitative description of the speed of sound while keeping comparable results for vapor-liquid equilibria for the investigated binary mixtures.

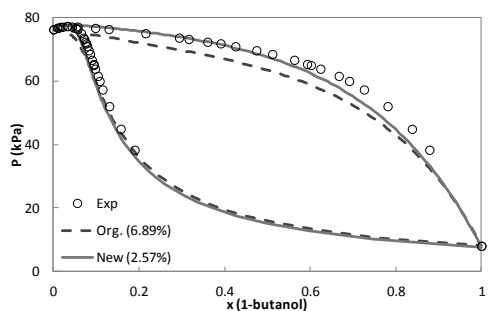


**Figure 6:** Vapor-liquid equilibria of binary 1-butanol and n-Hexane at 333.15K. Line symbols are the same as Figure 1. Data is taken from Skrzecz et al. [23]

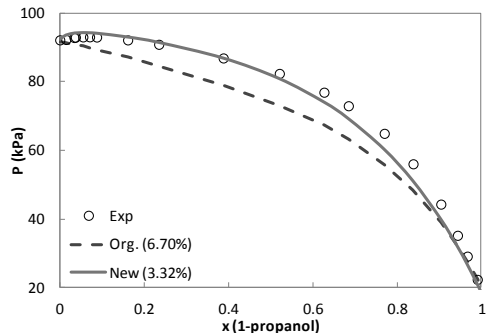


**Figure 7:** Vapor-liquid equilibria of binary 1-pentanol and n-Heptane at 368.15K. Line symbols are the same as Figure 1. Data is taken from Skrzecz et al. [23]

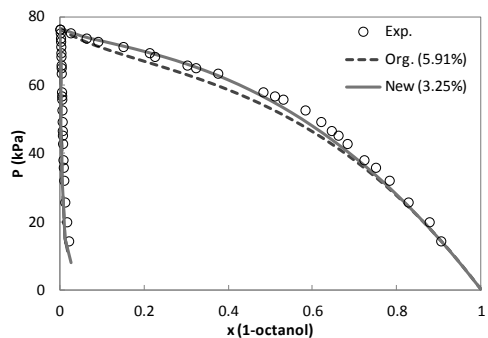


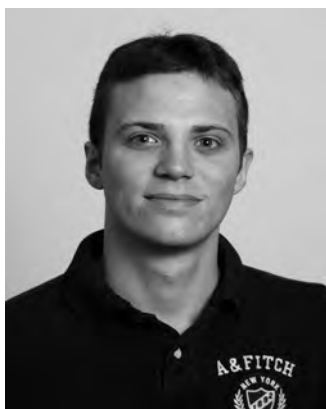
**Figure 8:** Vapor-liquid equilibria of binary 1-octanol and n-Hexane at 333.15K. Line symbols are the same as Figure 1. Data is taken from Skrzecz et al. [23]

#### Acknowledgements

Xiaodong Liang acknowledges Dr. Peter Jørgensen Herslund for many fruitful discussions. This PhD project is funded by the Danish National Advanced Technology Foundation (DNATF) and the Department of Chemical and Biochemical Engineering, Technical University of Denmark.

#### References

1. J. Gregorowicz, J.P. O'Connell, C.J. Peters, *Fluid Phase Equilibria*, 116 (1996) 94-101.
2. G. Soave, *Chem. Eng. Sci.*, 27 (1972) 1197-1203.
3. D.Y. Peng, D.B. Robinson, *Ind. Eng. Chem. Fundam.* 15 (1976) 59-65.
4. J. Gross, G. Sadowski, *Ind. Eng. Chem. Res.* 40 (2001) 1244-1260.
5. J. Gross, G. Sadowski, *Ind. Eng. Chem. Res.* 41 (2002) 5510-5515.
6. N. von Solms, M.L. Michelsen, G.M. Kontogeorgis, *Ind. Eng. Chem. Res.* 42 (2003) 1098-1105.
7. G. M. Kontogeorgis, G.K. Folas, *Thermodynamic models for industrial applications – from classical and advanced mixing rules to association theories*. John Wiley and Sons, Inc., New York, USA, 2010.
8. C. Held, T. Neuhaus, G.Sadowski, *Biophys. Chem.* 152 (2010) 28-39.
9. B.A. Wolf, S. Enders, *Polymer Thermodynamics – Liquid Polymer-Containing Mixtures*. Springer-Verlag Berlin Heidelberg, 2011, pp. 389-418.
10. F. Ruether, G. Sadowski, *J. Pharm. Sci.* 98 (2009) 4205-4215.
11. T. Lafitte, D.Bessieres, M.M. Pineiro, J.L. Daridon, *J. Chem. Phys.* 124 (2006) 024509 (1-16).
12. T. Lafitte, M.M. Pineiro, J.L. Daridon, D.A. Bessieres, *J. Phys. Chem. B* 111 (2007) 3447-3461.
13. I. Polishuk, M. Katz, Y. Levi, H. Lubarsky, *Fluid Phase Equilib.* 316 (2011) 66-73.
14. X.D. Liang, B. Maribo-Mogensen, K. Thomsen, W. Yan, G.M. Kontogeorgis, *Ind. Eng. Chem. Res.* 51 (2012) 14903-14914.
15. A. Grenner, G. M. Kontogeorgis, N. von Solms, M. L. Michelsen, *Fluid Phase Equilib.* 258 (2007) 83-94.
16. M.L. Michelsen, J.M. Mollerup, *Thermodynamic Models: Fundamentals & Computation Aspects*. Tie-Line Publications, Holte, Denmark, 2007, p.63.
17. NIST Chemistry Webbook, <http://webbook.nist.gov/chemistry>.
18. T.F. Sun, J.A. Schouten, S.N. Biswas, *Int. J. Thermophys.* 12 (1991) 381-395.
19. F. Plantier, J.L. Daridon, B. Lagourette, *J. Phys. D: Appl. Phys.* 35 (2002) 1063-1067.
20. B. Orge, A. Rodriguze, J. M. Canosa, G. Marino, M. Iglesias, J. Tojo. *J. Chem. Eng. Data* 44 (1999) 1041-1047.
21. M. Dzida, S. Ernst, *J. Chem. Eng. Data* 48 (2003) 1453-1457.
22. M. Dzida, *J. Phys. Chem. B* 113 (2009) 11649-11661.
23. A. Skrzecz, A. Bok, A. Mączynski, *J. Phys. Chem. Ref. Data*, 31 (2002) 701-748.



## Kasper Linde

Phone: +45 2249 6663  
E-mail: kaspli@kt.dtu.dk

Supervisors: Anker D. Jensen  
Brian B. Hansen  
Peter A. Jensen  
Pär L.T. Gabriëlsson, Haldor Topsøe A/S

### Industrial PhD Study

Started: July 2013  
To be completed: June 2016

## Catalytic Materials for Combined Particulate and NO<sub>x</sub> Removal from Vehicles

### Abstract

In order to reduce the size and cost of the overall diesel exhaust aftertreatment system, it is desired to combine the particulate filter with selective catalytic reduction of NO<sub>x</sub>. This project will identify catalytic formulations with the required combination of soot oxidation and selective catalytic reduction properties without unwanted side reactions such as NH<sub>3</sub> oxidation. The CeNb oxide system has shown promising results and will be the focus of the initial work.

### Introduction

Heavy duty diesel (HDD) vehicles handle a substantial part of the global transport and logistics. Harmful pollutants, such as nitrogen oxides (NO<sub>x</sub>), hydrocarbons (HC), particulate matter (PM), and carbon monoxide (CO), are however formed. The diesel exhaust aftertreatment (DEA) system has been developed to treat the pollutants in the exhaust gas.

Figure 1 illustrates the current standard DEA system consisting of a series of catalytic units. The Diesel Oxidation Catalyst (DOC) oxidizes CO and HC to CO<sub>2</sub> and H<sub>2</sub>O, as well as generates NO<sub>2</sub> from NO. The Diesel Particulate Filter (DPF) is a wall-flow filter, entraining PM in its monolith walls. The DPF can be regenerated actively by increasing the exhaust gas temperature using post-injection of fuel, or passively using a catalyst. NO<sub>2</sub> generated by the DOC also assists regeneration. NO<sub>x</sub> is treated through Selective Catalytic Reduction (SCR) using NH<sub>3</sub> as the reducing agent. NH<sub>3</sub> is supplied to the system through urea dosing, regulated by the onboard Model Predictive Control (MPC) unit. Excess NH<sub>3</sub> is controlled with Ammonia Slip Catalyst (ASC). Upon exiting the DEA system, the emissions should meet the restrictions imposed by the Euro VI regulations.

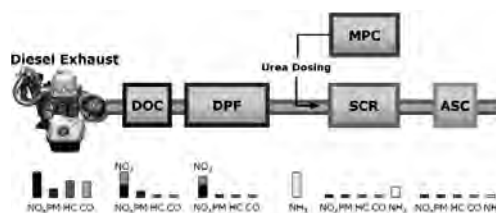


**Figure 1:** Example of a standard design of the DEA system, consisting of the DOC, DPF, SCR component, urea dosing MPC unit, and the ASC.

The DEA system is very complex, requiring efficient exhaust treatment for a wide range of operating conditions, corresponding to cold start, stop-and-start driving (inner city), and high speed driving (highways). As a result, DTU Chemical Engineering and Haldor Topsøe A/S are collaborating on the development of the next generation DEA system, with funding from The National Danish Advanced Technology Foundation. The underlying PhD projects concerns the development of new DOC and ASC formulations (Thomas Klint Hansen at CHEC, pg. 81-82), the combination of the DPF and SCR components (present project) and model development of the control unit for efficient urea dosing system (Andreas Åberg at CAPEC, pg. 259-260).

### Specific Objectives

The two largest components of the DEA system are the DPF and the SCR. A combination of these could therefore result in a considerable reduction in both cost

and size of the overall system. In order to achieve this, the present project will develop catalytic materials for combined particulate and NO<sub>x</sub> removal. This will be done by applying catalyst synthesis, characterization, kinetic lab-scale studies and pilot scale tests.

In order to develop a DPF with catalytic activities for combined soot and NO<sub>x</sub> removal, one can choose between two approaches: Zone coating of the filter, allowing for different catalytic formulations deposited in different zones of the filter (e.g. entrance or exit); or a multi-function catalyst, which have activities for both reactions simultaneously. Both approaches have pros and cons, but the one step multi-function coating makes its production much simpler.

Initially a literature survey of current state of the art will be performed. Next catalyst synthesis and screening of formulations will be performed alongside kinetic lab-scale studies of promising formulations. Finally monolithic substrates will be prepared based on the developed materials and tested in pilot-scale.

## Results and Discussion

CeNb based catalysts have in the literature been associated with promising activities for soot oxidation and SCR. The system is active for SCR of NO with NH<sub>3</sub>; hydrolysis of urea to NH<sub>3</sub>; and oxidation of soot [1]. With regards to the SCR reaction, the NO conversion was similar to a commercial reference V<sub>2</sub>O<sub>5</sub>/WO<sub>3</sub>-TiO<sub>2</sub> (VWTi) catalyst at 250-450°C, with 72% conversion at 250°C and almost full NO conversion between 300-450°C, see Figure 2. These conversions have been confirmed by other authors [2,3], who also found that Nb-oxides enhanced the total acidity, and NbCe/WO<sub>3</sub>-TiO<sub>2</sub> was found to be more temperature stable than VWTi.

In order to improve the NbCe based systems, dopants can be useful: For soot oxidation Nd-doping has been shown to increase the activity of CeZr-oxides [4] while doping with Mn has been found to improve low-temperature SCR of Ce based systems [5].

The literature on the subject is currently not covering the following aspects: More often than not NO is used as NO<sub>x</sub>, ignoring the effects of NO<sub>2</sub>; and no articles have been identified to test for both soot oxidation and SCR simultaneously, or even under the same reaction conditions (e.g. soot presence, gas concentrations). These issues will have to be addressed in order to evaluate if a catalytic formulation is useable as multi-purpose catalyst for a coated DPF.

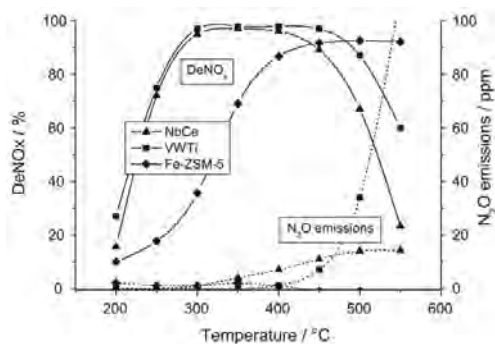


**Figure 2:** DeNO<sub>x</sub> and N<sub>2</sub>O emissions recorded for NbCe, VWTi and Fe-ZSM-5 vs. temperature. Model gas: 1000ppm NO, 100ppm NH<sub>3</sub>, 5% H<sub>2</sub>O, 10% O<sub>2</sub>, and N<sub>2</sub>. [1]

## Conclusions

Based on the literature study, the first experimental series will focus on synthesizing and testing the NbCe/WO<sub>3</sub>-TiO<sub>2</sub> system doped with Zr, Mn, Nd, or combinations of these, and comparing them to reference materials, such as the commercial VWTi system.

Furthermore, materials with known SCR activity (V) and materials with known soot oxidation activity (Ce) will be combined (VCeO<sub>x</sub>/WO<sub>3</sub>-TiO<sub>2</sub>) to investigate if the activities of the individual species remain to produce a bi-functional catalyst.

## Acknowledgements

This project is carried out in cooperation between Haldor Topsøe A/S, the CHEC group at DTU Chemical Engineering and The Danish National Advanced Technology Foundation.

## References

1. M. Casapu, A. Bernhard, D. Peitz, M. Mehring, M. Elsener, O. Kröcher, *Appl. Catal., B* 103 (2011) 79-84.
2. R. Qu, X. Gao, K. Cen, J. Li, *Appl. Catal., B* 142-143 (2013) 290-297.
3. Z. Ma, D. Weng, X. Wu, Z. Si, B. Wang, *Catal. Commun.* 27 (2012) 97-100.
4. A.M. Hernández-Giménez, L.P. dos Santos Xavier, A. Bueno-López, *Appl. Catal., A* 462-463 (2013) 100-106
5. M. Casapu, O. Kröcher, M. Elsener, *Appl. Catal., B* 88 (2009) 413-419.

**Asger Lindholdt**

Phone: +45 4525 2837  
E-mail: asli@kt.dtu.dk

Supervisors: Søren Kiil  
Kim-Dam Johansen  
Stefan M. Olsen, Hempel A/S  
Diego M. Yebra, Hempel A/S

PhD Study  
Started: December 2011  
To be completed: December 2014

## Fuel Efficiency and Fouling Control Coatings in Maritime Transport

### Abstract

The skin friction of antifouling coatings change over time and the initial friction for clean coatings are therefore not sufficient to accurately estimate the fuel efficiency of an antifouling coating over a typical dry-docking period. Furthermore, it is found that the skin friction increases significantly faster during static immersion compared to dynamic immersion. The immersion conditions are therefore of importance when determining the most fuel efficient antifouling coatings. The need for better prediction tools of the fuel efficiency is desired because the often applied route via surface friction measurements of antifouling coatings in clean condition and after static immersion are inadequate. An experimental method has therefore been developed to measure surface friction of antifouling coatings over a desired time period under conditions which can mimic the vast majority of ship profiles (speed and activity) in today's market. The experimental method consists of two parts, i.e. an aging setup and a laboratory scale rotor capable of measuring surface on coated cylinders. It was found that the surface friction was significantly lower for a hydrogel fouling release coating compared to a fluorinated fouling release coating.

### Introduction

The maritime transport sector is responsible for transporting huge amounts of goods all around the world which unfortunately has two primary negative side effects. Firstly, a vast amount of fuel is being consumed causing harmful emission of e.g. CO<sub>2</sub>, NO<sub>x</sub> and SO<sub>x</sub> particles. Secondly, toxic components are released from antifouling coatings to the surrounding seawater. Surface friction constitutes a large part of a ship's total resistance which, however, depends on several factors such as e.g. the condition of the antifouling coating and the ship's speed. Marine biological fouling is known to have an undesirable impact causing a ship's drag to increase. The drag performance (fuel efficiency) of antifouling coatings are today often being evaluated based on static immersion of coated objects followed by hydrodynamic drag measurements in e.g. a towing tank. Larger ships are only rarely static, e.g. in ports, and a static test is therefore only a mediocre method when evaluating antifouling coatings drag performance. Static exposure followed by hydrodynamic exposure has been applied and it is an improved test method compared to only static exposure because this test method more closely resembles the conditions a ship is exposed to during a typical voyage. However, further improvements are desirable in order to evaluate the long term drag performance of antifouling coatings in conditions which

mimic those antifouling coatings experience during voyages.

### Specific Objectives

The purpose of this project is to improve drag test methods for antifouling coatings applicable to a typical dry-docking period, e.g. 5 years. The focus is therefore primarily on long term drag performance determination of antifouling coatings. Furthermore, the specific objectives are to develop an experimental method capable of mimicking the aging process of antifouling coatings closely and measure the drag performance over a long time. During the aging process it is desired to continuously or frequently measure the drag performance via the determination of the surface friction coefficient for a number of antifouling coatings and their development over time.

The laboratory cylindrical rotor setup, which is seen in Fig. 1, is used to measure surface friction. The system consists of a large tank where the rotating cylinder is placed. A static cylinder is placed outside the inner rotating cylinder to obtain a controlled flow, i.e. Couette type flow. The torque sensor is used to measure the torque due to rotation of the system, i.e. bearings, shaft and cylinder. The surface friction of the coating can be determined by measuring the effects due to friction from the top and bottom of the cylinder, friction of the shaft and the bearings.

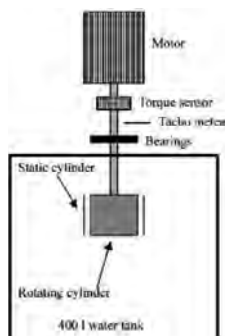


**Figure 1:** Laboratory cylindrical rotor setup

The seawater setup is seen in Fig. 2 where the antifouling coatings are aged in conditions mimicking those ship hulls experience during voyage. Flow conditions similar to that a ship hull experiences arises due to the rotational speed of the shaft where the coated cylinders are attached. Furthermore, the biological conditions are similar to that a ship hull experience due to the seawater immersion.



**Figure 2:** Cylindrical seawater test setup.

The advantage of the seawater setup compared to other setups used in the field of antifouling coating drag performance prediction is that the coating's aging process resembles the one a ship experiences due to the hydrodynamic immersion in the sea. Furthermore, the drag measurements are recorded with short time intervals, i.e. every 2 to 3 weeks, resulting in a large amount of drag measurements over time capable of making a drag performance over a long time interval.

### Results and Discussion

The skin friction coefficient determined in the laboratory rotor setup due to the aging in the seawater test setup has shown that changes over time can be determined, see Fig. 3. In Fig. 3 the skin friction coefficient from two similar antifouling coating technologies over a period of 26 weeks at 15.8 knots is seen. Week zero (designated by round dots) is the skin friction prior to immersion. The triangles designate that prior to skin friction measurement a period of two weeks static immersion had taken place. The squares designate that prior to skin friction measurements the coatings had been dynamically immersed at

approximately 10 knots for 3 weeks. The flat lines at week 26 designate that prior to skin friction measurements mechanical cleaning of the coatings had taken place.

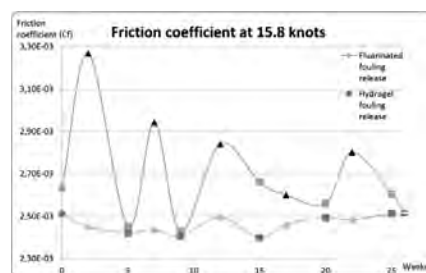


**Figure 3:** Skin friction coefficient over 26 weeks for fluorinated and hydrogel fouling release coatings. Round dots represent the coating condition prior to immersion, triangles represent static immersion for two weeks, squares represent 3 weeks of dynamic immersion at 10 knots and the flat lines at week 26 represent that the coatings had been mechanically cleaned.

The measurements show significant differences in the skin friction over time. Furthermore, it is seen that static immersion increase friction more than dynamic immersion, especially for the fluorinated fouling release coating. It was found that mechanical cleaning brought the coatings back to a similar skin friction coefficient value. The reason for a decrease in the skin friction coefficient after immersion at week zero might be explained by the uptake of water in the coatings (swelling).

### Conclusions

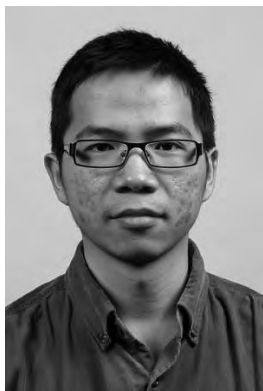
The developed test setup has proven capable of measuring significant surface friction differences between antifouling coating systems which is valuable when determining the optimal choice of coating with respect to fuel efficiency. It was found that the surface friction was significantly lower for a hydrogel fouling release coating compared to a fluorinated fouling release coating, especially after the periods with static immersion. The decrease in surface friction compared to condition prior to immersion shall be investigated further.

### Acknowledgements

This PhD project is supported both financially and knowledge wise from Hempel A/S which is greatly appreciated.

### References

1. C.E. Weinell, K.N. Olsen, M.W. Christoffersen, S. Kiil, *Biofouling* 19 (Supplement) (2003) 45–51.
2. M.P. Schultz, G.W. Swain, *Biofouling* 23, 3 (2007) 164-170.
3. K.A. Zargiel, G.W. Swain, *Biofouling*, (2013)

**Baoguang Ma**

Phone: +45 4525 6813  
E-mail: baom@kt.dtu.dk

Supervisors: Anne Ladegaard Skov  
Søren Hvilsted

**PhD Study**

Started: Aug 2011  
To be completed: Aug 2014

## Preparation and Characterization of Poly (Methyl Methacrylate) (PMMA) Microcapsules for PDMS Crosslinking Reaction

**Abstract**

Thermally activated microcapsules were designed by entrapping HMS-301 crosslinker within PMMA. The spherically shaped microcapsules contained ca. 25% of HMS-301 and had a mean diameter of ca. 50 $\mu$ m. A mixture containing vinyl functional PDMS polymers and PMMA/HMS-301 microcapsules remained fluidic at 50°C but gelled rapidly when heated to 120°C as a result of HMS-301 release and formation of the crosslinked silicone network.

**Introduction**

Polydimethylsiloxane (PDMS) elastomers have attracted much attention in research and applications due to their high thermal stability, high durability and good mechanical properties.<sup>1-3</sup> PDMS elastomers can be obtained from the crosslinking reaction between PDMS polymers and crosslinkers. One of the most commonly used type of PDMS elastomers is Room Temperature Vulcanizing (RTV) silicone, which is obtained from the crosslinking reaction between vinyl terminated PDMS polymers and a crosslinker with hydride groups. At the presence of the platinum catalyst, the two components will start to crosslink through the hydrosilylation reaction and form a network.

The controlled crosslinking reaction between the vinyl terminated PDMS polymers and the hydride crosslinkers is of considerable interest in applications such as self-healing materials<sup>5</sup>, smart materials<sup>6</sup> and nutrient preservations<sup>7</sup>. The control of the crosslinking reaction refers to the crosslinking reaction taking place in response to external stimuli, which include photo activation, chemical stimuli and thermal initiation.<sup>8</sup> In this study, the crosslinking reaction will be controlled by thermal initiation of the encapsulation of hydride crosslinker.

Microencapsulation is the capture of a compound inside a coating shell in order to isolate it, protect it or control its release. The core materials of the microcapsules can be metals, nutrients, perfumes or reactive compounds, while the coating materials are usually polymers, proteins or hydrogels. The applications of the

microcapsules are versatile, such as self-healing systems, triggered drug release and tuneable catalysis.<sup>5-9</sup> Microcapsules are prepared by several methods including emulsification polymerization, coacervation and phase inversion precipitation. Emulsification polymerization is commonly used in the preparation of microcapsules through the polymerization of monomers at the aqueous/organic interface in an emulsion.<sup>10</sup> Coacervation is also widely used in preparing microcapsules in food and fragrance applications.<sup>11</sup> Emulsion polymerization is commonly used in research, but the commercial applications are few since it does not allow for continuous processing. Meanwhile, coacervation requires opposite charge of the polymers in solution. Compared to the previous methods, phase inversion precipitation is widely used in the preparation of fragrance microcapsules where high productivity and continuous processing are required.<sup>12</sup> The advantages of the phase inversion precipitation not only include the high productivity and the potential for the continuous process, but the method also results in high strength shell walls and designable size distribution.<sup>12,13</sup> In this study, microcapsules will be prepared by use of a spray technique, which is based on the phase inversion precipitation mechanism. By splitting the homogenous polymeric solution into micro droplets from spraying, microcapsules can be obtained when the polymers precipitate and migrate to the surface of the micro droplets.

Several mechanisms are capable of initiating changes in microcapsule shells, resulting in release of core

materials from the microcapsules. These mechanisms can be grouped into two categories based on the reception mechanism of the external signals: (1) the polymers have functional groups which are sensitive to the external stimuli. (2) the structure of the polymer shells are disintegrated or created upon the external stimuli.<sup>6</sup>

In this study, thermal initiation based on changes in the polymer structure will be used. For temperatures lower than the glass transition temperature ( $T_g$ ) of the polymer shell, the interactions between polymer chains are strong and the core materials can not be released from the rigid polymer. When the temperature is higher than the  $T_g$  of the polymer, the polymer will become soft, resulting in the release of the core materials. The core material used in this study is hydride crosslinker, which can be used as a curing agent in the reaction with vinyl terminated PDMS.

## Experimental

### Materials

The chemicals used in the experiment were listed in the following: poly (methyl methacrylate) (PMMA) ( $M_w=15,000$ , Aldrich), 25%–35% (methylhydrosiloxane) with 65%–70% (dimethylsiloxane) copolymer (HMS-301) ( $M_w=2,000$ , 8-functional crosslinker, Gelest), platinum cyclovinyldimethylsiloxane complex (SIP 6832.2 catalyst, Gelest), vinyl-terminated polydimethylsiloxane (DMS-V35) ( $M_w=49,500$ , Gelest), chloroform (>99%, Aldrich) and methanol (>99%, Aldrich).

### Apparatus

The air compressor (#1A) and airbrush (DH-201) were purchased from Sparmax (Germany). The air flow of the compressor ranged from 7 to 11 litres per minute and the maximum pressure provided by the compressor in the air compressing process was 40psi. The diameter of the nozzle in the airbrush was 0.8mm.

### Microcapsule preparation (standard procedure)

The polymeric solution was prepared by dissolving 10% (wt) of HMS-301 and 10% (wt) of PMMA in chloroform. The polymeric solution was stirred at 700 rpm in a magnetic stirrer for 24h at room temperature. Afterwards, the polymeric solution was sprayed into a beaker containing 200ml methanol by use of the airbrush. The micro droplets formed from the polymeric solution precipitated, resulting in the encapsulation of the HMS-301. The microcapsules were then washed by methanol for several times to remove the residual HMS-301 on the surface. Finally, the microcapsules were collected by filtration. Figure 1 shows the scheme of the setup.

### Microcapsules preparation with different HMS-301 concentrations

In order to compare the encapsulation efficiency of the microcapsules, different concentrations of HMS-301 were used in the preparation as follows. a) 10% (wt) of HMS-301 and 10% (wt) of PMMA in chloroform b) 15% (wt) of HMS-301 and 10% (wt) of PMMA chloroform c) 20% (wt) of HMS-301 and 10% (wt) of

PMMA in chloroform. The abbreviations of the obtained microcapsules were MP10H10C, MP10H15C and MP10H20C.

For comparison purpose, microcapsules without HMS-301 were prepared by the same procedure from a polymeric solution containing 10% (wt) of PMMA and 90% (wt) of chloroform.

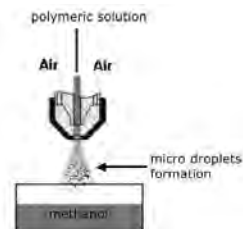


**Figure 1.** Schematic diagram of the spraying setup

## Results and discussions

### Morphological characterization

Morphological characterization of the PMMA/HMS-301 microcapsules was carried out by SEM analysis. Figure 2a shows a typical image of the microcapsules washed with heptane. It could be seen that the HMS-301 inside the PMMA shell had been washed away by heptane, leaving the hollow structure in the microcapsules. The empty space inside the PMMA shell should allow for the storage of the HMS-301. Besides, the PMMA shell had a porous structure, meaning that the PMMA shell was not perfect when microcapsules were prepared by spray technique. This was in good agreement with the morphology of the microcapsules prepared by use of spray.<sup>12,13</sup> Figure 2b shows a representative image of the microcapsules after washing with methanol. It could be seen that the microcapsules were spherically shaped and that few microcapsules were broken. This indicated that methanol remove the HMS-301 on the surface without destroying the microcapsules.

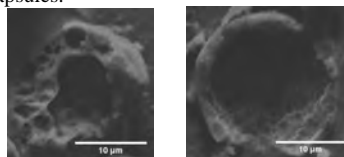


**Figure 2a.** SEM image of PMMA/HMS-301 microcapsules after washing with heptane

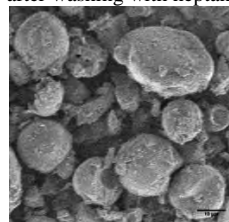


**Figure 2b.** SEM image of PMMA/HMS-301 microcapsules after being washed by methanol



### Size distribution of PMMA/HMS-301 microcapsules and PMMA empty capsules

As discussed in Morphology Characterization Section, most of the microcapsules were spherical when they were washed with methanol. Thus, the size distribution of the microcapsules could be investigated by Mastersizer based on laser diffraction. Figure 3 shows the size distribution of the microcapsules after washing with methanol. As shown in Figure 3, the mean diameter of the microcapsules ranged from 47 $\mu$ m to 58 $\mu$ m and the size distributions among all samples were similar.

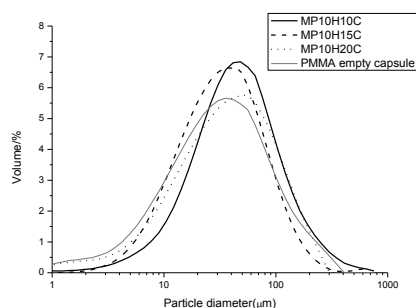


**Figure 3.** Size distribution of the PMMA/HMS-301 microcapsules and the PMMA empty capsules suspended in methanol

### Determination of weight fraction of HMS-301 in microcapsules

The weight fraction of HMS-301 was determined by using  $^1\text{H}$  NMR. As the  $-\text{O}-\text{CH}_3$  groups and the  $\text{Si}-\text{H}$  groups have  $^1\text{H}$  chemical shifts of 3.6ppm and 4.7ppm, the mol ratio between the PMMA and the HMS-301 could be calculated from the integrated signals at the corresponding areas. Figure 4 shows the integrated signals of the  $-\text{O}-\text{CH}_3$  groups and the  $\text{Si}-\text{H}$  groups in the  $^1\text{H}$  NMR measurements. The weight fraction of the HMS-301 estimated by  $^1\text{H}$  NMR was 28%, 21% and 14% in MP10H10C, MP10H15C and MP10H20C, respectively.

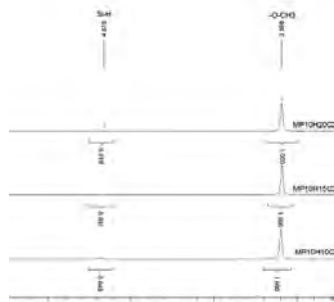


**Figure 4.**  $^1\text{H}$  NMR spectra of microcapsules by using different concentrations of HMS-301

### Reactivity of PMMA/HMS-301 microcapsules in vinyl functional PDMS polymer and catalyst

A typical mixture containing 0.01g PMMA/HMS-301 microcapsules with 1g V35 and catalyst was made. The mixture was placed in a vial, which was inserted into an oven at 50 $^\circ\text{C}$  for several days. Figure 5a shows that the mixture remained fluidic and had a low viscosity. This suggested that there was hardly any crosslinking reaction between the HMS-301 and the V35, as the HMS-301 was sequestered inside the rigid PMMA shell, leaving the system inactive. For comparison, a mixture of 0.01g PMMA/HMS-301 microcapsules and 1g V35 and catalyst was placed in a vial and inserted into an oven at 120 $^\circ\text{C}$  for several days. Figure 5b shows that a crosslinked gel was obtained. This indicated that extensive crosslinking reaction between the HMS-301 and the V35 occurred. After cooling down to the room temperature, the material remained a gel, indicating that the gelation did not arise from the physical association between the PMMA/HMS-301 microcapsules and the V35.



**Figure 5a (left), 5b (right).** Reactivity of PMMA/HMS-301 microcapsules in V35 and catalyst at 50 $^\circ\text{C}$ (left) and 120 $^\circ\text{C}$ (right)

To characterize the rheological behaviour of the mixture of the PMMA/HMS-301 microcapsule and the V35 quantitatively, time sweep rheological measurements were made at 50 $^\circ\text{C}$  and 120 $^\circ\text{C}$ . The measurements were performed with a low amplitude strain to minimize the disruption of the gel network during the formation process. Table 1 shows the composition and the stoichiometry of the mixture in the measurement.

**Table 1.** Compositions and the stoichiometry in rheological measurement

Syst em ID	m(V <sub>35</sub> ) /g	Microcapsule	m(microcapsule)/g	Weight fraction of HMS-301 (%)	Stoichiometry (r)
A	1	MP10H10C	0.010	28	0.24
B1	1	MP10H15C	0.010	21	0.18
B2	1	MP10H15C	0.013	21	0.24
C1	1	MP10H20C	0.010	14	0.12
C2	1	MP10H20C	0.020	14	0.24

The stoichiometry ( $r$ ) is the ratio between mol number of hydride and vinyl groups.  $r$  is calculated from:

$$r = \frac{n_{\text{hydride}}}{n_{\text{vinyl}}} = \frac{\frac{m_{\text{HMS-301}}}{M_{\text{HMS-301}}} * f_{\text{HMS-301}}}{\frac{m_{\text{V35}}}{M_{\text{V35}}} * f_{\text{V35}}} \quad (1)$$

Figure 6 shows representative curves of the storage modulus at 50°C and 120°C of mixture containing PMMA/HMS-301 microcapsule and V35. As shown in Figure 6, the storage modulus of the mixture remained low (<500Pa) at 50°C, indicating that the mixture maintained fluid-like characteristic. On the other hand, the reaction between the HMS-301 and the V35 took place to a small degree. The reaction was related to the leakage of a small portion of the HMS-301 from the porous PMMA shell, which was shown in Figure 2a. When the experiment was made at 120°C, the storage modulus of the mixture increased rapidly, eventually reaching the plateau within 5h, after which further increase in storage modulus was minimal. This suggested that there was substantial degree of crosslinking reaction during the measurement, which was in good agreement with the visual observation in Figure 5b. Considering the different rheological behaviour of the mixture at 50°C and 120°C, the results were indicative of that the HMS-301 was sequestered in the PMMA shell at 50°C, and that HMS-301 was released from the soft PMMA shell at 120°C. When the measurements were made at 120°C, the temperature was higher than the  $T_g$  (105°C) of the PMMA, resulting in the softening of the PMMA in the microcapsules. Therefore, the HMS-301 was able to penetrate through the PMMA shell and react with the V35 at the presence of catalyst.

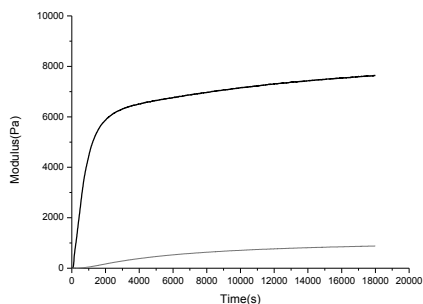


**Figure 6.** Thermally triggered gelation of PMMA/HMS-301 microcapsules and V35 mixture. The red curve and black curve represent the measurement at 50°C and 120°C, respectively.

## Conclusions

Microcapsules have been prepared by a spray process, which allows for upscale in industry. The morphology of the microcapsules is investigated by SEM, showing

the core shell morphology of the microcapsules. The content of the HMS-301 crosslinker in the microcapsules is estimated by  $^1\text{H}$  NMR. Finally, the reactivity of the microcapsules in vinyl functional PDMS polymer is investigated by the time sweep rheological measurements.

## Reference

- (1) Jerschow, P. *Silicone Elastomers*; Springer: Shropshire, UK, 2001; Vol. 12.
- (2) Keith, E. P. In *Rubber Division*, American Chemical Society; Cleverland, US, 1987; pp. 470–502.
- (3) Larsen, A. L.; Hansen, K.; Hassager, O.; Bach, A.; Ndoni, S.; Jørgensen, M. *Macromolecules* 2003, 36, 10063–10070.
- (4) Esteves, a. C. C.; Brokken-Zijp, J.; Laven, J.; Huinink, H. P.; Reuvers, N. J. W.; Van, M. P.; de With, G. *Polymer (Guildf)*. 2009, 50, 3955–3966.
- (5) Motornov, M.; Roiter, Y.; Tokarev, I.; Minko, S. *Prog. Polym. Sci.* 2010, 35, 174–211.
- (6) Murphy, E. B.; Wudl, F. *Prog. Polym. Sci.* 2010, 35, 223–251.
- (7) Madene, A.; Jacquot, M.; Scher, J.; Desobry, S. *Int. J. Food Sci. Technol.* 2006, 41, 1–21.
- (8) Johnston, A. P. R.; Such, G. K.; Caruso, F. *Angew. Chem. Int. Ed. Engl.* 2010, 49, 2664–6.
- (9) Kim, H.-J.; Matsuda, H.; Zhou, H.; Honma, I. *Adv. Mater.* 2006, 18, 3083–3088.
- (10) Tiarks, F.; Landfester, K.; Antonietti, M. *Langmuir* 2001, 17, 908–918.
- (11) Esser-kahn, A. P.; Odom, S. A.; Sottos, N. R.; White, S. R.; Moore, J. S. *Macromolecules* 2011, 44, 5539–5553.
- (12) Peña, B.; Panisello, C.; Aresté, G.; Garcia-Valls, R.; Gumí, T. *Chem. Eng. J.* 2012, 179, 394–403.
- (13) Panisello, C.; Garcia-Valls, R. *Ind. Eng. Chem. Res.* 2012, 51, 15509–15516.



**Christine Malmos**

Phone: +45 4525 2892  
E-mail: mmos@kt.dtu.dk

Supervisors: Nicolas von Solms  
John M. Woodley

PhD Study  
Started: August 2011  
To be completed: May 2015

## Inhibition of Gas Hydrate Formation by Antifreeze Proteins

### Abstract

Antifreeze proteins (AFPs) have shown in the literature to be promising green and environmentally benign inhibitors for gas hydrate formation. Especially insect AFPs express high antifreeze activities which is their ability to prevent ice from freezing. In this study we showed that AFP from the long horn Danish bark beetle, *Rhagium mordax*, can perform as an effective kinetic hydrate inhibitor (KHI) on the same level as the commercial synthetic inhibitor polyvinylpyrrolidone (PVP).

### Introduction

Gas hydrates are crystalline solid compounds of gas molecules and water which forms at low temperature and high pressure. In the oil and gas industry gas hydrates block flow lines and pipelines in oil and gas production causing huge production losses and safety problems. Hydrate formation is a stochastic time-dependent process consisting of the steps of nucleation and growth. Several theories and hypothesis are suggested in order to describe the nucleation mechanism of hydrates. One is by Sloan et al. 2007 the 'labile cluster nucleation' hypothesis. A labile cluster is an unstable entity (cavity occupied by a guest molecule) that readily undergoes changes. According to the hypothesis the nucleation of hydrates proceeds in 4 steps which are shown in Figure 1.

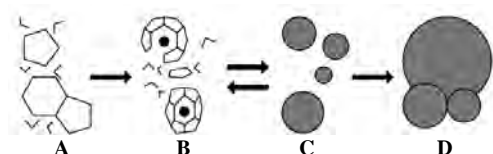


**Figure 1:** Schematic model of hydrate cluster growth. [1]

First pressure and temperature are at hydrate forming conditions but no gas is dissolved. Then gas dissolve into the water and labile clusters form. These clusters undergo agglomeration and finally hydrate growth begins when the size of clusters reaches a critical value. [2]

Hydrate formation was visually observed and pictures taken during the hydrate formation experiment with natural gas and water corresponding to the steps illustrated in Figure 1 are shown in Figure 2.

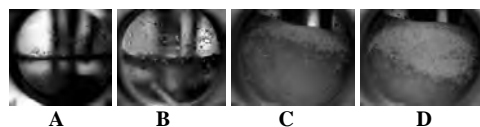


**Figure 2:** Photographs of hydrate nucleation and growth.

To provide flow assurance the industry use thermodynamic inhibitors as methanol, which are uneconomical and not environmentally friendly as large amounts are needed. Low dosage hydrate inhibitors are developed as an alternative which can be applied in much lower concentrations. Most of these suffer from low biodegradability which means that they cannot be applied in the North Sea. Recent studies have shown that antifreeze proteins may hold a promising potential to work as a low-dosage hydrate inhibitors in both natural gas [3-6] and methane gas [7,8] systems while at the same time being environmentally benign. AFPs protect organisms from deep freezing temperatures by preventing ice from growing upon cooling below the melting point. Especially AFPs from insects show considerable higher antifreeze activities than AFPs from other organisms. The long horn Danish bark beetle *Rhagium mordax* (RmAFP) can express antifreeze activity in excess of 8°C which is more than other insect proteins.[9]

### Specific Objectives

The objective of this PhD project is to investigate if AFPs can be applied in field conditions to control the formation of gas hydrates i.e. can AFPs substitute conventional types of chemicals like methanol as hydrate inhibitors. This objective will be achieved by setting up laboratory scale experiments to simulate realistic hydrate formation scenarios using three different experimental apparatus: high pressure micro-Differential Scanning Calorimeter (HP- $\mu$ DSC), Rocking Cells, and a pressurized stirred autoclave. Different types of water soluble polymeric commercial low-dosage hydrate inhibitors will be evaluated and the performance will be compared to AFPs. Synergy effects between inhibitors and other production chemicals will be studied and an evaluation of health, safety and environmental matters related to AFPs will be carried out. Finally a feasibility study will be carried out to investigate if AFPs can be implemented in field applications. In this study methane hydrate inhibition using AFP from *Rhagium mordax*, two amino acids: L-threonine and L-valine, Bovine Serum Albumin (BSA) and the synthetic inhibitor PVP (MW 10.000) in the new equipment Rocking Cells were investigated. The two amino acids and the non- antifreeze protein BSA were used as test controls. In AFP-I (type I AFP that exists in fish) hydroxyl groups of threonine residues have been shown to be essential to make antifreeze protein-ice interaction permanent. Replacement of the threonine hydroxyl-groups with methyl-groups (threonine to valine mutation) indicated that the hydrophobic methyl-group could be involved in water exclusion at the adsorption site of the protein. This means that the hydrophobic methyl-group could be important in the antifreeze inhibition mechanism of ice.[10]

### Equipment and method

Measurements of the onset of hydrate nucleation temperatures by constant cooling experiments were studied in Rocking Cells. The aim was to obtain the difference in delay of hydrate nucleation for synthetic and biological KHIs compared to a non inhibitor system in order to investigate how effective AFP is as an inhibitor. The methodology applied is based on the precursor (memory effect) method described by Duchateau et al. [11]. The results obtained are compared to results using fresh solutions. All inhibitors were tested in a concentration of 2770 ppm. The hydrate nucleation experiments were conducted in a Rocking Cells produced by PSL Systemtechnik (Figure 3). The apparatus consists of 5 test cells placed on a cell drive in the cooling bath. Each cell has a working pressure up to 200 bar. The temperature is adjusted by the external cooling bath in the range  $-20^{\circ}\text{C}$  to  $+60^{\circ}\text{C}$ .



**Figure 3:** Rocking Cells produced by PSL Systemtechnik. The picture shows the Rocking Cells setup consisting of the cooling bath with 5 test cells and the high pressure panel.

The stainless steel test cells with a volume of 40 ml and have a stainless steel ball that freely rolls over the entire length of the cell when it is rocking. The cells can rock with an angle of  $-45^{\circ}$  to  $+45^{\circ}$ . The measuring principle is based on a uniform rocking movement of the test cells. When the cell is rocked the ball inside the cell is rolling along the length of the cell and thereby blends the test mixture. Through movement of the ball shear forces and turbulences are created in the cell. Thereby the conditions in the pipelines can be reproduced. Each test cell was loaded with 10 ml of test liquid. To eliminate the air in the cells they were evacuated. All the systems were initially pressurized to 95 bar of methane gas. For the non inhibitor systems, the constant cooling/heating cycle was from  $20.5^{\circ}\text{C}$  to  $2^{\circ}\text{C}$  to  $20.5^{\circ}\text{C}$ . For the KHI experiments the  $13^{\circ}\text{C}$  to  $2^{\circ}\text{C}$  to  $14^{\circ}\text{C}$  in order to maintain the stability of the protein while fully melting the hydrates in the cells. The equilibrium temperature for the methane-water system at this pressure was determined using laboratory experiments by standard slow hydrate dissociation [12]. Experiments conducted resulted in an equilibrium temperature of  $12.9^{\circ}\text{C}$ . The experiments were programmed and temperature and pressure data were logged throughout the experiment. Two cycles were set up for each experiment in order to perform a non precursor and precursor test. The cells were set to rock and cooling at a constant rate. During cooling down the pressure decreases at a constant rate as the temperature decreases until hydrate nucleation which is observed as a fast pressure drop. The temperature at which hydrate nucleates is called the onset temperature,  $T_o$ .

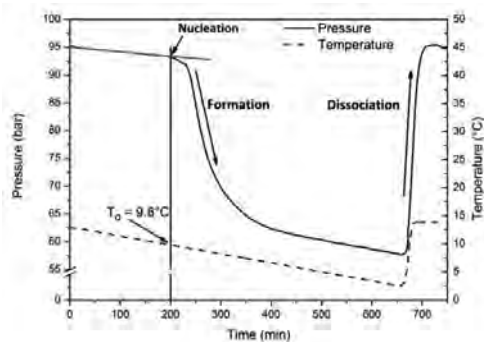


**Figure 4:** Temperature and pressure recorded during the constant cooling test of PVP10 in 50 mM NaCl-MilliQ. The red line indicates the pressure decrease as the temperature decreases. The measured pressure will deviate from the red line as hydrates nucleate. This is indicated by a black arrow pointing at the onset temperature ( $T_0$ ).

We maintained the temperature at 2°C for 1h to ensure complete conversion to hydrates. The cells were then heated at a fast rate in order to dissociate the hydrates. The temperature was maintained for 30 min to ensure fully dissociation of the hydrates before repeating the cycle for the precursor test. As the pressure and temperature reach the initial setting and stabilizes all the hydrates are dissociated.

### Results and Discussion

Previous studies showed that AFPs do inhibit hydrate nucleation and change the growth profile of hydrates [4,5,7,8]. How effective AFPs delay hydrate nucleation depends on the AFP type and concentration. In Figure 5 and Figure 6 onset hydrate nucleation temperatures for non-precursor tests and precursor tests are shown. In both the non-precursor test and precursor test the results show that L-valine and L-threonine do not exhibit any KHI effect in the form of amino acids as they do not delay hydrate nucleation compared to the non-inhibitor system. It should be noted that only one AFP non-precursor test was performed due to limited amount of AFP. Although, AFP shows a very promising result as a KHI compared to PVP. As can be seen from Figure 5 and Figure 6 the observed onset hydrate nucleation temperatures are very similar for the non-precursor and precursor test indicating that the memory effect did not affect the nucleation.

Daraboina et al. 2011 observed a similar result for PVP and AFP for inhibition of natural gas hydrates. Using an isothermal nucleation procedure to obtain the nucleation time (time delay of hydrate formation) it was shown that PVP and AFP obtained very similar nucleation times using both a stirred tank and the HP  $\mu$ DSC. [4,5]. This indicates that the AFPs are performing similarly for both methane systems (SI hydrates) and natural gas systems (SII hydrates). For antifreeze proteins at equimolar concentrations an increase in size of protein

decreases the solubility of the protein in the water phase which will lead to increased antifreeze activity [10]. We speculate that the observed KHI effect of BSA could be due to decreased solubility as the molecular weight of BSA (67 kDa) is significantly higher compared to RmAFP (14 kDa).

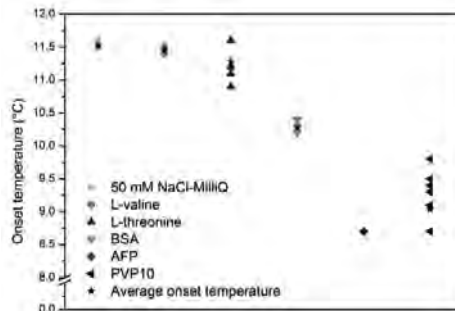


**Figure 5:** Onset hydrate nucleation temperatures for non-precursor constant cooling tests using KHIs at a concentration of 2770 ppm.

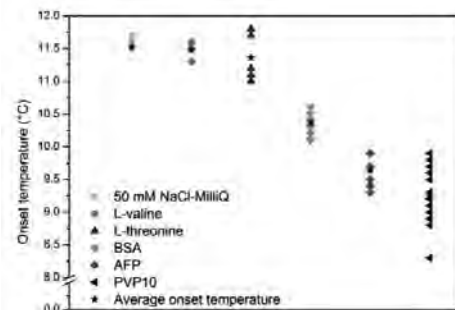


**Figure 6:** Onset hydrate nucleation temperatures for precursor constant cooling tests using KHIs at a concentration of 2770 ppm.

In Figure 7 normalized hydrate growth profiles for the non-precursor tests and the precursor tests are shown. The controls MilliQ water + NaCl, L-valine and L-threonine show very similar growth profiles in both the non-precursor test and precursor test.

In the non-precursor test BSA shows increased growth compared to the controls. AFP shows even more hydrate growth and grows fast initially in contrast to the other KHIs. However, the greatest growth of hydrates is observed when using PVP10 whereas the controls showed the least growth. This indicates that the KHIs promote hydrate growth although they significantly delay hydrate nucleation. In the precursor test the growth profile of AFP changes significantly by showing the least growth of hydrates which means AFP changes from promoting to inhibiting the hydrate growth.

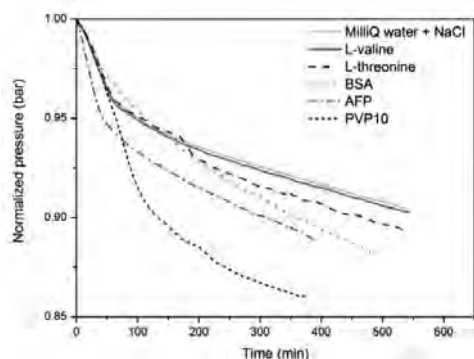


**Figure 7:** Hydrate growth profiles for non-precursor constant cooling tests using KHIs at a concentration of 2770 ppm.

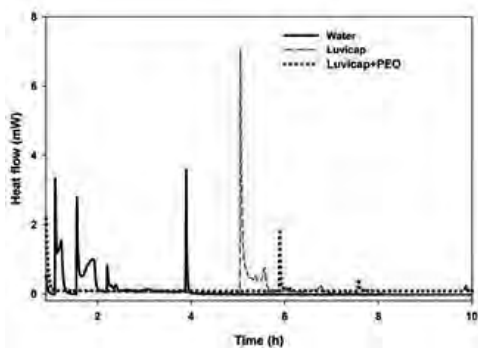


**Figure 8:** Typical DSC heat flow and temperature signal in fresh water, Luvicap and Luvicap+PEO samples obtained during hydrate formation (A) and decomposition (B) using an isothermal program [13].

Again, PVP10 shows significant growth but BSA shows even greater growth although at a slower rate. Inhibition of methane hydrate growth was also reported by Jensen et al. 2010 when using similar methodology and the insect AFP, *Tenebrio molitor*. In addition the AFP performed as a more effective inhibitor compared to PVP. However, both KHIs were performing as inhibitors of hydrates growth.[7]. Our study shows that AFP performs as an effective hydrate nucleation inhibitor and not any protein or amino acid can perform as an inhibitor. Figure 8 presents new results using a high pressure microcalorimeter to test known inhibitors. The delay in formation is clearly seen as a time lag in the heat signal [13].

## Conclusions

In both hydrate nucleation tests the AFP from the long horn Danish bark beetle, *Rhagium mordax*, (RmAFP) perform as an effective hydrate nucleation inhibitor at the same level as the synthetic inhibitor PVP. All inhibitor systems promoted the hydrate growth except

the AFP in the precursor test which showed to inhibit the growth. By comparing onset nucleation temperatures and growth profiles it is observed that no clear correlation between the effectiveness of KHIs. However, AFP in the precursor test performs as an effective inhibitor in both hydrate nucleation and growth. Further tests are needed to verify the performance of the AFP. To simulate realistic scenarios moreover, experiments are planned to be carried out in different salinity levels in order to simulate the variations observed in the fields. The biodegradability of AFP compared to synthetic inhibitors will be studied as it is of great importance for selection of future KHIs.

## Acknowledgements

The project is a part of the advanced technology project 'Biotechnology in Oil Recovery', funded by the Danish National Advanced Technology Foundation, the Technical University of Denmark, Maersk Oil A/S, Dong Energy A/S, Novozymes A/S, Danish Technological Institute and Roskilde University.

## References

1. Jr E.D. Sloan, C. Koh, Clathrate hydrates of natural gases, CRC Press, Boca Raton, USA, 2007, p. 133.
2. R.L. Christiansen, Jr E.D. Sloan, Annals of the New York Academy of Sciences 715 (1994) 283-305.
3. L. Jensen, K. Thomsen, N. von Solms, Energy Fuels 25 (2011) 17-23.
4. N. Daraboina, P. Linga, J. Ripmeester, V.K. Walker, P. Englezos, Energy Fuels 25 (2011) 4384-4391.
5. N. Daraboina, J. Ripmeester, V.K. Walker, P. Englezos, Energy Fuels 25 (2011) 4392-4397.
6. H. Ohno, R. Susilo, R. Gordienko, J. Ripmeester, V.K. Walker, Chem. Eur. J. 16 (2010) 10409-10417.
7. L. Jensen, H. Ramløv, K. Thomsen, N. von Solms, Ind. Eng. Chem. Res. 49 (2010) 1486-1492.
8. S. Al-Adel, J.A.G. Dick, R. El-Ghafari, P. Servio, Fluid Phase Equilib. 267 (2008) 92-98.
9. E. Kristiansen, C. Wilkens, B. Vincents, D. Friis, A.B. Lorentzen, H. Jenssen, A. Løbner-Olesen, H. Ramløv, J. Insect Physiol. 58 (2012) 1502-1510.
10. E. Kristiansen, K.E. Zachariassen, Cryobiology 51 (2005) 262-280.
11. C. Duchateau, J.-L. Peytavy, P. Glénat, T.-E. Pou, M. Hidalgo, C. Dichary, Energy Fuels 23 (2009) 962-966.
12. B. Tohidi, R.W. Burgass, A. Danesh, K.K. Ostergaard, A.C. Todd, Annals of the New York Academy of Sciences 912 (2000) 924-931.
13. N. Daraboina, C. Malmos, N. von Solms, Energy Fuels 2013, 27, 5779-5786



## **Seyed Soheil Mansouri**

Phone: +45 4525 2907  
E-mail: seso@kt.dtu.dk

Supervisors: Rafiqul Gani  
John M. Woodley  
Jakob K. Huusom

PhD Study  
Started: September 2013  
To be completed: August 2016

## **Design, Control and Analysis of Intensified Biochemical Processes**

### **Abstract**

The aim of this project is to develop a comprehensive systematic framework for simultaneous design, control and analysis of intensified chemical/biochemical processes. As a result of integration of functions/operations into one system the controllability region of intensified equipment is smaller and consequently the control options may be limited. To overcome these challenges, the systematic framework that will be developed in this PhD-project will include all considerations to generate existing and/or innovative intensified unit operations that are controllable, sustainable and economically profitable.

### **Introduction**

The current societal requirements and the state of environment, call for accelerated development of more sophisticated and efficient process systems. Process Intensification (PI) is one of the many options to match current and future challenges of the (bio)chemical industry and it has the potential to improve existing as well as conceptual processes to achieve a more sustainable and economic production [1–3]. However, to date only a few intensified technologies have been implemented in the industry such as reactive distillation, dividing wall columns and reverse flow reactors. One of the major reasons has been that the identification of the best intensified option is neither simple nor systematic. Lutze has [4] developed a systematic methodology to generate and evaluate intensified process options by application of computer-aided techniques. Lutze et al. [5] have shown that the application of their phenomena-based methodology can result in significant process improvements that totally new and innovative intensified unit operations can be generated and evaluated. Furthermore, a new concept of process synthesis is based on process intensification and actuation improvement. The concept enables integration of process operation, design and control through dynamic optimization. This simultaneous synthesis approach should provide optimal operation and more efficient control of complex intensified systems. It may also suggest innovative process solutions which are more economically and environmentally efficient and agile.

### **Framework**

Advancements in economic, sustainability and safety of intensified chemical processes can be obtained if control and operation of intensified equipment is considered systematically together with different PI options. The phenomena based technique of Lutze [4] will be used as a starting point. To apply their method, a given base case design is represented in terms of tasks (operations) that need to be performed and the phenomena associated with each task are then identified. By applying the phenomena based method [4], new process alternatives with PI-options can be generated. These options are then further reduced through economic and life cycle assessment (LCA) analysis to determine the most promising alternative that best matches the specified design targets, thereby improving the performance criteria. It should be noted that their method does not consider uncertainties or control and operation. Therefore, the method of Hamid [6] that presents a systematic framework work for integrated design and control will be used also as starting point; however, his method does not consider intensified processes. Note that currently there is no generic framework for simultaneous design, control and analysis of intensified processes [7]. Therefore, this project aims at incorporating process synthesis, design, intensification and control into one comprehensive computer-aided framework. One of the obstacles in course of developing the framework would be that intensified and/or multifunctional unit operations have less degrees-of-freedom which may limit the control options or may result in a more difficult to operate control

structure. Due to the integration of functions/operations into one system the controllability region of intensified equipment is smaller. By application of this proposed framework the intensified design option must be controllable and it the new framework has to account for environmental impacts, sustainability and performance of the intensified processes.

### **Project objectives**

The main objectives that are being sought in this project are as follows:

- 1) To develop a systematic methodology to obtain intensified processes that are optimal in terms of static and dynamic performance, economic, performance, safety, and LCA metrics
- 2) To extend the method and tool of Hamid [6] to design controllable processes with PI. This done by applying the integrated design-control algorithm of Hamid to process design obtained after phenomena based intensification using the method of Lutze [4]. Based on this study the phenomena based process design/synthesis method of Lutze may be adjusted.
- 3) To apply the developed methodology on a set of carefully selected case studies with a special emphasis on biochemical processes (for example batch processes).

### **Conclusions**

A systematic computer-aided framework for simultaneous design, control and analysis of intensified chemical/biochemical processes will be developed in course of this PhD-project. The application of this framework will be highlighted through a set of carefully selected case studies. The application of this framework will result in intensified design options that are not only controllable, but are also sustainable and profitable.

### **References**

1. P. Lutze, A. Román-Martínez, J.M. Woodley, R. Gani, *Compt. Chem. Eng* 36 (1) (2012) 189-207.
2. S.S. Mansouri, M.I. Ismail, D.K. Babi, L. Simasatitkul, J.K. Huusom, R. Gani, *Processes* 1 (2) (2013) 167-202.
3. P. Lutze, R. Gani, J.M. Woodley, *Chem. Eng. Process* 49 (6) (2010) 547-558.
4. P. Lutze, *An Innovative Synthesis Methodology for Process Intensification*, PhD Thesis, Technical University of Denmark, Kgs. Lyngby, Denmark, 2011.
5. P. Lutze, D.K. Babi, J.M. Woodley, R. Gani, *Ind. Eng. Chem. Res.* 52 (22) (2013) 7127-7144.
6. M. Hamid, *Model-Based Integrated Process Design and Controller Design of Chemical Processes*, PhD Thesis, Technical University of Denmark, Kgs. Lyngby, Denmark, 2011.
7. N.M. Nikacevic, A.E.M. Huesmana, P.M.J. Van den Hof, A.I. Stankiewicz, *Chem. Eng. Process* 52 (2012) 1-15.





**Michele Mattei**  
Phone: +45 4525 2959  
E-mail: micu@kt.dtu.dk

Supervisors: Rafiqul Gani  
Georgios M. Kontogeorgis

PhD Study  
Started: August 2011  
To be completed: July 2014

## A Systematic Methodology for Design of Emulsion-Based Chemical Products

### Abstract

The consumer oriented chemical based products are used every day by millions of people. They are structured products constituted of numerous chemicals, and many of them are emulsions where active ingredients, solvents, surfactants and additives are mixed together to determine the desired target properties. These products are still mainly designed through trial-and-error based experimental techniques, therefore a systematic approach for design of these products can significantly reduce both time and cost connected to the product development by doing only the necessary experiments. The methodology consists of a model-based framework, involving four hierarchical tasks, with associated models, tools, structured databases and algorithms. Three conceptual case-studies have been developed to highlight the application of the methodology.

### Introduction

The chemical industry is changing, going beyond commodity chemicals to higher value added products [1]. These structured products are still mainly designed on an experimental base, with a consequent large amount of time and money needed. A systematic methodology for design of these products is then considered a big improvement since the whole design procedure speeds up, saving time and money, and the optimum formulation can be identified, since a broad spectrum of alternatives has been virtually investigated. Such a procedure has been successfully developed recently with regards to liquid formulated products [2] and tailor-made blends [3]. Many of the consumer oriented products, however, especially household and personal care products, are emulsions and therefore a dedicated methodology is needed for their design. Moreover, data regarding several important emulsion properties are not available in the open literature and/or appropriate models for their prediction are not readily available. Consequently, dedicated pure component and mixture property models are needed.

### Specific Objectives

The objective of this project is to develop a systematic methodology for the design of emulsion-based chemical products, with associated tools, models, structured databases and algorithms, to be then implemented into a computer-aided framework to allow virtual formulation design and verification of emulsified products. In this

way, the design and development of these products can be made less costly and introduced to the market earlier, while using the experimental resources only for verification of the product.

The methodology consists of five hierarchical tasks: starting with the identification of the consumer needs and their translation into appropriate target properties; then building up the formulation by adding, one-by-one, the different classes of chemicals needed for specific functions: from the active ingredients (defined as the ingredients satisfying the main needs of the product), passing through the solvents mixtures, and finishing with the additives (defined as the ingredients satisfying the secondary needs of the product), and finally verifying the stability of the formulation, as shown in Figure 1.

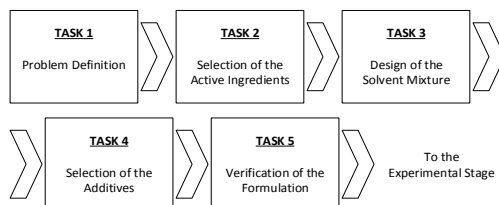


**Figure 1:** Work-flow of the model-based stage of the methodology for design of emulsion-based chemical products

The selection of the active ingredients and of the additives is done through rule-based selection criteria, centered on structured databases, where the relevant properties (e.g. safety or toxicity related), if not available, are predicted through dedicated pure component property models. The design of the solvent mixture, consisting of an oil phase, a water phase, and surfactants, is driven by selection criteria based on the functional properties of the chemical as well as consideration of effectiveness, safety, toxicity and cost. This is done through a data-model based computer aided molecular design technique. Once all the most advantageous ingredients have been chosen, the recipe candidates are identified through a knowledge-based mixture design method, where economic considerations are included together with appropriate boundaries related to solubility, stability, toxicity and safety issues. Once the above mentioned model-based methodology provides candidate formulations, an experimental stage is needed, in order to validate and/or refine the proposed formulations.

Special structured databases of chemicals, classified according to their function and associated properties have been developed. Also, a model library consisting of pure component and mixture property models have been developed so that the needed functional properties can be reliably predicted when their data cannot be found in the database. Table 1 gives an overview of the models needed for the target properties defined at Step 1 of the methodology in relation to the three case-studies developed so far [4], [5], [6].

**Table 1:** Performance criteria considered in this work and translation into target properties and symbols

Performance Criteria	Target Property	Symbol
Cleaning Performances	Hydrophilic-lipophilic balance, solubility parameters, surface tension	$HLB, \delta_D, \delta_P, \delta_H, \delta_T, \sigma$
Cost	Cost	$C$
Foam-ability	Critical micelle concentration, surface tension	$CMC, \sigma$
Safety	Open cup flash point	$T_f$
Solubility	Solubility parameters	$\delta_D, \delta_P, \delta_H, \delta_T$
	Hydrophilic-lipophilic balance (surfactants only)	$HLB$
Skin care	Solubility parameters	$\delta_D, \delta_P, \delta_H, \delta_T$
Spray-ability	Density, kinematic viscosity	$\rho, \nu$
Spread-ability	Density, kinematic viscosity	$\rho, \nu$
	Vapor pressure (solvents)	$P^{vap}$
Stability	Critical micelle concentration, cloud point, Krafft temperature, Hydrophilic-lipophilic deviation (surfactants)	$CMC, T_C, T_K, HLD$
	Toxicity	Toxicity parameter

One of the main issues to face when applying this methodology, though, is the availability of the needed

properties. Experimental data are often scarce and therefore the development of dedicated models for reliable prediction of pure component and mixture properties is necessary [7]. Table 2 and 3 give a detailed summary of the pure component and mixture property models, respectively, used in this project, where the highlighted rows indicate the newly developed models in this project.

**Table 2:** Pure component properties considered in this project and models employed for their estimation. Highlighted in grey, the property models developed in this project.

Pure Component Property	Model Used
$T_C$	M&G GC <sup>+</sup> method [8] - This work
$C$	Correlation
$CMC$	M&G GC <sup>+</sup> method [9] - This work
$\rho$	Modified Rackett EoS
$\mu$	M&G GC <sup>+</sup> method
$\delta_D, \delta_P, \delta_H$	M&G GC <sup>+</sup> method
$\delta_T$	M&G GC <sup>+</sup> method
$HLB$	Definition
$\nu$	Definition
$T_K$	M&G GC <sup>+</sup> method - This work
$T_f$	C&G GC method
$\sigma$	M&G GC <sup>+</sup> method
$LC_{50}$	M&G GC <sup>+</sup> method

**Table 3:** Mixture properties considered in this project and models employed for their estimation. Highlighted in grey, the property models developed in this project.

Mixture Property	Model used
$C$	Linear mixing rule
$\rho$	Linear mixing rule on the molar volume
$\mu$	GC(UNIFAC)-based method
	Dedicated model (emulsions only)
$\delta_D, \delta_P, \delta_H$	Linear mixing rule
$\delta_T$	Linear mixing rule
$T_f$	GC(UNIFAC)-based method
$\sigma$	GC(UNIFAC)-based method
	GC-based method (emulsions) - This work
$T_f$	Linear mixing rule

## Results and Discussion

One of the main objectives of this project, as already pointed out, concerns the property modeling. As from Table 2 and 3, three pure component properties and one mixture property have been modeled in this work and all the models are group-contribution based methods. In particular, the Marrero&Gani GC<sup>+</sup> method [10] has been applied. In this method, like other M&G methods, a physico-chemical property is predicted considering that each compound can be described by groups at three levels: first order-groups, second-order groups and third-order groups. The (first) basic level uses contributions of

first-order groups that describe a wide variety of organic compounds. The higher (second) level provides additional structural information, not provided by the first-order groups and thus corrects the estimates at the first level. A further correction (adjustment) to the predictions is provided through the third-level, where the contributions of parts of the structure of complex molecules are calculated.

The M&G estimation model has the form of the following equation:

$$F(\xi) = \sum_i^{NG1} N_i C_i + y \sum_j^{NG2} M_j D_j + h \sum_k^{NG3} O_k E_k$$

Where  $F(\xi)$  is a function of the estimated property  $\xi$ ;  $C_i$  is the contribution of the first-order group of type  $i$ ;  $N_i$  is the occurrence of the first-order group  $i$ ;  $D_j$  is the contribution of the second-order group of type  $j$ ;  $M_j$  is the occurrence of the second-order group  $j$ ;  $E_k$  is the contribution of the third-order group of type  $k$ ;  $O_k$  is the occurrence of the third-order group  $k$ ;  $y$ ,  $h$  are binary variables,  $NG1$ ,  $NG2$  and  $NG3$  are the number of first-, second- and third-order groups, respectively.

The abovementioned approach has been applied for the modeling of several properties: cloud point, critical micelle concentration and Krafft temperature as pure component properties of surfactants and surface tension of the mixture between water and surfactant. The M&G GC<sup>+</sup> approach, strictly, is applicable only to pure component properties, but in this particular case, even though all these properties are peculiar of the mixture between water and surfactants, estimating them at constant temperature (and pressure) and since the second component is fixed as water, it is possible to model these properties as pure component properties of the surfactant. Some results are shown in the following Figure 2 and 3.

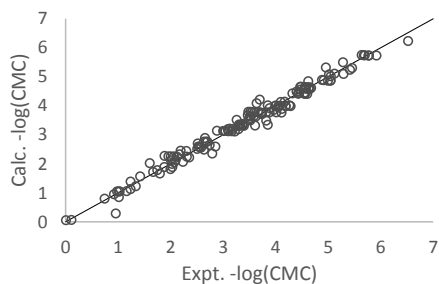


**Figure 2:** Predicted critical micelle concentration versus experimental data for ionic surfactants.

On the basis of the property models developed in this project and other considered for the different target properties listed in Table 2 and 3, dedicated structured databases for the different categories of ingredients and appropriate algorithms, it has been possible to test the methodology with a new conceptual case-study dealing with a tank cleaning detergent for palm oil removal. Following the methodology shown in Figure 1:

- Task 1: The main needs of this product are satisfactory cleaning performances and low foam-

ability. As secondary needs, the product is desired to be stable in its emulsified form before and during its application, to have a low impact on the surface, to be easily applicable and to have a determined color. The above product needs are translated into the following target properties: surface tension ( $\sigma < 25$  mN/m), Hansen solubility parameters ( $\delta_D = 17.7$ ,  $\delta_P = 3.5$ ,  $\delta_H = 3.7$  MPa<sup>1/2</sup>), hydrophilic-lipophilic balance (HLB > 12), critical micelle concentration (CMC > 0.01 mol/L), cloud point ( $T^c > 80^\circ\text{C}$ ), hydrophilic-lipophilic deviation (HLD  $\neq 0$ ) and kinematic viscosity ( $\nu < 75$  cS). Moreover, the presence of a proper preservative, a bleaching agent, a pigment and a builder are needed.

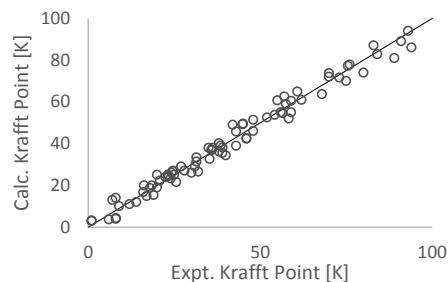


**Figure 3:** Predicted Krafft temperature versus experimental data for ionic surfactants.

- Task 2: The active ingredients needed for detergents are surfactants, and non-ionic surfactants are usually preferred because of their lower foam-ability and flexibility. Employing the non-ionic surfactant database and the target values of Task 1, the selection of the most advantageous active ingredient is made by simultaneously minimizing the cost and maximizing the performance in terms of palm oil dissolution. The most advantageous candidate obtained is Decyl Ethaethylene Oxide.
- Task 3: The oil phase in this problem is palm oil. As regards to the water phase, the database is screened for candidates and the decision, realized by minimizing the cost once boundaries on safety and toxicity are set, gives water as the most advantageous water phase ingredients. Also, a surfactant must be added to the formulation in order to improve the stability of it in the emulsified form. Since a surfactant has already been chosen as active ingredient, a co-surfactant is considered instead. It is necessary that the designed co-surfactant is compatible with the surfactant identified as active ingredient and Butyl Glycol is then chosen.
- Task 4: To match the secondary needs of Task 1, a suitable preservative, a bleaching agent, a pigment and a builder are needed. The selection is made through a rule-based search, where boundaries on safety and toxicity are applied and the cost is then minimized. Sodium Silicate, Potassium Hydroxide, Sodium Triphosphate and Titanium Oxide are the selected.

- Task 5: In order to estimate the optimal composition, boundaries on the overall kinematic viscosity and on the hydrophilic-lipophilic deviation are set, while the solubility of the active ingredients and additives in the two liquid phases are calculated with UNIFAC. The results are summarized in Table 4.

**Table 4:** Optimal formulation for a tank cleaning detergent for the removal of palm oil

Ingredient	Mole%	Ingredient	Mole%
Decyl Esaethylene Oxide	12.3	Sodium Triphosphate	2.5
Sodium Silicate	1.9	Potassium Hydroxide	8.4
Water	67.8	Titanium Oxide	3.4
Butyl Glycol	3.6		

Before going to the experimental stage for the validation and/or refinement of the optimal formulation obtained, a model-based verification of the thermodynamic stability of the product as an emulsion is performed. This consists of the analysis of the behavior of ternary systems of the type water-oil-surfactants. In relation to emulsion-based chemical product design, the most useful way to represent such a phase envelop consists in the so-called fish diagram. Here, ternary water-oil-surfactant data are drawn in an X-Y diagram, at constant water-oil ratio, where the surfactant content (usually in weight percentage) is in the X-axis, while the temperature is in the Y-axis. These diagrams represent a valid tool for emulsion-based product design since different types of products can be recognized and the possibilities for the formation of each of them are easily identified, given the temperature and the composition of the formulation.

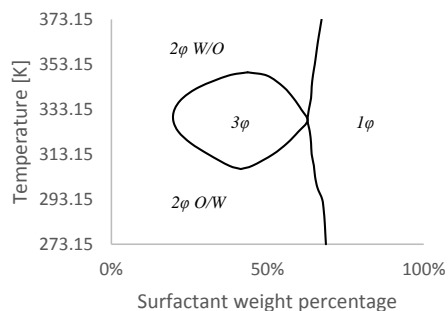


**Figure 4:** Representation of a standard fish-diagram

In Figure 4 different areas can be identified: the region defined with the symbol  $1\phi$  represents the area where a micro-emulsion can be formed, the regions defined with the symbol  $2\phi$  are the areas where emulsified products can be formulated, while the region identified by the symbol  $3\phi$  is a hybrid domain, where an emulsion and a micro-emulsion may coexist. As a part of an emulsion-based chemical product design procedure, it is necessary to make sure that the designed formulation lies in the  $2\phi$

$W/O$  area when a water-in-oil emulsion is desired or in the  $2\phi O/W$  area if an oil-in-water emulsion is wanted.

## Conclusions

A model-based framework for emulsion-based chemical product design has been developed and has been applied to three different case-studies. The application range of the methodology, however, is broad: once the formulation-structure and the structure-property relationships are available and the consumer assessments are given by the knowledge-base, any emulsion-based product can be designed through it. Because of uncertainties in the prediction of the composition of the formulated product, a second experiment-based stage of verification is necessary and is in development. The work-flow methodology with associated models, tools, structured databases and algorithms have been developed and they are being implemented into a computer-aided framework for emulsion-bases formulation design.

Future work will be regarding the prediction of the phase behaviors of both binary and ternary mixtures of water, oil and surfactants and the implementation of the whole methodology in the software "The Virtual Process-Product Design Laboratory" (Virtual PPD Lab) as a new feature, allowing users to perform virtual formulation design and verification for emulsified products is also in development. Moreover, another case-study, developed integrating the model-based and the experiment-based stages will be then developed.

## References

- [1] E.L. Cussler, G.D. Moggridge, Chemical Product Design, Cambridge University Press, Cambridge, UK 2011.
- [2] E. Conte, R. Gani, K.M. Ng, AIChE Journal 57 (2011), 2431-2449.
- [3] N.A. Yunus, K.V. Gernaey, J.M. Woodley, R. Gani, Computers and Chemical Engineering (2013), submitted.
- [4] M. Mattei, G.M. Kontogeorgis, R. Gani, Computer Aided Chemical Engineering 31 (2012), 220-224.
- [5] M. Mattei, G.M. Kontogeorgis, R. Gani, Computer Aided Chemical Engineering 32 (2013), 817-822.
- [6] M. Mattei, G.M. Kontogeorgis, R. Gani, Computer Aided Chemical Engineering, submitted.
- [7] M. Mattei, E. Conte, G.M. Kontogeorgis, R. Gani, Prediction of Thermophysical Properties of Liquid Formulated Products, in U. Brockel, W. Meier, G. Wagner, Product Design and Engineering – Formulation of Gels and Pastes, Wiley-VCH, Weinheim, Germany, 2013.
- [8] M. Mattei, G.M. Kontogeorgis, R. Gani, Fluid Phase Equilibria, in press.
- [9] M. Mattei, G.M. Kontogeorgis, R. Gani, Industrial and Engineering Chemistry Research 52 (2013), 12236-12246.
- [10] J. Marrero, R. Gani, Fluid Phase Equilibria 183-184 (2001), 183-208.
- [11] M. Kahlweit, R. Strey, Angewandte Chemie International Edition English 24 (1985), 654-668.



**Piotr Mazurek**

Phone: +45 4525 6196  
E-mail: pioma@kt.dtu.dk

Supervisors: Anne Ladegaard Skov  
Søren Hvilsted

PhD Study  
Started: January 2013  
To be completed: January 2016

## Thiol-ene “Click Chemistry” as a Powerful Tool for Preparation of Lab-on-Chip Flow Focusing Microfluidic Devices

### Abstract

Thiol-ene polymer composition was used to prepare lab-on-chip flow focusing microfluidic devices. The thiol-ene chemistry was proved to be a powerful tool not only for fabrication of crosslinked materials but also for selective surface modification via grafting reaction. Both of these features were exploited to prepare flow focusing microfluidic chips that allowed preparation of core-shell microspheres.

### Introduction

Many novel applications have been presented in literature since the first core-shell microspheres were prepared. They are mainly used in the pharmaceutical and biotechnological industries and self-healing materials. Due to their great potential many researchers still work on this topic trying to optimize the preparation procedure, which in many cases is very complicated. One of the main issues that one needs to face is the size distribution of the core-shell microspheres, which is a vital factor that ultimately defines possible applications of the product. The best results so far have been obtained by using microfluidic device systems consisting of a set of capillaries or a combination of different types of channel junctions (hydrophobic or hydrophilic) in microfluidic chips. Both methods are reported as tools capable of producing core-shell microspheres of extremely narrow size distribution [1,2].

The composition used for preparation of microfluidic chips presented in this report is based on thiol and allyl terminated compounds mixed in stoichiometric imbalance and then crosslinked under UV-irradiation. The procedure was presented and described by Haraldsson et al. [3]. The thiol-ene chemistry used in this system is a good alternative to PDMS chips, which possess a number of disadvantages, e.g. susceptibility to many organic solvents as well as elasticity which is a barrier for many applications. The curing process of thiol-ene

composition described here proceeds rapidly when exposed to UV-light in the presence of very little or even no photoinitiator. Moreover the reaction does not require any solvents or elevated temperatures, exhibits delayed gelation, low volume shrinkage and low stress development [3,4]. Furthermore, the crosslinked material is resistant to many solvents and mechanical properties can easily be altered simply by mixing reagents in different ratios. Introduction of the stoichiometric imbalance e.g. excess of thiol groups over allyl groups, results in presence of unreacted thiol groups (both in bulk and on the surface), which enables grafting of different compounds on the surface of the cured material, which is a key factor for preparation of double emulsions with the microchip [3,4,5].

The thiol-ene composition is additionally extended with an epoxy-containing component, which works as a bonding agent that increases adhesion between two wafers of microfluidic chip. The bonding process based on the thiol-epoxy “click chemistry” mechanism efficiently prevents leakages when using the chip [6].

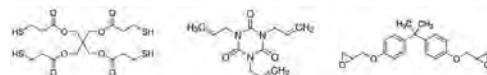


**Figure 1:** Structural formulas of compounds used for preparation of lab-on-chip devices (tetra-thiol, triallyl, diepoxy).

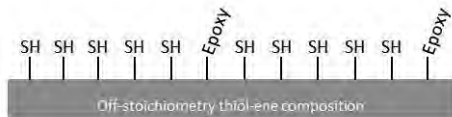


**Figure 2:** Schematic illustration of UV-cured network resulting from off-stoichiometric mixture of tetrathiol, triallyl and diepoxy compounds (2 : 1 : 0.15 respectively).

The abbreviations given to off-stoichiometry thiol-ene composition and the same composition extended with BADGE are OSTE and OSTE+ respectively.

### Materials

Sylgard 184 silicone kit used for preparation of mirror-image mold was purchased from Dow Corning. All three monomers used for preparation of the microfluidic chip polymer matrix (pentaerythritol tetrakis(3-mercaptopropionate) (PETMP), triallyl-1,3,5-triazine-2,4,6(1H,3H,5H)-trione (TATATO) and bisphenol A diglycidyl ether (BADGE)) as well as monomers used for grafting reactions (acrylic acid, allylmalonic acid, sodium hydroxide, 2,2,3,3,4,4,5,5,6,6,7,7-dodecafluoroheptyl acrylate (DFHA)) were purchased from Sigma Aldrich. Thiol-ene reaction photoinitiator Lucirin TPO-L was obtained from BASF GmbH Germany and 2,2-dimethoxy-2-phenylacetophenone (DMPA) was obtained from Sigma Aldrich. Thiol-epoxy reaction catalyst 1,5-diazabicyclo(4.3.0)non-5-ene (DBN) was purchased from Sigma Aldrich. All solvents used in this study were obtained from Sigma Aldrich.

### Microfluidic chip preparation

**Mold preparation.** After the master-mold was designed, all channels and geometries were micro-milled in PMMA plate. Sylgard 184 silicone kit was used for producing of mirror-image mold. Base and crosslinker were mixed together in 10 : 1 weight ratio respectively, degassed and casted on the PMMA master-mold. The PDMS curing reaction was allowed for two hours at 120 °C.

### Designing of initial composition for microfluidic chip.

As a starting point simple thiol-allyl mixtures were prepared and tested. Compositions with different stoichiometric ratios of reactive groups were investigated in terms of DSC. The results presented in Figure 3 show that when thiol and vinyl groups are in balance, the glass transition temperature is the highest, which is attributed to the highest degree of crosslinking in this composition and presumed absence of dangling chains. When a stoichiometric imbalance is introduced, the glass transition temperatures (T<sub>g</sub>) decrease due to the increasing number of dangling chains with unreacted functional groups. It can also be concluded

that the excess of allyl monomer (triallyl-1,3,5-triazine-2,4,6(1H,3H,5H)-trione) results in formation of a stiffer structure than in the case of excess of thiol monomer, which is finally attributed to the structure of monomers (shorter dangling chains and cyclic nature of allyl monomer). The presence of both thiol and vinyl groups in different compositions was proven by FTIR tests which for  $r=2.0$  exhibit a peak at wavenumber of around  $2550\text{ cm}^{-1}$  attributed to S-H stretch of thiol groups and no peaks in the range between  $3095 - 3010\text{ cm}^{-1}$  attributed to  $\text{sp}^2$  C-H stretch of vinyl group and vice versa in case of composition with excess of allyl monomer (see Figure 4).

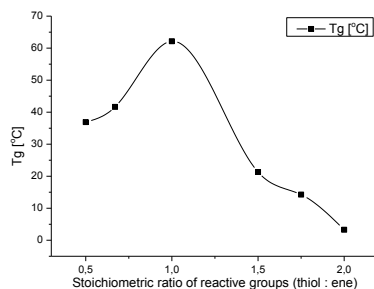


**Figure 3:** Glass transition temperatures of different OSTE compositions.

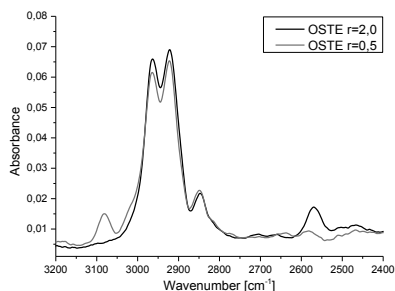


**Figure 4:** FTIR spectra of OSTE compositions with  $r=2,0$  and  $r=0,5$ .

Due to the efficiency of the thiol-ene “click” reaction that is initiated at the mercapto groups, the composition with excess of thiol groups was chosen as it will allow precise and efficient surface modifications for producing microfluidic chips for single and double emulsions.

**Crosslinking reaction step.** The off-stoichiometric mixture used for preparation of microfluidic chip consisted of pentaerythritol tetrakis(3-mercaptopropionate), triallyl-1,3,5-triazine-2,4,6(1H,3H,5H)-trione and bisphenol A diglycidyl ether (BADGE) (molar ratio of reactive groups 2 : 1 : 0.15 respectively). Lucirin TPO-L was used as

a photoinitiator for the thiol-ene crosslinking reaction and DBN was introduced to accelerate the thiol-epoxy reaction. Schematic thiol-ene and thiol-epoxy reactions are presented in Figure 5.

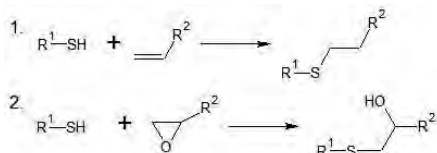


**Figure 5:** 1) thiol-ene photoinitiated reaction; 2) DBN catalyzed thiol-epoxy reaction.

The composition of all five compounds was thoroughly mixed, degassed and transferred onto the PDMS mirror-image mold and exposed to UV-irradiation for few minutes at light intensity of  $\sim 4\text{mW}/\text{cm}^2$ . After both wafers of microfluidic chip were demolded, they were assembled together (avoiding creation of air voids) and placed in the oven for 2 hours at  $80^\circ\text{C}$ . In this step the thiol and epoxy groups present on the surfaces of both wafers react with each other assuring covalent bonding of the two wafers. The amount of BADGE used in this system was kept at lowest possible level leaving as many thiol groups left on the surfaces of the channels as possible. The remaining thiol groups made it possible to modify the surface of the channels later, which is a crucial step in the preparation of flow-focusing microfluidic chips.

Surface modification of thiol-ene films and channels of the chip. The surface grafting reaction follows the same thiol-ene chemistry mechanism as presented above for the crosslinking reaction of the main matrix. In this system we take advantage of the thiol groups remaining on the surface of the material and introduce the reaction by immersing the polymer film into the grafting solution with present vinyl group containing compound. A series of grafting reactions was performed in order to find the most suitable chemicals that would effectively and permanently change the wetting properties of the material towards highest possible hydrophobicity and hydrophilicity respectively. Results of the experiments supported with static contact angle measurements are presented in Figure 6.

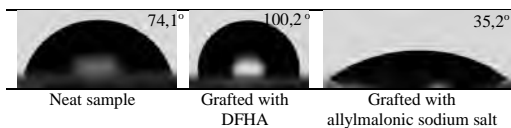


**Figure 6:** Wetting properties of thiol-ene samples grafted with different compounds in terms of static contact angle.

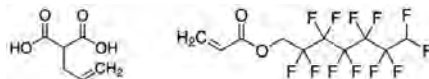


**Figure 7:** Structural formulas of allylmalonic acid and 2,2,3,3,4,4,5,5,6,6,7,7-dodecafluoroheptyl acrylate

The above described experiments allowed for determination of the best possible set of compounds that are to be used in the microfluidic chip channel surfaces modification reaction. In the first step of the process the 10 wt.% solution of DFHA in ethanol with additional 1 wt.% DMPA as photoinitiator was prepared. After the channels were filled with the solution, a part of the chip that was intended to remain hydrophilic was masked with stencil mask in order to block the grafting reaction in that area. Subsequently the chip was exposed to UV-irradiation at light intensity of  $\sim 4\text{mW}/\text{cm}^2$ . In the next step channels were thoroughly washed with substantial amounts of ethanol to dispose of the grafting solution. Afterwards the 10 wt.% solution of allylmalonic acid in ethanol with 1 wt.% DMPA was prepared and injected into the channels of the chip. The area of the chip that was designed to be hydrophobic was masked with stencil mask to avoid grafting reaction of allylmalonic acid in that area. The chip was again exposed to UV-irradiation and after the reaction was complete, it was flushed with ethanol. Subsequently a 0,01M NaOH water solution was injected into the channels in order to replace protons of carboxylic groups with sodium cations. This process was proved to significantly increase the hydrophilicity of the material. The two-step grafting process is presented in Figure 8 and the scheme of resulting wetting properties of the chip channels is shown in Figure 9.

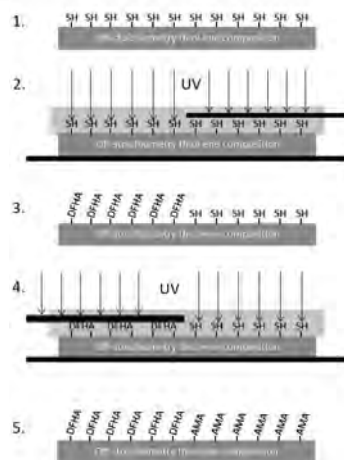


**Figure 8:** Schematic visualization of the two-step surface modification with DFHA and AMA.

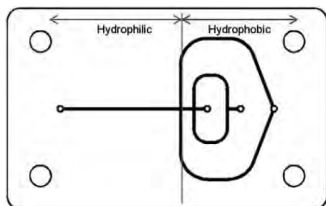


**Figure 9:** Schematic visualization of wetting properties of the channel surfaces in microfluidic chip used for preparation of w/o/w emulsion.

In some cases it was possible to observe progress of the grafting reactions from Fourier transform infrared spectroscopy. It was proved that the grafting reaction of small molecules takes place not only on the surface of the material but also to some extent in bulk. It is attributed to the fact that the polymer network contains a substantial amount of dangling chains due to a relatively high off-stoichiometry ratio of initial composition. The beam of FTIR analyzer usually penetrates through the first few microns of samples tested, so the spectra obtained should in principle show a small peak for the thiol group at the wavenumber of  $2550\text{ cm}^{-1}$  as it is in the case of the initial network. Spectra obtained for e.g. OSTE+ grafted with sodium acrylate show no peaks in that region. Additionally, other strong peaks are observed at different wavenumbers, e.g. stretches typical for carboxylic salts at around  $1600\text{ cm}^{-1}$  and  $1400\text{ cm}^{-1}$  (Figure 10). In the case of grafting of larger molecules like DFHA, there are no significant changes in FTIR spectra, although contact angle measurements show substantial divergence in wetting properties.

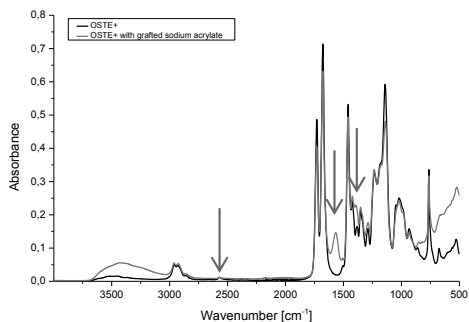


**Figure 10:** FTIR spectra of OSTE+ and OSTE+ grafted with sodium acrylate, showing changes in absorbance at wavenumbers of  $2550\text{ cm}^{-1}$ ,  $1600\text{ cm}^{-1}$  and  $1400\text{ cm}^{-1}$ .

## Conclusions

Thiol-ene chemistry was proved to be an easy to handle and effective tool for the preparation of polymer networks as well as for the chemical surface modification of materials. Increasing the variety of commercially available thiol and allyl-terminated compounds, as well as the high selectivity and low energy consumption of the thiol-ene reaction, gives a practically infinite amount of potential applications, making this chemistry extremely attractive.

## References:

1. Abate A.R., Weitz D.A., Faster multiple emulsification with drop splitting, *Lab Chip*, 2011, **11**, 1911
2. Adams L.L.A., Kodger T.E., Kim S., Shum H., Franke T., Weitz D.A., Single step emulsification for the generation of multi-component double emulsions, *Soft Matter*, 2012, **8**, 10719
3. Carlborg C.F., Haraldsson T., Öberg K., Malkoch M., van der Wijngaart W., Beyond PDMS: off-stoichiometry thiol-ene (OSTE) based soft lithography for rapid prototyping of microfluidic devices, *Lab Chip*, 2011, **11**, 3136
4. Hoyle C.E., Bowman C.N., Thiol-Ene Click Chemistry, *Angewandte Chemie*, 2010, **49**, 1540-1573
5. Kasprzak S.E., Wester B.A., Raj T., Allen M., Gall K., Photopatterning of Thiol-ene-Acrylate Copolymers, *Journal of Microelectromechanical Systems*, 2013, **22**, 339-348
6. Saharil F., Forsberg F., Liu Y., Bettotti P., et al., Dry adhesive bonding of nanoporous inorganic membranes to microfluidic devices using the OSTE(+) dual-cure polymer, *Journal of Micromechanics and Microengineering*, 2013, **23**





## Kresten Troelstrup Meisler

Phone: +45 4525 2912  
E-mail: kretm@kt.dtu.dk

Supervisors: Rafiqul Gani  
Krist V. Gernaey  
Nicolas von Solms

PhD Study  
Started: March 2011  
To be completed: September 2014

## Multi-Dimensional Population Balance Models of Crystallization Processes

### Abstract

The kinetics in crystallization operations are modeled and used in population balance models within a generic modeling framework. This modeling allows better insight into the mechanisms of crystallization and allows process analysis, operation policy design and optimization of crystallization operations. A systematic approach for the use of collected data is suggested in order to analyze the processes.

### Introduction

Crystallization is an efficient separation process for separation of compounds, which are solid in their pure form at the given separation conditions [1]. Depending on the system, high purities can often be obtained in a crystallization step. However, the product characteristics usually also involve a description of the particle distribution. The crystallization operation can be described from a thermodynamical point of view without considering the kinetics, or the kinetic phenomena can be involved through population balances. The kinetic phenomena enter the population balance through the constitutive model equations, and understanding of these phenomena and interactions has gained interest as it is recognized that this affects several properties of the final product. The polymorph, the size distribution and derivative properties of these (such as filterability) are strongly influenced or even governed by the kinetics of the chemical system. The relation between the balance, model and constitutive equations is shown in figure 1.

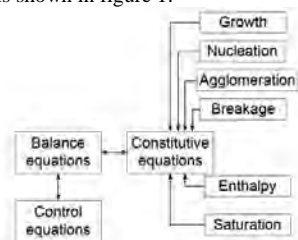


**Figure 1:** The relation between the kinetic phenomena and the model equations

Modeling the kinetic phenomena and their interaction through a population balance approach could help increase the understanding about and hence improve the optimization and design of crystallization operations. In order to accommodate the wide range of crystallization systems being in operation a generic procedure is established for the systematic development of models for use in design, analysis and simulation of crystallization operations. This procedure is used within a generic modeling framework for crystallization operations that allows the specific tasks for a crystallization operation scenario to be carried out independently (for example for analysis of a single phenomenon model) or in combination for simulations of complex problems with operations involving multiple phenomena [2]. The framework allows its user to model a crystallization operation very fast as the model structure supported with guidance to the phenomena is present, and thus both crystallization novices and experts can benefit from the use of the generic framework. A generic framework facilitates the use of the models in combination with other simulation tools, as the necessary specifications can be given overall, for example within commercial simulation software, where the crystallization operation can be combined with other unit operations and more complex chemical processes can be modeled.

### Specific Objectives

The project aims at developing models for the description of crystallization operations including the necessary phenomena in order to describe a process

completely within the generic framework. A systematic multi-dimensional population balance approach is used. A workflow guides the user through the modeling steps in the generic framework where the scenario is defined (for example single phenomenon analysis, model discrimination, crystallization operation analysis). The crystallization operation can be described with variations in the growth rate for different directions which adds dimensionality to the crystals for descriptions of different shapes. Other kinetic phenomena such as nucleation, breakage and agglomeration can be included in the model for the complete description of the kinetics, and with the possibility of evaluation of models at this stage, the detailed simulation of the population balance is not necessary to investigate the kinetic models. The kinetic models can be used for the constitutive equations in the population balance model and, in combination with mass and energy balances, the crystal size distribution from the operation can be calculated. With this result the simulation and practical operations can be compared and the models and experiments can be evaluated. In case of a mismatch between the experimental result and the model result it is possible to re-evaluate the parameters for the model.

## Results and Discussion

In order to establish the kinetics of the crystallization operations kinetic data are necessary. For industrial operations different technologies are used in order to monitor crystallizations. The use of the data from these sources allows a better understanding of the process; however, these data must be translated in order to give the necessary information. This data-translation can be non-trivial, which for example is the case for the translation of Focused Beam Reflectance Measurements (FBRM) from which a chord length distribution is obtained. This chord length distribution is not directly transferrable to a particle size distribution and several challenges have been identified in connection with the translation of data from FBRM measurements. Guidelines for experiments from which the necessary data can be obtained will be developed in the project. One such experiment is the monitoring of a controlled crystallizer in which conditions for promotion of certain phenomena are maintained. With this approach, the specific phenomena can be studied and their relative importance be assessed. In general, however, the reliability of parameters estimated on this data type can be questionable. For this purpose an investigation into the identifiability of the models is undertaken with statistical methods. At the same time, the knowledge that phenomena models are describing actual physical properties is used to decide on constraints for the parameters. Investigations into the relation between the concentration and the supersaturation curves and the kinetic phenomena have been undertaken and are currently in progress. A number of scenarios have been modeled to investigate kinetic models for chemical and technical systems. Examples include simple growth

models for paracetamol-ethanol and more complex models for the calcium oxalate-water system. Examples are given below.

### Scenario

The chemical system paracetamol/ethanol is analysed in order to establish growth kinetics

### Model criteria

The paracetamol-ethanol system has been studied. For this system a growth rate model is needed.

### Model choice

Worlitschek and Mazzotti [3] provide data. The authors have proposed a growth model (eq. 1) which includes a direct temperature dependency expression as an Arrhenius expression; the supersaturation description is reported as the absolute supersaturation often encountered for experimental work.

### Model data criteria

$$G = k_{g0} \cdot e^{-\frac{Ea}{RT}} (\Delta C)^g \quad \text{Eq. 1}$$

The kinetic parameters for the equation are stated in table 1.

**Table 1:** The kinetic parameters for the paracetamol-ethanol system from Worlitschek and Mazzotti [3]

Parameter
$k_{g0} = 21m/s(m^3/mol)^{1.9}$
$Ea = 41.6 kJ/mol$
$g = 1.9$

## Results

The growth rate for the system is plotted as function of temperature for a set of supersaturation values ( $\Delta C = \{1,2,3\} mol/m^3$ ). The plot is shown in figure 2.

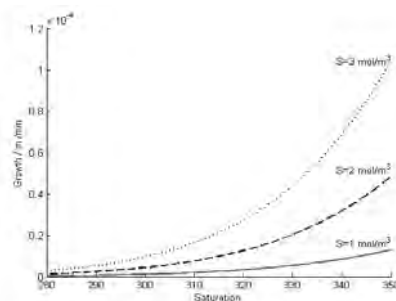


**Figure 2:** The growth rate as function of temperature at three levels of supersaturation.

The growth rate of the paracetamol in the paracetamol-ethanol system increases

The growth expression of paracetamol includes an exponent  $g = 1.9$ , which is near second order growth. This growth order suggests that the inclusion of solute into the crystal structure is important. From the kinetic model database and similar results the paracetamol-ethanol system can be compared to the sucrose-water system. A growth model for this system is Eq. 2, for which Ouiazane et al. [4] provide the kinetic data and matching parameters (table 2).

$$G = k_{g0} \cdot e^{-\frac{Ea}{RT}} \left( \frac{\gamma X - \gamma_{eq} X_{eq}}{\gamma_{eq} X_{eq}} \right)^g \text{ Eq. 2}$$

**Table 2:** The kinetic parameters for the sucrose- water system from Ouiazane et al. [4]

Parameter
$k_{g0} = 2.24 \text{ m/min}$
$Ea = 46.5 \text{ kJ/mol}$
$g = 1$

The systems show similarities in the activation energy. However, in the temperature range that was investigated the paracetamol shows a different response to changes in supersaturation as well as a different value of the rate constant, partly due to the numerical value of the supersaturation. The database allows comparisons across systems and with the beginning integration of model data and thermodynamic and kinetic parameters, the different models can be seen together for different chemical systems to spot trends and gain new system information.

#### Multiple phenomena

Including multiple phenomena in the population balance equation allows more complex systems to be studied. Modeling the single kinetic phenomena on exclusive basis where a single phenomenon is assumed to dominate has been done for several systems. The approach is illustrated through the calcium oxalate-water system.

#### Scenario

Initially a scenario, where the kinetic models for the specific kinetic phenomena are obtained, is defined. This includes models for the growth, nucleation, agglomeration and breakage. The scenarios for the nucleation and growth rate are similar to those of the growth rate discussed above. Extracting relevant parameters from the model library from [5] and [6] the phenomena can be analyzed.

For the agglomeration and breakage a scenario is built to obtain the relevant model.

#### Model criteria

For the agglomeration and breakage both a particle size distribution and rate of particles are necessary.

#### Model choice

In this case the distribution is assumed to be uniform, i.e. the probability of a particle agglomerating with another particle is independent of the volume and all sizes of daughter particles from a breaking particle have the same probability of occurring.

The rate of particle breakage is assumed to increase linearly with the volume of the particle. For both phenomena stirring of the vessel is assumed to affect the rate; however, other phenomena are not included.

#### Model data criteria

Rate kernels are needed for describing the phenomena. The rate kernels are calculated from the data provided by Zauner & Jones [5]. The data for the agglomeration is shown in figure 3 with the plot of the model (eq 3).

$$\log_{10}(\alpha_{\text{agglomeration}}) = -0.6534(\log_{10}(\epsilon))^2 - 2.466 \log_{10}(\epsilon) - 18.02 \text{ Eq 3}$$

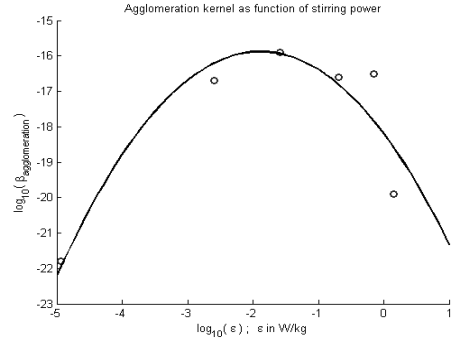


**Figure 3:** Plot of the data from [5] used to obtain an expression for the agglomeration rate.

$$\text{Growth rate } G = k_g X^g$$

$$\text{Nucleation rate } B = k_b X^b$$

Agglomeration Birth

$$\frac{1}{2} \int_0^v \alpha n(v-u, u) n(u) du$$

Agglomeration Death

$$n(v) \int_0^v \alpha n(u) du$$

Breakage Birth

$$\int_v^\infty \beta W(u) n(u) du$$

Breakage Death

$$W(v) n(v)$$

#### Results

With this model established the phenomena are combined. Under the assumption of constant temperature and supersaturation, the interactions of the kinetic phenomena can be explored. Seeding is assumed and a starting value is entered. The evolution in particle distribution is shown in figure 4 and 5.

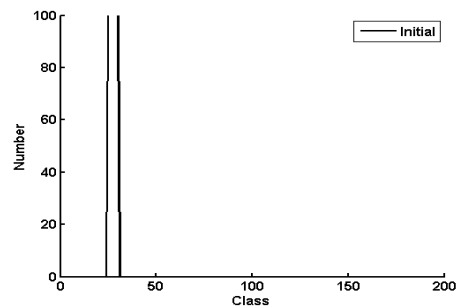


**Figure 4:** Initial seeding

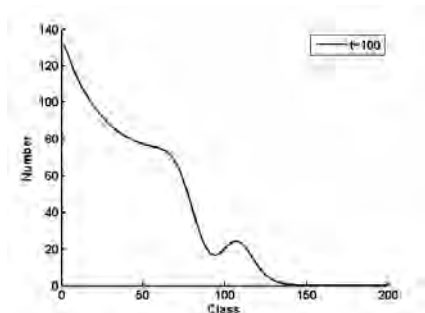


**Figure 5:** The evolution in particle distribution

As the phenomena are combined the nucleation results in a considerable formation of particles in the smaller class range and the growth and agglomeration moves the distribution to larger sizes. The breaking of particles results in a lower number of large particles and contributes to the increasing number of mid-range and small particles.

#### Model library

The model library contains the kinetic phenomena models for the studied systems. Through the model library where the models are stored for application, similarities in systems can be discovered and exploited. The analyzed scenarios can be stored as well and models rated based on their performance in case of multiple models for the same phenomena. Systems with similar kinetics can show similar responses when subjected to similar conditions. This can be utilized to plan new operations and make initial estimates for a new process based on limited information of a chemical system. Changes in the technical system or operation policy may also show responses known prior due to knowledge of kinetically similar systems operated under conditions that are analogous to the desired operating conditions. The combination of phenomena can mask the effects of a single phenomenon in a combined response. The selected approach allows both single and multiple phenomena for better analysis and possible promotion of a desired phenomenon over an undesired phenomenon. As full simulations of crystallization operations may be time consuming depending on the desired level of details and solution method [1] it can be advantageous to draw on similarities, which can be established when the relevant system parameters are known.

#### **Conclusion**

A framework for crystallization operations is being developed, which when complete will handle all operations related to crystallization. So far the overall framework has been developed and case studies with simulation of crystallization of various chemical systems have been investigated.

#### **Acknowledgements**

DTU Chemical Engineering for funding this research

#### **References**

- [1]: Samad, N. A. F. A.; R. Singh; G. Sin; K. V. Gernaey and R. Gani: A generic multi-dimensional model-based system for batch cooling crystallization processes, *Computers and Chemical Engineering* 35, 2011 p. 828-843
- [2]: Meisler, K. T. ; N. A. F. A Samad; K. V. Gernaey; N. von Solms and R. Gani: Generic Model and Data Based Framework for Analysis and Development of Crystallization Processes, Conference contribution, AIChE Annual Meeting, 2011
- [3]: Worlitschek, J. and Mazzotti, M.: Model-based optimization of particle size distribution in batch-cooling crystallization of paracetamol, *Crystal Growth and Design*. 4, 2004,p. 891–903.
- [4]: Ouaizane, S. B. Messnaoui, S. Abderafi, J. Wouters and T. Bounahmidi: Estimation of sucrose crystallization kinetics from batch crystallizer data. *Journal of Crystal Growth* 310, 2008, 798–803.
- [5]: Zauner, R. and A. G. Jones: Determination of nucleation, growth, agglomeration and disruption kinetics from experimental precipitation data: the calcium oxalate system. *Chemical Engineering Science* 55, 2000, p. 4219–4232
- [6]: Millan, A. O. Söhnel, F. Grases: The influence of crystal morphology on the kinetics of growth of calcium oxalate monohydrate, *Journal of Crystal Growth* 179, 1997, p. 231-239

#### **List of Publications**

1. K. T. Meisler, N. von Solms, K. V. Gernaey, R. Gani, *Crystallization Kinetics within a Generic Modelling Framework*, Proceedings of 20th International Workshop on Industrial Crystallization (BIWIC2013), Odense, 2013, p. 176-183.
2. N. A. F. bin Abdul Samad, K. T. Meisler, G. Sin, K. V. Gernaey, R. Gani: *A Generic Framework for Systematic Design of Process Monitoring and Control System for Crystallization Processes*; Proceedings of the 22<sup>nd</sup> European Symposium on Computer Aided Process Engineering, London, 2012.
3. N. A. F. bin Abdul Samad, K. T. Meisler, N. von Solms, K. V. Gernaey, R. Gani: *Systematic identification of crystallization kinetics within a generic modelling framework*, Proceedings of the 11<sup>th</sup> International Symposium on Process Systems Engineering, p. 945-949, 2012, Elsevier BV.



**Malwina Michalak**

Phone: +45 4525 6892  
E-mail: mmi@kt.dtu.dk

Supervisors: Jørn Dalgaard Mikkelsen  
Gunnar Jonson  
Manuel Pinelo

PhD Study  
Started: November 2008  
To be completed: January 2014

## Enzymatic Production and Purification of Prebiotic Oligosaccharides by Chromatography and Membrane Systems

### Abstract

Prebiotics are non-digestible food ingredients that stimulate the microbiota associated with health benefits in the host. One of the most known examples of prebiotics are galactooligosaccharides (GOS). Their production methods are well established in the industry. Galactooligosaccharides are enzymatically synthesized from lactose in trans-galactosylation reaction. Another group of prebiotic oligosaccharides are human milk oligosaccharides (HMO), which are so far not produced in a large scale. The objective of the present study was to generate and fractionate or purify potentially prebiotic oligosaccharides from agricultural and dairy waste or side streams and thereby create value-added products. Galactooligosaccharides were enzymatically produced by hydrolysis from two substrates: isolated galactan and galactan contained in potato pulp. Human milk oligosaccharides were synthesized with transferase from casein glycomacropeptide and an appropriate glycan. Furthermore, oligosaccharides similar in structures to HMO were generated with another enzyme catalyzing transfer of monosaccharide.

### Introduction

Prebiotics are “selectively fermented ingredients that allow specific changes, both in the composition and/or activity in the gastrointestinal microbiota that confers benefits upon host well-being and health”. GOS are widely studied bifidogenic compounds. They are produced from lactose in reaction catalyzed by a  $\beta$ -galactosidase. Besides their prebiotic properties GOS are known to have many other beneficial effects on human body, like stimulation of immune system [1], improvement of the absorption of calcium and magnesium [2, 3], reduction of incidence of allergies [4], as well as, protection from development of colorectal cancer [5]. GOS are often used in infant formulas. Their task in these products is to stimulate the growth of probiotic microorganisms and thus provide microflora similar to that present in breast-fed infants. The addition of GOS to the formulas should result in prevention of diseases and atopy, and stimulation of immune response. Another group of prebiotic oligosaccharides which could have even larger application in infant formulas than GOS could be human milk oligosaccharides. These compounds, however, are not produced at an industrial scale. There is no doubt that they would have positive effect on the well-being of infants. At first because they would be the same as natural compounds of human milk, which

constitute the third most abundant component of human milk. Secondly, because they have not only prebiotic properties, but also a wide range of other beneficial effects. HMO constitute an immunologic mechanism by which human milk confers breast-fed infants some level of protection against infection [4]. They function as soluble receptors that inhibit pathogens such as *Campylobacter jejuni* and *Escherichia coli* K1 from adhering to the receptors on the mucosal surface of the host gastrointestinal tract, and therefore help to reduce the incidence of diarrhea and other diseases in breast-fed infants [4, 6]. Due to these important biological properties the invention of method of production of HMO which could be performed at an industrial scale is of great interest. The production of GOS from an agricultural waste is worth an attention as well.

### Production and characterization of endo-1,4- $\beta$ -galactanase from *Emericella nidulans* expressed in *Pichia pastoris*

A novel endo-1,4- $\beta$ -galactanase from *Emericella nidulans*, GH family 53, was produced in a recombinant *Pichia pastoris* strain. The enzyme was purified by Cu<sup>2+</sup> affinity chromatography and after the purification the yield of protein was 1.6 g/L, which can be considered as high. The optimal reaction conditions of the endo-1,4- $\beta$ -galactanase were determined in a

statistically designed, quadratic central composite experiment. They appeared to be pH 5 and 49 °C. The specific activity of the *E. nidulans* enzyme expressed in *P. pastoris* was 73.3 U/mg protein, which was similar to that of an endo-1,4-β-galactanase from *Aspergillus niger* used as benchmark.

The influence of metal ions on the enzyme activity was tested too and revealed that the activity was not affected much by the metal ions. The strongest negative influence had Al<sup>3+</sup> (activity reduced to 51.3%), whereas the strongest positive effect was achieved by incubation with Zn<sup>2+</sup> (activity increased to 107.5%). A minor increase in the enzyme activity occurred also in case of treatment with Ca<sup>2+</sup> and Mn<sup>2+</sup>. The literature usually describes the influence of metal ions on fungal galactanases as weak, but inhibitory. The explanation of improvement of endo-β-1,4-galactanase activity in the presence of divalent metal ions, especially Zn<sup>2+</sup>, was found out during crystallization of the enzyme.

Diffraction data extending to 2.0 Å resolution were collected from a crystal of 1,4-β-galactanase from *E. nidulans* expressed in *P. pastoris*, which was grown from conditions containing 0.2 M zinc acetate. None of the other screening conditions gave any crystalline material. The crystal structure showed a high similarity between the investigated enzyme and other endo-β-1,4-galactanases belonging to GH53. The crystal structure revealed 15 zinc ions bound to the protein, one of which is located in the active site, whereas the majority of the ions are located on the surface of the enzyme, in some cases with side chains from two different molecules as ligands. This explained why the presence of zinc ions was essential for crystallization. Since the crystal structure did not suggest any catalytic role of the zinc ions, the increased activity of the endo-1,4-β-galactanase in the presence of the zinc ions may be explained by their stabilizing effect on the enzyme structure by neutralization of the surface charge and by better interactions of neutral enzyme with the substrate.

### Release of poly- and oligosaccharides from potato galactan and high molecular weight solubilized potato pulp polysaccharides (SPPP), and stimulation of bacterial growth

The optimized reaction conditions for the endo-1,4-β-galactanase were used to enzymatically create potentially prebiotic poly- and oligosaccharides from potato galactan and SPPP. The reactions were performed in 100-mL scale and the products were separated according to molecular weight using 3 kDa, 10 kDa or 100 kDa membranes. The produced fractions are described in Table 1. The accumulation of galactose and galactobiose in the obtained samples coincided with extended incubation time and high E/S ratio of 0.3 %.

The potential prebiotic properties of the fractionated saccharides were evaluated by measuring their growth promoting activity on selected pure cultures using a Bioscreen microtiter system.

The growth performance expressed as area under the growth curve [7] was assessed for five different bacteria

comprising three probiotic strains, *L. acidophilus*, *B. longum*, and *B. lactis*, one pathogenic strain of *C. perfringens*, and one commensal *E. coli* strain. Fructooligosaccharides (FOS) were used as a control due to their prebiotic properties on bifidobacteria and lactobacilli.

The growth of each individual test bacterium was affected differently by the different compounds. In addition, the different bacteria also responded differently to the same substrate (Figure 1).

**Table 1.** Details of produced galactan and SPPP fractions.

sample	sample details
PG1	galactan, 0.03%, 60 min, less than 3 kDa
PG2	galactan, 0.03%, 60 min, between 3 and 10 kDa
PG3	galactan, 0.03%, 15 min, less than 10 kDa
PG4	galactan, 0.03%, 15 min, between 10 and 100 kDa
PG5	galactan, 0.03%, 270 min, less than 3 kDa
SPPP1	SPPP, 0.3%, 15 min, less than 10 kDa
SPPP2	SPPP, 0.3%, 15 min, more than 10 kDa

The analysis of the bioscreen data showed that among the tested samples the lower molecular weight fractions exhibited more and various potentially prebiotic features. The data clearly suggest that β-galactooligosaccharides possess promising beneficial properties in relation to gut health. The available data also suggest that different sub-structures of these β-galactosides, e.g. certain molecular sizes and/or branching patterns, exhibit differential prebiotic effects.

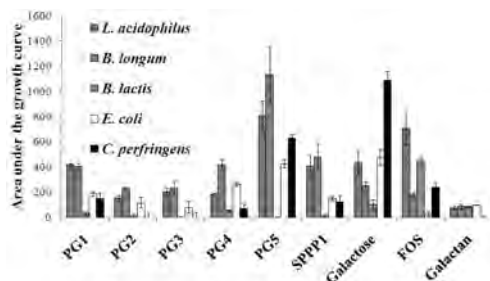


**Figure 1.** Differential growth of bacterial strains on *E. nidulans* endo-1,4-β-galactanase catalyzed hydrolysis products from potato galactan and SPPP. Data are given as average values of 3–6 growth assay replicates and shown ± S.D.

### Production of mutant sialidase Tr6 and tuning the reaction conditions for maximizing trans-sialidase activity

Mutated sialidase from *Trypanosoma rangeli* containing 6 point mutations was generated by rational design. The enzyme Tr6 was expressed in *Pichia pastoris* and produced in 5L fermentor. The wild type sialidase from *T. rangeli* and the Tr6 mutant enzyme have a high level of sialidase activity, but a relatively low level of trans-

sialidase activity [8]. To find out the reaction conditions that promote the trans-sialidase activity several statistically designed experiments were performed. The best found conditions were pH 5.5, 25°C, 117 mM acceptor and 4.6 mM sialic acid contained in the donor compound, casein glycomacropeptide (cGMP). The model acceptor of sialic acid was lactose. The product generated by Tr6 from lactose and cGMP was 3'-sialyllactose. The enzyme was selectively producing this isomer of sialyllactose and had high specific trans-sialidase activity, which was determined to 16.2 nmol min<sup>-1</sup> per µg of pure protein.

The 3'-sialyllactose was then produced in 5L scale. The product was purified by anion exchange chromatography using ammonium formate as an eluent. The quality of the separation and identity of 3'-sialyllactose was confirmed by capillary LC/MS and NMR spectroscopy. In order to remove the ammonium formate, the samples were lyophilized six times. The final yield of 3'-sialyllactose was 3.6 g, and the amount of obtained free sialic acid was 133 mg. Only approximately 50% of the sialic acid residues contained in the cGMP are bound at the 3'-position, and the rest is bound at the 6'-position [9]. Since the Tr6 catalyzed only the production of 3'-sialyllactose, it can be assumed that only 3'-bound sialic acid, i.e. ~50% of the total sialic acid in cGMP, was available for this enzyme. Therefore, the molar yield of 3'-sialyllactose was ~50% based on the available 3'-sialic acid in cGMP. The molar yield of the sialyllactose was 1% based on the lactose, and the yield of free sialic acid was ~2% based on the total sialyl-residues in the cGMP.

Tr6 catalyzed also sialylation of other HMO molecules: two lacto-N-tetraoses (LNT and LNnT) and two fuco-N-pentaoses (LNFP I and LNFP V), which structures are shown in Figure 2. These reactions were, however, performed in much smaller scale than the synthesis of 3'-sialyllactose due to the low availability of the substrate acceptors. 5–12 mg of sialylated LNT, LNnT, LNFP I and LNFP V were obtained employing the optimal reactions conditions for the Tr6 (pH 5.5, 25 °C), and as high as possible acceptor/donor ratio. LC/MS analysis confirmed the structures of the products.

#### Expression of mutant sialidase Tr13 in *P. pastoris* and production of sialylated glycans

Tr6 enzyme was used as a parent clone to generate another mutant Tr13. Tr13 was created by introduction of 7 additional mutations to the Tr6 sequence. Its optimal trans-glycosylation conditions were determined by statistical design experiments. These conditions were following: pH 3, 20°C and 351 mM acceptor. The acceptor used in the optimization study was lactose. The donor of sialic acid – cGMP was constant in all the experiments and it was 8 mM cGMP-bound sialic acid.

The advantage of Tr13 over Tr6 was the very low hydrolytic activity of Tr13. Tr13 produced higher concentration of sialylated oligosaccharides, due to much lower degradation of the products in comparison

with Tr6. As Tr6, Tr13 produced selectively only 3'-sialyl-glycans.

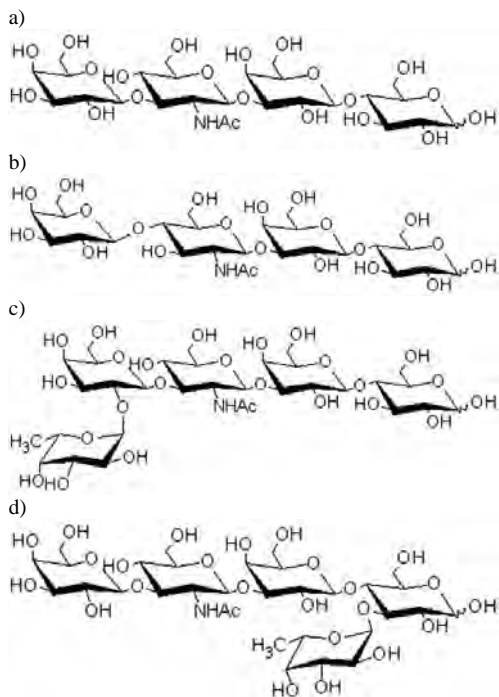


**Figure 2.** Structures of acceptor substrates used for production of sialylated oligosaccharides catalyzed by Tr6; a) lacto-N-tetraose, LNT; b) lacto-N-neotetraose, LNnT; c) lacto-N-fucopentaose I (LNFP I); d) lacto-N-fucopentaose V (LNFP V).

The optimal trans-glycosylation conditions were used for synthesis of sialylated glycans by Tr13. Well-documented prebiotics such as GOS, IMO and lactulose, as well as, three other compounds: melibiose, maltose, and fucose were sialylated with this enzyme (Table 2). The products were purified by anion exchange chromatography, as in case of products generated by Tr6. The LC/MS analysis proved that the sialylated compounds were completely separated from sialic acid, and the acceptor used in the reaction. The highest products yields were achieved when fucose (1.5 mM) and lactulose (1.9 mM) were used as the sialic acid acceptors. The yields of sialylation products of GOS and iso-maltooligosaccharides (IMO) were lower. GOS and IMO preparations were mixtures of oligosaccharides of different chain length. The yields for the different chain lengths might have differed from the average. Four and five sialylated compounds were obtained from GOS and IMO, respectively. The fact that Tr13 could sialylate not only terminal galactose, like *T. cruzi* trans-sialidase, but also terminal glucose and even glucose and fucose monomers was surprising. It indicated a high level of acceptor substrate promiscuity.

This broad substrate specificity can potentially be a valuable asset for enzymatic synthesis of a broad range of sialylated glycans.

**Table 2.** Products of sialylation of glycans by Tr 13 analysed by LC/MS.

acceptor	m/z [MH] <sup>-</sup>	product
GOS	632	SA- $\alpha$ -Gal-1,4- $\beta$ -Glc
	794	SA- $\alpha$ -Gal- $\beta$ -Gal-1,4- $\beta$ -Glc
	956	SA- $\alpha$ -Gal- $\beta$ -Gal- $\beta$ -Gal-1,4- $\beta$ -Glc
	1118	SA- $\alpha$ -Gal- $\beta$ -Gal- $\beta$ -Gal- $\beta$ -Gal-1,4- $\beta$ -Glc
fucose	454	SA- $\alpha$ -Fuc
melibiose	632	SA- $\alpha$ -Gal-1,6- $\alpha$ -Glc
lactulose	632	SA- $\alpha$ -Gal-1,4- $\beta$ -Fru
maltose	632	SA- $\alpha$ -Glc-1,4- $\alpha$ -Glc
IMO	470	SA- $\alpha$ -Glc
	632	SA- $\alpha$ -Glc-1,6- $\alpha$ -Glc
	794	SA- $\alpha$ -Glc- $\alpha$ -Glc- $\alpha$ -Glc
	956	SA- $\alpha$ -Glc- $\alpha$ -Glc- $\alpha$ -Glc- $\alpha$ -Glc
	1118	SA- $\alpha$ -Glc- $\alpha$ -Glc- $\alpha$ -Glc- $\alpha$ -Glc- $\alpha$ -Glc

### Conclusions

The results of this work have provided a positive foundation for biocatalytic design of  $\beta$ -galactooligosaccharides from potato pulp with potential health effects. The work has also shown a direction for potential valorization of the potato pulp byproduct. Moreover, the mutant sialidase from *T. rangeli* Tr6 has been successfully tuned into trans-sialidase and a few structures of human milk oligosaccharides were produced by this enzyme. This paves the way to develop new functional food ingredients from industrial side streams. Application of another *T. rangeli* enzyme with 13 point mutations, Tr13, for the synthesis of sialylated glycans demonstrates a novel opportunity to produce a range of oligosaccharides. These new sialylated glycans could be used in infant formula as potent prebiotics, or combat the food-born pathogens by adhesion (decoy molecules). Use of Tr13 ensures not only relatively high reaction yields but also, on the contrary to production of HMO, possibility of employing cheap acceptor compounds.

### Acknowledgements

The project was carried out within the Center for Biological Production of Dietary Fibers and Prebiotics at DTU ("Prebiotics Center") and as a part of "Enzymatic Production of Human Milk Oligosaccharides" project supported by The Strategic Research Council.

### References

1. V.M.C. de Sousa, E.F. dos Santos, V.C. Sgarbieri, Food Nutr Sci 2 (2011) 133-144
2. G.T. Macfarlane, H. Steed, S. Macfarlane, J Appl Microbiol 104 (2008) 305-344

3. C.M. Weaver, B.R. Martin, C.H. Nakatsu, A.P. Armstrong, A. Clavijo, L.D. McCabe, G.P. McCabe, S. Duignan, M.H.C. Schoterman, E.G.H.M van den Heuvel, J Agric Food Chem 59 (2011) 6501-6510
4. L. Bode, Glycobiology 22 (2012) 1147-62.
5. D. Charalampopoulos, R.A. Rastall, Prebiotics and probiotics science and technology, Springer, 2009
6. A.L. Morrow, G.M. Ruiz-Palacios, X. Jiang, D.S. Newburg, J Nutr 135 (2005) 1304-7.
7. H. Mäkeläinen, M. Saarinen, J. Stowell, N. Rautonen, A.C. Ouwehand, Benefic Microb 1 (2010) 139-48
8. G. Paris, L. Ratier, M.F. Amaya, T. Nguyen, P.M. Alzari, A.C.C. Frasch, J Mol Biol 345 (2005) 923-34.
9. T. Saito, T. Itoh, J Dairy Sci 75 (1992) 1768-74

### List of Publications

1. M. Michalak, L.V. Thomassen, H. Roytio, A.C. Ouwehand, A.S. Meyer, J.D. Mikkelsen, Enzyme Microb Technol 50 (2012) 121- 129
2. H. Otten, M. Michalak, J.D. Mikkelsen, S. Larsen, Acta Crystallogr Sect F 69 (2013) 850-854
3. M. Michalak, D.M. Larsen, C. Jers, J.R.M. Almeida, M. Willer, H. Li, F. Kirpekar, L. Kjærulff, C.H. Gotfredsen, R.T. Nordvang, A.S. Meyer, J.D. Mikkelsen, Process Biochem (2013), <http://dx.doi.org/10.1016/j.procbio.2013.10.023>
4. C. Jers, M. Michalak, D.M. Larsen, K.P. Kepp, H. Li, Y. Guo, F. Kirpekar, A.S. Meyer, J.D. Mikkelsen, PLOS ONE, in press
5. Holck J., Larsen D.M., Michalak M., Li H., Kjærulff L., Kirpekar F., Gotfredsen C.H., Forssten S., Ouwehand A.C., Mikkelsen J.D., Meyer A.S, New Biotechnol, in press
6. H. Gavlighi, M. Michalak, A.S. Meyer, J.D. Mikkelsen, J Agric Food Chem 61 (2013) 1272-78





**Aleksandar Mitic**

Phone: +45 4525 2949  
E-mail: asmi@kt.dtu.dk

Supervisors: Krist V. Germaey  
Kim Dam-Johansen  
Tommy Skovby (H. Lundbeck A/S)

Started: November 2010  
To be completed: February 2014

## Operational Aspects of Continuous Pharmaceutical Production

### Abstract

Establishment of continuous production is a great challenge in the modern pharmaceutical industry. Traditional batch and semi-batch processes have plenty of disadvantages which can be avoided by applying eco-friendly and economical continuous manufacturing. Furthermore, Process Analytical Technology (PAT) can reach its full benefits in this type of production system. The main aim of this PhD thesis is to accelerate slow chemical reactions in the production of zuclopenthixol, a product of H. Lundbeck A/S, as well as to complete continuous manufacturing and establish in-line process monitoring and control. Production of zuclopenthixol involves several steps: Grignard alkylation, hydrolysis, liquid-liquid separation, dehydration and hydroamination. Applications of mini- and micro-sized devices, as well as microwave assisted organic synthesis (MAOS) have been tested.

### Introduction

Organic synthesis is essential for the production of an important class of pharmaceuticals. Implementation of organic chemistry on an industrial scale is a great challenge and it has been mainly based on batch and semi-batch processes. However, besides their flexibility and versatility there are many disadvantages compared to continuous production, such as the risk of occurrence of hot spots, non-ideal mixing, undesirable temperature gradients, difficulties in implementing PAT applications, and so on.

The main aim of this PhD project is to complete continuous manufacturing of zuclopenthixol. The overall process flowsheet is depicted in Figure 1.

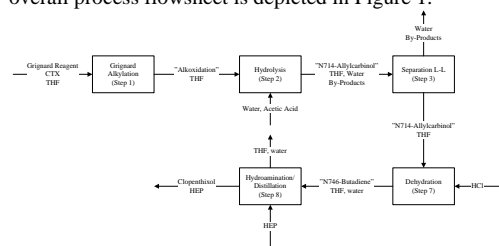


**Figure 1:** Zuclopenthixol production flowsheet

Furthermore, chemical reactions involved in the synthesis of zuclopenthixol are shown in Figure 2. The desired API is shown in the black frame.

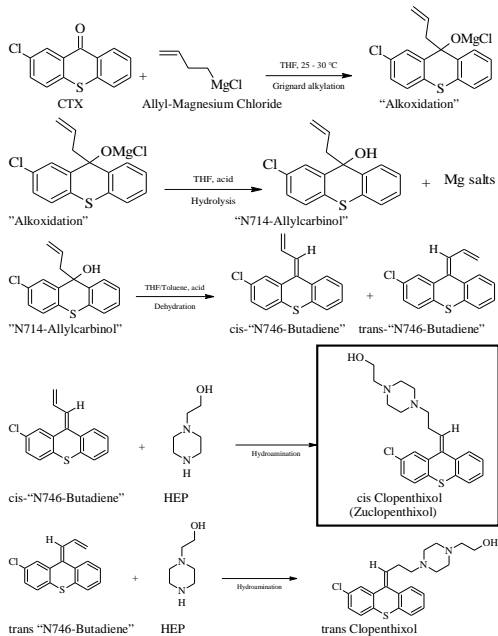


**Figure 2:** Chemical reactions involved in the Zuclopenthixol synthesis. The active pharmaceutical ingredient is shown in the black frame

### Specific Objectives

Different process solutions were tested with the main focus on micro- and mini-sized devices. For instance, Grignard alkylation is a very fast reaction which occurs almost in the mixing zone [1]. Application of a mini-sized tubular reactor by forcing laminar flow was proven to be a great choice. This reaction was followed by immediate hydrolysis of the obtained intermediate product. After hydrolysis, water and water soluble by-products needed to be separated before performing the dehydration reaction. To this purpose, a membrane PTFE micro-separator was used which showed a very high efficiency in practice [2, 3].

In order to complete continuous production of zuclopenthixol, it was necessary to increase the reaction rates of the two last steps – dehydration and hydroamination. In general, acceleration of slow reactions in organic synthesis can be performed by applying different methods. Sometimes, applications of homogeneous catalysis are defined as good manufacturing practices, but difficulties in finding suitable purification methods of final products are a major drawback of this approach. Furthermore, combination of heterogeneous catalysis and pressure increase is a good approach for very slow reactions, but possible deactivation of chemical catalysts due to a long-time exposure at very high temperatures actually forms a limitation to this approach. In addition, selectivity in these steps should be improved also because just the cis-isomer is desired as the product.

Acceleration of chemical reactions in the zuclopenthixol synthesis was performed by using physical effects. More precisely, the dehydration reaction was carried out in a tubular reactor under increased pressure (5 bars) which allowed higher temperature of the reaction media and a higher reaction rate at the same time. Lastly, hydroamination of “N746-Butadienes” showed quite good efficiency under microwave irradiation. This approach has actually shown plenty of advantages in the last decade of the 20<sup>th</sup> century because of faster heating caused by electromagnetic radiation and the specific temperature profile inside reactors. A new field in the organic chemistry was even introduced - microwave assisted organic synthesis (MAOS).

### Results and Discussions

Dehydration of “N714-Allylcarbinol” into the mixture of geometrical isomers of “N746-Butadiene” was performed by using sulfuric acid as the chemical catalyst. For this purpose, a meso-flow chemistry approach was used. The experimental setup is schematically depicted in Figure 3 and it involves in-line process monitoring with FT-NIR. All the results were compared and validated with off-line HPLC analysis.

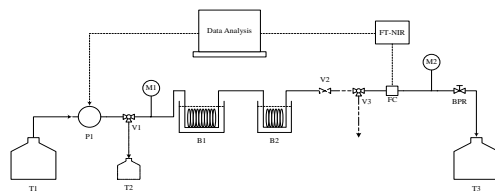


**Figure 3:** Experimental setup for performing dehydration of “N714-Allylcarbinol” in “N746-Butadienes”. Process Flow sheet includes: T1, T2, T3 – tanks; P1 – pump; V1, V2, V3 – valves; B1, B2 – oil and ice baths, respectively; FC – flow cell; M1, M2 – manometers; BPR – back pressure regulator.

The initial step in performing such a reaction successfully was to develop a suitable calibration of the instruments used for the data acquisition. FT-NIR spectrums are depicted in Figure 4 together with the defined areas where “N714-Allylcarbinol”, then “N746-Butadienes” and water absorb the near infrared.

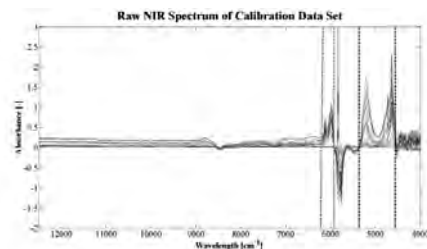


**Figure 4:** Raw spectrums of “N714-Allylcarbinol”, “N746-Butadienes” and water. The areas bordered with red dashed lines, as well as with black dashed lines, imply on absorptions of the mentioned constituents.

However, the raw data was not very accurate for making a PLS model. In order to extract all the useful information from the NIR spectrums, it was necessary to perform a mathematical pre-treatment. For this particular example, the Savitzky-Golay 2<sup>nd</sup> derivative with 15 points showed the lowest error of prediction. The treated spectrums are shown in Figure 5.

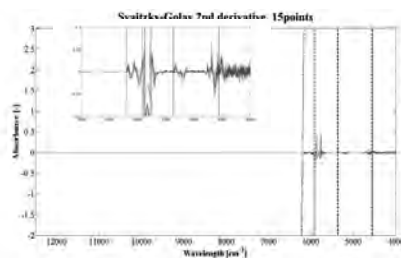


**Figure 5:** Treated spectrums of “N714-Allylcarbinol”, “N746-Butadienes” and water, with Savitzky-Golay 2<sup>nd</sup> derivative and 15 points.

All the acquired data was additionally analyzed with the off-line HPLC analysis, as well as with a new set of FT-NIR instrumentation, a so-called at-line instrument. The results for “N714-Allylcarbinol” are depicted in Figure 6, and it was concluded that a very good correlation was established between the different analysis modes.

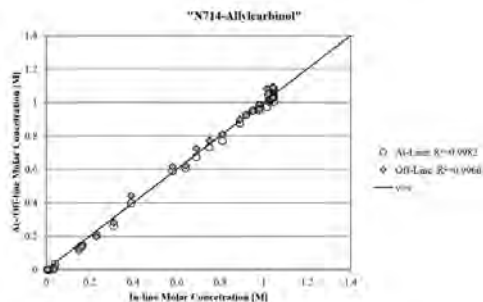


**Figure 6:** External validation of the experimental data obtained with in-line monitoring. At-line analysis is performed with a new set of the FT-NIR instrumentation whereas off-line analysis was performed by using HPLC.

A very good conversion of the substrate was recorded in a reasonable short reaction time – just 3 min. As shown in Figure 7, the total conversion of the tertiary alcohol was achieved regardless which molar concentration of the chemical catalysts was used.

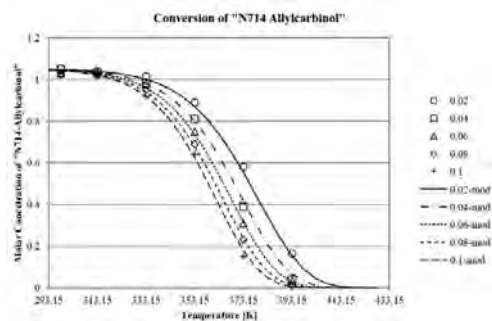


**Figure 7:** Conversion of “N714-Allylcarbinol” into “N746-Butadienes” at different temperatures and different concentrations of the chemical catalyst. The graph additionally compares experimental data with the achieved kinetic model.

Although fast and useful dehydration of the tertiary alcohol was achieved, selectivity to the desired cis isomer was just 42%. Therefore, big losses of the desired API intermediate were faced in this reaction step. Consequently, different combinations of Lewis acids and Lewis bases were tested. The results are depicted in Figure 8.

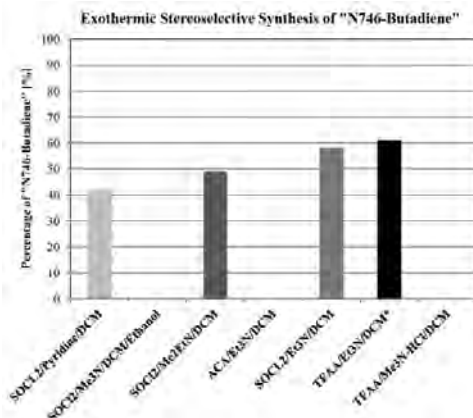


**Figure 8:** Stereo-selective dehydration of “N714-Allylcarbinol” into cis-“N746-Butadienes” by using different Lewis acids and bases. SOCL2-Thionyl Chloride, DCM-Dichloromethane, Me3N-Triethylamine, Me2Et-Dimethylethylamine, ACA-Acetic acid anhydride, Et3N-Triethylamine, TFAA-Trifluoroacetic acid anhydride.

A significant increase in the selectivity was achieved by using trifluoroacetic acid anhydride, triethylamine and dichloromethane as the reaction media. More precisely, an increase from 42% to 62% of the cis isomer was achieved. However, the very harsh reaction conditions together with the user unfriendly solvent used make this approach unsuitable for further implementation in a full-scale zuclopenthixol production.

The following step in the zuclopenthixol reaction is a very slow hydroamination reaction, which is known as a big challenge in the modern chemical catalysis. Acceleration of such reaction was successfully performed by using microwave irradiation, instead of applying different chemical catalysts. As shown in Figure 9, increasing temperatures caused very fast conversion of “N746-Butadienes”.

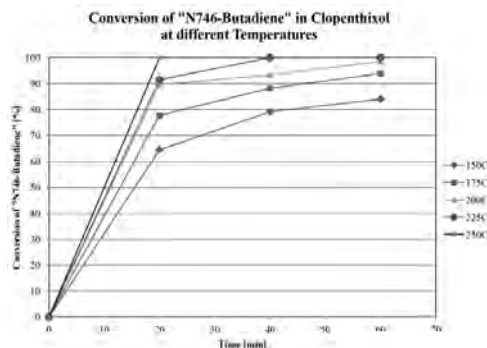


**Figure 9:** Conversion of “N746-Butadienes in Clopenthixol at different temperatures by applying different residence times in batch reactors.

It could be seen that a very fast conversion was achieved if a temperature of 250°C was applied. This approach would significantly accelerate synthesis of clopenthixol. However, a major issue in this reaction step is the very low thermal stability of the desired API. More precisely, very fast conversion of “N746-Butadienes” at high temperatures resulted in a mixture containing plenty of by-products.

Consequently, temperature screening was performed and a temperature of 120°C appeared as the most suitable reaction conditions. At such temperature, no by-products were formed according to the LC-MS analysis. Further investigations were performed and results are summarized in Figure 10.

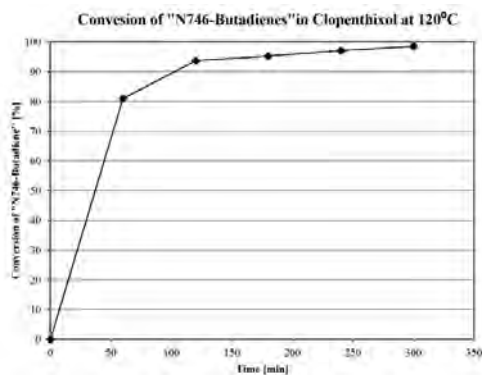


**Figure 10:** Conversion of “N746-Butadiene” in Clopenthixol at 120°C without using chemical catalysts and without any by-product formations.

It can be easily noticed that there are no significant improvements in the conversion after 2h. Therefore, the most optimum reaction time for such chemical reaction was 120 minutes. It is important to note that 15 equivalents of 1-(2-hydroxyethyl)piperazine were used causing pseudo-first order kinetics. In addition, a huge polarity of that compound was very beneficial because absorption of the microwave radiation was easily achieved. Very high temperatures were achieved very fast – the heating rate was 5°C/s.

Small scale trials in a microwave oven were done in the Biotage Initiator device.

### Conclusions and future work

Applications of meso-scale flow chemistry for dehydration purposes showed a good performance. The chemical reaction was accelerated from 2h which was typical for batch modes and reflux conditions down to just 3 min. However, a temperature increase was performed from the boiling point of THF up to 120°C. Furthermore, successful implementation of process chemometrics was performed which gave very accurate data. External validation with additional instrumentation was performed successfully. It is important to note that

all the instruments were calibrated independently of each other.

However, a low stereo-selectivity caused plenty of issues seen from an economic perspective. Therefore, different chemical catalysts together with different reaction conditions were tested. The best results were achieved by using trifluoroacetic acid anhydride together with triethylamine and dichloromethane at -68°C. An increase from 42% to 62% of the cis-isomer was achieved, but very harsh reaction conditions were needed, thus limiting practical applicability.

Lastly, the hydroamination reaction was accelerated from 24 h to just 20 min, however with formation of a significant amount of by-products. Therefore, a successful temperature screening was done and the optimum temperature was found to be 120°C with a reaction time of 2h. Although still slow, a significant speeding up was achieved.

Further work would be associated with establishing process control in the dehydration step. For this purpose, MATLAB Simulink will be used as software for performing simulation. In addition, potential applications of the ABB FTSW1000 Process Software for real-time process monitoring and automation will be tested.

Considering the hydroamination reaction, applications of the meso-scale flow chemistry will be tested within the reaction conditions defined by applying microwave irradiation. Real-time process monitoring and simulation of process control might be performed as well.

### References

1. A. E. Cervera-Padrell, J. P. Nielsen, M. J. Pedersen, K. M. Christensen, A. R. Mortensen, T. Skovby, K. D. Johansen, S. Kiil, K. V. Germaey, *Org. Process Res. Dev.* 16 (2012) 901-914
2. J. G. Kralj, H. R. Sahoo, K. F. Jensen, *Lab Chip* 7 (2007) 256-263
3. A. E. Cervera-Padrell, S. T. Morthensen, D. J. Lewandowski, T. Skovby, S. Kiil, K. V. Germaey, *Org. Process Res. Dev.* 16 (2012) 888-900
4. E. Sinkovec, M. Krajnc, *Org. Process Res. Dev.* 15 (2011) 817-823

### Acknowledgment

DTU is acknowledged for financial support of the project. H. Lundbeck A/S is acknowledged for financial and technical support of the project.

### Publications

- A. Mitic, S. Heintz, R. H. Ringborg, V. Bodla, J. M. Woodley, K.V. Germaey, *Chimica Oggi-Chemistry Today*, 31(4) (2013), 4-8.



**Bjørn Maribo-Mogensen**

Phone: +45 4525 2869

E-mail: bmm@kt.dtu.dk

Supervisors: Georgios Kontogeorgis  
Kaj Thomsen

PhD Study

Started: August 2010

To be completed: March 2014

## Development of an Electrolyte CPA Equation of State for Applications in the Petroleum and Chemical Industries

### Abstract

Complex mixtures of associating/polar components and electrolytes are often encountered in the oil- and gas and chemical industry. By modeling the phase behavior of these mixtures it is possible to reduce the environmental impact of natural gas processing, to optimize the performance of CO<sub>2</sub> capture and sequestration, and to improve purification of complex chemicals in the pharmaceutical and biochemical industries. This PhD project has developed a new equation of state for modeling phase behavior of complex mixtures containing electrolytes.

### Introduction

Complex mixtures of associating/polar components and electrolytes are often encountered in the oil- and gas and chemical industry. The presence of salts will decrease solubilities of gases in water-hydrocarbon mixtures (salting-out effect), and furthermore, the presence of electrolytes enhances the inhibitory effect of methanol and glycol on the formation of gas hydrates in natural gas pipelines. Salts may enhance corrosion of pipelines and the precipitation of salts (scaling) may occur as the brine composition, temperature or pressure changes from reservoir conditions. In the pharmaceutical and biochemical industry, electrolytes, associating and polar compounds are present during downstream processing and can here salts can be used to enhance separation of macromolecules (e.g. by salts inducing liquid-liquid phase separation in water-PEG). Electrolytes are also very important in the energy industry e.g. with regards to wet flue gas desulphurization or CO<sub>2</sub> capture from power plants using aqueous solutions of alkanolamines.

### Overview of Research Activities

A new equation of state for electrolytes in mixed solvents has been developed based on the Cubic Plus Association (CPA) equation of state (EoS) [1].



**Figure 1:** Energy contribution for the Electrolyte CPA equation of state.

The e-CPA model reduces to CPA in the absence of electrolytes, and to SRK in the absence of associating compounds.

When developing models for electrolyte solutions it is essential to account for the long-range electrostatic interactions between ions. It was demonstrated that the two competing theories for electrostatic interactions gave very comparable results for the electrostatic energy, but that the dielectric constant was the most important factor in calculating the electrostatic interactions [Publication A and Yearbook 2011].

However, there were no predictive models for the dielectric constant of complex mixtures that could be readily implemented in an equation of state, so a new model was developed [Publication D and Yearbook 2012].

This paper summarizes the work done in the past year to model the dielectric constant of mixtures containing salts [Publication E]. Results for parameter estimation with the e-CPA model will be presented along with applications to prediction of vapor-liquid and solid-liquid equilibrium.

### Modeling of the Dielectric Constant

The dielectric constant,  $\epsilon_r$  is the most important physical property for thermodynamic models that account for the electrostatic interactions between ions. The interaction energy is inversely proportional to  $\epsilon_r$  (Coulomb's law) and so is the Gibbs energy of hydration, which explains

why ions tend to go towards the most polar phase with a high value of  $\epsilon_r$  (as it results in the smallest energy):

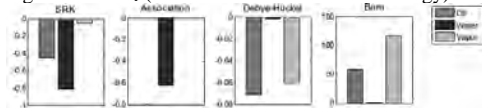


**Figure 2:** Contributions to the reduced Gibbs energy of hydration ( $\Delta_{\text{hyd}}G/RT$ ) for NaCl at infinite dilution in different phases. The major contributions origins from the Born term, which is inversely proportional to  $\epsilon_r$ .

The dielectric constant is related to the effective polarization of the fluid, which is related to the dipole moment and structure of the fluid. We may determine the dielectric constant of a mixture from the framework by Onsager/Kirkwood/Fröhlich [D,E]:

$$\frac{(2\epsilon_r + \epsilon_\infty)(\epsilon_r - \epsilon_\infty)}{\epsilon_r(\epsilon_\infty + 2)^2} = \frac{N_A}{9\epsilon_0 k_B T} \sum_i \rho_i g_i \mu_{i,0}^2 \quad (1)$$

Where  $\epsilon_\infty$  is the permittivity at infinite frequency,  $\epsilon_0$  the vacuum permittivity,  $N_A$  is Avogadro's constant,  $T$  is the temperature,  $k_B$  is the Boltzmann constant,  $\rho_i$  is the molar density of component  $i$ , and  $\mu_{i,0}$  is the vacuum dipole moment of component  $i$ .

The Kirkwood  $g$ -factor accounts for the increase in dipole moment due to the presence of structure in the fluid. The hydrogen bonding network is represented by the simplified geometrical model shown in Figure 3:

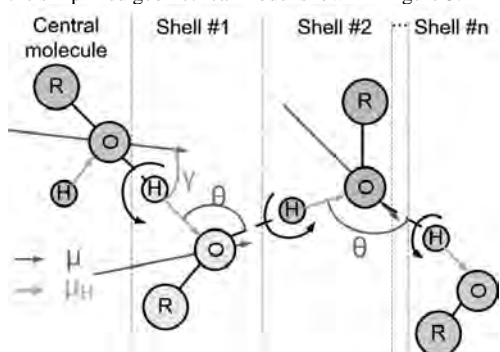


**Figure 3:** Sketch of important dipole moments and angles in a hydrogen-bonding system.

Using this simplified picture we may calculate the Kirkwood  $g$ -factor using Eq. (2) [D].

$$g_i = 1 + \sum_j \frac{z_{ij} P_{ij} \cos \gamma_{ij} \mu_{0,j}}{P_i \cos \theta_{ij} + 1 \mu_{0,i}} \quad (2)$$

Where  $z_{ij}$  is the coordination number of molecule  $j$  around a central molecule  $i$ ,  $P_{ij}$  is the probability that molecule  $i$  is associated to molecule  $j$ ,  $\mu_{i,0}$  is the vacuum dipole moment of molecule  $i$ , the angle  $\cos \gamma$  corresponds to the angle between the dipole moments of molecule  $i$  and  $j$  in the hydrogen bond network.

Using this new model and the degree of hydrogen bonding, we can correlate the static permittivity of pure compounds over wide ranges of temperature and

pressure. We can also predict (no fitting of binary parameters) the dielectric constant of mixtures as shown in Figure 4:

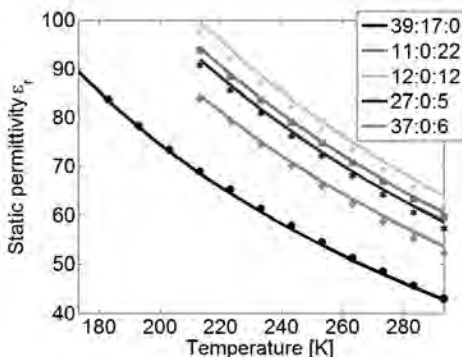


**Figure 4:** Comparison of experimental data to the predicted dielectric constant of ternary mixtures of water with different mole fractions of methanol:ethanol:ethylene glycol [D]. Data from [2].

In addition to water, alcohols, and glycols, the model can be used for e.g. 1,4-dioxane – a water-miscible, and non-polar cyclic ether as shown in Figure 5.

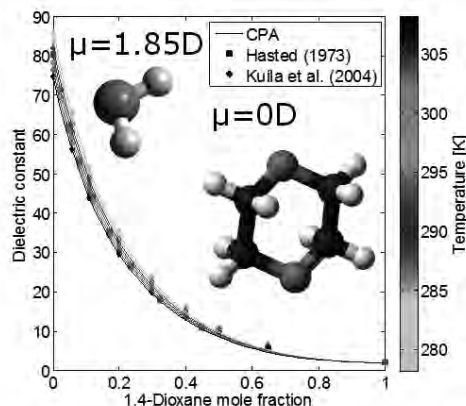


**Figure 5:** Dielectric constant of water-1,4-dioxane which is fully miscible in water at these conditions.

In all cases, the degree of hydrogen bonding is calculated with parameters obtained from fitting of the CPA model parameters to vapor-liquid equilibrium data.

### Extension of Model to Mixtures With Salts

When salts are present in the mixture, the dielectric constant is observed to decrease mainly due to two distinct effects: a thermodynamic effect due to hydration of ions and a dynamic effect known as kinetic depolarization (see Figure 6).

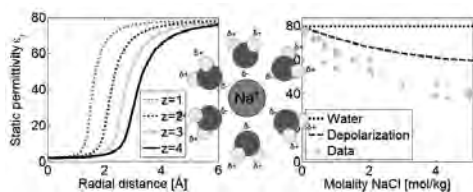


**Figure 6:** Dielectric saturation effect (left), ion hydration (center) and kinetic depolarization (right).

The dynamic effect is a consequence of the measurement technique for assessing the dielectric constant, and should not be included in thermodynamic models. Unfortunately, we cannot easily distinguish between either effect [E]. We may however be able to model the effect of ion hydration on the dielectric constant by only including the free water molecules in Eq. (1), and so by fixing the hydration number around each ion to 6 for monovalent cations, 8 for divalent cations and 5 for anions, we are able to get reasonable predictions of the total decrease of the dielectric constant (putting an upper bound on the hydration numbers), as seen in Figure 7:

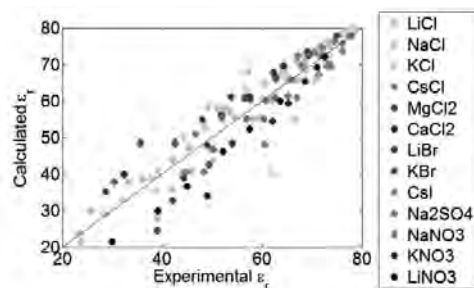


**Figure 7:** Good predictions of the dielectric constant of mixtures with water and salt. The effect of the model for the static permittivity on the derivatives of Debye-Hückel was investigated [E] by setting up four cases:

- A = Constant static permittivity of the solvent
- B = Solvent permittivity w/ empirical ion effect
- C = EoS permittivity from new theory
- D = C + effect of ion-solvent association

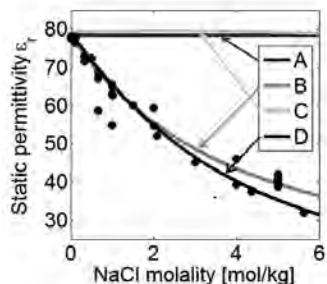


**Figure 8:** Dielectric constant with different models.

While model A yields similar results as model C, and model B yields similar results as model D, the derivatives of the Helmholtz energy are very different, giving rise to noticeable differences in the pressure

(Figure 9) and especially in the chemical potential of water (Figure 10). The new model for the static permittivity ensures a physically correct behavior of the contributions from electrostatics.

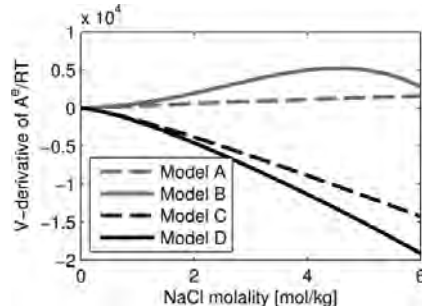


**Figure 9:** Reduced pressure (P/RT) from Debye-Hückel using different models for the static permittivity.

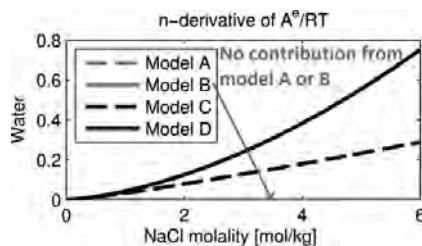


**Figure 10:** Chemical potential of water from Debye-Hückel using different models for the static permittivity.

### Thermodynamic Modeling with e-CPA

As the framework of the equation of state has been established, it is now possible to determine parameters for different systems. The Helmholtz energy is calculated from Eq. (3):

$$A = A^{id} + A^{CPA} + A^{Electrostatics} \quad (3)$$

Where  $A^{id}$  is the ideal gas contribution,  $A^{CPA}$  is the contribution from CPA (which consists of  $A^{SRK}$  and  $A^{Association}$ ), and the electrostatics are given by Debye-Hückel and the Born energy. As a first approximation, we neglect ion hydration and the effect of salts on the permittivity.

The attractive interactions between ions and the solvent (water) is modeled through the interaction energy  $\Delta U_{iv}$ . We use the Huron-Vidal/NRTL mixing rules for the attractive term of SRK and let the interaction energy be temperature dependent. The interaction energy between ions is assumed to be dominated by electrostatics, and we therefore define the attractive interactions between ions as  $\Delta U_{ij} = 0$ . By fitting ion-specific parameters to the osmotic coefficients and water activity data for  $\text{Li}^+$ ,  $\text{Na}^+$ ,  $\text{K}^+$ ,  $\text{Mg}^{++}$ ,  $\text{Ca}^{++}$ ,  $\text{F}^-$ ,  $\text{Cl}^-$ ,  $\text{SO}_4^-$ ,  $\text{NO}_3^-$ . In the range from 0.1-20 molal and 200-400K, the average relative deviation in the osmotic coefficient from 200-400K with 3 parameters is 3.5%. The deviations at 25°C are summarized in Table 1:

**Table 1:** Deviation with e-CPA model for the osmotic coefficient data at 25°C from 0.1-20 molal.

RAD [%]	F <sup>-</sup>	Cl <sup>-</sup>	NO <sub>3</sub> <sup>-</sup>	SO <sub>4</sub> <sup>-</sup>
Li <sup>+</sup>	-	2.1	2.7	3.8
Na <sup>+</sup>	0.7	0.7	0.8	1.2
K <sup>+</sup>	0.4	1.3	0.8	1.0
Mg <sup>++</sup>	-	2.8	3.4	2.3
Ca <sup>++</sup>	-	3.7	1.4	2.5

Figure 11 shows the calculated effect of salts on the solubility of NaCl in water and Figure 12 shows the temperature dependence of the osmotic coefficient of MgSO<sub>4</sub>:

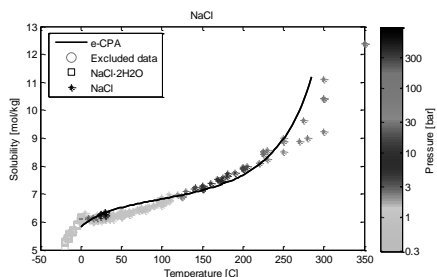


**Figure 11:** Solubility of NaCl with the e-CPA model. Data from [3].

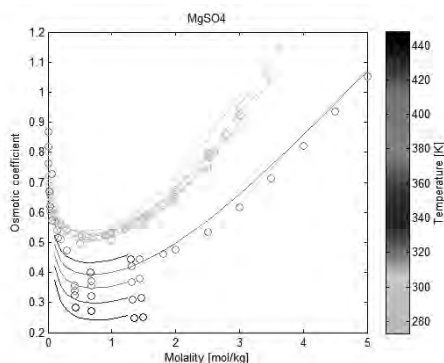


**Figure 12:** Osmotic coefficients as a function of temperature for MgSO<sub>4</sub> with the e-CPA model. Data from [3].

Once the model has been parameterized it can be used to predict e.g. the effect of salts on solubility of light gases as shown in Figure 13.

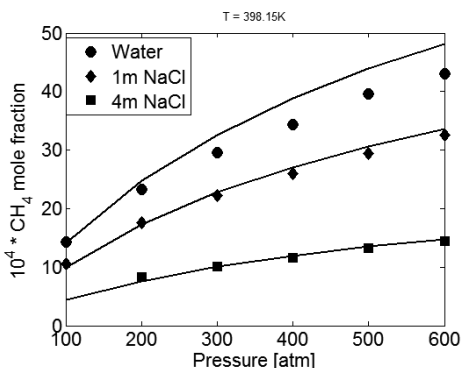


**Figure 13:** Predicted effect of salts on solubility of methane in water at 125°C.  $k_{ij,CH_4-H_2O}=0.7988-236.5/T$ . Data was taken from Sullivan et al. (1970) [4].

## Conclusions and Future Work

This PhD study has set up a practical framework for handling electrolytes in an equation of state. A new model for the dielectric constant has been developed that gives excellent predictions of the temperature, pressure, and composition dependence.

The model will be applied to modeling of the effect of salts on vapor-liquid, liquid-liquid, thermal properties, and solid-liquid equilibrium, including gas hydrate formation in mixed solvents. Finally it will be shown how this model can be implemented and used in commercial process simulators using the CAPE-OPEN standard.

## References

1. G.M. Kontogeorgis, G.K. Folas, Thermodynamic Models for Industrial Applications- From Classical and Advanced Mixing Rules to Association Theories, Wiley, 2010
2. Landolt-Börnstein Database Volume IV/17, IV/6
3. CERE Electrolyte Database, [www.cere.dtu.dk/Expertise/Data\\_Bank/Search](http://www.cere.dtu.dk/Expertise/Data_Bank/Search), Kaj Thomsen
4. T. D. O'Sullivan, N. O. Smith, J. Phys. Chem. 74 (7), 1970, 1460-1466

## List of Publications

- A. B Maribo-Mogensen, G Kontogeorgis, K Thomsen, Ind. & Eng. Chem. Res. 51 (14), 2012, 5353-5363
- B. V. Darde, B. Maribo-Mogensen, WJM van Well, E. H. Stenby, K. Thomsen, Int. J. Greenhouse Gas Control, 10, 2012, 74-87
- C. X. Liang, B. Maribo-Mogensen, K. Thomsen, G. M. Kontogeorgis, Ind. Eng. Chem. Res., 51 (45), 2012, 14903-13914
- D. B Maribo-Mogensen, G Kontogeorgis, K Thomsen, J. Phys. Chem. B, 117 (12), 2013, 3389-3397
- E. B Maribo-Mogensen, G Kontogeorgis, K Thomsen, J. Phys. Chem. B, 117 (36), 2013, 10523-10533
- F. PL Fosbøl, B Maribo-Mogensen, K Thomsen, Energy Procedia (GHGT-11), 37, 2013, 844-859





**Ane Loft Mollerup**

Phone: +45 4525 2907  
E-mail: molle@kt.dtu.dk

Supervisors: Gürkan Sin  
Peter Steen Mikkelsen, DTU Environment  
Dines Thornberg, Udviklingssamarbejdet

Industrial PhD Study  
Started: August 2011  
To be completed: December 2014

## Obtaining a Piecewise Linear Model of the Sewer System for Control Purposes

### Abstract

For control design purposes one needs two models: One model for the evaluation and another model for controllability analysis. Most tools used in control engineering for the controllability analysis needs a linear model. It is therefore of interest to obtain a linear model that describe the relationship between the manipulated variables and the possible controlled variables. However, this is not a straight forward with a system like the sewer system that is transient in nature and has large stochastic disturbances acting on it. In this contribution the method for obtaining a simplified model of the sewer system that can be used to obtain a linear model is discussed and it is shown that the virtual tank model can provide a good approximation to the detailed models.

### Introduction

One way of minimizing overflows from the sewer system and the risk of flooding is to control the system in an effective manner (Schilling, 1989). However, to design control is a complex problem, due to the number of actuators, uncertain measurements and the stochastic nature of the rain events.

For control design purposes one needs two models: One model for the evaluation and another model for controllability analysis. Most tools used in control engineering for the controllability analysis (such as the condition number and relative gain array), needs a linear model (Seborg et al., 2011). It is therefore of interest to obtain a linear model that describe the relationship between the inputs ( $u$ ) and the outputs ( $y$ ) of the system through a transfer function matrix,  $G(s)$ , as depicted in Figure 1.

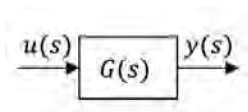


**Figure 1:** A linear model for control

Based on the transfer function matrix, the steady state gain matrix can be derived from (Seborg et al., 2011):

$$K = G(s = 0)$$

In this contribution, we discuss the linear model development.

### Method

As a case study, a subcatchment of Copenhagen's sewer system is used. It has a size of 80 hectare and is equipped with 3 pumping stations, 2 storage tanks, 1 pipe basin and 5 combined sewer overflow structures (CSOs). The sewer system is modelled with a simple Virtual Tank model (Ocampo-Martinez, 2010) in Matlab/Simulink and will be used for control strategy evaluation purposes. The Virtual Tank model is mainly based on mass-balances. A schematic representation of the case area modelled with the Virtual Tank approach is shown in Figure 2.

The calibration of the Virtual Tank model is done by fitting the computed CSO volumes to "observed" values, which are computed with a detailed deterministic model. For the calibration and validation a 20 year rain series is used (SVK rain gauge 5740). From this rain series rain events with a return period of more than two years are extracted (with respect to the mean 30 minute intensity and the depth). This results in a list of 20 rain events that are used for the calibration and validation.

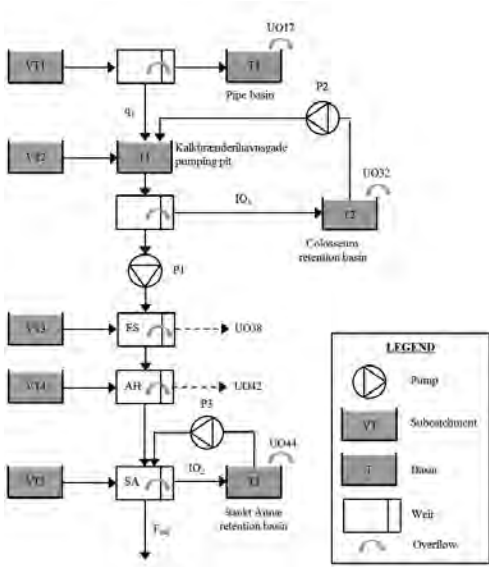


**Figure 2:** Schematics of the Virtual Tank model of the case area

The linear model approximation is obtained using the linear analysis tool in Simulink. Since the system does not have a steady-state operating point, a piece linear model was obtained for different operation point in the sewer system such dry weather, filling, emptying, etc. Using this tool snapshots of the system states are recorded at different operation points (i.e. time steps), to be used as the initial conditions, and the model is linearized at each of those time steps

### Results

The validation results in Figure 3 show that the simplified Virtual Tank model is able to capture the dynamics of the system in a satisfying way. The Virtual Tank model can therefore be used as the model for evaluation purposes.

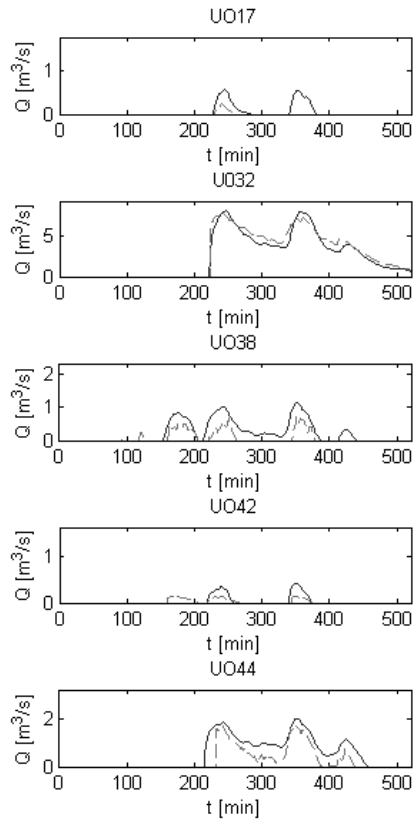


**Figure 3:** Example of the validation results (rain gauge 5740, rain event from 14/08-2010 13:40). The blue line is the “observed” data and the red line is the validation results.

Based on this model, a piecewise linear model for different operation point was obtained successfully (results not shown due to space limitation). The results of the linearisation show how the linear model changes due to changes in the linearisation point giving valuable insight to the system operation and derivation of control structures for the regulatory layer.

### References

1. Ocampo-Martinez, C. 2010, *Model predictive control of wastewater systems*, 1st edn, Springer, London, UK.
2. Schilling, W. (ed.). 1989 *Real-Time Control of Urban Drainage Systems. The state-of-the-art*. IAWPRC Task Group on Real-Time Control of Urban Drainage Systems. London
3. Seborg, D. E., Edgar, T. F., Mellichamp, D. A. and Doyle, F. J., 2011, *Process dynamics and control*, 3rd edn, John Wiley & Sons, Asia.

**Peter Mølgaard Mortensen**

Phone: +45 4525 2809  
E-mail: pmm@kt.dtu.dk

Supervisors: Anker Degn Jensen  
Peter Arendt Jensen  
Jan-Dierk Grunwaldt, KIT (Germany)

**PhD Study**

Started: August 2010  
To be completed: December 2013

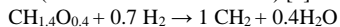
## Stability and Resistance of Catalysts for Hydrodeoxygenation of Bio-oil

**Abstract**

Fast pyrolysis of biomass to produce bio-oil followed by hydrodeoxygenation (HDO) of the bio-oil constitutes a prospective path to biofuels. One of the biggest challenges of HDO of bio-oil is to find an active catalyst with a sufficient stability during prolonged operation, as carbon deposition and bio-oil impurities readily may deactivate the catalyst. Ni/ZrO<sub>2</sub> and Ni-MoS<sub>2</sub>/ZrO<sub>2</sub> have been evaluated in long term HDO experiments with bio-oil model compounds. Without impurities, both catalysts had good stability over >100 h of operation. However, both catalysts were persistently deactivated by potassium. Chlorine caused a reversible inhibition of both catalysts. Ni/ZrO<sub>2</sub> was severely deactivated by sulfur, but in contrast Ni-MoS<sub>2</sub>/ZrO<sub>2</sub> lost activity if sulfur was not present. Overall, Ni-MoS<sub>2</sub>/ZrO<sub>2</sub> showed the best resistance, but Ni/ZrO<sub>2</sub> is an attractive catalyst due to the low price and milder operating conditions.

**Introduction**

Production of sustainable fuels and chemicals has been identified as one of the biggest challenges of the 21<sup>st</sup> century [1]. A prospective route to biofuels usable in the current infrastructure is the combination of flash pyrolysis and hydrodeoxygenation (HDO) [2]. By flash pyrolysis, the volumetric energy density of the biomass can be increased by a factor of up to 8 [2]. The bio-oil in itself is a poor fuel due to its high content of a variety of oxy-compounds (10-40 wt% oxygen) and a high water content (up to 30 wt%). Furthermore the oxy-compounds in the bio-oil make it unstable during storage, immiscible with crude oil, and acidic, among others [2]. Thus, upgrading of the bio-oil is needed, which can be done by HDO. Here high pressure hydrogen (up to 200 bar) is used to remove the oxygen functionality of the oil. The HDO reaction can be described as (normalized to feed carbon) [2]:



Here CH<sub>2</sub> is an unspecified hydrocarbon product.

Traditional hydrotreating catalysts, as Co-MoS<sub>2</sub> and Ni-MoS<sub>2</sub>, have been among the most tested catalysts [3]. This group of catalysts is already industrially established catalysts in hydrodesulfurization (HDS) [4].

Alternatively, Nickel catalysts have received increasing attention in recent years due to their relatively low price combined with good activity at relative low temperatures [5,6].

Common for both groups of catalysts, little work has been devoted to evaluating long term stability or resistance toward impurities during HDO [2,3]. Carbon on the catalyst is formed because many of the oxy-compounds present in bio-oil can undergo polymerization and condensation reactions on the catalyst surface, forming polyaromatic species which can lead to blocking of both the pore structure and the active sites of the catalyst [7].

As the bio-oil is derived from biomass, it will contain traces of a range of inorganic compounds like alkali metals, transition metals, chlorine, sulfur, and phosphorus [8]. Especially potassium, chlorine, and sulfur can be found in relative high amounts in the bio-oil with concentrations up to 0.3 wt%, 0.6 wt%, and 0.8 wt%, respectively [9].

Both carbon deposition and the presence of inorganic impurities in the oil are of significant concern, as this leads to catalyst deactivation. Finding a sufficiently stable HDO catalyst is one of the greatest challenges of the process.

The current work has evaluated the stability and resistance of Ni/ZrO<sub>2</sub> and Ni-MoS<sub>2</sub>/ZrO<sub>2</sub> for HDO of bio-oil model compounds in the presence of sulfur, chlorine, and alkali metals.

**Specific Objectives**

The objectives of the project are to develop catalysts for HDO, which should be evaluated both with respect to

activity, stability, and resistance towards impurities in bio-oil.

### Experimental

The experiments were performed at a high pressure continuous flow setup with separate high pressure liquid and gas feed lines, depicted in Figure 1. The gas product was analyzed by on-line GC-TCD measurements and the liquid product was collected and analyzed on GC-MS/FID.

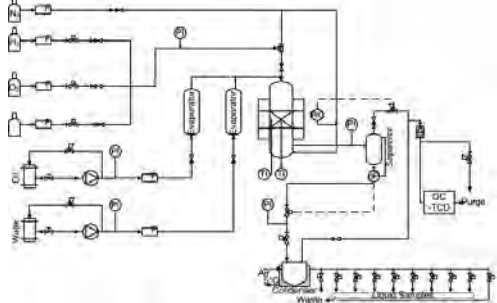


**Figure 1:** Flow sheet of continuous flow high pressure setup.

5 wt% Ni/ZrO<sub>2</sub> was prepared through the incipient wetness method from Ni(NO<sub>3</sub>)<sub>2</sub>. Reduction and calcination was done in the setup prior to the experiments at 500 °C with 500 Nml/min 50% H<sub>2</sub> in N<sub>2</sub> for 2 hours.

Ni-MoS<sub>2</sub>/ZrO<sub>2</sub> (3 wt% Ni and 15 wt% Mo) was prepared through sequential incipient wetness, initially impregnating Mo from (NH<sub>4</sub>)<sub>6</sub>Mo<sub>7</sub>O<sub>24</sub> and then Ni from Ni(NO<sub>3</sub>)<sub>2</sub>. The catalyst was calcined at 400 °C. Sulfidation was done in the setup prior to the experiment at 350 °C for 2.5 h with 800 Nml/min H<sub>2</sub> and 0.2 ml/min dimethyl disulfide (DMDS).

In the experiments, 2.5 g of catalyst diluted in 250 µm glass beads was loaded in the reactor. The nickel catalyst was tested at 250 °C and 100 bar with a gas flow of 400 Nml/min H<sub>2</sub> and 100 Nml/min N<sub>2</sub> and a liquid flow of 0.2 ml/min 10 vol% guaiacol in 1-octanol.

The sulfide catalyst was tested at 280 °C and 100 bar with a gas flow of 200 Nml/min H<sub>2</sub> and 50 Nml/min N<sub>2</sub> and a liquid flow of 0.2 ml/min 70 g/l phenol in 1-octanol.

Analysis of the product was done with a Shimadzu GCMS/FID-QP2010UltraEi fitted with a Supelco Equity-5 column. Identification was made on the mass spectrometer (MS) and quantification was done on the flame ionization detector (FID).

### Nickel Catalyst

Over the Ni/ZrO<sub>2</sub> catalyst, the sequential reaction scheme shown in Figure 2 was observed. For guaiacol, hydrogenation to 2-methoxy-cyclohexanol took place initially, followed by hydrogenolysis of the ether bond to form cyclohexanol and methanol. Cyclohexanol was

subsequently hydrodeoxygenated to produce cyclohexane.

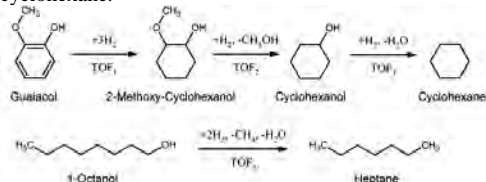


**Figure 2:** Reaction scheme of guaiacol and 1-octanol HDO over a Ni/ZrO<sub>2</sub> catalyst.

Heptane was the primary product from 1-octanol (as shown in Figure 2). This was produced by an initial dehydrogenation to form the aldehyde, which could then undergo decarbonylation to produce heptane and CO.

Testing the stability of the catalyst with the pure feed, good stability over a period of >100 h could be achieved with this catalyst, as shown in Figure 3. The degree of deoxygenation (DOD) only dropped from 92% to 90% over 104 h of operation. This slight deactivation was due to formation of coke on the catalyst, with a deposition of 1.5 wt% carbon on the catalyst at the end of testing. Overall showing good stability of the catalyst.

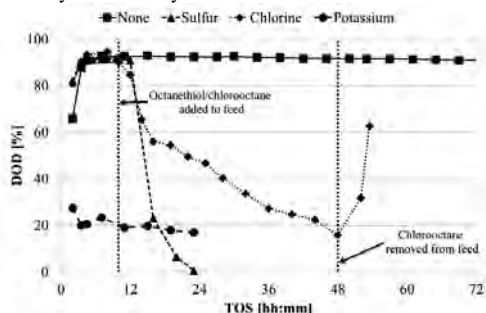


**Figure 3:** Development in the degree of deoxygenation (DOD) over a Ni/ZrO<sub>2</sub> catalyst during HDO of 10% guaiacol in 1-octanol exposed to sulfur, chlorine, and potassium. 1-octanethiol and 1-chlorooctane were added to the feed in concentrations of 0.05 wt% S and 0.05 wt% Cl, respectively, after 8 h of TOS as indicated in the figure. 1-chlorooctane was removed from the feed after 48 h of TOS. KNO<sub>3</sub> was impregnated in stoichiometric amounts relative to nickel on a fresh batch of catalyst prior to testing. Catalyst: Ni/ZrO<sub>2</sub>, T = 250 °C, P = 100 bar, WHSV = 4.0 h<sup>-1</sup>.

Exposing the catalyst to sulfur resulted in an immediate loss of activity, as shown in Figure 3. The loss of activity was due to formation of NiS<sub>x</sub>. This was evidenced by XAS and TEM-EDX. In Figure 4 the TEM-EDX micrograph shows the overlap of nickel and sulfur, revealing the interaction of nickel and sulfur.

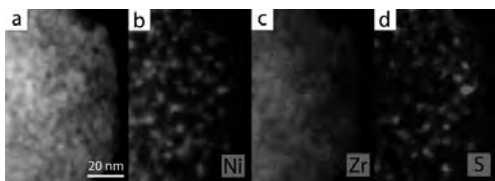


**Figure 4:** (a) TEM micrograph of a portion of the sulfur poisoned catalyst with (b) nickel, (c) zirconium and (d) sulfur EDX elemental distributions.

Chlorine was also found to cause deactivation of the catalyst when present, as seen from Figure 3. However, this was only an inhibiting effect, as the activity was regained when chlorine was removed from the feed.

Impregnating potassium on the catalyst led to severe deactivation of the catalyst, as shown in Figure 3. As the DOD only was ca. 20% compared to 90% in the un-poisoned case. This deactivation was persistent throughout 24 h of testing.

Table 1 summarizes and compares the deactivation of the individual reactions shown in Figure 2 in the three deactivation cases compared to the un-poisoned case. As already discussed, sulfur led to complete loss of activity. Chlorine and alkali metals deactivated the catalyst to the same extent. In these cases the hydrogenation reaction was unaffected ( $TOF_1$ ), but the deoxygenation reaction severely affected. This indicates that only the low coordinated nickel sites are affected by these species, as these previously have been identified as the active sites for this reaction [6].

**Table 1:** TOF's for the four reactions in Figure 2 in the three cases with different poisons relative to the case shown in Figure 3 with no poison. Catalyst: Ni/ZrO<sub>2</sub>, T = 250 °C, P = 100 bar, WHSV = 4.0 h<sup>-1</sup>.

Poison	Exposure	TOF <sub>1</sub> [s <sup>-1</sup> ]	TOF <sub>2</sub> [s <sup>-1</sup> ]	TOF <sub>3</sub> [s <sup>-1</sup> ]	TOF <sub>4</sub> [s <sup>-1</sup> ]
	$\frac{mol_{poison}}{mol_{Ni}}$				
None	-	>110	10	6	>110
Sulphur	1.1	0	0	0	0
Alkali	1	>110	2	0.1	1
Chlorine	3.2	>110	1	0.5	1

### Nickel Molybdenum Sulfide Catalyst

Ni-MoS<sub>2</sub>/ZrO<sub>2</sub> required higher temperatures than the Ni/ZrO<sub>2</sub> catalyst for HDO, and therefore 280 °C was used when testing this. At these conditions, cyclohexane was observed as the primary product from phenol, but also benzene, cyclohexanol, and cyclohexene were detected. HDO of phenol can take place through two paths as summarized in Figure 5: a direct deoxygenation of phenol to benzene, followed by hydrogenation to cyclohexane, or an initial hydrogenation of phenol to cyclohexanol followed by dehydration to cyclohexene and then hydrogenation to cyclohexane. The actual reaction path will be dependent on catalyst and reaction conditions [10]. Apparently, the hydrogenation path was preferred under the given conditions, as evidenced by

high fractions of cyclohexanol and cyclohexene in the product.

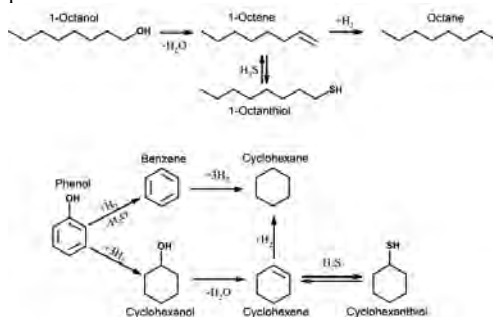


**Figure 5:** Reaction scheme of phenol and 1-octanol HDO over a Ni-MoS<sub>2</sub>/ZrO<sub>2</sub> catalyst.

Octane was the primary product from 1-octanol, but 1-octene was also found as an important byproduct. Thus, HDO of 1-octanol over this catalyst proceeds through a dehydration reaction scheme, producing 1-octene. This subsequently reacts with hydrogen to form octane as the final product, as shown in Figure 5.

This type of catalyst is highly dependent on the presence of sulfur, in contrast to the Ni/ZrO<sub>2</sub> catalyst, to obtain long term stability. This was evidenced by two experiments adding sulfur from different sources and different concentrations, as shown in Figure 6. 0.3 vol% 1-octanethiol in the feed was found insufficient to maintain stability of the catalyst, as the DOD decreased from 74% to 44% over 109 h of operation. Much better stability was obtained when adding 2 vol% DMDS to the feed, here the DOD only dropped from 90% to 82% over 96 h of operation.

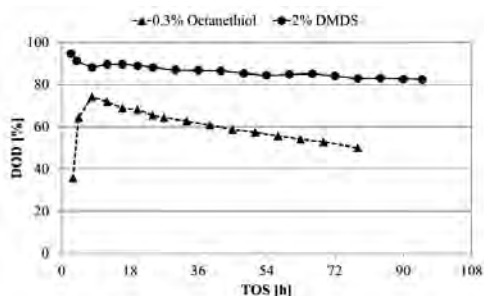


**Figure 6:** Stability of NiMoS<sub>2</sub>/ZrO<sub>2</sub> during HDO of phenol and 1-octanol in two cases with different types and concentrations of feed sulfur. Catalyst: Ni-MoS<sub>2</sub>/ZrO<sub>2</sub>, T = 280 °C, P = 100 bar, WHSV = 4.0 h<sup>-1</sup>.

Analysis of the spent catalyst samples revealed that the catalyst co-fed with 0.3 vol% 1-octanethiol was partly oxidized to MoO<sub>3</sub>. Thus, co-feeding insufficient sulfur will replace the framework sulfur atoms in the MoS<sub>2</sub> with oxygen.

Adding sulfur will however result in a byproduct of sulfur containing compounds if the residence time is

insufficient, as indicated in Figure 5. With 0.3 vol% 1-octanethiol in the feed, 13 ppm<sub>w</sub> sulfur was found in the product, but this increased to 381 ppm<sub>w</sub> in the case of co-feeding 2 vol% DMDS. It was found that to sufficiently decrease the sulfur content in the product, the WHSV should be <1.5 h<sup>-1</sup>, corresponding to more than a doubling of the residence time.

Adding chlorine or alkali metal to the catalyst was found to cause a decrease in the DOD, as shown in Figure 7. Potassium caused a severe persistent deactivation, decreasing the DOD to ca. 5%. DFT calculations by Andersen et al. [11] showed that potassium saturates the vacancy sites along the edges of the MoS<sub>2</sub> slabs, which probably explains the severe deactivation. Thus, both Ni and MoS<sub>2</sub> based catalysts are severely deactivated by potassium, indicating that this should be removed from the bio-oil before long term operation can be achieved.

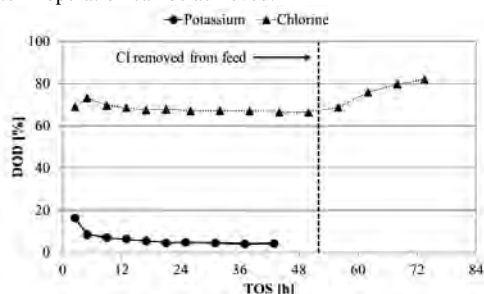


**Figure 7:** Development in the degree of deoxygenation (DOD) over a Ni-MoS<sub>2</sub>/ZrO<sub>2</sub> catalyst during HDO of 70 g/l phenol and 2 vol% DMDS in 1-octanol exposed to chlorine and potassium. 1-chlorooctane was added to the feed in a concentration of 0.05 wt% Cl. 1-chlorooctane was removed from the feed after 50 h of TOS. KNO<sub>3</sub> was impregnated in stoichiometric amounts relative to Ni and Mo on a fresh batch of catalyst prior to testing. Catalyst: Ni-MoS<sub>2</sub>/ZrO<sub>2</sub>, T = 280 °C, P = 100 bar, WHSV = 4.0 h<sup>-1</sup>.

Addition of chlorine to the feed was found to inhibit the reaction, and only decreased the DOD from 91% in the un-poisoned case to 74% in the chlorine poisoned case. Removing the chlorine from the feed increased the activity toward the un-poisoned case again, showing a non-persistent nature of the chlorine, similar to the findings of Ni/ZrO<sub>2</sub>.

## Conclusion

This work has evaluated the stability and resistance of Ni/ZrO<sub>2</sub> and Ni-MoS<sub>2</sub>/ZrO<sub>2</sub> as catalysts for HDO of bio-oil model compounds with special emphasis on the effect of bio-oil impurities. With pure feeds, both catalysts were quite stable during >100 h of operation. However, Ni-MoS<sub>2</sub>/ZrO<sub>2</sub> did require co-feed of sulfur to avoid oxidation and thereby maintain activity. Sulfur was on the contrary a severe poison for the Ni/ZrO<sub>2</sub> catalyst, leading to complete deactivation.

Potassium was a severe poison for both catalysts. This indicates that removal of potassium from bio-oil is a requirement before HDO can be done.

Chlorine inhibited both types of catalysts, but Ni/ZrO<sub>2</sub> was most severely deactivated. In both cases the activity could be completely regained when the chlorine was removed from the feed, showing that the chlorine was competing for the active sites by a reversible adsorption.

Both catalysts are interesting catalysts for HDO. Ni/ZrO<sub>2</sub> is attractive as this catalyst can function at lower temperatures than Ni-MoS<sub>2</sub>/ZrO<sub>2</sub> and does not require co-feed of sulfur. However, Ni-MoS<sub>2</sub>/ZrO<sub>2</sub> appears to be more resistant toward impurities in the bio-oil, especially sulfur.

Future work should focus on testing these catalysts for HDO of real bio-oil and this work is ongoing.

## Acknowledgments

The present work is financed by DTU and The Catalysis for Sustainable Energy initiative (CASE), funded by the Danish Ministry of Science, Technology and Innovation.

## References

1. T. Werpy, G. Petersen, A. Aden, J. Bozell, J.E. Holladay, J. White, A. Manheim, D. Eliot, L. Lasure, and S. Jones. Top value added chemicals from biomass. Volume 1 - results of screening for potential candidates from sugar and synthesis gas. Technical report, Department of Energy, 2004.
2. P.M. Mortensen, J.-D. Grunwaldt, P.A. Jensen, K.G. Knudsen, A.D. Jensen, *Appl. Catal. A*, 407 (2011) 1-19.
3. E. Furimsky, *Catal. Today*, 217 (2013) 13-56.
4. P. Raybaud, *Appl. Catal. A*, 322 (2007) 76-91.
5. V.A. Yakovlev et al., *Catal. Today*, 144 (2009) 362-366.
6. P.M. Mortensen, J.-D. Grunwaldt, P.A. Jensen, A.D. Jensen, *ACS Catal.*, 3 (2013) 1774-1785.
7. E. Furimsky, F.E. Massoth, *Catal. Today*, 52 (1999) 381-495.
8. G.W. Huber, S. Iborra, and A. Corma, *Chem. Rev.*, 106 (2006) 4044-4098.
9. T.N. Trinh, P.A. Jensen, H.R. Sørensen, K. Dam-Johansen, and S. Hvilsted, *Energy Fuels*, 27 (2013) 1399-1409.
10. B.S. Gevert, J.-E. Otterstedt, and F.E. Massoth, *Appl. Catal.*, 31 (1987) 119-131.
11. A. Andersen, S.M. Kathmann, M.A. Lilga, K.O. Albrecht, R.T. Hallen, and D. Mei, *J. Phys. Chem. C*, 115 (2011) 9025-9040.

## List of Publications

1. P.M. Mortensen, J.-D. Grunwaldt, P.A. Jensen, K.G. Knudsen, A.D. Jensen, *Appl. Catal. A*, 407 (1-2) (2011) 1-19.
2. P.M. Mortensen, J.-D. Grunwaldt, P.A. Jensen, A.D. Jensen, *ACS Catal.*, 3 (2013) 1774-1785.



**Line Munk**  
Phone: +45 4525 2979  
E-mail: lmun@kt.dtu.dk

Supervisors: Anne S. Meyer  
Jørn D. Mikkelsen

PhD Study  
Started: October 2012  
To be completed: October 2016

## Biorefining of Lignocellulosic Biomass

### Abstract

Lignin from lignocellulosic biomass holds the potential to generate energy and other valuable compounds. However, the resistant nature of lignin towards degradation, constitute a significant challenge to utilize this potential source. By investigating the action of laccase on lignin, it is sought to clarify if and how laccases can promote an environmentally beneficial utilization of lignin in lignocellulosic biomass.

### Introduction

Among the main components of lignocellulosic biomass, lignin is the most challenging part to utilize, because it is highly resistant to breakdown. Though lignin usually complies 20-32% of the biomass [1], it is treated as a contaminant in industry, e.g. pulp/paper production and biofuel conversion. Improving ways of refining and valorizing lignin would greatly improve overall utilization and application of lignocellulosic biomass.

### Specific objectives

This PhD project is supported by the Danish National Advanced Technology Foundation via the Technology Platform "Biomass for the 21st century - B21st". The objective is to elucidate mechanisms of potentially lignin active enzymes with focus on laccase in particular. A better understanding of these enzymes and their putative role in lignin modification, may clarify how they can assist in a more environmentally desirable conversion of lignocellulosic biomass.

### Lignin in lignocellulosic biomass

Lignin is a very complex biopolymer and is the second most abundant carbon source - only exceeded by cellulose. It is found in almost every type of biomass where it fills the spaces in the cell wall between cellulose, hemi-cellulose, and pectin biopolymers. Lignin contribute to the protection of the plant against the surrounding environment and acts as a filler and stiffener in the plant cell wall [2]. Unlike other biopolymers from lignocellulosic material, lignin comprises a large amount of aromatic units and has a very irregular structure without any defined backbone.

Increased interest in lignin utilization has resulted in a number of comprehensive studies, which provide insight into lignin structures and mechanisms involved in the synthesis. Lignin is primarily built of 3 monomeric precursors, which becomes p-hydroxyphenyl (H), guaiacyl (G), and syringyl (S) units, when incorporated in the lignin polymer (Fig. 1). Currently, the most widespread way of defining lignin, is to establish the ratio between these 3 units. The lignin polymer is formed by a radical polymerization process of the 3 precursors. Due to resonance delocalization of electrons in the aromatic ring structures, the polymer forms a three dimensional, irregular matrix [3]

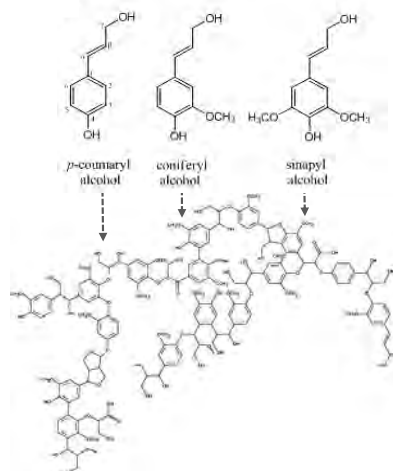


**Figure 1:** Lignin structure based on radical polymerization of the monomeric precursors for H, G and S units.

## Laccases

Laccases (EC 1.10.3.2) belongs to the multicopper oxidase family, a group of enzymes that is widespread in numerous fungi, plants, and bacteria [4]. Laccases have various functions that chemically relates to the oxidation of a wide range of aromatic substrates with the concomitant reduction of  $O_2$  to two molecules of  $H_2O$ . The fact that these phenol oxidases use  $O_2$  as the final electron acceptor rather than  $H_2O_2$ , differentiate them from other ligninolytic enzymes and make them more qualified in potential industrial applications with regard to economy and sustainability. Laccases contain four copper ions: type 1 (T1) or blue copper, type 2 (T2) or "normal" copper and type 3 (T3), an antiferromagnetically coupled binuclear copper pair (Fig 2). The T2 and T3 centers are close together and form a trinuclear cluster. T1 is the site where substrate oxidation takes place (Fig 2). From T1 electrons are shuttled along a pathway containing cysteine and histidine residues to the trinuclear cluster, which is the site of oxygen reduction [5]. The redox potentials of laccases range from 0.5 to 0.8V vs. NHE depending on the type of organism from which the enzyme has been isolated.

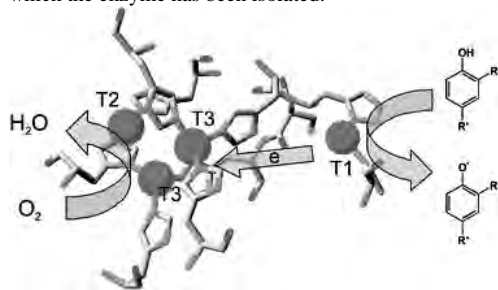


**Figure 2:** Copper centers in laccase from *Melanocarpus albomyces* [6].

The direct action of laccases on lignin appears to be restricted to phenolic units, which only represent a small percentage of the total lignin polymer. However, by means of small molecules called mediators, the range of substrates for laccases expand. It is believed that mediators act as electron carriers and diffuse into the plant cell wall to oxidize lignin [7].

## Challenges in assaying activity of laccase on lignin

It has been shown, that addition of laccase in the enzymatic conversion of lignocellulose to glucose increases the final yield of glucose [8]. The reason for this remains uncertain, but one explanation may be that laccase act on lignin to open the complex lignin network, which otherwise restrict the access to cellulose. Because of the intensive color, size, and hydrophobic nature of lignin, it is a difficult substrate to dissolve and analyse. For this reason, the activity and action of laccases are commonly studied on substrates, which resembles lignin very poorly in either size or structure and do not provide a conclusive picture of how and to what extent, laccases act on lignin. Another issue, that complicates the

elucidation of laccases action on lignin, is that laccase creates free radicals as products, which subsequently continue to react with no influence of the laccase. This is reflected in the literature, where there have been examples of laccase treatments that have resulted in depolymerization as well as in polymerization [5].

## Conclusion

In spite of comprehensive studies of both lignin and laccases, it is still uncertain how these enzymes affects lignin in relation to biomass conversion. A contributory cause to the uncertainty of this matter may be due to the difficulty in dissolving and analyzing lignin. A well-defined, easily analyzable, and representative model substrate in terms of size, structure and binding types, may be a way to unravel the mechanisms that occurs when laccase interacts with lignocellulosic biomass. This may also facilitate knowledge of how most efficiently to apply laccase treatment in biomass, and how to control and optimize surrounding conditions to promote any preferred outcome.

## References

1. M. Chen, G. Zeng, Z. Tan, M. Jiang, H. Li, L. Liu, Y. Zhu, Z. Yu, Z. Wei, Y. Liu, G. Xie. PLoS One 6(9) (2011) 1-8.
2. S. Barsberg, Handouts: Fundamentals of Polymer Material Science for Biomass and Bio-based Materials, KU, DK (2013).
3. A. U. Buranov, G. Mazza G. Industrial Crops and Products 28(3) (2008) 237-259.
4. A. Virk, Biotechnol Prog. 28 (2011) 21-32.
5. S. Shleev, J. Tkac, A. Christenson, T. Ruzgas, A.I. Yaropolov, J.W. Whittaker, L. Gorton. Biosens Bioelectron. 20 (2005) 2517-54.
6. N. Hakulinen, L.-L. Kiiskinen, K. Kruus, M. Saloheimo, A. Koivula J. Rouvinen Nature Struct. Biol. 9 (2002) 601-605.
7. D. Rochefort, D. Leech, R. Bourbonnais, Green Chemistry 6(1) (2004) 14-24.
8. W. Qui, H. Chen, Bioresource Technology 118 (2012) 8-12.





**Vikas Narayan**

Phone: +45 4525 0361336  
E-mail: vina@kt.dtu.dk

Supervisors: Peter Glarborg  
Peter Arendt Jensen  
Ulrik Birk Henriksen

PhD Study  
Started: July 2011  
To be completed: July 2014

## Ash Chemistry in Circulating Fluidized Bed

### Abstract

A Low Temperature Circulating Fluidized Bed System gasifier allows pyrolysis and gasification to occur at low temperatures thereby improving the retention of alkali and other elemental species within the system. The aim of the PhD project is to study the behavior of alkali metals and biomass ash in a Low Temperature Circulating Fluidized Bed System. The focus of the study is ash transformation in the reactor system and bed de-fluidization.

### Introduction

Gasification of herbaceous based fuels poses a large potential for power generation. Herbaceous fuels however, contain high amounts of alkali metals which get volatilized at high temperatures and form salts of low melting points and thus condense on pipelines, reactor surfaces and cause de-fluidization. The low Temperature Circulating Fluidized Bed Gasifier [1-2], functions without in-situ ash sintering and deposit problems and most potassium and chlorine are simply retained in a separate biomass ash stream. In this way a fuel-gas with low alkali content and a relatively high calorific value is produced that can be used for power production by use of a boiler.

### Low Temperature Circulating Fluidized Bed System

As shown in Figure 1, the LT-CFB process consists of two reactors. The biomass fuel enters the first reactor which is the pyrolysis chamber. The fuel is pyrolysed at around 650°C due to good thermal contact with mainly re-circulated sand and ash particles from the char reactor. The heat for the pyrolysis reaction is thus provided by the sand bed particles and hot re-circulated char and ash particles. The residual char, pyrolysis gases and inert particles are led to the primary cyclone, which separates char and inert particles to a bubbling bed char reactor. In this reactor, the char is exposed to air to undergo gasification, at temperatures typically around 730°C. Some steam or water may also be added in order to improve the conversion of char and limit the reactor temperature.

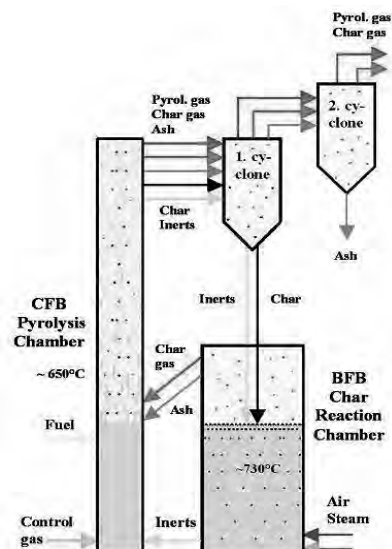


**Figure 1:** LT-CFB flow diagram [1-2]

The exit stream out of the pyrolysis chamber has a lower temperature compared to the temperature in the char reactor. Consequently, only small amounts of alkali species and ash components get carried off with the product gas and can therefore be separated efficiently in the cyclones. Moreover, the relatively low temperatures in the process limit the tendencies of de-fluidization in the system.

## Objectives of the PhD Study

The aim of the PhD project is to study the behavior of alkali metals and biomass ash in a Low Temperature Circulating Fluidized Bed System. The focus of the study is release of ash species with exit gas from the reactor system, ash transformation and bed de-fluidization.

## Experiments on the LTCFB Gasifier

To understand the behavior of alkali and ash in LTCFB reactors, available test data from runs made on a 100 kW plant at Risø and a 6 MW plant at Kalundborg, were analyzed by a preliminary mass balance. It was seen from the mass balance analysis that, the data were not sufficient to give a good understanding of the ash behavior in the system. It was therefore suggested to have direct measurements done on the product gas. The main aim of the measurements was to measure the concentration of K, Cl and S in the exit gas.

In addition to the gas phase measurements, bed material and cyclone ash samples were also collected and analyzed for the composition of the inorganic elemental species within the same. Mass balance calculations were thus made using the above results. The fuel used for all the plant runs was Danish Wheat Straw.

## Observation and Results

The first analysis was done using the dust measurements was to determine the particle concentration and dust load in the output gas.

**Table 1:** Dust Load in product in the various Plant runs made in Risø and Kalundborg

	Dust Load, g/Nm <sup>3</sup>
Risø (100 kW Plant)	8-11
Kalundborg (6MW Plant)	20-30

As can be seen from Table 1, the dust loading in the product gas leaving the LTCFB gasifier for the 100 kW plant at Risø was 8-11 g/Nm<sup>3</sup>. In the 6 MW plant at Kalundborg, the particle concentrations were found to lie within the range of 20-30 g/Nm<sup>3</sup>. The ash content of the collected samples were also analyzed using TGA. The TGA analysis of the cyclone ash collected from the secondary cyclone bottoms and dust samples in the exit gas showed that the samples were reasonably similar. Both the samples were found to contain about 35-40% char and 45-50% ash, with low percentage of volatiles (5-6%).

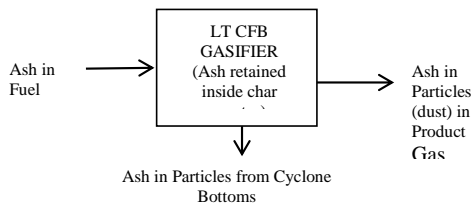


**Figure 2:** Distribution of ash in the LTCFB system

An overall ash balance on the LTCFB system was done as shown in Figure 2.

**Table 2:** Fraction of ash in the fuel released with the dust in the product gas and that retained within the cyclone ash.

% in Product gas	% in Cyclone	% Unaccounted
8-10 %	40-50 %	40-50%

It was seen that about 8-10% of the total ash in the fuel was found as dust in the product gas and 40-50% retained in the cyclone bottoms. The rest was retained within the system. To develop a preliminary understanding on the behavior of the inorganic species within the LTCFB gasifier, an overall mass balance of the inorganic elemental species within the LTCFB system was done.

**Table 3:** Results of mass balance from measurements at Kalundborg

1.	Element i	Si	K	S	Cl	Ca
2.	Fraction in cyclone ash	0,85	0,55	0,18	0,45	0,47
3.	Fraction accumulated in bed material (inside char reactor)	-0,18	-0,21	-0,009	-0,01	-0,16
4.	Fraction in product dust	0,07	0,07	0,03	0,09	0,08
5.	Unaccounted	0,27	0,60	0,79	0,48	0,62
6.	Sum total output	1,00	1,00	1,00	1,00	1,00

Table 3 shows the fraction of the major inorganic elemental species in the fuel that got retained in cyclone ash, in the dust particles in exit gas, in the bed material samples taken out for analysis and that got accumulated within the reactor. Rows 1,2 and 3 in Table 3 (the mass fractions determined from the samples analyzed during the plant runs) are based on the measured values whereas values in row 5 are the unaccounted mass fractions of the species calculated by closing the mass balance.

It can be seen from Table 3 that the mass balance closed poorly for most of the species. One of the main issues with the closure of the mass balance can be observed to be the uncertainty in the values for the accumulation of the species within the reactor. Bed material samples taken for analysis may be non-representative of the bed material inside the system. Though the accumulation of the species within the char reactor was uncertain, an analysis on the release of the ash forming species in the dust particles in the exit gas and that retained in cyclone ash could still be made. It can be seen from Table 3 that, 50% of K in the fuel was retained in the cyclone ash along with Cl (25%) and Si (49%) which indicates the possibilities of presence of chlorides and silicates in the same. A high fraction of Cl and S, (70-80% of the amounts in fuel) were found to be unaccounted for the mass balance. The unaccounted mass fractions could be due to the non-measured concentrations of S and Cl in the gaseous form (HCl or methyl chlorides). The sulfur may appear as reduced species COS, H<sub>2</sub>S or as SO<sub>2</sub>.

A study on the composition of the major inorganic elemental species in the cyclone ash and the dust particles further showed that the samples were reasonably similar, as shown in Table 4. The remaining fractions in the cyclone ash and dust (not shown in the Table) included char (as also evident from the TGA analysis).

**Table 4:** Composition of the inorganic elemental species in cyclone ash and dust

	Si	K	Ca	S	Cl
Cyclone Ash	16%	7,3%	2,5%	0,15%	0,96%
Dust	10,5%	6,7%	2,9%	0,19%	1,5%

As can be seen from Table 4, both the cyclone ash and the dust particles in exit gas were found to be mainly dominant in Si (10 -15%), K (6 -7%) and Ca (2,5 - 3%). Cl (1-1,5%) and S (0,15-0,2%) were present in lower amounts.

A study on the molar ratios of the inorganic elemental species in the samples analyzed further explained the behavior of the species in the system.

**Table 5:** Molar ratios of the inorganic elemental species in the cyclone ash obtained from the plant run in 100 kW LTCFB Gasifier at Risø on 4<sup>th</sup> June, 2012

	K/Cl	K/Si	K/S	K/P
Molar Ratio	6,9	0,3	38,8	5,8

Table 5 shows the molar ratios of the inorganic elemental species in the cyclone ash obtained from the plant run in the 100 kW LTCFB Gasifier at Risø on 4<sup>th</sup> June, 2012. It can be seen from Table 5 that the molar ratios of K/Cl (6,9) is high. This indicates that K was present in substantial amounts in other forms apart from being bonded to Cl. The high K/Cl ratios also indicate

that Cl, which was present in substantial amounts in the feed straw, was present in other (gaseous) forms in the product gas such as HCl or methyl chlorides, which agrees with the unaccounted fractions observed in mass balance results, mentioned earlier. As mentioned earlier, Si is mostly bonded to K as silicates as could be seen from the lower K/Si ratios (0, 3) from Table 4.

The tar in the exit gas was also analyzed for the inorganic elemental composition as shown in Table 6.

**Table 6 :** Composition of inorganic elements in tar in exit gas

Tar, % by wt				
Ca	K	Si	Cl	S
< 0,0005	< 0,004	< 0,01	< 0,0046	0,0060
< 0,0005	< 0,004	< 0,01	< 0,0048	0,0032

As can be studied from Table 6, the tar present in the product gas contained very low amounts (< 0,004%) of the inorganic elements. The above results indicate a low release of the major inorganic elements with tar in the gasifier during the above plant runs.

Furthermore, the exit gas was also analyzed for the presence of methyl chlorides, to confirm the presence of Cl in gaseous forms as shown in Figure 3.

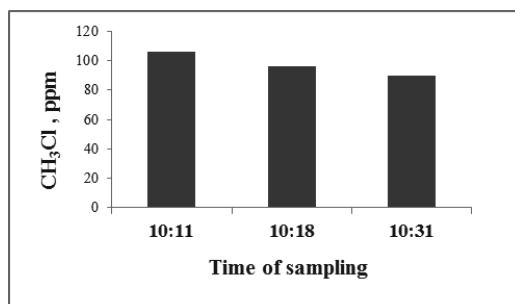


**Figure 3:** Composition of methyl chloride in the exit gas

It can be seen from the figure that, the analysis of the exit gas showed consistent presence of methyl chlorides which were in the range of 90-100 ppm. The amount of Cl in the exit gas thus measured was about 15% of the Cl present in the fuel. The presence of gaseous Cl in the exit gas as seen above (which were not included in the mass balance results shown in Table 3), could thus also partially explain the unaccounted fractions of Cl (70-80%) observed in the mass balance results explained earlier.

## Conclusions

To predict the overall ash distribution and behavior of the inorganic elemental species within the LTCFB system, particle sampling measurements were made on the exit gas leaving the LTCFB Gasifier.

There were exit gas particle measurements made at Risø and Kalundborg and dust particles, cyclone ash bottoms and the bed material samples from the gasifier were collected and analyzed with respect to the inorganic elemental composition.

It was seen from the measurements made on the LTCFB gasifier, that of the total ash that enters the system, 40 - 50% the ash was retained in the cyclone bottoms and a lower amount (8-10%) was released as dust in the exit gas.

A mass balance calculation was performed on the inorganic elemental species within the LTCFB system. It was seen from the mass balance results that about 30-40% of K, 25-30% of Ca and 45% of Si in the fuel was retained in the cyclone ash. About 20-25% of Cl in the fuel was also found to be retained in cyclone ash. Similar trends were observed in the dust particles in the exit gas, though the values for the retention of the inorganic elements in the dust were lower as compared to the cyclone ash. About 7-10% of K and Ca and 10% of Cl and Si, present in the fuel were retained in the exit gas dust particles.

It was also seen that high fractions of Cl and S (60 - 70%) were unaccounted in the mass balance results which could be due to the unmeasured concentrations of Cl and S in gaseous form. Cl could be present as methyl chlorides or HCl and S as COS or H<sub>2</sub>S. 15% of Cl in the fuel was found to be present as methyl chlorides (90-100 ppm).

A study on the composition of the cyclone ash and dust particles in the exit gas further showed that the samples were reasonably similar. Both the cyclone ash and the dust particles in exit gas were found to be mainly dominant in Si (10 -15%), K(6 -7% ) and Ca(2,5 - 3% ). Cl (1-1,5%) and S(0,15-0,2%) were present in lower amounts.

The retention of the inorganic elements in cyclone ash and dust was further studied by observing the molar ratios of the elements within them. The molar ratios of K/Cl were found to be high in cyclone ash and dust (5-7) which indicated that K is present in other forms apart from chlorides.

The tar in the exit gas was also collected during the plant runs at Risø and analyzed for the inorganic elemental composition. It was seen that the tar present in the product gas contained very low amounts of the inorganic ash species (less than 0,004%). This thus indicates that probabilities of release of K and other inorganic species in tar in the LTCFB gasifier are low.

## Future Work

The above studies do provide useful information on the release of the inorganic species in the LTCFB system. Based on the above analysis and literature studies, efforts towards developing an understanding on the

mechanism of transformation and release of the inorganic elements within the LTCFB system are being made. A simplified model that can describe the behavior of ash species in the LT-CFB system is being developed.

Experiments are also being performed to study the de-fluidization and agglomeration tendencies of bed material samples in a fluidized bed reactor set up. Ash (Bed material samples) obtained from Pyroener Gasifier running on Wheat straw are used as the feed.

## References

1. P. Stoholm, R. G. Nielsen, The Low Temperature CFB Gasifier-Latest 50 kW Test Results and New 500kW Plant, Proceedings of World Conference and Technology Exhibition on Biomass for Energy and Industry (ISBN), ETA-Florence & WIP-Munich, Rome, 2004.
2. P. Stoholm, J. Cramer, J. Krogh, R. G. Nielsen, B. Sander, J. Ahrenfeldt, U. Henriksen, The Low Temperature CFB Gasifier-100 kW<sub>th</sub> Tests on Straw and new 6 MW<sub>th</sub> Demonstration Plant, International Biomass Conference, Lyon, 2010.
3. Analysis Report on the inorganic elemental composition from Enstedværket Laboratory, Dong Energy
4. Analysis Report on methyl chloride concentration in tar, Zsuzsa Sárosy, Jesper Ahrenfeldt.
5. J.R. Pels, D.S. de Nie, J.H.A. Kiel, Improvement of the economics of biomass/waste gasification by higher carbon conversion and advanced ash management, E.C.N.,2006



**Hiep Dinh Nguyen**

Phone: +45 9175 1192  
E-mail: hing@kt.dtu.dk

Supervisors: Georgios Kontogeorgis  
David Löf, PPG Industries  
Anders Egede Daugaard

PhD Study  
Started: August 2012  
To be completed: July 2015

## Synthesis of Novel Biobased Binders for Alkyd Paint Systems

### Abstract

Alkyds are popular in coatings due to the versatility of the preparation methods, the ease of use and for economical reasons. Most alkyds today are partly fossil based, but there is an increasing demand from the market for a biobased alternative. The purpose of this PhD project is replacing petrochemical ingredients with renewable ones to produce highly durable alkyd. An optimized system for enzymatic synthesis of polyesters from activated polybasic acids and polyalcohols is successfully established, which allows producing of various backbones from different biobased feed components.

### Introduction

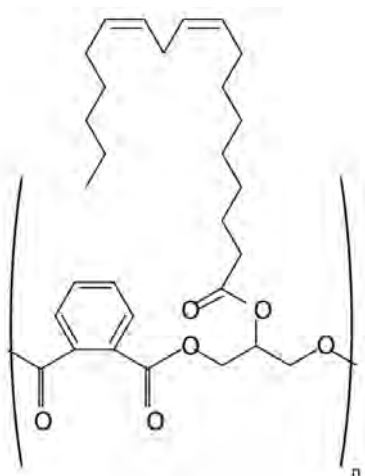


**Figure 1.** The structure of a typical alkyd produced from phthalic anhydride and glycerol grafted with linoleic acid.

Wood has long been widely used in outdoor application. Without protection, wood exposed outdoors are attacked through many different processes such as UV light, moisture and microorganisms. Therefore,

coatings have long been used in protecting wood as well as giving it a more appealing appearance, and the most popular one is the alkyd coating system.

An alkyd coating system comprises of four major components. The alkyd binder is the base of the system, and its role is forming a tough and continuous film covering the wood surface that requires coating. This film is also able to expand and collapse due to outside temperature to avoid cracks and protect the wood surface. Because of the versatility of the method, the ease of use and for economical reasons, around one million tons of alkyds are produced annually all over the world [2]. The second major part is the solvent, which acts as an environment for the formulation. The current trend is shifting from solvent-based paints to water-based paints, which are more friendly to the environment and safer for people to handle. Another component is the fillers, which can be particles to give reinforcement or components that reduce the cost of the coating. Filler can also be the pigments account for the color of the coating. The last component is the additives, which are put into the coating system for other purposes. That could be a biocide to eliminate microorganisms degrading the coating system or a UV stabilizer protecting the lignin in the wood from harmful UV light.

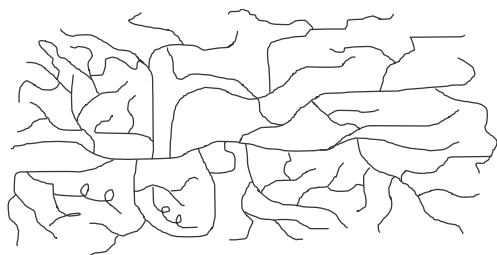


**Figure 2.** Illustration of a hyperbranched product from conventional synthesis method

As can be seen from Figure 1, alkyds can be considered as a polyester grafted with fatty acids, which account for drying properties of alkyds. The term alkyd has the origin from the AL of polyhydric alcohols and the CID in polyprotic acids (or polybasic acids, which is modified to KYD), two components creating the backbone of the resin [2]. One major issue of recent alkyds is that the petrochemical part accounts for 50wt% of the alkyd composition, as phthalic acid and iso phthalic acid are the two most frequently used polybasic acids [1]. Another issue is that consumers are starting to show an interest in materials that are more friendly to the environment. Therefore, the objective of this project is synthesis of new highly durable alkyds from renewable materials.

There are two methods which are usually used for synthesizing of alkyds. The first method is called the monoglyceride process, a two stage process in which firstly a mixture of glycerol and vegetable oil or animal oil is heated in the reactor under high temperature of 200-300°C with chemical catalyst. Some of the oils often used in alkyds are linseed oil, manhaden oil, safflower oil, sunflower oil, dehydrated castor oil, soybean oil, coconut oil and tung oil. The alcoholysis process here converts the initial feed compositions into a mixture of mono and di glyceride. At completion of the alcoholysis stage, which is defined by solubility of product in anhydrous methanol, polybasic acids are added to reaction mass and heating at high temperature continues. Reaction are generally considered completes when products reach sufficient acid and hydroxyl numbers.

The other conventional method in alkyd synthesis is the fatty acid process, a one stage process in which glycerol or other polyhydric alcohols, polybasic acids and fatty acids are mixed together in the reactor. Direct polyesterification is then carried out at high temperature of 200-250°C until products obtain sufficient acid and hydroxyl numbers. Compared with the monoglyceride process, the fatty acid process has shorter reaction time, higher reproducibility and better control with molecular weight and molecular weight distribution. However, the monoglyceride process has an economical advantage because vegetable oils are cheaper than fatty acids derived from these oils. The fatty acid process is preferred in cases where resins with higher qualitative parameters are required [8].

The similarities between these two processes are that they are all carried out by heating a complex mixture at high temperature to make a hyperbranched product with quite high poly dispersity index (PDI) (Figure 2). There are a number of issues with these two conventional synthesis process. High PDI brings significant problems in product characterization & structure elucidation, which make it quite difficult and time consuming for establishing the direct relationship between structures and wood protection properties. Difficulties in structure controlling are apparent since synthesis is carried out with complex feed components. The high temperature employed in polycondensation is also an issue since many compounds are unable to sustain such conditions and decompose, which can also lead to gelation.

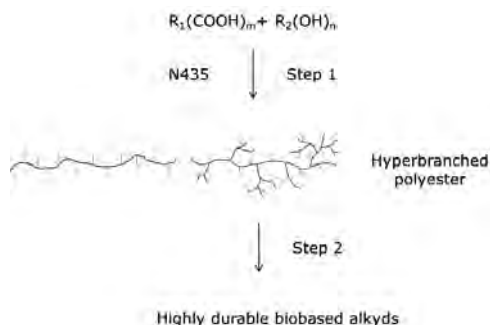


**Figure 3.** Illustration of two steps of the “Model system”

In order to efficiently achieve our goal in a limited amount of time, it was decided to use an enzymatic synthesis method employing Novozym 435 (N435), a heterogeneous biocatalyst that consists of *Candida antarctica* lipase B (CALB) physically immobilized within a macroporous resin of poly(methyl methacrylate). CALB has a molecular weight of 33 kD and comprises 317 amino acids with two important positions where esterification takes place, the catalytic triad with three amino acids (Ser105, His224 & Asp187) and the oxyanion hole with two amino acids (Gly106 & Thr40) [3]. N435 is able to catalyze polycondensation with high regioselectivity for primary hydroxyl groups [4]. Esterification starts with binding of a carboxylic acid to a free enzyme to make a noncovalent enzyme-acid complex, which later releases a water molecule and a modified enzyme. An alcohol then reacts with this modified enzyme to create a complex which then release the final ester product and the free enzyme. This process then starts again between this free enzyme and a new acid molecule [5]. Selectivity of N435 can be controlled by the combination of feed components, ratio, solvents, and temperature [4, 6, 7]. The enzymatic synthesis method can handle most of the issues arising from conventional ones. Because products achieved from the enzymatic process has much lower PDI compared with that from conventional synthesis processes, it is much easier for

product characterization & structure understanding. In addition, since the enzymatic reaction is carried out at temperature below 100°C, this method should maximize the choice of feed components and avoid the trouble from gelation.

The initial studies are focused on development of a model system (Fig 3), which includes three steps, to thoroughly establish the direct relationship between polyester structures and wood protecting properties. In the first step, polyesters with sufficient molecular weight & degree of branching are synthesized using the enzymatic catalyst N435. By regulating feed composition, ratio, time and temperature, from the same feed components linear, branched and hyperbranched polyesters with controlled molecular weight can be synthesized. After that, fatty acids of different structures and concentrations can be grafted to adequate backbones forming biobased renewable alkyds. Dividing the synthesis process this way help handle the issue with structure controlling in conventional methods. Effective structures for wood protection will then be identified with various testing methods and optimization will be carried out again and again until highly durable biobased alkyds are found. At this point the project will proceed to the final stage where conversion to conventional methods will be carried out for direct industrial application. The model system with use of enzymes as catalyst allows fast and effective screening since all the issues from conventional methods are handled.

## Results and discussion

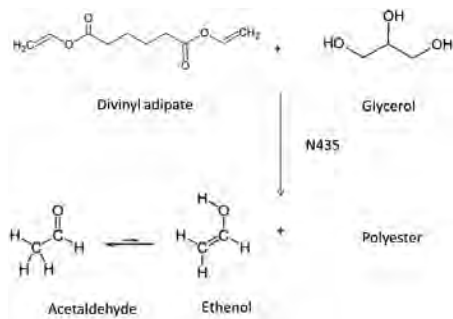


**Figure 4.** Enzymatic bulk polycondensation between divinyl adipate and glycerol

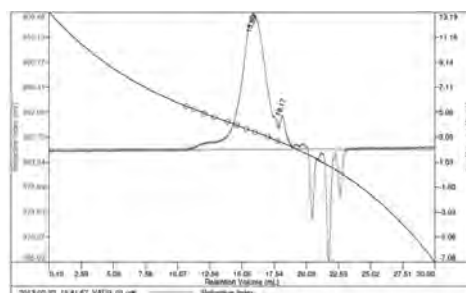


**Figure 5.** Size exclusion chromatogram of the initial linear polyester backbone.

The first objective in our project is establishing of an optimized system for the enzymatic polycondensation reaction between activated polybasic acids and polyalcohols. Once this system is established, different polyester backbones can be obtained by varying feed components. The quite popular biobased polyalcohol glycerol and divinyl adipate [4] were chosen as starting materials (Figure 4). This vinyl ester accelerates the rate of acyl transfer and shift the reaction equilibrium towards polymer synthesis since the byproduct ethenol rapidly tautomerizes to acetaldehyde, which automatically fly out of reaction mass due to its low boiling temperature of 20.2°C. Through this approach, a linear polyester with number average molecular weight ( $M_n$ ) of 2,628 g/mol and PDI of 3.274 was achieved.

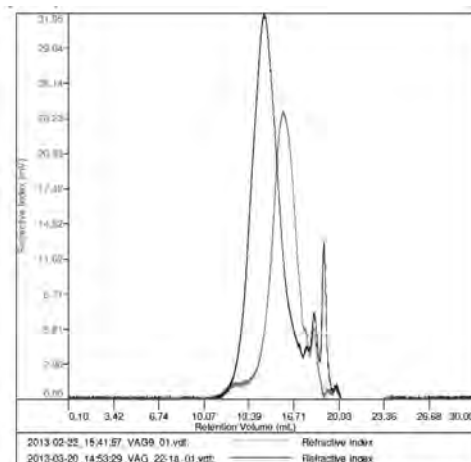


**Figure 6.** Overlay Size exclusion chromatogram of the polyester achieved from initial procedure (red) and optimized method (blue)

As can be seen from Figure 5, this product can be considered as bimodal with the main peak and a fraction of high molecular weight molecules at the left of the main peak. This fraction can be a problem for identification of the direct relationship between structures and wood protecting properties. Therefore, the system was optimized to remove this fraction as

well as to increase the molecular weight. Different factors that may affect the products, including feed composition, reaction time, energy providing method, pretreatment of enzyme, stirring method were then varied systematically. While a number of factors have positive effects, others behaves contradictorily. The best product was achieved with optimized stirring method (Figure 6). The linear polyester product here is unimodal, which can allow establishment of the direct relationship between structures and wood protecting properties. Compared with the initial product, the optimized one has much higher  $M_n$  of 6,906 g/mol and lower PDI of 2.372. IR spectrum of the optimized product (Fig 7) exhibited absorption bands at 3438 (H-bonded alcohols), 1730 (C=O of ester) and 1135  $\text{cm}^{-1}$  (secondary C-O), which confirm the linear structure of the polyester achieved.

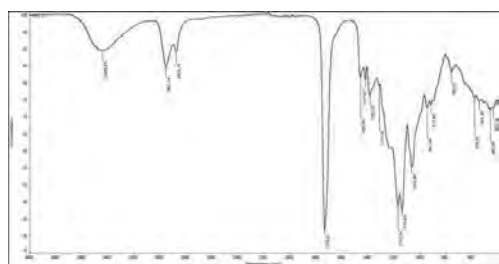


**Figure 7.** IR spectrum of the polyester achieved from optimized method

### Conclusion

Optimized system for the enzymatic polycondensation between activated polybasic acids and poly alcohols was successfully established. By exchanging feed components to other biobased compounds, various polyesters can be synthesized in the future using this system.

### Acknowledgement

The authors acknowledge the financial support from the Danish National Advanced Technology Foundation (DNATF) as well as the technical & financial support from other project partners including PPG Industries, Emmelev A/S, Palsgaard, Danish Technological Institute and Copenhagen University

### References

1. N.F. Jones, *Alkyd Resins*, Ullmann's Encyclopedia of Industrial Chemistry, Wiley-VCH, 2003.
2. R.V. Gorkum, E. Bouwman, *Coordination Chemistry Reviews* 249 (2005) 1709–1728.
3. K. Loos, *Biocatalysis in Polymer Chemistry*. Wiley-VCH, 2011.
4. B.J. Kline, E.J. Beckman, and A.J. Russell, *Journal of the American Chemical Society* 120 (1998) 9475-9480.
5. G.D. Yadav, P.A. Thorat, *Journal of Molecular Catalysis B: Enzymatic* 83 (2012) 16– 22.

6. Zh.Q. Duan, W. Du, D.H. Liu, *Bioresource Technology* 101 (2010) 2568–2571.
7. A.S. Kulshrestha, W. Gao, and R. A. Gross, *Macromolecules* 38 (2005) 3193-3204.
8. J. Kaska, F. Lesek, *Progress in Organic Coatings* 19 (1991) 283-331.





**Anne Veller Friis Nielsen**

Phone: +45 4525 6892  
E-mail: avfn@kt.dtu.dk

Supervisors: Anne S. Meyer

#### PhD Study

Started: September 2012  
To be completed: September 2015

## Phytase-Mediated Phytate Dephosphorylation to Improve Bioavailability of Iron

### Abstract

Iron bioavailability from particularly whole grains is low due to the presence of phytic acid in the bran layer. Phytic acid chelates iron and makes it unavailable for absorption in the small intestine. The bioavailability of iron can be increased by action of the enzyme phytase, which catalyses the hydrolysis of phosphate groups from phytic acid, thereby lowering the chelation strength towards iron and making it more readily available for absorption. In this PhD project, enzyme kinetics of different phytases in gastric conditions will be elucidated and compared with the purpose of evaluating the potential of *in vivo* phytase catalysis for improved iron bioavailability.

### Introduction

Iron deficiency anaemia is the most common nutritional deficiency disorder globally with particularly women of the childbearing age, children and the elderly being vulnerable groups. Vegetarians and people with a low consumption of meat rely on vegetables, legumes and cereals for mineral absorption. Grains often contain significant amounts of iron (e.g. 3.9 mg/100 g for oatmeal [1]), but this iron has been shown to be poorly bioavailable, meaning that an absorption efficiency of 2-3 % [2] is common, whereas for meat, the absorption of iron ranges from 15-35 % [3].

### Phytic acid

The low bioavailability of iron from grains is presumably caused by the chelation of iron by phytic acid (*myo*-inositol (1,2,3,4,5,6)-hexakisphosphoric acid) in the grains. Phytic acid is the main phosphorous storage compound of plants. Having six phosphate groups, the molecule is negatively charged at physiological pH values ( $pK_a$  values ranging from 1.1 to 12 [4]), whereby it is able to chelate positively charged compounds, e.g. minerals, notably iron, but also larger compounds such as peptides and starch. During seed development, phytic acid is deposited as phytate salts in protein-containing globoids. The phytate globoids are primarily located in the outer layers of the grains, meaning that both mineral and phytate contents are higher in whole grain compared to refined grain products.

### Phytate and Intestinal Iron Absorption

For barley, ~90 % of the iron content has been found to be associated with phytic acid [5]. It has also been shown that the ratio of phytate:iron in the complex found in barley was 4.6 [6]. The phytate salts are poorly soluble at the neutral to slightly acidic pH of the small intestine, where iron absorption takes place. Except from iron bound in protein complexes such as haemoglobin or ferritin, iron needs to be soluble in order to be absorbed by the intestinal cells. Therefore, iron chelated to phytic acid resulting in insoluble phytate complexes will not be available for absorption.

### Phytase

Phytases (mainly enzyme classes E.C. 3.1.3.8 and E.C. 3.1.2.26) are enzymes that catalyse the hydrolysis of phosphate groups from the *myo*-inositol ring of phytic acid. Phytases are widely used in feeds of monogastric animals (e.g. pigs, chicken, fish), where they are active in the stomach, resulting in improved phosphate utilisation from the feed and thereby minimising the need for addition of inorganic phosphate to the feed and also decreasing phosphorous content of manure. At the low pH values of the stomach, the phytates are more soluble, making the substrate more readily available to the phytases. Most of the commercially available phytases have activity optima in the low pH range. Hydrolysis of phytic acid results in a combination of lower inositol phosphates, i.e. *myo*-inositols with up to five phosphate groups. The fewer phosphate groups, the weaker the chelation strength and thus, more iron will

be in a soluble form – either loosely chelated to lower inositol phosphates or free in solution. It is not fully elucidated to which extent phytic acid should be dephosphorylated in order to eliminate the inhibitory effect on iron absorption, but it seems to be consensus that three or more phosphate groups should be cleaved off in order to sufficiently improve iron absorption. A simplified reaction scheme is shown in Figure 1.

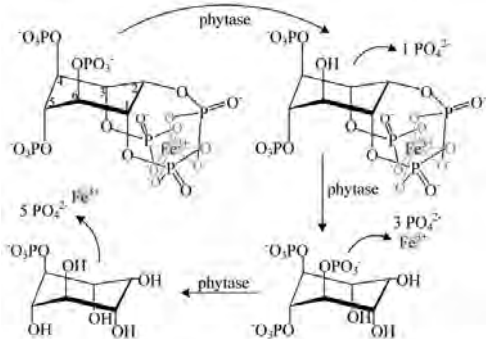


**Figure 1:** Simplified phytate hydrolysis with resulting iron release. Only some steps in the dephosphorylation are shown and the iron phytate complex is shown in a simplified form with 1:1 stoichiometry.

This means that the kinetics of the enzyme-mediated hydrolysis as well as the extent of reaction under gastric conditions are very important factors in order to fully understand the mechanism and potential of the phytase-mediated enhanced iron absorption.

Recently, the 3-phytase (meaning that the dephosphorylation starts at the phosphate group bound to the 3-carbon, see Figure 1) from the fungus *Aspergillus niger* has been approved for use in food for humans by the World Health Organisation with an acceptable daily intake “not specified” [7]. In addition, a patent has been granted to DSM Nutritional Products for an iron fortification nutritional blend containing phytase, corroborating the industrial potential and topicality of these enzymes for defying iron deficiency in humans [8].

### Specific Objectives

In this PhD project, it is a specific objective to elucidate the enzyme kinetics of different phytases under gastric conditions. These conditions comprise the presence of the proteolytic enzyme pepsin and low pH values. Usually, gastric conditions are simulated with a pH of 2, but as the relevant catalysis in this case may occur under fed conditions (when the substrate is present) pH values of ~3-5 are also realistic.

### Results and Current Work

Preliminary studies have shown good activity retention of three different commercially available microbial phytases (from *Eschericia coli*, *Peniophora lycii* and *Citrobacter braakii*) evaluated by phosphate release in gastric conditions (simulated here with pH values of 2

and 4 and a pepsin concentration of 800 activity units/mL).

Upcoming and current experimental work revolves around evaluation of the specific kinetics of different phytases in gastric conditions. The analyses are based on an ion chromatography method that allows the quantification of the different inositol phosphates using post-column reaction and UV detection. An example of a chromatogram showing the various inositol phosphates resulting from acid hydrolysis of phytic acid is shown in Figure 2. This sample is used as a reference standard for peak identification.

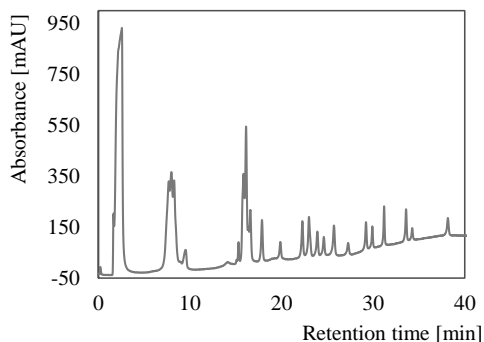


**Figure 2:** Chromatogram showing the various inositol phosphates resulting from acid hydrolysis of a phytic acid reference standard.

This method can be used to elucidate the sequential dephosphorylation and will give a more accurate picture of the iron release potential compared to the measurements of phosphate release alone.

### References

1. Danish Food Composition Databank, version 7.0, 2008. Website: <http://www.foodcomp.dk/>
2. R.F. Hurrell, J. Nutr. 133 (2003) 2973S–2977S.
3. R.F. Hurrell, I. Egli, Am. J. Clin. Nutr. 91 (2010) 1461S–1467S.
4. A.J.R. Costello, T. Glonek, T.C. Myers, Carbohydr. Res. 46 (1976) 159–171.
5. D.P. Persson, T.H. Hansen, R.P. Thomsen, K.H. Laursen, S. Husted, J.K. Schjørring, BioZoom 1 (2009).
6. D.P. Persson, T.H. Hansen, K.H. Laursen, J.K. Schjørring, S. Husted, Metallomics 1(5) (2009) 418–426.
7. World Health Organization. Safety Evaluation of Certain Food Additives. In WHO Food Additives Series: 67; WHO Press: Geneva, Switzerland, 2012.
8. K. Kraemer, G. Steiger, T. Wierprecht, Iron Fortification Nutritional Blend. EP 2166876 B1, 10 April 2013.

### List of Publications

- A.V.F. Nielsen, I. Tetens, A.S. Meyer, Nutrients 5 (2013) 3074–3098.



## Joachim Bachmann Nielsen

Phone: +45 4525 2922  
E-mail: jobni@kt.dtu.dk

Supervisors: Anker Degn Jensen  
John Nielsen, KU  
Niels Ole Knudsen, DONG Energy  
Matthias Josef Beier, Haldor Topsøe

PhD Study  
Started: September 2012  
To be completed: September 2015

## Direct Liquefaction of Lignin: Solvent Effects

### Abstract

The process of converting solid biomass in a solvent under high pressure in order to obtain a liquid product is called direct liquefaction. It is desired to develop a process for direct liquefaction of lignin to obtain a liquid diesel product with low oxygen content. Processes for solvolytic depolymerization of lignin have been investigated by conducting experiments in a high pressure batch autoclave. Oil yields of up to 84% have been achieved by treatment of lignin in ethanol at 400°C. Complete dissolution of the ash free fraction of lignin has been observed in alkaline solvents at 300°C. The oxygen content in the obtained lignin-oils was lowered by up to one third compared to the lignin feed.

### Introduction

There is an increasing pressure on the transport sector to lower the CO<sub>2</sub> footprint by blending fossil fuels with biofuels. Over the recent years there has been an increased focus on liquid fuel production from lignin. Lignin is of particular interest as it is found in quantities up to 30wt% in lignocellulosic biomass and the majority is burned as a low value fuel [1]. In order to transform solid lignin to a liquid fuel the lignin polymer needs to be depolymerized and the oxygen content lowered. Depolymerization can be obtained by direct liquefaction where lignin is dissolved in a solvent at elevated temperatures. Subsequent upgrading by hydrodeoxygenation (HDO) may be required in order to sufficiently lower the oxygen content and improve fuel quality [2].

At the CHEC research center at DTU-Chemical Engineering experiments on lignin depolymerization are carried out in batch autoclaves. Solvolysis at high temperature has been carried out at a range of different conditions with alcohols, water and heptane as solvent.

### Specific Objectives

It is desired to transform solid lignin from a low value fuel to a higher value liquid transport fuel. It will be satisfactory to obtain a product that can satisfy a 10vol% blend with a marine diesel. This requires a depolymerization of the lignin polymer and lowering of the oxygen content from about 30wt% to a level where blending with a nonpolar diesel is possible. Furthermore it is important to ensure a very low ash content of the

obtained liquid product as ash particles can cause excessive wear to internal combustion engines.

### Experimental Setup

A 500ml stirred HT 4575 Parr batch autoclave capable of handling temperatures up to 500°C and pressures up to 345bar has been used for lignin solvolysis experiments. The lignin used is a hydrothermally extracted lignin from a 2G bioethanol plant. Experiments have been carried out by mixing a weighed amount lignin with different solvents. The reactor is sealed and an inert N<sub>2</sub> atmosphere inside the vessel is ensured prior to heat up. Reaction time was 4 hours for all experiments except for experiments at alkaline conditions where the reaction time was only 10 minutes. After the reaction the vessel is rapidly cooled in an ice bath. The product mixture is filtered and the filtrate is subjected to centrifugation (3min at 11.000 rpm) prior to removal of solvent by rotary evaporation. When alkaline solvent (5wt% NaOH) has been used the filtrate is first acidified to pH=2 followed by extraction with diethyl ether, ethyl acetate or toluene prior to rotary evaporation in order to avoid sodium salts in the heavy fraction. The remaining heavy fraction is the obtained liquid oil which is subjected to a series of analyses. Oil yields are determined on a dry ash free basis.

### Results and Discussion

#### 1. Oil Yields

A suitable process for lignin to liquid conversion requires a high liquid yield. Oil yields obtained from

treating lignin at temperatures ranging from 190-400°C in ethanol, water or heptane are shown in Figure 1. At all temperatures ethanol yielded the highest oil yield. Effects of solvent polarity are believed to play a major role and the polarity of ethanol may resemble that of lignin due to the relative abundance of hydroxyl groups. Seemingly treatment in ethanol or heptane favors the highest temperature 400°C. For treatment in water a decline in recovered oil yield was observed when increasing the reaction temperature from 350°C to 400°C. The supercritical temperature for water is  $T_c=374^\circ\text{C}$  and passing the supercritical point imposes different physical properties of the solvent such as density, ion product and polarity which all may affect lignin solubility.

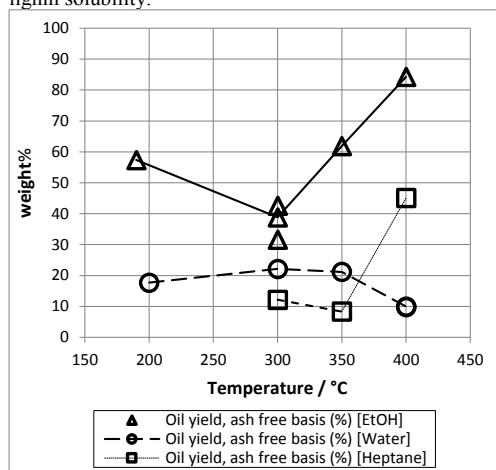


**Figure 1** Oil yields from treatment of 2g of lignin in 100ml of solvent in an  $\text{N}_2$  atmosphere for 4 hours at different temperatures and autogenous pressure.

Alkaline treatment of lignin is of special interest. Alkaline solvents are believed to react predominantly by cleavage of ether linkages in the lignin polymer by nucleophilic attack by  $\text{OH}^-$  on neighboring C-atoms [3]. Experiments conducted in alkaline solvent (5wt% NaOH in either ethanol or water) yielded complete dissolution of the ash free fraction of lignin after only 10 minutes. It was however not possible to recover more than 35% of the produced lignin oil after acidification and extraction procedures.

## II. Oxygen Content

Elemental composition of selected oils can be seen in Table 1. The elemental analysis indicates that treatment in ethanol at 400°C and alkaline treatment yields a reduction of oxygen content by up to one third compared to the lignin feed. The oxygen content still needs to be reduced further in order to satisfy fuel standards.

**Table 1** Elemental composition of oils obtained at different conditions. Oxygen determined by difference.

Sample	C	H	N	S	O	Ash
<b>Lignin</b>	<b>49</b>	<b>5.5</b>	<b>1.9</b>	-	<b>31</b>	<b>13</b>
Oil (EtOH, 400°C)	68	9.3	1.6	-	20	1
Oil (NaOH/water)	66	6.9	1.0	-	26	0.2
Oil (NaOH/ethanol)	69	8.7	1.2	-	21	0.4

## III. Mass Distribution

Size exclusion chromatography has been conducted on obtained lignin oils. The detection wavelength of 280nm primarily registers aromatic species. Figure 2 shows SEC data on lignin oils obtained from treatment in ethanol at different temperatures. Phenol has been added for reference roughly indicating the size of a lignin monomer. Calibration with regards to molecular mass is still required. When ethanol is heated to above the supercritical temperature ( $T_c=241^\circ\text{C}$ ) a shift towards lower molecular mass fractions is observed.

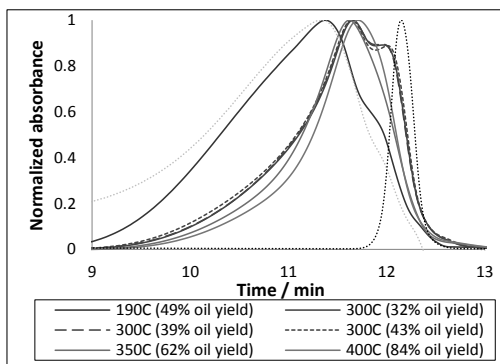


**Figure 2** Molecular mass distribution from SEC on lignin oils obtained from treatment in ethanol. The lignin used and phenol are added for reference.

## Conclusions

Oil yields of up to 84% have been achieved by treatment of lignin in ethanol at 400°C. This treatment and treatment in alkaline solvent at 300°C yielded a reduction of oxygen content by up to one third compared to the lignin feed. Supercritical solvent properties are believed to play a key role in lignin depolymerization.

## References

- Zakzeski, J., Bruijninx, P.C.A., Jongerius, A.L. and Weckhuysen, B.M., *Chem. Rev.*110 (2010) 3552-3599.
- Pandey, M.P., Kim, C.S., *Chem. Eng. & Technol.*34 (2011) 29-41.
- Gierer, J., *Wood Sci. Technol.* 19 (1985) 289-312.



**Mads Willemoes Nordby**

Phone: +45 4525 2809  
E-mail: mwnor@kt.dtu.dk

Supervisors: Kim Dam-Johansen  
Weigang Lin

PhD Study  
Started: December 2012  
To be completed: January 2016

## Understanding Agglomeration Behavior in Fluidized Bed Gasification

### Abstract

Biofuels high in potassium and silica content, such as wheat straw, are problematic when used for combustion or gasification in fluidized bed reactors as there is a high risk of bed agglomeration. The fundamental mechanisms for agglomeration are still not fully understood, and this is especially true for gasifying conditions. Therefore the purposes of this project are to gain a better understanding of alkali release and the ash chemistry, more specifically the role of phosphorus, during biomass gasification and how this might affect agglomeration.

### Introduction

The utilization of biomass with a high alkali metal and/or silica content in fluidized bed reactors have often proven to be problematic due to bed defluidization. This defluidization occurs due to the presence of melt-phases containing mixtures of reacting silica and potassium, and to a lesser extent the presence of sodium. The interacting potassium and silica forms low melting eutectics that are "sticky", and can cause bed particles to adhere to each other forming agglomerates.

Two main mechanisms for bed agglomeration have been identified. The first type of agglomerate is the result of *melt-induced* agglomeration where a separate ash-derived melt phase adhere two bed particles directly together ((2) in figure 1). The second type results from *coating-induced* agglomeration where a coating is formed on the bed particles after which individual particles may adhere to each other and form necks ((1) in figure 1). These two types of agglomerates can also be combined if after the first necks are formed, partial defluidization occurs leading to hotspots in the bed where melt phases can occur.

In most commercial scale installations melt-induced agglomeration has been observed to be the dominant process, but both bed material and fuel type has a significant influence on the type of agglomeration. For a high-quartz sand bed material both mechanisms are likely to occur, especially at large scale, while for inert bed material only melt-induced agglomeration is present.

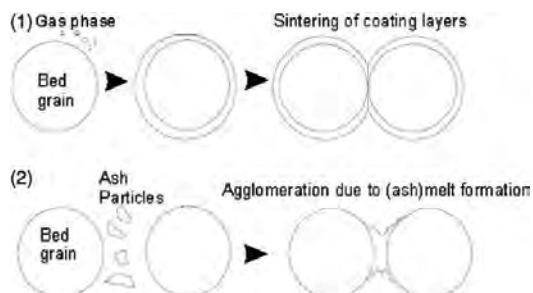


**Figure 1:** Agglomeration of bed material after coating formation from the gas phase (1) or melt formation of ash components (2).

### Specific Objectives

As the effects of gasifying conditions on volatile release and ash chemistry in biomass are not currently well understood, this PhD project aims to investigate some of the fundamentals of agglomeration during gasification in fluidized bed reactors.

- Investigate how the release of alkali metals is affected under gasifying conditions.
- Determine the effects of various operating conditions such as temperature, gas flow, fuel composition, etc., on the agglomeration tendency and product gas composition.
- Determine what role phosphorus plays in the ash chemistry.

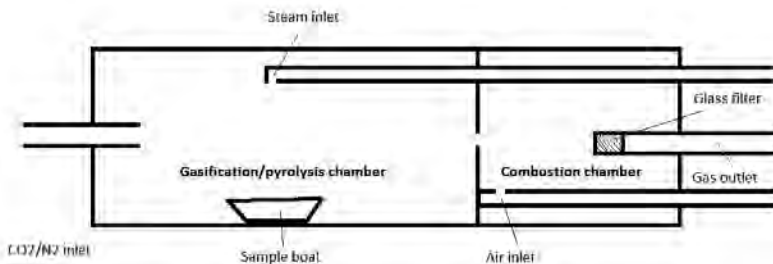


**Figure 2:** Schematic illustration of fixed bed oven setup used for planned experiments.

### Discussion

The release characteristics of alkali metals during pyrolysis and subsequent char gasification have shown that 53-76 % of the alkali metals were volatilized during the pyrolysis step, while during the char gasification it was 12-34 %. Expanding upon these results showed that during pyrolysis the evaporation was partly with the decomposition of lignin, hemicellulose and cellulose, and partly due to char-volatile interactions [1].

Research has also shown that during gasification the majority of the released alkaline species are combined with tar, primarily in the water-soluble fraction. At a temperature of 873 K 65 % of sodium and 63 % of potassium were released and present in the tar. Increasing the gasification temperature lead to secondary decomposition of the water-soluble tar, where the resulting released alkali species, could not be captured by quartz glass filter, which indicated that the alkaline species were released as very fine particles during secondary decomposition of the water-soluble tar. The yield of condensed alkaline species also increased significantly along with increasing gasification temperature [2].

Char reactivity has also been seen to drastically reduce during contact with steam. This was due to changes in the char structure, and was found to have no connection to the volatilization of the catalytically active alkali metals [3].

During combustion phosphor has been shown to react with potassium, reducing the amount available to volatilize or react with the bed material. However some of the phosphate rich ash particles were found to form low-temperature –melting alkali-rich phosphates promoting agglomeration behavior. A general observation is that phosphor plays a controlling role in ash transformation reactions during biomass combustion, due to the high stability of phosphate compounds [4, 5].

### Experimental Work

The release of alkali metals under CO<sub>2</sub> and steam gasifying conditions will be investigated using a fixed-bed oven. The oven is separated into two chambers; a primary pyrolysis/gasification zone and a combustion zone where problematic particulates, i.e. tars, are

combusted. An illustration of the setup can be seen in figure 2.

Furthermore the effects of phosphor additives will be tested in both the fixed bed oven and in a lab-scale fluidized bed reactor, where agglomeration conditions and the product gas composition can be monitored.

Using the results from these experiments, a release mechanism for the alkali metals and a reaction mechanism for phosphor under gasifying conditions are to be proposed.

### Acknowledgements

This project is part of DANCNGAS, and I would like to thank the Sino-Danish Center for Education and Research and the Technical University of Denmark for funding it, as well as the Chinese Academy of Sciences for their support.

### References

1. L. Jiang, S. Hu, J. Xiang, S. Su, L.-S. Sun, K. Xu, Y. Yao, *Bioresour. Technol.* 116 (2012) 278-284.
2. O. Hirohata, T. Wakabayashi, K. Tasaka, C. Fushimi, T. Furusawa, P. Kuchonthara, A. Tsutsumi, *Energy Fuels* 22 (6) (2008) 4235-4239.
3. D. M. Keown, J.-I. Hayashi, C.-Z. Li, *Fuel* 87 (2008) 1127-1132.
4. A. Grimm, N. Skoglund, D. Boström, M. Öhman, *Energy Fuels* 25 (2011) 937-947.
5. A. Grimm, N. Skoglund, D. Boström, C. Boman, M. Öhman, *Energy Fuels* 26 (2012) 3012-3023.



## Kristian Petersen Nørgaard

Phone: +45 4525 2843  
E-mail: kpno@kt.dtu.dk

Supervisors: Søren Kiil  
Kim Dam-Johansen  
Pere Català, Hempel A/S

### PhD Study

Started: January 2011  
To be completed: February 2014

## Design and Testing of Efficient and Robust Intumescent Coatings

### Abstract

Although steel is a non-combustible material, a weakness when used as load bearing material in constructions, is reduced mechanical stability which becomes critical at temperatures around 400 to 550 °C. At these temperatures, which occur in the event of a fire, the steel cannot support its own weight, and a collapse is likely. A method to prolong the time before collapse is to protect the steel with intumescent coatings. Intumescent coatings, is a kind of passive fire protection which expands and form a thermally insulating layer when exposed to heat. The expansion happens according to a complex reaction mechanism and in addition to the intumescent coatings, other parameters, such as performance of a primer, between the intumescent coating and steel may influence the coating. In this document, results based on a special electric oven, with controlled gas composition are presented. The results are concerned with the use of primers for intumescent coatings.

### Introduction

In this document, an overview of the results obtained in the Ph.D. project, relating to oxygen content and primers, is given. For detailed background information please refer to the list of publications. As the project title shows robust systems are being investigated. To get a good performance of the system, it is important to understand failures which can happen during a fire and reasons behind such failures. Examples of failures are damages of the char, due to falling or moving objects during the fire or detachment from the substrate, which will lead to a rapid temperature increase of the steel. An important requirement for intumescent coatings is expensive and time consuming third party approval tests, in which primers and topcoats are also tested. In this yearbook contribution, an overview of work with primers for intumescent coatings is collected.

### Specific objectives

The main objectives of this Ph.D. project is to investigate the effect of external parameters, such as gas composition or heating rate as well other coating layers such as primers, and to some extent, internal coating parameters, such as reaction chemistry is studied.

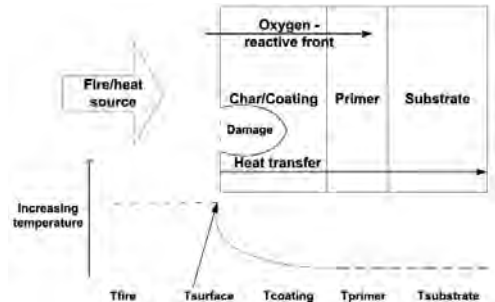


**Figure 1:** Drawing showing the intumescent coating system, with primer, and access of heat and oxygen after damage. After [1].

### Intumescent reaction mechanism

From the literature, a generic reaction mechanism with increasing temperature has been collected [1], and is briefly summarized in condensed form below. Intumescent coatings generally consist of five basic compounds, blowing agent (e.g. melamine), carbon source (e.g. pentaerythritol), acid source (e.g. ammonium polyphosphate), binder (e.g. acrylic) and pigments (e.g. TiO<sub>2</sub>).

1. At temperatures between 150 – 215 °C, an inorganic acid is released from the acid source

- which can degrade into  $\text{NH}_3$ , water and acidic phosphoric groups [2-4].
- At temperatures slightly higher than those of bullet 1, the phosphoric acid groups react with hydroxyl groups on the carbon source and form a phosphoric ester [4, 5]. This reaction is often referred to as esterification or phosphorylation (alcoholysis) [6-8].
  - At temperatures between step 1 and 2, the binder melts [3].
  - At temperatures from 280 to 350 °C, the phosphoric ester degrades and forms a carbon-inorganic residue [4].
  - Meanwhile, the blowing agent (e.g. melamine) decomposes and emits gases such as  $\text{NH}_3$ ,  $\text{CO}_2$ , water, and  $\text{NO}_2$  [9, 10] which makes the coating swell [4, 11].
  - Following the expansion, solidification, through cross-linking of the melted compounds, takes place and a solid char is formed [3].
  - At higher temperatures, thermal decomposition and/or oxidation of the char take place [4, 12]. The degradation could for instance be oxidation of the carbon.

### Primer and intumescent coatings

In addition to the mechanisms described above, intumescent coatings also need to interact with other coating layers, as for instance a primer. The primer is applied both to ensure good adhesion and to prevent corrosion of the underlying metal. As well, third party approval of a primer is necessary before it can be used with the intumescent coating.

### Experimental methods

#### Materials

Two commercial primers and a generic solvent-borne acrylic intumescent coating are used in the study. Primer A, a shop primer, contains polyhydroxyether epoxy/polyamide with zinc aluminum phosphate pigment. Primer B contains bisphenol-A epichlorhydrin/phenalkamine primer with zinc phosphate and micaceous iron oxide pigments.

#### Gas-fired furnace tests

At first the primers were tested in a gas-fired furnace, below an intumescent coating. The gas-fired furnace has an inner volume of 0.65 m<sup>3</sup> and follow the ISO834 time-temperature curve. The coatings were applied to the large face of steel panels with dimensions of 300x200x6 mm<sup>3</sup>. The oxygen content of the gas in the furnace is approximately 1 Vol%.

#### Oven with controlled gas composition

To test the mechanisms causing the failure, a special test oven was used, and samples with the two primers were prepared. The samples were heated at a heating rate of approximately 10 °C/min to 500 °C in either

atmospheric air or pure nitrogen. A photograph of the oven is seen in Figure 2. Samples for the oven test were 10x10 mm squares, coated with different primer thicknesses (without intumescent coating). Twelve samples were heated in the oven, at once.



**Figure 2:** Photograph of oven with controlled gas composition.

#### Thermogravimetric analysis.

Thermogravimetric measurements were performed in a Netzsch Jupiter F1 STA, in alumina crucibles with an inner diameter of 7 mm. The gas flow was 100 NmL/min and consisted of either pure nitrogen or 10% oxygen and 90% nitrogen (reduced oxygen). The samples were powders of either the intumescent coating, primer A or primer B. Mixtures were not tested.

### Results

#### Thicknesses for gas-fired furnace

The thickness of primer A was 25 µm, and primer B was in the range of 113-119 µm. The intumescent coating was applied at a dry thickness of 1000 µm.

#### Temperatures in gas-fired furnace

In the gas-fired furnace, primer A showed good adhesion properties, whereas primer B failed. Figure 3 shows the steel and gas temperatures. The failure can be seen from the sudden temperature increase for primer B in the steel temperature.

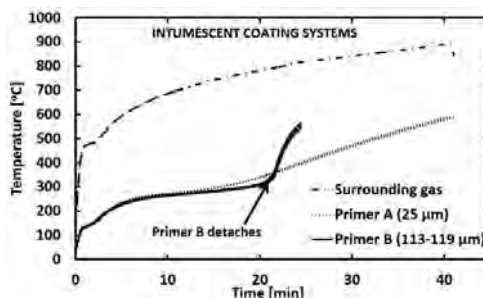


**Figure 3:** Steel and gas temperatures for the primers tested below an intumescent coating. After [1].



### Thermogravimetric analysis

The results from the thermogravimetric analyses are seen in Figure 4. From all the samples, except primer B in reduced oxygen, the curves are seen to follow the same qualitative trend. This could be interpreted, as some inherent property and mismatch in the degradation of intumescent coating and primer led to the failure in the gas-fired furnace. However, from the results obtained in the electric oven, this does not appear to be the case, as will be shown in the next paragraph.

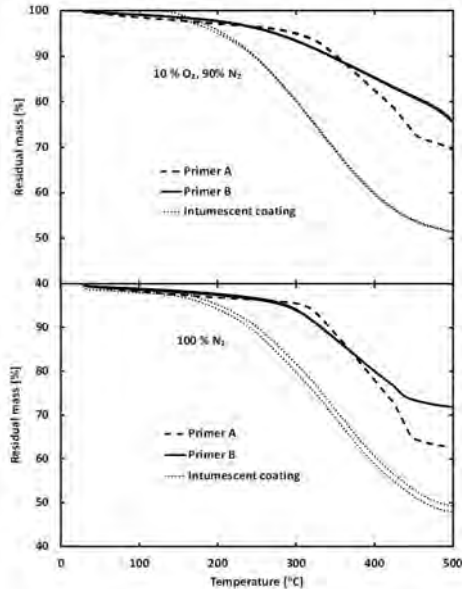


**Figure 4:** Mass loss curves (TGA) for the two primers and intumescent coating (all individual one-coat layer). The top plot shows mass loss under reduced oxygen and the bottom plot mass loss in nitrogen. For each sample, two data series are shown, verifying a good repeatability. After [1].

### Electric oven with controlled gas composition

Some selected results from the investigation of the primers for intumescent coatings are shown in Figure 5. The results showed that the primer changed to black in the presence of nitrogen, and in oxygen the damages increased with thickness. This was both the case for primer A and primer B. Due to the sake of brevity, only selected results are shown here, full documentation can be found in reference [1].

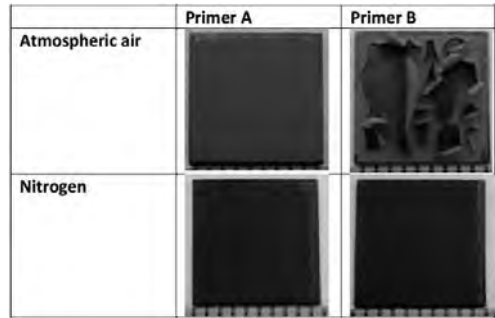


**Figure 5:** Examples of primers (without intumescent coating) after heating to 500 °C in atmospheric air and nitrogen in the electric oven. Both primers changed color to black but stayed attached in the presence of nitrogen. In oxygen one primer stayed attached and the other failed. The thicknesses are between 16 and 26 μm.

### Discussion

The results from the primer analyses showed that in the presence of oxygen primer performance decreases with film thickness. Another observation is that in the absence of oxygen, the primers changed color to black. Although it has not been experimentally verified, this may potentially be used as a practical test method to see if the primer has been exposed to oxygen. It is noted that the tests in atmospheric air constitutes a worst case scenario with 21% oxygen. From the thermogravimetric analysis it could seem that the failure was due to an incompatibility between primer B and the intumescent coating in the presence of oxygen. However, it is noticed that the thermogravimetric behavior may not be sufficient to describe the failure, because with increased thicknesses, primer A also fails.

### Conclusions

Intumescent fire protective coatings, which expand to form a thermally insulating char, react according to a complex temperature triggered reaction sequence. Apart from this reaction sequence other parameters such as additional coating layers or damages due to falling objects and gas compositions, are important. In this document a fast screening method to test the influence of oxygen content and primer performance is presented. The test methods which are investigated in the present Ph.D. project, are supplements to the existing standard tests, and investigates parameters differing from the parameters such as steel temperatures traditionally investigated in standard tests.

### Acknowledgments

Financial support by the Hempel Foundation is gratefully acknowledged. The Hempel R&D Group – Fire Protection, is gratefully acknowledged for performing the tests in the gas-fired furnace.

## References

- [1] K.P. Nørgaard, K. Dam-Johansen, P. Català, S. Kiil, Laboratory and gas-fired furnace performance tests of epoxy primers for intumescent coatings, *Prog. Org. coat.* (Accepted October 2013).
- [2] G. Camino, L. Costa, L. Trossarelli, Study of the mechanism of intumescence in fire retardant polymers: Part V--Mechanism of formation of gaseous products in the thermal degradation of ammonium polyphosphate, *Polym. Degrad. Stab.* 12 (1985) 203-211.
- [3] K.M. Butler, Physical modeling of intumescent fire retardant polymers. 669 (1997) 214-230.
- [4] S. Bourbigot, S. Duquesne, Fire retardant polymers: recent developments and opportunities, *J.Mater.Chem.* 17 (2007) 2283-2300.
- [5] M. Władyka-Przybylak, R. Kozłowski, The Thermal Characteristics of Different Intumescent Coatings, *Fire Mater.* 23 (1999) 33-43.
- [6] B.K. Kandola, A.R. Horrocks, Complex char formation in flame-retarded fibre-intumescent combinations--II. Thermal analytical studies, *Polym. Degrad. Stab.* 54 (1996) 289-303.
- [7] Z. Lei, Y. Cao, F. Xie, H. Ren, Study on surface modification and flame retardants properties of ammonium polyphosphate for polypropylene, *J Appl Polym Sci.* 124 (2012) 781-788.
- [8] G. Camino, L. Costa, L. Trossarelli, F. Costanzi, G. Landoni, Study of the mechanism of intumescence in fire retardant polymers: Part IV—Evidence of ester formation in ammonium polyphosphate-pentaerythritol mixtures, *Polym. Degrad. Stab.* 8 (1984) 13-22.
- [9] C. Branca, C. Di Blasi, H. Horacek, Analysis of the combustion kinetics and thermal behavior of an intumescent system, *Ind Eng Chem Res.* 41 (2002) 2107-2114.
- [10] Z. Han, A. Fina, G. Malucelli, G. Camino, Testing fire protective properties of intumescent coatings by in-line temperature measurements on a cone calorimeter, *Progress in Organic Coatings.* 69 (2010) 475-480.
- [11] Z. Wang, E. Han, W. Ke, An investigation into fire protection and water resistance of intumescent nano-coatings, *Surface and Coatings Technology.* 201 (2006) 1528-1535.
- [12] G. Griffin, The Modeling of Heat Transfer across Intumescent Polymer Coatings, *J. Fire Sci.* 28 (2010) 249-277.

## List of Publications (Articles)

K.P. Nørgaard, K. Dam-Johansen, P. Català, S. Kiil, Investigation of char strength and expansion properties of an intumescent coating exposed to rapid heating rates, *Progress in Organic Coatings* 76 (2013) 1851-1857

K.P. Nørgaard, K. Dam-Johansen, P. Català, S. Kiil, Laboratory and gas-fired furnace performance tests of epoxy primers for intumescent coatings (accepted for *Progress in Organic Coatings* 11/10-2013)

K.P. Nørgaard, K. Dam-Johansen, P. Català, S. Kiil, Intumescent coatings under fast heating, *European Coatings Journal* 06/2012. (Also translated to publication in *Russian Coatings Journal*)

## List of Publications (Conferences)

Poster and oral presentation at 8<sup>th</sup> and 9<sup>th</sup> Coatings Science International conference, Noordwijk, The Netherlands

Poster presentation at 14<sup>th</sup> European Meeting on Fire Retardancy and Protection of Materials, Lille, France

Presentation at "European Coatings conference – Fire retardant coatings", Berlin, 13<sup>th</sup> and 14<sup>th</sup> of March 2012.



## Anders Nørregaard

Phone: +45 4525 2990  
E-mail: andno@kt.dtu.dk

Supervisors: Krist V. Gernaey  
Brian Madsen, Novo Nordisk  
Stuart M. Stocks, Novozymes  
John M. Woodley

### PhD Study

Started: January 2013  
To be completed: January 2016

## Mixing and Oxygen Transfer Processes in Bioreactors

### Abstract

Biotechnological production in stirred tank reactors suffers from the limited knowledge that is available about the oxygen mass transfer properties and flow patterns in the fermentation broth. This knowledge could be valuable in order to design and optimize the fermentation processes that account for production of a large variety of products. This project investigates the concentration gradients that emerge in the fermentors, and more specifically the focus will be on characterising the oxygen concentration in the broth. New experimental techniques with minimal impact on the process together with mathematical modeling are necessary in order to investigate this problem in more detail. Experiments will be performed in industrial scale fermentors.

### Introduction

Biochemical production by suspended aerobic fermentation processes is nowadays used to produce most industrial enzymes, many pharmaceuticals and chemical precursors. The processes are based on the conversion of a carbon substrate by a microorganism, in the presence of oxygen, to form biomass, products and carbon dioxide. During production, mass transfer of oxygen to the fermentation broth is the rate-limiting factor which has large importance for the process. Due to the large size of the industrial-scale fermentation vessels, concentration gradients inside the reactor will occur, and thereby the often made assumption of perfect mixing in the reactor - usually applied in process models - does not apply. Differences in pressure, agitation intensity and viscosity together with organism growth differentiation make this heterogeneity difficult to predict. The purpose of this project is therefore to investigate the properties of mixing and oxygen transfer in large scale fermentation vessels in order to better understand the processes and phenomena that take place in these vessels.

Modelling large-scale bioreactor systems is challenging because only a limited experimental basis in large scale vessels exists, and significant differences between laboratory scale and production scale are often observed.

Since the processes take place inside a sealed steel vessel, sampling from the vessel is limited to probes that can tolerate the high temperature of the initial heat

sterilization of the vessel together with surface growth of the production organism. A limited number of ports are available for these kinds of probes, often limited to ports in one location in the bottom of the fermentor. The fermentation broth is also opaque which limits the applicability of many optical methods.

Fermentors of 20.000 L or larger are expensive to operate, and their availability is limited. The industries operating such reactors usually do not reveal any details related to the dimensions of the reactor. Furthermore, they are normally part of existing industrial processes which means that they cannot be modified for academic reasons due to the risk of disturbing the production.

The time scale of oxygen consumption in the fermentor is measured in seconds. That is, if the oxygen supply to the fermentor is shut off it will be starved for oxygen within seconds. That makes oxygen a good process parameter for the fermentor, but it also makes it difficult to measure the dissolved oxygen concentration since a sample cannot be removed from the fermentor without the organisms consuming the oxygen before it can even be analysed.

The volumetric mass transfer coefficient ( $k_L a$ ) is dependent on many of the physical factors of the process and is described by eq. 1, an empirically derived correlation proposed by Cooke et al. [1]

$$k_L a = C \cdot \left(\frac{P}{V}\right)^a \cdot v_g^b \cdot \mu_{app}^c \quad \text{Eq. 1}$$

Here  $P/V$  is the volumetric power input from agitation ( $W/m^3$ ),  $v_g$  is the superficial gas flow rate if plug flow is assumed ( $m/s$ ), and  $\mu_{app}$  is the apparent viscosity of the broth ( $Pa \cdot s$ ).  $C$ ,  $a$ ,  $b$  and  $c$  are empirically derived constants that are dependent on the fermentor design, production organism and process conditions.

The expression is a further development of a classical empirical correlation for  $k_L a$  described by Brown et al. [2] similar to the above equation but without the part containing apparent viscosity. The issue with the empirical correlations is that some viscous fermentation broths show non-Newtonian behavior which means that the apparent viscosity is difficult to predict since it is dependent on fermentor configuration and production organism phenotype. Figure 1 describes the typical flow patterns inside the fermentor depending on different impeller configurations. Each set of empirically derived constants for eq. 1 is therefore specific for a given process. Another dynamic factor of the oxygen transfer is the pressure inside the vessel that changes depending on the height of the liquid column. Oxygen is absorbed during the rise of the air bubbles which changes the driving force for oxygen transfer along the height of the fermentor.

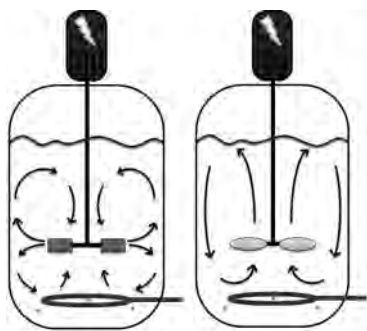


**Figure 1:** Typical flow patterns inside the fermentor depending on axial (left) and radial (right) pumping impellers.

### Specific Objectives

The first part of the project is focused on finding a proper way to establish informative measurements in the bioreactor with the lowest degree of disruption of the fermentation process in the reactor. The first processes to be investigated are the production of cellulase enzyme from cultivation of the filamentous fungus *Trichoderma reesei*, and insulin production with the yeast *Saccharomyces cerevisiae*. These production methods both utilize pure cultures of fungi to produce a secreted protein, but differ significantly in the morphology of the production strain together with the product purity requirements and value.

Knowledge about the spatial heterogeneity in the fermentor can be put into a compartmentalized model, similar to the existing process models e.g. the one presented by Albæk et al. [3], but with differentiation regarding the oxygen transfer in the different areas of

the fermentor. This could improve the model accuracy and could also be represented in downscaled experiments that utilize several small fermentors in series each with appropriate oxygen mass transfer to mimic the spatial heterogeneity of the larger fermentors. This method can not only be applied to improve existing models, but also facilitates design of new processes and screening of new production strains. It can also be used to rethink some of the more practical aspects of the equipment design, such as where to add substrate and pH control in order to reduce the concentration gradients.

### Results and Discussion

An experimental method for oxygen measurement has been proposed and is now being tested in lab scale. It is the goal to test this equipment in production scale as well as project.

### Conclusions

The issue concerning characterization of the spatial heterogeneity in fermentors has long been known and several studies to investigate the problem by means of mathematic modeling supported with pilot scale experiments have been carried out. These experiments often suffer from the highly dynamic and complex issue of scalability of the processes. Characterization of the spatial heterogeneity in a production scale fermentor has still not been carried out, and the potential benefits of such a characterization cover all aspects of cultivation of suspension cultures in large vessels, including design of production equipment, production organisms and process conditions.

### Acknowledgements

The project is carried out in collaboration with Novo Nordisk A/S and Novozymes A/S. The project is financed by the BIOPRO project, and by the Technical University of Denmark

### References

1. D.A.R. Brown, P.N. Jones, J.C. Middleton, G. Papadopoulos, E.B. Arik, Experimental Methods in E.L. Paul, V.A. Atiemo-Obeng, S.M. Kresta, Handbook of Industrial Mixing, Wiley Interscience, Hoboken, New Jersey. 2004, p. 145-201.
2. M. Cooke, J.C. Middleton, J.R. Bush. Mixing and mass transfer in filamentous fermentations. 2nd International Conference on Bioreactors. Cambridge, UK 1988.
3. M.O. Albæk, K.V. Gernaey, M.S. Hansen, S.M. Stocks. Modeling enzyme production with *Aspergillus oryzae* in pilot scale vessels with different agitation, aeration, and agitator types, Biotechnol. Bioeng. 108 (2011) 1828-1840.

### List of Publications

A. Nørregaard, S.M. Stocks, K.V. Gernaey, J. Woodley, Filamentous fungi fermentation. In Meyer, H.P. & Schmidhalter, D. (eds.) Industrial scale suspension culture of living cells, Wiley-VCH, 2014.



**Brian Kjærgaard Olsen**

Phone: +45 4525 2830  
E-mail: bria@kt.dtu.dk

Supervisors: Anker Degn Jensen  
Francesco Castellino, Haldor Topsøe A/S

PhD Study  
Started: June 2011  
To be completed: June 2014

## Deactivation of Selective Catalytic Reduction Catalysts in Biomass Fired Power Plants

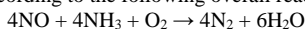
### Abstract

Selective catalytic reduction of nitrogen oxides by ammonia over vanadia based catalysts has proved to be an effective method for reducing the emissions from stationary, coal fired sources. However, due to the release of alkali elements during biomass firing, accelerated deactivation of these catalysts has been observed.

In order to study this alkali poisoning, four series of plate shaped, vanadia based catalysts have been exposed to aerosols of potassium chloride in a bench scale setup. Activity measurements on exposed catalysts show vast deactivation regardless of exposure temperature (150 or 350 °C) and time (300 or 600 hours). However, a lower exposure temperature does seem to slow down the deactivation.

### Introduction

Selective catalytic reduction (SCR) of nitrogen oxides ( $\text{NO}_x$ ) with ammonia ( $\text{NH}_3$ ) is a well established method for controlling the  $\text{NO}_x$  emissions from stationary sources such as coal fired heat and power plants [1,2]. In the presence of oxygen ( $\text{O}_2$ ), nitrogen oxide ( $\text{NO}$ ) is catalytically converted into molecular nitrogen ( $\text{N}_2$ ) according to the following overall reaction [1]:



The most widely used catalysts for stationary applications consists of titania ( $\text{TiO}_2$ ) supported vanadia ( $\text{V}_2\text{O}_5$ ), promoted with either tungsten oxide ( $\text{WO}_3$ ) or molybdenum oxide ( $\text{MoO}_3$ ), in the shape of honeycomb monoliths [2].

Topsøe *et al.* [3-5] proposed a widely accepted mechanism for the SCR reaction over  $\text{V}_2\text{O}_5$  based catalysts. The mechanism, which is schematized in Figure 1, consists of two catalytic cycles, each of which involves a type of active site – the so called Brønsted acid sites ( $\text{V}^{5+}\text{-OH}$ ) and the redox sites ( $\text{V}^{5+}=\text{O}$ ).

In a time with great focus on the release of carbon dioxide ( $\text{CO}_2$ ), firing (or co-firing) of biomass (straw, wood chips, etc.) and waste products such as sewage sludge and municipal waste, is being applied in order to reduce the net  $\text{CO}_2$  emissions.

Unfortunately, the industrially applied SCR catalysts have a significantly reduced life-time when used in connection with such fuels. The shortened duration of the catalysts is due to an accelerated deactivation by a high amount of poisonous components in the fuels.

Alkali and alkaline earth metals, which can be present in biomass in high concentrations, are examples of components that can severely deactivate commercial SCR catalysts [6].

Potassium, released e.g. during firing of straw, may reach the SCR catalyst in the form of aerosols of potassium chloride ( $\text{KCl}$ ) or potassium sulfate ( $\text{K}_2\text{SO}_4$ ) which deposit on the catalyst surface and diffuse into the pore system [7]. It is believed that potassium, due to its alkaline nature, poisons the SCR catalyst by reacting with the acidic  $\text{V}^{5+}\text{-OH}$  sites [8,9]. Research has furthermore shown that the reducibility of  $\text{V}^{5+}$  species is inhibited upon alkali poisoning [10].

While the effect of alkali metal on commercial SCR catalysts is generally understood, a more systematic study of the deactivation mechanism has yet to be performed. Such a study will provide useful information during development of new alkali resistant catalysts and/or improved means of operation.

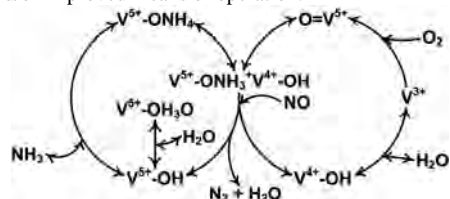


**Figure 1:** The proposed mechanism for the reduction of  $\text{NO}$  by  $\text{NH}_3$  over  $\text{V}_2\text{O}_5$  based catalysts. Adapted from [5].

### Specific Objectives

The main objective of this PhD study is to investigate the influence of catalyst composition and operating conditions on the rate of deactivation during alkali poisoning. It is particularly of interest to study the relationship between surface –OH sites and the rate of alkali penetration.

### Experimental

Through four campaigns, four series of plate shaped SCR catalyst, supplied by Haldor Topsøe A/S, have been subjected to KCl aerosols at various conditions in a bench scale SCR reactor. The catalysts were based on fiber reinforced TiO<sub>2</sub> impregnated with V<sub>2</sub>O<sub>5</sub> to various levels (0-6 wt.%). Some of the plates were doped with WO<sub>3</sub> as well.

A schematic overview of the SCR exposure pilot is presented in Figure 2. The setup consists of a natural gas burner, a flue gas duct perpendicular to the burner outlet, a heat exchanger section where the reactor temperature can be adjusted, and the reactor itself. A second heat exchanger cools the flue gas further before it is led to the stack. A water cooled injector probe equipped with a two-fluid nozzle can be introduced into the flue gas duct at the end adjoining the burner outlet. At the opposite end of the duct, a bayonet heat exchanger can be inserted.

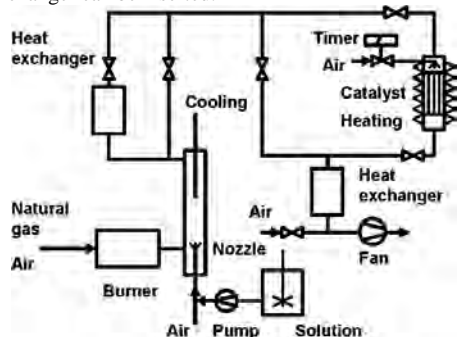


**Figure 2:** Schematic drawing of the SCR exposure pilot. Adapted from [9].

The four exposure campaigns mainly differed by the reactor temperature, the total exposure time and the position of the injector nozzle, as stated in Table 1.

**Table 1:** Main parameters of the four exposure campaigns.

Parameter	Campaign No.			
	1	2	3	4
Nozzle position [cm]	40	40	40	142
Reactor temperature [°C]	350	150	350	300
Exposure time [h]	600	300	300	300

The aerosols were created by pumping an aqueous solution of KCl (with a concentration of 7.4 g/L) through the injector probe (at a rate of 420 mL/h) and injecting it into the hot flue gas by the aid of pressurized air. In three of the campaigns the solution was injected

close to the burner outlet (40 cm into the flue gas duct) where the gas temperature typically was 1050-1100 °C. In one instance, the injection point was moved further downstream the burner (142 cm from the insertion point) where the temperature was significantly lower (<550 °C). In general it is believed that mainly the ultrafine (<100 nm) potassium rich particles are harmful to the SCR catalysts [11]. It has thus been of interest to expose the samples to aerosols of various characteristics.

### Results and Discussion

The characteristics of the KCl aerosols were measured using a Scanning Mobility Particle Sizer (SMPS) and a Low Pressure Impactor (LPI) by sampling the flue gas just above the reactor inlet. Depending on the position of the injector probe (i.e. the gas temperature at the point of injection) the characteristics of aerosol can be affected as indicated from the LPI results reported in Figure 3.

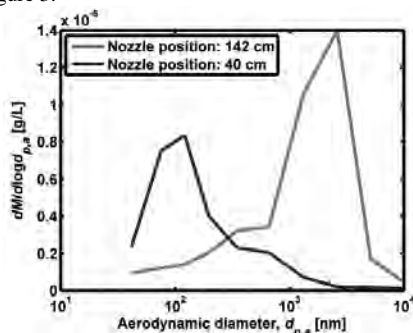


**Figure 3:** Mass based size distributions measured for different nozzle positions.

As seen from the figure, the distribution measured for a nozzle position at 142 cm peaks at an aerodynamic diameter of 2600 nm, while the one for the 40 cm position peaks at 120 nm. Moving the two-fluid nozzle further into the flue gas duct clearly results in a shift of the mass based size distribution towards larger particles. Nevertheless, a significant amount of ultrafine particles may still be present in the flue gas, as seen from the SMPS results in Figure 4.

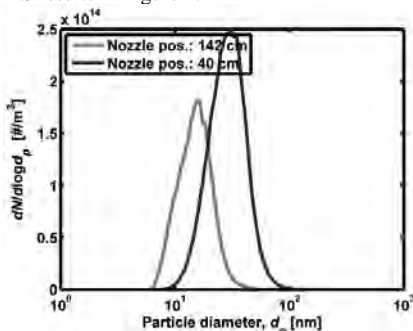


**Figure 4:** Number based size distributions measured for different nozzle positions.

The figure shows a number based size distribution obtained with an injection nozzle position of 142 cm, measured at conditions identical to those of campaign 4, as well as a distribution measured during campaign 3. The submicron particles measured with nozzle at a position of 142 cm peaks at a particle diameter of 16 nm and amounts to a total number based concentration of  $6.4 \cdot 10^{13} \text{ \#}/\text{m}^3$ . These particles may originate from old salt deposits in the setup.

The catalytic activities of the exposed samples as well as of fresh, unexposed counterparts have been measured in a laboratory reactor. The samples were crushed down, diluted with sand and loaded into a quartz reactor between two layers of quartz wool. A total flow of about 2800 NmL/min was used during the measurements and the gas was composed of 500 ppmv NO, 600 ppmv NH<sub>3</sub>, 5 vol.% O<sub>2</sub>, about 1.4 vol.% H<sub>2</sub>O and balance N<sub>2</sub>. The activity of fresh catalysts generally increased with the V<sub>2</sub>O<sub>5</sub> loading. At temperatures below 300 °C the activity of fresh, WO<sub>3</sub> free catalysts was found to be comparable or even higher than that of WO<sub>3</sub> promoted catalysts with the same V<sub>2</sub>O<sub>5</sub> loading. At elevated temperatures, the promoted catalysts showed the highest activities.

Figure 5 shows the catalytic activity, as a function of temperature, of 3% V<sub>2</sub>O<sub>5</sub>-7% WO<sub>3</sub>/TiO<sub>2</sub> samples exposed in the four campaigns, as well as that of an unexposed sample. The figure reflects the general trends observed for all exposed the catalyst formulations.

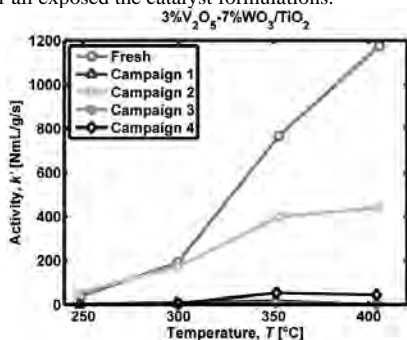


**Figure 5:** Catalytic activities of powdered 3% V<sub>2</sub>O<sub>5</sub>-7% WO<sub>3</sub>/TiO<sub>2</sub> catalyst plates as functions of temperature.

The catalysts exposed in the four campaigns all show significant deactivation. The remaining activity of the respective catalysts exposed in campaign 1 and 3 is comparable and in most cases insignificant. The samples exposed in campaign 2 show the highest remaining activities of all the exposed samples, which may indicate that the mobility of potassium is lower at reduced temperatures. In most cases the activity of these samples increases with temperature in the entire temperature range, however, for the samples loaded with 6 wt.% V<sub>2</sub>O<sub>5</sub> (both with and without WO<sub>3</sub>), the activity peaks at 350 °C. This indicates that potassium poisoned SCR catalysts with high V<sub>2</sub>O<sub>5</sub> loadings act as NH<sub>3</sub> oxidation catalysts [6]. The samples which have

been exposed to an aerosol containing larger particles (campaign 4) are more or less inactive. Beforehand, the deactivation was expected to be less severe since larger particles are less likely to enter the pore systems of the catalysts and since the contact area between catalyst surface and potassium rich particles, deposited on the catalyst exterior, will be lower. The reason why we still have significant deactivation may be due to the continued presence of ultrafine particles in the pilot, as pointed out earlier.

To assess the mobility of potassium at the given exposure temperature, the potassium concentration through the thickness of catalyst plates from campaign 1 and 2 have been measured by Scanning Electron Microscopy in combination with Energy Dispersive X-ray Spectroscopy (SEM-EDS). Figure 6 shows the potassium and vanadium concentration profiles through the 3%-V<sub>2</sub>O<sub>5</sub>-7% WO<sub>3</sub>/TiO<sub>2</sub> sample from campaign 1.

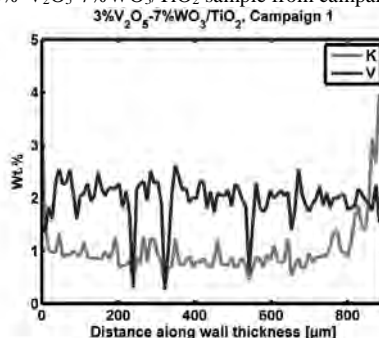


**Figure 6:** Potassium and vanadium concentration profiles along the thickness of the 3% V<sub>2</sub>O<sub>5</sub>-7% WO<sub>3</sub>/TiO<sub>2</sub> plate from exposure campaign 1.

As seen from the figure, the potassium concentration through the centre of the sample is approximately constant and assumes a value of about 0.8 wt.%. Near the edges of the sample the concentration increases, most likely due to deposits of potassium rich particles at the surface. A similar potassium concentration level was observed in a 6% V<sub>2</sub>O<sub>5</sub>-7% WO<sub>3</sub>/TiO<sub>2</sub> sample from the same campaign. Figure 7 shows the potassium concentration in a TiO<sub>2</sub> sample, also from campaign 1.

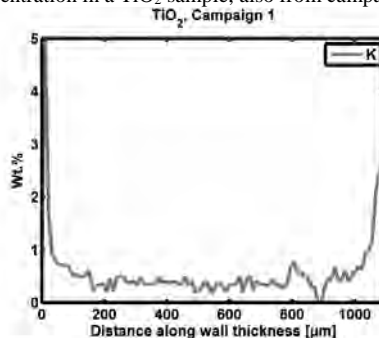


**Figure 7:** Potassium concentration profile along the thickness of the TiO<sub>2</sub> plate from exposure campaign 1.

The potassium concentration at the centre of the sample is around 0.4 wt.% which is about the detection limit of the microscope. Like for the 3%V<sub>2</sub>O<sub>5</sub>-7%WO<sub>3</sub>/TiO<sub>2</sub> sample, large quantities of potassium, amounting to several wt.%, is present near the edges. The fact that the potassium concentration inside the sample is low, even though plenty of potassium is available, may indicate that potassium have less sites to latch on to in TiO<sub>2</sub>. Low potassium concentrations, close to or below the detection limit, have been found in the samples from campaign 2.

In order to further study the transport potassium in SCR catalysts, a series of pellet based experiments have been devised. The concept is to produce a series of pellets consisting of two layers – one layer pressed from fresh, pulverized SCR catalyst, and one layer of the same catalyst impregnated with e.g. KCl. After exposure to a flowing gas at elevated temperatures, the potassium profile through the two layers can be studied by SEM-EDS, hopefully providing a description of the potassium movement, from one layer to the other, as a function of exposure time, temperature, etc. A preliminary experiment has been conducted. Here, a series of two-layer pellets were exposed in a horizontal oven to a flow (1 L/min) of N<sub>2</sub>, O<sub>2</sub> (6%) and H<sub>2</sub>O (about 3%) at 350 °C for up to 7 days. The pellets were made from a 3%V<sub>2</sub>O<sub>5</sub>-7%WO<sub>3</sub>/TiO<sub>2</sub> catalyst and the impregnated layer contained roughly 1.6 wt.% K. The potassium concentration profiles in two pellets, exposed for 2 and 7 days respectively, are shown in Figure 8.

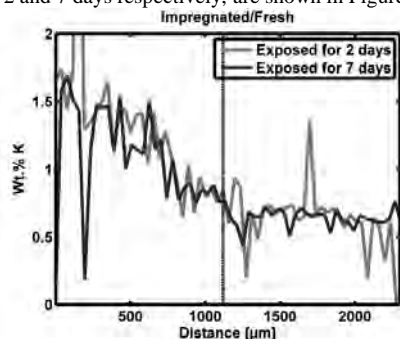


**Figure 8:** Potassium concentration profiles across two-layer pellets.

As seen from the figure, the profiles are more or less overlapping. In both cases the potassium concentration drops from around 1.6 wt.% at the surface of the impregnated layer to a constant level of about 0.7 wt.% in the fresh part. The fact that two profiles are that similar indicates that the potassium diffusion is very fast and/or that potassium is mobile even at room temperature (i.e. further potassium diffusion in the period between ended experiment and time of SEM-EDS measurement). The potassium concentration in the fresh part of the pellets is comparable to the level found in the particle exposed catalyst plate of similar composition (Figure 6). This may indicate that there exists saturation level of potassium. An interesting point

is that no chlorine was found in the exposed samples – neither in the impregnated part nor in the fresh layer. This indicates that chlorine readily leaves at elevated temperatures, e.g. as Cl<sub>2</sub>, and that potassium is bound to something else during diffusion.

A transient model for the potassium poisoning of a single monolith channel of an SCR catalyst is being developed. The model can describe the concentrations of NO and NH<sub>3</sub> along the channel as well as through the catalyst wall, the deposition of potassium rich particles on the catalyst surface, the diffusion and build-up of potassium in the wall, and the resulting loss in SCR activity.

## Conclusion

Vanadia based catalyst plates have been exposed to KCl aerosols in a bench scale reactor through four exposure campaigns, differing only by reactor temperature, exposure time or aerosol characteristics. All exposed catalysts show significant deactivation, however samples exposed at lower temperature (150 °C versus 300/350 °C) have higher remaining activity. Perhaps due to a continued presence of ultrafine particles, plates exposed to an aerosol containing mainly (on a mass basis) particles above 1 micron had lost the majority of their activity. SEM-EDS measurements of the potassium profiles through the thickness of plates exposed at 350 °C for 600 hours show complete penetration of potassium with a constant level across the centre of up to about 0.8 wt.%. A similar potassium concentration was found in the fresh side of exposed two-layer pellets, indicating the existence of a potassium saturation level.

## Acknowledgements

This PhD project is a part of the GREEN Research Center (Center for Power Generation from Renewable Energy) financed by the Danish Council for Strategic Research.

## References

1. H. Bosch, F. Janssen, *Catal. Today* 2 (1988), 369-532
2. P. Forzatti, *Appl. Catal. A* 222 (2001), 221-236
3. N.-Y. Topsøe, *Science* 256 (1994), 1217-1219
4. N.-Y. Topsøe, J.A. Dumesic, H. Topsøe, *J. Catal.* 151 (1995), 241-252
5. J.A. Dumesic, N.-Y. Topsøe, H. Topsøe, Y. Chen, T. Slabiak, *J. Catal.* 163 (1996), 409-417
6. Y. Zheng, A.D. Jensen, J.E. Johnsson, *Ind. Eng. Chem. Res.* 43 (2004), 941-947
7. Y. Zheng, A.D. Jensen, J.E. Johnsson, *Appl. Catal. B* 60 (2005), 253-264
8. J.P. Chen, R.T. Yang, *J. Catal.* 125 (1990), 411-420
9. Y. Zheng, A.D. Jensen, J.E. Johnsson, J.R. Thøgersen, *Appl. Catal. B* 83 (2008), 186-194
10. L. Chen, J. Li, M. Ge, *Chem. Eng. J.* 170 (2011), 531-537
11. Å. Kling, C. Andersson, Å. Myringer, D. Eskilsson, S.G. Järås, *Appl. Catal. B* 69 (2007), 240-251



**Emmanouil Papadakis**

Phone: +45 4525 2808  
E-mail: empap@kt.dtu.dk

Supervisors: Rafiqul Gani  
Krist V. Germaey  
Gürkan Sin

PhD Study  
Started: October 2013  
To be completed: September 2016

## **Modeling and Synthesis of Pharmaceutical Processes: Moving from Batch to Continuous Manufacturing**

**Abstract**

Pharmaceutical manufacturing has been dominated by batch-wise processes which served well both pharmaceutical industries and regulatory bodies in the past. Batch processing has a number of drawbacks which can be eliminated by shifting to continuous manufacturing. The transition from batch to continuous manufacturing can be assisted by using Process Systems Engineering methods and tools. The aim of this PhD study is to use these methods and tools to facilitate the shift towards the continuous manufacturing.

**Introduction**

The delay with the introduction of innovative systems into pharmaceutical manufacturing can be attributed to the regulatory uncertainty. Generally the batch processes are not good for product quality assurance and possess a number of drawbacks such as poor process understanding, low productivity, high energy consumption, high capital cost, low product purity, scalability and waste production [1].

However, over the last decade the regulatory bodies (FDA in USA, EMA in Europe etc.) require the pharmaceutical companies to demonstrate more process understanding in order to improve the efficiency, to reduce the cost and the waste of the development of new pharmaceuticals. Moreover, the pharmaceutical companies need to meet their profit expectations due to increasing research and development (R&D) costs and the competition from generic manufactures [2, 3].

Continuous pharmaceutical manufacturing (CPM) is an attractive option for the pharmaceutical companies. The use of continuous processes naturally eliminates the drawbacks of the batch processes while the flexibility of batch processes can be maintained. Smaller equipment is usually used for continuous processing which mean lower capital cost, less plant space and less utilities requirements. The use of micro-technology and micro-reactors for the continuous synthesis of pharmaceutical products improves the mass and heat transfer in the reactor which results in higher process yield, selectivity, improved safety and scaling up becomes easier. The implementation of on-line control can increase the quality assurance of the final product. Continuous

processing also leads to more sustainable processes development [2].

However, unlike other industries such as chemical, petrochemical or the polymer industry where the continuous manufacturing has been applied and used from many years, pharmaceutical industry is incipient to apply continuous manufacturing. Methods and tools that can be used to model, synthesize, design, optimize and control pharmaceutical manufacturing processes are not advanced, are not mature and have not been used in pharmaceutical processes. This means that currently the pharmaceutical industry relies on previous experience and/or experimental-based methods in order to design and optimize a process; hence the developed process can be expensive, inefficient and time consuming. Therefore, the trend towards to continuous pharmaceutical manufacturing for the production of multiple products increases the need for model-based approaches [4].

Process Systems Engineering (PSE) tools and methods can have essential role in the transition from batch to continuous manufacturing in the pharmaceutical industries. Predictive process models can be developed and used as complement to experiments, to assist the process/product development and to improve the process understanding. Modeling and computational tools such as flow-sheet simulations, global and local sensitivity analysis can assist for the identification of the important process parameters. Application of process analytical technology (PAT) methods and quality by design (QbD) approaches can assist the development of

continuous pharmaceutical processes by improving and ensuring the product quality [4, 5, 6].

### Research Challenges

In the literature numerous examples of cases that the batch process has been converted to continuous process has been reported [3, 6]. However there are still research challenges which need to be overcome in order continuous processing to be applied in pharmaceutical industry. These research challenges have been identified by several authors and are presented in the Table 1.

**Table 1:** Identified challenges which the pharmaceutical industry needs to overcome to move from batch to continuous processing.

Research Challenges
What are the conditions of moving to continuous manufacturing
Development of Process Predictive Models
Predictive solvent selection tools
Development of Dynamic plant wide models
Scale up
Economic Analysis and Sustainability Analysis
Multipurpose production line
Startup and Shut down
Tablet prediction properties
Process intensification and hybrid systems
Research on chemistry
Development of systematic approaches
Required time to change production
Definition of Design Space
Monitoring and control
Development of new chemical synthesis routes

### Objectives

Computer aided methods and tools can be beneficial for the development or retrofit continuous pharmaceutical process because it provides a rapid indication of the economic performance of each process which can be really useful in early decision stage.

The development of a systematic methodology based on computer aided method and tools, is to be studied in this project. This is expected to serve as enabling technology for the industry to facilitate moving from batch to continuous pharmaceutical processing is required. The generic approaches will assist the multipurpose pharmaceutical industry to systematically solve the multiple complex problems. Development of such a methodology requires a knowledge database and a model library. The knowledge library should provide all the relevant information for pharmaceutical product/process development such as reaction mechanisms, reaction kinetics, reactants (substrates, catalysts, and solvents), reaction conditions, properties, and process efficiency. The model library should contain information to describe many unit operations involved in pharmaceutical processes such as filtration, distillation, precipitation (reactive crystallization), crystallization, drying and milling, to describe different kind of reactors and reaction kinetic models and properties prediction models.

Development of plant wide models involving both upstream (synthesis, reaction, etc) and downstream (separation, purification, tableting, etc) unit operations could describe the performance of the integrated process by evaluating the possible disturbances, the cost, and the environmental impact. Plant wide modeling can serve as a tool to evaluate the required time for a certain production line to change between products (multipurpose production line) and to evaluate the amount of the produced waste during the startup and shut down of the process. The systematic framework could be integrated with QbD approaches and PAT methods which need to be developed during the development of the pharmaceutical process in order to guarantee the quality of the product at each stage of the process development.

### Conclusion

In conclusion the objective of the study is the proposal of an integrated framework which can facilitate the move from batch towards the continuous pharmaceutical manufacturing by using process predictive models, solvent selection tools, dynamic plant wide models, process intensification principles, PAT and QbD approaches, and to be applicable in multipurpose production line. The integrated framework is intended as an enabling technology for the development of greener pharmaceutical processes with higher economic feasibility, safer and improved product quality.

### References

1. K. Plumb, Chem. Eng. Res. Des., 83 (6), (2005), 730-738.
2. C. Jiménez-González, P. Poehlauer, Q. B. Broxterman, B.-S. Yang, D. am Ende, J. Baird, C. Bertsch, R. E. Hannah, P. Dell'Orco, H. Noorman, S. Yee, R. Reintjens, A. Wells, V. Massonneau, and J. Manley, Org. Process Res. Dev. 15(4), (2011), 900-911.
3. S.D. Schaber, D.I. Gerogiorgis, R. Ramachabdran, J.M. Evans, P.I. Barton, B. L. Trout., Ind. Eng. Chem. Res. 50 (17), (2010), 10083-10092
4. K.V. Gernay, A. E. Cervera- Pardell, J. M. Woodley, Comput. Chem. Eng., 42, (2012) 30-47
5. A. Rogers, A. Hashemi, M. Ierapetritou, 1, (2013), 67-127
6. A. E. Cervera- Pardell, T. Skovby, S. Kiil, R. Gani, K.V. Gernay, Eur. J. Pharm. Biopharm., 82 (2), (2012), 437-456.



## Michael Jønch Pedersen

Phone: +45 36 43 70 56  
E-mail: mjped@kt.dtu.dk  
mjhp@lundbeck.com  
Supervisors: Kim Dam-Johansen  
Søren Kiil  
Tommy Skovby, H. Lundbeck A/S  
Michael J. Mealy, H. Lundbeck A/S

### Industrial PhD Study

Started: August 2011  
To be completed: July 2014

## Design of Continuous Reactor Systems for API Production

### Abstract

Grignard alkylation of a carbonyl functional group is a very important method for forming new carbon-carbon bonds in the synthesis of small molecule pharmaceuticals. A reevaluation of the synthesis has demonstrated potential for adaptation of the existing batch synthesis to a continuous PFR setup. The active compound Melitracen could be isolated in 86% yield and >99% purity.

### Introduction

The pharmaceutical industry has experienced a significant change over the last decade regarding their manufacturing methods due to regulatory changes. Continuous manufacturing and flow chemistry are believed to cause a major impact on the industry, enabling more safe processes, cheaper production, and conducting chemistry previously not possible in batch, to mention a few. H. Lundbeck A/S has aggressively pursued these new methods, and already has two continuous reactor setups operating in full-scale.

A powerful reaction that is highly suited for being conducted in flow is Grignard reactions, due to the exothermic behavior and fast reaction kinetics. Furthermore, it is a widely applied method for forming of new carbon-carbon bonds. The formation of the antidepressant **4** in figure 1 illustrates such a synthesis that is currently produced by a batch process at Lundbeck.

The reaction between 10,10-DMA (**1**) and DMPC-MgCl (**2**), results in the formation of magnesium alkoxide intermediate **3**. Upon hydrolysis and dehydration, the final product can be precipitated with HCl gas to achieve the salt form of Melitracen HCl (**4**).

The current batch process can be improved in several ways. The existing process uses a two-solvent system for the alkylation, a large molar excess of Grignard reagent **2** compared to ketone **1** is required, and the reaction temperature is relatively high for a simple alkylation. In addition to these potential improvements, the subsequent operation to achieve the final API may be simplified, if the hydrolysis and dehydration steps could be combined. This would furthermore eliminate a phase separation.

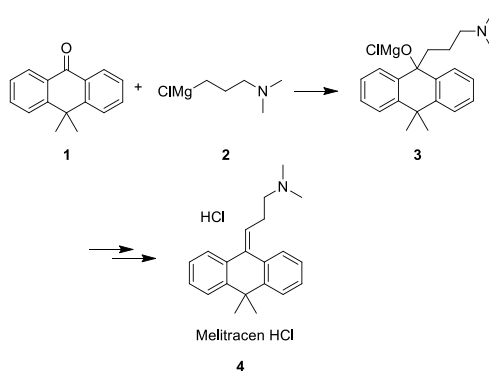


**Figure 1:** The synthesis of the intermediate active pharmaceutical ingredient **3** in Melitracen. A Grignard alkylation between 10,10-DMA (**1**) and DMPC-MgCl (**2**) forms the desired enol intermediate **3**. Upon hydrolysis and dehydration, the final compound is precipitated with HCl gas as its salt form **4**.

### Results

Considering flow chemistry and continuous manufacturing, it is desired that simple flow reactor such as PFR can be used. In order for this to be the case, it requires high solubility of the used reactants and formed products. Given the complexity of a two-solvent system, it is desired to identify if a simpler one-solvent system can be used.

Three potential solvents were screened: toluene, THF and MeTHF. It was found that all of these could be suitable for full-scale manufacturing. In the case of

toluene, trace amounts of ether are still required to stabilize the Grignard reagent. The solubility screening was further done at up to room temperature, as this is the limited temperature for storing the stock solution without the need for heat tracing pipes, etc. THF revealed to have the highest solubility close to 500 g/L at 20 °C for the ketone **1**. The high solubility of **1** in THF, and the possibility to use only one solvent were the main argument for THF as solvent.

The next challenge was to verify if it was possible to separate THF from the aqueous phase after quenching the reaction, while keeping the product in the organic THF phase. Upon aqueous hydrolysis, the system is basic and is a one-phase. The hydrolysis was completed with diluted acetic acid. Ammonium hydroxide solution (25%) was used to adjust the pH to 8, and this operation elicited a phase separation. The product at this pH has distributed itself between the aqueous and the organic phase in the ratio 40:60. The pH was further adjusted to 10, which led to an almost full separation of product into the organic phase.

Based on the initial screening experiment, a set of different acids was tried, to verify if it was possible to do both hydrolysis and dehydration in the same step, and still achieve separation. If possible, a phase separation could be eliminated from the full-scale synthesis. The results of the DoE for one-step hydrolysis and dehydration are presented in table 1. All mixture was adjusted to pH 10 with Ammonium hydroxide solution (25%).

**Table 1:** The products and separation by use of different acids for one-step hydrolysis and dehydration.

Acid (aq)	Product	Separation
HCl	Dehydrated 100%	>99%
AcOH	Alcohol 100%	>99%
HCl/AcOH (1:1)	Dehydrated 90%	>99%
	Alcohol 10%	

A challenge for the hydrochloric acid system was the precipitation of white solid compound after adjusting the pH for the phase separation. No solid can be accepted if a PFR is intended as the flow reactor. The white solid turned out to be magnesium salt of which many are known to have very low solubilities in water. However, they do form a complex with acetic acid that changes their solubility drastically. Another test was done with first adding hydrochloric acid for hydrolysis and dehydration, afterwards adding acetic acid to keep the magnesium salt in solution upon adjusting the pH to 10. This test gave the same desirable results as the pure hydrochloric acid.

The final achievement to overcome before having a setup that could be tested for actual flow chemistry was if the formed Melitracen could be precipitated as its HCl salt form from THF. In that way the last solvent exchange could be avoided likewise the first after the hydrolysis. This was verified by using 2M HCl in DME. The crystallization of the API was not optimized and

conducted at room temperature. Fine white crystals precipitated under these conditions, with a loss in the mother liquid of about 14%. Preliminary analyses indicate that the product is essentially identical to material currently used for tablet manufacturing.

The next step in the process is to verify the flow setup that is seen on figure 2. At present, IR models are generated to follow the conversion of **1** with **2** to form **3**. For the hydrolysis and dehydration, pH will be sufficient enough to follow the process, and IR could be used after phase separation to verify the purity of the Melitracen before HCl precipitation.

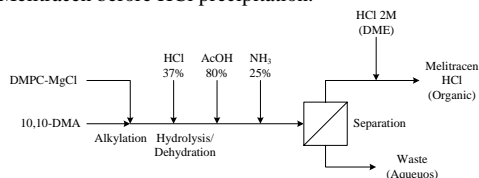


**Figure 2:** Conceptual layout of a setup for continuous manufacturing of Melitracen HCl.

## Conclusion

Exploratory studies to identify a potential continuous manufacturing setup to produce the antidepressant Melitracen hydrochloride have been completed. The new PFR method intended for continuous manufacturing needs to be tested in flow setup in laboratory. Based on the initial demonstration in the screening experiments; it is highly likely to succeed.

## List of Publication

- M.J. Pedersen, T.L. Holm, J.P. Nielsen, T. Skovby, M.J. Mealy, K. Dam-Johansen, S. Kiil, Grignard Alkylation in a Continuous Heterogeneous Reactor Setup, FROST3, Budapest, Hungary, 2011.
- K.M. Christensen, M.J. Pedersen, K. Dam-Johansen, T.L. Holm, T. Skovby, S. Kiil, Design and operation of a filter reactor for continuous production of a selected pharmaceutical intermediate, Chem. Eng. Sci. 71 (2012) 111-117.
- A. Cervera-Padrell, J. Nielsen, M.J. Pedersen, K.M. Christensen, A. Mortensen, K. Dam-Johansen, S. Kiil, K. Gernaey, Monitoring and control of a continuous Grignard alkylation reaction for the synthesis of an active pharmaceutical ingredient intermediate using in-line NIR spectroscopy, Org. Process Res. Dev. 16 (5) (2012) 901-914.
- M.J. Pedersen, T.L. Holm, J.P. Rahbek, T. Skovby, M.J. Mealy, K. Dam-Johansen, S. Kiil, Full-Scale Continuous Mini-Reactor Setup for Heterogeneous Grignard Alkylation of a Pharmaceutical Intermediate, Org. Process Res. Dev. 17 (9) (2013) 1142-1148.

**Thomas Petersen**

Phone: +45 4174 8010  
E-mail: tpet@kt.dtu.dk

Supervisors: Ole Hassager  
Thorvald Ullum,  
GEA Process Engineering A/S  
Jakob Sloth,  
GEA Process Engineering A/S

**Industrial PhD Study**

Started: September 2012  
To be completed: August 2015

## Model of Stickiness in Spray Drying

**Abstract**

Wall deposits are a primary concern in the design of spray drying equipment and the most troublesome type is a result of a property referred to as 'stickiness'. The cause for stickiness is currently not determined conclusively and no accurate models exist for describing stickiness in spray drying quantitatively. It is the purpose of this study to understand the phenomena causing stickiness in spray drying, using modelling tools and rheological measuring equipment. Finally a model which can accurately predict stickiness for the purpose of equipment design is to be produced.

**Introduction**

Spray drying is a well described method for drying particles used in many applications, ranging from food and dairy, through chemicals to pharmaceuticals. Amongst other things it has the advantage of relatively low drying temperatures and well-controlled, uniform particle size distribution. In spite of this some challenges remain with the method, one of the most dominant of which is wall deposits [1]. Deposits can occur for various reasons depending on the condition of the impacting droplet or particle and various techniques are already in use in order to avoid it. Wet particle-wall impact is avoided by use of controlled flow conditions and dry particles that are deposited because of contributions from Van der Waals and electrostatic forces can be removed by using pneumatic hammers or air brushes. However one type of wall deposits remains a problem, namely those caused by what is known as stickiness in the industry. The term stickiness refers to the condition when a material is very close to dry and yet still adheres. Several studies of sticky materials have shown that stickiness of a substance occurs at a temperature close to and above its glass transition temperature  $T_g$  – a point at which a substance changes from a glassy (below) to a rubbery (above) state – some of which are reviewed in [2]. However the range of temperatures (even within the same study) varies between 5-40 °C with no conclusive reason found. Furthermore most of these measuring techniques fail to match the conditions seen during spray drying. As such the phenomena determining stickiness in spray drying

remain unidentified and an accurate measuring technique has yet to be published.

**Specific Objectives**

The purpose of this study is to identify the phenomena determining stickiness. This will be done through both experimental work and mathematical modelling.

The modelling will consist of simulating the impact between a dried droplet and a wall. The material function of the droplet will be described based on empirical rheological measurements. A map of the particles adherence or bounce will be produced with varying parameters such as viscosity, elasticity and surface properties.

Obtaining the rheological data in the relevant regime is a little difficult though given that the materials of interest tend to crystallize in that same regime. As such new methods for measuring these parameters must be developed as well.

The simulations will be validated using a new experimental setup in which drying can be controlled and the impact between the droplet and the wall will be monitored using a high-speed camera.

**Results and Discussion**

In [3] a method for measuring stickiness is presented but more importantly a theory for the relation between glass transition and stickiness is presented which also takes into account the varying temperature difference between stickiness occurring and  $T_g$ . Here it is suggested that the determining parameter is in fact

viscosity which decreases rapidly for increasing temperature just above  $T_g$ . This allows for the formation of liquid bridges between a particle of the sticky substance to a wall or another particle. As such initial model studies using a Finite Element Method (FEM) with the Level Set Method (LSM) will look into the formation and break-up of liquid bridges at various viscosities. This will be combined with rheological techniques used to investigate how the material properties vary near the stickiness point. Based on this it should be possible to determine whether liquid bridges are a primary or minor factor in determining overall stickiness.

A look into the existing stickiness measuring techniques will reveal that they are often associated with a number of problems that make them different from conditions experienced by a particle in spray drying during sticking [2]. The best example is the so-called stirring technique in which a dry powder is stirred with a rod while slowly being wetted at constant temperature. At a certain point the force required to stir the rod will increase sharply and this temperature and moisture content will make up the so-called sticky-point. This technique shows limited reproducibility but there are more distinct problems with it that exemplify the methods used in the literature. First off the technique uses an initially dry powder and wets it. During drying it is obvious that this is reversed thus the history of the particle is different and this could have a significant effect. The second point is that the stirring technique uses a significant number of particles, which makes it difficult to evaluate the stickiness for a single particle meaning it is difficult to discern which phenomena causes the behaviour. An example of where these two problems have been attempted solved is shown in figure 1. Here a particle is dried using equipment at GEA Process Engineering A/S which measures drying conditions accurately and then moved into contact with a plate. Stickiness is then evaluated optically. Figure 1 shows a sticky particle. This method however does not solve the third major problem with the typical technique and showed low reproducibility in the current set-up.

The third major problem is that the system is much less dynamic than the impact of particles with equipment wall during spray drying. This means that the kinetic energy is much lower and contact times are much higher meaning stickiness would most likely occur much easier in the stirring technique than during spray drying. Another technique called the particle gun measuring technique ([4]) exists where dry particles are shot through a moist gas before hitting a plate. The amount of material stuck to the wall is the measure of the degree of stickiness. This technique solves problems 2 and 3, but the conditions for the drops are not as well-known and the first problem is not solved either. As such it is desired to develop a technique during this project which can measure stickiness of particles that are being dried before impacting a wall.

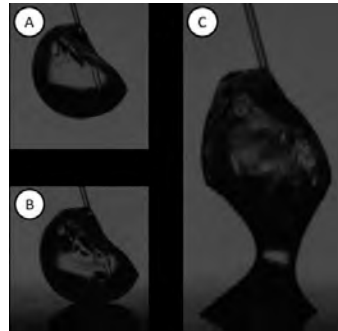


**Figure 1:** Picture exemplifying a sticky particle. A: Partially dried particle hangs from a pin. B: The particle is moved into contact with a plate. C: The liquid bridge is unbroken and the particle sticks to the plate.

### Conclusions

An accurate model would allow improved equipment design for avoiding stickiness in spray drying during operation. Such a model would require knowledge of the phenomena which determine stickiness; however this is not currently available.

Some published results suggest a relation between the change in viscosity occurring at particle temperature just above  $T_g$ , which suggest that the primary cause is formation of strong liquid bridges between particle and wall. Whether this is actually the case can be explored using CFD tools and rheological measuring equipment. Similar approaches can be used to investigate the influence of other parameters on stickiness.

### Acknowledgements

This project is carried out in cooperation between GEA Process Engineering A/S and the DPC group at DTU Chemical Engineering. Furthermore it is partially funded by the Danish Industrial Ph.D. Fellowship Programme administered by the Danish Agency for Science Technology and Innovation.

### References

1. K. Masters, Deposit-Free Spray Drying: Dream or Reality? Proc. Tenth International Drying Symposium IDS '96; Vol. A, 52-60; Krakow, Poland, 1996
2. B. Adhikari, T. Howes, B.R. Bhandari, V. Truong, International Journal of Food Properties, 4 (1) (2001) 1-33
3. K.D. Foster, J.E. Bronlund, A.H.J. (Tony) Paterson, Journal of Food Engineering, 77 (4) (2006) 997-1006
4. J.Y. Zuo, A.H. Paterson, J.E. Bronlund, R. Chatterjee, International Dairy Journal, 17 (3) (2007) 268-273



## Jason Price

Phone: +45 4525 2992  
E-mail: japr@kt.dtu.dk

Supervisors: John M. Woodley  
Jakob Kjøbsted Huusom  
Mathias Nordblad

### PhD Study

Started: September 2011  
To be completed: October 2014

## Fed-Batch Feeding Strategies for Enzymatic Biodiesel Production

### Abstract

In this work a kinetic model for the enzymatic transesterification of rapeseed oil using a solubilised lipase (Callera Trans L-*Thermomyces lanuginosus*) was developed from first principles. The model is then used to evaluate various feeding strategies to improve the enzymatic biodiesel production. The feeding strategies investigated, gave insight into how the methanol should be fed to potentially mitigate enzyme deactivation while improving the reactor productivity and reducing the excess methanol used. The best experimental results gave a yield of 700.6 g FAME L<sup>-1</sup> and a reactor productivity of 29.19 g FAME L<sup>-1</sup> h<sup>-1</sup>. In comparison, to reach the same yield, the optimised two step feeding strategy took 1.28 hours less, which equates to an increase the reactor productivity of 5.6 %.

### Introduction

Descriptions of the various kinetic models for enzymatic transesterification of vegetable oils are quite numerous [1-7]. In terms of determining the optimal methanol feeding profile, the current kinetic models in literature are not able to predict the concentration of the major species over the entire course of the reaction, for changes in the process conditions such as:

1. Alcohol/oil molar ratio
2. Water and Free fatty acid concentrations
3. Different enzyme loadings
4. Interfacial area of the oil–water interface

The aim of this work is to:

- Develop a mechanistic model from first principles that takes into consideration the effects of the process conditions outlined.
- Use the proposed model to evaluate various feeding strategies to improve the biodiesel production while constraining the maximum allowable concentration of methanol in the reactor.

### Model Formulation and Methods

**Model formulation:** The mathematical model describing the transesterification reaction in the biphasic oil–water system with a soluble lipase (Callera Trans L-*Thermomyces lanuginosus*) was formulated on the basis of the following assumptions:

1. The reaction proceeds via a Ping-Pong Bi-Bi mechanism
2. No inhibition by the substrate
3. Competitive alcohol inhibition
4. The interfacial and bulk concentrations of the substrate and products are the same (mass transfer from the bulk to the interface is instantaneous)
5. Acyl migration can be ignored
6. All reaction steps are reversible

By including the interfacial enzyme concentration ( $E$ ), the reaction scheme then proceeds as shown in Table 1. The total specific interfacial area of a droplet ( $a_T$  [m<sup>2</sup>/m<sup>3</sup>]) can be represented as:

$$a_T = \frac{6 V_p}{d_s V} \quad (1)$$

Where  $d_s$  is the Sauter mean diameter of the droplets in the system -  $5.88 \times 10^{-6}$  [m],  $V_p$  is the size of the polar volume [m<sup>3</sup>] and  $V$  is the bulk volume [m<sup>3</sup>].

Given the enzyme coverage  $A_e$  [m<sup>2</sup>/mole], it is possible to calculate the free specific interfacial area,  $a_f$  [m<sup>2</sup>/m<sup>3</sup>] as seen in (2). Note, it is assumed the size of the various enzyme substrate complexes don't vary significantly from the size of the free enzyme [8].

$$a_f = a_T - A_e \cdot (E + EX + ET + ED + EM + ECH) \quad (2)$$

The free specific interfacial area can then be expressed as a concentration ( $A_f$  [mol/ m<sup>3</sup>]) by using the enzyme coverage to estimate a theoretical upper limit of the moles of enzyme molecules that can occupy the interface.

$$A_f = a_f / A_e \quad (3)$$

The mass balance for the system is then combined with the kinetics to give the system of ordinary differential equations presented in Table 1. An illustration of the enzyme and its complexes is presented in Fig. 1.

**Parameter Estimation:** The 20 unknown kinetic constants ( $k_1$ - $k_{10}$ ,  $k_{-1}$ - $k_{-10}$ ) were estimated by minimizing the squared-sum of the relative errors between the simulated and experimental values for  $T$ ,  $D$ ,  $M$ ,  $BD$  and  $FFA$ . Six sets of experimental data and a seventh validation data set (Exp. 1-7) are used to judge the quality of the fitting.

**Methanol Feeding Optimization:** Given that the transesterification reaction is reversible, an excess of methanol is needed to push the reaction to its equilibrium conversion. For this enzyme formulation, at least 1.5 molar equivalents (Eq.) of methanol are necessary (1 Eq. of methanol corresponds to the ratio of 3 moles of methanol to 1 mole of triglyceride).

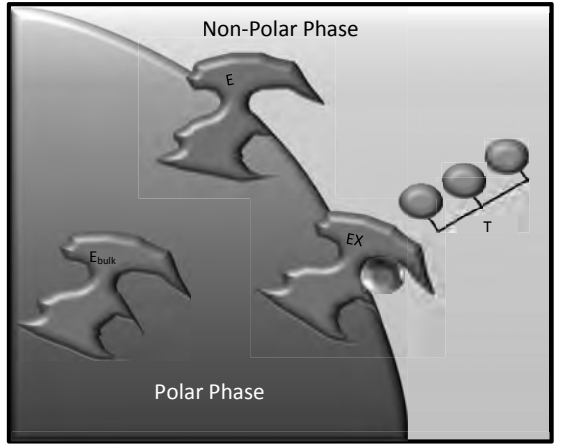


**Fig. 1.** Diagrammatic representation of the enzyme at the oil water interface. The polar phase contains water, methanol, glycerol and the Free enzyme ( $E_{bulk}$ ). The non-Polar phase contains the oil components along with the biodiesel formed. At the interface is the penetrated enzyme ( $E$ ) and the Acyl Enzyme complex ( $EX$ )

Table 1. Rate and differential mass balance equations for a feed batch reactor

	Reactions	Rate of reaction ( $r_i$ )	Differential mass balance Eqns. for Fed-Batch
1	$E_{bulk} + A_f \leftrightarrow E$ Enzyme in bulk absorbed at the interface	$k_1 \cdot [E_{bulk}] \cdot [A_f] - k_{-1} \cdot [E]$	$d([T]V)/dt = -V(r_2)$
2	$T + E \leftrightarrow E.T$	$k_2 \cdot [T] \cdot [E] - k_{-2} \cdot [E.T]$	$d([D]V)/dt = V(r_3 - r_4)$
3	$E.T \leftrightarrow EX + D$	$k_3 \cdot [E.T] - k_{-3} \cdot [EX] \cdot [D]$	$d([M]V)/dt = V(r_5 - r_6)$
4	$D + E \leftrightarrow E.D$	$k_4 \cdot [D] \cdot [E] - k_{-4} \cdot [E.D]$	$d([BD]V)/dt = V(r_9)$
5	$E.D \leftrightarrow EX + M$	$k_5 \cdot [E.D] - k_{-5} \cdot [EX] \cdot [M]$	$d([FA]V)/dt = V(r_8)$
6	$M + E \leftrightarrow E.M$	$k_6 \cdot [M] \cdot [E] - k_{-6} \cdot [E.M]$	$d([G]V)/dt = V(r_7)$
7	$E.M \leftrightarrow EX + G$	$k_7 \cdot [E.M] - k_{-7} \cdot [EX] \cdot [G]$	$d([W]V)/dt = -V(r_8)$
8	$EX + W \leftrightarrow FFA + E$ The acyl enzyme complex can then react with water or methanol (Pong) and then release the second product $FA$ or $BD$ (Ping)	$k_8 \cdot [EX] \cdot [W] - k_{-8} \cdot [FFA] \cdot [E]$	$d([CH]V)/dt = -V(r_9 + r_{10})$
9	$EX + CH \leftrightarrow BD + E$	$k_9 \cdot [EX] \cdot [CH] - k_{-9} \cdot [BD] \cdot [E]$	$d([E]V)/dt = V(r_1 + r_8 + r_9 - r_2 - r_4 - r_6 - r_{10})$
10	$CH + E \leftrightarrow E.CH$ Reversible competitive methanol inhibition	$k_{10} \cdot [CH] \cdot [E] - k_{-10} \cdot [E.CH]$	$d([EX]V)/dt = V(r_3 + r_5 + r_7 - r_8 - r_9)$
Note:			$d([E.T]V)/dt = V(r_2 - r_3)$
1. $T, D, M, G, CH, BD, W, FFA, A_f, E_{bulk}, E, EX, F_a, R_G,$ and $R_W$ are Triglyceride, Diglyceride, Monoglyceride, Glycerol, Alcohol, Biodiesel, Water, Free fatty acid, Free Interfacial area, Free enzyme bulk concentration, Penetrated enzyme, acyl enzyme complex, volumetric flow rate of methanol and the volumetric net rates of production of Glycerol and Water respectively. $E.T$ represents the Enzyme Triglyceride complex formed and extends to the other complexes formed. Units for the concentrations are in mol/ m <sup>3</sup> .			$d([E.D]V)/dt = V(r_5 - r_6)$
2. Intermediate steps for reactions 2 - 9 were grouped together given interest is in the overall rate			$d([E.M]V)/dt = V(r_6 - r_7)$
3. The differential equation to estimate the polar volume neglects the change in density of the system.			$d([E.CH]V)/dt = V(r_{10})$
			$d([E_{bulk}]V)/dt = -V(r_1)$
			$d(V)/dt = (F_a)$
			$d(V_p)/dt = R_o + R_v$



However, high concentrations of methanol will cause the activity of the enzyme to decrease due to methanol inhibition and irreversibly deactivate the enzyme [9]. The mechanism for methanol inhibition is covered in the model presented, however deactivation of the enzyme is not, due to insufficient experimental data to characterise the phenomena. Samukawa and co-workers found that they can increase the reuse of the immobilised enzyme (a clear indication of a reduction in enzyme deactivation), by using a stepwise feeding strategy. This kept the methanol content in the reactor below the concentration that gave the highest initial rate of FAME production [10]. Hence we wished to extend their work by actually being able to maintain the concentration of methanol in the reactor ( $\{CH_{critical}\}$ ) that gave the best initial rate, at each time increment  $t_i$ , while maximizing the objective function in (4).

$$\max_F J_{BD} = \int_0^{t_f} BD \cdot dt - \mu \quad (4)$$

$$\text{Where } \mu = \begin{cases} 0, & CH_{critical} < 0 \\ 1 \times 10^3, & CH_{critical} > 0 \end{cases}$$

The control vector for the methanol feed rate is,  $F = [F_1, F_2 \dots F_N]^T$ , [L/min] and the same experimental settings in Exp. 1-7 are used to investigate how the lower number of feed increments (Opt.1, N=2) and upper number of feed increments (Opt.2, N=20) affects the process.

In Exp. 1-7 the initial amount of methanol dosed was 0.2 Eq. The optimal initial amount of methanol to be dosed is found by using the objective function in (5), by maximizing the initial rate of FAME production ( $IR_{FAME}$ ). A value of 0.525 Eq. is found, and is used in the rest of the simulations as  $CH_{critical}$ .

$$\max_{CH_0} J_{IR} = IR_{FAME} \quad (5)$$

## Results and Discussion

**Parameter Estimates and model validation:** In Fig. 2 the performance of the parameter estimates on the validation data set (Exp.7) is shown. The model captures the dynamics for the five components quite well, however the prediction for the FFA and the MAG show some deviation from the experimental data. The model mismatch observed may be due to the process phenomena not taken into consideration as well as the uncertainty in the parameter estimates. How the uncertainty in the parameter estimates affects the model outputs can be quantified via Monte-Carlo simulations but is outside the scope of this work.

**Feeding Strategy Simulations:** The two feeding strategies simulated (Opt.1 and Opt.2) are able to satisfy the objective function in (4) at each time increment for  $N=2$  and  $N=20$ . One possible measure to ascertain which feeding strategy is better, is to use the FAME yield. For the two feeding strategies simulated, it was possible to increase the FAME concentration throughout the entire course of the reaction as seen in the parity plot in Fig. 3. After 24 hours Exp.7 had the highest FAME yield (700.6 g/L) of all the experiments and a reactor productivity of 29.19 g FAME  $L^{-1} h^{-1}$ . For Opt.1 and

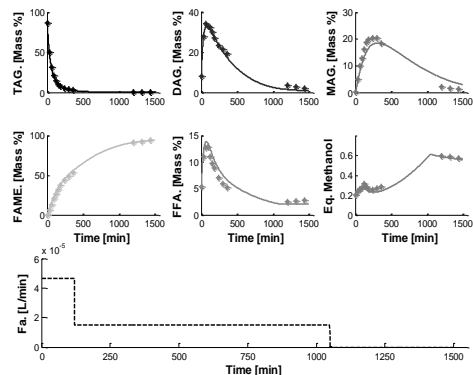


**Fig. 2** Results for validation data set. Squared-sum value of 150.4 [Mass %]<sup>2</sup>

Opt.2 the FAME yield was 704.4 g/L and 704.9 g/L respectively. What this means, from a production perspective, is that using Opt.1's feeding strategy, the reaction could be stopped 1.28 hours earlier and still have the same FAME yield as in Exp. 7. This equates to an increase in the reactor productivity of 5.6 %.

The increase in reactor productivity due to the optimal feeding of methanol can be explained by the plots shown in Fig. 4. For feeding strategies Opt.1 and Opt.2 the concentration of methanol in the reactor is below or at the optimal value of 0.525 Eq. which gave the fastest initial rate. It is known that initial reaction rate increases with increasing methanol content, reaches a maximum, and thereafter decreases when the methanol content is further increased [1]. From the simulations (not shown) this behaviour also occurs during the reaction. Given the methanol concentration never crosses the critical value of 0.525 Eq. for the two feeding strategies; the inhibition is not as severe, as compared to Exp.7 in the latter half of the reaction.

Opt.2 has the highest FAME yield in the end of the reaction compared to Opt.1. This is due to the fact in Opt.2 the methanol concentration stays very close to the critical value given the larger number of feed

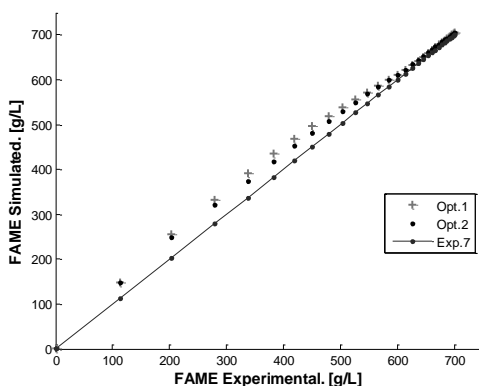


**Fig. 3** Parity plot of the Exp.7 vs. the two feeding strategies. Each point represents 50 minute increments.

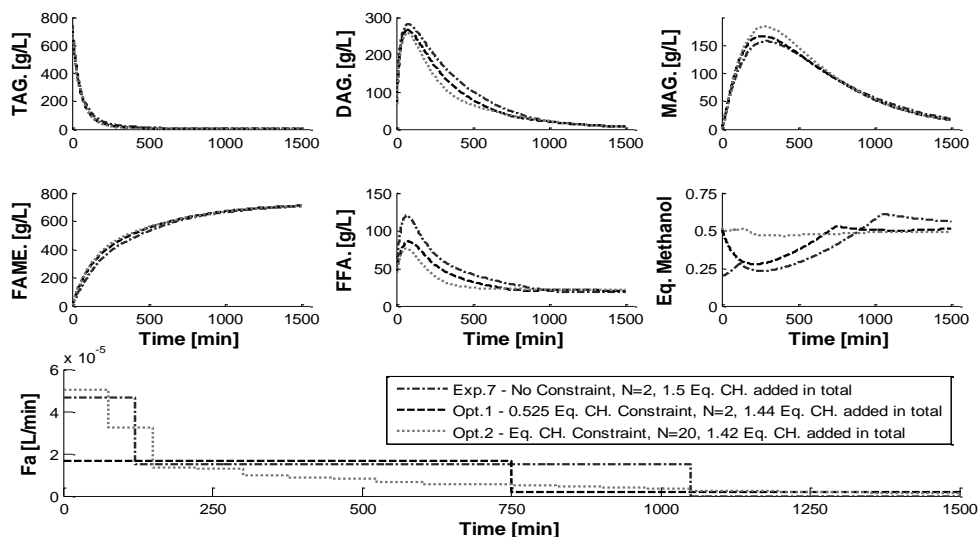


**Fig. 4** Simulation of the feeding strategies for Opt.1 and Opt. 2 along with the simulation results of Exp.7 for comparison

strategies increased the biodiesel yield while decreasing the amount of methanol that needs to be recovered in the downstream processing. For a medium sized 50,000 Ton/yr biodiesel plant this equates to a reduction of  $1.4 \times 10^4$  L of methanol used.

The increase in FAME production for Opt.1 and Opt.2 compared to Exp.7, in the first half of the reaction is due to the increase in methanol concentration. This means there is more methanol substrate to react, giving a faster reaction before the interface is filled with other competing enzyme substrate complexes, which ultimately slows down the reaction in the later half.

Another interesting observation is that Opt.1's (also Exp.7) methanol profile for the first 700 minutes stays below 0.525 Eq. This means the enzymes in Opt.1, is not exposed to as harsh conditions as the enzymes in Opt.2 during the first half of the reaction and may provide a better environment for the enzyme, thereby decreasing the amount of enzyme that is irreversibly deactivated. However this conclusion needs to be validated in the lab by repeated reuse of the enzyme.

## Conclusions

The developed mechanistic kinetic model combined with the reactor mass balance enabled the evaluation of various feeding strategies to improve biodiesel production. Increasing the number of feed increments won't necessarily give a better yield but is dependent on how the methanol is fed to the reactor. It is important that the methanol concentration in the reactor is very close to the critical value to maximize the reactor productivity. In the end, the two optimization feeding strategies, resulted in an increase in the biodiesel, lowered the amount of methanol that needs to be recovered and since the enzymes experiences much

lower methanol concentrations this strategy may very well serve to mitigate methanol deactivation.

## Acknowledgments

The authors will like to acknowledge the work of Vanessa Lampreia Silva and Björn Hofmann who's experimental and analytical work made this study possible. Also this work was partly supported by the Danish National Advanced Technology Foundation (DNATF) whose support is gratefully acknowledged.

## References

1. S. Al-Zuhair, *Biotechnol Progr* 21 (2005) 1442–1448.
2. M. Pilarek, K.W. Szweczyk, *J Biotechnol* 127 (2007) 736–744.
3. B. Cheirsilp, A. H-Kittikun, S. Limkatanyu, *Biochem Eng J* 42 (2008) 261–269.
4. V. Calabrò, E. Ricca, M.d. Paola, S. Curcio, G. Iorio, *Bioproc Biosyst Eng* 33 (2010) 701–710.
5. W. Li, R.-w. Li, Q. Li, W. Du, D. Liu, *Process Biochemistry* 45 (2010) 1888–1893.
6. D. Lv, W. Du, G. Zhang, D. Liu, *Process Biochem* 45 (2010) 446–450.
7. S.N. Fedosov, J. Brask, A.K. Pedersen, M. Nordblad, J.M. Woodley, X. Xu, *J Mol Catal B-Enzym* 85-86 (2012) 156–168.
8. E. Jurado, F. Camacho, G. Luzón, M. Fernández-Serrano, M. García-Román, *Biochem Eng J* 40 (2008) 473-484.
9. S. Al-Zuhair, F.W. Ling, L.S. Jun, *Process Biochem* 42 (2007) 951–960.
10. T. Samukawa, M. Kaieda, T. Matsumoto, K. Ban, A. Kondo, Y. Shimada, H. Noda, H. Fukuda, *J of Biosci and Bioeng* 90 (2000) 180–183.



**Daniela A. Quintanilla Hernández**

Phone: +45 4525 2990  
E-mail: danaquh@kt.dtu.dk

Supervisors: Krist V. Gernaey  
Ole Hassager  
Kim Hansen, Novozymes

PhD Study  
Started: November 2013  
To be completed: October 2016

## **Linking Strain Morphology to Rheology and Mass Transfer as a Means to Improve Fermentation Processes**

### **Abstract**

It is believed that the morphology of filamentous microorganisms at the microscopic and macroscopic level is one of the process variables that it is closely associated with productivity in a fermentation process. However, until now there is no clear evidence of this relation between morphology and productivity, and there is an ongoing discussion around the topic due to the poor understanding of fungal morphogenesis. Therefore as well, fungal morphology is usually a bottleneck for productivity in industrial production, and will be extensively studied in this work. This will allow us to determine whether a certain microorganism's phenotype has an influence on process performance, and how this performance can be influenced actively by manipulating different process variables or by genetic engineering, as a means of improving the design and operation of filamentous fungal fermentations.

### **Introduction**

Fermentation processes for the production of industrial enzymes are under continuous optimization so that the enzymes can be produced with a lower cost. Manipulation of media, strain improvements and various parameter optimizations (pH, temperature, etc.) are among the most relevant strategies for promoting the overproduction of bulk enzymes to meet the global demand [1]. However, further improvements are needed if enzyme cost has to be reduced to make some processes economically feasible. One example of such a process is the production of second generation bioethanol from renewable feedstock, where the enzymes represent one of the major expenses related with the utilization of cellulosic biomass [2].

Production of industrial enzymes is usually carried out as submerged aerobic fermentation, a process that is performed with a substrate, which is either dissolved or remains suspended in an aqueous medium in a closed fermentation vessel where the production microorganism is grown. Filamentous microorganisms are widely used as hosts in these processes due to their ability of secreting large amount of proteins, post-transcriptional modifications machinery and the fact that a large number of species are generally recognized as safe (GRAS). Nevertheless, they also present major disadvantages, due to the unavoidable oxygen transfer limitations as a consequence of the high viscosity of the medium that they develop, which is believed to be related to the biomass concentration, growth rate and

morphology [3]. This last variable is one of the most outstanding characteristics of the filamentous fungus due to its great complexity [4], and will be fully studied in this project.

### **Further Background**

In submerged cultivations one can recognize different types of morphology, which are usually classified as dispersed and pelletized, as shown in Figure 1. According to this first classification the biomass can be found in the form of freely dispersed hyphae or mycelial clumps. Pellets are highly entangled and dense spherical agglomerates of hyphae which can have diameters varying between several hundred micrometers up to several millimeters [5]. Depending on the desired product, the optimal morphology for a given bioprocess varies and cannot be generalized; in some cases both types of morphology are even combined in one process [6], as illustrated in Figure 2.

A pellet type morphology is preferred since it allows for simplified downstream processing and yields a Newtonian fluid behavior of the medium, which results in low aeration and agitation power input. However, the pelleted morphology results in nutrient concentration gradients within the pellet. This situation is obviously not observed in freely dispersed mycelia allowing for enhanced growth and production, which has been attributed to the fact that at the microscopic level the morphology has an influence on the production kinetics, e.g. on the secretion of enzymes. The latter was reported

by Spohr et al. (1997) who observed an increase in protein secretion from a more densely branched mutant of *Aspergillus oryzae* [7]. However, on the macroscopic level this type of morphology greatly affects the rheology of the fermentation broth, and therefore the transport process in the bioreactor increasing the power inputs [7][8].

### Specific Objectives

This project aims to improve fermentation processes by understanding and possibly controlling strain morphology, which is believed to be linked to process productivity. Therefore, the relationships between morphology and productivity will be extensively investigated in this project at the microscopic and macroscopic level, as a means of improving the design and operation of filamentous fungus fermentations. The specific project objectives are:

- In lab scale fermentations, conduct morphological characterization of a filamentous fungus strain at the microscopic and macroscopic level together with the determination of the rheological properties of the fermentation broth.
- Determination of the main process variables influencing the strain morphology and association of specific microscopic morphology with productivity.
- Linking morphology and rheology, and furthermore prove the applicability of the developed model in pilot scale and full scale fermentations.
- Investigate whether rheology can be influenced actively, by modifying strain morphology genetically or by changing process operating mode.

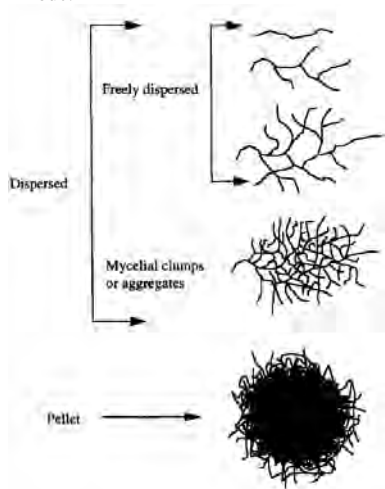


**Figure 1:** Forms of morphology found in typical submerged cultures of filamentous fungi. Adapted from [5].

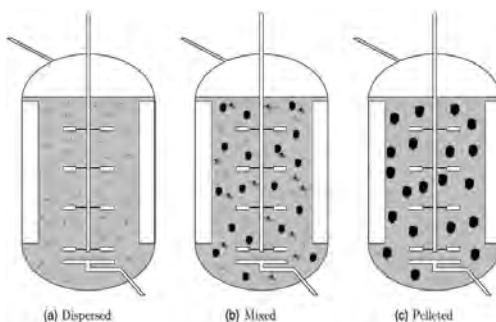


**Figure 2:** The morphology of filamentous microbes cultivated in bioreactors can range from dispersed hyphal elements to distinct pellets.. Adapted from [6].

### Strain

The studies will be conducted on the filamentous fungus *Trichoderma reesei*, specifically on the widely used strain RUT-C30 (ATCC 56765). This microorganism is the host for the production of cellulases, enzymes which are widely used in the production of second generation bioethanol. The strain was constructed after three rounds of random mutagenesis of the wild-type QM6a making it to achieve exceptional levels of protein secretion and activity, [9] which will also allow achieving conditions relevant to those found during full scale production.

### Acknowledgements

The project is funded by the Novo Nordisk Foundation, Novozymes A/S and the Technical University of Denmark.

### References

1. S. Sivaramakrishnan, D. Gandadharan, K. M. Nampoothiri, C. R. Soccol & A. Pandey. Food Technol. Biotechnol., 44 (2006) 173-184.
2. N. Patel, V. Choy, P. Malouf & J. Thibault. Process Biochemistry 44 (2009) 1164-1171.
3. J. J. Smith, M. D. Lilly & R. I. Fox. Biotechnol. Bioeng. 35 (1990) 1011-1023.
4. T. Wucherpfeing, T. Hestler and R. Krull. Microbial Cell Factories 10 (2011) 58.
5. P. W. Cox, C. G. Paul & C. R. Thomas. Microbiology. 144 (1998) 817-827
6. D. J. Barry & G. A. Williams. Journal of Microscopy 244 (2011) 1-20
7. A. Spohr, C. Dam-Mikkelsen, M. Carlsen, J. Nielsen & J. Villadsen. Biotechnol. Bioeng. 58 (5) (1998) 542-553.
8. T. Wucherpfeing, K. A. Kiep, H. Driouch, C. Wirmann & R. Krull. Advances in Applied Microbiology. Elsevier Inc. Oxford U.K., 2010 p. 92.
9. R. Peterson & H. Nevalainen. Microbiology 158 (2012) 58-68.



**Hemalata Ramesh**

Phone: +45 4525 2958  
E-mail: hemra@kt.dtu.dk

Supervisors: John M. Woodley  
Ulrich Krühne

PhD Study

Started: October 2011  
To be completed: September 2014

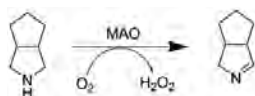
## Identification of Bottlenecks for Biocatalytic Oxidations

### Abstract

Several oxidation reactions are complex to achieve by pure chemical methods. This complexity provides the opportunity for biocatalysis, because biocatalysts provide the access to such oxidation reactions. Although fantastic chemistry is achieved, very few biocatalytic oxidations are implemented at scale. This is a result of several challenges that oxidation reactions pose, for example, inhibition and inactivation of the biocatalyst by substrate(s) and product(s), lack of stability of the biocatalyst and oxygen supply among others. This article provides a systematic methodology for identification of the bottleneck for a select oxidation reaction and provides the potential solutions for debottlenecking and subsequently implementation of this biocatalytic oxidation.

### Introduction

Products from oxidation reactions are increasingly being used for drug synthesis [1]. The combination of high selectivity and the replacement of corrosive oxidants (i.e., oxygen in place of chromates) have promoted the interest for using biocatalysts for industrial oxidations [2]. Several enzymes can be used for selective oxidations. Oxidases and oxygenases are particularly interesting as they have shown to have potential for industrial application [3,4]. These biocatalytic oxidations come with some innate challenges (product toxicity, challenges for oxygen supply etc.) which consequently provide opportunities for process development (such as the use of the so called *in situ* product removal strategy which removes the toxic product from the vicinity of the catalyst). Although cases of substrate and product inhibition and oxygen supply are not uncommon, they are certainly unique to each system. The bottleneck for one system is different from that of another. This project presents a methodology for identification of process related challenges for the implementation of the monoamine oxidase system (Scheme 1).



**Scheme 1:** Overview of the target reaction system chosen to validate the methodology

The reason for choosing this system as the target is that the product is used as an intermediate for producing telaprevir, a drug for the treatment of Hepatitis C [5]. Also, previous studies only serve as a proof of concept that monoamine oxidase can catalyse the reaction [6]. The following discussion represents the first steps towards quantification of the reaction system and consequently bottleneck identification.

### Framework for bottleneck evaluation

In this project, a framework for process evaluation was developed and used to identify the bottlenecks in the target system (Figure 1).

Bottleneck evaluation and process development start with the identification of a target system. Once the reaction system is chosen and the product value is known, we can classify the product into one of the three categories – pharmaceuticals, fine chemicals or bulk chemicals. Based on the product value, specific targets can be set for the reaction system in terms of product concentration required, reaction yield, enantiomeric excess (where relevant) etc. The targets for the select reaction (a pharmaceutical) can be set from literature and is depicted in Table 1[7,8].

Since most naturally occurring biocatalysts are not suitable for direct application, they need to be “improved” to work at process relevant conditions. Thanks to protein engineering strategies, this is now possible. Several mutants of the wild type enzyme can be obtained. These mutants still need to be screened for relevant properties (selectivity towards substrate,

stability etc.), which leads to the next step in the methodology where biocatalysts are screened. The screening can be as simple as the ability to convert the

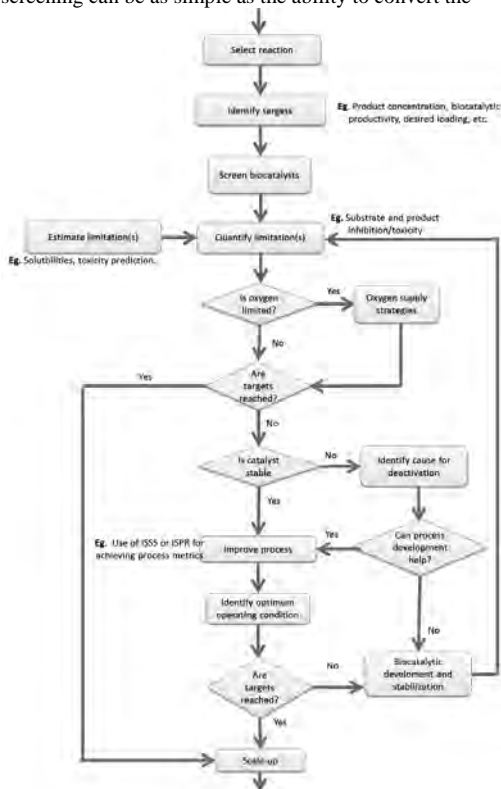


**Figure 1:** Framework used to identify bottlenecks in the target oxidase system.

substrate of interest to the product and then successful mutants can be subjected to further screening by obtaining time-point measurements through the reaction. This would give an insight towards the rate and stability of the catalyst and the best biocatalyst can be chosen.

**Table 1:** Targets for a pharmaceutical product

Parameter	Target
Product concentration	50 g/L
Space time yield (STY)	≥3.7gP/L/h
Biocatalytic yield	10gP/gcdw or 100gP/g free enzyme
Reaction yield	>95%
Optical purity	>99% e.e.
Duration of batch	≤20h

### Quantify limitations

Limitations to a reaction system can arise from reaction characteristics (e.g. thermodynamic limitation) biocatalyst characteristics (toxicity and inhibition) or

substrate and product characteristics (boiling and melting points, solubility, pH stability etc.). While some of these limitations can be identified *in silico* (solubility, thermodynamic equilibrium), others (substrate and product inhibition, stability of biocatalyst etc.) need to be experimentally tested.

### Inhibition of the biocatalyst

For the current case study, inhibition and toxicity of the substrate and the product to the enzyme were determined experimentally. Initial rate measurements at different substrate and product concentrations were used to identify inhibition (Figure 2). The studies indicated that substrate was inhibiting at concentrations above 14 g/L and the product seemed quite inhibitory (and toxic) at even low concentrations (<1 g/L). The by-product hydrogen peroxide also indicated inhibition (Figure 3), but the reaction progress curves indicated that the reaction reached complete conversion (results not shown).

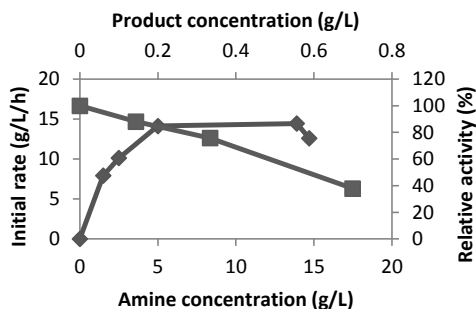


**Figure 2:** The figure depicts the inhibition trends for the substrate (red line) and product (blue line) of the target system. The reaction was carried out in baffled shake flasks which were incubated at 37°C at 150 rpm. The total working volume in the flasks was 20mL. The pH was maintained at 7.65 with 100mM phosphate buffer.

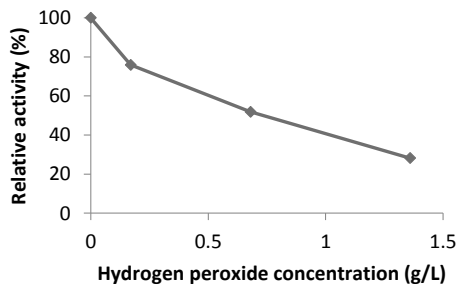


**Figure 3:** Indicates the inhibition of the enzyme by hydrogen peroxide. The figure indicates that the enzyme is inhibited by hydrogen peroxide. Reactions were carried out under the same conditions as substrate and product inhibition curves.

### Inactivation of the biocatalyst

It is of critical importance to estimate if the substrate and product cause irreversible inactivation of the biocatalyst. These phenomena compromise on the stability of the biocatalyst, consequently lowering the potential of using the biocatalyst in the reaction.

### Inactivation by the substrate (amine)

Inactivation of the enzyme by the substrate had to be measured indirectly. By choosing a concentration at which the substrate is not inhibiting the enzyme, the reaction was run in both batch and fed-batch mode. Figure 4 shows the inactivation of the biocatalyst by the substrate.

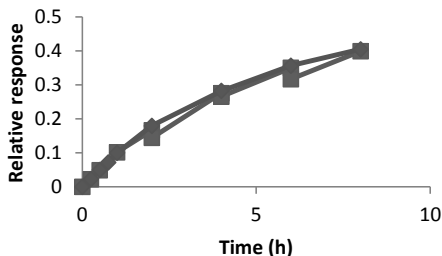


**Figure 4:** The figure represents the relative response obtained in batch (blue line) and fed-batch (red line). Since the batch and the fed-batch reaction follow the same trend, it indicates that there is no inhibition by the substrate.

### Inactivation by product (imine)

Inactivation by product was detected by incubating the cells in the presence of different concentrations of product at 37°C and 150 rpm in a shaker incubator. Table 2 indicates the loss in activity due to the product.

**Table 2:** Inactivation of biocatalyst by the product

[P] (g/L)	0	0.22	0.27
Activity (%)	100	93.06	75

### Inactivation by hydrogen peroxide

Inactivation by hydrogen peroxide was tested by adding a co-catalyst (catalase) to remove the hydrogen peroxide as and when produced. To rule out the issues related to the transport of the catalase to the site of hydrogen peroxide production, the conversion was also tested with crude extracts with catalase. The results are depicted in Figure 5. The figure indicates that the trend of the reaction progress is the same irrespective of the presence of catalase indicating that hydrogen peroxide is not toxic to the enzyme.

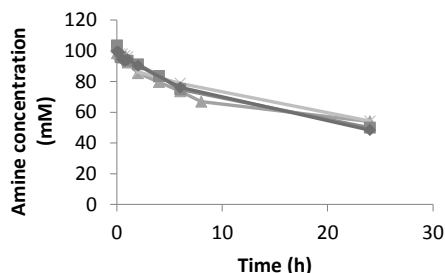


**Figure 5:** Test for hydrogen peroxide inactivation. Substrate concentration: 100mM, Biocatalyst concentration: 3gdcw/L, catalase concentration - 2.5mg/mL. (◇) - whole-cells (control), (Δ) - crude extract, (□) - whole cell with catalase, (○) - crude extract with catalase

### Test for oxygen limitation

Limitation of oxygen was tested by running the reactions at increasing concentrations of the biocatalysts. If the reaction was oxygen limited, the reaction rate will not increase linearly to the biocatalyst concentration. Figure 6 indicates that the reaction rate is linear to the function of cell concentration, indicating that oxygen transfer is not limiting. In a shake flask, 1.48 g/L/h of oxygen transfer is expected. This is less than the oxygen concentration that is required at the given rate of the reaction.

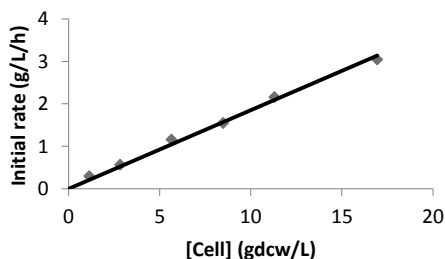


**Figure 6:** Reaction rate as a function of cell concentration to test for oxygen limitation

### Constraints identified

Based on these experiments several constraints have been identified for the system. For producing 50 g/L of the product, at least 68 g/L of the substrate need to be converted in a 20h batch reaction. This will subsequently lead to the order of the constraints explained further.

The first and foremost of these constraints is the expression of the enzyme. To reach the economic targets, about 3-fold improvement on the expression is required.

The subsequent constraint is toxicity and inhibition of the enzyme by the product. To cope with product inhibition, the so called *in situ* product removal strategy can be adopted. One of the possible strategies for exploitation here is the difference in charges between

the substrate and product at pH 9.5. The product is uncharged at this pH which allows the easy adaptation of ISPR using absorptive resins.

The next constraint that would be experienced is inhibition by the substrate. This can be overcome by feeding the substrate.

Following this, the stability might be limiting which can be improved by stabilization methods such as immobilization can be adopted.

Oxygen is not expected to be limited at the target space time yield and biocatalyst concentrations required to meet the economic targets for the system. Figure 7 summarizes the challenges to the system in the sequence they are expected to occur.

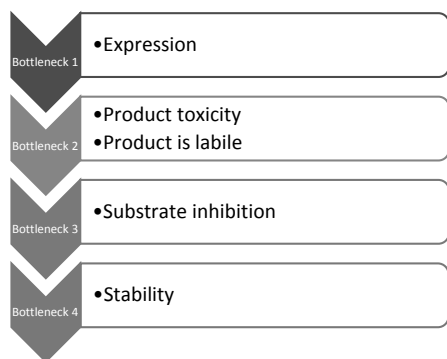


**Figure 7:** Bottleneck analysis for the target system.

### Conclusions

Although the MAO catalyses a very relevant industrial process, it is necessary for the protein expression to be improved for a successful industrial production. Furthermore, at the rate at which the reaction proceeds, it is not limited by oxygen and is therefore not a concern at this very moment. However, with an improvement in the protein expression, the situation is likely different and the focus will shift from the expression to potentially developing the means to keep the biocatalyst stable via process development.

### References

- [1] T. Matsuda, R. Yamanaka, K. Nakamura, *Tetrahedron: Asymmetry*. 20 (2009) 513-557.
- [2] S.G. Burton, *Trends Biotechnol.* 21 (2003) 543-549.
- [3] L. Pollegioni, G. Molla, S. Sacchi, E. Rosini, R. Verga, M.S. Pilone, *Appl. Microbiol. Biotechnol.* 78 (2008) 1-16.
- [4] V. Alphand, G. Carrea, R. Wohlgemuth, R. Furstoss, J.M. Woodley, *Trends Biotechnol.* 21 (2003) 318-323.

[5] A. Znabet, M.M. Polak, E. Janssen, F.J.J. de Kanter, N.J. Turner, R.V.A. Orru, E. Ruijter, *Chemical Communications*. 46 (2010) 7918-7920.

[6] V. Köhler, K.R. Bailey, A. Znabet, J. Raftery, M. Helliwell, N.J. Turner, *Angewandte Chemie International Edition*. 49 (2010) 2182-2184.

[7] J.M. Woodley, in: K. Drauz, H. Gröger, O. May(Eds.), *Enzyme Catalysis in Organic Synthesis*, Wiley-VCH Verlag GmbH & Co. KGaA. Weinheim, Germany, 2012, pp. 217-247. .

[8] P. Tufvesson, J. Lima-Ramos, J.S. Jensen, N. Al-Haque, W. Neto, J.M. Woodley, *Biotechnol. Bioeng.* 108 (2011) 1479-1493.



**Dominik Bjørn Rasmussen**

Phone: +45 4525 2922  
E-mail: dbjra@kt.dtu.dk

Supervisors: Anker Degn Jensen  
Jakob Munkholt Christensen  
Anders Riisager, DTU Chemistry  
Jan Rossmeisl, DTU Physics  
Burçin Temel, Haldor Topsøe A/S  
Poul Georg Moses, Haldor Topsøe A/S

**PhD Study**

Started: December 2011  
To be completed: December 2014

## Selective and Efficient Synthesis of Ethanol from Dimethyl Ether and Syngas

**Abstract**

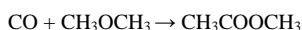
In the present work, carbonylation of dimethyl ether (DME) to methyl acetate (MA) over Mordenite is studied at atomic level with density functional theory (DFT) and experimentally in a high-pressure fixed-bed reactor. The DFT calculations show that MA is primarily formed in the side pockets of Mordenite. In the main channel trimethyloxonium (TMO) is formed, which blocks the active sites. TMO is not formed in the side pockets because of the sterical constraints. Additionally, it is shown experimentally that ketene is a reaction intermediate, in agreement with the DFT calculations. Finally, the amount of hard coke deposited on Mordenite in the DME carbonylation reaction, is found to decrease with increasing reaction pressure.

**Introduction**

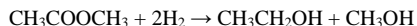
Currently, most transportation fuel is of fossil origin and its use is thereby not sustainable. The steadily increasing prices of fossil fuels and the vulnerability of the global economy to disruption of oil supplies are other factors, making it evident that the demand for alternative fuels will continue to increase. Ethanol (EtOH) can play an important role in this context as gasoline additive or substitute. Catalytic conversion of syngas to ethanol is an interesting option due to its flexibility considering the feedstock and energy efficiency. Syngas can be produced from biomass, making the entire process environmentally friendly.

Catalysts based on Co-MoS<sub>2</sub>, converting syngas directly to EtOH, have been developed [1-3], but their activity as well as selectivity to ethanol is fairly low. In addition, they suffer from the undesirable property of incorporating sulfur compounds into the product, making their industrial use unlikely.

Recently, an alternative, two-step process has been demonstrated [4-7], where DME, formed from syngas, and CO first react to MA:



MA in turn is hydrogenated to EtOH and methanol (MeOH):



MeOH can afterwards be easily converted to DME, using well-established processes. The main benefit of this method is its unprecedented selectivity towards ethanol, while MeOH, the primary by-product, and the unreacted syngas are easily recycled.

The principal challenges that need to be solved before this method can find industrial application are an increase of the activity and stability of the catalyst for MA synthesis. The subsequent hydrogenation of MA to MeOH and EtOH is facile.

A number of acidic zeolites such as H-MOR, H-ZSM-35 and H-FER may act as selective (> 99 mol %) catalysts for synthesis of MA [6, 8-10]. Mordenite has been identified to have the highest initial activity but there is evidence that H-ZSM-35 may have higher long-term stability [6].

The framework of Mordenite contains three types of cavities (Figure 1): 1) the main channel, circumscribed by 12 Si atoms (12 membered ring = 12-MR), 2) 8-MR parallel to the main channel and 8-MR side pockets (SP), which do not interconnect the 12-MR.

Previous experimental [10] study indicates that SP are the sole active sites for MA synthesis. The main reaction products in 12-MR are large aromatic compounds, which block the channels and are coke precursors. It has been shown that the resistance of Mordenite towards deactivation is significantly increased if the acidic sites in 12-MR are blocked [11] or removed [12]. Such a treatment does not affect the activity towards MA. To investigate the effects of the channels, all relevant species and reactions, considered in this work, are studied both in 12-MR and SP. Up to the pressure of 10 bar, MA synthesis has been proposed to be zero- and first-order with respect to the partial pressure of DME and CO, respectively [8].

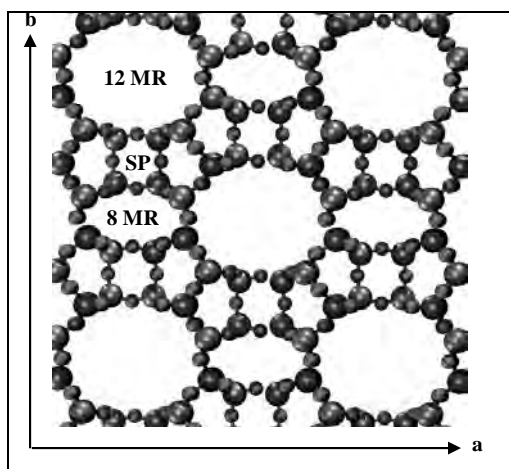


**Figure 1:** View of the main channel of Mordenite along the c-axis. Oxygen-red (small circles), Silicon-blue (big circles).

### Specific Objective

The objective of this work is to improve the understanding of DME carbonylation on Mordenite in a

dual experimental/theoretical study. The reaction is examined at the atomic level with density functional theory (DFT) and a microkinetic model will be developed using the data. Additionally, the activity and stability of Mordenite is tested in a high-pressure fixed-bed reactor to verify the theoretical predictions.

### Methods

All DFT calculations are performed using the GPAW DFT program [13] and the structure optimizations are done with the ASE [14] program package. For all systems, except molecules in vacuum, periodic boundary conditions are applied with a (1,1,2) k-point mesh of the Monkhorst-Pack type and the electronic temperature of 0.1 eV. The real-space grid spacing for all calculations is 0.18 Å. The RPBE [15] and BEEF-vdW [16] exchange-correlation (XC) functionals are employed for calculations on a pure DFT level (without dispersion forces) and DFT-D, including the dispersion forces, respectively. All geometry optimizations are done until the residual force component is below 0.03 eV/Å. In carbonylation reactions the formation energies of the initial/final state ( $E_i$ ) are calculated relative to the system with a methyl group, adsorbed at the same site (8MR or 12MR), and a CO molecule in vacuum. For reactions involving DME, the reference system is extended by a DME molecule in vacuum.

In the experimental work the Mordenite ( $\text{SiO}_2/\text{Al}_2\text{O}_3=20$ ) obtained from Zeolyst (CBV21A) is used. The initial ammonium form is converted to the acidic form, H-MOR, by heating it at 773 K (heating rate 1K/min) overnight in a flow of air. Before the experiments the catalysts are calcined at 773 K in 10%  $\text{O}_2$  in  $\text{N}_2$  for 3h (heating rate 1K/min). The experiments are performed in a high-pressure fixed-bed reactor setup (Figure 2) at a temperature of 438 K and at pressures 10-100 bar. The flow of the reactants (2% DME in CO) in all experiments is 300 Nml/min and the amount of catalyst is 1.500g (particle size 125-250  $\mu\text{m}$ ). The product characterization downstream from the reactor is conducted using an online GC/MS system.

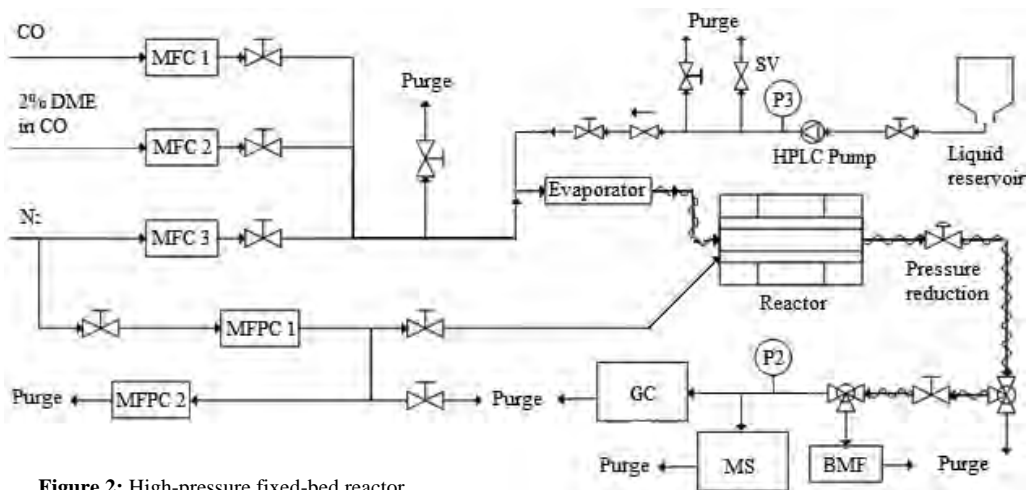


**Figure 2:** High-pressure fixed-bed reactor.

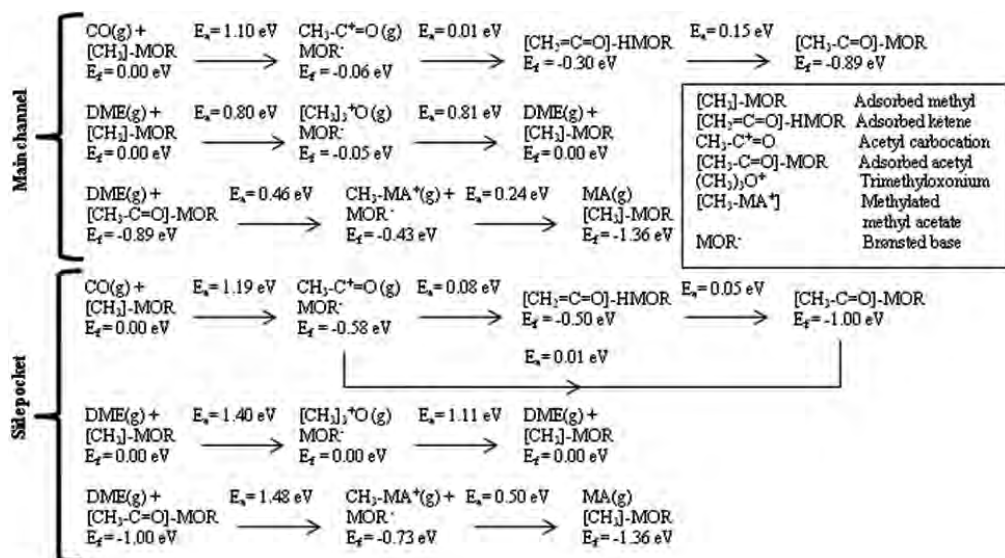


**Figure 3:** Reaction network for synthesis of methyl acetate on Mordenite.

## Results and Discussion

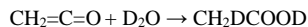
Figure 3 (all energies calculated using BEEF-vdW) shows that formation of methyl acetate mainly occurs in the side pockets because carbonylation of the surface methyl groups and the following formation of surface acetyl can only take place in the side pocket. In the main channel the methyl groups rather react with DME in the process called “DME scrambling”, in which a charged molecule, trimethyloxonium (TMO), is formed. The energy barrier for formation of TMO is 0.3 eV lower, than that for carbonylation, making DME scrambling a significantly faster reaction. TMO is only weakly bound to the surface but it may be enough to block the carbonylation reaction in the main channel. In the side pocket, when a methyl group is carbonylated, first, an acetyl carbocation is formed, which consequently reacts further to ketene and acetyl. The energy barriers for these reactions are very similar and below 0.1 eV so they presumably all occur at high rates.

These findings are in agreement with the literature and in a recent study of Li et al. [17] it has been observed, using in-Situ Solid-State NMR spectroscopy, that acetyl is only formed in the side pockets during DME carbonylation on Mordenite. Very small amounts of methyl acetate were detected in the main channel, which could mean that some of the methyl groups are carbonylated, and then, as Figure 3 shows, the subsequent reactions are swift. Mordenite is known to undergo a fast deactivation, which is attributed to coke formation in the main channel, whereas zeolites with smaller channels are more stable [6]. Deactivation of Mordenite may be related to the

presence of TMO in the main channel and/or oligomerization of ketene, which is relatively weakly bound and probably has some mobility. Bonati et al. [18] has studied aromatic acylation on zeolites, in which ketene is the acylating agent, and proposed that oligomerization of ketene in zeolite pores plays a important role in the deactivation of the H-Beta zeolite.

To verify the theoretical result that ketene is a reaction intermediate, an experiment with heavy water was performed. In the experiment, a DME carbonylation reaction was performed and at the time of maximum MA synthesis rate, heavy water was introduced to the reactant stream.

If heavy water ( $D_2O$ ) reacts with gas phase ketene ( $CH_2=C=O$ ), acetic acid with 2 deuterium atoms and mass 62u is formed:



All other reaction intermediates, which potentially can form acetic acid upon reaction with heavy water, create the isotope with mass 61u ( $CH_3COOD$ ). The results of the experiment are shown in Figure 4. It is seen that the ratio between signals  $m/z=62$  and  $m/z=61$  rapidly increases as heavy water is introduced. There is only a single top for  $t = [2.4-2.9h]$  because once water is added, it reacts with all ketene and acetyl in the system. Methyl groups react faster with water than they are carbonylated, so there is no ketene or acetyl formed as long as there is water in the system.

Figure 5 shows the dependence of the reaction rate of MA synthesis on the total pressure (gas mixture 2 vol% of DME in CO). It is seen that for pressures up to 50 bar, the data points lie on a straight line, in good agreement with the reaction mechanism proposed in the literature. However, for higher pressures the reaction rates are lower than expected, indicating that the true rate expression, also including high pressures, might be different.

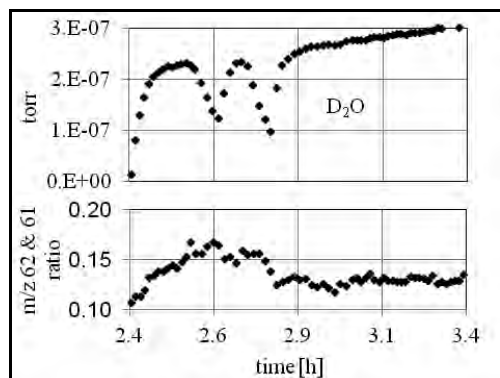


**Figure 4:** Experimental detection of ketene.

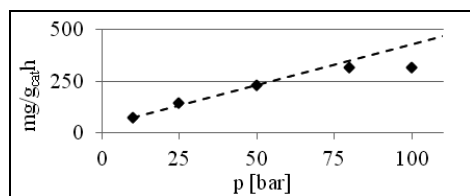


**Figure 5:** Pressure dependence of MA synthesis.

All spent catalysts from the carbonylation experiments have been analyzed in TPO experiments (Figure 6). It has been discovered that the relative amount of hard coke that is formed, is smaller the higher the reaction pressure is (not all data are included for the sake of brevity). The smaller amount of hard coke that is deposited can potentially make a regeneration of the catalyst easier.

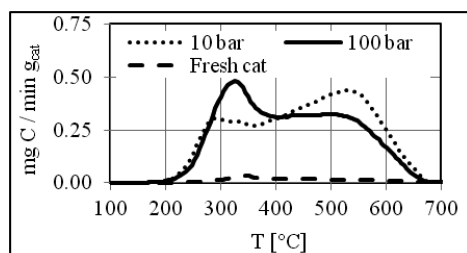


**Figure 6:** TPO analysis of spent catalysts.

## Conclusion

The present work shows that DME carbonylation on Mordenite primarily takes place in the side pockets. In the main channel the methyl groups react with DME,

forming bulky trimethyloxonium (TMO) molecules, which block the active sites. TMO is not formed in the side pocket because of sterical constraints. Additionally, it has been shown experimentally that ketene is a reaction intermediate, in agreement with the DFT calculations. Finally, the amount of hard coke deposited on Mordenite in the DME carbonylation reaction, was found to decrease with increasing reaction pressure.

## Acknowledgments

The project is financed by DTU and the Catalysis for Sustainable Energy research initiative (CASE), funded by the Danish Ministry of Science, Technology and Innovation.

## References

- [1] J.M. Christensen, P.M. Mortensen, R. Trane, P.A. Jensen, A.D. Jensen, *Appl. Catal., A* 366 (2009) 29.
- [2] J.M. Christensen, P.A. Jensen, N.C. Schiodt, A.D. Jensen, *Chemcatchem* 2 (2010) 523.
- [3] J.M. Christensen, P.A. Jensen, A.D. Jensen, *Ind. Eng. Chem. Res.* 50 (2011) 7949.
- [4] X. San, Y. Zhang, W. Shen, N. Tsubaki, *Energy Fuels* 23 (2009) 2843.
- [5] X. Li, X. San, Y. Zhang, T. Ichii, M. Meng, Y. Tan, N. Tsubaki, *Chemsuschem* 3 (2010) 1192.
- [6] J. Liu, H. Xue, X. Huang, Y. Li, W. Shen, *Catal. Lett.* 139 (2010) 33.
- [7] Y. Zhang, X. San, N. Tsubaki, Y. Tan, J. Chen, *Ind. Eng. Chem. Res.* 49 (2010) 5485.
- [8] P. Cheung, A. Bhan, G.J. Sunley, E. Iglesia, *Angew. Chem. Int. Ed.* 45 (2006) 1617.
- [9] A. Bhan, A.D. Allian, G.J. Sunley, D.J. Law, E. Iglesia, *J. Am. Chem. Soc.* 129 (2007) 4919.
- [10] P. Cheung, A. Bhan, G.J. Sunley, D.J. Law, E. Iglesia, *J. Catal.* 245 (2007) 110.
- [11] L. Junlong, X. Huifu, H. Xiumin, W. Pei-Hao, H. Shing-Jong, L. Shang-Bin, S. Wenjie, *Chin. J. Catal.* 31 (2010) 729.
- [12] H.F. Xue, X.M. Huang, E.S. Zhan, M. Ma, W.J. Shen, *Catal. Commun.* 37 (2013) 75.
- [13] J.J. Mortensen, L.B. Hansen, K.W. Jacobsen, *Phys. Rev. B* 71 (2005)
- [14] S.R. Bahn, K.W. Jacobsen, *Comput. Sci. Eng.* 4 (2002) 56.
- [15] B. Hammer, L.B. Hansen, J.K. Nørskov, *Phys. Rev. B* 59 (1999) 7413.
- [16] J. Wellendorff, K.T. Lundgaard, A. Mogelholm, V. Petzold, D.D. Landis, J.K. Nørskov, T. Bligaard, K.W. Jacobsen, *Phys. Rev. B* 85 (2012)
- [17] B.J. Li, J. Xu, B. Han, X.M. Wang, G.D. Qi, Z.F. Zhang, C. Wang, F. Deng, *J. Phys. Chem. C* 117 (2013) 5840.
- [18] M.L.M. Bonati, R.W. Joyner, M. Stockenhuber, *Microporous Mesoporous Mater.* 104 (2007) 217.



**Helena Rasmussen**

Phone: +45 99516262  
E-mail: heras@dongenergy.dk

Supervisors: Anne S. Meyer  
Hanne R. Sørensen, DONG Energy

Industrial PhD Study

Started: October 2012  
To be completed: September 2015

## Degradation Products from Pretreated Biomass

### Abstract

The degradation compounds formed during pretreatment when lignocellulosic biomass is processed to ethanol or other biorefinery products include furans, phenolics, organic acids, as well as mono- and oligomeric pentoses and hexoses. Depending on the reaction conditions glucose can be converted to 5-(hydroxymethyl)-2-furaldehyde (HMF) and/or levulinic acid, formic acid, and different phenolics at elevated temperatures. The reactions are of interest because the very same compounds that are possible inhibitors for biomass processing enzymes and microorganisms may be valuable biobased chemicals. Hence a new potential for industrial scale synthesis of chemicals has emerged. A better understanding of the reactions and the impact of the reaction conditions on the product formation is thus a prerequisite for designing better biomass processing strategies and forms an important basis for development of new biorefinery products from lignocellulosic biomass as well.

### Introduction

When lignocellulosic biomass is processed into biofuels - and potentially other biorefinery products - the biomass is usually pretreated in order to make the cellulose and hemicellulose amenable to enzymatic depolymerization. The biomass pretreatment, particularly pretreatment regimes involving acid and/or temperatures above 160-180 °C, induces formation of degradation products that may inhibit the cellulolytic enzymes and/or the ethanol producing microorganisms (notably yeast, *Saccharomyces cerevisiae*) that are required for the subsequent sugar conversion.

The advances in the recent two years have also revealed that the chemistry of formation of the putative inhibitors during thermal biomass pretreatment for biofuel production have many features overlapping with the discipline of industrial scale synthesis of biobased platform chemicals from glucose and potentially from other biomass monosaccharides [1]. The deliberate production of this type of products from biomass carbohydrates for industrial uses currently only appears feasible via targeted catalytic or biocatalytic technologies [1].

### Biomass Degradation during Hydrothermal Pretreatment

A summary overview of cellulose, hemicellulose and lignin degradation is shown in Figure 1.

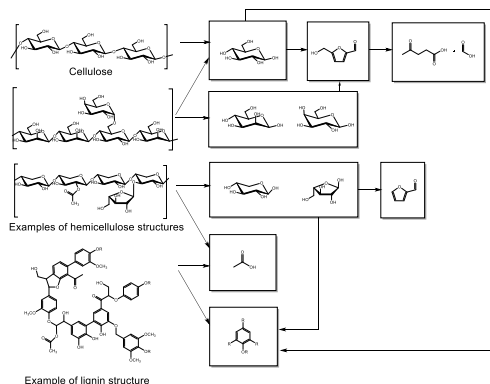


**Figure 1:** Biomass degradation summary overview.

The degradation products include furans, phenolics, organic acids, as well as mono- and oligomeric pentoses and hexoses. These compounds are moreover able to undergo various reactions with each other. Such intermolecular reactions can lead to several new products and polymerization reactions as pseudo lignin and humins.

Pseudo lignin is an aromatic material containing hydroxyl and carbonyl functional groups. In this way pseudo lignin resembles native lignin but is not derived thereof. Recent progress has confirmed that pseudo-lignin can form solely via carbohydrate degradation [2]. Humins are dark coloured substances that are formed during thermal hydrolysis of glucose. Formation of humins has been shown to arise from reaction of HMF with glucose [3] and/or via reaction of HMF with 2,5-dioxo-6-hydroxy-hexanal (hydrated HMF) [4] and subsequent polymerization. The formation of humins via HMF reactions have been reported relatively recently [3][4], and whether, and to which extent, humins impact cellulolytic enzymes and/or yeast during cellulosic ethanol production is at present uncertain.

### Mechanistic Considerations regarding Degradation

Via ab initio molecular dynamics simulations it has been shown that the rate limiting step in the reaction of glucose is protonation of hydroxyl groups on the glucose or direct protonation of the pyranose oxygen. Different protonation sites can lead to different reaction mechanisms and hence different subsequent degradation products [5] as illustrated for glucose in Figure 2.

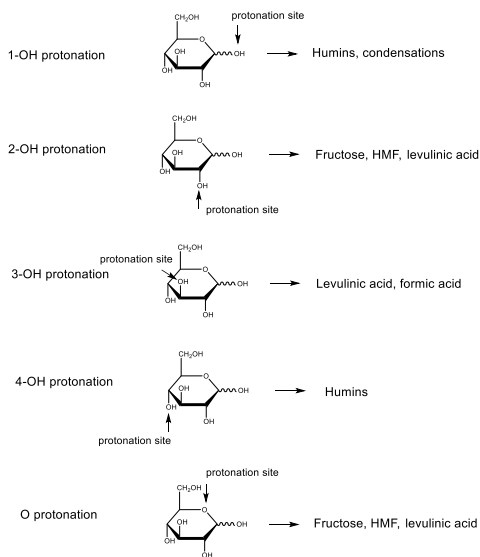


**Figure 2:** Site of protonation and subsequent degradation products from glucose determined by ab initio molecular dynamics in water and quantum mechanics modelling with solvent water.

Solvent water structure is crucial for the protonation site since water molecules compete for protons and hydrogen bond to the hydroxyl groups. In addition, reaction conditions (pH, solvent, salts etc.) can easily alter the water molecule surroundings and hence the

hydroxyl protonation site and the reaction mechanism and the following reaction.

In the literature it has long been discussed which degradation mechanisms and products that are correct [6][7][8] and the key point is that they may all be correct depending on reaction conditions.

It is still to be revealed how actual reaction conditions can be coupled to degradation mechanisms and routes in order to control the degradation product profile. Detailed knowledge about the impact of process conditions is important with respect to cost reduction of biofuel processes, but is also highly relevant for industrial scale synthesis of biomass derived chemicals where the aim is to increase the yield of one or more particular compounds of interest.

### Conclusions

Whether the goal is to reduce or increase degradation/synthesis compounds from lignocellulosic biomass, it is important to understand the chemistry of the degradation or synthesis of compounds.

It has long been discussed which exact reaction routes and mechanisms that lie behind monosaccharide degradation during hydrothermal pretreatment of lignocellulosic biomass. In fact the different reaction routes proposed in the literature may all be correct and may even occur side by side. The site of protonation initiating the monosaccharide degradation determines the mechanism and degradation route and hence the biomass degradation products. Protonation site is depending on solvent water structure surroundings, which in turn depend on the reaction conditions. The key point is thus that degradation product profile is depending on reaction conditions and may potentially be controlled by controlling the process parameters

### References

1. P. Gallezot, *Chem. Soc. Rev.* (41) (2012) 1538-1558.
2. R. Kumar, F. Hu, P. Sannigrahi, S. Jung, A.J. Ragauskas, C. Wyman, *Biotechnol. Bioeng.* (110) (2013) 737-753.
3. J. S. Dee, A. T. Bell, *Chemsuschem* (4) (2011) 1166-1173.
4. R. K. S. Patil, C. R. F. Lund, *Energy Fuels* (25) (2011) 4745-4755.
5. X. Quian, M. Nimlos, M. Davis, D. Johnson, M. Himmel, *Carbohydr. Res.* (340) (2005) 2319-2327.
6. G. Yang, E. A. Pidko, E. J. M. Hensen, *J. Catal.* (295) (2012) 122-132.
7. H. Kimura, M. Nakahara, N. Matabayasi, *J. Phys. Chem* (115) (2011) 14013-14021.
8. X. Qian, *Top Catal.* (55) (2012) 218-226.

### Publications

1. H. Rasmussen, H. R. Sørensen, A. S. Meyer, *Carbohydr. Res* (2013) DOI <http://dx.doi.org/10.1016/j.carres.2013.08.029>



**Helle Christine Ravn**

Phone: +45 4525 6892  
E-mail: hcrv@kt.dtu.dk

Supervisors: Anne S. Meyer  
Lars G. Kjørboe

PhD Study

Started: December 2010  
To be completed: September 2014

## Time of Harvest Affects the Yield of Soluble Polysaccharides Extracted Enzymatically from Potato Pulp

### Abstract

Potato pulp is a co-processing product from potato starch production. The potato pulp pectin is dominated by galactan branched rhamnogalacturonan I which after enzymatic solubilization has shown promising properties as bifidogenic prebiotic fibers. The potato starch processing campaign is based on processing of fresh potatoes (in Denmark the campaign lasts from September to December). Data suggest that potato pulp produced late in the campaign would be preferable for upgrading to the bifidogenic fibers.

### Introduction

Potato pulp is a high-volume, low value by-product resulting from industrial production of potato starch. Currently, this pulp is not upgraded to any significant degree, and the enormous amounts available create a large incentive for developing effective processes for its utilization and valorization. A key feature of the potato pulp cell wall polysaccharides is their high content of galactose and galacturonic acid. The main type of cell wall polysaccharides in potato pulp is pectin in the form of homogalacturonan (HG) and notably rhamnogalacturonan I (RG I), of which the latter is predominantly branched with high molecular weight, linear ( $\beta$ 1,4-)galactan and arabinogalactan side chains. The high-molecular weight RG I galactan polysaccharides may make up a high-value functional food ingredient product, due to their documented effects as fermentable dietary fibers in humans [1]; weight gain retarding effects in rats [2], and prebiotic bifidogenic potential [3] [4]. In order to particularly target the solubilization of the high-molecular weight galactan fibers of the RG I region of the potato pectin, we recently developed a minimal enzymatic treatment procedure based on catalyzing the breakdown of the HG surrounding the RG I regions by use of a combination of mono-component pectin lyase (EC 4.2.2.10) attacking mainly the  $\beta$ 1,4 bonds of methoxylated galacturonic acids and polygalacturonase (EC 3.2.1.15) attacking mainly the bonds between non-methoxylated galacturonic acid residues in HG [3]. During the potato starch campaign, which e.g. in Denmark usually sets off in early September and terminates in the middle of

December, and is based exclusively on processing of freshly harvested potatoes, potatoes of slightly different ripeness or maturity are processed. Hence, the optimal time point for obtaining maximal yields of enzymatically solubilized potato polysaccharides within the potato starch campaign may be hypothesized to be dependent on a possible inherent effect of the potato maturity and may also depend on the potato pulp composition. The objective of this study was to test this hypothesis by examining if the yields of enzymatically solubilized potato polysaccharides correlated with the pulp composition, and whether an optimal time, i.e. early or late in the campaign, could be identified for this enzymatic upgrading of the pulp.

### Methods

The monosaccharide compositions of seven crude potato pulp samples as well as the monosaccharide compositions and sizes of the released potato polysaccharides from the seven potato pulp samples were determined in order to characterize and map any differences in the enzymatically released potato polysaccharides during the potato starch campaign.

### Characteristics of enzymatically released potato polysaccharides

The building blocks of the galactan RG I structure, i.e. the contents of arabinose, galactose and galacturonic acid – were all found to significantly ( $p < 0.05$ ) increase within the potato starch campaign, whereas the content rhamnose was found to be constant ( $p > 0.05$ ). Some variation in the yields of the enzymatically released

potato polysaccharides (calculated in percent as total amounts of polysaccharides relative to the initial amount of starch free dry matter) was seen across the campaign (see Figure 1). From the compositional analysis, and as expected, the majority of the enzymatically released high molecular weight potato polysaccharides were presumably made up of galactan, subsidiarily arabino-galactan.

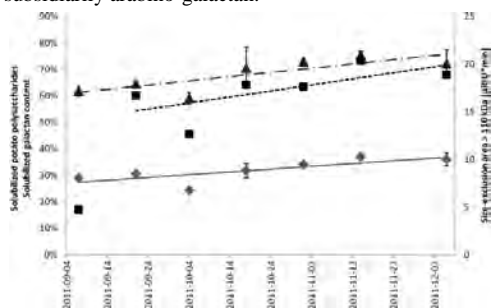


**Figure 1:** Plots and statistical analysis of enzymatically solubilized potato polysaccharide characteristics: Straight-line relationships between time within the potato starch campaign and solubilized potato polysaccharides (—●—), solubilized galactan content (---▲---), and the size-exclusion area of structures of more than 110 kDa (---■---). The size-exclusion data point for the time point 2011-09-07 was not included in the statistical data analysis, as it was considered as an outlier. Solubilized potato polysaccharides and solubilized galactan content are displayed on the primary axis, whereas the size-exclusion data is displayed on the secondary axis. The following parameters and fits were given by the modeling of the straight-line relationships in SAS JMP®: solubilized potato polysaccharides:  $y = -41.28 + 1.22 \times 10^{-8}x$ ,  $R^2 = 0.539$ , and  $p = 0.0002$ , solubilized galactan content:  $y = -62.21 + 1.85 \times 10^{-8}x$ ,  $R^2 = 0.507$ , and  $p = 0.0003$ , and size-exclusion area >110 kDa:  $y = -2455.78 + 7.2686 \times 10^{-7}x$ ,  $R^2 = 0.454$ , and  $p = 0.1423$ .

## Discussion

The monosaccharide composition of the crude potato pulp did not influence to the yield of enzymatically extracted potato polysaccharides. However, the polysaccharide solubilization efficiency was significantly higher late in the potato starch campaign, regardless of the approach to evaluation. The total amount of solubilized potato polysaccharides thus increased during the campaign, just as the sum of the amounts of monosaccharide solely deriving from rhamnagalacturonan I with hairy regions, and the proportion of solubilized galactan also increased. Especially the increase in proportion of solubilized galactan is important as the bifidogenic effect is mainly triggered by the galactan side chains [3]. The presence and location of the galactan and arabinan side chains of RG I are usually correlated with stages of cell and/or tissue development. Potato microsomal membranes contain enzymes that both initiate and elongate  $\beta$ 1,4-

galactan side chains of RG I [5]. Even if this theory has not been unequivocally proven for the actual plant cell wall galactans, the findings that galactan yields increased during the campaign thus may be explained by the potentially higher levels of available galactan after longer action of elongating enzymes as the potato matures during season. The increase in solubilized potato polysaccharides late in the potato starch campaign is probably caused by natural modifications during maturation of the potatoes, such as either a “loosening” of the HG backbone egg-box structures, e.g. via cessation of potato pectinmethyl esterase (EC 3.1.1.11) expression involved in developing robust HG egg box structure zones during potato tuber maturation [6]. Other more indirect effects such as those resulting from e.g. down-regulation of the expression of cell wall strengthening “tyrosine-and lysine-rich protein” (StTLRP) involved in developing the cell wall robustness of potatoes during growth (notably the skin layer cell walls) [7] cannot be excluded.

## Conclusion

These results provide a guide for optimal biorefining of potato pulp for the industrial production of soluble polysaccharides. Only minor variations were detected in the crude potato pulp samples collected during the potato starch campaign. However, the yield of soluble potato polysaccharides increased during the potato starch campaign just as the proportion of solubilized galactan suggesting collecting potato pulp for production of soluble potato polysaccharides at the end of the potato starch campaign.

## References

1. M. Olesen, E. Gudmand-Hoyer, M. Norsker, L. Kofod, J. Adler-Nissen. *Eur. J. Clin. Nutr.* 52 (2) (1998) 110-114.
2. H.N. Lærke, A.S. Meyer, K.V. Kaack, T. Larsen, *Nutr. Res.* 27 (3) (2007) 152-160.
3. L.V. Thomassen, L.K. Vignsnaes, T.R. Licht, J.D. Mikkelsen, A.S. Meyer, *Appl. Microbiol. Biotechnol.* 90 (3) (2011) 873-884.
4. M. Michalak, L.V. Thomassen, H. Roytio, A.C. Ouwehand, A.S. Meyer, J.D. Mikkelsen, *Enzyme Microb. Technol.* 50 (2) (2013) 121-129.
5. B.L. Ridley, M.A. O'Neill, D. Mohnen, *Phytochemistry* 57 (6) (2001) 929-967.
6. R.P. Sabba, E.C. Lulai, *J. Am. Soc. Hortic. Sci.* 130 (6) (2005) 936-942.
7. J.D. Neubauer, E.C. Lulai, A.L. Thompson, J.C. Suttle, M.D. Boltona, I.G. Campbella, *J. Plant Physiol.* 170 (4) 2013 413-423.

## List of Publications

- H.C. Ravn, M.L. Damstrup, A.S. Meyer, *Biocatal. Agr. Biotechnol.* 1 (2012) 273-279.  
H.C. Ravn, A.S. Meyer, *Food Bioprod. Process.* (2013) *In Press.*  
H.C. Ravn, O. Bandsholm, A.S. Meyer, *Process Biochem.* (2013) *In Press.*





**Rolf H. Ringborg**

Phone: +45 61663013  
E-mail: rolri@kt.dtu.dk

Supervisors: John Woodley  
Ulrich Krühne  
Krist V. Gernaey

PhD Study

Started: October 2012  
To be completed: September 2015

## $\mu$ -Tools for Development of $\omega$ -Transaminase Processes

### Abstract

The focus of this project is to develop  $\mu$ -technology and toolboxes that can be used for feasibility screening of new processes. The development will focus on the enzyme  $\omega$ -transaminase, this catalyst has shown challenging difficulties in relation to thermodynamics and economic feasibility. It is believed that the use of microtechnological methods will contribute to the exploitation of  $\omega$ -transaminase based technology significantly. Microtechnology will reduce the quantity of expensive and/or scarce resources needed for evaluation of potential process candidates. The technology should also potentially help to reduce the development time of biocatalysis based processes. The project is part of a European collaboration called BIOINTENSE and also features a consortium of 14 partners

### Introduction

Biochemical process development is currently based on screening. The investigation is most likely performed in shake flasks or in well plates. These techniques often yield poor control and low data density (end-point measurements). Most of all is highly labor intensive and yields often in an uncertain foundation for selection. It is the vision of this project to fabricate an easy building block process tool, that will yield the possibility to quickly and with high confidence analyze the potential of a biocatalyst. For transaminase processes it is explicitly essential to have a flexible design space as each reaction requires a unique design. The project will therefore focus on development of such a platform as a tool for transaminase exploitation. The biocatalyst  $\omega$ -transaminase ( $\omega$ -TA) is asymmetrically exchanging a ketone with an amine group [1], see **Figure 2**.

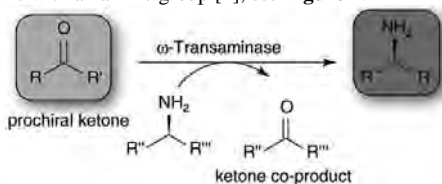


**Figure 1:** Asymmetric synthesis of prochiral ketones [1]

This transformation produces chiral amines of 99% enantiomeric excess (ee), which is essential for the production of pharmaceuticals [2]. Compared to traditional organic chemistry this feature is

unprecedented, that normally produces racemic mixtures. These mixtures are very difficult to separate due to the similarity between the two enantiomers. On top of that, the maximum yield is halved as one of the aminated enantiomers renders useless [3]. The unfavorable downstreaming and loss of product is the downside of traditional amination. The downside to  $\omega$ -TAs is that they have in many cases unfavorable thermodynamics, yielding low product concentration. It will therefore be a requirement to shift the equilibrium to the more advantageous side. In this project, both standard and newly developed procedures of product removal, substrate delivery and even cascade reactions will be tested. An example of a cascade reaction is the synthesis of 1-phenylamine from acetophenone is conducted L-alanine as amine donor (see **Figure 2**).

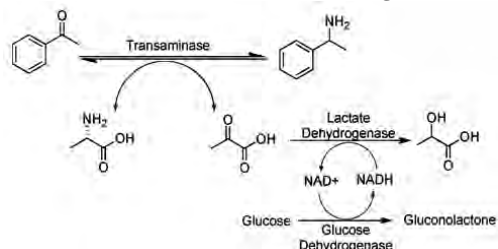


**Figure 2:** displaying the reaction scheme for synthesis of 1-phenylamine by  $\omega$ -TA [4]

The amine donor will be converted to pyruvate as a co-product and can further be removed by lactate dehydrogenase (LDH). The LDH reaction is NADH dependent and NADH has to be regenerated for the process to become economically feasible. Glucose dehydrogenase (GDH) can be added and will promote the NADH regeneration. This specific cascade reaction, consisting of three biocatalyst facilitated reactions, is shown in the reaction scheme, in **Figure 2**. The complexity of the transaminase reactions is high and requires accordingly a high level of control. This can be provided with microscale equipment due to the miniaturization. When changing from lab to micro scale the majority of the effects can be described by. In particular the smaller intrinsic volume, larger surface-to-area ratio and small characteristic length. The microchannels will have well defined laminar flow, where heat and mass transfer will mainly be governed by diffusion/convection. Furthermore the heat and mass transfer will also be rapidly completed due to short diffusion distances (channel width).

The science of biocatalysts is based on empirically validated models, and the most effective way to obtain data for these is by screening, which is another reason to use microscale setups. Due to the small volumes it is possible to reduce the substrate and enzyme consumption significantly. This is especially suitable for screening of biocatalysts, as newly expressed enzymes will only be available in small quantities. The developed platform is therefore envisaged to be a very cost effective method for biocatalyst evaluation. The following parameters have been identified by the PROCESS group in order to reach overall economy of a biocatalytic process (**Table 1**).

**Table 1:** Success factors for the economic feasibility of a biocatalytic process [5]

<b>Biocatalyst formulation</b>	
Retention of activity	High
Stabilization	Improve catalyst productivity > 5 times
<b>Reaction</b>	
Product concentration	>50 g/L
Catalyst productivity	100-250 g product/ g free enzyme (crude) 50-100 g product/g immob. Enzyme
Stereoselectivity	> 98% ee
Yield	>90%

These parameters will be used as a minimum requirement for the development of the platform. A protocol will hereafter be made for data collection, the procedure will be done in an iterative manner where a structured framework will be developed and tested. This is done to direct future labwork towards collecting only essential data for process development.

### Specific Objectives

- Develop a microtechnology platform with reactor, analytics and downstreaming.
- Numerical evaluation of the platform by computational fluid dynamics
- Create protocols for experiments and data collection
- Test and develop  $\omega$ -TA process
- Create a decision algorithm for biocatalytic process development
- Investigate methods for shifting the equilibrium towards product formation
- Evaluate sources of amine donors

### Results, Discussion and Conclusions

The projects consortium consists of leading scientists and companies within transaminase and microtechnology. It has competences within fabrication, process development, sensor development, computational fluid dynamics, microreactor development, strain engineering, enzyme expression etc. The project is made with a very pragmatic view on the problem of biocatalyst development, the consortium associated with the project has also been chosen strictly related to the technology that they offer. Integrating the different parts of the consortium yields great possibilities for a success of the project. The end product is desired to be more than a Ph.D thesis, it should be a biocatalyst process development manual. It should be noted that the technology's scope is focused at the fine chemical and pharmaceutical industry as these will be the main producers of optical pure solutions of chiral amines.

### Acknowledgements

Many thanks to the European Union for funding this project.

### References

1. D. Koszelewski, K. Tauber, K. Faber and W. Kroutil, Trends in Biotechnology 28 (2010) 324-332.
2. J. M. Woodley, Trends in Biotechnology, 26 No. 6 (2008) 321-327
3. P. Tufvesson, J. Lima-Ramos, J. S. Jensen, N. Al-Haque, W- Neto, J. M. Woodley, Biotechnology and Bioengineering, 108 (2011) 1479-1493.
4. M. D. Truppo and N. J. Turner, Org. Biomol. Chem. 8 (2010) 1280-1283.
5. P. Tufvesson, W. Fu, J. S. Jensen, J. M. Woodley, Food Bioprod. Process, 83 (2010) 3-11



## Inês Pereira Rosinha

Phone: +45 4525 2993

E-mail: inros@kt.dtu.dk

Supervisors: Ulrich Krühne  
John M. Woodley  
Krist V. Gernaey  
Anders Daugaard

### PhD Study

Started: November 2012

To be completed: October 2015

## Optimisation of a Microbioreactor Configuration for Enzymatic Production of Chiral Amines

### Abstract

The synthesis of chiral amines plays an important and growing role in the development of new pharmaceutical and agrochemical and building blocks. Most of the biocatalytic reactions for chiral amine production take place under unfavourable equilibrium conditions such as product and reactant inhibition. This project focuses on the development of procedures for shape and topology optimisation of miniaturized reactor geometry in order to improve the yield of chiral amine production inside of a microreactor. This project consists of a development of a systematic shape optimisation procedure for a YY-microreactor using an interface between Matlab and ANSYS CFX®. From the results, it was possible to evaluate the influence of the mixing versus the kinetics in the shape optimisation.

### Introduction

Optically pure chiral amines are valuable compounds for a wide range of applications; they can for example serve as intermediates for synthesis of pharmaceutical and agrochemical active ingredients. The current synthesis of optically pure chiral amines is dominated by chemical processes which are rarely enantiomerically selective enough. Biocatalytic synthesis of these compounds using for example  $\omega$ -transaminase ( $\omega$ -TAm) as a biocatalyst has several advantages such as versatility regarding the substrates, mild reaction conditions, high stereoselectivity and high enantioselectivity.<sup>[1,2]</sup> Although the use of  $\omega$ -TAm, for production purposes, is very attractive for industrial application, limitations inherent TO the whole process development make it a very challenging reaction system. These limitations include the unfavourable equilibrium and substrate and product inhibition.

The challenges concerning the biocatalytic process development are the high cost of the enzymes at an early stage, as well as limited enzyme availability, preventing bench-scale process screening. For this reason, microsystems are a good alternative, since they enable a high throughput or high content screening of process parameters, reaction kinetics, solvents or materials. However they are thus far broadly used in the field. Microfluidic systems in particular have demonstrated several advantages in (bio)chemical processes, especially due to the very large surface-area-to-volume-ratio, combined with very effective heat and

mass transfer, easier control of process parameters and the potential of introducing new synthesis concepts by numbering up, instead of scale-up for the increase of production capacity.

The complexity of enzymatic reactions, combined with the versatility of microsystems fabrication, gives a clear motivation to explore the influence of the microreactor shape on the production yield.<sup>[3,4]</sup> The purpose of this mathematical optimisation study is to configure beforehand an optimal reactor design and to test right away the best predicted geometry. Hence, it should be possible to cut down on the fabrication costs of the miniaturized reactor system while demonstrating the validity of the mathematical optimisation procedure.

### Optimisation Case Study

This computational fluid dynamics (CFD) simulation investigated a microbioreactor for the production of optically pure chiral amines.

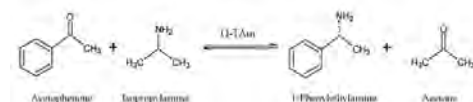
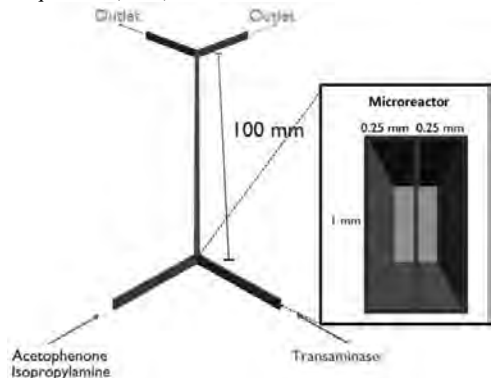


Figure 1: Model reaction for microreactor optimisation

The chosen model reaction consisted of the synthesis of the chiral product (*S*)-1-phenylethylamine from acetophenone by using  $\omega$ -transaminase as biocatalyst.

Isopropylamine is the amino donor which is converted into acetone by the same reaction.  $\omega$ -TAM is known for following the Ping Pong Bi Bi mechanism. The kinetic parameters specific for this reaction system were determined and fit to the enzymatic mechanism by Al-Haque *et al.* (2012).<sup>[4]</sup>



**Figure 2:** Initial configuration of the microreactor.

The initial shape of the studied microreactor consisted of a YY-microchannel with a rectangular cross-section

where the inlet and the outlet are located at the respective ends of the reactor (Figure 2).

Both inlet and outlet consisted of a Y shape where two streams meet at the entrance of the flow chamber and are split into two streams at the exit of the chamber. The flow chamber consists of a channel without divisions. The initial configuration has the following dimensions: 0.25 mm of width for each inlet and outlet, 1 mm of height and 100 mm of length. (See Figure 2) The optimisation routine focuses on the modification of the microreactor shape parameters such as height and width of the inlet and outlet. The length is maintained constant during the optimisation routine.

The residence time inside of the microreactor is 30 minutes for all simulations. Since the volume of the microreactor varies from simulation to simulation, the flowrate has to be adjusted in order to maintain the residence time.

For an optimisation it is necessary to define the objective function and restrictions. In this study, the objective function is the concentration of product at the outlet of the microreactor because it is the parameter that is not related to the modifications of the reactor configuration and therefore it is possible to compare it between simulations. For example, the amount

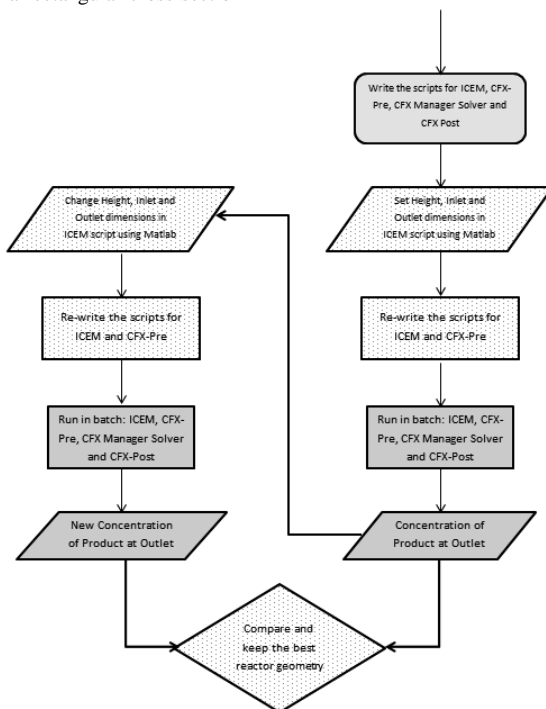


**Figure 3:** Detailed optimisation procedure of the microreactor using an interface between Matlab and ANSYS CFX®: operation made by Matlab and operation performed by ANSYS CFX®

produced depends on the flowrate and the last one is adjusted for each simulation. Therefore, the amount produced cannot be used as objective function. The established restrictions were linked to the width of inlet and outlet (sum of both inlet/outlet channels) and the height of the reactor. The lowest dimension was decided on the basis of the fabrication limitations and the highest were based on the limitations of a microsystem (1000  $\mu\text{l}$ ). The limiting dimensions are summarized in Table 1.

**Table 1:** Geometry restrictions for the simulation setup

	Height (mm)	Inlet (mm)	Outlet (mm)
<b>Minimum</b>	0.4	0.2	0.2
<b>Maximum</b>	10	1	1

At the inlet, the concentrations are the following: 10 mM of Acetophenone, 0.5 M of Isopropylamine and 0.0759 M of  $\omega$ -TAM. In microfluidics, mixing by diffusion plays an important role. In this case, there were considered two slow diffusing compounds: Acetophenone ( $1 \cdot 10^{-13} \text{ m}^2 \text{ s}^{-1}$ ) and  $\omega$ -TAM ( $1 \cdot 10^{-12} \text{ m}^2 \text{ s}^{-1}$ ). All the other compounds involved in this reaction system were considered to have the same diffusion coefficient,  $1 \cdot 10^{-9} \text{ m}^2 \text{ s}^{-1}$ .

### Optimisation Procedure

The routine implemented kinetic models into a CFD

framework (ANSYS CFX<sup>®</sup>) which has been coupled with a Matlab routine performing the optimisation by making changes to the geometry of the reactor and running the simulation. This optimisation routine consists of a systematic procedure. This means for example that a variable was tested along all the dimensions listed by the user. For example, even if the increase of the variable value has not improved the production previously, it will still test for all the higher values. A detailed optimisation procedure and the interaction between Matlab and ANSYS CFX<sup>®</sup> are presented in the Figure 3. The scripts for running the geometry and meshing, setup and postprocessing were prepared by ANSYS CFX<sup>®</sup>. Matlab opened these files and the changes were made according to parameter definition. After modifying the scripts, Matlab ran ANSYS CFX<sup>®</sup> in batch in order to create the geometry and meshing and setup definition files from the scripts. Subsequently, Matlab started also the solver and the postprocessing module in batch. Ultimately, the performance of the system was evaluated by the objective function (concentration of Phenylethylamine at the outlet) and compared with the previous configuration. If the changes in the geometry result in a better reaction yield, the geometry was selected as the best and the old configuration was discarded. Matlab ran for all the combinations of dimension values of height, outlet, inlet that the user decided beforehand.

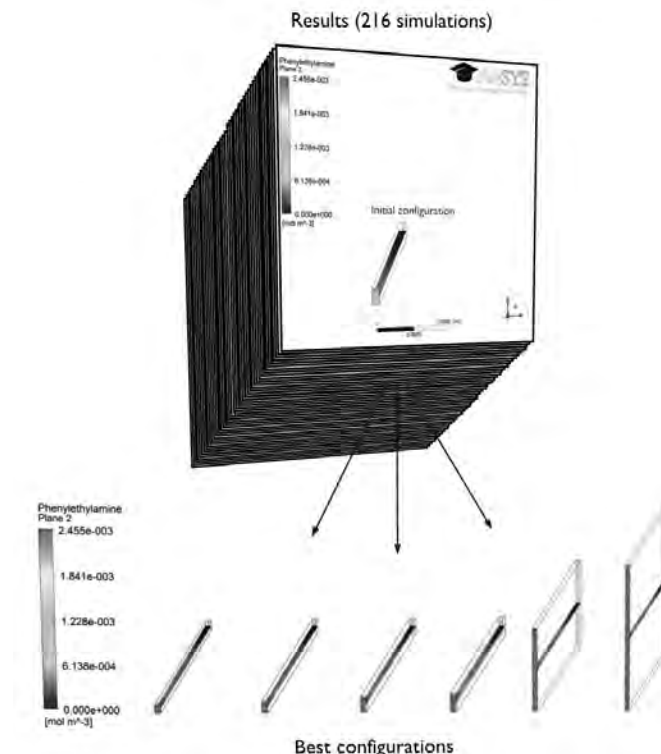


**Figure 4:** Optimisation simulation results and simulation results of best configurations from ANSYS CFX<sup>®</sup>.

## Results and Discussion

This optimisation study included 216 simulations and from there was not only one best result but a range of best results. In fact the height has no influence on the predicted yield. Although, there is larger contact surface between the two streams with the height increase, there is also an increase of the molar flow rate ( $\text{mol s}^{-1}$ ) in order to maintain the residence time inside of the microreactor. For this reason, the yield will be the same for the whole range of height values.

Regarding the inlet and outlet widths, the best configurations have the following dimensions: 0.2 mm for the inlet and 0.2 mm outlet. This means that the best configurations have the minimum width established for this simulation. As a matter of fact, the minimum width of the channel allows a better mixing because there will be a higher diffusion of slowly diffusing molecules such as Acetophenone and  $\omega$ -transaminase than in wider microreactors.

## Conclusions

From this optimisation study, it was possible to gain understanding regarding the mixing mechanism inside of the microsystem and the crucial role it plays for the yield of an enzymatic reaction.

From this simulation, it was also possible to comprehend how important the role of the kinetic model is in comparison to mixing. In fact, in this particular case it seems that the kinetic model does not influence the shape optimisation. Although there are inhibitions at substrate and product level and unfavourable equilibrium, mixing was revealed to be the crucial factor to achieve high yields.

The understanding from this optimisation study is very useful for the experimental work and it allowed avoiding unnecessary experimental studies which can otherwise result into waste of material.

However, the concentration of phenylethylamine from this simulation does not correspond to the same results obtained by Bodla *et al.* (2013) by applying this kinetic model to the microreactor. Therefore, it is important to study enzymatic kinetic models in microsystems.

## Future Work

Since the kinetic model applied in this optimisation study was determined at bench scale, it is necessary to determine it in a microreactor. In fact, there is no knowledge on whether the enzymes perform in the same way in microscale as in bench scale.

Another possible procedure for the shape optimisation is the use of an evolutionary optimisation routine. For the evolutionary procedure, the shape will only develop further into a testing direction if there is an improvement of the objective function. Otherwise, the configuration for the next simulation will be the best configuration and it will be developed into another shape direction.

The shape optimisation is not the only type of optimisation that can improve the yield of a reaction. The topology optimisation can also influence of the improvement of a reaction. Topology optimisation consists of the spatial distribution of the enzymes inside of the microreactor (e.g. immobilization on the surface(s)). This project will also include studies on topology optimisation of microreactors.

## References

1. N.J. Turner, M.D. Truppo, Biocatalytic Routes to Nonracemic Chiral Amines, Chiral Amine Synthesis, 2010, p. 431-459
2. M. Hoehn, U.T; Bornscheuer, Biocatalytic Routes to Optically Active Amines, ChemCatChem, 1 (1) (2009), 42-55
3. J.S. Shin, B.G. Kim, *Biosci Biotechnol Biochem* 65 (8) (2001) 206-211
4. Koszelewski D, Tauber K, Faber K, Kroutil W. *Trends Biotechnol.* 28 (6) (2010) 324-332
5. N. Al-Haque, P.A. Santacoloma, W. Neto, P. Tufvesson, R. Gani, J.M. Woodley, 28 (5) (2012), 1186-1196
6. Bodla, V. K., Seerup, R., Krühne, U., Woodley, J. M., & Germaey, K. V.. Chem. Eng. & Tech. 36 (6) (2013) 1017-1026



**Koldo Saez de Bikuña Salinas**

Phone: +45 24648965  
E-mail: ksde@kt.dtu.dk

Supervisors: Andreas Ibrom  
Michael Zwicky Hauschild  
Kim Pilegaard  
Ulrik Birk Henriksen  
Gürkan Sin

PhD Study  
Started: December 2012  
To be completed: May 2016

## **Land Use in Life Cycle Impact Assessment: Terrestrial Carbon Pools Modeling for Prediction of Impacts on Climate and Biotic Production.**

### **Abstract**

In order to have a better estimate of all the relevant environmental impacts caused by bioenergy along its whole life cycle, land use (LU) effects on soils need to be considered. Life Cycle Assessment (LCA) is an important Quantitative Sustainability Assessment tool for consistently accounting for all these impacts. However, it has been lacking a consistent methodology for LU impact assessment until late 2013. The present study focuses on improving such methodology through carbon pool modeling under different agricultural management scenarios. Changes in stocks of terrestrial carbon under different LU will be translated into Biotic Production Potential (BPP) and Climate Regulation Potential (CRP) impacts.

### **Introduction**

Environmental impacts derived from land occupation and transformation have largely been bypassed within the LCA community due to soils' multifunctionality and the interconnectedness between the ecosystem services (ES) they provide. These inherent modeling complexities have traditionally forced LCA practitioners to content with a mere quantification of LU as surface area and duration (in m<sup>2</sup> or ha and years) appropriated by humans, without further analysis of the impact pathways derived from those land uses. Milà i Canals established the first comprehensive, basic framework for taking soil quality aspect into Life Cycle Impact Assessment (LCIA) that reached acceptance among the LCA community [1]. Through contributions from UNEP-SETAC's special task force on LU, great progress has ensued in developing further such LCIA [2, 3, 4, 5, 6].

Several notorious authors have long claimed the importance of approaching ecosystem assessment through dynamic modeling [7, 8, 9]. This is beyond the reach of LCA [10], but the implementation of more accurate soil modeling results are needed to check the sensitivity of existing Life Cycle Inventories [11] and impact Characterization Factors (CF) for CRP [5].

On the other hand, 1<sup>st</sup> order loop impacts across impact categories are deemed significant but nevertheless neglected in LCIA modeling. Inter-

category CF will be derived from literature and computed for Danish conditions. The following midpoint impact categories have shown a potential to add on to effects on Biotic Production and Climate Change and will be further studied and assessed: Erosion Regulation Potential, Acidification, Ecotoxicity and Photochemical Ozone Formation.

### **Specific Objectives**

The specific objectives for the whole PhD are:

- To compare results from validated soil carbon model C-tool with the rough CF estimates on place used for Climate impact assessment in LCA.
- To compare results from measured data on nitrous oxide emissions with the estimates on place used for Climate impact assessment in LCA.
- To assess first order loop effects across impact categories and illustrate their significance on final results.
- To address shortcomings and pitfalls in Sustainability Assessment of bioenergy systems within LCA through systematic analysis of key sensitive aspects of Allocation, Functional Unit, Reference System, Marginal Lands and Value Choices.

## Project Outline

Focusing on the stated objectives, the project will proceed from improvement proposals of LCIA methodology on LU, to the development and application of those on several study cases. The goals will change, addressing one main objective each time, but the scope will remain the same: bioenergy from dedicated willow cropping in Danish farmlands, thermal gasification as conversion technology for Heat and Power production, and amendment of original lands with bio-ash and bio-char.

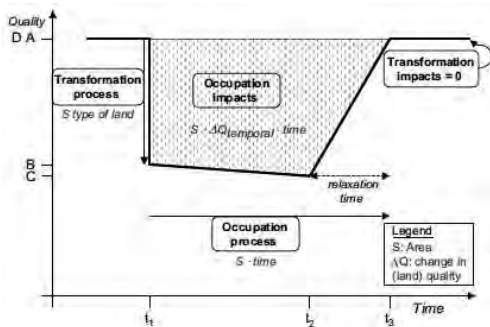


**Figure 1:** UNEP-SETAC framework for Land Use Impact Assessment to be used in the project.

## Discussion and Future Work

Implementing impact assessment from land use into LCA is a challenging task, as it needs to reach an elusive but harmonic solution, balancing out simplicity with accuracy in a compromise set of indicators. The present project will try to shed light on the life cycle accounting of environmental impacts incurred by bioenergy systems. In order to reinforce the systems perspective on sustainability assessment, trade-offs and hidden utilities of environmental services and products will be elucidated along the PhD.

## References

[1] Milà i Canals L, Bauer C, Depestele J, Dubreuil A, Freiermuth, Knuchel R, Gaillard G, Michelsen O, Müller-Wenk R, Rydgren B. (2007a). Key elements in a framework for land use impact assessment within LCA. *Int J Life Cycle Assess* 12:5–15

[2] Koellner T, de Baan L, Beck T, Brandão M, Civit B, Margni M, Milà i Canals L, Saad R, de Souza DM, Müller-Wenk R (2013a). UNEP-SETAC guideline on global land use impact assessment on biodiversity and ecosystem services in LCA. *Int J Life Cycle Assess*

[3] Koellner T, Geyer R (2013b). Global land use impact assessment on biodiversity and ecosystem services in LCA. *Int J Life Cycle Assess*

[4] Brandão M, Milà i Canals L (2013). Global characterisation factors to assess land use impacts on biotic production. *Int J Life Cycle Assess*

[5] Müller-Wenk R, Brandão M (2010). Climatic impact of land use in LCA—carbon transfers between vegetation soil and air. *Int J Life Cycle Assess* 15:172–182

[6] Beck T, Bos U, Wittstock B, Baitz M, Fischer M, Sedlbauer K (2010). LANCA—land use indicator value calculation in life cycle assessment. Fraunhofer, Stuttgart.

[7] Costanza R, Wainger L, Folke C, Mäler KG (1993). Modeling complex ecological economic systems.

[8] Gunderson CS, Holling LH (2002). Panarchy : Understanding transformations in human and natural systems.

[9] Odum H (1973). *Energy, Ecology and Economics*

[10] Hofstetter P (1993). Perspectives in life cycle assessment.

[11] Hamelin, Lorie, Uffe Jorgensen, Bjorn M. Petersen, Jorgen E. Olesen, and Henrik Wenzel. Modelling the Carbon and Nitrogen Balances of Direct Land Use Changes From Energy Crops In Denmark: a Consequential Life Cycle Inventory. *GLOBAL CHANGE BIOLOGY BIOENERGY* 4.6 (2012): 889-907. Web.





**Catarina Seita**

Phone: +45 4525 2926  
E-mail: casse@kt.dtu.dk

Supervisors: John Woodley  
Joana Lima-Ramos

PhD Study

Started: December 2013  
To be completed: December 2016

## Bioprocess Evaluation Tools

### Abstract

There is an increasing interest, both from academia and industry in developing new bioprocesses. These bioprocesses focus on production of chemicals from renewable sources and it is frequently claimed that their synthetic routes are “greener” and generate less toxic by-products and waste. It is also often argued that the mild conditions used in bioprocesses (ambient temperature and pressure, neutral pH and aqueous-based media) lead to environmental friendly production processes. However, to date few reports have documented the economics or environmental profiles of such processes. This project aims to develop a range of adequate tools to evaluate bioprocesses in different development stages from three different perspectives – technical, economic and environmental.

### Introduction

During the last few years considerable progress has been made in the production of organic compounds by means of fermentation or biocatalysis [1]. These bioprocesses have emerged as an alternative to conventional chemical synthesis driven by the need for selective synthetic routes, with high reaction yield and few side reactions, as well as the use of renewable and biodegradable raw materials and catalysts and the fact that biocatalytic reactions run under mild conditions (ambient temperature and pressure and neutral pH) in aqueous solutions. All these features make bioprocesses as alternatives with great potential for “green” and selective processes and its application is steadily increasing at an industrial scale [2].

However, since it is a relatively new technology and given the complexity of the development process, many bioprocesses do not fulfill the economic requirements for industrial operation (high reaction yield, high biocatalyst yield, high product concentration and high space-time yield) [3].

Also, the claim that bioprocesses are more sustainable and environmental friendly than the conventional chemical route can be misleading.

To date few reports have been published with economic and environmental profiles of bioprocesses. There is a need for more evaluation tools to identify process bottlenecks and to assess the feasibility of such processes in different development stages [2].

This PhD project aims to evaluate the feasibility of 3-5 case studies and establish a set of tools that can be used to evaluate processes in several stages of development. These tools can provide guidance for research and development and ultimately can lead to a reduced process development time. The project is carried out in collaboration with the strategic Alliance NatLifE 2020 coordinated by BRAIN AG, Zwingenberg. The consortium is funded by the German Federal Ministry of Education and Research and consists of 22 companies and academic partners developing new bioprocesses using different technologies.

### Specific Objectives

The following specific objectives were defined:

- To establish suitable bioprocess evaluation tools for early stage technical, economic and environmental feasibility tests;
- To establish a suitable bioprocess evaluation tool for late stage technical, economic and environmental assessment tests;
- To develop the tools using suitable case studies from the NatLifE partners;
- Prepare a development plan, including targets for biological and process improvements;
- When appropriate to test the concepts at pilot scale.

### Introduction to case studies

The first case study to be evaluated is the production of R-(+)-perillic acid via biotransformation of R-(+)-

limonene using a whole-cell biocatalyst (see Figure 1) [4].

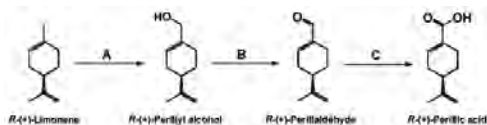


**Figure 1:** Bioconversion of R-(+)-limonene to R-(+)-perillic acid by *P. putida* DSM 12264: (A) monooxygenase; (B) alcohol dehydrogenase; (C) aldehyde dehydrogenase.

Perillic acid is a monoterpeneic acid present in the plants *Perilla mint* and *Perilla frutescens*, which has a broad growth-inhibitory effect on bacteria, yeast and moulds. Thus it is an attractive candidate to be used in substitution of conventional preservatives, particularly in cosmetic industry. Since it is present in very low concentrations in natural sources its extraction is not economically feasible. Additionally, the chemical synthesis has several disadvantages – it involves four low-yielding reaction steps, the use of toxic reagents and a high energy input. Hence biocatalysis appears as an interesting alternative due to its inherent selectivity and environmental friendly reaction conditions [4].

However, the bioprocess faces numerous challenges, namely substrate and product inhibition, low biocatalyst activity, low water solubility of limonene and its derivatives and high volatility of limonene.

To overcome these limitations there are several solutions, which include *in situ* product removal (ISPR) as well as solutions involving biocatalyst improvement.

An evaluation of the several alternatives will be made to determine the process bottlenecks and define the metrics that need to be achieved in order to allow its industrial application.

## Conclusions

It is still a challenge to develop bioprocesses given the complexity of the systems. Communication between chemists, biologists and engineers is crucial to channel research efforts which can lead to a better use of resources, reduced process development time and better understanding of the systems limitations. Given the multidisciplinary nature of this consortium, there is a great potential to overcome the current limitations in bioprocesses development.

## Acknowledgements

This project is carried out in collaboration with the Innovation-Alliance NatLifE 2020 funded by the German Federal Ministry of Education and Research. The PhD fellow would like to thank in particular to the German company BRAIN AG for all the support.

## References

[1] B. G. Hermann, M. Patel, Today's and tomorrow's bio-based bulk chemicals from white biotechnology, *Appl. Biochem. Biotechnol.* 136 (2007) 361–388.

- [2] P. Tufvesson, J. Lima-Ramos, M. Nordblad, J. M. Woodley, Guidelines and cost analysis for catalyst production in biocatalytic processes, *Org. Process Res. Dev.* 15 (2011) 266-274.
- [3] J. Lima-Ramos, A methodology for development of biocatalytic processes, Technical University of Denmark, 2013.
- [4] M. A. Mirata, D. Heerd, J. Schrader, Integrated bioprocess for the oxidation of limonene to perillic acid with *Pseudomonas putida* DSM 12264, *Process Biochemistry* 44 (2009) 764-771.



**Aamir Shabbir**

Phone: +45 4525 2971  
E-mail: aash@kt.dtu.dk

Supervisors: Ole Hassager  
Anne Ladegaard Skov

PhD Study  
Started: October 2013  
To be completed: September 2013

## Supramolecular Polymeric Rheology

### Abstract

The objective of this PhD is to understand the nonlinear rheology of responsive materials. In particular, we are interested to investigate their complex multiscale structure and dynamics at a fundamental level. We utilize the unique filament stretch rheometer (FSR) developed by the Hassager group here at the DTU for this project. In addition, special complementary fixtures (known as SER and EVF) mounted on commercial rheometers will also be used.

### Introduction

Supramolecular polymers are relatively new class of polymers, with attractive groups that offer reversible interactions and thus the possibility of turning the properties on will. These associative polymers present superior versatility compared to their covalent polymeric counterparts. They include charged polymers (ionomers, polyelectrolytes, metal-ligands), block copolymers in strongly selected solvents, and polymers with hydrogen bonding [1].

Supramolecular polymeric materials are capable of displaying stimuli- response, because of the nature of the noncovalent interactions. Therefore, unlike their high molecular weight counterparts, their processing is easy. Furthermore, selfhealing characteristics are attained because of the noncovalent bonds in these materials [2].

The non-linear rheology of these materials remains yet to be well established. In the future work, we seek to investigate the influence of molecular characteristics on the extensional strain hardening, role of external stimuli (temperature and pH) on their dynamics and the role played by the association/dissociation on the non-linear rheology of transient polymeric networks. Here we report the preliminary results of transient extensional viscosity of 210k PnBA melt.

### Filament Stretch Rheometer (FSR)

The extensional rheometer used in this project is a filament stretch rheometer, designed by Bach et al. [3] at the DTU. Besides measuring uniaxial extension, the FSR can measure stress relaxation, creep, reverse flow, large amplitude oscillatory extension (LAOE) and planar extension [4].

After an elongational experiment, the hencky strain and the mean value of the stress difference over the mid-filament plane are calculated from the measured radius of the filament  $R(t)$ , and the force on the bottom plate  $F(t)$ , as:

$$\epsilon(t) = -2 \ln((R(t)/R_0))$$

$$\langle \sigma_{zz} - \sigma_{rr} \rangle = \frac{F(t) - m_f g / 2}{\pi R(t)^2}$$

Where  $R_0$  is the radius of the sample at the start of the extension,  $g$  is the acceleration due to gravity and  $m_f$  is the weight of the polymer filament.

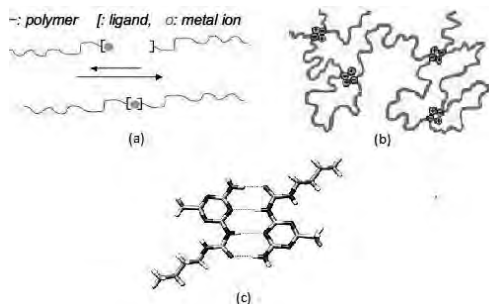


**Figure 1:** (a) Metal-ligand supramolecules, (b) Ionomers, (c) Hydrogen bonded supramolecules.

The transient elongational viscosity is defined as:

$$\eta^{\mp} = \frac{\langle \sigma_{zz} - \sigma_{rr} \rangle}{\dot{\epsilon}}$$

In this work the elongational measurements are presented in the uncorrected form.

### Materials

The starting material 210k Poly-n-butylacrylate was supplied by our research partner. Sample of mass 0.4 g was used, which gives length  $L_0=2.12$  mm, giving aspect ratio  $A_0 = L_0/R_0 = 0.394$ .

### Preliminary results

The uniaxial extension experiments were performed at 21.5 °C and at different strain rates from 0.01 1/s to 5 1/s.

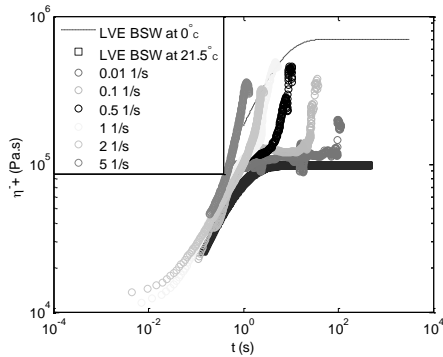


**Figure 2:** Uncorrected average extensional viscosity of pure PnBA melt as a function of time at 21.5 °C at different strain rates.

### Conclusion

Pure PnBA melt displayed strain hardening as evidenced from figure 2.

### Future work

The current work will proceed by performing uniaxial extensional measurements on hydrolyzed PnBA samples. We are particularly interested to investigate the extensional behavior of PnBA with increasing the acid groups via hydrolysis. We also hypothesize that with increasing the hydrolysis the strain hardening would increase.

### Acknowledgment

This project is a part of SUPOLEN, funded under the Initial Training Network in the Seventh Framework Marie Curie Programme.

### References

1. M. Rubinstein, A. V. Dobrynin, TRIP 5 (6) (1997) 181-186.

2. A. Bach, H. Rasmussen, O. Hassager, J. Rheol. 47, (2003) 429–441.
3. M.J. Cortese, Organisations dans les polymères supramoléculaires : du comportement en solution au comportement en masse, PhD thesis.
4. Q. Huang, Molecular rheology of complex fluids, PhD thesis.



**Laura Snip**

Phone: +45 4525 2990  
E-mail: lasn@kt.dtu.dk

Supervisors: Krist V. Gernaey  
Ulf Jeppsson, Lund University  
Xavier Flores-Alsina  
Benedek Plósz, DTU Environment  
Ulrich Krühne

PhD Study  
Started: May 2012  
To be completed: April 2015

## Practical Application of Models in the Urban Water System: Simulation Based Scenario Analysis

### Abstract

Nowadays a wastewater treatment plant is challenged to not only provide clean water but also to take its carbon footprint into account. Another ‘new’ challenge is the removal of so called micropollutants. In order to further optimize the performance of the wastewater treatment plant a good understanding of the production of greenhouse gases and the removal of micropollutants is required. Modeling these processes contributes to the development of a proper understanding of the main mechanisms involved, and enables to test different plant operation scenarios on their efficiency *in silico*. As a result new evaluation tools can be developed concerning the production of greenhouse gases and the removal of micropollutants.

### Introduction

With the increasing awareness of global warming also wastewater treatment plants (WWTPs) have to monitor and if possible reduce their production of greenhouse gases (GHGs). In a WWTP, three different GHGs are produced, namely  $\text{CO}_2$ ,  $\text{CH}_4$  and  $\text{N}_2\text{O}$ . The global warming potential (a measure to compare the effect of different chemicals on the global warming) of  $\text{CH}_4$  is 23 kg equivalent  $\text{CO}_2$  and that of  $\text{N}_2\text{O}$  is 296 kg equivalent  $\text{CO}_2$  [1]. This shows that a small production of  $\text{N}_2\text{O}$  will have a higher impact compared to a small production of  $\text{CO}_2$  and therefore it is important to take those emissions into account.

Besides GHG emissions, a WWTP has a relatively new challenge. Indeed, the development of methods to measure chemicals at low concentrations has resulted in a growing awareness of the presence of low concentrations of the so-called micropollutants in the aquatic environment. These micropollutants can originate from medication, illicit drugs and personal care products. Recent studies have shown that these chemicals can influence aquatic life by inducing sex reversal and/or intersexuality [2], or that the reproductive behavior is reduced [3]. WWTPs are traditionally not designed to remove micropollutants; however a change in operational conditions such as increasing the sludge retention time can increase the removal of micropollutants in a WWTP [4].

In order to face these challenges the Benchmark Simulation Model 2 (BSM2) will be

extended to include the processes concerning GHGs and micropollutants.

The BSM2 is a general plant wide model of a WWTP that was developed with the purpose of comparing different control strategies [5]. The model includes a plant layout, shown in Figure 1, a simulation model, influent loads, test procedures and evaluation criteria. When using the same plant layout, influent loads, test procedures and evaluation criteria, the outcome of different control strategies will be comparable in an objective way.

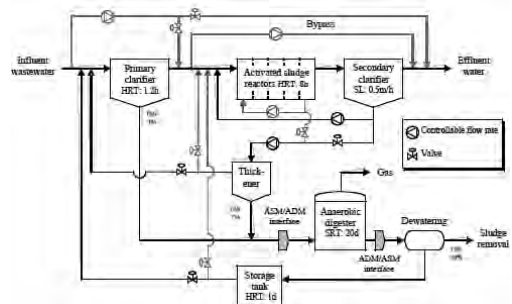


**Figure 1:** A schematic overview of the plant layout of BSM2.

### Objective of PhD study

The objective of this PhD study is to extend the BSM2 with processes involving the GHG production and processes concerning the micropollutants. Once this

extension is made different operating scenarios will be compared in silico according to newly developed evaluation tools. These evaluation tools should include criteria concerning GHG emissions and micropollutants besides the current effluent quality index and operational cost index. Also, different control strategies will be tested to investigate potential improvements of plant operation.

### Carbon footprint of the WWTP

Nitrous oxide is being produced in a WWTP as an intermediate during heterotrophic denitrification, which is an anoxic process. Also it can be produced in the aerobic tanks by ammonia oxidizing bacteria. This can happen during nitrifier denitrification and by chemical reactions; however it is not yet known precisely how these processes work and to what extent they contribute to the overall production of N<sub>2</sub>O [6]. Ni *et al.* [7] have developed four different mathematical models that can describe the N<sub>2</sub>O production. These models were implemented into the BSM2 in order to account for N<sub>2</sub>O production by ammonia oxidizing bacteria (AOB). The dynamic simulation results of the different models are shown in table 1.

**Table 1:** The dynamic results of the four different models published by Ni *et al.* [7] with the BSM1.

	AOB denitrification		Incomplete oxidation of hydroxylamine (NH <sub>2</sub> OH)		Units
	Model	Model	Model	Model	
	A	B	C	D	
S <sub>O<sub>2</sub></sub>	2.61	4.01	2.78	3.33	g O <sub>2</sub> .m <sup>-3</sup>
S <sub>NH<sub>4</sub></sub>	2.81	0.04	4.42	0.28	g N.m <sup>-3</sup>
S <sub>NO<sub>3</sub></sub>	14.15	4.51	8.95	11.14	g N.m <sup>-3</sup>
S <sub>NO<sub>2</sub></sub>	1.30	1.12	0.02	2.86	g N.m <sup>-3</sup>
S <sub>NO</sub>	0.022	0.63	0.003	0.0005	g N.m <sup>-3</sup>
S <sub>N<sub>2</sub>O</sub>	0.26	1.32	0.76	0.31	g N.m <sup>-3</sup>
X <sub>AOB</sub>	0.42	0.46	0.19	0.81	g COD.m <sup>-3</sup>
X <sub>NOB</sub>	0.12	0.08	0.11	0.12	g COD.m <sup>-3</sup>
G <sub>N<sub>2</sub>O</sub>	<b>44.98</b>	<b>152.95</b>	<b>71.50</b>	<b>39.14</b>	kg N <sub>2</sub> O. N.d % N <sub>2</sub> O produc ed of N- influen t
	<b>4.5%</b>	<b>15.2%</b>	<b>7.1%</b>	<b>3.9%</b>	

As can be seen in the table, the different models predict a different percentage of N<sub>2</sub>O produced with model B having the highest percentage (15.2%) and model D the lowest of 3.9%. This indicates that more research is needed to establish the pathways involved in N<sub>2</sub>O production. During an external stay at a wastewater treatment company in Belgium, real plant data will be used to calibrate the models. This can help identify which pathway of the AOB is the dominant pathway.

For now the CO<sub>2</sub> production is mainly calculated by conversion factors and the CH<sub>4</sub> production by the anaerobic digester is already calculated in the BSM2. The emissions that are taken into account when calculating the carbon footprint are emissions during: i) treatment, namely biological treatment, endogenous respiration, BOD oxidation, nitrification (CO<sub>2</sub> credit) and nitrogen removal; ii) energy use of the plant; iii) sludge digestion; iv) sludge disposal; v) power credit by use of biogas; and, vi) chemical usage. The emissions during the building of the WWTP are not taken into account as those are not controllable. Once the BSM2 is extended with the production of the three GHGs, different control strategies can be compared in order to decrease the carbon footprint of the plant.

### Micropollutants

There are many different micropollutants present in the wastewater with each compound having its own characteristics. Therefore every compound has to be modeled with different parameters. However the same processes are responsible for the removal of the micropollutants. The processes removing the micropollutants are sorption and biotransformation [8]. Other processes that also occur with the micropollutants are desorption and retransformation into parent compound. These processes can take place in the aerobic and in the anoxic phase; however there are different parameters for the aerobic and anoxic phase. These processes will lead to three different forms of the micropollutant in the wastewater, namely the liquid form, C<sub>LI</sub>, the sorbed form, C<sub>SL</sub>, and the conjugated form, C<sub>CJ</sub>. There is then also a fraction of the micropollutants that can not be removed because it is sequestered (C<sub>SL1</sub>). These are just the processes concerning the micropollutants in the activated sludge reactors. To model the fate of the micropollutants in an urban water system context, also the behavior in the sewer system, the settlers, the anaerobic digester and the receiving waters should be taken into account.

There are different studies on the removal of micropollutants in a WWTP, however not all include a mathematical model, and the published models differ largely. For this study the framework published by Plósz *et al.* [8, 9] was chosen. This framework takes the above-mentioned processes and variables into account, and has been tested in lab scale and full scale. With this framework, the occurrence, transport and fate of five different pharmaceuticals could be simulated. The occurrence of the pharmaceuticals was modeled by extending the influent generator of the BSM2 [10]. This generator consists of a model block calculating the flow rate, a block calculating the pollutant loads and a block calculating the temperature. These calculations are put together and passed through a transport block where the sewer system is defined. This is schematically shown in figure 2. To calculate the loads of pollutants a daily profile is combined with a weekly and a seasonal profile, which is multiplied with the number of Person Equivalent (PE) that are in the catchment.

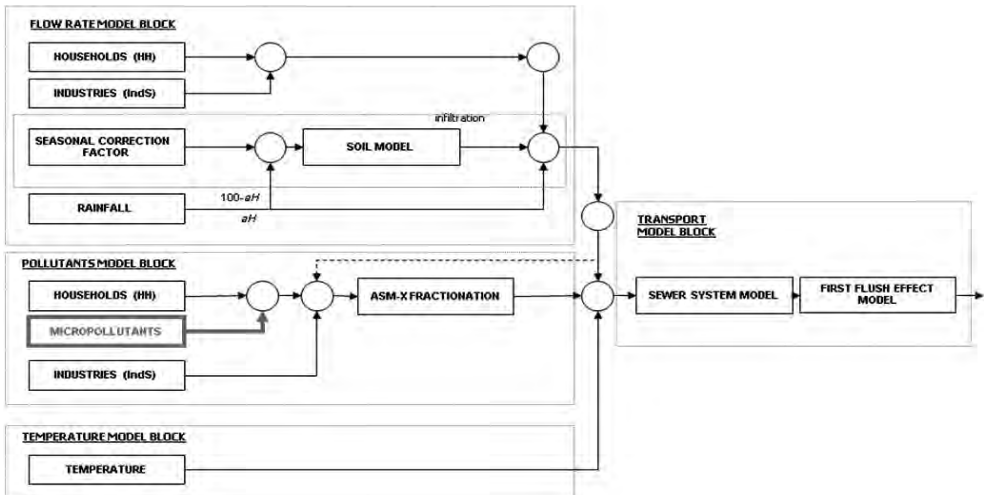


**Figure 2:** Schematic representation of the influent pollutant disturbance scenario modelling approach with the addition of micropollutants.

The occurrence of micropollutants is generated with two different approaches. Daily, weekly and seasonal influent dynamics for the micropollutant sulfamethoxazole (SMX) are generated following a phenomenological approach based on user-defined pollutant profiles. For compounds which are known to have more random patterns/dynamics in the influent, like diclofenac (DCF), a stochastic approach based on Markov Chains is used. Drug administration patterns, bioavailability, half-time and total annual consumption rates are the basis to generate the user defined profiles, while the Markov Chains are constructed assuming a set of transition probabilities. As mentioned before, the daily, weekly and seasonal variation is combined and multiplied with the PE. To obtain more realistic results, noise is added to the occurrence of SMX. As the stochastic approach based on Markov Chains already shows a high level of randomness, there is no additional noise needed. The obtained occurrences for SMX and DCF over a week can be seen in figure 3.

The transport conditions could also have an effect on the occurrence of the micropollutants at the inlet of a WWTP. To examine the effects, different oxygen concentrations, different sewer lengths and different TSS loading rates were simulated and the results were compared. Figure 4 shows the results of different sewer lengths on the variable  $C_{LI}$  of SMX. It can be observed that the longer the sewer is, the less variation is observed in the  $C_{LI}$  concentration.

After modeling the occurrence and investigating the effect of different transport conditions, the effect of different treatment scenarios in a WWTP was examined. Five micropollutants were examined under three or four different operating conditions; 1) the default scenario; 2) an addition of carbon; 3) a step feed configuration; and 4) increase of the sludge retention time.

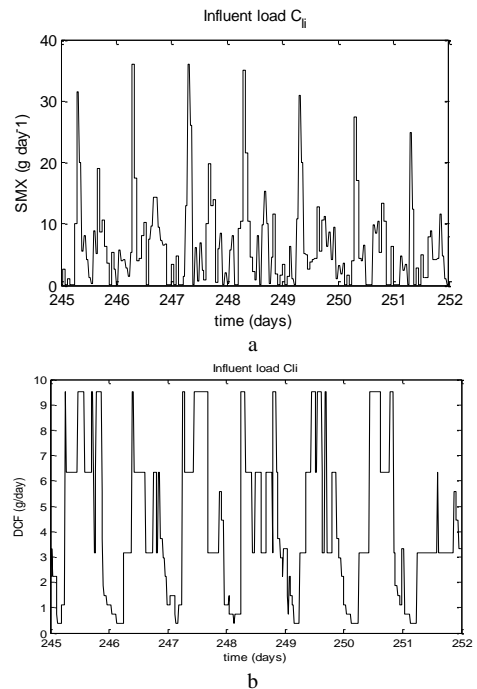


**Figure 3:** Dynamic influent load of SMX (a) and DCF (b) during a week generated with the extended BSM2 influent generator.

The results of the SMX and DCF variables  $C_{LI}$  and  $C_{SL}$  can be seen in table 1. It can be seen that the different configurations have some effect on the concentrations of  $C_{LI}$  and  $C_{SL}$ ; however the differences are not large. After performing an uncertainty analysis, it was shown that the differences could also be attributed to uncertainty in the model parameters.

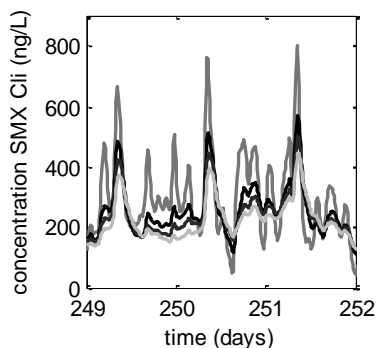


**Figure 4.** Effect of sewer length (red: 2 subareas, black: 4 subareas, blue: 6 subareas, green: 8 subareas) on the concentration of the SMX variable  $C_{LI}$  in the inlet to the WWTP.

The results on the occurrence of the micropollutants obtained with the extended influent generator will be calibrated and validated with data during an external stay at the University of Girona, Spain. In order to evaluate the different control strategies of a WWTP regarding the removal of micropollutants, the traditional performance evaluation criteria have to be extended. This can be done by including removal indexes based on percentages of micropollutant removed, or sorbed, but also by including a receiving water model. With a receiving water model, concentrations of the micropollutant after discharge can be calculated and compared with concentration limits of toxic compounds.

**Table 2:** Influent and effluent concentrations showing the effect of different operating conditions on SMX and DCF.

	$C_{LI}$ (ng/L)	$C_{SL}$ (ng/L) Over/Underflow
<b>SMX</b>		
<b>Influent</b>	321	0
<b>SC1<sub>fate</sub></b>	632	2/1187
<b>SC2<sub>fate</sub> (Increase OM)</b>	652	2/1075
<b>SC3<sub>fate</sub> (Stepfeed)</b>	601	2/1197
<b>DCF</b>		
<b>Influent</b>	234	0
<b>SC1<sub>fate</sub></b>	340	0/30
<b>SC2<sub>fate</sub> (Increase OM)</b>	290	0/22
<b>SC3<sub>fate</sub> (Stepfeed)</b>	334	0/31
<b>SC4<sub>fate</sub> (Increase SRT)</b>	169	0/18

#### Acknowledgements

Laura Snip acknowledges the People Program (Marie Curie Actions) of the European Union's Seventh Framework Programme FP7/2007-2013 under REA agreement 289193 (SANITAS) and REA agreement 329349 (PROTEUS), respectively. This article reflects only the authors' views and the European Union is not liable for any use that may be made of the information contained therein.

#### References

1. IPCC, Climate Change 2001: The Scientific Basis, Cambridge University Press, 2001, chapter 4.
2. A. Lange, G.C. Paull, T.S. Coe, Y. Katsu, H. Urushitani, T. Iguchi, C.R. Tyler, Environmental Science and Technology, 43 (4) (2009) 1219-1225.
3. T.S. Coe, P.B. Hamilton, D. Hodgson, G.C. Paull, J.R. Stevens, K. Sumner, C.R. Tyler, Environmental Science and Technology, 42 (13) (2008) 5020-5025.
4. M. Clara, N. Kreuzinger, B. Strenn, O. Gans, H. Kroiss, Water Research, 39 (1) (2005) 97-106.
5. U. Jeppsson, M.-N. Pons, I. Nopens, J. Alex, J. Copp, K.V. Gernaey, C. Rosen, J.-P. Steyer, P.A. Vanrolleghem, Water Science and Technology, 56 (8) (2007) 67-78.
6. M.J. Kampschreur, H. Temmink, R. Kleerebezem, M.S. Jetten, M.C. van Loosdrecht, Water Research, 43 (2009) 4093-4103.
7. B.-J. Ni, Z. Yuan, K. Chandran, P.A. Vanrolleghem, S. Murthy, Biotechnology and Bioengineering, 110 (1), (2013) 153-163
8. B.Gy. Plósz, K.H. Langford, K.V. Thomas, Biotechnology and Bioengineering, 109 (11) (2012) 2757-2769
9. B.Gy. Plósz, H. Leknes, and K.V. Thomas, Environmental Science and Technology, 44 (2) (2010) 734-742.
10. K.V. Gernaey, X. Flores-Alsina, C. Rosen, L. Benedetti, and U. Jeppsson, Environmental Modelling & Software, 26 (11) (2011) 1255-1267.

#### List of Publications

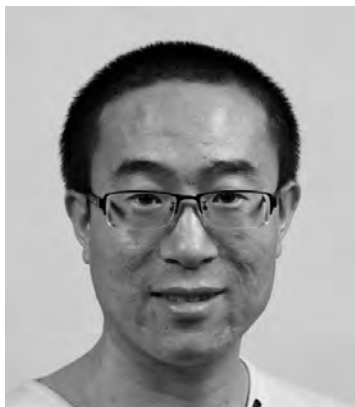
Flores-Alsina, X., Arnell, M., Amerlinck, Y., Corominas, L.L., Gernaey, K.V., Guo, L., Lindblom, E., Nopens, I., Porro, J., Shaw, A., Snip, L., Vanrolleghem, P.A. and Jeppsson, U. (2014). Balancing effluent quality, economic cost and greenhouse gas emissions during the evaluation of (plant-wide) control/operational strategies in WWTPs. *Science of the Total Environment*, 466-467, 616-624.

Snip, L., Flores-Alsina X., Plósz B.G., Jeppsson U. and Gernaey, K.V. (2013). Extending the BSM platform with occurrence, transport and fate of micropollutants using the ASM-X framework. *Environmental Modelling & Software* (submitted).

Arnaldos, M., Castro-Barros, C.M., Meng, F., Rehman, U. and Snip, L.J.P. (2013). Modelling for addressing emerging challenges of the urban water system", *10<sup>th</sup> IWA Leading Edge Technology Conference (LET2013)*, Bordeaux, France, 2-6 June, 2013.

Snip, L., Boiocchi, R., Flores-Alsina X., Jeppsson U. and Gernaey, K.V. (2013). Expanding activated sludge models with additional processes: A case study based on nitrous oxide production by autotrophic ammonia-oxidizing bacteria. *11<sup>th</sup> IWA Conference on Instrumentation, Control and Automation (ICA2013)*, Narbonne, France, 18-20 September 2013.





**Guotao Sun**

Phone: +45 4525 2946  
E-mail: sngu@kt.dtu.dk

Supervisors: Anne S. Meyer  
Anders Thygesen

PhD Study  
Started: December 2011  
To be completed: November 2014

## Establishment of Bioelectrochemical Systems (BESs) for Production of Electricity and Hydrogen Peroxide from Pretreated Energy Crops

### Abstract

Microbial fuel cells (MFCs) are considered to be a promising yet challenging technology to contribute in covering the increasing energy requirement. MFCs are the major type of bioelectrochemical systems (BESs) which convert biomass into electricity through metabolic activity of bacteria. Despite the fact that in the recent 10 years the power generation from MFCs have reached the level of primary power targets in lab-scale systems, the practical application of MFCs for electricity production is still a big challenge. However, alternative applications of a MFC could be useful in practice. The present PhD project will thus focus on optimization of MFCs to produce electricity and hydrogen peroxide from waste residue after bioethanol fermentation of energy crop.

### Introduction

Microbial fuel cells (MFCs) are considered a promising future technology for capturing energy from organic materials in waste streams, i.e. for converting this energy to electricity. Opposite to classical electrolysis, where the electric current is used to drive a chemical reaction, MFCs rely on formation of electric current by microbial conversion of organic material. MFCs are thus principally similar to chemical fuel cells (CFCs) encompassing an anode and a cathode reaction for driving the redox process resulting in production of electricity. However, in MFCs bacteria serve as the biocatalyst to convert an organic substrate to electricity. For the MFC to work, in addition to electron transfer, ions present in the electrolyte, must be able to diffuse between the anode and cathode chambers in order to maintain charge balance for the system. The anode and cathode chambers are therefore separated by an ion-exchange membrane, which restricts oxidant diffusion but allows ion migration. In MFCs (Fig 1), the anode chamber is in practice maintained under anaerobic conditions, while the cathode chamber is usually kept aerobic, often directly exposed to air. The bacteria grow anaerobically in the anode chamber and must form a biofilm on the surface of the anode in order to oxidize the organic substrate fed to the anode chamber to release electrons. In turn, these electrons are collected by the anode and then transferred through the external circuit to the cathode where the reduction reaction takes place (Fig 1). At the same time, positively charged ions

(as the cations in Fig 1) must cross the membrane from the anode chamber to the cathode chamber to balance the circuit.

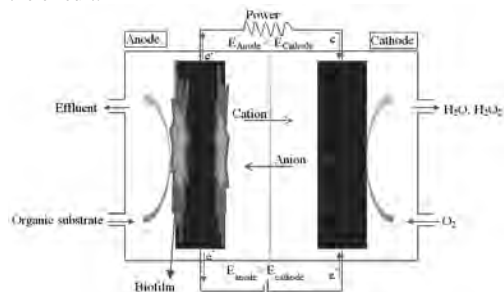


**Figure 1** Schematic of microbial fuel cell system containing anaerobic bacteria formed biofilm in anode and chemical cathode.

### Principles of bioelectricity generation in MFCs

Bacteria capable of complete oxidation of organic substrates by electron transfer in a biofilm on an anode electrode surface are termed as electrogenic bacteria<sup>1-3</sup>. Fig 2 shows a qualitative summary of the bioelectrochemical reaction, which electrogenic bacteria (i.e. *Geobacter Sulfurreducens*) obtain energy via the anaerobic respiration processes start with electrons being donated by an organic substrate followed by a serial electron transport chain from intracellular to

extracellular. The anode is intermediate acceptor and through an external circuit, finally terminates with reduction of an electron acceptor like  $O_2$  in the cathode.

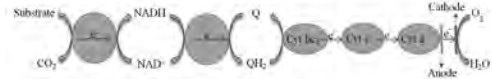


**Figure 2** Schematic illustration of electron transport from substrate to electrode in *Geobacter S.* biofilm. Substrate/ $CO_2$  is the respiratory oxidation process; NADH/NAD<sup>+</sup> is the intermediate for transporting released electrons during respiration;  $QH_2/Q$  transfer electron in the inner cell membrane; Cyt bc1, cyt c and cyt c1 are serial cytochrome agents in the outer cell membrane; Anode serves as the intermediate electron acceptor;  $O_2$  serves as the terminal electron acceptor in cathode. (Figure drawn with modification from Lovley et al. (2004)<sup>4</sup>)

### Reactor design with consideration of internal resistance

In an MFC, the anode acts as electron acceptor for bacteria, which oxidize organic substrate to release electrons. The electrons are transferred from anode chamber to cathode chamber where the electrochemical reaction terminates with electricity generation. The redox reaction rate on both anode and cathode surface lead to overpotentials, which result in a big voltage loss. The overpotential losses are classified as activation losses, ohmic losses and concentration losses as illustrated in Fig 3.

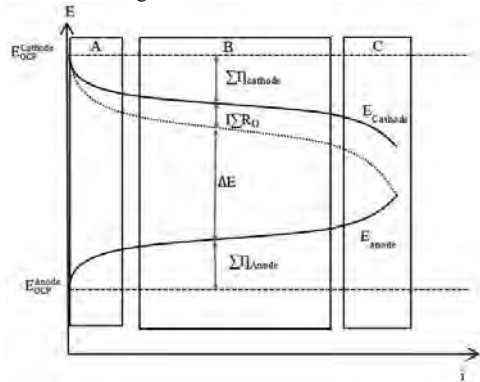


**Figure 3** An anodic ( $E_{anode}$ ) and cathodic ( $E_{cathode}$ ) polarization curve indicating the region of activation losses (region A), the ohmic losses (region B) and concentration losses (region C). The open circuit potential is indicated by ( $E_{OC}^{cathode}$  and  $E_{OC}^{anode}$ ). The activation losses is presented by ( $\Sigma\Pi_{cathode}$  and  $\Sigma\Pi_{anode}$ ), cell voltage by  $\Delta E$  and ohmic losses by  $I\Sigma R_{\Omega}$ . (Modification after (Clauwaert et al. 2008)<sup>5</sup>).

In the concept of MFC, the electrical current flowing through the external circuit can spontaneously drive the charged ion transportation in the electrolyte. The charge transportation from the anode surface to the cathode surface via the electrolyte needs to overcome the

resistance from the electrode overpotentials, electrolyte and membrane. The ion transportation (especially proton) is the major limiting step when ionic conductivity and membrane permeability are poor. Under the limited proton transfer condition, microbial activity is reduced due to proton accumulation in anode chamber, and meanwhile the insufficient proton supply in cathode slows down the cathode reaction<sup>6,7</sup>. MFC with high power density correspondingly have low internal resistance. The internal resistance is considered as a key parameter to evaluate the system performance. As shown in Fig 4, the internal resistance order is  $A>B>C>D$ .

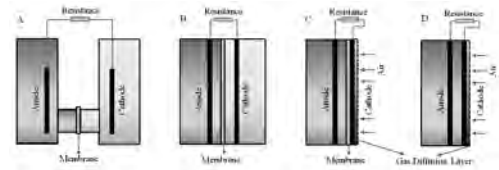


**Figure 4** Types of MFCs: (A) H-shape two chamber system showing anode and cathode connected by tube with membrane as separator; (B) Cube-shape reactor where the two chambers separated by a membrane (without tube connection); (C) Single chamber air-cathode reactor with MEA; (D) Membrane-less air-cathode reactor .

### Current Work

1. Optimization of electrogenic biofilm formation by selecting inoculum and substrate.
2. Production of  $H_2O_2$  in cathode chamber of BES.
3. Scale up of MFCs by novel reactor configuration.

### Acknowledgements

The author is grateful to Danida Fellowship Centre for supporting the research project (Biobased Electricity in Developing Countries, DFC No. 11-091 Risø)

### Reference

1. Bond DR, Lovley DR. *Appl Environ Microbiol* 69(3) (2003)1548-1555.
2. Lovley DR. *Nat Rev Microbiol* 4 (2006) 497–508.
3. Lovley DR. *Curr Opin Biotech* 19 (2008) 564–571.
4. Lovley DR, Holmes DE, Nevin KP. Academic Press (2004) 219–286
5. Clauwaert P, Aelterman P, Pham TH, De Schampelaire L, Carballa M, Rabaeq K, Verstraete W. *Appl Microbiol Biotechnol* 79 (2008) 901–913.
6. Gil G, Chang I, Kim BH, Kim M, Jang J, Park HS, Kim HJ *Biosens Bioelectron* 18 (2003) 327–334.
7. Rozendal RA, Hamelers VMH, Buisman CJN *Environ Sci Technol* 40 (2006) 5206–5211.



**Sune Tjalfe Thomsen**

Phone: +45 2132 5181  
E-mail: sunt@kt.dtu.dk

Supervisors: Hanne Østergård  
Zsófia Kádár

PhD Study  
Started: December 2010  
To be completed: January 2014

## Bioenergy from Lignocellulosic Waste Resources in Ghana

### Abstract

The distinctive resources of a tropical, developing country introduces new and complex issues within the conversion of biomasses into energy carriers. In order to assess these, the knowledge gained within the last decades in this area must be transferred, adjusted and further developed. The focus is on characterising Ghanaian bioresources, as well as development of conversion technologies within both pretreatment of the different biomasses and the biological transformation of pretreated material into energy carriers.









### Introduction

In recent years, the focus on sustainable biofuel production from agricultural bioresidues has increased considerably. However, the scientific work within this field has predominantly been concentrated upon bioresources from industrialised and newly industrialised countries, while the residues from many developing countries remain unstudied.

Using Ghana as a model country, this project will focus on making sustainable bioenergy solutions in a third world context. An initial mapping of Ghanaian waste resources that are relevant for production of bioenergy have been carried out based on reviewing the literature [1]. A broad selection of biomasses has been obtained through our Ghanaian partners (Table 1), where after the resources have been characterized with regard to chemical composition and the bioenergy potentials have been evaluated.

In the next phase of the study, the lignocellulosic biomasses have been subjected to pretreatment such as hydrothermal treatment, soaking in aqueous ammonia, boiling pretreatment and biological pretreatment with white rot fungi. Thereafter, the pretreated biomasses were converted to bioenergy in the laboratory where both ethanol production and biogas production have been tested. Based on the results different concepts specially adapted for third world conditions will be developed such as innovative reactor setups. Finally, but very importantly, an evaluation of most suitable bioenergy technology will be carried out, in order to assist our Ghanaian partners in pilot scale trials.

**Table 1:** List of analysed Ghanaian bioresources.

Crop	Residue	
Yam	Peelings	
Cassava	Peelings	
	Stalks	
Plantain	Peelings	
	Trunks	
	Leaves	
Cocoa	Husks	
	Pods	
Oil palm	Empty fruit bunches	
Maize	Stalks	
	Cobs	
Rice	Straw	
Groundnut	Straw	

## Results and discussions

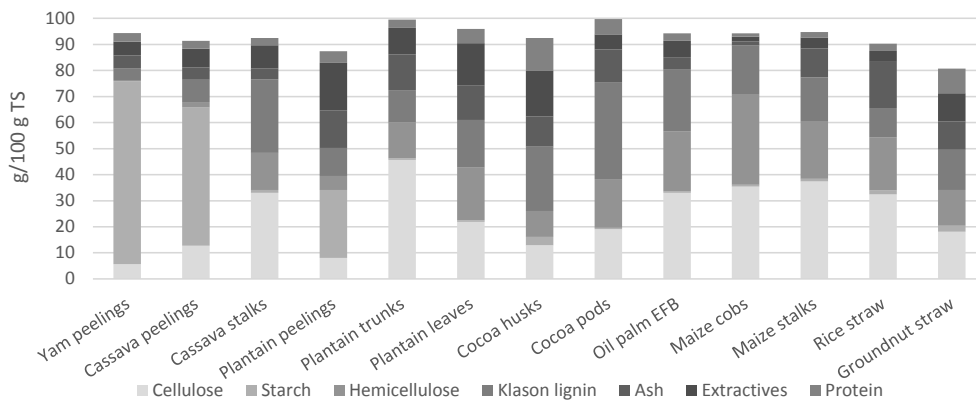


**Fig. 1.** Composition of common Ghanaian biomasses

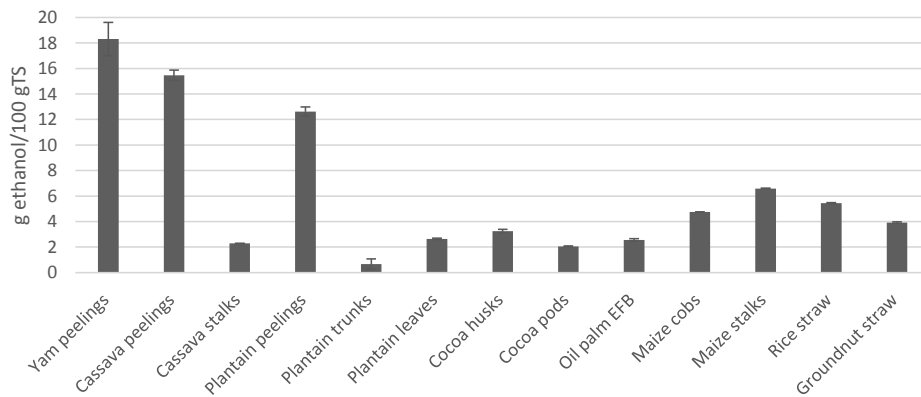


**Fig. 2.** Bioethanol potentials of common Ghanaian biomasses

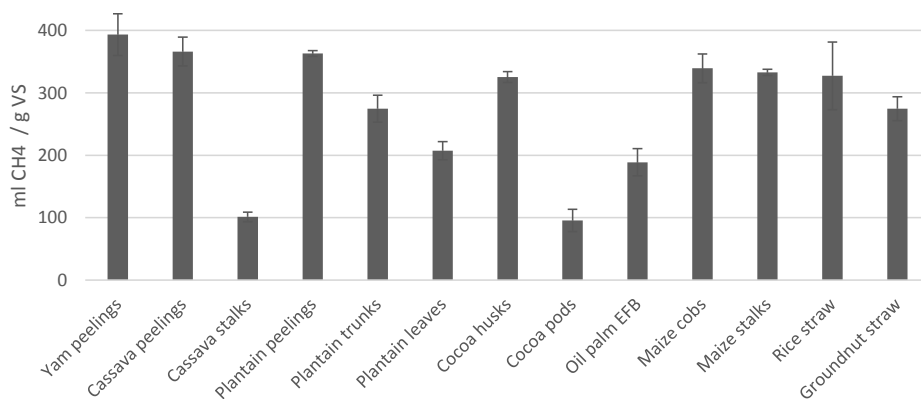


**Fig. 3.** Biomethane potentials of common Ghanaian biomasses

Asking a bioenergy researcher about the composition of wheat straw, he would know it by heart. However, if enquiring about typical African biomasses – it would be another case. Until now, biomasses common to African countries have not received the same scientific attention as biomasses from Europe, North America or Brazil. For that reason, it is difficult to estimate bioenergy potentials in the African region.

13 common African agricultural residues have been thoroughly compositionally analysed, these were yam peelings, cassava peelings, cassava stalks, plantain peelings, plantain trunks, plantain leaves, cocoa husks, cocoa pods, maize cobs, maize stalks, rice straw, groundnut straw and oil palm empty fruit bunches (EFB). This was done to establish detailed compositional mass balances (Figure 1), enabling estimations of accurate bioenergy potentials for bioethanol and biogas. Furthermore, biomasses high in specific biomass constituents, such as hemicellulose or lignin, have been identified for future biorefinery applications.

The composition of the residues shows significant differences. Yam-, cassava-, and plantain peelings have very high a high starch content, which causes high theoretical bioenergy potentials of up to 41 g bioethanol (100 g TS)<sup>-1</sup> and 439 L methane (kg TS)<sup>-1</sup>. Plantain trunks have the highest amount of cellulose, 46 g (100 g TS)<sup>-1</sup>, which can hold potentials in relation to biomaterials as well as bioenergy. Cocoa pods are unusual rich in lignin (Figure 1), thus poor in carbohydrates and will therefore not be optimal for fermentative processes such as in biogas and bioethanol production. However, this residue might be favourable for biorefinery purposes where a phenol rich starting material is desired. Cocoa husks and groundnut straw are among the residues with least carbohydrates and therefore they hold low ethanol potentials, however these residues are relatively high in protein, which makes them more attractive as livestock feed.

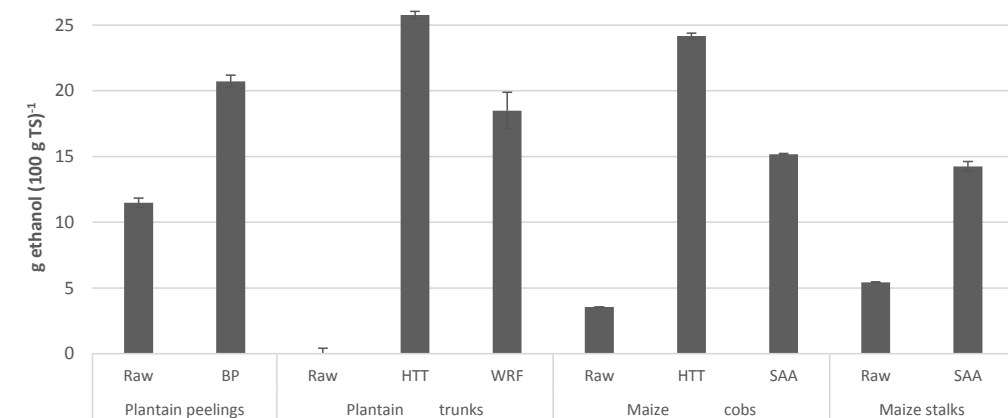
The theoretically bioenergy potentials based on the composition of the residues, and did not take biomass

recalcitrance are not taking into account. This might have resulted in over-estimations in the presented results. Therefore, laboratory pretreatment and fermentation test of the most attractive residues have been done.

Bioethanol potentials of the Ghanaian biomasses are presented in Figure 2, where the composition-derived differences for bioethanol potential are evident. For instance when comparing the residues from plantain, where the easy degradable starch fraction in the peelings give rise to a fair amount of potential product, the quite high level of cellulose in the trunks shows the highest bioethanol potential. However, this would imply a more complicated 2<sup>nd</sup> generation bioethanol technology, which might not be feasible in Ghana. Full utilisation of the plantain leaves or trunks would include the conversion of C5 sugars by using technology that is even more complex. Due to the differences in recalcitrance in different biomasses, this study will give special emphasis to potential pretreatment methods within both biogas and bioethanol production in third world countries.

Biomethane potentials on the biomasses are presented in Figure 3. Similar to the bioethanol case, the starchy biomass residues are also giving the highest potentials, thus it is clear that those easy degradable residues should be utilised first when possible. However, in anaerobic digestion the need for pretreating is not as profound as for ethanol, and lignocellulosic biomasses such as cocoa husks, maize cobs, maize stalks, and rice straw, performs almost as well as the starchy residues, thus these biomasses also holds prospects for biogas production. On the other hand, some biomasses such as cassava stalks, cocoa pods and oil palm fruit empty fruit bunches have biomethane yields far below what could be expected when looking at the content of methane-yielding biomass constituents such as cellulose, hemicellulose, proteins and lipids. This effect is caused by the recalcitrance of the biomasses, which is related, to the lignin content of the biomasses.

The most promising of the Ghanaian biomasses have been selected for further studies with pretreatment of the



recalcitrance are not taking into account. This might have biomasses prior to ethanol fermentation. Tree different

**Fig. 4.** Bioethanol potentials of selected pretreated Ghanaian biomasses. Boiling pretreatment (BP), hydrothermal treatment (HTT), white rot fungi pretreatment (WRF), and soaking in aqueous ammonia pretreatment (SAA).

methods applicable for Ghanaian conditions were tested. That were, soaking in aqueous ammonia (SAA), boiling pretreatment (BP) and fungi assisted pretreatment with white rot fungi (WRF). These methods were benchmarked against the well-known method of hydrothermal treatment (HTT).

HTT refers to the use of hot water in either the gaseous or the liquid phase to pretreat lignocellulosic biomass. HTT is most often done at 160-220°C where autohydrolysis of the hemicellulose is taking place and where degradation of glucan is limited. Autohydrolysis occurs when water acts as a weak acid that causes depolymerisation of hemicellulose by hydrolysing glycosidic linkages in the hemicellulose side-chains. Thus, the main effect of HTT is solubilisation of hemicellulose consequently increasing cellulose digestibility, while most of the cellulose and lignin of a biomass remain in the solid phase after HTT. SAA takes advantage of a mild alkali effect on the biomass and the major effects of SAA are swelling of the cellulose and delignification due to cleavage of ether bonds in lignin, as well as the ether and ester bonds coupling lignin to hemicellulose. Boiling pretreatment (BP) is performed without pressurised equipment and unlike HTT it cannot exceed temperatures of 100°C. This substantially limits the effect on lignocellulosic materials since the autohydrolytic effect does not take place. When BP has been applied as lignocellulose pretreatment method, it has been with a limited effect. However, BP can be performed in small-scale low-tech set-ups, applicable for Ghanaian circumstances. WRF of biomass takes advantage of the unique and extracellular oxidative enzymes produced by white rot fungi. These enzymes are efficient to degrade lignin and open the phenyl rings, thus increasing the accessibility to the carbohydrates in the biomass. Fungal pretreatment is an aerobic process, initiated by inoculating fungal mycelia in moist biomass. The degradation process is preferential as it is interdependent on both the type of pretreated biomass and the fungal species used.

There is a clear effect of pretreating apparent in the ethanol yields after fermentation, where all the pretreatments are significantly increasing the ethanol yields (Fig. 4). It is well-known that degradation products of certain pretreatments will act as a fermentation inhibitor if they exceed certain levels. However, there is no sign of inhibition in any of the fermentations. Most of the fermentations have final ethanol concentrations corresponding to utilisation of 80 to 90 % of the glucose liberated in the preceding enzymatic convertibility.

### Conclusions

The findings in this study will be linked to results from project partners who have assessed availability of the agricultural residues, possible up-scaling of the low tech pretreatment technologies, and sustainability of the agricultural systems.

The results of the study suggest that 4 out of the 11 addressed West African lignocellulosic biomasses were found to be feasible for cellulosic ethanol production,

which should be taken into account when estimating cellulosic ethanol potentials of the region.

The technologies and products will be developed to give positive environmental consequences (e.g. more efficient use of biomass resources, decrease in greenhouse gas emissions, and better fertility of agricultural soil) and they will be ranked to improve the knowledge base on which the Ghanaian society can select the best context specific strategy depending on the community structure.

### Acknowledgements

The PhD is a part of a development research project titled: Biofuel production from lignocellulosic materials – 2GBIONRG, funded by the Danida Fellowship Centre of the Danish Ministry of Foreign Affairs.

### References

1. F. Kemausuor, A. Kamp, S.T. Thomsen, E.C. Bensah, H. Østergård, Assessment of biomass residue availability and sustainable bioenergy yields in Ghana, resubmitted after review to Resources, Conservation and Recycling (2013)
2. S.T. Thomsen, Z. Kádár, J.E. Schmidt, Compositional analysis and theoretical biofuel potentials from various West African agricultural residues, resubmitted after review to Biomass & Bioenergy (2013)
3. M. Ambye-Jensen, S.T. Thomsen, Z. Kádár, A. Meyer, Ensiling of wheat straw decreases the required temperature in hydrothermal pretreatment, *Biotechnology for Biofuels* (2013) 6:116
4. S.T. Thomsen, J.E.G. Londoño, J.E. Schmidt, Z. Kádár, Screening of pretreatments of common West African lignocellulosic biomass residues for ethanol production, submitted to *Renewable Energy* (2013)
5. S.T. Thomsen, H. Spliid, H. Østergård, Statistical prediction of biomethane potentials based on the composition of lignocellulosic biomass, resubmitted after review to *Bioresource Technology* (2013)



**Anna Trubetskaya**

Phone: +45 4525 2952  
E-mail: atru@kt.dtu.dk

Supervisors: Peter Glarborg  
Peter Arendt Jensen  
Anker Degn Jensen

PhD Study  
Started: April 2012  
To be completed: March 2015

## Single Biomass Particle Combustion and Fuel Characterization

### Abstract

Coal fired power plants contribute significantly to greenhouse gas emissions, particularly CO<sub>2</sub>. An attainable way to reduce CO<sub>2</sub> emissions is to replace coal with biomass in power plants. Biomass has traditionally been fired in grate and fluidized bed boilers, while experience with pure pulverized biomass combustion is limited. The objective of this PhD research is to establish accurate simplified one-dimensional mathematical models, which will be possible to use for the prediction of main combustion processes for biomass particles of different sizes and shapes. The accuracy of these models will be validated against the experimental data provided by the measurements on the wire mesh reactor, drop tube reactor and entrained flow reactor.

### Introduction

Biomass as an environmentally friendly and CO<sub>2</sub> neutral fuel is increasingly used for power production. On the global scale biomass contributes currently roughly 10 % to the primary energy demand [1].

Biomass combusted in boiler can be used for the production of heat, power and electricity. There are a variety of biomass residues available around the world. The most abundant of these are crops, forestry and livestock residues [2].

The most common ways of biomass combustion in power plants are grate firing and pulverized wood combustion. Suspension firing of pulverized fuel has been used for coal combustion for many decades. One of the challenges in the pulverized biomass combustion is to keep the power plant production energy efficient and stable in operation. The reactivity of the chars produced in the pyrolysis stage influences significantly the power plant production.

The nature of the virgin fuel and the reaction conditions during the pyrolysis stage have a strong impact on the char reactivity [3]. The impacts of pyrolysis reaction conditions on the char reactivity have been studied by many researchers. However, only limited amount of work is available to relate the pyrolysis conditions and char reactivity.

Another challenge by using biomass in a suspension firing plant is the presence of large top size biomass particles (0.5-2 mm) where the coal particles size are maximum 0.1-0.3 mm, causing problems with the flame stability and burnout. The research dealing with the char reactivity and biomass particles larger 0.5 mm at the pyrolysis conditions has not been carried out in a larger extent.

### Objectives

A major focus of this work is to investigate the different stages of a single particle biomass combustion behavior (ignition, pyrolysis and char oxidation) for particles of different type, size and shape. The char reactivity and burnout will be studied on fuels with the various ash contents and on different particle size fractions to relate the pyrolysis conditions with the char reactivity through the structural evolution and morphological changes of the char.

The accurate simplified one-dimensional mathematical single-particle model for biomass fast pyrolysis will be developed for thermally thin and thermally thick particles based on conservation of mass, energy and momentum. The developed model will additionally include influences of heating rate, final temperature and organic/

inorganic composition on the char formation and yield.

The accuracy of the model will be validated against the experimental data provided by measurements on the wire mesh reactor, drop tube reactor and entrained-flow reactor.

## Results and discussion

The experimental setup used in this study, has been designed and used at TU Muenchen. The reactor is presented schematically in figure 1:

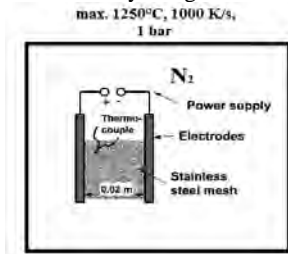


**Figure 1:** Wire mesh reactor setup

The wire mesh reactor was operated can be operated at temperatures up to 1250°C and atmospheric pressure. The heating rate is controllable up to 1000K/s. The mesh is constantly swept by nitrogen to remove any pyrolysis products and to prevent the re-condensation of tars. After the heating period the mesh was cooled down only by thermal radiation and the nitrogen sweep stream. The experimental work was carried out to investigate the influence of the heating rate, final temperature and organic/inorganic content on the char yield and char formation. In all experiments a sample mass of 10mg is used. In the reference measurements the sample mass of 10mg is verified to be low enough to ensure uniform distribution of biomass particles between wire meshes. The final temperatures of 600, 1000 and 1250°C and heating rates 10, 100, 300, 600 and 1000K/s with the additional holding time 1.0s which was found sufficient to complete the devolatilization process of 50-200µm biomass particles. Several different biomasses were used in this experimental work: pinewood (0.26%, ash), beechwood (1.3%, ash), wheat straw (3.8%, ash), washed wheat straw (1.5%) and rice husks (19.7%, ash).

The result of this investigation in terms of the heating rate influence on the char yield is shown in figure 2.

From the figure 2, the increase in the char yield is observed for all three samples when the heating rate stepped up from 10K/s to 1000K/s.

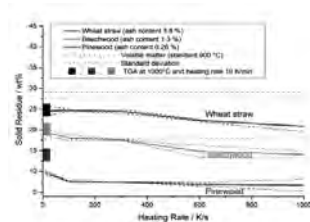


**Figure 2:** Influence of heating rate on char yield In figure 3, a significant influence of the final pyrolysis temperature is noticed.

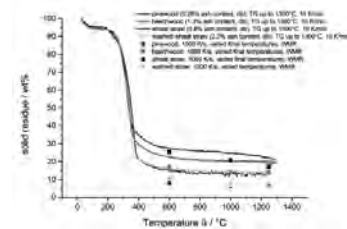


**Figure 3:** Influence of final temperature on char yield

In comparison to the slow heating rate TGA measurements (10K/s, 1300°C, N<sub>2</sub>), the WMR data showed 4-5% more of yielded char.

## Conclusion and future work

From the investigations on the wire mesh reactor, it can be concluded that the final temperature has more significant influence on the char yield than the heating rate. The further work will be conducted on the evaluation of the char structural changes by application of biomass samples with the different organic/inorganic content. The 1D mathematical model will be established.

## Acknowledgements

This PhD project is a part of the GREEN Research Center (Center for Power Generation from Renewable Energy) financed by the Danish Strategic Research Council.

## References

1. M. Kaltschmitt, Biomass for energy in Germany: status, perspectives and lessons learned, Journal of Sustainable Energy and Environ. Special Issue (2011) 481-490.
2. M. Balat, G. Ayar, Biomass Energy in the World, Use of biomass and Potential Trends, Energy Sources, 27 (10) (2006) 931-940.
3. E. Cetin, B. Moghtaderi, R. Gupta, T.F. Wall, Influence of pyrolysis conditions on the structure and gasification reactivity of biomass chars, Fuel, 83 (2004) 2139-2150.





**Anjan Kumar Tula**

Phone: +45 4525 2817  
E-mail: antu@kt.dtu.dk

Supervisors: Rafiqul Gani  
Gurkan Sin

PhD Study

Started: December 2013  
To be completed: December 2016

## Process Synthesis and Design Using Process Group Contribution Methodology

### Abstract

Process synthesis and design is the step in which an engineer will select the optimal flow sheet from the numerous alternatives for converting specific raw materials to specific desired products subject to predefined performance criteria. This work includes development of a systematic framework to simultaneously model, design, and synthesize chemical and biochemical processes using principles of the group-contribution. This new approach can be applied to both new process design problems and retrofits problems. The application range will be highlighted by various case studies.

### Introduction

Process synthesis can be considered as the cornerstone of the process design activity, it provides a systematic way to identify the types of equipment, flow rates, operating/design conditions and optimal interconnections among different units that create the best total flow sheet. In chemical process synthesis two types of problems exist, in the first type, one seeks to improve an existing process flow sheet (also known as the retrofit problem), while in the second type, one seeks to find a completely new process flow sheet. This work describes the development and application of a framework which will address both the problems. This framework concept applies the principles of the group contribution [1] approach from chemical property estimation to the synthesis and design of chemical processes.

### Process Groups Methodology

The process group methodology is analogous to CAMD (computer aided molecular design) where feasible molecules are designed through rigorous framework comprising preselected groups, target properties and structural feasibility constraints [2]. In CAMD molecules are represented using descriptors (graph representing the atoms and bonds, set of molecular groups) and the properties are evaluated using methods capable of predicting properties based on the descriptors used to represent the molecules. In the case of CAMD, the building blocks are molecular

groups, whereas for process flow sheet synthesis the building blocks could be distillation columns, mass or heat exchange modules, specific unit operations which we define as "Process groups". The bonds among the process groups represent the streams connecting the unit operations, in an analogous way to the bonds combining (molecular) functional groups. As in group contribution based molecular property prediction (where the same molecular groups may be used to represent many molecules), the process groups are also not component dependent, but component property dependent. Therefore, the use of the same process groups to represent different components having similar properties is also valid in the case of process flow sheets of a process. For example, in Figure 1, a simple process flow sheet composed of a distillation column, followed by an extractive distillation column to separate a binary azeotropic mixture by using ionic liquids as entrainer (with the addition of a makeup of solvent), followed by a flash drum and a stripping column to recover the solvent, could be represented with process groups.

The feed mixtures are represented by two process groups; one inlet process group (iC), and the inlet containing two compounds (iAB). The end products are represented by two outlet process groups (also process groups with one attachment), (oA), (oB) and one outlet process group containing two compounds (oBC). The two process groups representing a distillation (AB/B) and a solvent based separation (cycB/C) have at least one inlet and one outlet stream. Once the process groups

are identified a feasible flow sheet structure can be created as shown in Figure 1(b/c) where a binary azeotropic mixture is separated with a downstream separation process in which the feed mixture is concentrated up to its azeotropic point and then by a special process group, A and B are obtained as pure products (a product of purity  $\geq 99.5\%$ ).

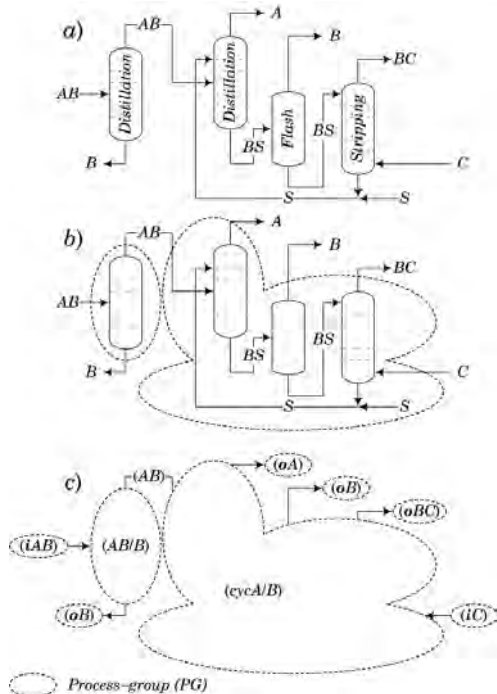


**Figure 1:** a) Representation of a simple process flow sheet; b, c) with process groups

### Frame work

The entire framework consists of 6 steps as shown in figure 2. Step 1 Problem definition: In this step the user provides the necessary information of the inlet and outlet stream data (for example, pressure, temperature, compositions and individual flow rates) along with the specs (property targets) for optimization. Step 2 Problem Analysis: This step generates all the needed information for the process alternatives synthesis and design steps by using several models. Reaction kinetics of the components is analyzed by reaction model and mixture analysis like finding azeotropes, eutectic points, binary ratios and feasible unit operation are done by mixture analysis model. Step 3 Process Group selection: In this step the various process groups are selected based upon the feasible unit operation analysis [3] done in step 2. This step uses process groups database [4] developed for this framework. Step 4 Flow sheets generation: The objective in step four is to combine the process groups selected in step three according to a set

of connectivity rules and specifications [5] to generate flow sheet structures. Each process group has outlet specifications, which are guaranteed to be met if the connectivity rules of the process group are satisfied. The output specifications are based on mass balance rules.

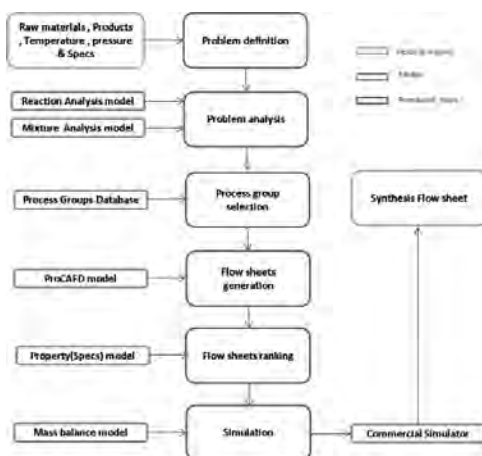


**Figure 2:** Workflow diagram of the Framework

Step 5 Flow sheet Ranking: The objective of this step is to test the generated flow sheet structure candidates with respect to their target property values(specs) chosen in step one, using the corresponding flow sheet property model. Flow sheets can be ranked based upon energy consumption, CAPEX or OPEX. Step 6 Simulation: simulation step involves three tasks: i) the resolution of the mass balance through each process group in a process flow sheet and ii) the calculation of the flow sheet design parameters of the process unit operations through reverse simulation in the flow sheet structure. iii) With the information from above two tasks, rigorous simulation is done through commercial simulators to refine the most promising process flow sheet.

### References

1. Marrero,J, Gani.R. Group-contribution based estimation of pure component properties (2001) Fluid Phase Equilibria, 183-184, pp. 183-208.
2. P.M. Harper. A Multi-Phase Multi-Level Framework for Computer Aided Molecular Design. PhD thesis, Technical University of Denmark, 2000.
3. C. Jaklsland, PhD Thesis, Department of Chemical Engineering, DTU, Denmark, 1996.
4. Merlin Alvarado-Morales, Krist V. Gernaey, John M. Woodley, Rafiqul Gani, Synthesis, Design and Analysis of Downstream Separation in Bio-refinery Processes through a Group-Contribution Approach, Computer Aided Chemical Engineering, Elsevier, 2010, Volume 28, Pages 1147-1152.
5. Loïc d'Anterrosches, PhD Thesis, Department of Chemical Engineering, DTU, Denmark, 2006.



**Fragkiskos Tzirakis**

Phone: +45 4525 2821  
E-mail: frtz@kt.dtu.dk

Supervisors: Georgios Kontogeorgis  
Nicholas von Solms  
Christophe Coquelet, MINES ParisTech

PhD Study

Started: June 2013  
To be completed: June 2016

## An Experimental and Theoretical Study of CO<sub>2</sub> Hydrate Formation Systems

### Abstract

CO<sub>2</sub> capture and sequestration (CCS) is nowadays an important area of research for alleviating CO<sub>2</sub> emissions worldwide. According to literature, CO<sub>2</sub> is globally the largest pollutant to which the global warming is attributed. Therefore, hydrates can become of great importance as they form the basis for a new technology that concerns CO<sub>2</sub> capture from flue gases (hydrate crystallisation). The understanding of the problems caused by hydrates, and their possible use, requires experimental data of high quality and advanced models. In order to enhance hydrate stability and decrease the cost of hydrate technology, several promoters are currently under examination. The experimental and theoretical results of this project should be applied over a wide range of temperatures and pressures so that more efficient and economical separation processes can be designed in the future.

### Introduction

The capture of CO<sub>2</sub> and sequestration (CCS) has become an important area of research for treating CO<sub>2</sub> emissions. CO<sub>2</sub> separation is the most expensive step of the CCS process [4], the effort is to develop energy efficient and environmental friendly technologies to capture the CO<sub>2</sub> produced in large scale power-plants, where flue gas typically contains mostly CO<sub>2</sub> and N<sub>2</sub> [1]. One novel approach to separate CO<sub>2</sub> from combustion flue gas is via gas hydrate crystallization technique [4], [1]. This technique allows hydrate crystals to be formed from a mixture of CO<sub>2</sub>+gases and CO<sub>2</sub> is captured. Then the hydrate crystals dissolve through imposition of increased temperature and CO<sub>2</sub> is concentrated in one stream. [4]

### Project Objectives

This project aims to close the gap of experimental and theoretical knowledge on CO<sub>2</sub> hydrates concentrating mainly on promoters. To achieve this objective, two research groups, one from DTU and one from the École des Mines (France), are going to work on closely, developing a new theory for the thermodynamic treatment of CO<sub>2</sub> hydrates (DTU) as well as producing new experimental data (France) for enhancing hydrate formation. More particularly, the project core is the execution of experiments on gas hydrate-formation systems e.g. for mixtures of CO<sub>2</sub>+N<sub>2</sub>+H<sub>2</sub>O+promoter. The exact systems will be decided upon the completion of the literature study. This work will be conducted in collaboration with the Laboratory of Thermodynamics

of the Center for Energy and Processes in MINES ParisTech, where the experimental work is expected to be implemented. The results obtained will be then modeled using an extension of van der Waals-Platteeuw's theory along with an association model for fluid phases in DTU.

### CO<sub>2</sub> Hydrates

CO<sub>2</sub> hydrates are solid non-stoichiometric inclusion compounds formed by a lattice structure, composed of water molecules (named *host* molecules) linked together by hydrogen bonding, and stabilized by encapsulating CO<sub>2</sub> molecules (named *guest* molecules). The most common gas hydrates belong to the three crystal structures: cubic structure I (sI), cubic structure II (sII) and hexagonal structure H (sH), Fig.1. CO<sub>2</sub> forms sI structure.

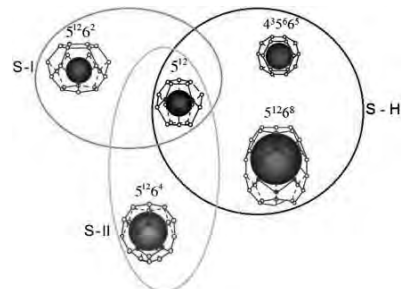


**Figure 1:** Illustration of the three common hydrate cages for sI, sII, sH

## Hydrate promoters

Currently various promoters (or formers) and mixtures of them are under examination. Thermodynamic promoters extend the hydrate formation region in a  $P, T$  diagram. Thermodynamic promoters are considered as kinds of ionic liquids (ILs). ILs are organic salts that are generally liquid at room temperatures [7]. The disadvantage of using these thermodynamic promoters is that the amount of  $\text{CO}_2$  captured in the hydrate form decreases since the thermodynamic promoters occupy some water cavities [8]. The most well experimentally examined example is the cyclic aliphatic ether: tetrahydrofuran (THF). THF in water forms nonideal mixture which shows high immiscibility at low-temperatures and complex liquid-phase behavior at high temperature [5]. Some tetra-alkylammonium halides, which are water-soluble, such as tetrabutyl ammonium bromide (TBAB), of fluoride (TBAF), of chloride (TBAC) and some tetra-alkylphosphonium halides like tetra-butylphosphonium bromide (TBPB) have already been proposed as promoters of gas hydrates. Especially, the TBAB is generally considered as promising materials for various innovating processes.

## Macroscopic and microscopic techniques for hydrate phase equilibria

For macroscopic hydrate experiments, the most common techniques used are by name: High pressure visual autoclave cell, Quartz Crystal Microbalance (QCM) in high pressure cell, rocking cell, and High-pressure Differential Scanning Calorimetry (HP-DSC). High pressure visual autoclave cell can determine  $P_{diss}$ ,  $T_{diss}$ , gas consumption rate during growth/decomposition and visual imaging of growth/decomposition. Quartz Crystal Microbalance (QCM) is also used for  $P_{diss}$ ,  $T_{diss}$ . Its major advantage is the small samples (in the order of mg) so equilibration times (hence experimental time) reduced [6]. Finally, High-pressure Differential Scanning Calorimetry (HP-DSC) can delimitate  $T_{diss}$ , heat capacities, heat of dissociation, emulsion stability and hydrate agglomeration [6].

For microscopic hydrate experiments techniques, Solid-state NMR spectroscopy, Raman spectroscopy with high pressure windowed cell, X-ray diffraction are widely applied. NMR spectroscopy can delimitate guest occupancy, structure, structural transitions, dynamics, hydration number, hydrate formation and dissociation kinetics. Raman spectroscopy can determine guest occupancy ratios, structure and structural transitions. X-ray diffraction can specify structure and structure transitions, hydrate crystal growth, decomposition and thermal expansivity [6].

## Hydrate modeling

One of the first and most important models for solid phases is the so called *van der Waals - Platteeuw (1959) model*. This is a statistical model which was applied for hydrate formation and calculates  $\mu^H - \mu^G$  of Eq. 1. The concentration of nonwater species in the hydrate was treated in a manner similar to the Langmuir adsorption

of a gas onto a solid. Thus, for a single guest molecule it arises:

$$\mu^H - \mu^G = RT \sum_i v_i / n (1 - Y_i) \quad (1)$$

Another important model for fluid phases is called *Cubic-Plus-Association (CPA) Equation of state (EoS)*. Association in chemistry describes the effect of hydrogen bonding upon a molecule (self-association) or upon two different molecules (cross-association) in a solution. The model is comprised of two contributions: a physical and association term, Eq. 2.

$$P = \frac{RT}{V_m - b} - \frac{a(T)}{V_m(V_m + b)} - \frac{1}{2} \frac{RT}{V_m} \left( 1 + \rho \frac{\partial \ln g}{\partial \rho} \right) \sum_i x_i \sum_j (1 - X_{ij}) \quad (2)$$

The physical term measures the deviation from ideality due to physical forces (mainly attractive) and can be cubic or non-cubic EoS [2].

## Conclusions

The climate change urges the researchers discovering new techniques for  $\text{CO}_2$  capture. Hydrate crystallization could become a promising technology. Therefore, the experimental data of this study for  $\text{CO}_2$  hydrate promotion will try to give a boost to that research field. The results obtained will be then modeled using an extension of van der Waals-Platteeuw's theory along with an association model (CPA EoS) for fluid phases so that a more comprehensive insight can be acquired.

## Acknowledgments

The project is part of "CO<sub>2</sub> Hydrates – Challenges and possibilities" (Project ID: 50868) and is financed by 2/3 through Danish Research Council for Independent Research and by 1/3 through DTU.

## Reference

- [1] Belandria V., Eslamimanesh A., Mohammadi A.H., Richon D., Ind. Eng. Chem. Res. 50 (2011) 4722–4730.
- [2] Kontogeorgis G.M., Folas G.K., Muro-Suñé N., Roca Leon F., Michelsen M.L., Oil & Gas Science and Technology – Rev. IFP 63 (3) (2008) 305-319.
- [3] Mayoufi N., Dalmazzone D., Fürst W., Elghoul L., Seguatni A., Delahaye A., Fournaison L., J. Therm. Anal. Calorim. 109 (2012) 481–486
- [4] Mohammadi A.H., Eslamimanesh A., Belandria V., Richon D., J. Chem. Eng. Data, 56 (2011) 3855–3865.
- [5] Ricaurte M., Torré J.-P., Asbai A., Broseta D., Dicharry C., Ind. Eng. Chem. Res. 51 (2012) 3157–3169.
- [6] Sloan E.D. and Koh C.A., 2008, Clathrate Hydrates of Natural Gases, third ed., CRC Press, Taylor & Francis Group, New York.
- [7] Tumba K., Reddy P., Naidoo P., Ramjugernath D., Eslamimanesh A., Mohammadi A. H., D. Richon J. Chem. Eng. Data, 56, (2011) 3620–3629.
- [8] Zhang, J., Lee J.W., Industrial & Engineering Chemical Research 48 (2009) 5934–5942.



**Sindhu Vudayagiri**

Phone: +45 4525 6825

E-mail: sivu@kt.dtu.dk

Supervisors: Anne Ladegaard Skov  
Ole Hassager

PhD Study

Started: August 2011

To be completed: July 2014

## Surfactants to Ease the Release of Thin Polydimethylsiloxane Films from Difficult Substrates

### Abstract

Silicone elastomers are used as dielectric electroactive polymers for making actuators, generators, sensors and as artificial muscles in medical applications. Current requirements in the actuator manufacturing put a strict limitation on the thickness of the elastomers, such that a maximum permissible thickness is around 25-50  $\mu\text{m}$ . The relatively small Young's modulus for these elastomers is a requirement for actuation capabilities. However, peeling and release of such films during manufacture processes are very difficult. To ease the release of the films, techniques like grafting of low surface energy functionalities, addition of low surface energy di-block copolymer, release agents like detergents and surfactants have been used and performance of the films tested. The methods used are required not to interfere with the Young's modulus and the dielectric permittivity in a negative way. Polysorbate-20, a non-ionic surfactant fulfils all requirements of such a release agent.

**Introduction:** Danfoss PolyPower A/S has established a large scale manufacturing process for making DEAP films.[1] The manufacture process involves the coating of elastomer mixture (PDMS + cross linker + Platinum catalyst) on a carrier web (roll) to make a thin film of thickness 25 to 50  $\mu\text{m}$  (Figure 1). The carrier web is 20 cm in width and moves at an approximate speed of 2.5m/minute in the roll to roll process. The carrier web has micro-scale corrugation lines on the surface on which the elastomer is coated. The carrier web with the elastomer coating is then heated in an oven to approximately 100oC for 2 minutes to cure the elastomer mixture. [1] The elastomer cures by hydrosilylation reaction to form an elastomer network. The cured elastomer film is then peeled from the carrier by a delaminator at a speed of 1m/minute. The microstructures on the carrier web are imprinted on the film as it cures. The flat surface of the peeled film is transferred to a nonwoven backer with the corrugated surface facing upwards. Electrode material, usually silver, is then deposited on the films by vacuum deposition. The entire manufacture process is done in a clean room environment in order to minimize defects in the fabricated elastomer films, which may manifest themselves as breakdown voltage failures. [1] The release and peeling of the films from carrier webs in the delaminator may also induce some defects in the film if the peel force is high enough to induce pre-strain. The peeling in a delaminator is much different from that of a

lab scale peeling by hand. The speed of the delaminator equipment and force with which the film is peeled have to be optimized to produce films without defects or uncontrollable pre-strain. Reducing the delamination speed, which is already quite low is not economically viable as the production line needs to operate at a profitable speed. Hence, reducing the peel forces and making release easy is a prime focus. Though PDMS has a surface energy of 19-21 mJ/m [2], the films made from the silicone systems stick too well to the substrate/carrier web owing to their low Young's modulus and thin geometry [3]. Furthermore, since the surface of the carrier web consists of microscale corrugations, the surface area is significantly high requiring high peel force to remove the PDMS film. Detergents and non-ionic surfactants are tested as release agents (Figure 2 & 3). To reduce the strain induced on the film during the peeling, release agents are good alternatives to minimize the peel force. Non-ionic surfactants are chosen in this case, in order to avoid ionization of the surfactant under electric field since the application of films as actuators requires use of high voltage.

### Materials

#### *Detergent*

The detergent tested is Akuta dish washing machine cleaning liquid. The contents of this detergent are water,

fatty alcohols, sodium cumenesulfonate, potassium cumene sulfonate, citric acid and trisodium citrate.

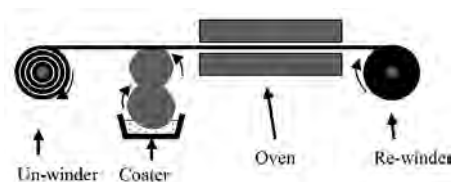


**Figure 1:** Industrial manufacture process of DEAP films[1]

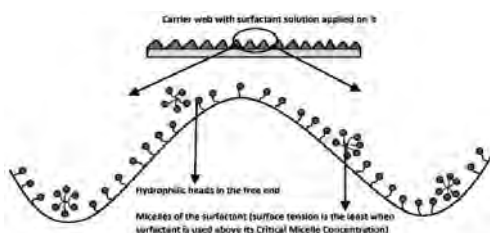


**Figure 2:** PDMS film on the treated carrier web

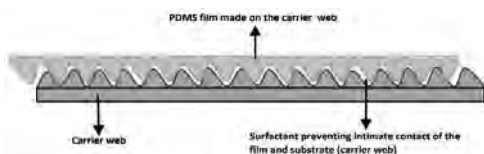


**Figure 3:** Surfactant on carrier web

#### **Non-ionic surfactants**

1. Polysorbate-20 (Polyoxyethylene (20) sorbitan monolaurate) from Sigma-Aldrich, St.Louis, MO, USA. The molecular mass of Polysorbate-20 is 1227.54 g/mol. The CMC of Polysorbate-20 is 0.06 mg/ml. [4]
2. Triton<sup>TM</sup> X-100 (Polyethyleneglycol tert-octylphenyl ether) from Sigma-Aldrich, St.Louis, MO, USA. The molecular mass of Triton X-100 is 647g/mol. The CMC of Triton is 0.129- 0.582 mg/ml. [5]
3. Tergitol<sup>®</sup> solution (Nonylphenol Ethoxylate) NP-40s from Sigma-Aldrich, St.Louis, MO, USA. The molecular mass of Tergitol is 1982.47 g/mol. The CMC of tergitol is 0.232 mg/ml. [6]
4. Cetomacrogol-1000 (Polyethylene glycol monocetyler, PO841) from Tokyo Chemical Industrial Co. Ltd., Kita-ku, Tokyo, Japan. The molecular mass of cetomacrogol is 1123.5 g/mol. The CMC of cetomacrogol is 0.0063 mg/ml. [7]

#### **Silicone networks**

Elastosil<sup>®</sup> RT 625 (Room temperature vulcanizable (RTV) silicone), Powersil Fluid TR50 and Inhibitor PT

88, respectively, were obtained from Wacker Chemie AG, Germany. Elastosil is supplied as two parts, part A is a mixture of vinyl terminated PDMS and cross-linker while Premix B is a mixture of vinyl terminated PDMS and catalyst amongst other components such as fillers. The mixing ratio of Elastosil is 9:1. The oil added is 15% and inhibitor is 0.8% by mass of the elastomer mixture. Elastosil<sup>®</sup> LR 3043 / 50 (Liquid Silicone Rubber (LSR or LR)) was obtained from Wacker Chemie AG, Germany. OS-20 (an ozone-safe volatile methylsiloxane (VMS) fluid) was obtained from Dow Corning<sup>®</sup>, USA. Elastosil is supplied as two parts A and B. The part A has PDMS and platinum catalyst and part B has the PDMS cross-linker. The mixing ratio of Elastosil A, B and OS-20 is 5:5:7 by mass.

POWERSIL<sup>®</sup> XLR<sup>®</sup> 630 A/B (a low viscosity LSR) and Belsil<sup>®</sup> TMS 803, a resin were both obtained from Wacker Chemie AG, Germany. XLR630 is supplied as two parts A and B. The part A has PDMS and platinum catalyst and part B has the PDMS cross-linker. The mixing ratio of parts A and B is 1:1. Belsil TMS 803 is an MQ type silicone resin commonly known as trimethylsiloxysilicate. It is a white powder with a particle size of 10  $\mu\text{m}$ . It is also mixed in a mass ratio of 1, 3 and 5% with XLR 630 mixture.

#### **Results and discussions:**

##### **Rheological tests:**

The Young's moduli values calculated with  $G'$  at the lowest frequency ( $\omega \rightarrow 0$ ) are as follows. 1) Elastosil LR3043/50 is 536 kPa, 2) Elastosil RT625 is 107 kPa, 3) XLR 630 with 1% Belsil is 2550 kPa, 4) XLR 630 with 3% Belsil is 5860 kPa and 5) XLR 630 with 5% Belsil is 3630 kPa

##### **Dielectric breakdown:**

The use of any release agent or technique for easing the release should not lead to a decrease in the dielectric breakdown of the films. Akuta decreased the breakdown strength of the films (Figure 4) from 82 V/ $\mu\text{m}$  to 73 V/ $\mu\text{m}$ , which is a significant reduction.[8] The Akuta detergent has sodium/potassium cumenesulfonate which are zwitterionic surfactants with Na<sup>+</sup>/K<sup>+</sup> and O<sup>-</sup> in the hydrophilic head. The detergent adsorbs into the PDMS films. The surfactants and salts in Akuta get ionized/charged under electric field. Since the detergent percolates into the films (network), they make the films conductive as the surfactants get ionized and conduct electricity under high voltage.[9] Also, Akuta had a corrosive effect on films as it is observed that the films became sticky over a period of time which makes them unusable. Such conductive films cannot be used for making actuators. Hence, usage of Akuta as a release agent was discarded. For further tests non-ionic surfactants (10% solutions) were chosen. Non-ionic surfactants do not have conducting ions. For both Elastosil RT 625 and LR 3043/50 films, Polysorbate-20 shows the least influence on breakdown strength, compared to other surfactants (Figure 4). The addition of

resin depreciates the breakdown strength of the XLR 630 films, the maximum depreciation being 16% for 5% resin. The error bars mark the difference in the measurements between two identical samples

### Peel tests

The peel test results are shown in Figure 5. Akuta reduced the R between RT 625 film and carrier web from 20.9 N/m to 14.9 N/m, but since Akuta lowered the breakdown strength of the films, its further use was however discarded. For RT 625 films the value of R is reduced from 21 N/m to a lowest of 6.3 N/m with Triton X-100 (20% solution). RT 625 films show lower R values (20 N/m) than LR 3043/50 films overall. The low R values of RT 625 films can be attributed to the presence of 15% oil in the formulations which was a trend observed in the work by Vudayagiri et al. [3] The 2.5, 5 and 7.5% Polysorbate-20 solutions gave very high R values for Elastosil LR 3043/50 films as the surfactant content is too low and does not reduce the R effectively. For LR 3043/50 films the value of R is reduced from 116.4 N/m to a lowest 2.8 N/m with Polysorbate-20 (10% solution), which is a decrease of more than 4000%. For XLR630 films the value of adhesive force (R) reduced from 20.7 N/m to a lowest of 10.5 N/m with 3% with Belsil resin. From Figure 7c it is seen that as Young's modulus of the films increase their peel/adhesive force decreases. [3] Belsil TMS 803 is a trimethylsiloxy silicate MQ type resin [10] which when compounded with PDMS networks makes them more hydrophobic. The resins can be incorporated with the reactive Si-H or Si-Vinyl groups so that they can bond with the elastomer matrix via the hydrosilylation reaction. [11] At 3% resin, the cross-linking density is optimum and a high Young's modulus is attained by the cured elastomer as seen from. When the resin is increased to 5% the Young's modulus decreases which could be attributed to Belsil interfering negatively with the crosslinking of the elastomer matrix.

### Discussion

Polysorbate-20 (10% solution) is the optimum surfactant to be used as a release agent as it gave low peel forces and had negligible effect on the dielectric breakdown strength of the films. Polysorbate-20 caused the blackening of the silver electrode that is sputtered on it. Initially, the color change suggested oxidation of the silver electrode. On the contrary, Polysorbate-20 is a reducing agent and undergoes self-oxidation. Polysorbate-20 and 80 are used as reducing agents to reduce silver salts to silver metal nanoparticles. [12] The possibility of silver metal getting oxidized by Polysorbate-20 is therefore excluded and Polysorbate-20 may rather work as protective sacrificial layer. Polysorbate-20 is obtained from Sigma-Aldrich Corporation, St. Louis, MO, USA for 397 DKK per kg. The amount of Polysorbate-20 required is 3.5g/m<sup>2</sup> of the surface area of carrier web (real surface area, including corrugations), which translates to 1.4 DKK/m<sup>2</sup>. The calculations are made considering a 50% wastage of the surfactant, since there is wastage during the application

and evaporation process. The use of Polysorbate-20 is therefore a cheap and environmentally friendly alternative as opposed to fluorinated elastomers and liners. In comparison to Belsil resin, Polysorbate-20 is a cheaper alternative and it doesn't interfere with the crosslinking reaction.

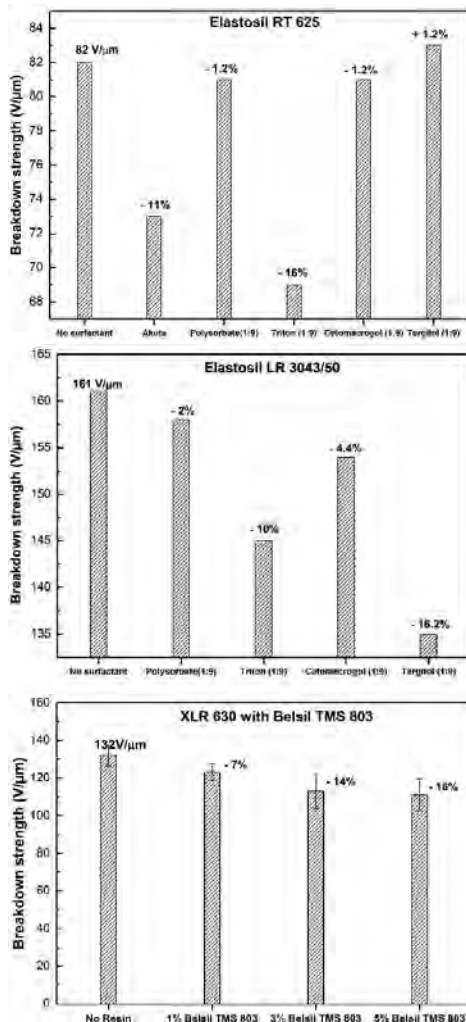


Figure 4: Breakdown test results

### Conclusions

Though Akuta detergent reduced the peel forces to 14.9 N/m, it had a corrosive effect on the films and decreased the breakdown strength of the films. It is therefore not suitable to be a release agent.

The Belsil resin at 3% concentration reduced the peel forces to 10.5 N/m and had a negative influence on the breakdown strength of the XLR630 films. Hence, this method will compromise the quality of the DEAP films.

The adhesive force between the film and the carrier web is the lowest (2.8 N/m) with the Polysorbate-20: water (1:9) formulation. Also, Polysorbate-20 does not interfere with the breakdown of the films unlike Akuta or Belsil resin. In all the methods tested, using Polysorbate-20 solution is the best and the most economical method for easy release of very thin polydimethylsiloxane films from microstructured carrier webs in the current manufacturing process set up.

## Acknowledgements

The authors gratefully acknowledge the financial support from the Danish National Advanced Technology Foundation and the technical support from Michael Daniel Junker, Process Engineer, Danfoss Polypower A/S.

## References:

- [1] H. Kiil, M.Y. Benslimane, *Proc. of SPIE, San Diego, California, USA*. **2009**; 72870R-1 – 72870R-10
- [2] A.C.M. Kuo, *Poly (dimethylsiloxane) Polymer Data Handbook*, Oxford University Press, **1999**, pp. 411–435.
- [3] S. Vudayagiri, M.D. Junker, A.L. Skov, *Polymer Journal*. **2013**; 45(8), 871-878.
- [4] K.L. Mittal, *Journal of Pharmaceutical Sciences*. 1972; 61(8): 1334-1335.
- [5] K.S. Hait, S.P. Moulik, *Journal of surfactants and detergents*. 2001; 4(3): 303-309.
- [6] F.L. Bautista, R.M. Sanz, C.M. Molina, N. Gonzalez, D. Sanchez, 14th International Biodeterioration and Biodegradation Symposium. 2009; 63(7): 913-922.
- [7] P.H. Elworthy, *Research Papers*. 1960; 293-299.
- [8] P. Sommer-Larsen, A.L. Larsen, *Proc. of SPIE*, **2004**; 5385, 68-77.
- [9] D. López-Díaz, M.M. Velázquez, *The Chemical Educator*. **2007**; 12, 5.
- [10] J.M. Zeigler, F.W.G. Fearon, *Silicon-Based polymer Science: Advances in Chemistry*. American Chemical Society, **1990**, pp. 181-199.
- [11] H. Mayer, *Farbe + Lack*. **1991**; ISSN 0014-7699, 97(10): 867-870.
- [12] H.J. Li, A.Q. Zhang, Y. Hu, L. Sui, D.J. Qian, M. Chen, *Nano Express*. **2012**; 7(612): 1-13.

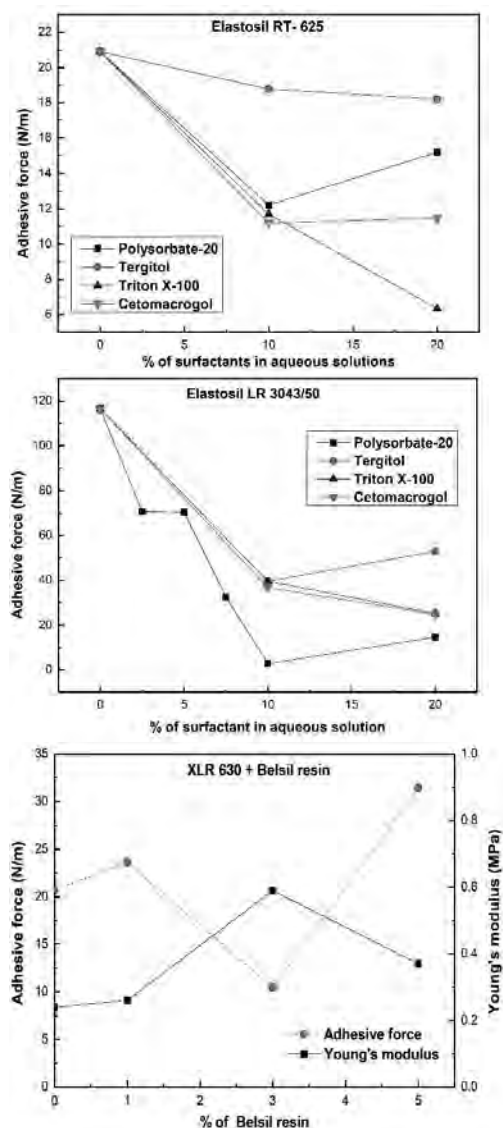


Figure 5: Peel test results





**Rui Xue**

Phone: +45 4525 2993  
E-mail: rxue@kt.dtu.dk

Supervisors: John M. Woodley  
Anne S. Meyer  
Jørn D. Mikkelsen

PhD Study  
Started: December 2010  
To be completed: June 2014

## Reaction and Reactor Design for Multi-step Biocatalysis

### Abstract

Enzyme cascades (which mimic nature) using two or more enzymes sequentially for the synthesis of useful chemical compounds are attracting increasing interest as a potential means of production. Such schemes overcome many of the conventional difficulties integrating biocatalysis into chemical synthetic schemes, such as changes of media, temperature and pH. In this project, the synthesis of sialic acid derivatives and useful oligosaccharides will be taken as an example for the design of an enzyme cascade. Laboratory scale-down tests will be carried out to characterize the enzymatic systems. Engineering tools for selection of reactors and processes for multi-enzymatic synthesis will be developed.

### Introduction

During the past decade, biocatalysis has become increasingly attractive for the development of more efficient and cleaner chemical synthetic processes [1]. Higher selectivity and specificity, as well as the use of mild reaction conditions in general gives an excellent 'green' profile to reactions catalyzed by enzymes. Enzymatic synthesis can either involve a single enzyme or can make use of more than one enzyme operating either sequentially or in parallel for the synthesis of more complex compounds (Figure 1) [2,3].

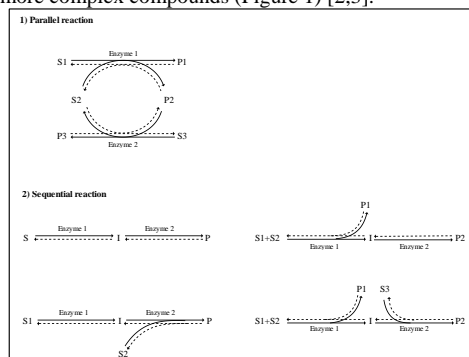


**Figure 1:** Scheme of different multi-enzymatic reactions. S: substrate, I: intermediate, P: product [3].

The interesting concept of using multi-enzymatic synthesis mimics the chemical processes in nature.

According to the applications, multi-enzymatic systems can be classified into four categories, including cofactor regeneration (parallel reactions), equilibrium shift (sequential reactions), renewable biomass feedstock degradation (mixed reactions) and macromolecule synthesis (mixed reactions). Multi-enzymatic processes have been deemed as an alternative to chemical-catalysis in the production of a number of pharmaceuticals and fine chemicals. In principle, they may also be applied in the field of bulk chemicals (and even biofuels and bio-polymers), although the cost structure in these sectors makes application challenging [3].

The purpose of this project is to develop tools for the selection of synthetic routes, reactors, process and operations for the reactions which involve multi-step biocatalysis.

### Process options

Multi-enzymatic syntheses can be carried out in either a single reactor or several reactors. In theory, for an n-step multi-enzymatic reaction, the number of possible processes is  $2^{n-1}$ . Hence, reducing the size of the search space is highly desirable [3]. Developing an engineering tool to accelerate the selection process is one of the main goals in this project.

For the reactions in which the combination of enzymes may come from different hosts, the enzymes may not share similar optimal temperatures, optimal pH values and other conditions, or even more importantly they may not have similar reaction rates at similar

concentrations of reagents. Hence, it might be preferable to divide the cascade into several groups [3, 4].

On the other hand, a one-pot process uses more than one enzyme in a single reactor. The concentrations of the intermediates are usually low so that the possibility of intermediate inhibition may be reduced. Additionally, one-pot processes may also reduce downstream processing and operating costs [5]. However, the limitation of a one-pot process is that the conditions in each reaction (such as media, temperature, pH, catalyst stability) should be well balanced and optimized for maximum productivity [3].

### Reactor options

The selection of an optimal reactor for an enzymatic reaction is usually based on cost, space, mass transfer, kinetics, and reusability of the catalyst [6, 7]. The same principles apply for multi-enzymatic processes.

The number of factors affecting the kinetics of a multi-enzymatic reaction is much more than that in a kinetic model for a single enzymatic reaction. The evaluation and selection of reactors for a multi-enzymatic process, based on the kinetic model, is therefore more difficult. Experimental work can be carried out to examine the performance of different reactors. For the purposes of understanding the mechanisms of the biocatalysis and better experimental design, however, it is also important to establish the theoretical basis first [3]. Integral kinetic models describing the reactions in different reactors are desirable and give rise to a new challenge in the project.

### Chemo-enzymatic synthesis of sialic acids

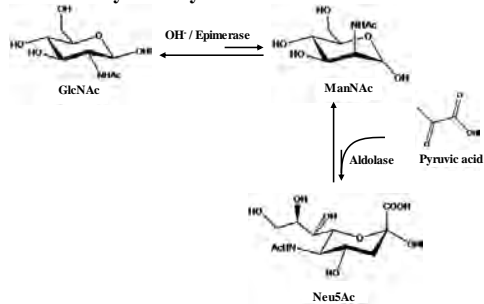


**Figure 2:** Scheme of the reactions involved in the synthesis of sialic acid. GlcNAc: N-acetyl-glucosamine; ManNAc: N-acetyl-mannosamine; Neu5Ac: N-acetyl-neuraminic acid.

The case studies involve the synthesis of sialic acid. Sialic acid has been attracting much interest due to its potential applications as the compounds of interest in the pharmaceutical industry [8]. The reactions involved in the production of sialic acid are shown in Figure 2. Both of the two reactions are thermodynamically unfavorable in the desired direction. In this project, a two-step chemo-enzymatic system for sialic acid (Neu5Ac) production has been investigated.

### Kinetic study

The research revealed the key properties in the reactions as well as pH/temperature/substrate concentration dependency on substrate stability and reaction kinetics.

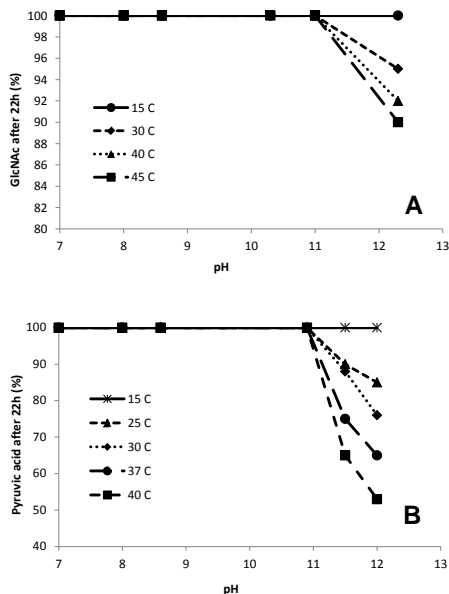


**Figure 3:** Stability of N-acetyl-glucosamine (A) and pyruvic acid (B) at different temperature and pH.

As shown in Figure 3, stability of N-acetyl-glucosamine (GlcNAc) and pyruvic acid depended on the temperature and pH chosen for the reactions. The more alkaline the conditions were, the more unstable the compounds were. Temperature may largely influence the stability of the compounds as well.

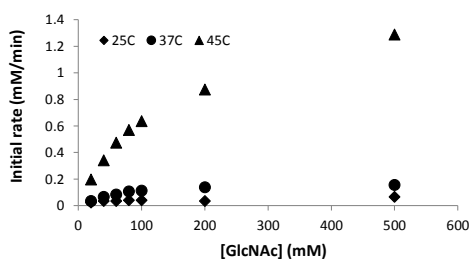


**Figure 4:** Initial reaction rates of the first reaction (epimerization) versus initial concentration of GlcNAc: 25°C NaOH pH 12.0 (◆), 37°C NaOH pH 12.0 (●), 45°C NaOH pH 12.0 (▲).

In Figure 4, it is shown that increasing temperature markedly increased initial rate of the first reaction (alkali-catalyzed epimerization). It also shows that an increase in GlcNAc concentration decelerates the reaction, resulting in non-linear curves.

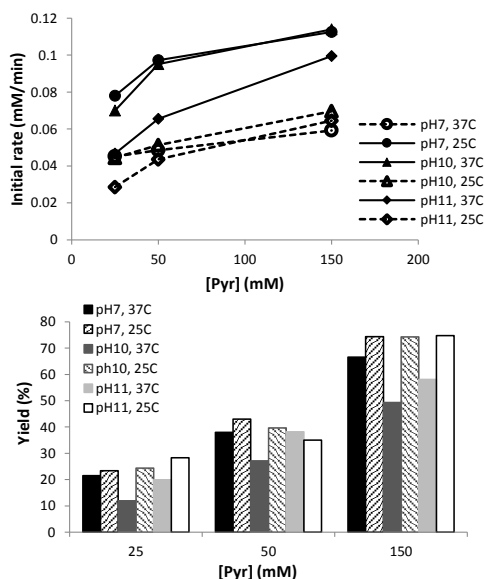


**Figure 5:** Initial rates and yield of Neu5Ac for the second reaction (aldol-condensation) versus initial concentration of pyruvic acid and pH.

Figure 5 shows the initial rates and product yields of the second reaction (enzyme-catalyzed aldol-condensation) under different conditions. The rates were higher at a higher temperature, and they were lower at higher pH. The enzyme worked faster under more neutral pH settings. From low to high pyruvic acid concentrations, the reaction rates showed a general increasing trend. It was likely to be caused by the increased concentration of enzyme-pyruvate complexes that can react. The rate increase might also stem from increased enzyme stability from pyruvate decomposition products. The enzyme was thermo stable in the examined region as yield did not vary significantly as temperature increased. A tendency of lower Neu5Ac yield can be seen in Figure 5 at higher temperature. The reaction from ManNAc to Neu5Ac is an exothermic reaction. The final yields should be lower at higher temperatures as the equilibrium is shifted towards the endothermic ManNAc product.

#### Different operation strategies

As aldol condensation is exothermic, increasing the temperature lower the conversion of pyruvic acid and ManNAc into Neu5Ac. However, epimerization favors high temperature. High temperatures can also accelerate reaction rate. In addition, epimerization can only occur at high pH, however, aldolase may be deactivated under the same condition. As a result, a temperature shift and/or a pH shift may be required, if one-pot process is applied.

Different operation strategies with temperature and/or pH shifts have been investigated as shown in Figure 6.

In Experiment 5, temperature shift was applied. The yield of Neu5Ac had an increase of 15.9% comparing to the control experiment. In the experiments with pH shift (Experiment 2-4), the results indicated that pH shifts did work but only at low temperature (15°C or 30°C). The higher the temperature was, the lower the yield increase was for a pH shift. It may be due to that aldol condensation is an exothermic reaction. It may be also caused by the deactivation of enzymes at high temperature.

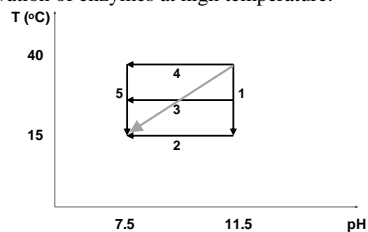


**Figure 6:** Experiments with temperature or pH shift (black arrow), and both temperature and pH shift (gray arrow).

Aldolases might be partially deactivated under alkaline conditions. This deactivation might be reversible as yields increased in Experiments 2 and 3 with pH shift. However, epimerization stopped when pH was shifted from 11.5 to 7.5. Insufficient amount of intermediate (ManNAc) may reduce the overall yield of Neu5Ac. In the experiment with both temperature and pH shift, the results are similar to the results from the experiments with only temperature shift.

Different substrates and/or catalysts feeding strategies have been also investigated to further optimize the process, as shown in Figure 7.

In the case of pyruvic acid fed-batch (Figure 7A), the yield of Neu5Ac was increased by 27.3% comparing to the control experiment. Smaller amount of pyruvic acid degradation products was observed as well. In the experiment of aldolase fed-batch (Figure 7A), the yield was increased by 21.8% which is lower than pyruvic acid fed-batch. It may be due to the inhibitory effect caused by high pyruvic acid concentration. In this case, more substrate degradation was observed comparing with pyruvic acid fed-batch. A combination of these two strategies was also tested. In the aldolase-pyruvic acid fed-batch (Figure 7B), around 20% increase in the product yield was obtained, and the level of substrate degradation was low. Interestingly, a complete consumption of the intermediate (ManNAc) was also been observed in this scenario. In all of these three cases, temperature shift was necessary and pH should be maintained at 11.5 before pH shift.

Feeding GlcNAc was also carried out (Figure 7A). Only temperature shift was applied, because the reaction should be kept at alkaline condition to prompt epimerization. In this case, concentration of GlcNAc was kept at low level and the inhibitory effect of GlcNAc on aldol condensation was reduced. However, the yield of Neu5Ac after three days was lower than it in the control experiment. Slower reaction might be

caused by low substrate concentration. Aldolase might also have lower activity under alkaline condition.

At last, two-pot processes were investigated as well (Figure 7C). Low yield of Neu5Ac was observed, due to

high inhibition of GlcNAc and pyruvic acid on the aldol condensation. ManNAc was accumulated in the reaction mixture.

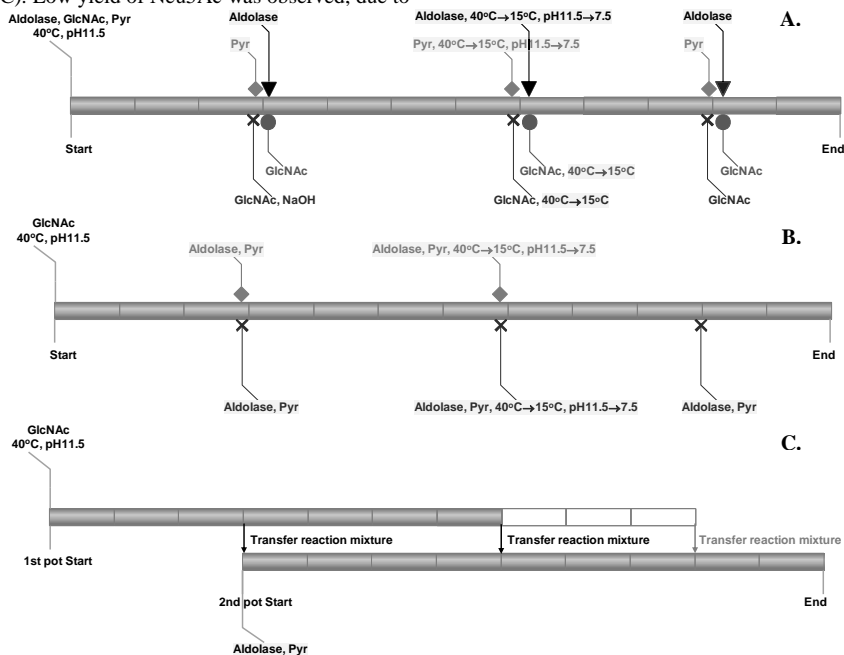


**Figure 7:** Experiments with different feeding strategies. A. pyruvic acid feeding ( $\blacklozenge$ ), aldolase feeding ( $\blacktriangledown$ ), GlcNAc and NaOH feeding ( $\times$ ), GlcNAc feeding ( $\bullet$ ); B. aldolase and pyruvic acid feeding: two steps ( $\blacklozenge$ ), tree steps ( $\times$ ); C. Two pots process, transfer reaction mixture from the first pot to the second pot twice (gray) or three times (white).

### Conclusion

According to the experimental analysis for the reaction kinetics, different operation strategies for sialic acid production have been proposed and validated in the laboratory. Neu5Ac yield has been increased by more than 20% in pyruvic acid fed-batch compared to those without temperature/pH shift and pyruvic acid feeding. Further optimization can be done in the future.

### Acknowledgements

The author would like to express her gratitude to Technical University of Denmark for the financial support.

### List of publication

1. R. Xue, J.M. Woodley, *Bioresour. Technol.* 115 (2012) 183-195.
2. R. Xue, J.D. Mikkelsen, A.S. Meyer, J.M. Woodley, 10th International Symposium on Biocatalysis and Biotransformations, Sicily, Italy, 2011.
3. R. Xue, J.D. Mikkelsen, A.S. Meyer, J.M. Woodley, Zing Conference on Biocatalysis, Xcaret, Mexico, 2012.
4. R. Xue, J.M. Woodley, 11th International Symposium on Biocatalysis and Biotransformations, Manchester, UK, 2013.

5. R. Xue, J.M. Woodley, *Enzyme Engineering Conference XXII*, Toyama, Japan, 2013.

### References

1. D.J. Pollard, J.M. Woodley, *Trends Biotechnol.* 25 (2007) 66-73.
2. A. Bruggink, R. Schoevaart, T. Kieboom, *Org. Process Res. Dev.* 7 (2003) 622-640.
3. R. Xue, J.M. Woodley, *Bioresour. Technol.* 115 (2012) 183-195.
4. D. Monti, E.E. Ferrandi, I. Zanellato, L. Hua, F. Polentini, G. Carrea, S. Riva, *Adv. Synth. Catal.* 351 (2009) 1303-1311.
5. P.A. Santacoloma, G. Sin, K.V. Gernaey, J.M. Woodley, *Org. Process Res. Dev.* 15 (2010) 203-212.
6. J.F.A. Fernandes, M. McAlpine, P.J. Halling, *Biochem. Eng. J.* 24 (2005) 11-15.
7. J.M. Woodley, M.D. Lilly, in: J.M.S. Cabral, D. Best, L. Boross, J. Tramper (Eds.) *Applied Biocatalysis*, Harwood Academic, 1994, p. 371.
8. R. Schauer, *Glycoconj. J.* 17 (2000) 485 - 499.



**Shamsul Bin Zakaria**

Phone: +45 256813  
E-mail: shaza@kt.dtu.dk

Supervisors: Anne Ladegaard Skov

PhD Study

Started: January 2013  
To be completed: January 2016

## The Electrical Breakdown of Thin Dielectric Elastomers: Thermal Effects

### Abstract

Dielectric elastomers are being developed for use in actuators, sensors and generators to be used in various applications, such as artificial eye lids[1], pressure sensors[2] and human motion energy generators[3]. In order to obtain maximum efficiency, the devices are operated at high electrical fields, which make the likelihood for electrical breakdown large. Hence for many applications the performance of the dielectric elastomers is limited by this risk of failure, which is triggered by several factors. Amongst others thermal effects may strongly influence the electrical breakdown strength[4]. In this study, we model the electrothermal breakdown in thin PDMS based dielectric elastomers in order to evaluate the thermal mechanisms behind the electrical failures. The objective is to predict the operation range of PDMS based dielectric elastomers with respect to the temperature at given electric field.

### Introduction

For power cables used in high-voltage applications, the mechanisms of the electrical breakdown in these solid insulators have been discussed for several decades. Several factors that might lead to electrical breakdown such as electric breakdown, thermal breakdown, electromechanical breakdown and partial discharge breakdown have been studied extensively[5]. Even though power cable and dielectric electroactive polymers (DEAP) are operated at high electrical fields, the differences in functionalities, applications and properties make them distinct from each others. Thus, currently studies of the mechanisms of electrical breakdown in DEAP are important in line with the development of DEAP technology and certainly this information can give numerous benefits especially for the manufacturers. For instance, in the early 1960s, polyethylene was chosen as an insulator for power cables as replacement for butyl rubber[6]. This hydrophobic material[7] was assumed to be a perfect insulator at that time. However, after a few years in service the cables started to break down[6]. Therefore, the investigations were performed to elucidate the mechanisms behind this failure. The investigations showed that the cable encountered water degradation which now is well-known as 'water treeing'. Consequently, a triple extrusion technique was introduced in order to prevent moisture and thereby reduced the water treeing problem considerably[5].

In thin dielectric films, when the power dissipation increases rapidly with the increasing applied voltage, at a certain point, it will achieve a critical voltage. Whitehead[8] termed this 'the maximum thermal voltage', i.e. the voltage before thermal runaway occurs. Analytical and numerical theories to predict thermal runaway for thin dielectric films have been developed. For instance, Qi (2003)[9] has studied thermal runaway of a thin polypropylene film between two metal electrodes using finite element method (FEM) where the temperature rise as function of electric fields for 10  $\mu\text{m}$  thick polypropylene film has been computed and the result shows the temperature increase slowly prior the critical field (875  $\text{V}/\mu\text{m}$ ) at which thermal runaway occurs.

### Specific Objectives

In this study, the effects of thermal to the electrical breakdown in thin PDMS film will be modeled. We assume the effect of temperature on electrical breakdown of thin PDMS film is different from polypropylene film as investigated by Qi (2003)[9]. The main difference is that the PDMS elastomer is chemically crosslinked and thus the Young's modulus will not decrease with temperature as for the thermoplastic. Furthermore, recent studies (Kollosche 2011)[10] have shown that the breakdown strength increases with the increasing Young's modulus.

The modeling will be based on experimental data of the influence of temperature on dielectric permittivity, elasticity and conductivity. Furthermore, thermogravimetric studies will also be performed to evaluate the thermal-stability of the materials with no applied electrical field.

## Results and Discussion

Figure 1 shows storage permittivity and loss permittivity of PDMS films with varying temperature from 25°C to 450°C. Meanwhile, figure 2 show electrical conductivity as function of temperature. The figures clearly indicate an increase in loss permittivity and electrical conductivity of PDMS films upon increasing the temperature. This can be attributed to the increase in the segmental mobility of PDMS chains[11], since the specific volume of the polymer is temperature dependent, i.e., it increases as the temperature increases. In other words, at lower temperature, as the dipoles are rigidly fixed in the film, the field cannot change the condition of dipoles to the same extent. As the temperature increases, the polarization increases as a result of the dipoles becoming more mobile and they will able to respond to the applied electric field[12].

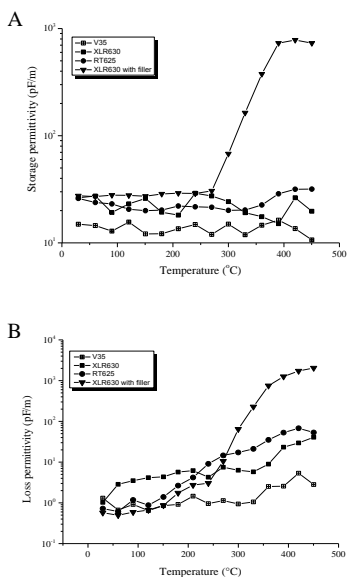


**Figure 1:** The dielectric properties as function of elevated temperatures for several PDMS films: (A) Storage permittivity (B) Loss permittivity.

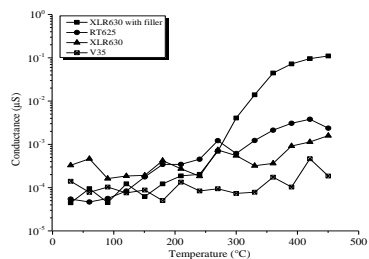


**Figure 2:** The electrical conductivity as function of temperature for several PDMS films.

The increases of the loss permittivity with increasing temperature are attributed to more dissipation of the electrical energy into heat[13]. At the same time, the increases of electrical conductivity on the elevated temperature cause more of the heat will be produced since the joule heating is directly proportional to the electrical conductivity[5]. Therefore these properties are likely affected by the electrothermal breakdown behavior in PDMS film. Hence, a model that evaluates the effect of temperature and electric field dependence of electrical conductivity on electrothermal breakdown in PDMS film has been developed in this study and will be discussed in the next section.

Beside the purpose of the TGA analysis to determine the percentages of silica loaded into various PDMS films, it was also performed in order to ensure the electrothermal breakdown occurring before the film degrading. As shown in figure 1 and 2, there is a significant increase in the loss permittivity and the electrical conductivity when the temperature of PDMS films is above 150°C. In the meantime, the PDMS films start to degrade at 300°C with the percentage of weight loss is 2% (Table 1). Hence, these properties ascertain that electrothermal breakdown in PDMS film will occur before the degradation will take place.

**Table 1:** The percentages of silica and the filler inside PDMS films and the temperature where 2% of weight of the films have moved out.

PDMS films	Weight of fillers (%)	Temperature at 2% of weight degradation (°C)
XLR630 with filler	40	313
XLR630	53	419
V35	0.2	451
RT625	62	305

For a PDMS film, the heat production rate by applied voltage across the film can be calculated as[5]

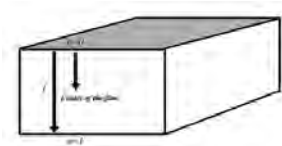
$$P = \sigma \cdot E^2 \quad (1)$$

where  $\sigma$  is the electrical conductivity and  $E$  is the electric field. In the model we assume that voltage across the film is increased in small increments, and assuming that at each voltage step, thermal steady state is reached. The surface temperatures were fixed and the initial temperature and boundary temperatures are set to room temperature.

As illustrated in figure 3, with the electric field applied along the  $x$  axis, the thickness of the film was given by  $l$ , one boundary of the film is at  $x=0$ , another boundary at  $x=l$ . The temperature distribution at steady state is then given by[14]

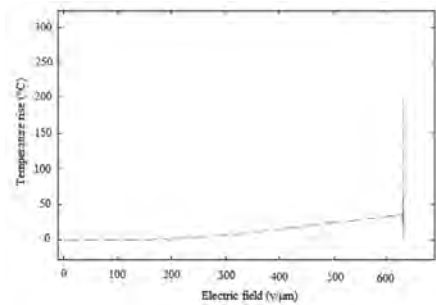
$$dT = \frac{A_0}{2K} (x(l-x)) \quad (2)$$

where  $K$  is the polymer thermal conductivity and  $A_0$  is the averaged volumetric power dissipation. Then the average film temperature was calculated in order to be applied in computing a new average electrical conductivity ( $\sigma$ ).



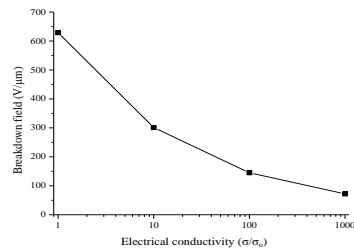
**Figure 3:** The PDMS film with  $l$ = the thickness of the film and  $x$ = the position where the thermal breakdown occurs. The maximum temperature will be achieved at the center of the film ( $x=\frac{l}{2}$ ) as predicted by Qi (2003)[9].

Figure 4 shows the general behavior of temperature versus electric field for PDMS film which the temperature at the center of the sample just before thermal runaway is only a few degrees above the boundary temperature. With only a few volts increase across the sample, thermal runaway occurs very rapidly. This is common characteristic of electrothermal instability which has also been observed in electrothermal computations[15, 16]. It is worth acknowledging that the results of this work demonstrate the breakdown fields that are enormously higher than the electrical breakdown strength typically reported for PDMS which in range from 19 to 133 V/ $\mu\text{m}$ [17]. Hence, thermal breakdown may not be the major factor that cause of electrical breakdown in thin PDMS based dielectric elastomers.



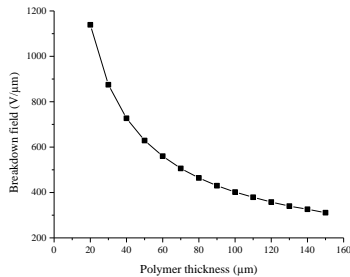
**Figure 4:** The temperature rise versus electric field for 50  $\mu\text{m}$  thick PDMS film as computed by quasi-steady state numerical method. The temperature increase slowly prior to critical field (629V/ $\mu\text{m}$ ) at which thermal runaway occurs.

Figure 5 shows the breakdown field as function of electrical conductivity for 50  $\mu\text{m}$  thick PDMS film. The graph illustrates that the higher electrical conductivity gives the breakdown field lower, as expected and this ensures that electrothermal breakdown is relevant in the room temperature where the heat production rate is strongly dependent on the electrical conductivity of the film (equation 4).



**Figure 5:** Breakdown fields as function of conductivity at room temperature. The initial electrical conductivity,  $\sigma_0$  of the 50  $\mu\text{m}$  thick PDMS film is  $2.45e^{-16}$  S/m at room temperature.

Figure 6 shows the affect of film thickness on breakdown field for PDMS film. The graph demonstrate the similar trend which the breakdown field exhibit hyperbolically decreases as the position where the breakdown field was measured is closer to the film surface as the result of the heat that generated inside the film can be removed rapidly to the surrounding. This characteristic of electrothermal breakdown in thin polymer films was predicted and have been shown the same behavior in Tröls (2013)[18].



**Figure 6:** The dependence of the polymer thickness on the breakdown field was computed as described in the text. The value of  $x$  was fixed as half of the film thickness.

### Conclusion

In this study, the effect of temperature on dielectric properties of different systems of PDMS dielectric elastomers has been studied experimentally and the model of electrothermal breakdown in thin PDMS based dielectric elastomers has been developed. From both methods, it can be concluded that electrothermal breakdown of the materials is strongly influenced by the increase in both dielectric permittivity and conductivity and the electrothermal breakdown may not be the major factor that cause of electrical breakdown in thin PDMS based dielectric elastomers.

### Acknowledgements

The authors gratefully acknowledge the financial support from the Ministry of Education of Malaysia and Universiti Malaysia Pahang.

### References

[1] S. H. Goodwin-Johansson, P. H. Holloway, G. McGuire *et al.*, "Artificial eyelid for protection of optical sensors," 225-231 (2000).

[2] Y. Iskandarani, and H. R. Karimi, "Pressure sensor development based on Dielectric Electro Active Polymers." 530-535.

[3] J. A. Paradiso, and T. Starner, "Energy scavenging for mobile and wireless electronics," *Pervasive Computing, IEEE*, 4(1), 18-27 (2005).

[4] J. O'Dwyer, "Breakdown in solid dielectrics," *IEEE Transactions on Electrical Insulation*(6), 484-487 (1982).

[5] J. C. Fothergill, and L. A. Dissado, [Electrical degradation and breakdown in polymers] IET, (1992).

[6] W. Thue, [Electrical power cable engineering] CRC Press, (2012).

[7] M. Ashraf Khan, and R. Hackam, "Loss of hydrophobicity of high density polyethylene." 2, 378-381 vol.2.

[8] S. Whitehead, [Dielectric breakdown of solids] Clarendon Press Oxford, (1951).

[9] Q. Xiaoguang, Z. Zhong, and S. Boggs, "Computation of electro-thermal breakdown of polymer films." 337-340.

[10] M. Kollosche, H. Stoyanov, S. Best *et al.*, "Parameter dependence of an electro-mechanical breakdown model for insulating elastomeric films." 79760S-79760S-7.

[11] M. Akram, A. Javed, and T. Z. Rizvi, "Dielectric properties of industrial polymer composite materials," *Turk J Phys*, 29(6), 355-362 (2005).

[12] O. G. Abdullah, S. A. Hussen, A. Alani *et al.*, "Electrical Characterization of Polyvinyl Alcohol Films Doped with Sodium Iodide," *Asian Transactions on Science & Technology (ATST ISSN: 2221-4283) Volume, 1*.

[13] A. R. Von Hippel, and A. R. Hippel, [Dielectrics and waves] Artech House, (1954).

[14] H. S. Carslaw, and J. C. Jaeger, [Conduction of Heat in Solids] Oxford University Press, 130 (1959).

[15] S. A. Boggs, S. Nishiwaki, M. Toyoda *et al.*, [Thermal Stability in High Current Contacts-Effect of silver thickness], Boston(2002).

[16] S. A. Boggs, S. Nishiwaki, M. Toyoda *et al.*, "Scaling of High Current Contact Thermal Stability," *IEEE Asia Pacific Transmission and Distribution Conference and Exposition*, 1, 99-103 (2002).

[17] A. P. Gerratt, and S. Bergbreiter, "Dielectric breakdown of PDMS thin films," *Journal of Micromechanics and Microengineering*, 23(6), 067001 (2013).

[18] A. Tröls, A. Kogler, R. Baumgartner *et al.*, "Stretch dependence of the electrical breakdown strength and dielectric constant of dielectric elastomers," *Smart Materials and Structures*, 22(10), 104012 (2013).





## Birgitte Zeuner

Phone: +45 4525 2610

E-mail: biz@kt.dtu.dk

Supervisors: Anne S. Meyer  
Anders Riisager, DTU Chemistry

### PhD Study

Started: December 2009

To be completed: December 2013

## Optimizing the Biocatalytic Productivity of an Engineered Sialidase from *Trypanosoma Rangeli* for 3'-Sialyllactose Production

### Abstract

Human milk oligosaccharides (HMOs) are a family of glycans that are highly abundant in human milk, but rare in milk from other mammals including bovine milk, which is the basis of most infant formula. Thus, the interest in producing HMOs from cheap, abundant sources is huge. A sialidase from *Trypanosoma rangeli* has been engineered to improve its trans-sialidase activity and has been used for production of 3'-sialyllactose, a model HMO compound, in gram quantities. Using enzyme immobilization and an enzymatic membrane reactor, the biocatalytic productivity of the engineered sialidase, Tr6, has been optimized for the production of 3'-sialyllactose.

### Introduction

Dairy side streams are obvious candidates for large-scale production of 3'-sialyllactose and other sialylated compounds from lactose, which is abundant in whey, and the sialylated CGMP (casein glycomacropeptide), which is the soluble glycosylated casein residue produced after chymosin action on  $\kappa$ -casein during cheese manufacture. Recently, it was shown that an engineered sialidase from *Trypanosoma rangeli*, Tr6, could be expressed at high yield in *Pichia pastoris* and used for production of 3'-sialyllactose in gram quantities using CGMP and lactose as substrates for the trans-sialidase reaction [1]. Furthermore, the biocatalytic productivity of Tr6, i.e. the amount of product (3'-sialyllactose) per amount of enzyme has been significantly improved through different enzyme recovery methods, namely enzyme immobilization and the use of an enzymatic membrane reactor (EMR) [2].

### Immobilization of Tr6

Tr6 was immobilized by three different methods [2]:

- 1) Encapsulation of cross-linked Tr6 in calcium alginate
- 2) His-tag-facilitated immobilization on imino-diacetic acid (IDA)-functionalized carbon-coated magnetic nanoparticles (MNPs)
- 3) Fouling-induced membrane immobilization in an EMR

Encapsulation of cross-linked Tr6 in calcium alginate resulted in immediate loss of enzyme activity, whereas membrane immobilization of Tr6 suffered from low

immobilization efficiency (35%). Immobilization of Tr6 on carbon-coated MNPs took place with high efficiency (94%) and resulted in an improved ratio between trans-sialidase activity and unwanted sialidase activity, giving a higher 3'-sialyllactose concentration than free Tr6 already in the first reaction run (Figure 1) [2].

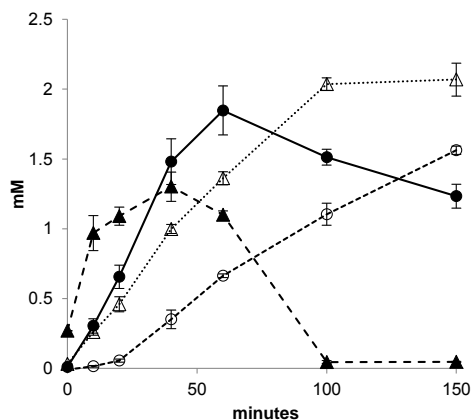


**Figure 1:** Batch production of 3'-sialyllactose (solid symbols) and free sialic acid (open symbols) from lactose and CGMP with Tr6 immobilized on MNPs (circles) and free Tr6 (triangles).

However, the recyclability of the Tr6-MNPs was low due to loss of enzyme from the carrier (Figure 2) [2].

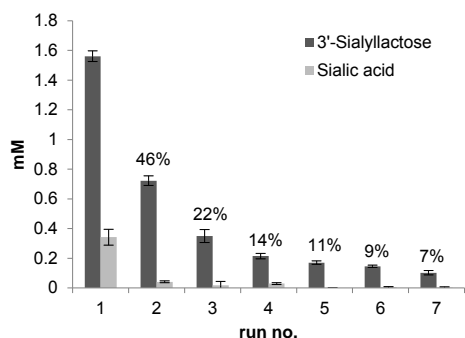


**Figure 2:** Production of 3'-sialyllactose (dark grey) and free sialic acid (light grey) with Tr6 immobilized on MNPs during seven consecutive 60-minute reaction runs. The percentages indicate the level of 3'-sialyllactose compared to the first reaction run.

### Free Tr6 in a membrane reactor

As an alternative to immobilization, free Tr6 was used in an EMR equipped with a 10 kDa regenerated cellulose membrane in order to retain the enzyme (and the CGMP substrate) in the reactor. The production of 3'-sialyllactose was high and constant throughout seven consecutive 60-minute reaction cycles (Figure 3) [2].

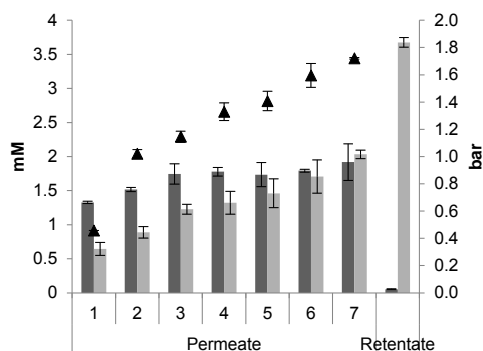


**Figure 3:** Permeate concentrations of 3'-sialyllactose (dark grey) and free sialic acid (light grey) with free Tr6 during seven consecutive 60-minute reaction cycles in the EMR. Retentate concentrations were measured after the end of the seventh cycle. Average pressure applied in each cycle is indicated (triangles; right-hand axis).

Due to CGMP fouling on the membrane, the average pressure applied during each cycle increased throughout the seven-hour reaction (Figure 3). However, CGMP was easily removed from the membrane, which recovered its permeability after simple washing. CGMP build-up inside the reactor also resulted in increased sialic acid concentrations. Even so, rejection of the desired product, 3'-sialyllactose, was low and almost all 3'-sialyllactose was recovered in the permeate (Figure 3) [2].

### Biocatalytic productivity and molar yield on donor

Using Tr6 immobilized on MNPs, the biocatalytic productivity was improved 2.5-fold. However, due to the low recyclability of the Tr6-MNPs, no significant increase in the biocatalytic productivity was obtained after seven reaction cycles compared to four. Instead, much higher yields were obtained with free Tr6 in the EMR: The biocatalytic productivity increased approx. 9-fold compared to the batch reaction, and the molar yield on the sialyl donor, CGMP, was 37% (Table 1) [2]. It may be hypothesized that Tr6 targets  $\alpha(2,3)$ -bound sialic acid only, which corresponds to 50% of the sialic acid present in CGMP [3, 4]. Consequently, the molar yield on the sialyl donor may be 74%.

**Table 1:** Biocatalytic productivity (mg 3'-sialyllactose per mg Tr6) and molar yield on the sialyl donor, CGMP (mol 3'-sialyllactose per mol sialic acid in CGMP) obtained with free Tr6 in batch reactor or in EMR and with Tr6 immobilized on MNPs (up to seven consecutive reaction runs). Superscript letters indicate significant difference ( $p < 0.05$ ).

	Biocatalytic productivity	Molar yield on sialyl donor
Free Tr6	33.5 <sup>a</sup>	28% <sup>f</sup>
Tr6-MNPs (1 run)	47.6 <sup>b</sup>	40% <sup>g</sup>
Tr6-MNPs (4 runs)	73.3 <sup>c</sup>	15% <sup>h</sup>
Tr6-MNPs (7 runs)	84.1 <sup>c</sup>	10% <sup>i</sup>
Free Tr6 in EMR (1 run)	34.3 <sup>a</sup>	29% <sup>f</sup>
Free Tr6 in EMR (4 runs)	164.7 <sup>d</sup>	35% <sup>g</sup>
Free Tr6 in EMR (7 runs)	305.6 <sup>e</sup>	37% <sup>g</sup>

**In conclusion,** the biocatalytic productivity of Tr6 was thus optimized for larger scale production of 3'-sialyllactose from dairy side stream components.

### References

1. Michalak M, Larsen DM, Jers C, Almeida JRM, Willer M, Li H, Kirpekar F, Kjærulff L, Gotfredsen CH, Nordvang RT, Meyer AS, Mikkelsen JD. Biocatalytic production of human milk oligosaccharides by use of a modified sialidase with superior *trans*-sialidase activity. *Process Biochem* 2013; doi:10.1016/j.procbio.2013.10.023.
2. Zeuner B, Luo J, Nyffenegger C, Aumala V, Mikkelsen JD, Meyer AS. Optimizing the biocatalytic productivity of an engineered sialidase from *Trypanosoma rangeli* for 3'-sialyllactose production. Accepted for publication, *Enzyme Microb Technol*, 2013.
3. Vandekerckhove F, Schenkman S, Pontes de Carvalho L, Tomlinson S, Kiso M, Yoshida M, Hasegawa A, Nussenzweig V. Substrate specificity of the *Trypanosoma cruzi trans*-sialidase. *Glycobiology* 1992;2:541-8.
4. Saito T, Itoh T. Variations and distributions of oligosaccharidically linked sugar chains in bovine  $\kappa$ -casein. *J Dairy Sci* 1992;75:1768-74.



**Shizhong Zhang**

Phone: +45 4525 2853  
E-mail: shiz@kt.dtu.dk

Supervisors: Søren Kiil  
Kim Dam-Johansen  
Sten Nørkjær, Hempel A/S

PhD Study  
Started: September 2011  
To be completed: August 2014

## Wind Turbine Blade Coatings with Anti-Erosion Properties

### Abstract

This yearbook contribution describes the correlation test of a new erosion test rig which is expected to supplement testing by the whirling arm rig. A continuous flat fan jet and a straight jet chopped by slotted disks were used in our rig to create erosion. Results have shown that the most important parameters for coating erosion are the water jet slug speed and the impact frequency. However, erosion results obtained so far could not be directly correlated with that obtained in the whirling arm rig.

### Introduction

The wind energy as one of the most potential new energy sources among bio-energy, solar power and nuclear power is attracting global interest [1]. Wind turbine blade coatings play a critical role in determining the durability and performance efficiency. It protects them from exposure to rain, solid particle, dust, UV radiation, salt water, extreme temperature fluctuation and ice accumulation [2]. Wind turbine blades are expected to have 20 years lifetime. Rain droplet impacting is one of the most important factors causing erosion. Rain field properties including droplet temperature, droplet shape, droplet size and density, attack angles, impact velocity and impact time can influence the erosion process in different ways [3].

It is difficult to perform the real erosion test for aircrafts and wind turbine blades, therefore, material anti-erosion properties are normally tested on an artificial erosion testing rig, which can provide an experimental simulation on the coating erosion process and predict the lifetime [4].

Whirling arm facility produces meaningful erosion evaluation which was verified during the research of aircraft materials [5], it is also adopted for rain erosion evaluation by paint companies nowadays, and however, this method with high cost and low test efficiency has confined the screening speed during the development of new coating formulations.

The attempt of this study is trying to construct a new erosion test rig with higher test efficiency and lower cost of both construction and operation if compared with whirling arm apparatus. The continuous flat fan jet was firstly investigated and then discrete straight jet was

used to involve the research of impact frequency. Parameters including impact speed, impact frequency and water jet size were evaluated in this study, and the erosion mechanism and reason of discrepancy of the test results with whirling arm rig are also discussed.

### Specific Objectives

A new rain erosion simulation rig by a water jet shown in Figure 1 was constructed at the first stage. The main goal of this work is to carry out correlation test; the results by the new rig should be able to be correlated with the test results by the whirling arm apparatus.

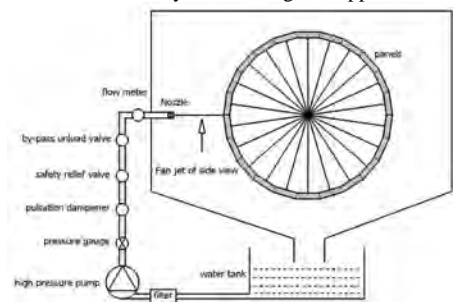


**Figure 1:** Cross sectional view of water jet erosion test.

### Strategy of investigation

The previous erosion tests by continuous even flat fan jet show different results with whirling arm test, therefore the rig was modified to incorporate impact frequency test. The strategy of investigation is shown in Figure 2.

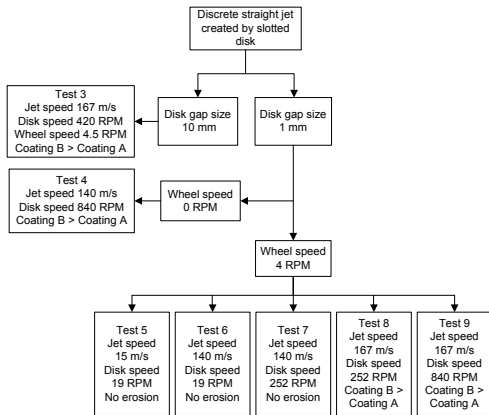


**Figure 2:** Strategy of investigation

### Specimen description

Flat steel panels with dimension  $7.0 \times 15.0$  cm were used as substrate. The steel substrate were firstly coated by the same epoxy primer and then further coated by two different polyurethane based topcoats. The panels were supplied with complete coated state, only the overall dry film thickness (DFT) of both primer and topcoat can be measured. The targeted DFT of primer and topcoats were  $200 \mu\text{m}$  and  $250 \mu\text{m}$ , respectively. The practical overall DFTs fluctuate between  $300$  and  $500 \mu\text{m}$  according to our measurements.

### Effect of water jet speed

In test 5, parameters are varied to equal the impact frequency of the two setups; however, there is no erosion. The impact speed was firstly increased to  $140$  m/s (test 6), and then frequency was increase to  $252$  RPM (test 7) with other parameters kept the same, however, there is still no erosion detected in 66 hours, after that, the speed was increased to  $167$  m/s and erosion of coating A was found to be at 60 hours, this indicates that there is a critical jet velocity for the initiation of erosion, below this speed, the coatings will not show erosion even after a long time exposure, impact speed is the most critical element governing the initiation of erosion, this observation is in accordance with the water hammer pressure.

### Effect of water jet slug size

Erosion increased rapidly with increase of jet size if test 3 and test 4 are compared, because slugs created in test 3 with  $10$  mm gap disk is  $84$  cm which is much bigger than  $3.5$  cm created by  $1$  mm slot disk in test 4. This is due to the reason that with bigger jet size, the pressure exerted on the coating surface will be longer, and bigger size also makes it easier to be distorted and therefore the radius of curvature is larger, this will also increase interaction time between the jet and coating.

### Effect of impact frequency

The elastic coatings have unique property compared with rigid material; their ability to recover between

impacts gives them their superior erosion resistance compared with other rigid polymeric coatings. When the frequencies are matched (test 5 and 6), there are still other differences between the two rigs. Those differences may also lead to discrepancy of erosion results. If the impact frequency is increased from  $252$  RPM (test 8) to  $840$  RPM (test 9), the initiation time of erosion is decreased to 25 hours, and thus, impact frequency is an important parameter governing the rate of erosion damage. However, if the jet speed is not high enough for erosion initiation, the increase of impact frequency exert on erosion on coating even after a long exposure time.

### Conclusions

A new water jet erosion test rig, expected for supplement of erosion test by whirling arm apparatus, was designed and constructed. Two coating systems tested by whirling arm were also investigated by the new rig. The new rig with its capacity of testing 22 panels simultaneously is more efficient than the whirling arm method of 3 samples tested each time. The water jet can create faster erosion and with more samples tested simultaneously than the whirling arm method. The water jet speed is found to be the most critical element for erosion initiation, the increase of impact frequency can increase the erosion rate, and the effect of impact frequency should be based on the existing jet speeds higher than the critical speed for the erosion initiation. The erosion was also accelerated tremendously by increasing the size of water jets slugs.

### Acknowledgement

The project is financially supported by the Technical University of Denmark and The Hempel Foundation.

### References

- [1] S. Gsänger, J.D. Pitteloud, World Wind Energy Report 2012 (2013) 1-19.
- [2] N. Dalili, A. Edrisy, R. Cariveau, A review of surface engineering issues critical to wind turbine performance, Renewable and Sustainable Energy Reviews. 13 (2009) 428-438.
- [3] W.F. Adler, The mechanics of liquid impact, in: C.M. Preece (Ed.), treatise on materials science and technology, Academic Press, New York, 1979, pp. 127-185.
- [4] C.J. Hurley, G.F. Schmitt, Development and calibration of a mach 1.2 rain erosion test apparatus, AFML. AFML-TR-70-240 (1970) 1-68.
- [5] G.F. Schmitt, Flight test-whirling arm correlation of rain erosion resistance of materials, AFML. AFML-TR-67-420 (1968) 1-31.

**Guofeng Zhou**

Phone: +45 4525 2853  
E-mail: guzho@kt.dtu.dk

Supervisors: Anker Degn Jensen  
Peter Arendt Jensen  
Niels Ole Knudsen, DONG Energy

**PhD Study**

Started: October 2012  
To be completed: September 2015

## Fast Pyrolysis of Wood and Lignin Using the New Pyrolysis Centrifuge Reactor

**Abstract**

Fast pyrolysis is a prospective thermal chemical route to produce liquid fuel, known as bio-oil, from biomass. Over the past 20 years, fast pyrolysis technology has been mainly developed using fluidized bed reactor systems. A new reactor design is developed in the CHEC Research Center, called the Pyrolysis Centrifuge Reactor (PCR). The biomass particles obtain a high heat transfer rate through direct contact with the hot reactor wall, and the reactor is further improved by a redesigned version of the PCR. The objectives of the project are to optimize the liquid yield from lignin pyrolysis and to test the use of hydrogen online upgrading of the pyrolysis oil.

**Introduction**

Fast pyrolysis is a thermal chemical method to decompose biomass at 450-600°C and short gas residence time (< 1 second) in the absence of oxygen, whereby a maximum yield of pyrolysis oil is achieved [1]. Three products are produced, *i.e.* char, bio-oil and pyrolysis gas. The obtained bio-oil is a mixture of water and oxygenated hydrocarbons.

The CHEC research Center at DTU has developed a fast pyrolysis technology called the Pyrolysis Centrifuge Reactor (PCR). The pyrolysis of various types of biomasses, including wood, straw, algae and lignin, has been investigated using the PCR. Up to about 70wt% bio-oil yield on dry basis is achieved using wood as a feedstock on the PCR setup. Based on the obtained experience, the PCR setup is renovated and a new improved reactor has been developed.

**Specific objectives**

The low quality of the produced bio-oil with respect to stability, immiscibility with hydrocarbons and low pH limits its usage as transport fuel. The objectives of this project are to optimize the liquid yield from lignin pyrolysis and to upgrade pyrolysis vapor using catalyst and hydrogen donor.

**Experimental setup**

The biomass particles are conveyed by a screw feeder into the centrifuge reactor. Biomass particles are forced onto the hot reactor wall in order to obtain a high

heating rate. After the reactor, the char particles are separated by a change-in-direction separator first, followed by a cyclone. Separator and cyclone are kept at 500°C by heat tracing. The bio-oil is condensed in a bubble chamber, which is kept below 40°C by cooling liquid. Isopropanol is added to the bubble chamber as a condensing solvent. The aerosols are collected by a coalescer filled with fibrous Rockwool®. The gas product is partially recycled back to the reactor by a gas pump. Prior to the reactor, the gas is heated up to 500°C by a gas preheater. The gas flow is controlled by a needle valve to maintain a desired gas residence time. The remaining gas passes through a gas meter and is sent to ventilation.

**Results and discussion****1. Comparison of new and old PCR**

To compare the performance of the new and old PCR, wood is used. The reactor temperature is kept at 550°C; the feeding rate is between 7-10 g/min; and the gas residence time is below 1 second.

The chars obtained from the two reactors were analyzed by a TGA (Thermal Gravimetric Analyzer). The samples were heated up to 1000°C under 100 ml/min nitrogen. The weight losses are 29% and 53% for chars from the new and old PCR respectively, as shown in Figure 1. This indicates that the wood particles processed by the new PCR are more devolatilized compared to the old one, due to a better heat transfer

from the reactor wall to the biomass particles. SEM images of the chars collected from the separators of the two reactors confirm this. As shown in Figure 2, wood particles without being completely pyrolyzed are found in the separator of the old reactor.

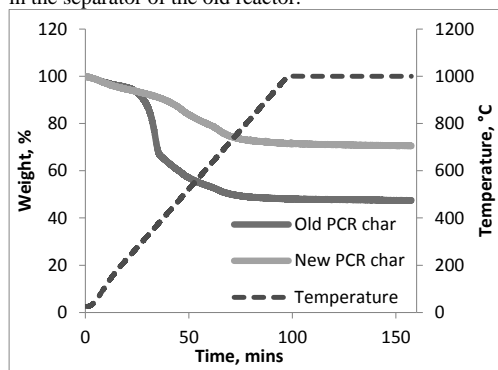


**Figure 1:** TGA profiles of wood derived chars from new and old PCR.

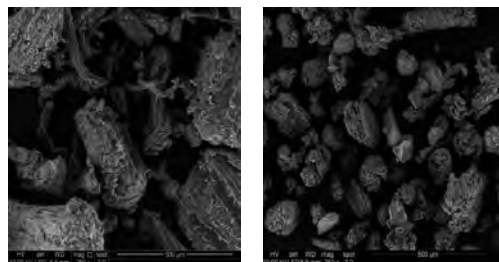


**Figure 2:** SEM images of the chars collected in the first separators of the old (left) and new (right) PCR. The scale bar is 500  $\mu\text{m}$ .

Good performance is achieved with lower char yield from the new PCR, and hence more oil and gas are produced, as shown in Figure 3. A reduction of the char yield of 46% is achieved using the new PCR, while 2.9% more wood derived bio-oil is gained.

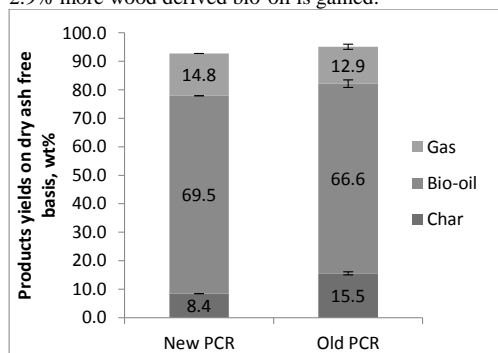


**Figure 3:** Products yields of wood fast pyrolysis using old and new PCR. The results are from three repeated runs.

## II. Lignin fast pyrolysis

Lignin is the second most abundant biomass component found in the nature [2]. It is a residue from the pulp and paper industry as well as the second generation bioethanol industry. In this project, lignin produced from Inbicon, a second generation bioethanol plant, is used. In the past 20 years, fast pyrolysis technology has been developed mainly using fluidized bed reactor system. Lignin is found difficult to process in such a reactor system, due to formation of adhered clumps of bed material and lignin char [2]. However, it is not a problem for the PCR, because it requires no bed material and the rotor inside the reactor continuously moves the lignin particles and removes lignin chars.

Initial experiments are conducted at three different reactor temperatures, 500°C, 550°C and 600°C. The feeding rate is kept at 11 g/min and the gas residence time is 0.73 second. The bio-oil is now divided into reaction water and organics. The maximum organic yield is found at 500°C. With increasing temperature, the organics are cracked and more gas products are produced as shown in Figure 4.

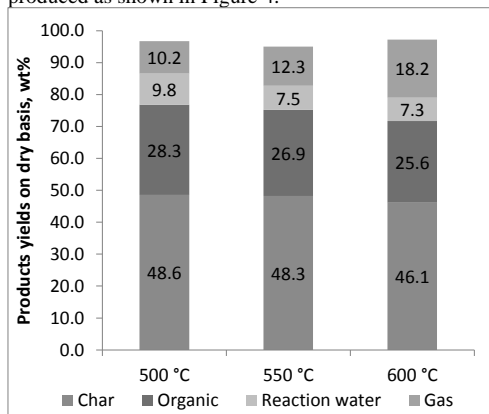


**Figure 4:** Products yields of lignin fast pyrolysis using the new PCR under different temperature.

## Conclusions

The PCR setup developed by the CHEC research Center is renovated and an improved reactor is built. Compared to the old one, the new PCR provides better heat transfer from the reactor wall to the biomass particles. This results in a higher degree of biomass pyrolysis and more bio-oil products. Lignin is also successfully processed by the new PCR without facing typical problems observed in fluidized bed reactor systems. The maximum organic yield (28.3 wt%<sub>db</sub>) from lignin fast pyrolysis is found at 500°C.

## References

1. A.V. Bridgwater, Biomass and Bioenergy 38 (0) (2012) 68-94.
2. D.J. Nowakowski, A.V. Bridgwater, D.C. Elliott, D. Meier, P. de Wild, Journal of analytical and applied pyrolysis 88 (1) (2010) 53-72.



**Andreas Åberg**

Phone: +45 4525 2912  
E-mail: aben@kt.dtu.dk

Supervisors: Jens Abildskov  
Jakob Kjøbsted Huusom  
Anders Widd, Haldor Topsøe

PhD Study  
Started: August 2013  
To be completed: July 2016

## Modeling and Operation of Diesel Engine Exhaust Gas Cleaning Systems

### Abstract

Diesel engine exhaust gases contain amongst other things nitrous gases such as NO and NO<sub>2</sub>. Reducing the amount of these gases is of great importance due to new legislation, and because of the effect they have on urban air quality. A promising and widely used technology for this is based on selective catalytic reduction (SCR) of the gases, with ammonia as a reducing agent. Challenges with this technology include dosing the right amount of urea to reach maximum nitrogen oxide conversion, but at the same time minimize ammonia slip. The aim of this project is to develop model based control algorithms for the dosing of urea to the catalyst. The project is in collaboration with Haldor Topsøe A/S.

### Introduction

Heavy duty diesel (HDD) vehicles handle a substantial part of the world's transport and logistics. Harmful pollutants are however formed, such as nitrogen oxides (NO<sub>x</sub>), hydrocarbons (HC), particulate matter (PM), and carbon monoxide (CO). The diesel exhaust aftertreatment (DEA) system has been developed to treat the pollutants in the exhaust gas. Figure 1 illustrates the current standard DEA system consisting of a series of catalytic units. The Diesel Oxidation Catalyst (DOC) oxidizes CO and HC to CO<sub>2</sub> and H<sub>2</sub>O, as well as generates NO<sub>2</sub> from NO. The Diesel Particulate Filter (DPF) is a wall-flow filter, entraining PM in its monolith walls. The DPF can be regenerated actively by increasing the exhaust gas temperature using post-injection of fuel, or passively using a catalyst. NO<sub>2</sub> generated by the DOC also assists regeneration. NO<sub>x</sub> is treated through Selective Catalytic Reduction (SCR) using NH<sub>3</sub> as the reducing agent. NH<sub>3</sub> is supplied to the system through urea dosing, regulated by the onboard Model Predictive Control (MPC) unit. Excess NH<sub>3</sub> is controlled with the Ammonia Slip Catalyst (ASC). Upon exiting the DEA system, the emissions should meet the restrictions imposed by the Euro VI regulations [1].

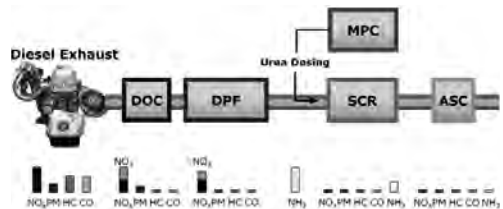


**Figure 1:** Example of a standard design of the DEA system, consisting of the DOC, DPF, SCR component, urea dosing MPC unit, and the ASC.

The DEA system is very complex, requiring efficient exhaust treatment for a wide range of operating conditions, corresponding to cold start, stop-and-start driving (inner city), and high speed driving (highways). As a result, DTU Chemical Engineering and Haldor Topsøe A/S are collaborating on the development of the next generation DEA system, with funding from The National Danish Advanced Technology Foundation. The underlying PhD projects concern the development of new DOC and ASC formulations (Thomas Klint Hansen, pg. 83-84), the combination of the DPF and SCR components (Kasper Linde, pg. 121-122), and the development of the MPC unit for efficient regulation of urea dosing in this project.

### Specific Objectives

The overall objective of this project is to develop models and model based control structures to control the urea injection to the catalyst demanded by enhanced legislation. Since a new catalyst design most likely will be developed by the other PhD-students in the overall project, it is important that the results in this project are generic and can be used for a new system as well. Therefore, the project will focus on developing a methodology on a currently used catalyst, to be able to tackle similar problems. Developing the methodology will involve several steps:

- Develop high fidelity simulation model based on first principles, parameter estimation and validation of the model
- Develop lower accuracy models, parameter estimation and validation of the models
- Quantify information loss in different models to understand the needed model complexity
- Develop and investigate several model based control schemes
- Validate the chosen control structure with full-scale engine tests using standardized test driving cycles.

Based on the progress in the other projects, the developed methodology will be used on a new system design.

### Current Results and Discussion

A high fidelity model based on first principles has been developed. The model can be described as a plug flow reactor model with diffusion terms describing the transfer into the washcoat, where the reaction takes place. The governing equations are as in Equations 1 through 4.

$$\frac{\partial c_{b,i}}{\partial t} = -u \frac{\partial c_{b,i}}{\partial z} + D_{ax,i} \frac{\partial^2 c_{b,i}}{\partial z^2} - \frac{4kg_i}{b} (c_{b,i} - c_{wcs,i}) \quad (1)$$

$$\frac{\partial c_{wc,i}}{\partial t} = \frac{D_{wc,i}}{\epsilon_{wc}} \frac{\partial^2 c_{wc,i}}{\partial x^2} + \frac{1}{\epsilon_{wc}} \sum_{i=1}^N r_i \quad (2)$$

$$\frac{\partial T_b}{\partial t} = -u \frac{\partial T_b}{\partial z} \frac{\lambda_{ax}}{\rho_b c_{p,b}} \frac{\partial^2 T_b}{\partial z^2} - \frac{4h_{heat}}{b \rho_b c_{p,b}} (T_b - T_{wcs}) \quad (3)$$

$$\frac{\partial T_{wc}}{\partial t} = \frac{\lambda_{wc}}{\epsilon_{wc} \rho_{wc} c_{p,wc}} \frac{\partial^2 T_{wc}}{\partial x^2} + \frac{1}{\epsilon_{wc} \rho_{wc} c_{p,wc}} \sum_{i=1}^N \Delta H_i r_i \quad (4)$$

The equations describe the change in concentration in the bulk and washcoat for the different species, and also the change in bulk temperature and washcoat temperature. Assumptions made when deriving the model is that there exist no radial gradients, the volumetric flow rate is constant, no reactions take place in the bulk phase, there is no convective flow in washcoat and that there is no energy loss to ambient. The reaction terms  $r_i$  can be given by several different kinetic expressions found in literature.

The above model has been implemented in MATLAB, using an equispaced finite volume method to discretize the set of partial differential equations (PDEs). The

species currently included in the model are NO, NO<sub>2</sub> and NH<sub>3</sub>, which in total gives 8 nonlinear PDEs that have to be solved simultaneously. Another candidate that is of interest is for example N<sub>2</sub>O, which depending on the project direction will be included later.

The number of physical parameters and reaction parameters that have to be estimated is large, and it is therefore important to have good initial guesses for these values. To estimate diffusions coefficients, thermal conduction constants, heat capacities etc. both theoretical methods and numerical correlations based on observations have been used. To estimate film transfer coefficients for heat and mass, relationships with dimensionless numbers such as Reynolds, Nusselts and the Sherwood number have been used.

The reason a high fidelity model has been developed, even though the end application will require a very fast model capable of running faster than real time, is firstly that it will give a good initial system understanding of how important different phenomena are. Secondly, it will make it possible to quantify how much information is lost with lower accuracy models compared to the best case. This will help to determine the required model accuracy in the control algorithm. Thirdly, a good simulation model will hopefully be accurate enough to reduce the amount of experimental data required to test control algorithms, since the control structures can be tested on the model before it is tested using a real engine.

### Conclusions and Future Work

The derived simulation model includes few major assumptions and will therefore with good parameter estimates represent reality well. The estimation of the parameters will however be critical for its performance. Due to the complexity, simulation time is high and estimation of the parameters will be time consuming and require good initial guesses. The work in the immediate future will include a numerical estimation of the parameters using real engine data. After this, the same will be done with lower accuracy models which will then be used in a model based control algorithm.

### Acknowledgement

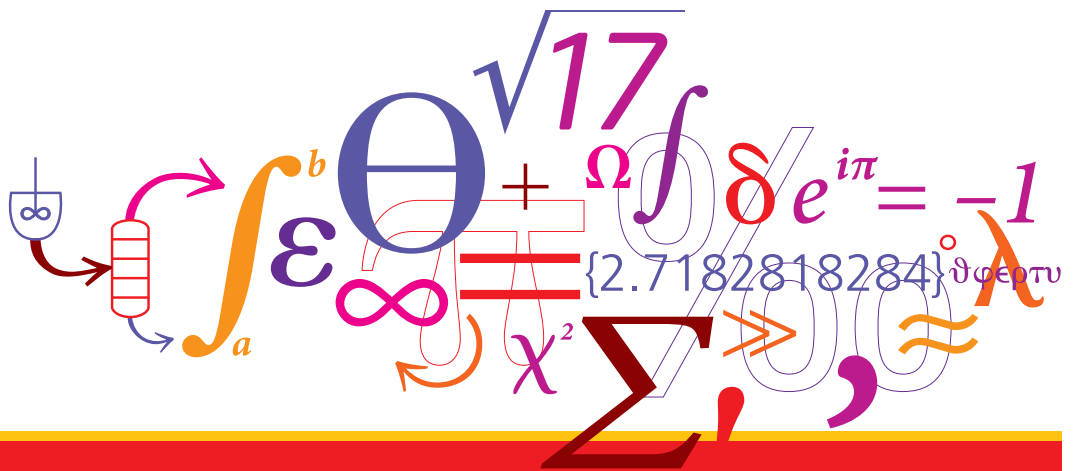
This project is a collaboration between the CAPEC research center of DTU Chemical Engineering, Haldor Topsøe A/S and the National Danish Advanced Technology Foundation.

### References

1. W. A. Majewski, M. K. Khair, Diesel Emissions and Their Control, SAE International, 2006.







## Chemistry at work

Bio Engineering

Catalysis

Combustion and Environmental Engineering

Ecosystem Modelling and Sustainability

Engineering Thermodynamics

Enzyme Technology

Petroleum Engineering

Polymer Technology

Process Technology and Unit Operations

Product Design

Reaction and Transport Engineering

Systems Engineering

Department of Chemical  
and Biochemical Engineering

DTU Building 229  
Søltofts Plads  
DK-2800 Kgs. Lyngby  
[www.kt.dtu.dk](http://www.kt.dtu.dk)